HORT PAPERS IN—

nalytical and laboratory methods

conomic geology

ngineering geology

ield equipment

eochemistry

eomorphology

eophysics

round water

ydrologic instrumentation

sotope geology

Marine geology

Mineralogy

aleontology

etrology

Quality of water

ock mechanics

edimentation

tratigraphy

tructural geology

# GEOLOGICAL SURVEY RESEARCH 1966

## Chapter C



GEOLOGICAL SURVEY PROFESSIONAL PAPER 550-C

# GEOLOGICAL SURVEY RESEARCH 1966

# Chapter C

GEOLOGICAL SURVEY PROFESSIONAL PAPER 550–C

*Scientific notes and summaries of investigations by members of the Geologic, Topographic, and Water Resources Divisions in geology, hydrology, and related fields*

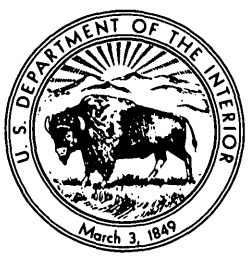


UNITED STATES GOVERNMENT PRINTING OFFICE, WASHINGTON: 1966

UNITED STATES DEPARTMENT OF THE INTERIOR

STEWART L. UDALL, Secretary

GEOLOGICAL SURVEY

William T. Pecora, Director

For sale by the Superintendent of Documents, U.S. Government Printing Office,
Washington, D.C. 20402 - Price $2.25

# CONTENTS

## GEOLOGIC STUDIES

# GEOLOGICAL SURVEY RESEARCH 1966

This collection of 43 short papers is the second published chapter of "Geological Survey Research 1966." The papers report on scientific and economic results of current work by members of the Geologic, Topographic, and Water Resources Divisions of the U.S. Geological Survey.

Chapter A, to be published later in the year, will present a summary of significant results of work done during fiscal year 1966, together with lists of investigations in progress, reports published, cooperating agencies, and Geological Survey offices.

"Geological Survey Research 1966" is the seventh volume of the annual series Geological Survey Research. The six volumes already published are listed below, with their series designations.

Geological Survey Research 1960—Prof. Paper 400
Geological Survey Research 1961—Prof. Paper 424
Geological Survey Research 1962—Prof. Paper 450
Geological Survey Research 1963—Prof. Paper 475
Geological Survey Research 1964—Prof. Paper 501
Geological Survey Research 1965—Prof. Paper 525

# DETACHMENT FAULTS IN THE CENTRAL SANTA MONICA MOUNTAINS, CALIFORNIA

By R. H. CAMPBELL, R. F. YERKES, and C. M. WENTWORTH,
Menlo Park, Calif.

*Work done in cooperation with Los Angeles County, Calif.*

*Abstract.*—The central Santa Monica Mountains are made up of sedimentary and volcanic rocks of Late Cretaceous through middle Miocene age that are probably underlain at depth by older metasedimentary and igneous rocks of the sort exposed in the core of the Eastern Santa Monica Mountains. Structurally, these strata form an autochthon(?) and three detachment thrust sheets that were emplaced during latest middle Miocene time, apparently from a source to the north. The thrust sheets are superimposed upon one another in a stratiform sequence which, in turn, has been folded and faulted, and dilated by igneous intrusion. On the south, these rocks and structures are truncated by the Malibu Coast fault, which trends east-west along the southern flank of the range.

The Santa Monica Mountains trend east-west along the north side of Santa Monica Bay and the northwest side of the Los Angeles basin (fig. 1). The range lies at the southern edge of the east-west-trending Transverse Ranges province; farther south of the range the general northwesterly trends of the Peninsular Ranges province predominate in the largely submerged continental borderland. The rocks of the Santa Monica Mountains are complexly folded and faulted, and the geology is further complicated by facies changes in several of the time-stratigraphic units. Since 1961, the U.S. Geological Survey, in cooperation with Los Angeles County, has been mapping the geology of the central part of the range at a scale of 1:12,000. Although the mapping is far from complete and many problems remain, the structural, stratigraphic, and paleontologic data gathered to date clearly demonstrate that thrust faults (detachment faults) dominate the structure of the main mass of the central Santa Monica Mountains. Low-angle thrust faults have not been recognized in this area by earlier investigators (Durrell, 1954; Bailey and Jahns, 1954; Soper, 1938; and Hoots, 1931); nevertheless, most of the rock distribution shown on their maps is readily reconciled with the structural framework described herein.

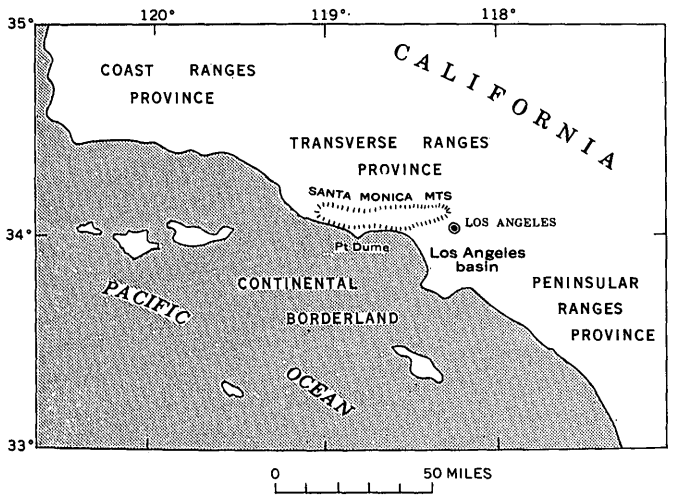


FIGURE 1.—Outline map of part of southern California, showing relation of the Santa Monica Mountains to geomorphic provinces.

The main mass of the central Santa Monica Mountains lies north of the west-trending Malibu Coast fault (fig. 2), where the strata consist of sedimentary and volcanic rocks of Late Cretaceous through middle Miocene age (fig. 3) that are probably underlain by older metasedimentary and igneous rocks of the sort exposed in the core of the eastern Santa Monica Mountains (Durrell, 1954). Structurally, these rocks form an autochthon(?) and three superimposed thrust sheets: in ascending order, the Tuna Canyon, Zuma, and Malibu Bowl thrust sheets, each of which is named for the thrust fault beneath it. This tectonic stacking

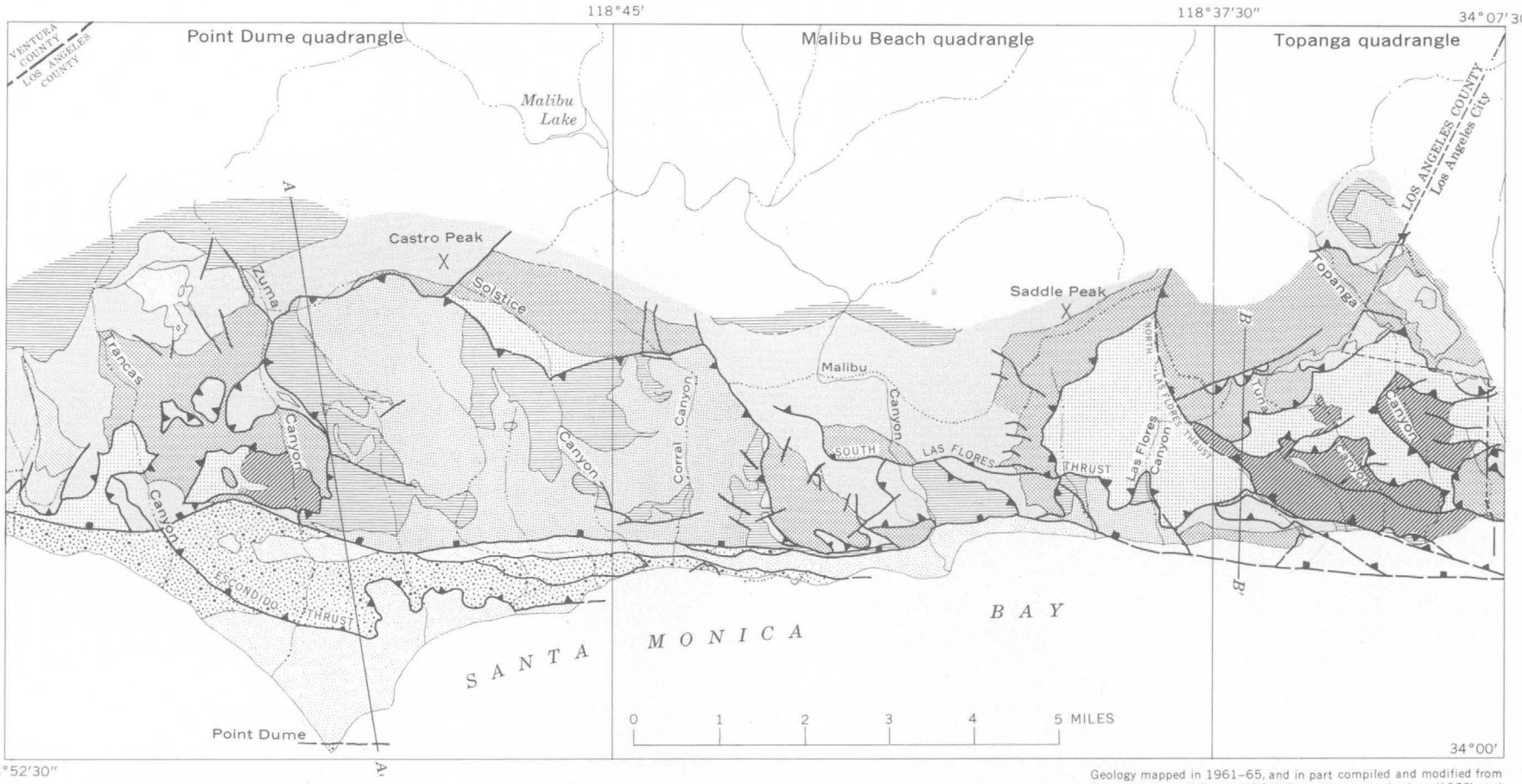


Geology mapped in 1961–65, and in part compiled and modified from Schoellhamer and Yerkes (1961), Schoellhamer and others (1962), and Yerkes and others 1964

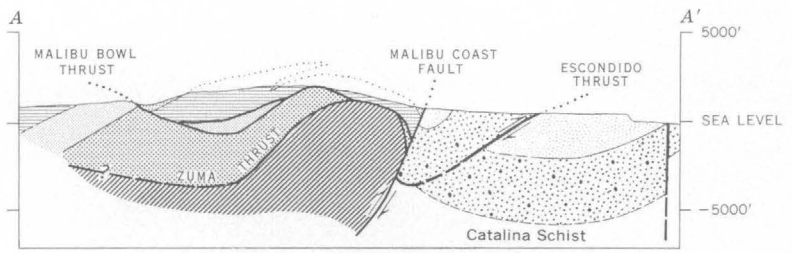


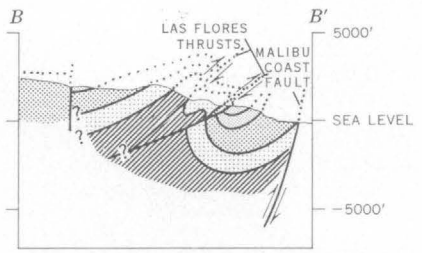


EXPLANATION

COASTAL SEQUENCE
(South of Malibu Coast fault)

Upper and middle Miocene marine sedimentary rocks (Monterey Shale)

Middle and lower Miocene marine sedimentary and volcanic rocks

MOUNTAIN SEQUENCE
(North of Malibu Coast fault)

Upper middle Miocene intrusive rocks

Upper middle Miocene marine sedimentary rocks (Upper Topanga Formation of Durrell, 1954)

Middle Miocene volcanic rocks (Middle Topanga Formation of Durrell, 1954)

Middle and lower Miocene sedimentary rocks, predominantly marine (Lower Topanga Formation of Durrell, 1954)

Middle Miocene to upper Eocene sedimentary rocks, predominantly continental (includes Sespe Formation)

Eocene and Paleocene marine sedimentary rocks

Upper Cretaceous marine sedimentary rocks

Contact
*Dashed where approximately located; dotted between formations in lithofacies units of this map*

Malibu Coast fault
*Dashed where approximately located*

Thrust fault
*Sawteeth on upper plate; dashed where approximately located*

High-angle fault
*Dashed where approximately located*

FIGURE 2.—Generalized geologic map and sections of the south-central Santa Monica Mountains, Los Angeles County, Calif.

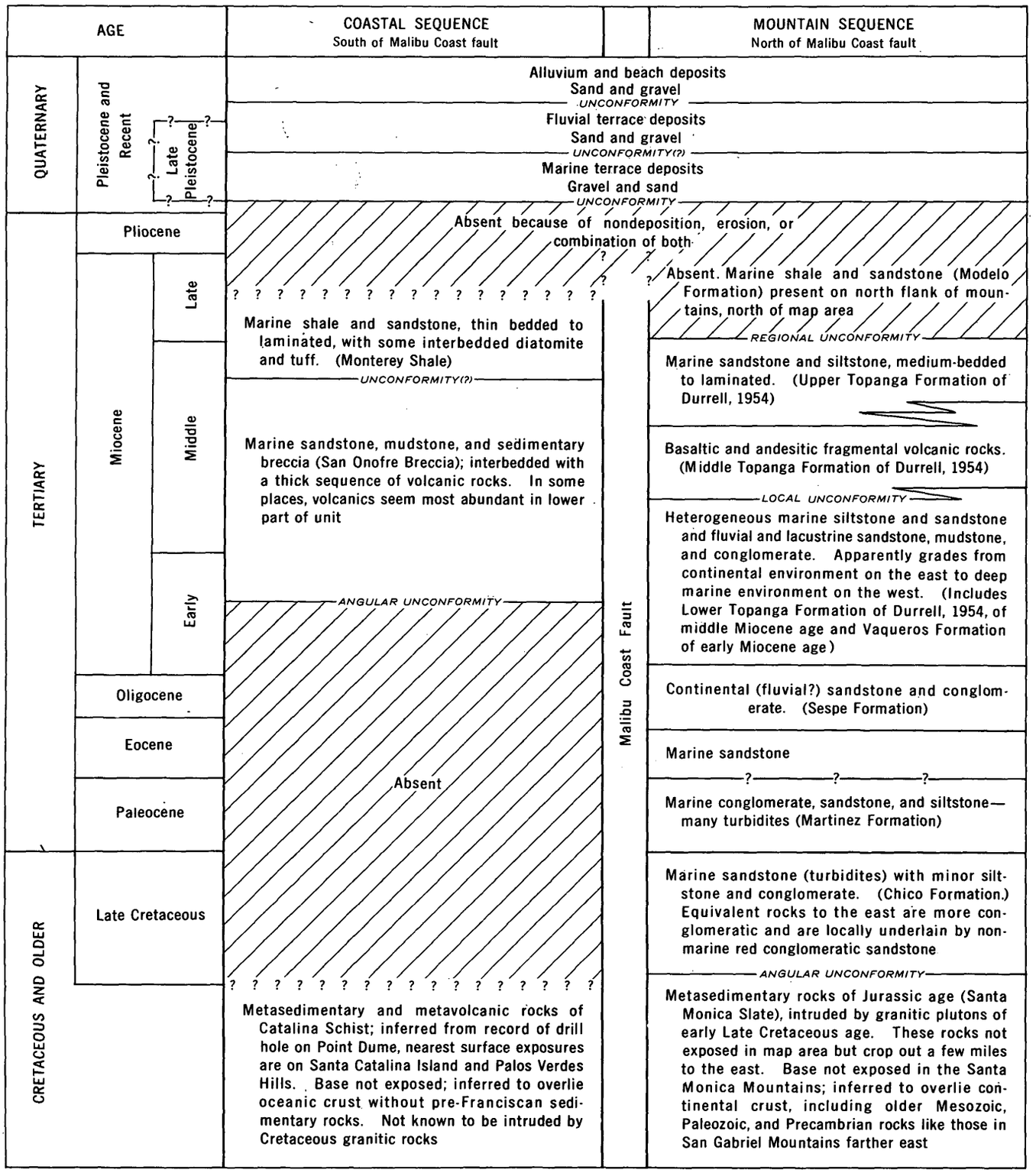


FIGURE 3.—Columnar chart showing the two stratigraphic sequences juxtaposed along the Malibu Coast fault.

has resulted in a stratiform sequence that has subsequently been folded and faulted, and dilated by the intrusion of mafic and intermediate igneous rock. The Zuma sheet is the most widely exposed of the thrust sheets; the autochthon(?) and the Tuna Canyon sheet are exposed in windows cut through it, and the Malibu Bowl sheet is represented by outliers on top of it. The north, east, and west limits of the thrust sheets have not as yet been ascertained. On the south, these rocks and structures end abruptly at the Malibu Coast fault.

The Tuna Canyon, Zuma, and Malibu Bowl thrusts are detachment faults (following the usage of Pierce, 1963, p. 1226) that, for the most part, bring younger rocks over older rocks along surfaces that are parallel or nearly parallel to bedding in the rocks of the upper plate. The thrusts are unambiguously recognizable only where they break across the bedding of the upper-plate rocks (for examples see figs. 4 and 6). From the relatively few localities where these discordant relations are found, the thrusts have been traced through contiguous areas of accordant relations, and correlated across discontinuities of exposure by the rather distinctive stratigraphic intervals associated with each thrust sheet. Exposures of the actual thrust surfaces are rare; the few found expose either a zone of brecciated rock (generally less than 2 feet thick, but locally thicker) or a filling of intrusive igneous rock. The traces of the faults are, however, sufficiently controlled by outcrops of the juxtaposed rock units to establish that gentle dips predominate. In localities where beds in the upper plate are accordant with the underlying fault surfaces, and where lower-plate rocks are older than upper-plate rocks, the detachment thrusts might be misinterpreted as unconformable sedimentary contacts, perhaps complicated by high-angle faults. In such areas consistency with the regional structural and stratigraphic framework is the best guide to the nature of unexposed contacts.

South of the Malibu Coast fault, a greatly different sequence of strata is present (fig. 3). Although undoubtedly widespread beneath the waters of Santa Monica Bay, the rocks are known best from exposures in the narrow strip of relatively low-lying coastland extending east and west from Point Dume. The strata of this coastal strip correlate with those of the western part of the Los Angeles basin (see Woodford and others, 1954), whereas the strata of the main mass of the mountains correlate with those to the north and east in the Transverse Ranges, and with those of the eastern part of the Los Angeles basin. The geologic structures of the coastal strip trend generally east, approximately parallel to the general trend of the Santa Monica Mountains. There is, however, no evident direct association of these structures (including at least one thrust fault—the Escondido thrust) with the thrust faults to the north. Indeed, the structures of the coastal strip involve rocks that are younger than the probable youngest thrusting of rocks in the main mountain mass. They are most probably intimately associated with the Malibu Coast fault.

## THE AUTOCHTHON(?)

The autochthon(?) is below the lowest of the recognized thrust faults of the tectonically layered sequence. It is exposed in windows through the overlying thrust sheets in Topanga Canyon and in an elongate irregular area extending about 3 miles west-northwest from the mouth of the Topanga Canyon. Windows in Zuma Canyon and Trancas Canyon (fig. 5) expose rocks that also belong to the autochthon(?) unless the Tuna Canyon thrust is present below the deepest exposures. The rocks of the autochthon(?) are chiefly sandstone of Late Cretaceous age, overlain conformably(?) in a few places by conglomerate and sandstone of Paleocene age. The beds are folded and faulted. Strikes and dips vary widely, but west to northwest strikes are most common, and a general asymmetry of the folding, with north-dipping axial planes, is suggested by the overall predominance of gentle dips of the north-facing beds and steeper dips of the south-facing beds. Moreover, the only recognized overturned beds face southward and dip steeply northward. In most places, exposures are inadequate to obtain a complete, detailed understanding of the structure within the autochthon(?). Nevertheless, the rocks seem to have been at least gently folded before the lowest overlying thrust sheet was emplaced.

## THRUST SHEETS

### Tuna Canyon thrust sheet

The Tuna Canyon thrust sheet and the Tuna Canyon thrust fault at its base are named for exposures in Tuna Canyon. The Tuna Canyon sheet is the lowest of the recognized thrust sheets. It is exposed in windows that have been eroded through the younger overlying thrust sheets in an irregular area extending from the east side of Topanga Canyon westward for about 4 miles. To the north and southeast it is overlain by the rocks of the two higher thrust sheets. It is inferred to be present southeast of Saddle Peak, in a window bounded by the North and South Las Flores thrust faults


FIGURE 4.—The Zuma thrust fault; view southwestward of the east side of a ridge east of Trancas Canyon. The fault here is a nearly flat surface as is well defined by its sinuous trace along a fixed altitude on the slope of the ridge; it is also found on the west side of the same ridge and on the hillside in the background. Marine Paleocene rocks (Tma) are exposed below the thrust. Above the thrust, marine lower Miocene rocks (Tva) overlie continental sandstone and conglomerate of the Sespe Formation (Ts) at *A*, an accordant depositional contact (dotted where concealed beneath landslide, Qls). Both the bedding within the Sespe (*B*) and the contact (*A*) are truncated at their contact—the Zuma thrust—with the older rocks below.

(fig. 5). It has not been recognized in the windows of Zuma and Trancas Canyons, and its continuation at depth is not inferred to extend that far west (structure section C–C′, fig. 5).

The rocks of the exposed segments of the Tuna Canyon thrust sheet are almost exclusively Paleocene in age. Conglomerate, overlain by sandstone and siltstone, predominates in the Topanga and Tuna Canyon areas. Farther west, conglomerate is less abundant and sandstone predominates. A small thickness of Cretaceous sandstone belonging to the Tuna Canyon sheet is exposed beneath Paleocene conglomerate in a small area in the head of Tuna Canyon. The contact appears to be conformable, except for minor scour features. The same depositional contact is exposed in the autochthon(?) on the east side of Topanga Canyon and on the east side of Tuna Canyon (fig. 2). The Tuna Canyon thrust sheet is the only one that contains rocks and a contact that are also found in the autochthon(?), and, therefore, it might be regarded as parautochthonous in comparison with the allochthonous Zuma and Malibu Bowl sheets.

Although the Tuna Canyon thrust fault is parallel or nearly parallel to the bedding of the upper-plate rocks in many places, it locally cuts across that bedding. The relations suggest gently folded beds cut by a nearly planar fault that was subsequently folded and faulted.

### Zuma thrust sheet

The Zuma thrust sheet and the Zuma thrust fault at its base are named for exposures between Zuma

and Trancas Canyons (figs. 4 and 5). There, the Zuma sheet overlies rocks that apparently belong to the autochthon(?). Farther east it overlies rocks of the Tuna Canyon thrust sheet except in a few small areas where it cuts out the Tuna Canyon sheet and lies directly on the autochthon(?).

The fluvial(?) continental sandstone and conglomeratic sandstone of the Sespe Formation (fig. 3) are the most distinctive and widespread rocks of the Zuma thrust sheet. The Sespe is known only in the Zuma thrust sheet and has not been found in the autochthon(?) or in the other thrust sheets. The Zuma sheet also carries marine and continental sandstone, siltstone, and mudstone of early and middle Miocene age (the Lower Topanga Formation of Durrell, 1954), which overlie the Sespe Formation and are, in turn, overlain by basaltic and andesitic volcanic rocks of middle Miocene age (the Middle Topanga Formation of Durrell, 1954) (fig. 3). The only place where pre-Sespe rocks are probably included in the Zuma thrust sheet is in the upper part of Solstice Canyon. There, fossiliferous conglomerate, sandstone, and siltstone of Paleocene and Eocene age underlie the Sespe apparently in a normal depositional sequence.

The rocks of the Zuma thrust sheet were probably folded before, as well as after, the displacement on the Zuma thrust occurred. Although the thrust fault is parallel or nearly parallel to the bedding of the upper-plate rocks in most places, it locally cuts across bedding and faults of the upper plate, with relations suggesting that previously folded and faulted beds were cut by a nearly planar fault. Locally, the Zuma thrust cuts out the Tuna Canyon thrust sheet (fig. 5, section *C–C'*; fig. 6). The Zuma thrust sheet was also folded and cut by high-angle faults prior to the emplacement of the higher Malibu Bowl thrust sheet (fig. 5, section *C–C*; fig. 6).

### Malibu Bowl thrust sheet

The Malibu Bowl thrust sheet and thrust fault are named for a topographic amphitheater at the head of Corral Canyon. Newton (1958) mapped the Malibu Bowl fault from there westward to Zuma Canyon and southeastward to its intersection with the Malibu Coast fault. The largest single exposure of the Malibu Bowl sheet is an elongate area about 2 miles wide, extending from about 1½ miles west of Malibu Canyon westward to the east side of Zuma Canyon. Exposures farther east are restricted to the extreme northeast corner of the map area (fig. 2), to small outliers in the Topanga quadrangle, and to a narrow strip near the coast.

The rocks exposed in the Malibu Bowl thrust sheet include lower and middle Miocene marine sandstone, siltstone, and minor conglomerate (Lower Topanga Formation of Durrell, 1954), overlain by basaltic and andesitic extrusive volcanic rocks of varying thickness (Middle Topanga Formation of Durrell, 1954) succeeded by and intertonguing with marine sandstone and siltstone of middle Miocene age (Upper Topanga Formation of Durrell, 1954) (fig. 3). Several outliers and horses (bounded by thrust faults), chiefly of lower Miocene marine sandstone and siltstone appear to be slivers peeled from the base of the Malibu Bowl sheet.

The Malibu Bowl thrust cuts both the Tuna Canyon and Zuma thrust faults. The Malibu Bowl thrust is commonly parallel or nearly parallel to the bedding in the upper plate. Although the fault locally cuts across bedding in the upper plate, there is no clear indication that upper-plate folds are truncated. The underlying thrust sheets, however, were probably folded prior to emplacement of the Malibu Bowl sheet. At the anticline that crosses Topanga Canyon, for example, the Zuma and Tuna Canyon thrust faults are arched with greater amplitude than that of the Malibu Bowl thrust (fig. 6).

### Age and origin

Crosscutting relations suggest a chronologic sequence of thrust sheets, with the Tuna Canyon thrust sheet first, followed by the Zuma and Malibu Bowl sheets. Nevertheless, they may be very close in age. The Malibu Bowl sheet includes rocks of middle Miocene age and, from interpretation of maps published by Hoots (1931) and Durrell (1954), the thrust faults are cut by the unconformity at the base of the Modelo Formation of late Miocene age, about 2 miles north of the map area of figures 2 and 5. The thrust sheets were, therefore, probably emplaced during late middle Miocene.

The thrust plates are tentatively inferred to have moved from north to south. This is based on the absence, south of the Malibu coast fault, of strata that could have provided the rocks in the thrust sheets, and on the present general east-west structural trends which are presumed to be approximately perpendicular to the direction of movement. This presumption assumes, of course, that the late middle Miocene trends were not greatly different from, nor obscured by, those formed in subsequent deformation. The general younger-over-older sense of displacement of the thrust sheets indicates detachment and translation of relatively shallow younger strata over more stable, deeper, older rocks, and, therefore, suggests that the thrusting was a near-surface phenomenon of the sort often considered to be associated with gravity tectonics. To the north, the nearest uplifted area that might have

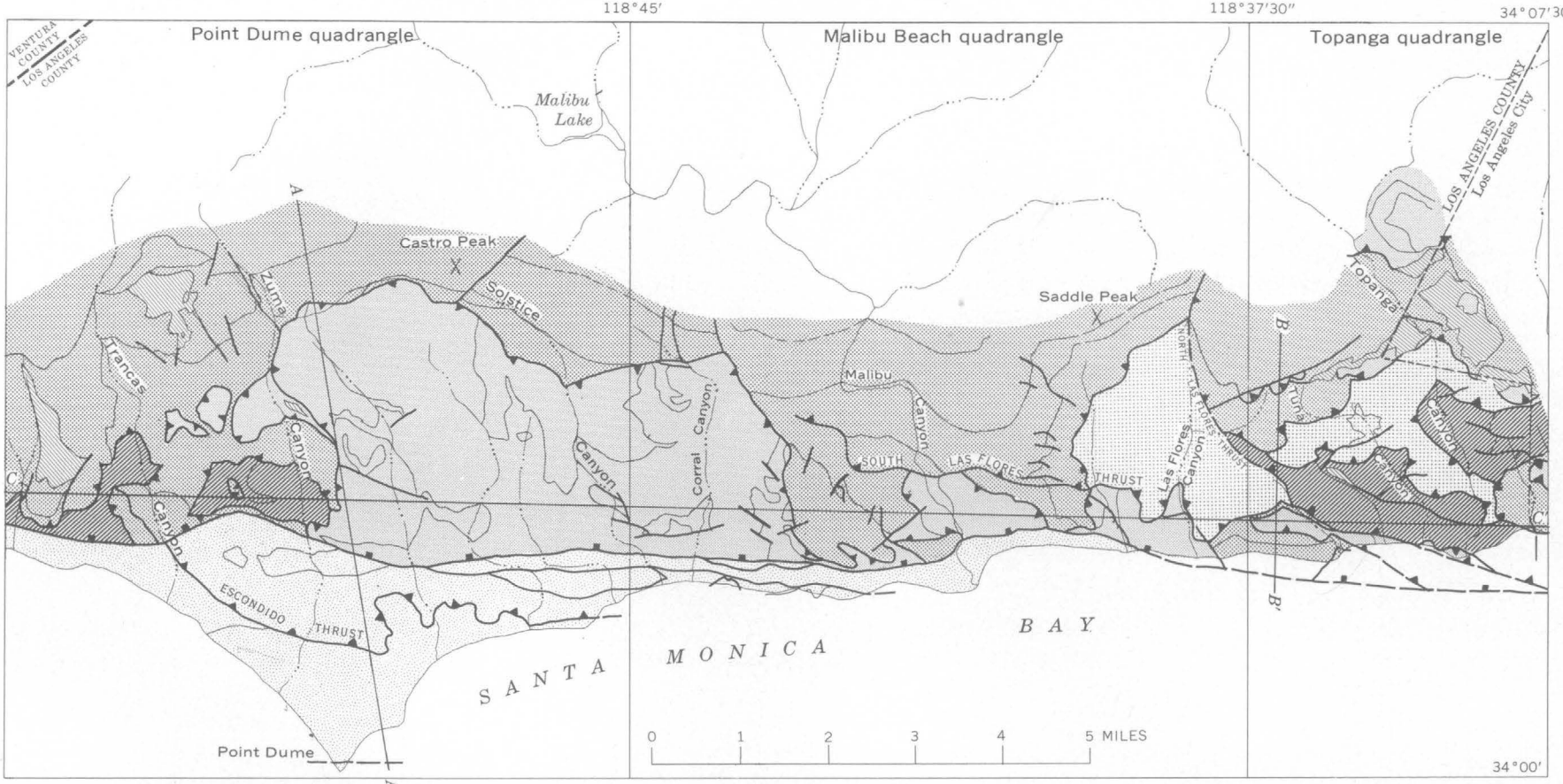


Geology mapped in 1961–65, and in part compiled and modified from Schoellhamer and Yerkes (1961), Schoellhamer and others (1962), and Yerkes and others 1964.

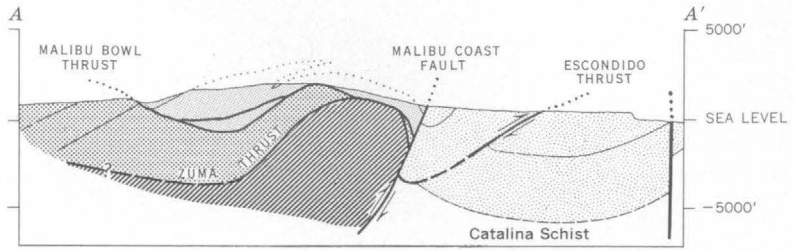


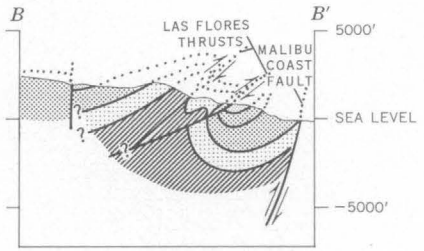


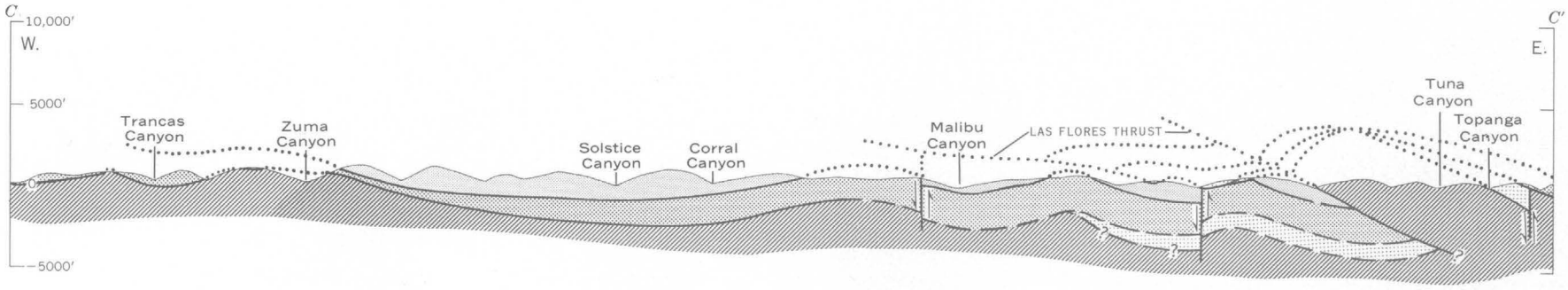


EXPLANATION

Rocks south of the Malibu Coast fault (coastal sequence)

Mafic intrusive rocks

Malibu Bowl thrust sheet

Zuma thrust sheet

Tuna Canyon thrust sheet

Autochthon(?)

Contact
*Dashed where approximately located*

Malibu Coast fault
*Dashed where approximately located*

Thrust fault
*Sawteeth on upper plate; dashed where approximately located*

High-angle fault
*Dashed where approximately located*

FIGURE 5.—Thrust sheets of the south-central Santa Monica Mountains, Los Angeles County, Calif. Formation contacts from fig. 2 shown for comparison.

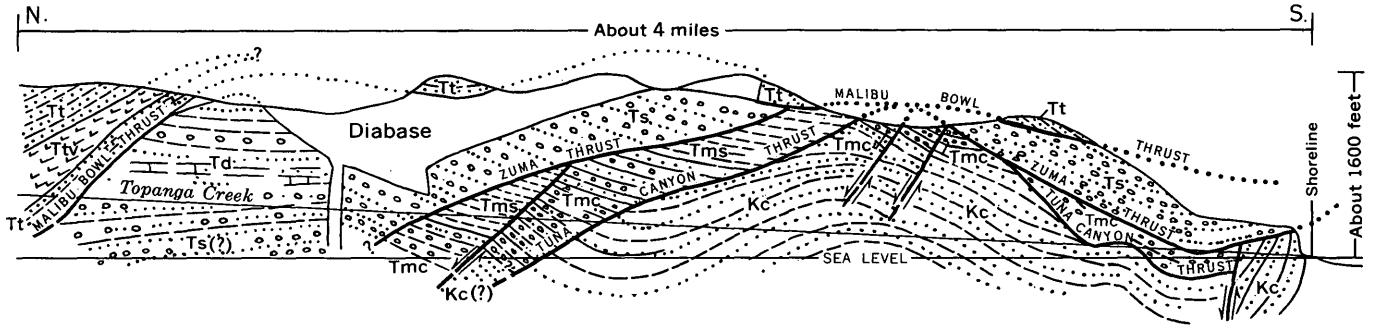


FIGURE 6.—Geologic sketch of the east wall of Topanga Canyon (not to scale). Tt, middle Miocene marine sandstone and siltstone; Ttv, interbedded volcanic rocks; Td, middle Miocene fluvial, lacustrine, and estuarine(?) sandstone, mudstone, and conglomerate; Ts, sandstone and conglomeratic sandstone (Sespe Formation); Tms, Paleocene siltstone and sandstone; Tmc, Paleocene conglomerate and sandstone; Kc, Upper Cretaceous sandstone and minor conglomerate.

served as a source for gravity thrust sheets is the Simi Hills; however, much more work must be done to test the validity of speculations concerning origin.

## LATER DEFORMATION AND IGNEOUS INTRUSION

Deformation of a different style followed the emplacement of the Malibu Bowl thrust sheet. A large asymmetric anticline, trending east-west and having a north-dipping axial surface, distorted the tectonically layered sequence (fig. 6). The anticline extends from as far west as Trancas Canyon eastward beyond the edge of the mapped area, and its crest commonly lies from 1 to 1½ miles north of the Malibu Coast fault (see sections A–A′ and B–B′, fig. 5). The anticline apparently began to form after the emplacement of the Tuna Canyon thrust sheet and continued to grow during and after the emplacement of the Zuma and Malibu Bowl sheets. The Las Flores thrust faults, which carried older rocks from the crestal zone of the anticline southward (section *B–B′*, fig. 5), are probably break thrusts associated with the late stages of the anticlinal folding.

Large quantities of diabase, andesite, and basalt were forcibly intruded, probably at about the same time or slightly later than movement along the Las Flores faults. Some intrusives were probably emplaced earlier, and intrusion may have begun even before the earliest thrusting; but one of the largest igneous masses was intruded along the Malibu Bowl thrust (fig. 6), and some small bodies were intruded along the Las Flores faults. The igneous rocks were forcibly emplaced, dilating the section. Dikes, most only a few feet thick, and small irregular bodies are abundant; the larger intrusive bodies are sill-like masses, filling thrust faults or bedding planes.

Very large displacement along the Malibu Coast fault postdates virtually all the structures of the mountain mass to the north of it. This fault clearly cuts many structures that intersect it from both sides, but their offset segments have not been recognized. The stratigraphic sections juxtaposed along the fault are greatly different (fig. 3), and Yerkes and Wentworth[1] conclude that it is a deep-seated thrust along which the southern margin of the Transverse Range province overrides the continental borderland to the south. Very large displacement along the Malibu Coast fault certainly postdates the deposition of the upper Miocene (Mohnian) beds of the Monterey Shale now exposed on Point Dume. Although the Malibu Coast fault may well have originated earlier, the local evidence does not require movement prior to latest Miocene.

Upper Pleistocene deposits are cut in a few places by minor faults that are probably associated with Malibu Coast fault deformation, but the deposits are generally not offset more than a few feet to a few tens of feet. The deposits are thus younger than the very large displacement of the upper Miocene rocks. In a few places, especially just east of the mouth of Topanga Canyon, minor displacement of Pleistocene deposits has occurred along segments of the older thrust faults that apparently provided preexisting planes of weakness along which there was some adjustment in response to the late deforming forces.

## REFERENCES

Bailey, T. L., and Jahns, R. H., 1954, Geology of the Transverse Range province, southern California [pt.] 6 *in* chap 2 *of* Jahns, R. H., ed., Geology of southern California: California Div. Mines Bull. 170, p. 83–106.

Durrell, Cordell, 1954, Geology of the Santa Monica Mountains, Los Angeles and Ventura Counties [California], map sheet 8 *of* Jahns, R. H., ed., Geology of California: California Div. Mines Bull. 170.

Hoots ,H. W., 1931, Geology of the eastern part of the Santa Monica Mountains, Los Angeles County, California: U.S. Geol. Survey Prof. Paper 165–C, p. 83–134.

[1] R. F. Yerkes and C. M. Wentworth, 1965, Structure, Quaternary history and general geology of the Corral Canyon area, Los Angeles County, California: U.S. Geol. Survey rept. prepared on behalf of U.S. Atomic Energy Comm., 215 p.

Newton, R. C., 1958, The Malibu Bowl fault area, Santa Monica Mountains: Univ. California at Los Angeles, unpub. M.A. thesis.

Pierce, W. G., 1963, Reef Creek detachment fault, northwestern Wyoming: Geol. Soc. America Bull., v. 74, p. 1225-1236.

Schoellhamer, J. E., and Yerkes, R. F., 1961, Preliminary geologic map of the coastal part of the Malibu Beach quadrangle, Los Angeles County, California: U.S. Geol. Survey open-file map, Sept. 6, 1961, scale 1:12,000.

Schoellhamer, J. E., Yerkes, R. F., and Campbell, R. H., 1962, Preliminary geologic map of the coastal part of the Point Dume quadrangle, Los Angeles County, California: U.S. Geol. Survey open-file map, Aug. 20, 1962, scale 1:12,000.

Soper, E. K., 1938, Geology of the central Santa Monica Mountains, Los Angeles County: California Jour. Mines and Geology, v. 34, no. 2, p. 131–180.

Woodford, A. O., Schoellhamer, J. E., Vedder, J. G., and Yerkes, R. F., 1954, Geology of the Los Angeles basin [California], [pt.] 5 *in* chap. 2 *of* Jahns, R. H., ed., Geology of southern California: California Div. Mines Bull. 170, p. 65–81.

Yerkes, R. F., Campbell, R. H., Schoellhamer, J. E., and Wentworth, C. M., 1964, Preliminary geologic map and sections of southwest part of the Topanga quadrangle, Los Angeles County, California: U.S. Geol. Survey open-file map, scale 1:12,000.

211-690 O—66——2

# MIOCENE STRUCTURAL MOVEMENTS IN THOMAS COUNTY, GEORGIA

By CHARLES W. SEVER, Tifton, Ga.

*Prepared in cooperation with the Georgia Department of Mines, Mining, and Geology*

*Abstract.*—Rocks of Oligocene and Miocene age in Thomas County, in the Coastal Plain province in southwestern Georgia, are gently folded and are transected by at least one northeast-trending fault. Maximum displacement along the fault is at least 190 feet and may be somewhat greater. Structural deformation began during Oligocene time, or at least before the Tampa Limestone (early Miocene) was deposited, and continued spasmodically through middle Miocene and possibly through late Miocene time. The trends of the Miocene structures parallel those of late Paleozoic structures in the Appalachian tectonic province in Georgia. The parallel trends suggest that the older Paleozoic structures in some way have controlled the Miocene structures.

Evidence for a northeast-trending fault and for downwarping to the northwest and upwarping to the southeast of it has been collected during a study of the ground-water resources of Thomas County, Ga. The purpose of this paper is to describe and name the structural features, to indicate their geologic age, and to relate them to the regional structural framework. Thomas County, which is in the southwestern part of the State at the Georgia-Florida boundary, is situated between the Chattahoochee anticline and the Ocala uplift, both of which are important structural features of the Coastal Plain physiographic province.

## LOCATION AND AGE OF GEOLOGIC STRUCTURES

The evidence of faulting and folding in Thomas County can be presented best in the form of structure-contour maps and a cross section which illustrate the folds and a break in each of two stratigraphic zones. These zones — the Suwannee Limestone of Oligocene age and the Tampa Limestone of early Miocene age — each are easily recognized stratigraphic units.

In Thomas County the Suwannee Limestone, the principal aquifer, generally is a white, nonsandy, porous, oolitic, fossiliferous limestone that at places is almost a microcoquina. The foraminifer *Pararotalia mexicana mecatepecensis* Nuttall (*Rotalia mexicana* of former usage) generally can be found in cuttings from the upper part of the Suwannee Limestone throughout Thomas County. This foraminiferal species is considered by Herrick and Vorhis (1963, p. 13) to be diagnostic of the Oligocene in Georgia. Other diagnostic species listed by them include *Quinqueloculina leonensis* Applin and Jordan, *Camerina dia* (Cole and Ponton), *Asterigerina subacuta* Cushman var. *floridensis* Applin and Jordan, and *Lepidocyclina mantelli* (Morton). The Suwannee Limestone can be distinguished from overlying Miocene limestone by the absence of sand in the Suwannee and by diagnostic Foraminifera.

Contour lines drawn on the top of the Suwanne Limestone (fig. 1) show that the formation is downfolded into a northeast-plunging basin near Meigs, in northwestern Thomas County. This structure, here named the Meigs basin, is part of a much larger, generally southwest-plunging trough called the Gulf trough by Herrick and Vorhis (1963, p. 55 and 67). The contour lines also show that in the central part of Thomas County the Suwanee Limestone has been unfolded along a northeast-trending arch. This structure is here named the Barwick arch. Separating these two structures is a northeast-trending fault that is here named the Ochlockonee fault, after the river of this name.[1] Rocks on the southeast side of the fault are upthrown; the amount of displacement generally increases to the northeast.

Along the Ochlockonee fault the top of the Suwannee Limestone has been displaced 100 to 190 feet.

[1] The U.S. Board on Geographic Names official spellings of the town and the river of this name are slightly different. The name of the town Ochlocknee, (figs. 1 and 2) does not contain a third "o."

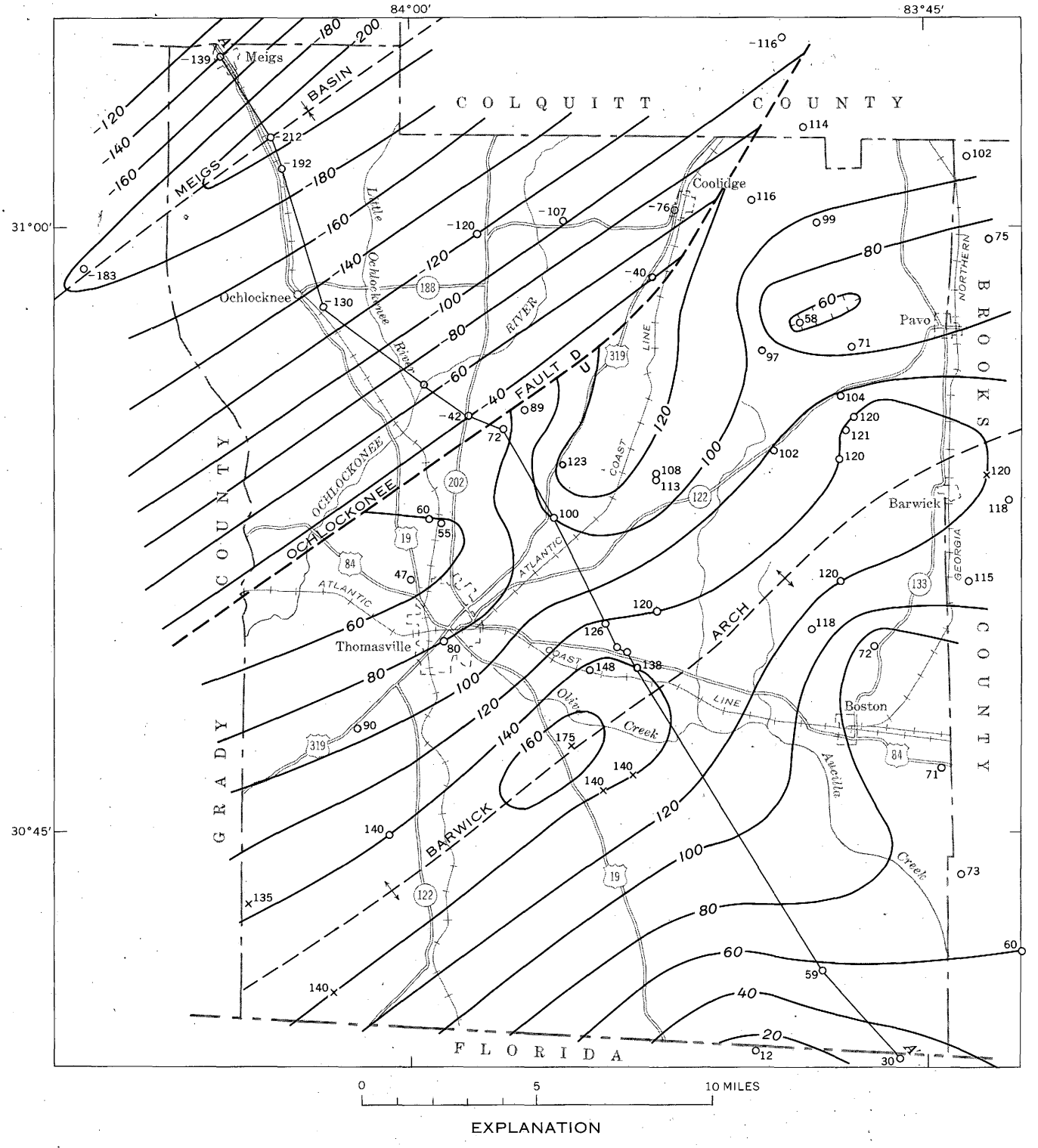


FIGURE 1.—Map showing contour lines on the top of the Suwannee Limestone in Thomas County, Ga. Line *A–A'* shows location of geologic section (fig. 3).

Thus faulting occurred after this formation was deposited. Although data are inadequate to determine whether any of the faulting occurred earlier, partial dolomitization of Eocene and Oligocene limestones within the Meigs basin, together with other evidence, indicates that the basin may have been downwarped prior to Miocene time.

Throughout Thomas County—except near the axis of the Meigs basin—the uppermost 3 to 10 feet of the Suwannee Limestone is very permeable. Probably the permeability is the result of solution during exposure of the formation to weathering during earliest Miocene time. That the weathering did not produce significant relief is indicated by the nearly uniform thickness (150 to 180 feet) of the Suwannee throughout the county. Upwarping of the Barwick arch southeast of the Ochlockonee fault is postulated tentatively because the contours on the top of the Suwannee (as well as those on the top of the overlying Tampa Limestone) indicate possible deformation of a weathered or erosional surface that presumably had been nearly horizontal.

The Tampa Limestone of early Miocene age overlies the Suwannee Limestone. The lower member of the Tampa is predominantly yellowish-gray to greenish-gray sandy marl with interbedded thin, white, very sandy beds of limestone, and the upper member is an easily recognized gray to brown, dense, cherty, phosphatic, sandy limestone. This upper member (the Chattahoochee Formation of previous usage) is easily distinguished from other Miocene limestone units by its color; by its sand content; by its dense cherty texture, which causes a prominent high anomaly on electric logs; by its phosphate, which contains traces of uranium that cause a distinctively high anomaly on gamma-radiation logs; and by its fossils, which include specimens of the Foraminifera *Archaias* sp. and *Sorites* sp., and numerous fragments of large shells.

Contour lines drawn on the top of the Tampa Limestone (fig. 2) show that it too is downfolded in the Meigs basin and upfolded along the Barwick arch. The upper member of the Tampa Limestone and, locally, the Suwannee Limestone are exposed along the crest of the Barwick arch. Along the Ochlockonee fault the top of the Tampa has been displaced about 80 to 100 feet, or about 20 to 100 feet less than the displacement of the top of the Suwannee Limestone. This difference in displacement indicates that some movement occurred along the Ochlockonee fault after deposition of the Suwannee and before deposition of the upper member of the Tampa. Differences in the thickness of the lower member of the Tampa Limestone (fig. 3) northwest of the fault, together with absence of the lower member southeast of the fault, indicate that at least part of the movement occurred during early Miocene time and was contemporaneous with deposition of the lower member northwest of the fault.

Because the upper member of the Tampa Limestone has about the same maximum thickness and the same lithology on both sides of the fault, this member must have been deposited during an interval of relative stability. However, displacement of this member across the Ochlockonee fault shows that additional movement along the fault occurred after this member was deposited.

Southeast of the Ochlockonee fault the Tampa Limestone was uplifted at the end of early Miocene time, and, at a few places (fig. 3), deep channels were incised through the Tampa and into the upper part of the Suwannee.

Sands and clays of the Alum Bluff Group of early and middle Miocene age, which were deposited on this irregular surface, filled the channels. Since deposition, beds of the Alum Bluff Group have been folded and at places faulted. Many of these structures obviously were caused by differential compaction within the Alum Bluff Group, and others probably were caused by continuing solution and collapse of the underlying limestones. However, some of these structures may have been caused by continued uplift of the Barwick arch during middle Miocene to late Miocene time.

Northwest of the Ochlockonee fault, the Alum Bluff Group appears to overlie the Tampa Limestone conformably. Within the Meigs basin this group is divisible into three mappable zones: a lower zone of sandy marl; a middle zone of phosphatic sandstone that causes a high anomaly on gamma-radiation logs; and an upper zone of fuller's earth. Changes in lithology and thickening of these zones within the basin indicate that folding and faulting probably occurred during middle Miocene time prior to or contemporaneous with the deposition of these zones. The lower zone cannot be traced with confidence across the Ochlockonee fault, but the lithology of the unit shown as undifferentiated Alum Bluff Group on figure 3 is similar to this zone. Possibly the thinning of the middle zone near the fault indicates that some movement occurred during deposition of this zone. Within the Meigs basin, commercial deposits of attapulgite and fuller's earth are present in the upper zone. Similar deposits are absent southeast of the Ochlockonee fault. Data are insufficient to determine whether the absence of these beds is due to their removal by erosion or to nondeposition.

Overlying the Alum Bluff Group within the Meigs basin is the Citronelle Formation, which consists of as much as 90 feet of gravel and coarse sand of terrestrial origin (fig. 3). On the Barwick arch this

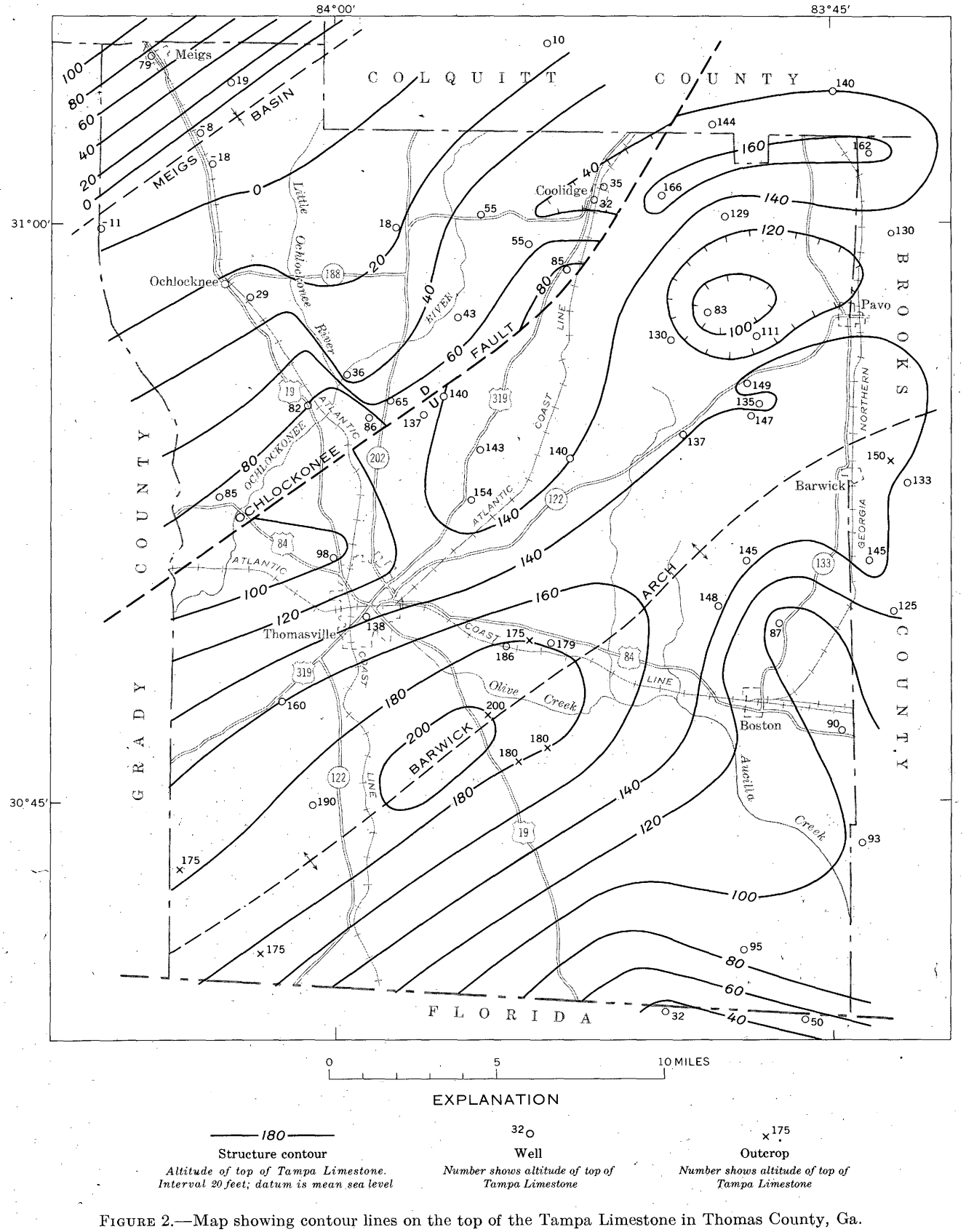


FIGURE 2.—Map showing contour lines on the top of the Tampa Limestone in Thomas County, Ga.

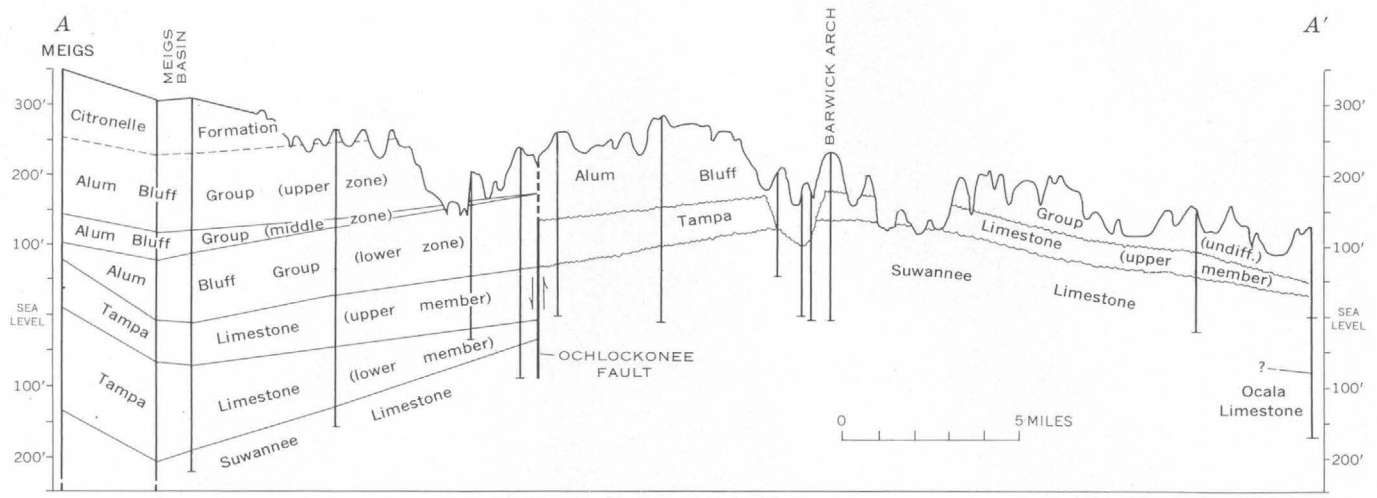


FIGURE 3.—Geologic section southeastward across Thomas County, Ga. Location of section shown on figure 1.

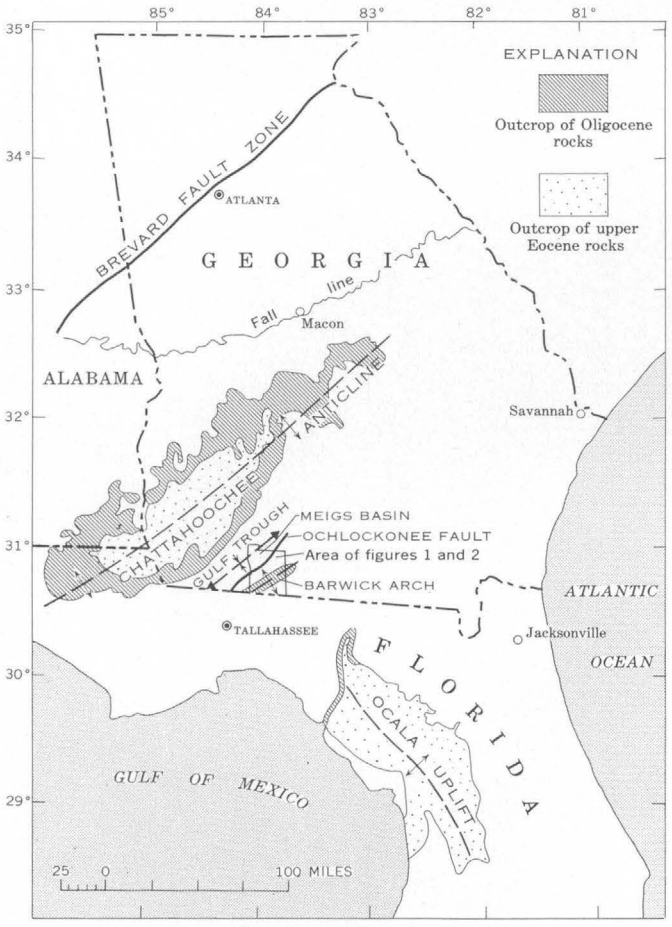


FIGURE 4.—Regional geologic structures in southwestern Georgia and adjacent areas.

formation generally is absent but is represented locally by as much as 20 feet of sand and gravel in what appear to be old river channels. Southeast of the Barwick arch, sands in the lower part of Citronelle intertongue with shallow-water marine beds in which the author and several others have found numerous fossil mammal teeth. The teeth were identified as *Merychippus* sp. and *Diceratherium* sp. by Olsen (1963), who considers them to be of late Miocene age. The areal distribution of the Citronelle indicates that the Barwick arch may have been uplifted again after the Citronelle was deposited.

## RELATION TO REGIONAL STRUCTURAL TRENDS

The Ochlockonee fault and the axes of the Meigs basin and Barwick arch trend parallel to the Chattahoochee anticline (fig. 4) as relocated by Sever (1965). All these structures are oriented parallel to the structural trend in the Appalachian tectonic province in Georgia, as it is shown on figure 4 by the trend of the Brevard fault zone. The parallel trends suggest that the older Paleozoic structures have controlled in some way the Miocene structures in Thomas County.

All these structural trends are almost normal to the general northwestern structural trend of the Ocala uplift in Florida.

## REFERENCES

Herrick, S. M., and Vorhis, R. C., 1963, Subsurface geology of the Georgia coastal plain: Georgia Geol. Survey Inf. Cir. 25, 78 p., 28 fig.

Olsen, S. J., 1963, An upper Miocene fossil locality in north Florida: Florida Acad. Sci. Jour., v. 26, no. 4, p. 308–314.

Sever, C. W., 1965, The Chattahoochee anticline in Georgia: Georgia Geol. Survey Min. Newsletter, v. 17, p. 39–43.

# PRE-MIDDLE DEVONIAN AND POST-MIDDLE DEVONIAN FAULTING AND THE SILURIAN-DEVONIAN UNCONFORMITY NEAR RICHMOND, KENTUCKY

By GEORGE C. SIMMONS, Berea, Ky.

*Work done in cooperation with the Kentucky Geological Survey*

*Abstract.*—Two periods of movement on northwest-trending faults are recognized by differences in amount of offset of Silurian and Devonian formations and by the results of pre-Middle Devonian erosion. Initial faulting occurred after deposition of the Crab Orchard Formation, and probably the Bisher(?) Limestone. Subsequent erosion almost completely removed the Bisher(?) and produced a nearly level surface on the Crab Orchard. Consequently, only lower parts of the Crab Orchard remain on upthrown sides of faults; thicker sections are present on downthrown sides. Faulting again occurred after the Boyle Dolomite and the lower part of the New Albany Shale were deposited.

Recent mapping has delineated a system of northwest-trending faults in Ordovician, Silurian, and Devonian strata near Richmond, Ky. The faults, including one which was recognized by Campbell (1898) and another by Jillson (1964), lie between the northeast-trending Kentucky River and Irvine fault zones (fig. 1). Two periods of movement on northwest-striking faults are recognized in the Palmer and Union City quadrangles (fig. 1). The first period of faulting occurred prior to the development of the unconformity at the base of Devonian rocks in central Kentucky; the second took place during or after Middle Devonian time. The formations exposed in the Palmer quadrangle are listed in table 1.

TABLE 1.—*Paleozoic formations exposed in the Palmer quadrangle, Kentucky*

| Series | Formation |
|---|---|
| Lower Mississippian | Borden Formation (lower part) |
| Middle and Upper Devonian and Lower Mississippian | New Albany Shale |
| Middle Devonian | Boyle Dolomite |
| Middle and Lower Silurian | Bisher(?) Limestone<br>Crab Orchard Formation<br>Brassfield Formation |
| Upper Ordovician | Drakes Formation<br>Ashlock Formation |

The pre-Boyle age of the first period of faulting is inferred from the relation of the Boyle Dolomite to the Crab Orchard Formation; the Boyle overlies thinner sections and older beds of the Crab Orchard on the upthrown side of each fault than on the adjacent downthrown side. In the geologic section (fig. 2) showing a fault in the Palmer quadrangle, a stratigraphic difference of 20 feet exists between the uppermost beds of the Crab Orchard on the opposite sides of the fault. An isopach map of the Crab Orchard Formation in the Palmer quadrangle (fig. 3) shows that this formation is thinner on the upthrown sides of faults than on the corresponding downthrown sides.

The second period of faulting was obviously younger than the Boyle Dolomite and the lower part of the New Albany Shale because these units were displaced. The upper possible age limit of this faulting is unknown because the upper part of the New Albany and younger rocks are absent in the faulted areas.

The total vertical displacement of the two periods of faulting is commonly about 40 feet; the maximum is about 80 feet. The amount of drag adjacent to the faults is relatively great, and the difference in the elevation of correlative beds within a few hundred yards of the faults is at some places three or more

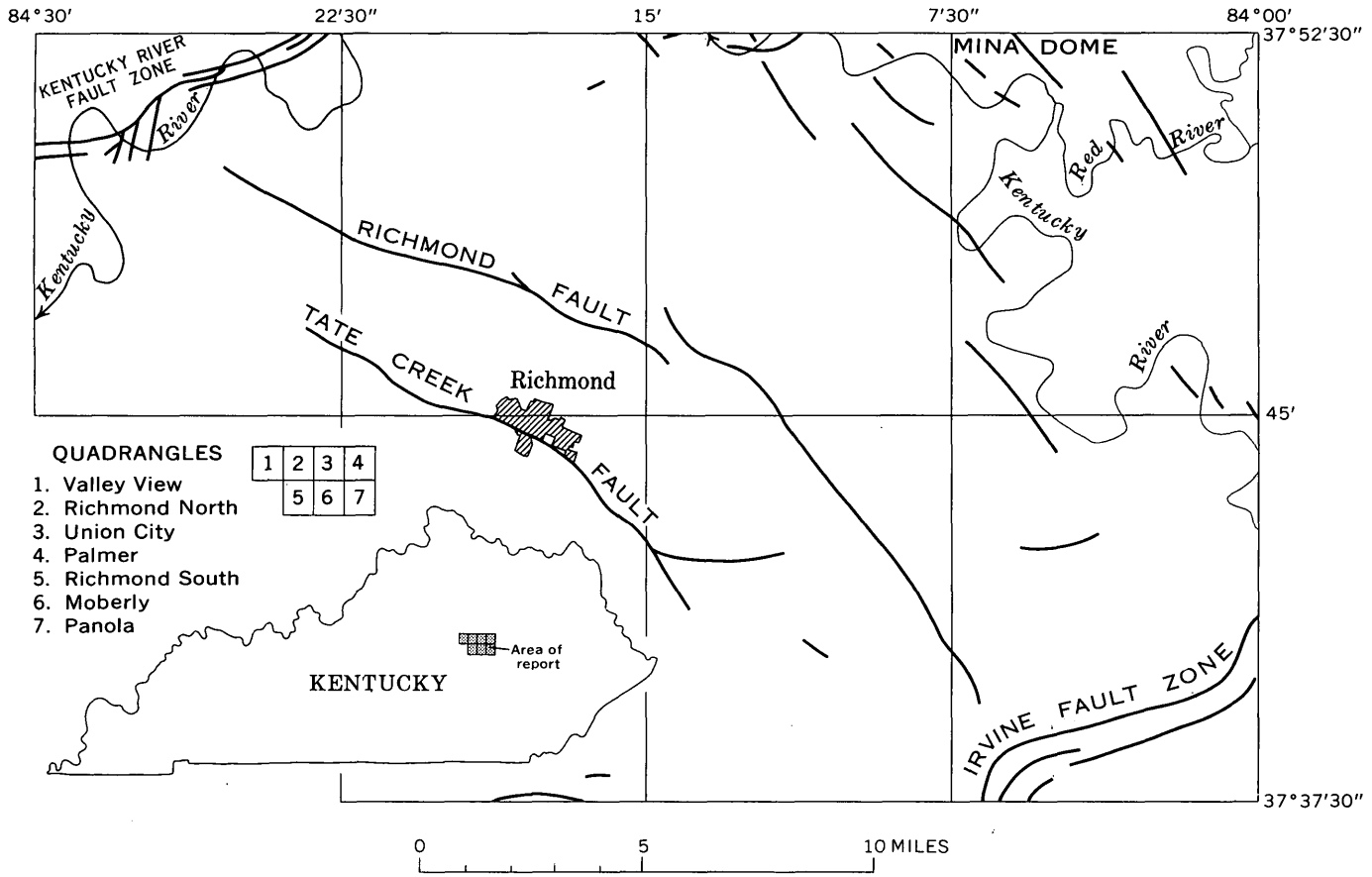


FIGURE 1.—Index map showing location of faults near Richmond, Ky.

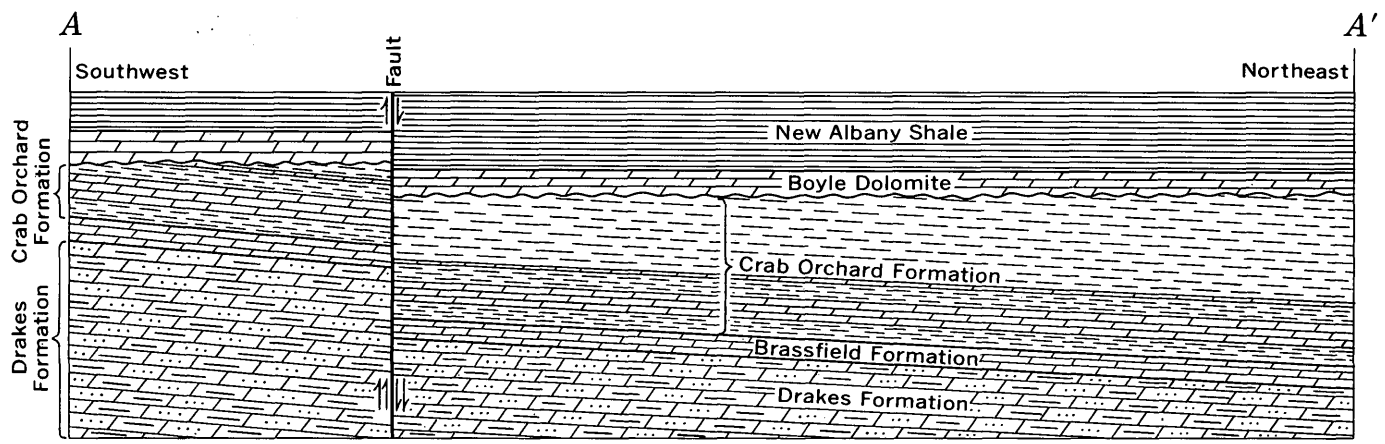


FIGURE 2.—Diagrammatic geologic section showing results of two periods of faulting and intervening erosion. The Crab Orchard Formation is 45 feet thick on the southwest (left) side of the fault, 65 feet thick on the northeast (right) side, 30 feet thick at *A*, and 90 feet thick at *A'*. The offset of the Crab Orchard Formation is 40 feet; the base of the Boyle Dolomite is offset only 20 feet. See figure 3 for location of geologic section.

times as much as the offset along the faults. In general, displacement during the first period of faulting was greater than displacement during the second, although local exceptions exist. The difference in offset is most easily determined in the field by comparing the displacement of the base of the Brassfield Formation with that of the base of the New Albany Shale. These contacts generally are well exposed, and the former was affected by both periods of faulting, whereas the latter was affected by only one.

At two places it is questionable whether the faults were active during post-Boyle time. Although Silu-

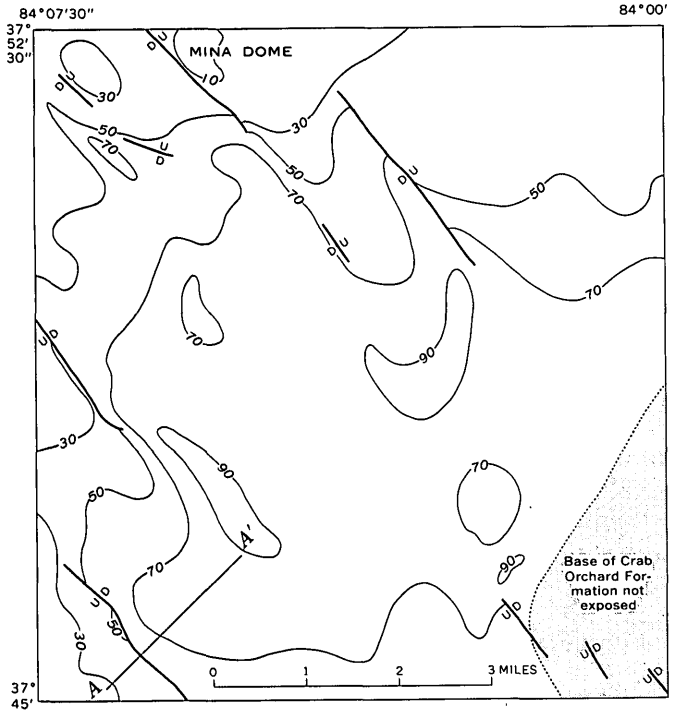


FIGURE 3.—Isopach map of the Crab Orchard Formation in the Palmer quadrangle, Kentucky. Contours, in feet, show that the formation is thinner on upthrown sides of faults than on adjacent downthrown sides. Geologic section *A–A'* shown in figure 2.

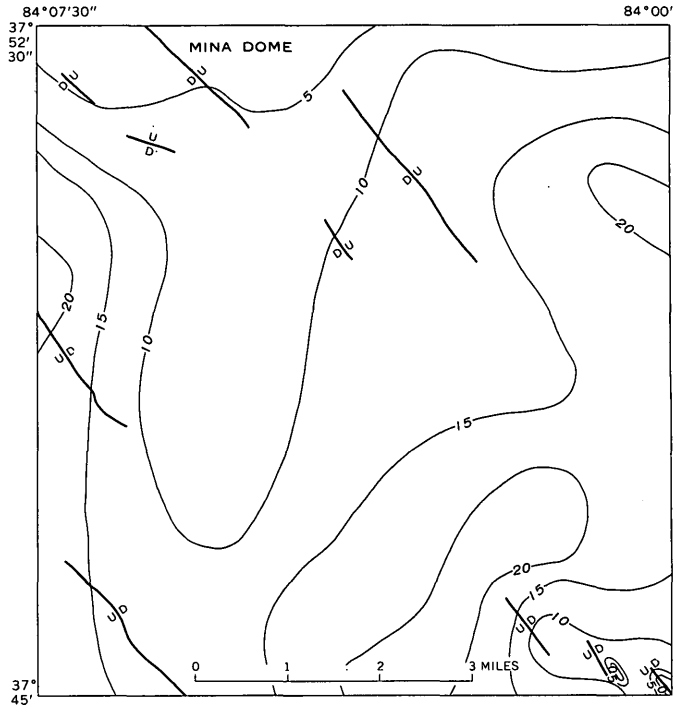


FIGURE 4.—Isopach map of the Boyle Dolomite in the Palmer quadrangle, Kentucky. Thickness shown in feet.

rian rocks are offset more than 20 feet by both faults, the difference in elevation of Devonian strata on opposite sides of the projections of the faults is only a few feet. As no faults are exposed in Devonian strata, the slight differences may result from post-Boyle tilting rather than faulting. Thus, the fault on the southwest side of the Mina dome (fig. 4) and the north part of the longer of the two faults southeast of the dome may have been inactive during the second period of faulting.

The faults have no apparent economic significance. Because their northwest-southeast strike is parallel to the regional (southeast) dip, the faults have not created large closed structures which might serve as oil reservoirs. Small structural closures exist adjacent to a few faults as the result of differential movement and drag. One fault increased the closure on the Mina dome. No mineralization has been found along the faults.

The regional unconformity at the base of the Devonian rocks in the Palmer quadrangle in central Kentucky is commonly the contact between the Boyle Dolomite and the underlying Crab Orchard Formation. Pre-Boyle erosion removed most of the Bisher(?) Limestone and cut an almost level surface on the Crab Orchard. An isopach map of the Boyle Dolomite in the Palmer quadrangle (fig. 4) shows that the Boyle was deposited as a thin layer on a surface of low topographic relief. In the southeast corner of the quadrangle two hills made up of Crab Orchard Formation and capped by Bisher(?) Limestone stood a few tens of feet above the Middle Devonian sea. The Boyle Dolomite was deposited around the hills and wedged out against the Crab Orchard Formation on the hill slopes. Consequently, the Bisher(?) Limestone on the ancient hilltops stood at higher elevations than the younger Boyle Dolomite and lowest part of the New Albany Shale.

## REFERENCES

Campbell, M. R., 1898, Description of the Richmond quadrangle [Kentucky] U.S. Geol. Survey Geol. Atlas, Folio 46.

Jillson, W. R., 1964, Discovery of Mid-Paleozoic faulting in eastern-central Kentucky: Frankfort, Ky., Roberts Printing Co., 13 p.

# DESCRIPTION AND RELOCATION OF PART OF THE ILSE FAULT ZONE, WET MOUNTAINS, COLORADO

By Q. D. SINGEWALD, Beltsville, Md.

*Abstract.*—New data on the Ilse fault zone, a major dislocation in the central Wet Mountains of Colorado, show that it extends northward and joins a fault previously known to cross the Arkansas River 1½ miles west of Parkdale. An ancestral Ilse fault antedated the Cambrian Period; it was a linear zone, variable in width and intensity of deformation, and transected the grain of Precambrian gneiss. Reactivation on a major scale, but not necessarily of equal intensity everywhere, moved the east wall relatively downward during Laramide, or later time. Several strong radioactive anomalies were found north of hitherto reported thorium mineralization in the fault and southeast of it.

The Ilse fault zone, an important dislocation in the central Wet Mountains, is shown on the 1935 geologic map of Colorado (Burbank and others, 1935) as being nearly 17 miles long and having a prevailing trend of approximately N. 30° W., except at the north end, where near Grape Creek it is shown as striking nearly due north. Because Precambrian rocks occupy both walls throughout this stretch, neither the age of the fault nor the direction and amount of movement along it could be determined in earlier studies.

Geologic reconnaissance during 1964 shed new light on the character and age of the Ilse fault. The fault was found to extend 5 miles farther north-northwestward than thought previously and to connect with another fault that is shown 1½ miles west of Parkdale on the geologic map of Colorado. The existence of an eastward extension of the latter fault was determined to be in error. Incidentally to the structural study, radioactive anomalies were found at several places north of hitherto reported thorium deposits. The revised fault pattern is compared on figure 1 with the pattern on the 1935 map. On a larger scale map (fig. 2), part of the Ilse fault is shown in relation to streams and contours copied from the newest topographic maps, and the prevailing foliation at different places is given.

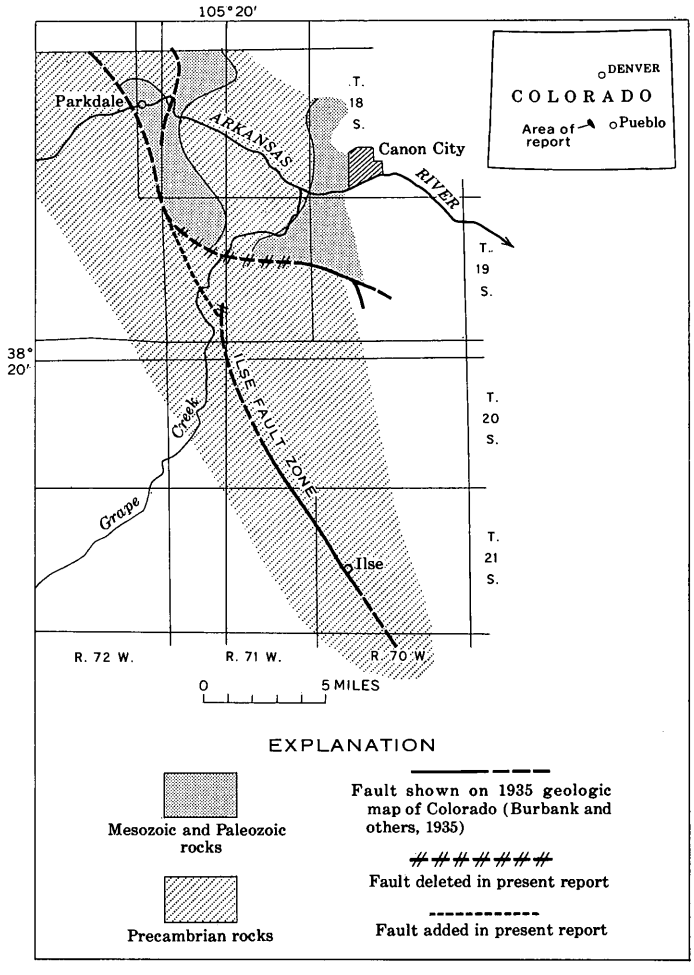


FIGURE 1.—Ilse fault zone between Ilse and Parkdale, Colo.

## TOPOGRAPHIC EXPRESSION

The most striking aspect of the Ilse fault is its topographic expression. For 12 miles northward from Ilse, a fault-line scarp east of the fault boldly rises 1,000 to 2,000 feet above the fault trace and towers

above irregularly dissected lower ridges and hills west of the fault. This contrast between slopes is fairly evident from contours at even the very large, 400-foot contour interval of figure 2. Fewer veins and fissures and greater quantities of granite gneiss combine to make rocks east of the fault, along this 12-mile stretch, more resistant to erosion than rocks west of the fault. Farther north, where the scarp is missing, rocks on opposite sides of the fault are not notably dissimilar.

## BEDROCK ALONG FAULT

Mesozoic rocks, which are sharply uptilted in the east wall of the fault, lie east of the fault in the northern part of the area shown on figure 2 and continue northward for several miles. They include the Morrison Formation (Upper Jurassic), Dakota Sandstone (Lower and Upper Cretaceous), and Benton Shale (Lower and Upper Cretaceous), as modified from the 1935 geologic map of Colorado (Burbank and others, 1935).

Elsewhere, bedrock is a crystalline complex of Precambrian rocks cut by many dikes. These rocks have been described in the McKinley Mountain area (Christman and others, 1959, p. 493-512). Most widespread along the Ilse fault are biotite-quartz-plagioclase gneiss and associated migmatite, horneblende-plagioclase gneiss and amphibolite, and alaskitic granite gneiss. These gneisses commonly occur together in irregularly alternating layers that may pinch or swell, interfinger, or grade into one another. "Basic dikes," whose feldspar ranges from calcic labradorite to calcic andesine, are more numerous but less persistent than syenite dikes. Most of these dikes in the Wet Mountains are very late Precambrian or, more probably, Early Cambrian in age (M. R. Brock and R. F. Marvin, unpub. data).

The detailed pattern of foliation, fissures, and dikes close to the Ilse fault remains very imperfectly known because outcrops are scarce and tend to be slumped. At a few places, gneiss less than a hundred feet from the fault seems little disturbed or altered. Elsewhere, a disturbed zone hundreds of feet wide borders at least one side of the fault; dips in interlayered gneisses become more variable than in undisturbed areas and culminate locally in a chaotic pattern; fissures and dikes increase in abundance as the fault is approached. These features, which on a lesser scale also are visible along secondary faults, including branches of the Ilse, are well displayed in the valley of Grape Creek between Bear Gulch and the Ilse fault (fig. 2). Segments of rock between fissures exhibit sharp flexures and contortions of thin gneiss layers that must have been folded while the rock was plastic enough not to break. Fissures in the disturbed zone may be transverse, oblique, or parallel to the main fault.

## EXPOSURES AND OTHER EVIDENCE OF THE FAULT

Nearly a century ago, the Terrible mine at Ilse, and prospects farther south, exposed the Ilse fault. Ore in the fault was cerussite, devoid of galena to the greatest depth of mining, about 750 feet (C. L. Beach[1], oral commun., 1955); this, despite galena at the surface in nearby veins, and a water table only about 50 feet deep, suggest that the cerussite may be hypogene. The opencut of the Terrible mine, now partly filled by water, remains the best exposure of the Ilse fault in the Wet Mountains. Geologic details are recorded by Emmons (1896, p. 468) and by Hunter (1915, p. 32). Briefly, the rocks involved in the fault at the Terrible mine lie between granitic gneiss walls that dip 60° westerly and comprise: (1) a western barren zone, 15 to 40 feet wide, of greenish-gray to blue soft, crumbly "diorite," green clayey material, and clay gouge, all of which are variably permeated by a yellow and brown stain; and (2) a "pay zone," 70 to 80 feet wide, of crushed granitic rock "now altered beyond recognition, shattered into small lozenge-shaped fragments and stained by iron oxide" (Emmons, 1896, p. 468). Hunter (1915, p. 32) add that

> For 2 miles south of the Terrible mine, the so-called cerusite [sic] zone can be followed almost continuously and ranges from a belt 80 feet in maximum width at this mine to a mere band of slightly altered and iron-stained gneiss only a few feet across. In several places prospects reveal a narrow zone of intensely crushed rock consisting chiefly of clay gouge, feldspathic material, calcite, and chloritic micas with limonite and manganese stains. On either side of such a zone, which is rarely over 10 feet wide, the granite gneiss may be considerably altered, although as a rule it is but little crushed and grades into fresher rock.

The remarkable variations in thickness and intensity of crushing do not reflect a southward termination but are characteristic features of the fault.

Details about the fault between Ilse and locality 2 (fig. 2) have been learned from recently completed mapping in the Mount Tyndall quadrangle (M. R. Brock and Q. D. Singewald, unpub. data). Particularly noteworthy is a great difference in prevailing foliation attitudes of rocks on opposite sides of the fault, as shown on figure 2. A great difference in lithology also exists; hornblende gneiss predominates west of the fault, biotite gneiss and granite gneiss east of the fault. Along this 2½-mile stretch, the fault bends abruptly at 7 places, but only at 4 of them is the angle large enough to be apparent on figure 2. Although exposed only at localities 1 and 2, the fault

[1] Mr. and Mrs. C. L. Beach are now the only residents at Ilse; he worked in the Terrible mine during its last active period.

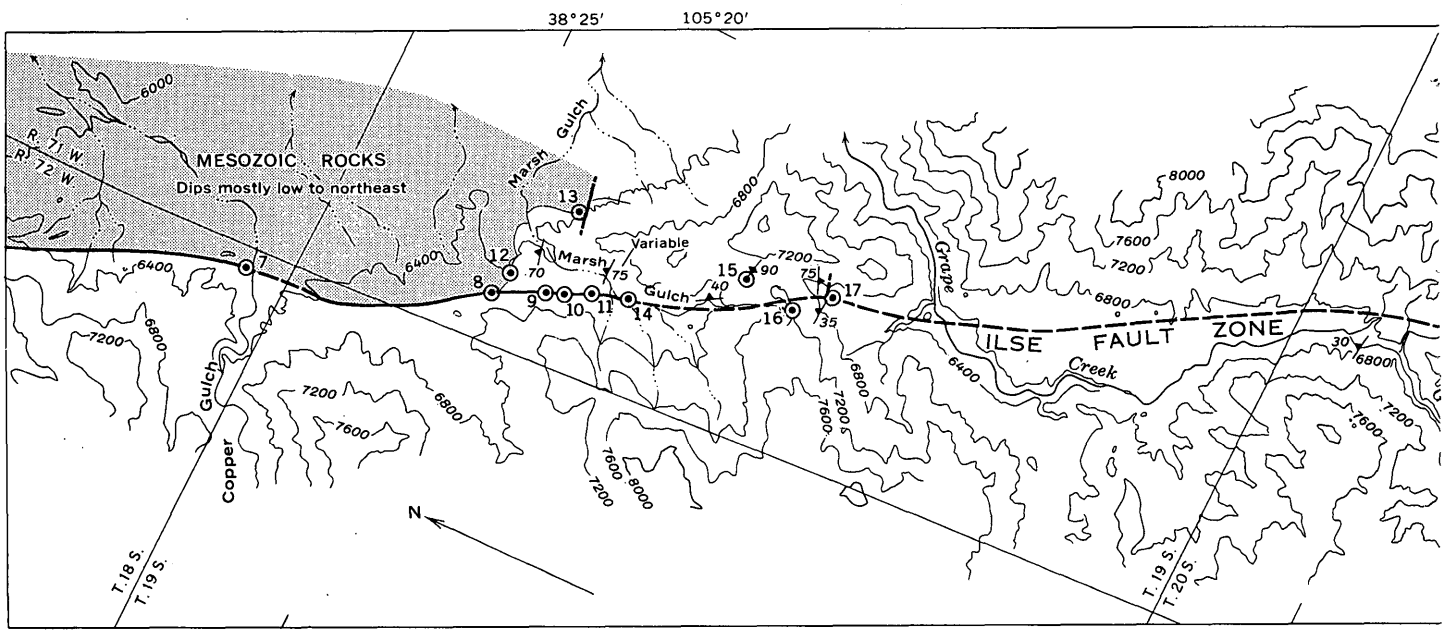


Base compiled from U.S. Geological Survey Royal Gorge 15-minute sheet, 1959; Mount Tyndall 7½-minute sheet, 1954; and Hardscrabble Mountain 7½-minute sheet 1963

FIGURE 2.—Part of Ilse fault zone, Colorado. Rocks of the map area are Precambrian except those shown to be Mesozoic in the northern part of the area.

between Ilse and locality 2 can be located within an estimated 100 to 200 feet, owing in part, to its position at the upper edge of pediment benches along Oak Creek and, in part, to fairly numerous exposures of reddish feldspathized rock inferred to be in the eastern wall. An auxiliary fault that bends, or possibly even displaces, the Ilse fault at the south end of the Terrible mine, trends N. 50° W. Oak Creek follows this auxiliary fault for 2 miles, then wends its way back to the Ilse fault, at locality 3, where intensely fractured granite gneiss on the west tip of a gravel-covered bench is inferred to be in or adjacent to the Ilse fault.

Continuation of the Ilse fault northward from locality 3 to locality 5 beneath alluvium of Oak Creek is proved conclusively by marked divergence in attitudes of rocks. As shown on figure 2, the strike of the foliation is rather uniformly northwestward on the east side of the fault, and less uniform, yet prevailingly northeastward on the west side. At locality 4, two pits on a gravel-covered hill expose intensely sheared, altered hornblende gneiss dipping 70°–75° west, through which the Ilse fault is inferred to pass; at locality 5, the westernmost outcrops of virtually solid granite gneiss are inferred to be very near the fault. Except at these localities, the valley of Oak Creek is so broad that the trace of the fault generally can be located with an accuracy no greater than 0.2–0.25 mile.

Near locality 4, the Ilse fault bends 35° (fig. 2); if its trend from there to locality 5 continued northwestward, the fault would roughly coincide with the remarkably straight course of Bear Gulch. Moreover, the strike of interlayered gneisses along and near Bear Gulch is variable, yet prevailingly northwest. Analogous linear zones of northwest strikes, in mapped quadrangles to the south, are transverse to a regional northeast strike of gneisses west of the Ilse fault. These are regarded by the author as structural elements along which transverse displacement took place by rock flowage, as regional metamorphism waned and before the rocks became brittle. The Bear Gulch element probably absorbed a major share of the Ilse deformation, during at least the early stages of deformation, in this general area. The main Ilse zone, nevertheless, in this report as on the 1935 geologic map of Colorado is inferred to approximately follow, northward from locality 5, a lithologic boundary that also is a conspicuous topographic boundary between a high area of massive granite gneiss to the east and a lower area of fractured interlayered gneisses to the west. At locality 6, fracture and alteration along the

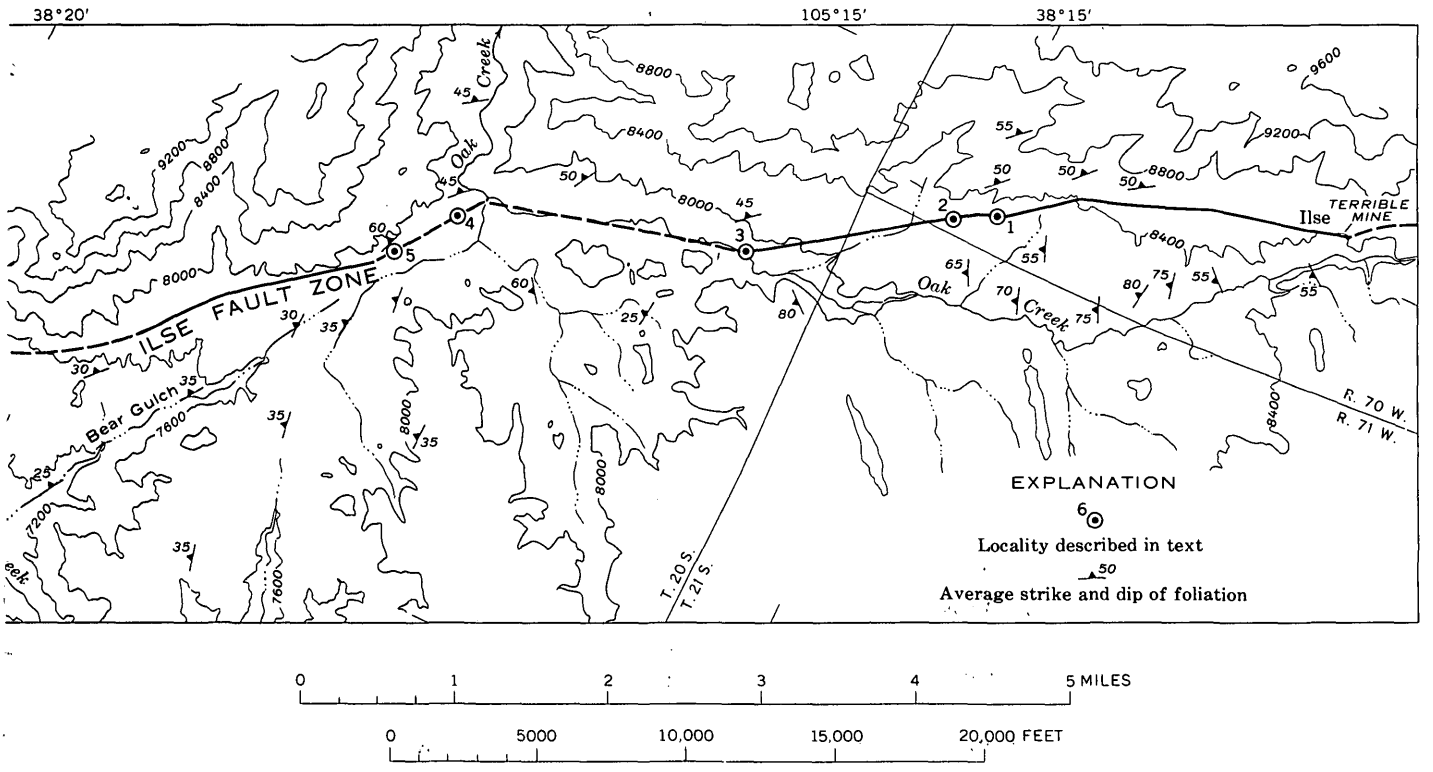


inferred Ilse fault are much less obvious than in a wide, radioctive shear zone that trends slightly east of north, about 0.1 mile to the west-northwest of locality 6.

The course of Grape Creek, where it approaches the Ilse fault, is deflected from northeast to northwest and opens from a narrow valley having nearly continuous exposures of bedrock into a wide valley in which unconsolidated material conceals most of the bedrock. Nearly 3 miles farther downstream (northwestward), Grape Creek again curves northeastward through the northernmost trace of the Ilse fault-line scarp in a gorge so narrow and rocky as to be named "The Tights." The valley in the northern part of the northwest-flowing segment attains a width of 0.5 to 0.6 mile, because the stream itself flows away from the scarp at a small oblique angle along a zone of auxiliary fractures. Between the stream and the escarpment is a dissected pediment bench, where nonresistant, fractured and slumped, interlayered gneiss is covered at most places by unconsolidated debris.

At the northern part of the area of figure 2, uptilted Mesozoic rocks occupy the east wall of the Ilse fault. Although the fault was traced in this study only as far as shown on figure 2, it is known to continue northward, across the Arkansas River, as shown by the 1935 geologic map of Colorado. At locality 7, where the fault zone is wider than normal, alluvium covers all sedimentary rocks except a ledge of limonite-permeated, sericitized(?), shattered, white quartzite. Gneiss, to a distance of 500 feet west of the quartzite, is greatly altered and cut by breccia zones, dikes, and veins. At locality 8, whitish powdery soil in a low saddle reveals the approximate location of the fault at the southernmost point where the fault lies between Precambrian and Mesozoic rocks.

Relations at localities 9, 10, and 11 prove that the fault at locality 8 continues southward in a nearly straight line at least a mile, with Precambrian rocks in both walls. The contact at localities 12 and 13 is an unconformity, and not a fault as shown on the 1935 geologic map of Colorado. At locality 9, a prospect pit exposes part of a zone of comminuted and bleached rocks, on opposite sides of which the attitudes of foliation differ. At locality 10 an opencut 75 feet long, transverse to the fault, exposes shattered and altered gneiss that has erratic dips, is transected by countless fissures, and contains an irregularly distributed radioactive vein substance; the radioactivity of local spots exceeds 5 milliroentgons per hour, the highest reading of the scintillation counter. This radioactive zone crops out at several places between localities 9 and 10, and it almost certainly connects beneath talus with a conspicuous zone of sheared and iron-stained gneisses, dikes, and veins at locality 11. By contrast, at localities 12 and 13, poorly bedded,

slightly friable conglomerate lies unconformably on Precambrian gneiss, with no fault between them. At each locality, several tens of feet of green fissile shale and then tan, massive-bedded sandstone are above the conglomerate. The fault close to locality 13 on figure 2 displaces the contact, but is not along it.

In the broad valley of Marsh Gulch, which is 0.1–0.2 mile wide south of locality 11, outcrops are rare. The major fault may logically be drawn through a small outcrop of pulverized rock in the east bank of Marsh Gulch at locality 14, and two outcrops of shattered and intensely altered rock 800 feet and 2,300 feet, respectively, farther upstream, but the fault is concealed elsewhere. Where alluvium becomes thin and discontinuous southward, along the divide between Marsh Gulch and Grape Creek, the Ilse fault should again become obvious, yet it does not. Conceivably, the major fault could (1) terminate before reaching the divide between Marsh Gulch and Grape Creek, in which case the fault at locality 17 would be en echelon; (2) curve abruptly so as to pass first through locality 15, where a vein and dike zone trend N. 50° W., then through the saddle to the south, and finally down a rubble-filled ravine trending S. 5° E.; or (3) maintain a fairly straight course up Marsh Gulch, cross the divide 200 feet northeast of locality 16 as a relatively inconspicuous zone of mildly fractured and stained granite gneiss cut by few dikes, and then continue to locality 17. The author prefers the third explanation, because variations in the intensity of crushing are characteristic of the fault, as already mentioned.

Locality 17 is an outcrop of fissile, shattered, altered biotite gneiss in a gully wall; 200 feet upstream, radioactivity readings greater than the maximum recording range of the scintillometer were found on the dump of a mine in a vein nearly concordant with foliation in the east wall of the gully. The marked divergence in dips on opposite sides of the gully at locality 17 is proof of a major fault; presumably, the fault continues down the rubble-filled gully to Grape Creek.

## RECAPITULATION

To sum up, incipient development of the Ilse fault may have begun before the Precambrian gneisses were fully brittle; that is, while stress could be relieved more by folding, twisting, or stretching than by fracture. The concentration of excessive contortion, folding, and twisting—as represented by variable to chaotic dips unrelated to any specific faults—along transverse linear zones shows that deformation began to concentrate on the linear zones before the rocks were brittle enough to yield mainly by fracture. However, whatever may have been the date of its inception, the zone clearly antedates intrusion of Early Cambrian(?) dikes; otherwise, the dikes would not be more abundant along it than elsewhere. The ancestral fault transected the grain of its Precambrian rock wall. It is conceivable that at some places, zones such as the one along Bear Gulch, now regarded as a branch, absorbed as much of the Precambrian deformation as the main Ilse zone. The Paleozoic and Mesozoic history, after intrusion of the dikes, remain unknown. Renewed faulting on a major scale during Laramide, or later time, is shown by sharply uptilted and truncated Mesozoic rocks. At that time, the east wall moved relatively downward. The Tertiary deformation need not have been uniform; in fact, variation in the extent of crushing along the fault, first noted by Hunter (1915, p. 32), suggests nonuniformity. The total picture, then, is one of an ancestral fault of variable width, intensity of deformation, and rock alteration, that localized Tertiary movement, which, in turn, was strong at some places and weak or absent at others.

## REFERENCES

Burbank, W. S., Lovering, T. S., Goddard, E. N., and Eckel, E. B., compilers, 1935, Geologic map of Colorado: Published by U.S. Geol. Survey in coop. with Colorado State Geol. Survey Board and Colorado State Metal Mining Fund.

Christman, R. A., Brock, M. R., Pearson, R. C., and Singewald, Q. D., 1959, Geology and thorium deposits of the Wet Mountains, Colorado, a progress report: U.S. Geol. Survey Bull. 1072–H, p. 491–535 [1960].

Emmons, S. F., 1896, The mines of Custer County, Colorado: U.S. Geol. Survey 17th Ann. Rept., pt. 2, p. 405–472.

Hunter, J. F., 1915, Some cerusite deposits in Custer County, Colorado: U.S. Geol. Survey Bull. 580–C, p. 25–37.

# ELASTIC MODULI OF GRANITIC ROCK FROM IN SITU MEASUREMENTS OF SEISMIC VELOCITY

By RODERICK D. CARROLL, JAMES H. SCOTT, and D. R. CUNNINGHAM, Denver, Colo.

*Work done in part in cooperation with the Defense Atomic Support Agency*

*Abstract.*—Results of measurement of compressional and shear waves and calculations of dynamic elastic constants are presented for granitic rock in two tunnels in Colorado and Nevada. Inhole recording with near-surface detonation, and surface recording with near-surface detonation were used in this study. Neither method yielded consistent shear-wave generation. This lack in consistency is attributed to conditions around the energy source and in the transmission path.

Because of the relationship of shear waves to dynamic elastic moduli, studies of the generation, transmission, and detection of shear waves in various rock types have been reported by numerous investigators. White and others (1956), White and Sengbush (1963), and Jolly (1956) have described field investigations concerned with the nature of shear-wave generation and methods of detection. Values of dynamic elastic moduli, under in situ conditions, using measurements of compressional and shear-wave velocity have been determined for granite (Nicholls, 1961) and salt (Dickey, 1964). The writers have measured compressional and shear-wave velocities in two different granites in an attempt to determine the dynamic elastic properties of these rocks. Velocities were recorded in the Straight Creek pilot bore, an 8,000-foot tunnel in Colorado passing beneath the Continental Divide, and in tunnels of the Climax stock at the U.S. Atomic Energy Commission's Nevada Test Site, Mercury, Nev. The Test Site measurements were made at the site of the proposed PILE DRIVER nuclear test. Measurements were made using a linear array of accelerometers along the tunnel walls at the Colorado site and in shallow drill holes at the Nevada Test Site.

## INSTRUMENTATION

Instrumentation was practically the same at both the Colorado and Nevada localities, except for the sensitivity and orientation of the detectors. Diagrams illustrating the methods of measurement at the two sites are shown in figure 1.

Detection of the seismic velocities in the Straight Creek tunnel was accomplished by mounting accelerometers in studs grouted in ½-inch-diameter holes drilled 1 inch into the granite rib (fig. 1*A*). The useful range of these accelerometers was 3 to 3,500 cycles per second (c) with a resonant frequency of around 13 kilocycles per second (kc) and a sensitivity of approximately 8 millivolts per gravitational acceleration (mv/g). Because these accelerometers have a very high internal impedance, 4-foot cables were used to connect them to transistorized preamplifiers with variable gain (0.25 to 150). Low-pass (4-kc) filters were coupled to the preamplifiers, and outputs of the preamplifiers-filter pairs were fed to transistorized line drivers. The low output impedance of the latter enabled signals to be transmitted through cables several hundred feet long without voltage loss or waveform distortion. Power to the preamplifiers was provided by 27-volt mercury batteries. Output of the detector-amplifier system was fed into a 4-channel oscilloscope, and the display was recorded on Polaroid film.

Seismic caps and a few decigrams of powder were used to provide the seismic energy.

The accelerometers used at the Climax locality had a greater sensitivity (40 to 50 mv/g) and a flat response over the frequency range 10 to 10,000 c. In addition,

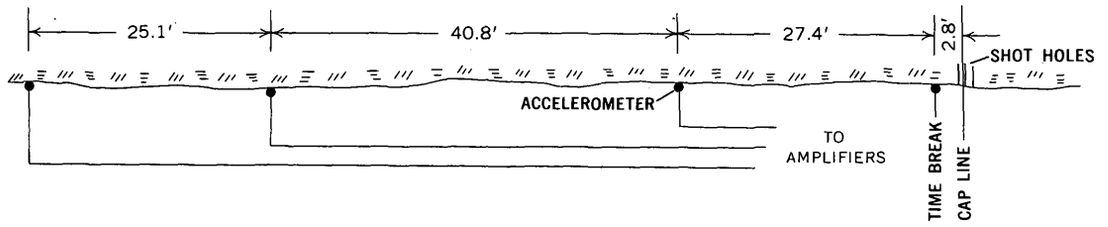


*A*. Plan view of detector layout in Straight Creek pilot bore, Colorado

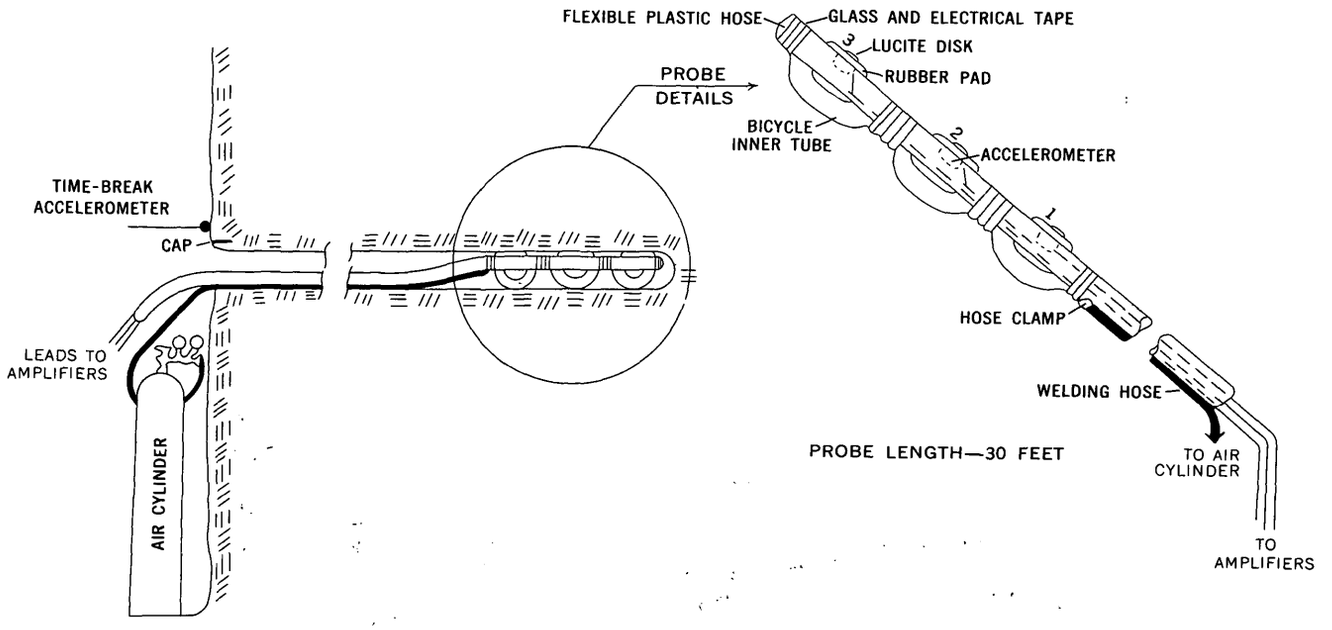


*B*. Details of inhole recording method in Climax-stock tunnels, Nevada

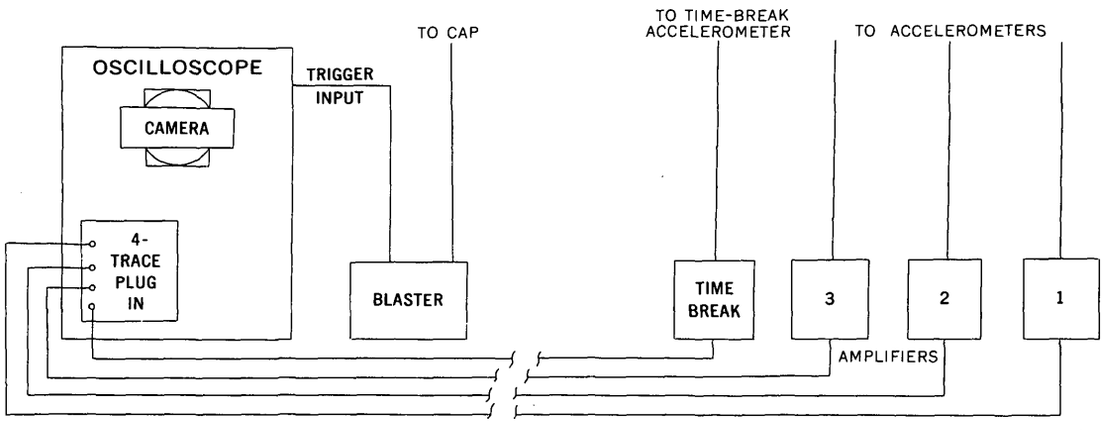


*C*. General block diagram of recording apparatus

FIGURE 1.—Details of seismic recording arrangements used in the study of elastic moduli of granitic rock.

the detectors were mounted at 2-foot intervals in plastic tubing which was inserted in 3-inch-diameter holes drilled 20 to 30 feet deep on the tunnel periphery. Contact between the accelerometers and the borehole walls was obtained by inflating a bicycle inner tube between the probe and the borehole wall (fig. 1*B*). Special 40-foot cables were used to connect the accelerometers in the probe to the preamplifiers at the hole collar.

For this arrangement, a 6-inch-deep shothole, ⅝ inch in diameter, was drilled near the collar of the instrument hole. Seismic energy was provided by a seismic blasting cap inserted in the shothole with water-soaked tissue used for stemming. In a few instances, when the accelerometers were positioned deep in the hole, the cap energy had to be supplemented by a small charge of dynamite wrapped in aluminum foil around the cap. Mostly, however, the single blasting cap yielded sufficient energy to obtain measurements throughout the length of the hole.

## MEASUREMENTS IN THE STRAIGHT CREEK PILOT BORE

The granitic rock in which the Straight Creek pilot bore was driven is considered to be equivalent to the Precambrian Silver Plume Granite (Robinson and Lee, 1962). A section of quartz monzonite relatively free of fractures was selected for the initial measurements. A sample record obtained over the interval indicated in figure 1*A* is shown in figure 2.

Consistent shear-wave generation with repeated shooting was not obtained even though numerous shothole orientations and loading conditions were tried. Although time limitations prevented the checking of alternative arrangements, it is tentatively concluded that the use of a water-filled hole with the charge detonated halfway in the hole is an effective means of generating a strong shear wave. Variations in the waveform character with repeated shots and the inability to consistently recognize a shear-wave arrival with repeated shots remains a problem. A recognizable shear-wave arrival on a number of records, however, allows elastic moduli to be calculated.

Table 1 lists values of dynamic moduli obtained at the Straight Creek site based on the standard formulas that relate these moduli (Dobrin, 1952, p. 181). A density of 2.67 grams per cubic centimeter which is the average density of 30 samples was used as a representative value for granitic rock in the calculations at both the Colorado and Nevada sites.

## MEASUREMENTS IN TUNNELS IN THE CLIMAX STOCK

The granitic rock comprising the Climax stock consists of both granodiorite and quartz monzonite

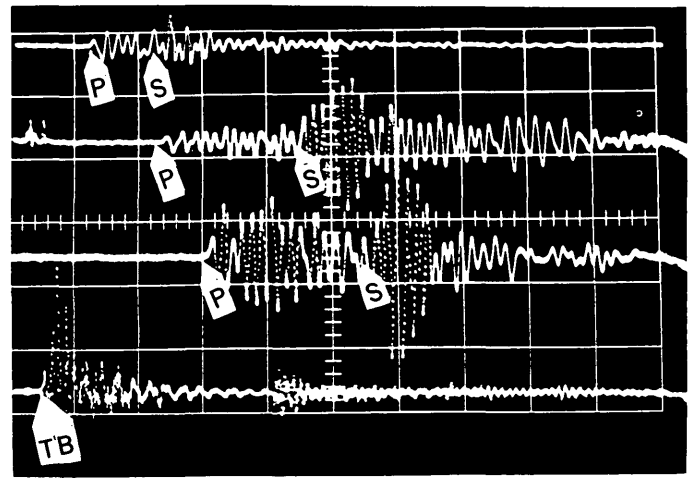


FIGURE 2.—Accelerometer record from Straight Creek pilot bore, showing compressional (P) and shear (S) waves and time break (TB). Time base—2 milliseconds per major division.

(Houser and Poole, 1960). In the tunnels of the Climax stock, measurements were obtained in quartz monzonite by the inhole method (fig. 1*B*). Sample records obtained at two locations in the quartz monzonite are shown in figure 3. As in the Straight Creek tunnel, shear waves were not generated consistently in a number of holes or even at different depths in the same hole. In areas of severe fracturing, shear waves were not detected by either the inhole method or the surface method.

The dynamic elastic constants calculated for the two locations in the tunnels in the Climax stock are listed in table 2. The total time (time break to each accelerometer) recorded at the shop-drift site (fig. 3) differs significantly from the interval time between detectors. This is because the shop-drift site exhibits low velocity layering on the tunnel periphery, owing to the enlargement of preexisting fractures in response to stress relief. Consequently, the velocities listed in table 2 for this hole represent the higher velocity layer behind the tunnel wall, and a velocity based on total time (time from shot instant at collar to last detector

TABLE 1.—*Dynamic elastic moduli obtained in Straight Creek pilot bore, Colorado*

| Interval (feet) | Compressional-wave velocity (ft/sec) | Shear-wave velocity (ft/sec) | Young's modulus ($10^6$ psi) | Shear modulus ($10^6$ psi) | Bulk modulus ($10^6$ psi) | Poisson's ratio |
|---|---|---|---|---|---|---|
| 2.8–27.4 | 18, 300 | 8, 300 | 6. 8 | 2. 5 | 8. 8 | 0. 37 |
| 27.4–69.2 | 17, 000 | 8, 200 | 6. 5 | 2. 4 | 7. 2 | . 35 |
| 69.2–94.3 | 17, 900 | 10, 900 | 10. 3 | 4. 3 | 5. 8 | . 21 |
| Value based on total time (2.8–94.3) | 17, 800 | 8, 900 | 7. 6 | 2. 8 | 7. 6 | . 33 |

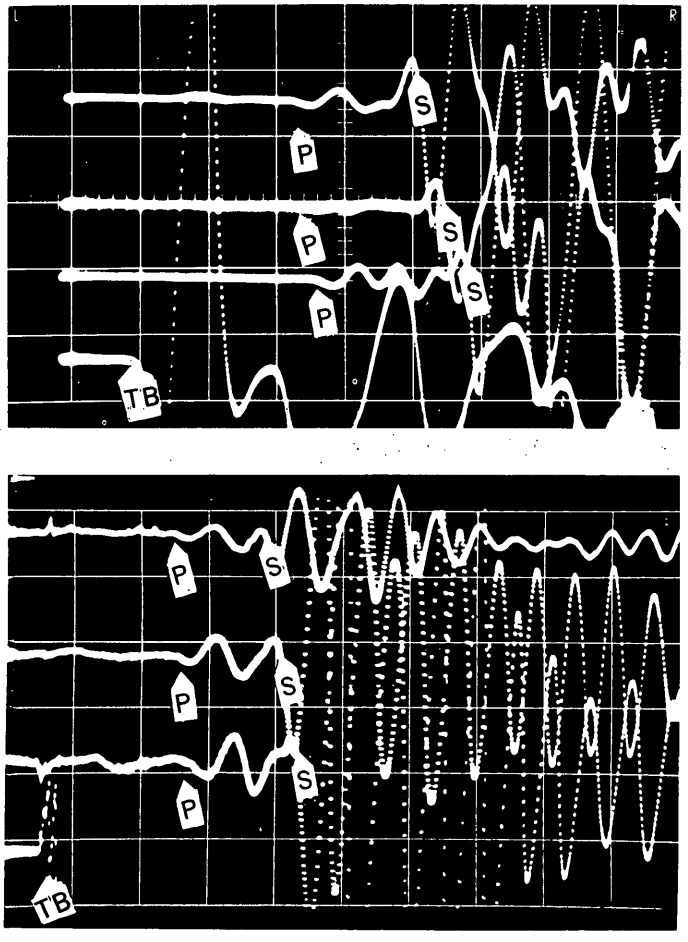


FIGURE 3.—Accelerometer records from two locations in the Climax stock, Nevada, showing compressional (P) and shear (S) waves and time break (TB). Time base—0.5 milliseconds per major division. *Top,* shop drift, first detector 23 feet from hole collar. *Bottom,* cross-drift AR, first detector 16 feet from hole collar.

in the hole) is not listed. No shear waves were detected when the detectors were located within the low-velocity layer.

## RESULTS AND CONCLUSIONS

On the basis of seismic studies on quartz monzonite from the Straight Creek tunnel in Colorado and on quartz monzonite of the Climax stock in Nevada, suitable values were obtained for the in situ dynamic elastic moduli at both locations. A direct comparison of the properties of the rocks based upon these moduli

TABLE 2.—*Dynamic elastic moduli obtained in tunnels in the Climax stock, Nevada Test Site, Nevada*

| Location | Compressional-wave velocity (ft/sec) | Shear-wave velocity (ft/sec) | Young's modulus ($10^6$ psi) | Shear modulus ($10^6$ psi) | Bulk modulus ($10^6$ psi) | Poisson's ratio |
|---|---|---|---|---|---|---|
| Shop drift | 20,000 | 11,400 | 11.8 | 4.7 | 8.2 | 0.26 |
| Cross drift | 20,000 | 12,300 | 13.0 | 5.4 | 7.1 | .20 |
| Value based on total times | 18,000 | 9,000 | 7.8 | 2.9 | 7.8 | .33 |

should be approached with caution, however, because the seismic velocity of rock is a function of stress, which may differ in the two environments. Additional research is needed (1) to relate the magnitude and direction of stress to relative changes in compressional and shear-wave velocities and (2) to determine the consequent effect on the dynamic elastic moduli.

The techniques used in this investigation could not consistently generate shear waves. Results indicate that the environment of the energy source and the presence of fractures in the transmitting media are critical. Another approach that may enhance the detection of shear waves (not tried in this investigation) would be the use of three-component detectors.

## REFERENCES

Dickey, D. D., 1964, Effects of the GNOME nuclear explosion upon rock salt as measured by acoustical methods, *in* Geological Survey Research 1964: U.S. Geol. Survey Prof. Paper 501–B, p. B108–B–111.

Dobrin, M. B., 1952, Introduction to geophysical prospecting: New York, McGraw-Hill, 435 p.

Houser, F. N., and Poole, F. G., 1960, Preliminary geologic map of the Climax stock and vicinity, Nye County, Nevada: U.S. Geol. Survey Misc. Geol. Inv. Map I–328.

Jolly, R. N., 1956, Investigation of shear waves: Geophysics, v. 21, p. 905–938.

Nicholls, H. R., 1961, In situ determination of the dynamic elastic constants of rocks: U.S. Bur. Mines Rept. Inv. 5888, 13 p.

Robinson, C. S., and Lee, F. T., 1962, Geology of the Straight Creek tunnel site, Clear Creek and Summit Counties, Colorado, and its predicted effect on tunnel construction: U.S. Geol. Survey open-file rept, 32 p.

White, J. E., Heaps, S. N., and Lawrence, P. L., 1956, Seismic waves from a horizontal force: Geophysics, v. 21, p. 715–723.

White, J. E., and Sengbush, R. L., 1963, Shear waves from explosive sources: Geophysics, v. 28, p. 1001–1019.

# RUPTURE PHENOMENA IN THE SILVER PLUME GRANITE, COLORADO

By FITZHUGH T. LEE and THOMAS C. NICHOLS, JR., Denver, Colo.

*Abstract.*—Fractures, slickensides, and gouge produced during laboratory compressive testing of cylinders of Silver Plume Granite resemble fractures noted in the granite during surface and subsurface mapping in the Straight Creek area, Colorado. Formation of gouge and slickensides in the laboratory is believed to be due primarily to energy release rather than to movement. Fault displacements in granitic terrane should be examined in the light of these findings.

A rock mechanics study of the Precambrian Silver Plume Granite has been undertaken in connection with a comprehensive geological and geophysical research program being conducted in the pilot bore of the Straight Creek Tunnel, 55 miles west of Denver, Colo. (fig. 1). The ultimate objective of these laboratory tests is the application of the results to engineering problems in surface and subsurface excavations.

Similarities were noted between slickensides and gouge produced in core samples before or during compressive failure and natural slickensides and gouge. These laboratory-produced features may shed new light on field criteria for recognition of faulting, as well as on determination of amount of displacement along faults. For example, Nevin (1949, p. 134) states that if other variables are equal, the amount of shattering and the thickness of associated breccia are proportional to the amount of displacement on a fault. It is generally assumed that slickensides and gouge are produced only by differential grinding movement along the two sides of a fault. However, these features can also be produced by internal strain adjustments in response to compressive forces.

The Silver Plume Granite was selected for an investigation of rock mechanics because it has been extensively studied in connection with the construction of the Straight Creek Tunnel pilot bore, and because samples could be selected from here that are relatively uniform in composition, structure, and fabric. According to Robinson and Lee (1962, 1965) the granite varies considerably in composition, principally as a result of partial to complete assimilation of metasedimentary rocks. Where uncontaminated, the rock is a quartz monzonite rather than a true granite. The granite is light gray to light pinkish gray and fine to medium grained. The following tabulation shows the average modal analysis of 31 samples from the Straight Creek area:

| Mineral | Amount (volume percent) |
|---|---|
| Microcline | 33.9 |
| Quartz | 28.9 |
| Plagioclase [1] | 25.4 |
| Biotite | 3.9 |
| Calcite | 2.9 |
| Chlorite | 1.8 |
| Muscovite | 1.6 |
| Opaque | 1.1 |
| Accessory | 0.3 |
| Sillimanite | 0.2 |
| Total | 100.0 |

[1] The average An content of the plagioclase feldspar in 25 samples was 25.5 percent.

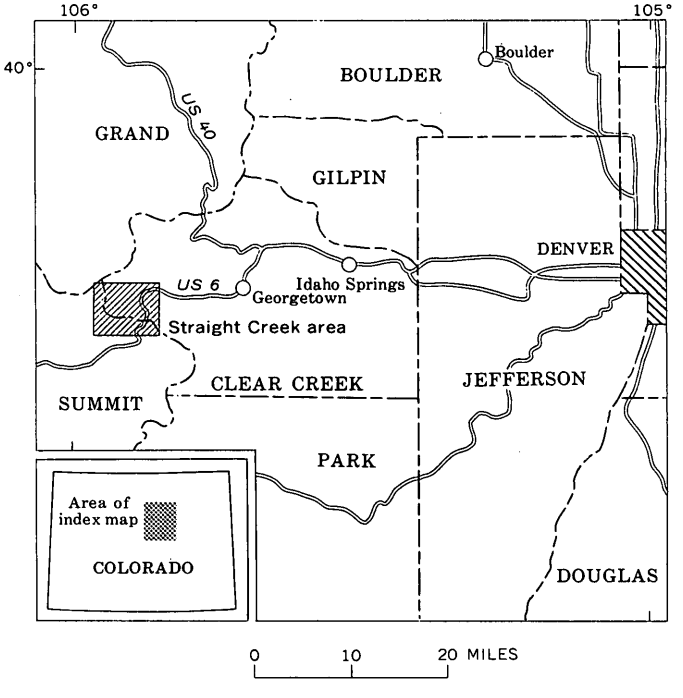


FIGURE 1.—Index map of Straight Creek area, Colorado.

## FRACTURES IN THE SILVER PLUME GRANITE

Rocks of the Straight Creek area are shattered along the southern part of the Berthoud Pass fault (Lovering and Goddard, 1950, p. 59–60), which is a north- to northeast-trending zone, about 2 miles wide, in which diversely oriented bodies of faulted and sheared rock are separated by relatively unfractured rock. According to Lovering and Goddard (1950, p. 79), episodes of shearing took place in Precambrian time and also in Late Cretaceous and Tertiary time.

In the pilot bore of the tunnel the Silver Plume Granite is sheared and altered in varying degrees. Contacts of shear zones are gradational—the intensity of shearing decreases outward from the center of the zone. Near the margins of the shear zones, the rock is broken into slivers 0.1 foot wide bounded by slickensided shear planes. Grooves 2 feet or more in length are also present. Much of the sheared surface is covered with clay gouge and broken feldspar and quartz grains. Figure 2 shows a closer view of a slickensided granite sample from the pilot bore. Microscopic examination indicates that grain fracturing, and commonly the shearing as well, extends entirely through some of the blocks. Where shearing was intense, the rock has been reduced to a coarse to fine sand, and the shear planes are from less than 0.01 foot to 0.1 foot apart and are oriented in many directions. In areas of most intense shearing the material is fault gouge consisting of clay with varying amounts of fine-grained feldspar, mica, and quartz grains. The fault gouge commonly shows some chemical alteration.

Many joints in the pilot bore are actually microfaults and shears (Robinson and Lee, 1965, p. 19).

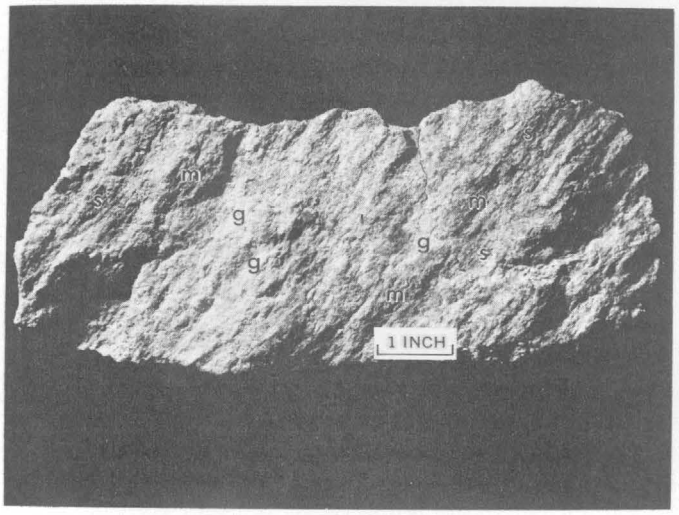


FIGURE 2.—Sample of Silver Plume Granite from wall of Straight Creek Tunnel pilot bore, showing slickensided surface (s), mullion structure (m), and clay gouge (g). Note similar features in figure 5.

Such joints typically are coated with biotite or chlorite and commonly are slickensided. The rock immediately adjacent to the joint is partially altered for a distance of 0.01 foot to 0.1 foot inward from the joint. Other joint surfaces are coated with calcite, dolomite, selenite, talc, or epidote. Locally, quartz coats the joint surfaces, and is commonly slickensided. A few tight uncoated joints are also present.

## LABORATORY RESULTS

The laboratory investigation of the Silver Plume Granite included both triaxial and unconfined compressive tests. Pressures ranged from atmospheric (unconfined) to 5,000 pounds per square inch (confined). Compressive strengths ranged from 15,000 to 65,700 psi. Thirty cylindrical cores were tested which had an average length of 4.01 inches and an average diameter of 1.99 inches. Figure 3 shows a typical core after failure. The test procedures and equipment are discussed elsewhere (Nichols and Lee, 1966). The core in figure 3 failed under a compressive stress of 65,700 psi and a confining pressure of 5,000 psi. The main failure surface forms an angle of 25°–35° with the vertical axis.

As the confined cores approached failure under compression, the middle of the cylinder bulged; this was reflected by an increase in the ratio of the radial strain to the longitudinal strain. In order to better understand the mechanics of deformation and failure, an accelerometer was fitted in a base platen (fig. 3) to detect seismic disturbances during axial and lateral loading. A recording oscillograph provided a photographic record of energy-producing events during loading (fig. 4). It is noteworthy that minor amounts of energy were released several minutes before failure, during which the rate of loading was about 60 psi per second. Megascopic and microscopic examination of features noted in cores which failed and in cores removed prior to failure suggests that the energy-producing events recorded may have been caused by grain dislocations and fractures (both shear and tensile) during the lateral bulging. Increase of the axial load eventually resulted in complete failure of the rock sample, during which a sudden large release of energy occurred, accompanied by a loud explosion and simultaneous breaking of the core. Inasmuch as gouge was found in cores removed before failure, some of the events from $t=-3.5$ seconds to $t=0$ second (fig. 4), and perhaps earlier, may be associated with rupture phenomena which produce gouge and slickensides before shear movement occurs.

Adjacent to the main failure surface a zone of subparallel rupturing about 0.5 inch wide contains clay-

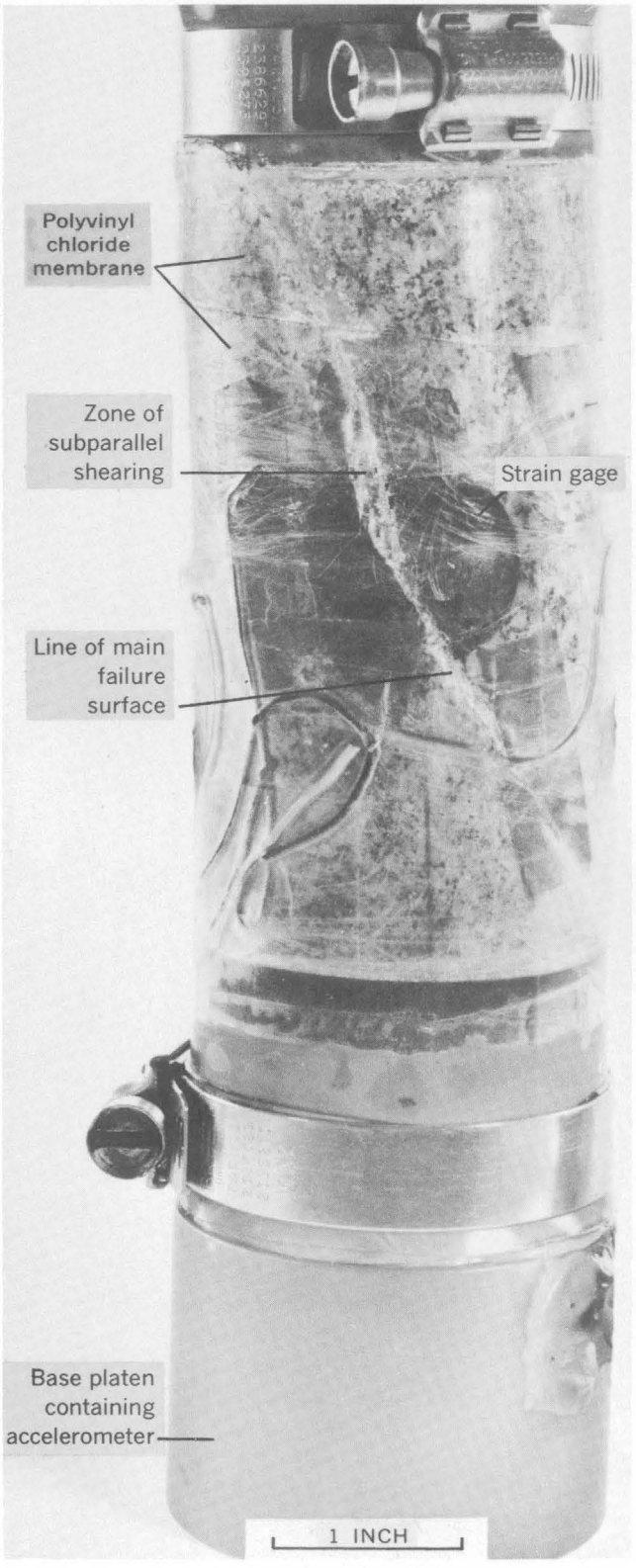


FIGURE 3.—Core of Silver Plume Granite, outfitted for a triaxial test, after failure under compression. A flexible polyvinyl chloride membrane encloses the core to prevent entry of hydraulic fluid. Two strain-gage rosettes, mounted on opposite surfaces, monitor lateral and longitudinal strain.

size gouge consisting of crushed quartz, feldspar, and biotite or chlorite grains. The maximum relative displacement measured along the dip of the ruptured zone is about 0.25 inch. The displacement is the amount of offset between reference lines marked on the core. The vinyl membrane has a negligible influence on displacement because of the high fluid confining pressure. Continuous slickensides on the surface of failure (fig. 5) are as long as 2 inches. Relative displacements are as long as 2 inches. Relative displacements are consistently about one order of magnitude less than observed slickenside length. The surfaces shown in figure 5 have coatings of "fault gouge" that consist of clay- to sand-sized particles. Other cores show continuous grooves as much as 4 inches long.

X-ray examination of the gouge found along faults in the Silver Plume Granite shows montmorillonite, kaolinite, and illite to be present, whereas the gouge produced in cores in the laboratory lacks montmorillonite and illite and has only a minor amount of kaolinite. This indicates that much of the gouge found in the pilot bore is the result of post-faulting alteration, perhaps caused by ground water, since the presence of clay minerals would not be anticipated in gouge material produced from dry, unaltered granite.

The "fault gouge" from the laboratory tests was carefully removed from the failure surfaces and weighed and compared with the original weight of the core to determine the percentage of "fault gouge." The amount of fresh rock reduced to clay size and fine sand ranged from less than 1 percent to about 3 percent (by weight) of the original core. The actual percentage was considerably higher in some instances in which observable gouge could not be collected from internal surfaces without causing abnormal breakage. In general, greater confining pressures caused the production of greater amounts of fine-grained material.

## CONCLUSIONS

The writers are as yet unable to provide a wholly adequate explanation of all the fracture phenomena described above. In general, they concur with the ideas of brittle crack growth during compression expressed by Brace and Bombolakis (1963), who believe that many faults may be formed by the interaction of en echelon arrays of cracks which are present before displacement along a fault. Brace and Bombolakis also point out that the applied stress necessary to start growth of cracks in brittle material is less than the stress required to produce ultimate macroscopic fracture; and, in at least a few cases, the stress required to produce macroscopic fractures is considerably less than the stress necessary to cause failure by faulting.

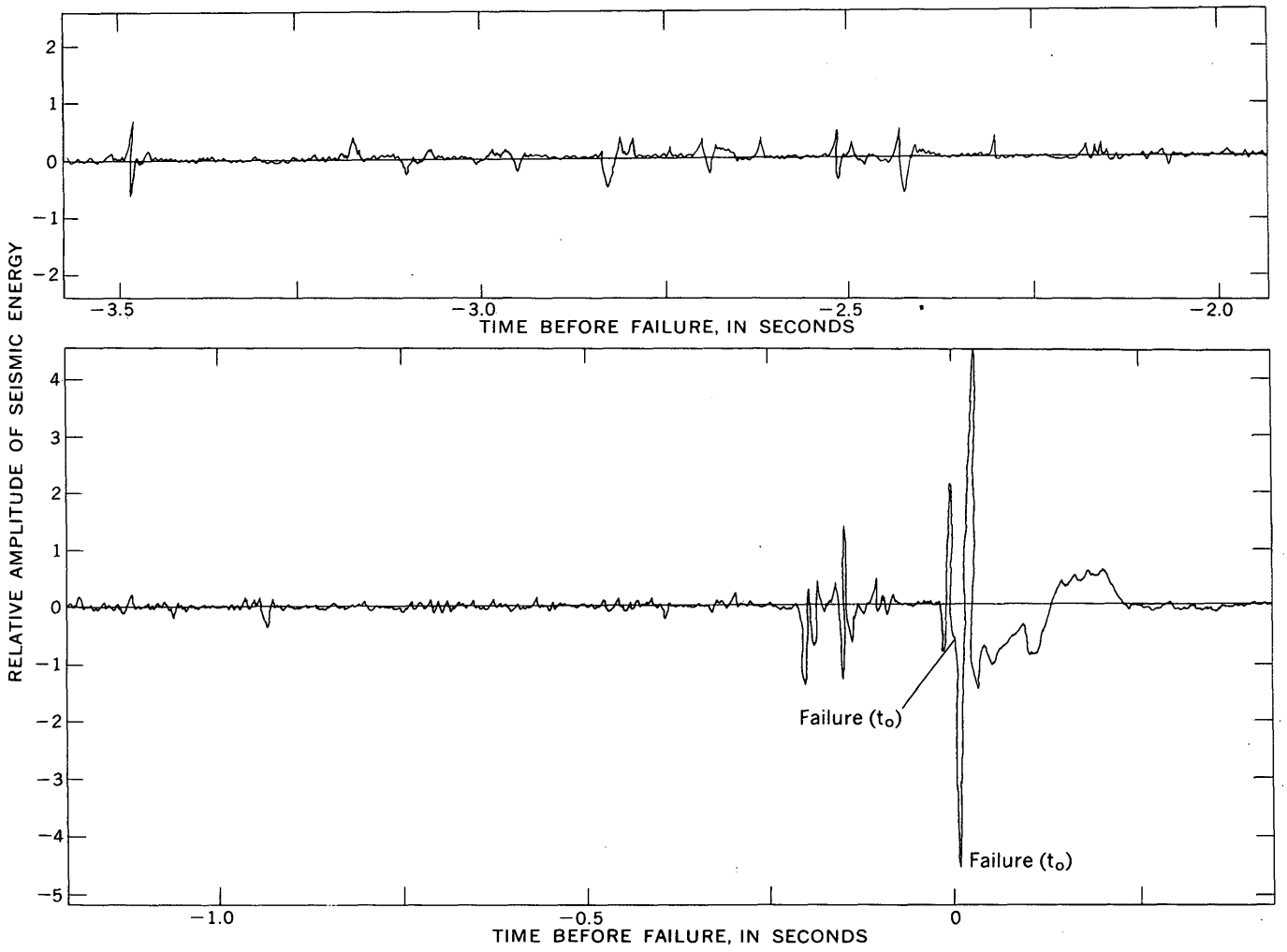


FIGURE 4.—Seismic record of triaxial test of core shown in figures 3 and 5. Vertical scale is arbitrary, and units on both sections are equal. That part of record between $t = -2.0$ seconds (upper part of figure) and $t = -1.0$ second (lower part of figure) has been omitted.

The results of our investigations support the following:

1. Under compressive stress in laboratory tests, fractures and fault gouge form in samples of Silver Plume Granite before the rock fails completely.
2. Maximum relative movement of adjacent displaced pieces of core is at least one order of magnitude less than the length of observed slickensides.
3. In laboratory tests, more than 3 percent by weight of some samples of fresh granite is converted to clay-, silt-, and sand-sized material along surfaces of rupture.
4. The occurrence of some fault gouge in the Silver Plume Granite may be the result of energy release under high compressive stress rather than granulation during movement along shear surface.
5. In granitic terrane, wide shatter zones are not nec-

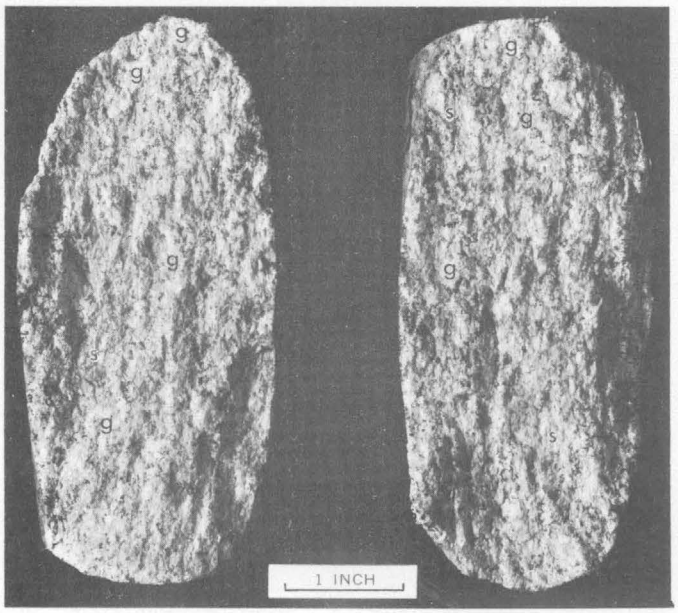


FIGURE 5.—Core of Silver Plume Granite shown in figure 3 with gouge (g) and slickensides (s) on inside surfaces of separated pieces.

essarily reliable indicators of faulting and fault displacement, nor are gouge and slickensides formed only by grinding action along fault surfaces.

## REFERENCES

Brace, W. F., and Bombolakis, E. G., 1963, A note on brittle crack growth in compression: Jour. Geophys. Research, v. 68, no. 12, p. 3709–3713.

Lovering, T. S., and Goddard, E. N., 1950, Geology and ore deposits of the Front Range, Colorado: U.S. Geol. Survey Prof. Paper 223, 319 p.

Nevin, C. M., 1949, Principles of structural geology: New York, John Wiley and Sons, 410 p.

Nichols, T. C., and Lee, F. T., 1966, Preliminary appraisal of applied rock mechanics research on Silver Plume Granite, *in* Geological Survey Research 1966: U.S. Geol. Survey Prof. Paper 550–C, p. C34–C38.

Robinson, C. S., and Lee, F. T., 1962, Geology of the Straight Creek Tunnel site, Clear Creek and Summit Counties, Colorado, and its predicted effect on tunnel construction: U.S. Geol. Survey open-file rept, 32 p., Dec. 1962.

——— 1965, Preliminary report on the engineering geology of the Straight Creek Tunnel pilot bore, Clear Creek and Summit Counties, Colorado: U.S. Geol. Survey open-file rept., 34 p., Feb. 1965.

# PRELIMINARY APPRAISAL OF APPLIED ROCK MECHANICS RESEARCH ON SILVER PLUME GRANITE, COLORADO

By THOMAS C. NICHOLS, JR., and FITZHUGH T. LEE, Denver, Colo.

*Abstract.*—A program of preliminary laboratory testing was conducted to determine elastic and physical properties of the Silver Plume Granite and certain types of rock associated with it. Data derived from laboratory tests were used to relate deformation to the structure, fabric, and mineralogy of the rock. Results of this investigation show: (1) how structural features such as strong lineations, foliations, joints, faults, and associated mineralogic variations are related to the deformation and failure of granitic rocks, and (2) how the knowledge of the physical behavior of a rock determined in the laboratory is significant to the engineer when it can be related to the behavior of the rock in the field.

Laboratory testing was conducted on a relatively undeformed, uniform rock of medium grain size, the Silver Plume Granite, to determine deformational and strength properties under various conditions. Information obtained from these tests was compared to structure, fabric, and mineralogy of the rock in an attempt to isolate factors related to deformation and strength. An attempt was also made to relate deformational phenomena observed in the laboratory to similar geologic phenomena observed in the field.

The Precambrian Silver Plume Granite specimens used for testing were relatively massive and of fairly uniform mineralogy and grain size. The granite has been described by Harrison and Wells (1959, p. 17–20). The specimens used for these tests contain medium-sized randomly oriented grains of quartz, feldspar, biotite, and muscovite, with a few large grains of feldspar that give a slightly porphyritic texture. Foliation of feldspar is faintly discernible. Individual mineral grains have microscopic and macroscopic fractures of apparent random orientation, although some apparent fractures are cleavages and grain interfaces. Samples for testing were obtained from an abandoned quarry near Silver Plume, Colo.

## METHODS OF STUDY

Laboratory tests consisted of measurements of triaxial compression, unconfined compression, and tensile strength, from which stress, strain, and seismic data were obtained at various stages of deformation.

All samples were prepared in the manner described below:

1. Samples not already existing as cores were cut with a 2⅛-inch core barrel.
2. Cores were trimmed and planed such that the length-to-diameter ratio was at least 2:1. The end parallelism was held to a tolerance of less than 0.001 inch. Orientation of foliation and planes of weakness were recorded. Samples for the tensile tests were trimmed to the size of the apparatus. Parallelism of the ends of these samples is unimportant.
3. For triaxial compression tests, strain gages were applied to the surface of each core midway between the top and bottom. Two rosette gages, each with two 90° components, were applied, one component being parallel and the other perpendicular to the long axis. The gages were mounted on opposite sides of the core with the parallel components connected in series to obtain average strain measurements. Radial strain was determined by comparing the ratio of the change in circumference ($\Delta C$) to the original circumference ($C$), or conversely the ratio of the change in radius ($\Delta R$) to the original radius ($R$). It can be shown that $\frac{\Delta C}{C} = \frac{\Delta R}{R}$ or that circumferential strain is equal to radial strain. Thus, radial strain was measured directly by circumferentially mounted strain gages. Axial strain was measured by gages mounted parallel to the long axis.

The cores for triaxial testing were covered with tough membranes of polyvinyl chloride (fig. 1) and placed between loading platens in a triaxial chamber capable of transmitting axial loads of 400,000 pounds and holding fluid pressures of 8,000 pounds per square inch. An accelerometer was mounted on the bottom

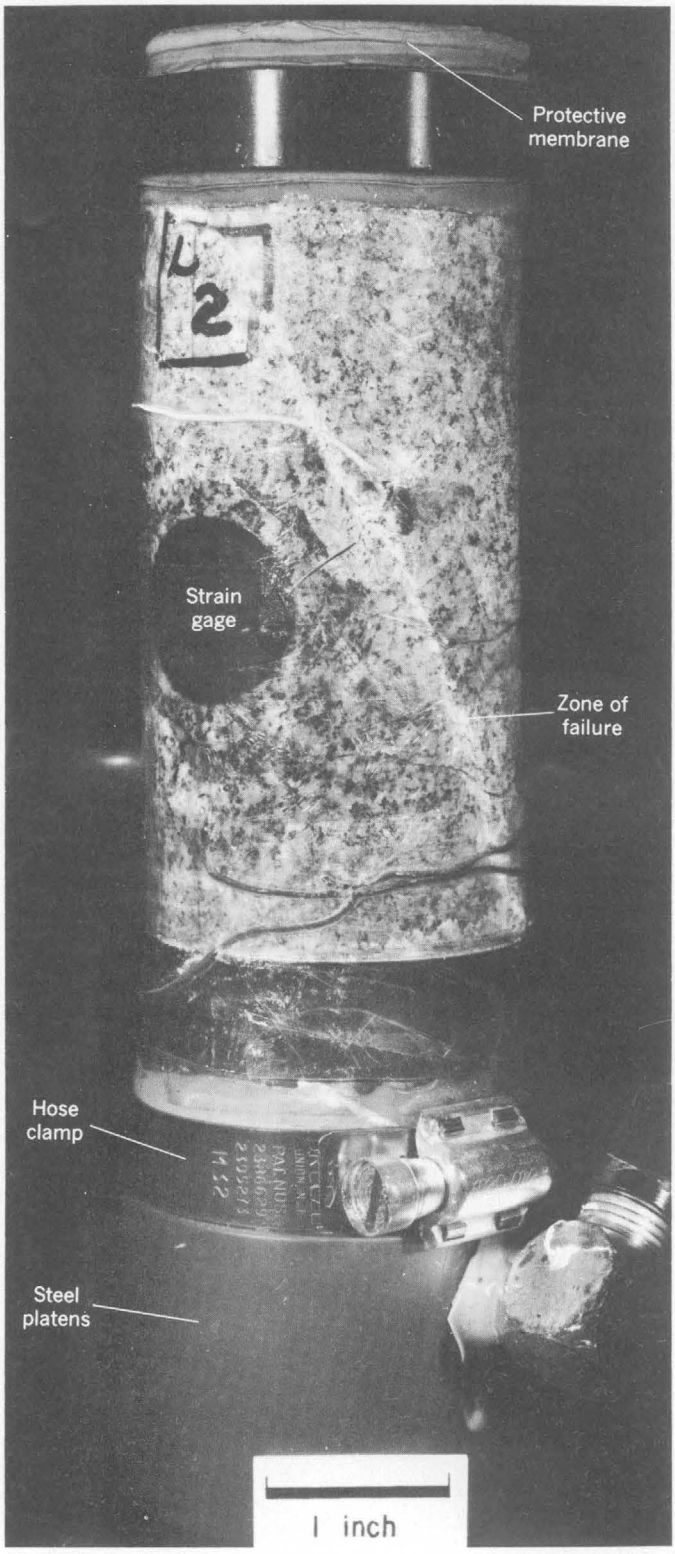


FIGURE 1.—Core after failure, showing steel platen, protective membrane, and strain-gage rosette.

platen within an air chamber and was oriented so that it was sensitive to the vertical component of seismic energy released as fracturing occurred. The triaxial chamber, after being filled with hydraulic fluid and sealed, was placed in a hydraulic press capable of exerting loads up to 400,000 pounds at uniform loading rates. Electrical connections necessary for monitoring strain measurements and accelerometer impulses were then completed. A strain indicator was used to measure strain, and an oscillograph was used to monitor accelerometer impulses. A diagrammatic sketch, figure 2, shows the entire loading and monitoring system.

### Types of tests

Triaxial loading tests were performed on the core to investigate the following:

1. The effect of increased confining pressures upon the elastic and physical properties of the samples.
2. The differences between physical measurements that can be expected within the Silver Plume Granite.
3. The applicability of Mohr's failure envelope in predicting strength and internal friction for various degrees of confining stress.
4. The probability and amount of creep under confining pressures.
5. The modes of failure, and fabric changes of the samples during stress applications.
6. How the modes of failure and fabric change can be related to natural geologic phenomena, such

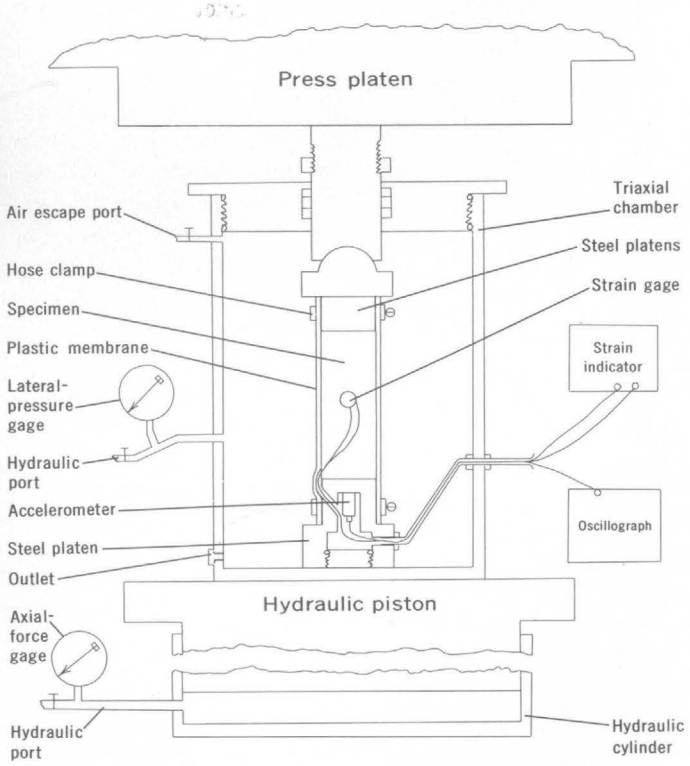


FIGURE 2.—Sketch of loading and monitoring system for triaxial testing.

as possible stiffening of rock, slickensides, fault planes, hardway and softway planes.

Unconfined compression tests and tensile tests were conducted on duplicate samples, primarily to correlate these test observations with triaxial test observations, and to provide data for Mohr's failure envelopes.

The unconfined compression tests were performed by loading cores axially until they failed. No attempt was made to induce permanent set in the cores by preliminary repeated loading. Strain measurements were made with calibrated mechanical extensometers.

The tensile tests were conducted on apparatus designed by Donald R. Reichmuth,[1] utilizing a point-loading method. Strain was not measured in these tests.

## RESULTS OF INVESTIGATIONS

### Compressive strength

The compressive strength of the Silver Plume Granite is quite high under all conditions of orientation and loading. The unconfined compressive strength ranges from 22,000 to 33,000 psi. Confining pressures ranging from 0 to 5,000 psi were applied to various cores of similar composition placed in different orientations with respect to foliation. As the confining pressures increased, the strength of the rocks also increased. At 5,000 psi some specimens of Silver Plume Granite reached a strength of 65,000 psi. The strengths and internal angles of friction under different confining pressures and core orientations were predictable in most instances using Mohr's failure-envelope plots (Sowers and Sowers, 1951, p. 42–44) (fig. 3). As suspected, the weak foliation in these cores had very little effect upon the strength. All test curves that were plotted, with the exception of curves 4 and 6, fit very closely to the failure envelope. The deviation of curves 4 and 6 can be explained by a probable decrease of cohesion or internal friction within the cores tested.

### Effect of mineral content and foliation on strength

To show the effect of mineral content upon the strength of the Silver Plume Granite, several cores were chosen that had a greater deviation of mineral content than those used for the Mohr's envelope plot. These cores were tested under identical confining pressures of 1,500 psi at similar orientations; their strength varies only slightly with composition change (fig. 4). With the exception of one apparently anomalous core that failed at 60,300 psi, core failure values are in a very narrow range. Thus, it appears that the incipient

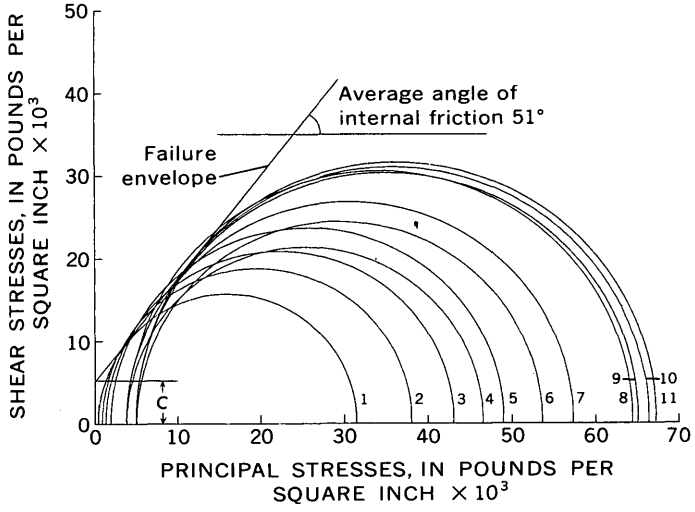


FIGURE 3.—Mohr's failure envelope for Silver Plume Granite. Numbers indicate individual tests; *c*, cohesion is approximately 5,200 psi.

foliation and slight variations in mineral content that occur in Silver Plume Granite have only a minor effect on rock strength.

The strength of migmatite, gneiss, and schist associated with the Silver Plume Granite, although high, varies considerably with respect to the orientation of well-developed foliation and lineation, joints, and with variations in mineralogy and grain size. Cores of metamorphic rock with foliation directions oriented subparallel to the direction of maximum shear stress failed along these foliations at relatively low com-

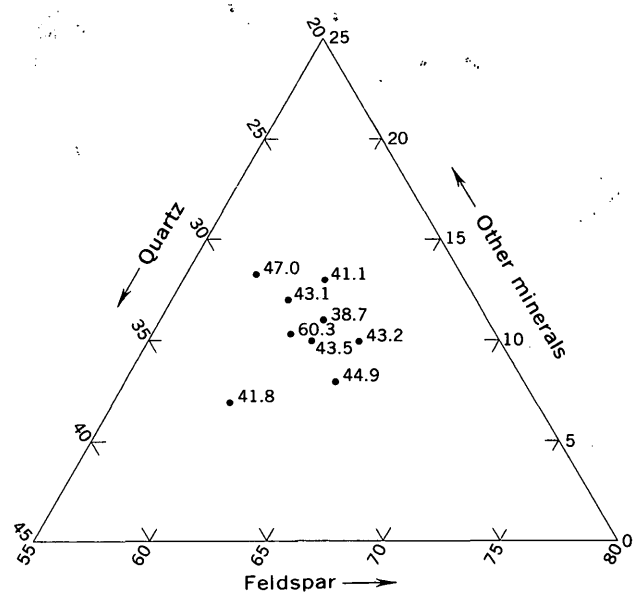


FIGURE 4.—Diagram showing mineral composition and strength of Silver Plume Granite cores under confining pressures of 1,500 psi. Solid circles show mineral content of individual specimens tested. Numbers represent strength of specimen tested in Kips per square inch.

[1] Mining Methods Research Engineer, Minneapolis Mining Research Center, Minneapolis, Minn.

pressive stress values. Also, the compressive strengths of these rocks changed with variations in mineralogy; as the biotite or quartz content increased, the strength lessened. In such rocks, Mohr's failure envelope could not be used with any great success to predict ultimate strengths of the rocks or their angles of internal friction.

### Elastic behavior

When the Silver Plume Granite was subjected to confining pressures of 0 to 5,000 psi during testing, a brittle elastic behavior was observed. Very little ductility was noticed, and the elastic behavior was seen to be very uniform, as described below.

In similar tests on Silver Plume Granite samples oriented in several different directions, the ratio of axial stress to axial strain varied a maximum of $\pm 6$ percent from the mean value. The mean value for the stress-strain ratio was approximately $7 \times 10^6$ psi for unconfined tests and approximately $8.6 \times 10^6$ psi for tests in which the confining pressures ranged from 1,500 to 5,000 psi. Thus, there was an initial increase of the stress-strain ratio when the confining pressure was changed from 0 to 1,500 psi, but no significant change as the confining stress was increased from 1,500 to 5,000 psi.

The ratios of radial strain to axial strain were consistently very close on samples of the Silver Plume Granite tested under similar conditions. In general, these ratios increased as the axial stress was increased, but decreased as the confining stress was increased. Cores that were repeatedly preloaded by axial and hydrostatic stresses had decreased radial- to axial-strain ratios. Also, permanent set was developed, the greatest amount occurring during the first preload.

Different conditions of repeated preloading of these specimens appear to uniquely change the elastic behavior of the samples. Although definite conclusions cannot be drawn from the limited data available, the following observations were made:

1. Those cores that were axially preloaded showed:
   a. permanent set primarily parallel to the axis of the specimen.
   b. a linear stress to axial-strain ratio.
   c. a nonlinear stress to radial-strain ratio. The change of stress generally did not increase as rapidly as the change of radial strain.
2. Those cores that were hydrostatically preloaded showed:
   a. permanent set of similar magnitude both in the axial and radial directions.
   b. a linear stress to axial-strain ratio that generally is greater than the stress to strain ratio of axially preloaded cores.
   c. a nearly linear stress to radial-strain ratio.

### Creep

Creep under confining pressures of as much as 5,000 psi is probably negligible within the Silver Plume Granite. Tests show that when a granite sample is loaded to 5,000 psi confining pressure and 51,000 psi axial stress for 3 days, the rate of creep slows to (1) approximately 25 microinches per inch per day on the second day and (2) to 15 microinches per inch per day on the third day. Yet, the amount of strain caused by a 1°C change in temperature is about 8 microinches per inch. Thus, creep apparently becomes negligible after stress has been applied for several days, after which small strain caused by temperature fluctuations will be dominant.

### Fabric changes

There was an initial attempt to make quantitative fabric measurements for this investigation, but because of excessive time required for these measurements it was felt that the following qualitative observations of gross features would suffiice for these preliminary investigations.

Immediately before and after failure of core samples there is a substantial increase of fracture density along many zones subparallel to or at conjugate angles to the main rupture zone. In all instances this fracturing took place along planes of high shear stress. Some of these zones of intense fracturing did not completely propagate through the cores, indicating that shear failure is not an instantaneous occurrence. Energy release, recorded as the specimens were loaded, indicated that small local failures along fractures took place at a uniform rate throughout the duration of the test until complete failure occurred. At the time of complete failure a very large amount of energy is released. This indicates that fracture density probably increased along planes of high shearing stress throughout the duration of the test and that movement along these planes possibly occurred before total failure. The failure planes had slickensides and well-developed gouge similar to that observed in the field along faults and fractures (Lee and Nichols, 1966).

## APPLICATION OF TEST RESULTS

The strength of the different rocks tested is great. Therefore, significant engineering problems in this terrane most likely will be related to faults, gouge zones, joints, strong lineations, and foliations rather than to the inherent strength of the rocks themselves.

The Mohr failure-envelope plots indicate that a uniform granite such as the Silver Plume has remarkably uniform strength and internal friction properties, which could be used to help solve structural problems in the field. For example, if the attitudes of shear fractures are measured in the field on similar rocks whose stress history is not known, then angles of friction computed from stress analyses in the laboratory might help define conjugate sets of shear joints. Such local information could be valuable in analyzing regional tectonic systems when used in conjunction with more sophisticated methods such as those described by Brace (1961) and Harrison and Moench (1961).

The knowledge of elastic behavior of the Silver Plume Granite gained from laboratory studies is probably not of any great value in itself without additional field information. In situ measurements using geophysical techniques to determine the elastic behavior before, during, and after disturbances caused by engineering construction are probably more meaningful. By comparing the elastic behavior of rocks measured in situ with the behavior of similar rocks tested in the laboratory it may be possible to study (1) the magnitude and nature of stress redistributions caused by engineering disturbances, and (2) the relation of these redistributions to existing geologic structures.

To corroborate these interpretations of elastic behavior, scale models simulating geologic structures should be made in the laboratory with built-in monitoring devices capable of sensing stress and temperature changes and microseisms. Similar devices should be used in the field. These laboratory models can be stressed to simulate the disturbances caused in the field by construction practices. Data obtained from these tests can then be compared with field data in an attempt to determine the effects of structural features upon stress behavior.

## CONCLUSIONS

In general, preliminary laboratory testing of the Silver Plume Granite has helped explain the behavior of this rock under certain stress conditions. More importantly, the test data have a practical application to engineering construction problems, and have provided a basis for planning future testing. Clearly, field measurements of rock behavior are needed in conjunction with future laboratory studies.

## REFERENCES

Brace, W. F., 1961, Mohr construction in the analysis of large geologic strain: Geol. Soc. America Bull., v. 72, no. 7, p. 1059–1080.

Harrison, J. E., and Moench, R. H., 1961, Joints in Precambrian rocks, Central City–Idaho Springs area, Colorado: U.S. Geol. Survey Prof. Paper 374–B, 14 p.

Harrison, J. E., and Wells, J. D., 1959, Geology and ore deposits of the Chicago Creek area, Clear Creek County, Colorado: U.S. Geol. Survey Prof. Paper 319, 92 p.

Lee, F. T., and Nichols, T. C., Jr., 1966, Rupture phenomena in the Silver Plume Granite, Colorado, *in* Geological Survey Research 1966: U.S. Geol. Survey Prof. Paper 550–C, p. C29–C33.

Sowers, G. B., and Sowers, G. F., 1951, Soil mechanics and foundations: New York, Macmillan Co., 284 p.

# STRATIGRAPHY, PALEONTOLOGY, AND ISOTOPIC AGES OF UPPER MESOZOIC ROCKS IN THE SOUTHWESTERN WRANGELL MOUNTAINS, ALASKA

By ARTHUR GRANTZ, D. L. JONES, and M. A. LANPHERE,
Menlo Park, Calif.

*Abstract.*—Reconnaissance field observations, fossils, and potassium-argon ages have provided new information on the upper Mesozoic strata of the Wrangell Mountains. The Kotsina Conglomerate is probably Middle or lower Upper Jurassic. Sandstone along the Chetaslina River may be Callovian (Jurassic), and nearby unfossiliferous shale and sandstone is probably also upper Mesozoic. A unit of sandstone, siltstone, conglomerate, and calcarenite, previously thought to be gradational downward into the Kotsina Conglomerate, yielded Hauterivian and Barremian (Lower Cretaceous) fossils. Similar rocks occur in the northern Chugach Mountains and at Kuskulana Pass, where they rest on granodiorite dated as 141±5 m.y. Sandstone and siltstone with Albian (Lower Cretaceous) fossils rest on the Hauterivian to Barremian rocks at Kuskulana Pass, and shale and arkose of similar age rest on granodiorite dated as 126±4 m.y. near Mount Drum.

The southwestern Wrangell Mountains, and the adjacent lower Chitina Valley, occupy an important position between geologically better known areas—the upper Chitina Valley to the southeast, and the Nelchina area to the west (fig. 1). A reconnaissance survey of the upper Mesozoic rocks in the report area was made to determine regional stratigraphic relationships and the age of certain poorly dated formations. Knowledge of these relationships may have an economic application in the nearby Copper River lowland, where poorly exposed upper Mesozoic rocks are a possible source of petroleum.

The upper Mesozoic rocks rest unconformably upon altered upper Paleozoic sedimentary and volcanic rocks, Triassic basalt, and Upper Triassic limestone, black shale, and argillite. The pre-Jurassic rocks were strongly folded, intruded by plutonic rocks, and uplifted and deeply eroded by late Mesozoic time. They supplied most of the detritus found in the upper Mesozoic formations. The upper Mesozoic formations occupy a synclinal belt between the Chokosna River and Mount Drum and rest on Paleozoic rocks in a small area of the Chugach Mountain front near Chitina (fig. 2).

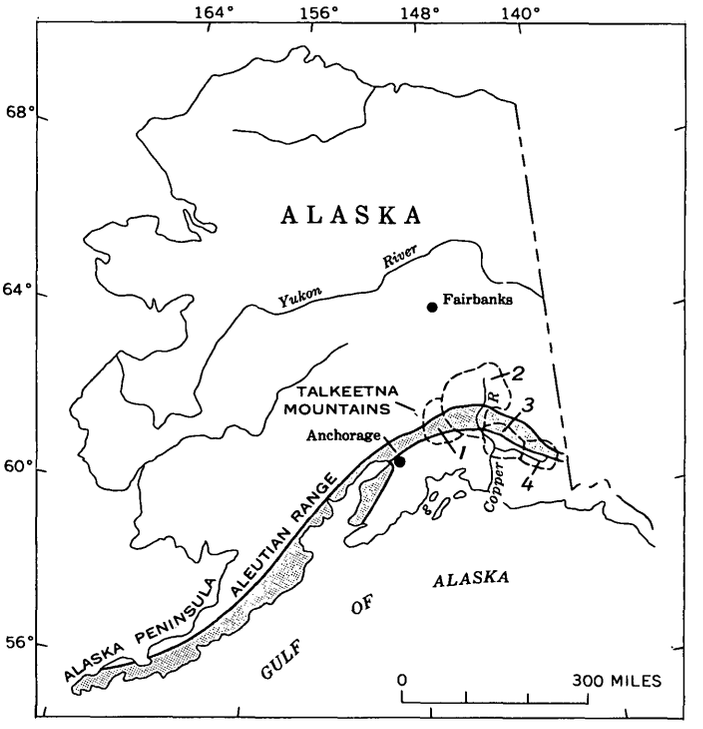


FIGURE 1.—Extent of upper Mesozoic rocks of the Matanuska geosyncline (shaded area) and area discussed in text. *1*, Nelchina area; *2*, Copper River lowland; *3*, southwestern Wrangell Mountains and lower Chitina Valley, (report area); and *4*, upper Chitina Valley.

## PREVIOUS WORK

Pioneer reconnaissance surveys by Rohn (1900), Schrader and Spencer (1901), and Moffit and Maddren

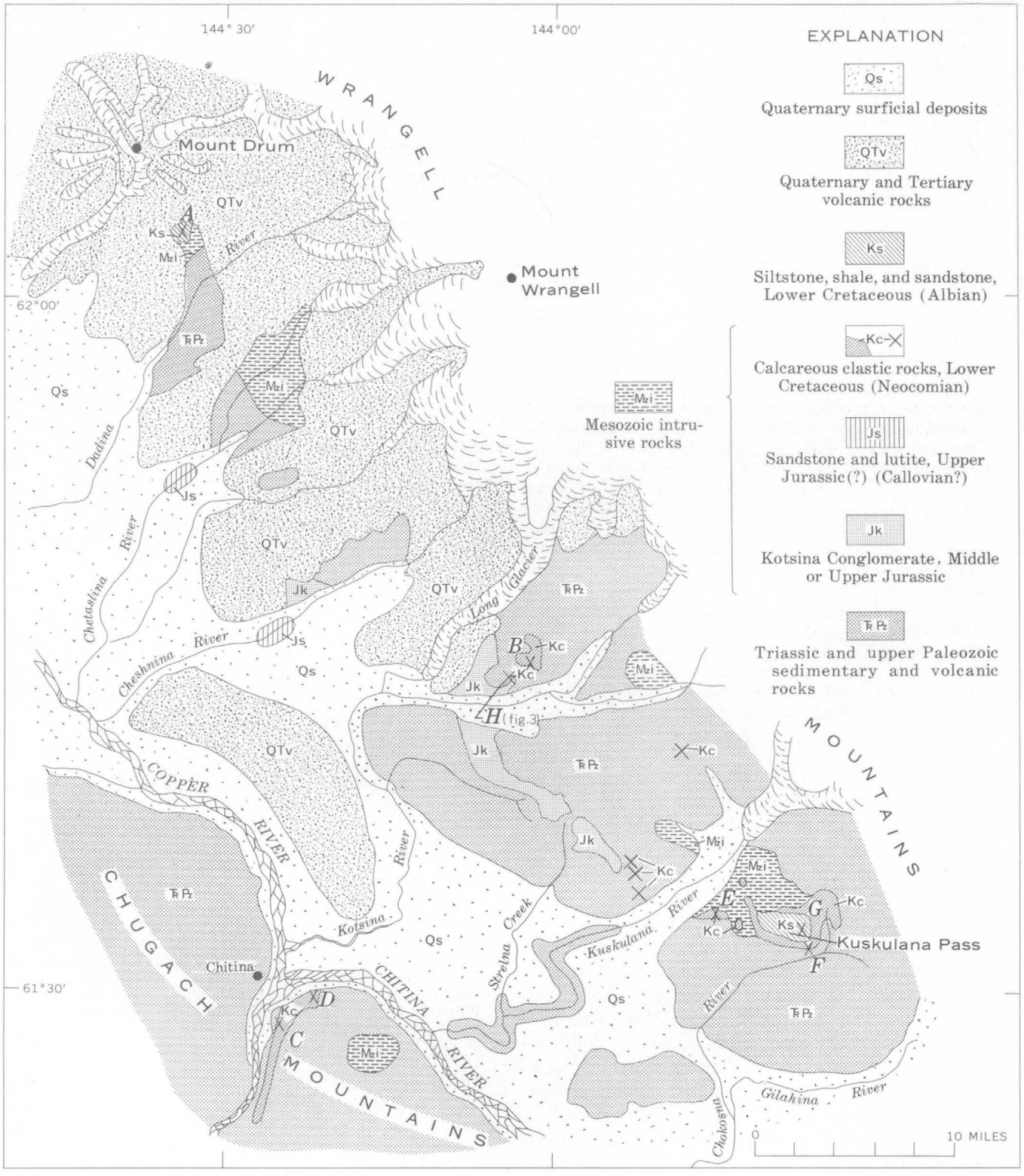


FIGURE 2.—Generalized geologic map of the southwestern Wrangell Mountains, Alaska, and generalized columnar sections of Cretaceous rocks in the area. Map after Moffit (1938). Large letters on map refer to stratigraphic sections on facing page.

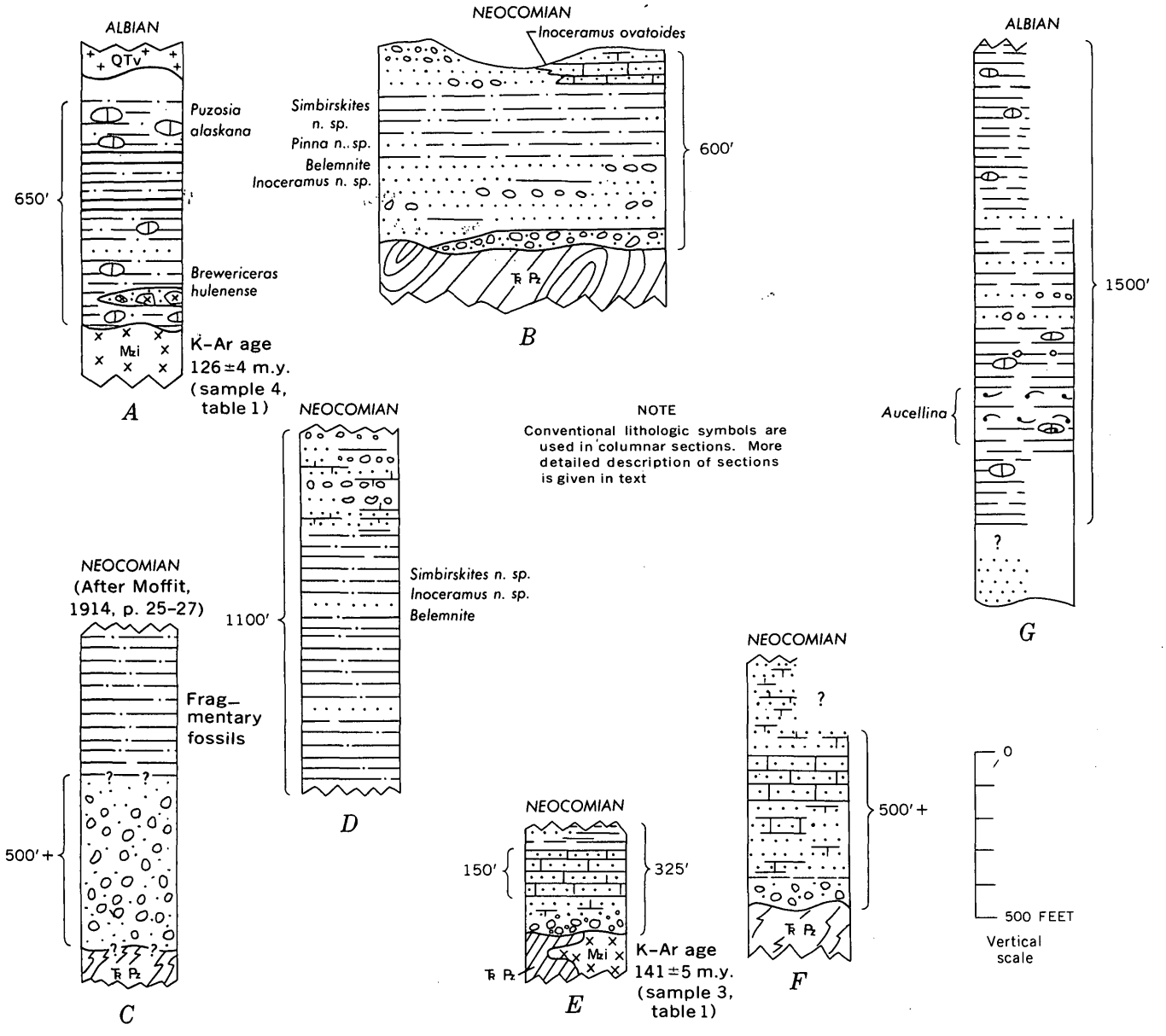


FIGURE 2.—Continued

(1909) resulted in the recognition of shale and limestone of supposed Late Jurassic or Early Cretaceous age in the Kotsina-Kuskulana Rivers area. These rocks were considered to be part of the Kennicott Formation, and of the thick Kotsina Conglomerate (Rohn, 1900, p. 431) of unknown age. In addition, Mendenhall (1905) mapped unaltered sedimentary rocks which he thought were Tertiary, in the Cheshnina, Chetaslina, and Dadina River drainage areas, but these rocks are now known to be upper Mesozoic. Near the mouth of the Chitina River, Moffit (1914) found two units of supposed Middle Jurassic age, a unit of "tuffaceous slate" overlying a "tuffaceous conglomerate".

In the Kotsina-Kuskulana Rivers district, Moffit and Mertie (1923) recognized three units of upper Mesozoic rocks to which they assigned a Late Jurassic age. The lowest unit is the Kotsina Conglomerate which unconformably overlies Upper Triassic shale and consists of massive conglomerate with rare shale lenses. The Kotsina was thought to be overlain by an unnamed unit of sandstone, conglomerate, and shale, and this in turn by an unnamed light-colored, highly fossiliferous limestone unit. Moffit and Mertie did not retain the name Kennicott Formation for the upper two units.

The sporadic distribution of these three units, and the fact that in no place were the upper two found in

stratigraphic sequence with the Kotsina Conglomerate, led to uncertainty as to their relationships. The massive Kotsina Conglomerate was thought to grade laterally into soft yellowish-brown fossiliferous sandstone of the middle unit to the north. The lack of thick conglomerate in some places between the upper limestone unit and the Triassic formations, however, suggested that either the Kotsina was deposited in a restricted area, or that it was removed by erosion prior to deposition of the limestone.

Moffit (1938) published a summary of the geology of the entire Chitina Valley and adjacent area, but the relationships of the upper Mesozoic rocks of the Kotsina-Kuskulana Rivers area and nearby areas to those in other parts of the region were puzzling; they could not be correlated either lithologically or faunally with any other known sequence. Likewise, the supposed Middle Jurassic tuffaceous beds exposed near the mouth of the Chitina River could not be correlated with any others within the Chitina Valley region.

Imlay and Reeside (1954, p. 231) correlated the Kotsina Conglomerate with the basal part of the Matanuska Formation of supposed Coniacian (Late Cretaceous) age. The fossiliferous limestone was not mentioned and presumably was also regarded as part of the Matanuska Formation. They also assigned an Albian (Late Cretaceous) age to the Kennicott Formation, which crops out eastward from Kuskulana Pass, at the east margin of the present study area.

## PRESENT INVESTIGATIONS

This report is based on 9 days of helicopter-supported fieldwork carried out by Grantz in the summer of 1963, and contains the results of paleontologic studies by Jones and isotopic age measurements by Lanphere. An abstract of the data resulting from this collaborative work has been published previously (Grantz and others, 1965). Geologic observations were made throughout an area of about 1,200 square miles, but time did not permit tracing contacts or thorough examination of all exposures.

It is assumed that the potassium-argon ages discussed are at least minimum ages, because there is no evidence that biotite or hornblende from granitic rocks incorporate significant amounts of radiogenic argon at the time of crystallization. The plus-or-minus value assigned to each age (table 1) is the estimated standard deviation of analytical precision.

Where possible the formations discussed below will be correlated with the standard stages of northwestern Europe; a list of these stages for the Upper Jurassic and Cretaceous is presented in table 2.

## JURASSIC ROCKS

### Kotsina Conglomerate

The Kotsina Conglomerate, named by Rohn (1900, p. 431) for exposures on and near the Kotsina River, also crops out near the headwaters of Strelna Creek,

TABLE 1.—*Potassium-argon ages and analytical data*

[Potassium analyses by H. C. Whitehead; argon analyses by M. A. Lanphere]

| Sample No. | Sample description | Mineral | $K_2O$ analyses (percent) | Average $K_2O$ (percent) | $Ar_{rad}^{40}$ ($10^{-10}$ moles/g) | $\frac{Ar_{rad}^{40}}{Ar_{total}^{40}}$ | Apparent age (millions of years) | Field No. | Location |
|---|---|---|---|---|---|---|---|---|---|
| 1 | Biotite granodiorite clast in Kotsina Conglomerate. | Biotite | 3. 97, 3. 97 | 3. 97 | 9. 633 | 0. 90 | 157±6 | 63ALe 14b | Valdez (C–1) quadrangle; lat 61°44′00″ N., long 144°02′50″ W. (loc. *H*, fig. 2; fig. 3). |
| 2 | Porphyritic hornblende microdiorite dike cutting Kotsina Conglomerate. | Hornblende. | . 668, . 672 | . 670 | 1. 460 | . 83 | 142±5 | 63AGz 213 | Valdez (C–1) quadrangle; lat 61°44′03″ N., long 144°03′02″ W. (loc. *H*, fig. 2; fig. 3). |
| 3 | Granodiorite near Kuskulana Pass. | do | . 767, . 784 | . 776 | 1. 684 | . 87 | 141±5 | 63ALe 15 | McCarthy (C–8) quadrangle; lat 61°32′45″ N., long 143°42′30″ W. (loc. *E*, fig. 2). |
| 4 | Biotite granodiorite near Mount Drum. | Biotite | 7. 29, 7. 30 | 7. 30 | 14. 11 | . 92 | 126±4 | 63AGz 162 | Gulkana (A–2) quadrangle; lat 62°03′09″ N., long 144°34′40″ W. (loc. *A*, fig. 2). |

Decay constants for $K^{40}$: $\lambda_\epsilon = 0.585 \times 10^{-10}$ year$^{-1}$; $\lambda_\beta = 4.72 \times 10^{-10}$ year$^{-1}$.
Atomic abundance of $K^{40} = 1.19 \times 10^{-4}$.

TABLE 2.—*Commonly used stage names of the Upper Jurassic and Cretaceous, including the stage names used in this report* [1]

| Series | Stage | |
|---|---|---|
| Upper Cretaceous | Maestrichtian | |
| | Campanian | |
| | Santonian | |
| | Coniacian | |
| | Turonian | |
| | Cenomanian | |
| Lower Cretaceous | Albian | |
| | Aptian | |
| | Neocomian | Barremian |
| | | Hauterivian |
| | | Valanginian |
| | | Berriasian |
| Upper Jurassic | Portlandian | |
| | Kimmeridgian | |
| | Oxfordian | |
| | Callovian | |

[1] Compiled from Imlay (1952, pl. 2) and Imlay and Reeside (1954, pl. 1).

and was found on the north side of the Cheshnina River valley during the present study (fig. 2).

The physiographic expression of the formation was aptly described by Moffit and Mertie (1923, p. 45) who noted that "The conglomerate mountains are rugged, with precipitous cliffs and a ragged skyline. Their dark color and rough surface give them a forbidding aspect, and in fact many of the ridges are practically impassable." The Kotsina is a very thick bedded, well-rounded, pebble-and-cobble conglomerate that contains boulders in some beds. Hand specimens are prevailingly dark or olive gray. The matrix is lithic or feldspathic sandstone which is poorly to fairly well sorted, or in some places dark, hard lutite. The formation contains interbeds and lenses of similar sandstone and of black lutite that commonly is carbonaceous and contains plant scraps. Some of the interbeds are tens of feet thick. The conglomerate clasts are principally dark rocks and of local origin, mostly altered volcanic rocks and Triassic limestone, argillite, and chert. Some light-colored and some mafic plutonic rocks, sandstone, and a little quartz are also present. The size of the clasts appears to decrease toward the southeast. The Kotsina Conglomerate rests unconformably upon rocks as young as latest Triassic. It is probably at least 2,000 to 2,500 feet thick, but its upper contact has not been recognized, and its full thickness is not known. Its estimated thickness and coarseness of grain size suggest that the Kotsina Conglomerate was deposited in a fault- or flexure-bounded basin, probably on or near shore.

The only fossils found in the Kotsina Conglomerate are plant scraps in the lutite layers and Late Triassic mollusks in limestone clasts. Earlier workers based its age upon mollusks found in supposedly equivalent or gradationally overlying marine clastic rocks now known to be of late Neocomian Early Cretaceous (Hauterivian) age. These fossiliferous rocks are unrelated to the Kotsina Conglomerate, and in fact could not be found in contact with it. The supposedly equivalent rocks have been variously considered to be Late Jurassic, Jurassic or Cretaceous, Early Cretaceous, or Late Cretaceous, and the age of the Kotsina Conglomerate varied with the age assigned to these beds.

The Kotsina Conglomerate is intruded by porphyritic hornblende microdiorite dikes that cut a post-Kotsina fault north of the Kotsina River (locality *H*, fig. 2) and are themselves unconformably overlain by beds of Hauterivian age. These relations are shown on figure 3. Assuming that a significant period of time was required to fault the Kotsina Conglomerate, intrude the dikes, erode the rocks on the west side of the fault to the level of the dikes, and then to submerge the area to receive the Hauterivian sediments, then a Jurassic age for the Kotsina Conglomerate seems likely.

Support for, and considerable refinement of, the stratigraphic age of the Kotsina Conglomerate is

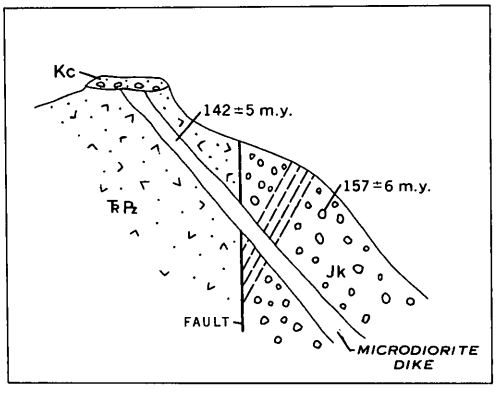


FIGURE 3.—Schematic geologic section showing the field relations critical to dating the Kotsina Conglomerate. Ages were determined by the potassium-argon method. The section is located on the north side of the Kotsina River (loc. *H*, fig. 2). Geologic units are identified by letter symbol on figure 2.

provided by potassium-argon ages determined for hornblende in one of the microdiorite dikes (sample 2, table 1) which cut the conglomerate and in a biotite grandiorite clast (sample 1, table 1) from the conglomerate in the same outcrop. The age determined for hornblende from the dike is 142±5 million years, and that for biotite from the clast is 157±6 m.y. These determinations indicate a minimum age of Late Jurassic and suggest a Middle or Late Jurassic age for the Kotsina Conglomerate. The biotite age is in good agreement with potassium-argon ages of biotite and hornblende from plutons in the Talkeetna Mountains (Grantz and others, 1963) and the Aleutian Range (Detterman and others, 1965). The stratigraphic evidence in these two areas suggests that emplacement of these plutons occurred in latest Early to earliest Middle Jurassic time. The biotite age for the Kotsina Conglomerate clast suggests that the plutonism which was widespread in the area of the Matanuska geosyncline also occurred locally in the area of the Kotsina Conglomerate.

An age of 141±5 m.y. (sample 3, table 1) was determined for hornblende from a granodiorite pluton near Kuskulana Pass (loc. *E*, fig. 2). This pluton intrudes latest Triassic rocks and is overlain unconformably by Lower Cretaceous (Hauterivian) rocks. Its indicated age is significantly less than the ages that have been measured for granitic rocks in the Talkeetna Mountains and Aleutian Range, which were noted above.

The ages of the hornblende from the pluton at Kuskulana Pass and from the dike which intrudes the Kotsina Conglomerate north of the Kotsina River (samples 2 and 3, table 1) are, however, in excellent agreement, and are considered to represent a Late Jurassic plutonic episode.

#### Sandstone and lutite

Other rocks in the southwestern Wrangell Mountains that may be Jurassic crop out in the bluffs along the Chetaslina and Cheshnina Rivers (fig. 2). These rocks consist mostly of sandstone and lutite and dip 25° to 30° SW. The outcrops along the Cheshnina River lie downdip from nearby outcrops of the Kotsina Conglomerate which they resemble more closely in degree of induration and deformation than they do the Cretaceous rocks of the area.

The most abundant rock type is greenish-gray, thick-bedded feldspathic and lithic graywacke that is locally crossbedded and calcareous. It ranges from fine-grained to very coarse grained and pebbly sandstone with angular to subrounded grains that are generally poorly sorted. The sandstone contains many interbeds and units of pebble-and-cobble conglomerate, dark-gray siltstone, and mudstone intraclasts. Most of the conglomerate clasts are volcanic rock fragments, but some are granitic, and others are sandstone or limestone. Plant scraps and a few marine fossils have been found in the sandstone and its siltstone interbeds.

Downstream from the main sandstone outcrops on the Cheshnina River, and possibly overlying them, are green to gray lutites with thin sandstone interbeds at some places. These interbeds of sandstone are dark greenish gray and fine grained, and they locally have graded bedding and sole markings. Apparently the stratigraphically highest rocks are shaly and silty claystone and siltstone that contain brownish gray-weathering limestone interbeds and concretions.

The sandstone beds are estimated to be more than 1,000 feet, and are possibly more than 2,000 feet thick. Neither the top nor the base of the section is exposed. The lutites are at least several hundred feet thick, but in places they are in tight southeast-striking isoclinal and chevron folds, and their thickness could not be determined during the present reconnaissance.

These rocks were mapped as nonmarine and of Tertiary age by others (Moffit, 1939, pl. 2; Mendenhall, 1905, pl. 4). During the present studies, however, a belemnite and *Inoceramus* scraps were found in sandstone on the Chetaslina River, and several small pelecypods and small ammonites in outcrops on the Cheshnina River. Ralph W. Imlay, of the U.S. Geological Survey, states (written commun., 1963) that although the ammonites cannot be positively identified, they resemble immature forms of *Kepplerites*, or some related genus, of Callovian age, and that an early Late Jurasic age seems probable.

## CRETACEOUS ROCKS

#### Clastic rocks of Early Cretaceous (Neocomian) age

Marine sedimentary rocks of Neocomian age form many small mountaintop outcrops between Long Glacier and Kuskulana Valley and constitute a larger area of continuous exposures near Kuskulana Pass (fig. 2). Correlative beds previously referred to as the tuffaceous units of Middle Jurassic age crop out south of the Chitina River in the northern Chugach Mountains. Moffit and Mertie (1923) described the Neocomian beds in some detail but were puzzled by their stratigraphic complexity and age and their relation to the Kotsina Conglomerate. Indeed, mollusks from these beds have been assigned by various paleontologists to the Middle Jurassic, Late Jurassic, Early Cretaceous, and Late Cretaceous (Moffit and Mertie, p. 44–48; Moffit, 1938, p. 66–70; Imlay and Reeside, 1954, p. 231).

The Neocomian beds are much less deformed than the latest Triassic and older rocks upon which they rest with angular unconformity, and near Kuskulana Pass (loc. *E*, fig. 2) they overlie granodiorite for which a potassium-argon age of 141±5 m.y. was obtained on hornblende (sample 3, table 1). They are overlain, apparently unconformably, by beds of Albian age.

The Neocomian rocks are clastic marine deposits, but they are characterized by an almost white calcarenite facies which is composed of finely comminuted prisms of *Inoceramus* shell. Sandstone beds with lower proportions of biogenic calcite grains are brownish gray, greenish gray, or olive gray. North of the Chitina River these rocks are mostly fossiliferous, cross-bedded, calcareous sandstone and conglomerate. The thickest sections are from 600 to almost 1,000 feet thick. The sandstone and conglomerate intertongue greatly, and the stratigraphic sections differ widely from place to place (see Neocomian columnar sections, fig. 2). As with the nearby Kotsina Conglomerate, the conglomerate and sandstone clasts are chiefly greenstone, limestone, and argillite, and were derived from the subjacent formations. These rocks are nearshore, high-energy, shallow-water deposits.

North of the Chitina River, from 0 to 200 feet of rounded cobble-and-boulder conglomerate with a calcareous matrix, and in places containing many mollusks, occurs at the base of the Neocomian sequence. In the section north of the Kotsina River (loc. *B*, fig. 2) beds overlying the basal conglomerate are at least 600 feet thick. The lower 200–300 feet consist of calcareous sandstone that is fine to coarse grained and conglomeratic. The sandstone is fossiliferous, cross-bedded, and contains beds and lenses of calcarenite and of coquinoid sandstone. It in turn is overlain by a similar thickness of medium-dark and greenish-gray sandy siltstone with many, commonly large, mollusks. The upper part of the section consists of fossiliferous coarse sandstone, conglomerate, and calcarenite. At one place, about 60 feet of sandstone and conglomerate at the base of the upper coarse clastic rocks is overlain by about 50 feet of thick-bedded, very light gray (almost white), generally fine grained calcarenite with large *Inoceramus* shell fragments and some lenses of terrigenous pebbles and sand. The calcarenite section is overlain by a small thickness of incompletely exposed calcareous sandstone. Within one large outcrop the calcarenite interfingers with calcareous conglomerate, and it is evidently supplanted by fossiliferous calcareous sandstone and conglomerate within a quarter of a mile to the west. At one place the basal 5 feet of the calcarenite interfingers with pebble conglomerate and lenses out within a horizontal distance of 6 to 8 feet. The calcarenite may represent a nearshore bar or bank of wave-comminuted shell fragments which abutted an area in which terrigenous detritus was being deposited in shallow water from a nearby stream mouth.

Correlative Neocomian beds in the northern Chugach Mountains south of the Chitina River and near its mouth (locs. *C* and *D*, fig. 2), are grossly similar in lithology to those north of the river. They are thicker, however, and include a thick unit of dark siltstone. Moffit (1914, p. 25-27) reported that these Neocomian rocks (loc. *C*, fig. 2) south of the Chitina River (which he considered Middle Jurassic) consisted of (1) a lower unit at least 500–600 feet thick composed of massive conglomerate with rounded pebbles and cobbles of argillite, diorite, greenstone, and quartz, set in a tuffaceous matrix, and (2) an upper unit several hundred feet thick of fossiliferous tuffaceous beds "... composed of dark fine-grained sandstone-like rock, slightly calcareous, and showing numerous small flakes of mica on the cleavage surface." Moffit mapped the upper unit as tuffaceous slate (1914, pl. 2), and tuffaceous shale (1938, pl. 2). He stated that the conglomerate appeared to rest unconformably upon Carboniferous(?) schist, but that the contact was poorly exposed and at many places appeared to be a fault. Moffit's description of these rocks suggests that they are calcareous conglomerate and siltstone lithologically like the Neocomian clastic rocks north of the Chitina River. However, three fossil collections from the upper unit were studied by T. W. Stanton (Moffit, 1914, p. 26), who referred them to the Middle Jurassic. These collections were reexamined during the present study and found to consist of fragmentary mollusks that could be either Jurassic or Cretaceous and that would not be out of place in the Hauterivian faunule collected from similar rocks about a mile to the east during the present study.

During the present reconnaissance the Neocomian rocks south of the Chitina River were examined only in a small stream at the east end of their outcrop area (loc. *D*, fig. 2) and their relationship to the rocks described by Moffit was not determined. Along this stream more than 800 feet of dark, fairly hard, fossiliferous glauconitic siltstone is exposed. It contains layers of thick *Inoceramus* shells and thin interbeds of calcareous sandstone and coarse siltstone crowded with *Inoceramus* prisms. This thick, fossiliferous siltstone probably was deposited somewhat farther from shore than the thinner and coarser equivalent rocks north of the river. The siltstone section is overlain by a few hundred feet of calcareous conglomerate and sandstone that contains abundant *Inoceramus* prisms

and has some interbeds of siltstone and of graywacke conglomerate and sandstone. As in the outcrops to the north, the conglomerate is dominated by clasts of altered volcanic rocks, limestone, black chert, and argillite, and contains some granitoid rocks and rarely quartz.

The abundant molluscan faunule in the lower and middle parts of the section (loc. *B*, fig. 2) north of the Kotsina River contains species of *Inoceramus*, *Pinna*, *Simbirskites*, and a belemnite which are probably of Hauterivian (late Neocomian) age. The same faunule was obtained from the dark siltstone south of the Chitina River (loc. *D*, fig. 2). The calcarenite near the top of the section north of the Kotsina River contains *Inoceramus ovatoides* of Anderson, which is of late Hauterivian to Barremian (late Neocomian) age. The genus *Simbirskites* in Europe is of middle to late Hauterivian age.

The Hauterivian beds of the southwestern Wrangell Mountains are correlative with the Nelchina Limestone and overlying dark sandstone in the Nelchina area of the Talkeetna Mountains, which Bergquist (1961) found to contain Hauterivian Foraminifera. The Nelchina Limestone is an almost white calcarenite characterized by *Inoceramus* shell fragments and prisms. The Nelchina Limestone overlies *Buchia*-bearing sandstone and conglomerate of Valanginian (early Neocomian) age which is absent in the Wrangell Mountains.

#### Siltstone, shale, and sandstone of Early Cretaceous (Albian) age

Albian-age rocks crop out in a broad syncline at Kuskulana Pass (loc. *G*, fig. 2), where they rest with apparent unconformity on the Neocomian beds just described, and in a small area on the southeast flank of Mount Drum (loc. *A*, fig. 2). The beds near Mount Drum have a moderate dip to the west and rest upon biotite granodiorite. Biotite from this pluton yielded a potassium-argon age of 126±4 m.y. (sample 4, table 1), suggesting intrusion during Neocomian (Early Cretaceous) time. The fact that the unconformity at the base of the Hauterivian (upper Neocomian) beds in the Kotsina-Kuskulana Rivers area represents a greater structural discordance and a longer hiatus than the unconformity at the base of the overlying Albian beds suggests that the pluton was intruded before deposition of the upper Neocomian beds of the Kotsina-Kuskulana Rivers area, and that it was unroofed by a combination of pre-Hauterivian and pre-Albian erosion.

The Albian rocks at Kuskulana Pass are similar to strata cropping out near Fourth of July Pass in the upper Chitina Valley that have been designated the Kennicott Formation. However, usage of the name Kennicott has been so varied that use of the term should be suspended until detailed mapping is accomplished in the type area. At Kuskulana Pass the Albian rocks (loc. *G*, fig. 2) are about 1,500 feet thick and are dominantly siltstone. Some sandstone may occur at the base of the section, but the lowest beds are poorly exposed at the place visited. The bulk of the section is siltstone, silty claystone, and shale that are slightly greenish gray and medium dark gray and weather to medium gray, brownish gray, or greenish gray. The siltstone contains limestone concretions and lentils and a few volcanic ash layers. An interval 150 feet thick in the lower part of the sequence contains abundant shells of the pelecypod *Aucellina* in limestone concretions and coquinoid beds. Another interval at least 200 feet thick in the middle of the sequence contains 5 to 10 percent of thin to thick interbeds of coarse siltstone, sandstone, and minor conglomerate. These interbeds resemble turbidites, being commonly graded, and many show sole markings, wavy bedding, small-scale crossbedding, and channeled bases. The uppermost exposed beds in this section are siltstone and silty claystone with limestone concretions, but the top of the section is not preserved. Fossils were not obtained from the highest beds, and thus their age is unknown. A few observations along the northeast side of the syncline at Kuskulana Pass suggest that sandstone and conglomerate interbeds in the middle of the sequence may increase in number and thickness to the north.

The Albian strata near Mount Drum are lithologically quite different from those at Kuskulana Pass, for they are characterized by very carbonaceous silt and clay shales and contain beds of granite wash. They are also slightly younger. The exposed section (loc. *A*, fig. 2) exceeds 650 feet in thickness. Its basal part is 350 feet thick and consists mostly of gray, soft siltstone and silt shale resting on granodiorite. It contains large limestone concretions with marine fossils, wood fragments, and glauconite grains. Medium to very thick interbeds of arkose, mostly coarse and pebbly, and of granite wash are distinctive features of this unit. The thickest of these interbeds are composed of angular and subangular granitic blocks mixed with intraclasts of sandstone and limestone, yet they are separated from the underlying granodiorite by tens of feet of shallow marine siltstone. These relationships suggest that the basal Albian sea floor had appreciable relief, and that the coarse detritus was dumped in and buried without significant reworking, even though the beds are apparently of shallow marine origin.

Dark, very carbonaceous, and commonly fissile brownish-gray-weathering shale and siltstone, 175 feet thick, overlie the basal unit. These rocks have yielded some animal trails but no other fossils. The carbonaceous character of these beds, the presence of trails, and the absence of mollusks within them suggest that they are of brackish-water or lagoonal origin. The uppermost 140 feet of the exposed section is dark, chunky, and platy weathering siltstone that contains large limestone concretions, some of which contain marine fossils. The top of the unit is unexposed, but the section is overlain by Cenozoic volcanic rocks.

The basal beds near Mount Drum contain *Brewericeras hulenense* and other ammonites of the *Brewericeras hulenense* local faunizone of late early Albian age. The upper beds contain *Puzosia alaskana* Imlay of probably the same age. *Aucellina*, which is restricted to the lower lower Albian zone of *Moffitites robustus*, is apparently absent from the Mount Drum section, which is therefore slightly younger than the *Aucellina*-bearing Albian beds at Kuskulana Pass. The Mount Drum section is also lithologically different from that at Kuskulana Pass; it more closely resembles the Albian beds of the northern part of the Nelchina area, which consist of coaly beds overlain by very fossiliferous shallow marine shale. The lithologic differences between the Albian rocks of Kuskulana Pass and Mount Drum suggest that the former should be named according to the formal stratigraphic nomenclature applied to the upper Chitina Valley, and the latter according to the nomenclature of the Nelchina area and Copper River lowland.

The upper Mesozoic rocks of the southwestern Wrangell Mountains record at least three episodes of deep erosion followed by sedimentation. These episodes are recorded at (1) the base of the Kotsina Conglomerate, (2) the base of the Neocomian beds, (3) the base of the Albian beds. These rocks also record evidence of plutonism of latest Early or earliest Middle Jurassic age, of Late Jurassic age, and of Early Cretaceous age within or near the Matanuska geosyncline. These rocks have some overall lithologic similarities to rocks of similar age in nearby areas, but their stratigraphic sequence is nevertheless quite different from that found in the nearby areas. These relations illustrate that these rocks were deposited in a tectonically active trough that typically produced rocks that are lithologically similar over wide areas, but which are arranged in highly distinctive and variable local sequences. Long-range extrapolation of local stratigraphic details in these rocks is, therefore, a risky enterprise.

## REFERENCES


Bergquist, H. R., 1961, Early Cretaceous (middle Neocomian) microfossils in south-central Alaska: Art. 374 *in* U.S. Geol. Survey Prof. Paper 424–D, p. D236–D237.

Detterman, R. L., Reed, B. L., and Lanphere, M. A., 1965, Jurassic plutonism in the Cook Inlet region, Alaska, *in* Geological Survey Research 1965: U.S. Geol. Survey Prof. Paper 525–D, p. D16–D21.

Grantz, Arthur, Jones, D. L., and Lanphere, M. A., 1965, Upper Mesozoic rocks of the lower Chitina Valley, Alaska [abs]: Geol. Soc. America Spec. Paper 82, p. 255 and 356.

Grantz, Arthur, Thomas, Herman, Stern, T. W., and Sheffey, N. B., 1963, Potassium-argon and lead-alpha ages for stratigraphically bracketed plutonic rocks in the Talkeetna Mountains, Alaska: Art. 16 *in* U.S. Geol. Survey Prof. Paper 475–B, p. B56–B59.

Imlay, R. W., 1952, Correlation of the Jurassic Formations of North America, exclusive of Canada: Geol. Soc. America Bull., v. 63, p. 953–992.

Imlay, R. W., and Reeside, J. B., Jr., 1954, Correlation of the Cretaceous formations of Greenland and Alaska: Geol. Soc. America Bull., v. 65, p. 223–246.

Mendenhall, W. C., 1905, Geology of the central Copper River region, Alaska: U.S. Geol. Survey Prof. Paper 41, 133 p.

Moffit, F. H., 1914, Geology of the Hanagita-Bremner region, Alaska: U.S. Geol. Survey Bull. 576, 56 p.

Moffit, F. H., 1938, Geology of the Chitina Valley and adjacent area, Alaska: U.S. Geol. Survey Bull. 894, 137 p [1939].

Moffit, F. H., and Maddren, A. G., 1909, Mineral resources of the Kotsina-Chitina region, Alaska: U.S. Geol. Survey Bull. 374, 103 p.

Moffit, F. H., and Mertie, J. B., Jr., 1923, The Kotsina-Kuskulana district, Alaska: U.S. Geol. Survey Bull. 745, 149 p.

Rohn, Oscar, 1900, A reconnaissance of the Chitina River and the Skolai Mountains, Alaska: U.S. Geol. Survey 21st Ann. Rept, pt. 2, sect. h, p. 393–440, pls, 51–54.

Schrader, F. C., and Spencer, A. C., 1901, The geology and mineral resources of a portion of the Copper River district, Alaska: U.S. Geol. Survey, spec. pub., 94 p.

# ALGAL STROMATOLITES OF THE UPPER CAMBRIAN COPPER RIDGE DOLOMITE IN UNION AND CLAIBORNE COUNTIES, TENNESSEE

By LEONARD D. HARRIS, Knoxville, Tenn.

*Abstract.*—Approximately 60 percent of the Upper Cambrian Copper Ridge Dolomite, which has an average thickness of 925 feet, is composed of algal stromatolitic structures. Two forms, each apparently indicative of a particular phase of intertidal environment, are readily discernible. The most abundant stromatolite occurs as discrete, vertically stacked hemispheroids in widespread lateral zones from 5 to 140 feet thick. These zones are composed of finely to medium crystalline dolomite with abundant vugs. The other form, composed of a series of laterally linked hemispheroids, is best developed in silt-sized to very finely crystalline dolomite. Persistence of porous stromatolite zones into the subsurface, inferred from study of drill cuttings, offers a potential site for the accumulation of hydrocarbons.

The Copper Ridge Dolomite of Late Cambrian age has been studied and mapped in Tennessee for over a half century (for historical development see Bridge, 1956, chart 1). Although the Copper Ridge has been known for a long time, few specific details of the stratigraphy and depositional environment have been learned because of the thick soil cover and the scarcity of naturally exposed continuous sections. Most descriptions of the Copper Ridge are based on details from a very few artificially exposed sections, supplemented by a study of residual products. Recently, four nearly complete sections of the Copper Ridge Dolomite have been measured by the author along a 9½-mile stretch of the south shore of Norris Reservoir, in Union and Claiborne Counties in eastern Tennessee (fig. 1). These exposures resulted from the removal of soil cover over a 29-year period by a repeated semiannual 50-foot fluctuation of the reservoir level. These exposures are significant because they are wide and nearly complete stratigraphically, and because the exposed weathered rock shows a high contrast between various constituents, thereby accentuating many important primary features. A study of these naturally etched rock surfaces has led to the conclusion that the algal stromatolites were significant rock builders in the Copper Ridge.

Recent authors (Rodgers, 1953; Miller and Fuller, 1954; Bridge, 1956) have characterized the Copper Ridge as being divisible into two parts or members—a lower, dark member and an upper, light member. The lower member is made up of massive beds of predominantly brownish gray, finely to medium crystalline dolomite that emits a petroliferous odor when freshly broken. The upper member, in general, is more thinly bedded, and is composed of olive-gray to light-olive-gray silt-sized to very finely crystalline dolomite that contains only a few zones of the darker dolomite typical of the lower member. Oolitic chert is common throughout the formation but is most abundant in the upper member. Thickness cited for the Copper Ridge ranges from 800 to 1,100 feet. *Cryptozoon*, an algal stromatolite, has been recognized as a minor constituent occurring throughout the forma-

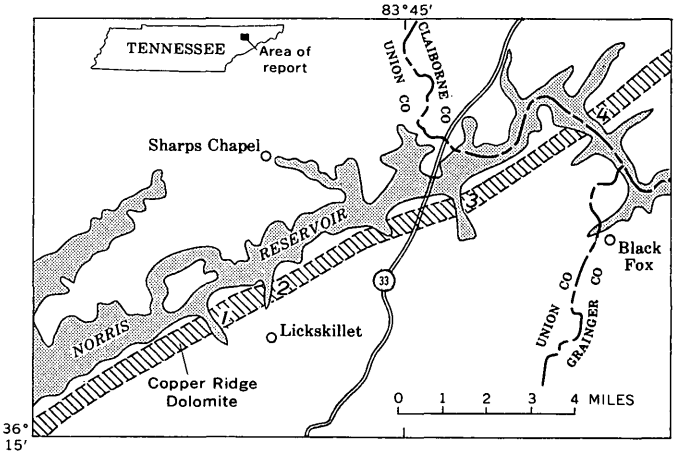


FIGURE 1.—Map showing part of the Norris Reservoir, outcrop pattern of Copper Ridge Dolomite along the shore, and numbered locations of four almost completely exposed sections of the Copper Ridge Dolomite.

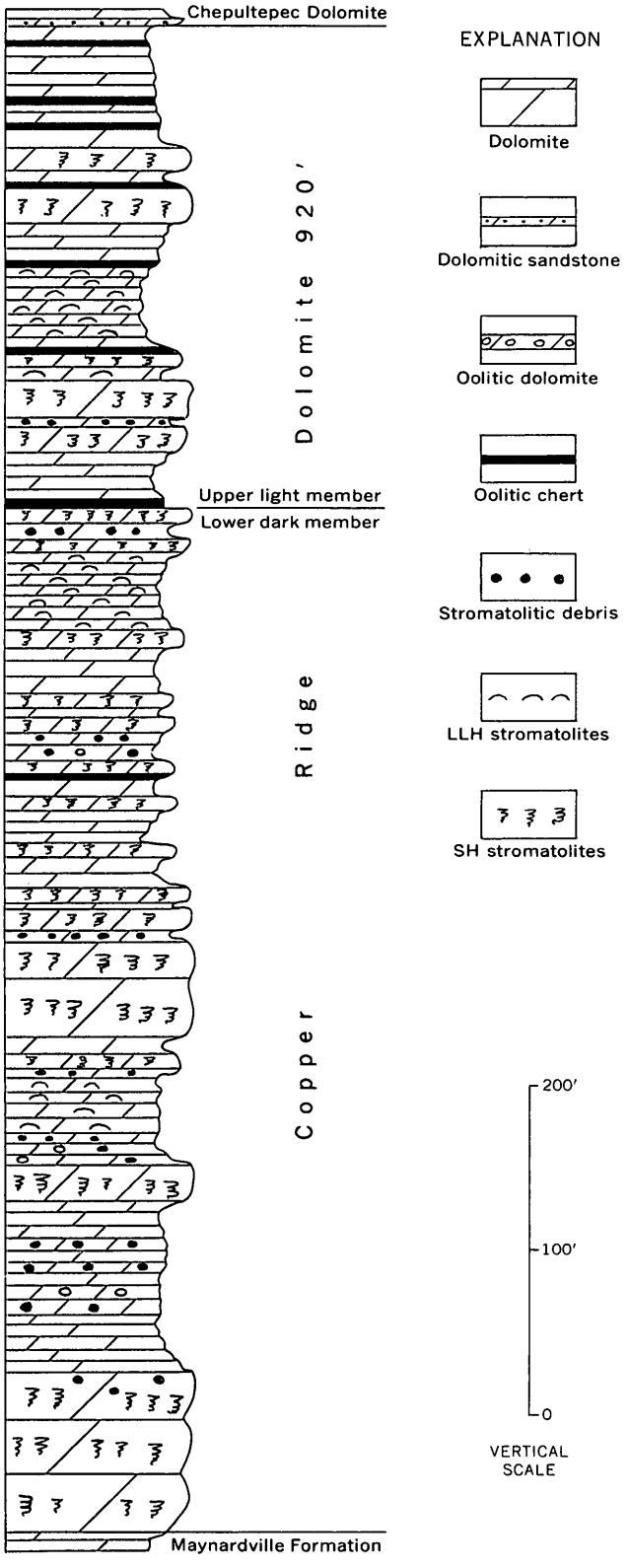


FIGURE 2.—Stratigraphic section of the Copper Ridge Dolomite at locality 3 (fig. 1).

tion, with local accumulations as much as 15 feet thick present 70 feet above the base of the formation (Miller and Fuller, 1954, p. 46). Other fossils are rare. Studies of the Copper Ridge along the Norris Reservoir have indicated that the formation is composed of at least 60 percent algal stromatolites in zones from 5 to 140 feet thick (figs. 2 and 3).

## STRUCTURE OF THE STROMATOLITES

An algal stromatolite is a laminated structure formed by the activity of algal film in trapping and binding sediment. Algal stromatolite deposits differ from calcareous algal deposits in that they consist of preexisting clastic material collected by, not precipitated by, a mucilaginous organic film (Black, 1933, p. 184). Thus, they are organosedimentary features in which only the gross structure of the algal film is preserved; cellular and other detail structures are not preserved. Recently Logan and others (1964, p. 68–83) published a significant paper concerning the classification and environmental significance of algal stromatolites. The stromatolites do not lend themselves to limited definitions of form genera or form species. As a result, attempts to apply a strict binominal nomenclature seem to have led to unwarranted complexity (Logan and others, 1964, p. 81), which in turn has tended to restrict the usefulness of algal stromatolites. Logan and others (1964, p. 73–74) propose to abandon all generic and specific names, substituting a descriptive nomenclature based on the arrangement of certain geometric forms. Their basic forms are the hemispheroid and the spheroid. At present three major arrangements are recognized: (1) laterally linked hemispheroids (LLH), which may be closely spaced (LLH–C or widely spaced (LLH–S); (2) discrete, vertically stacked hemispheroids (SH); and (3) discrete, spheroids (SS). Apparently each of these arrangements is simply a reaction of the algal material to specific environmental processes. Thus, in a fluctuating environment one could expect to find compound forms that exhibit multiple growth forms. Evidently the majority of algal stromatolitic structures are compound forms of LLH and SH types, and these forms may be large scale, small scale, or combinations of both (Logan and others, 1964, p. 76). Many combinations of the LLH and SH arrangements are illustrated by Logan and others (1964, table 5, p. 78), although they recognize that all arrangements cannot be shown and that it is possible other arrangements will be discovered.

Most algal stromatolite structures in the Copper Ridge Dolomite have been referred to as *Cryptozoon.*

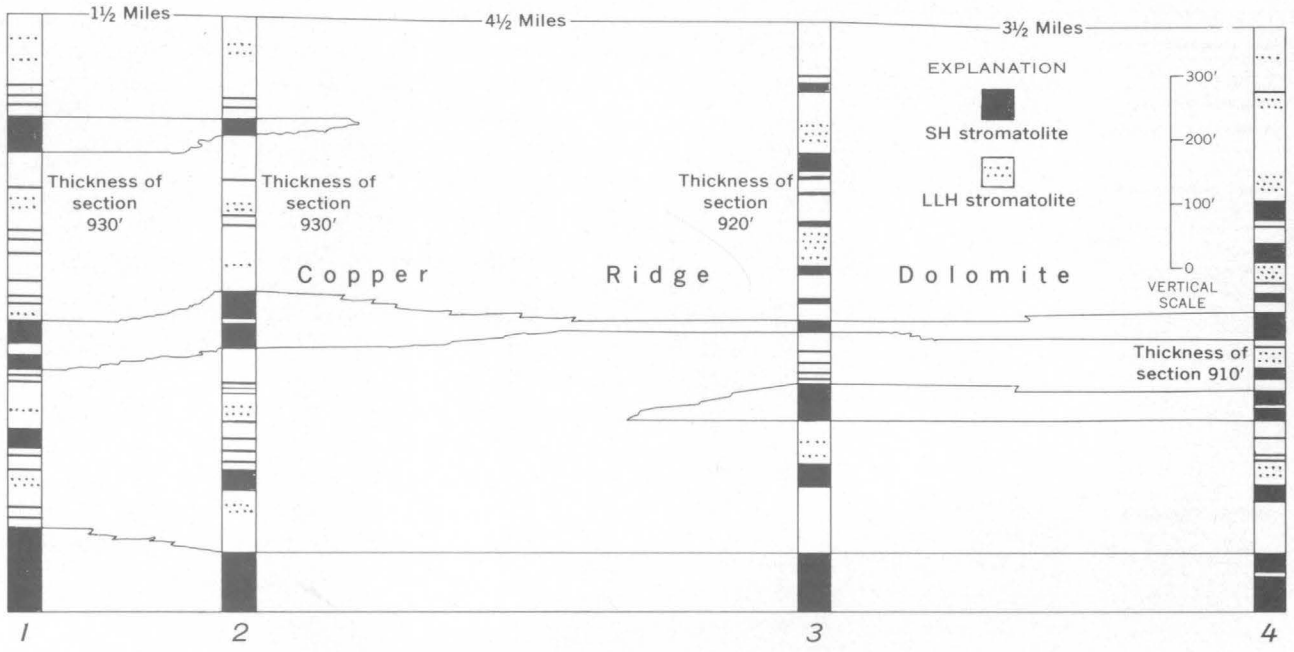


FIGURE 3.—Distribution of LLH and SH stromatolites in four measured sections of the Copper Ridge Dolomite along the Norris Reservoir. (Locations of sections shown in fig. 1.)

These structures include at least two basic arrangements (LLH and SH) and many compound variations. The simplest arrangement is the closely spaced, laterally linked hemispheriod (LLH–C). In cross section this form is composed of literally hundreds of paper thin, undulating laminae (fig. 4*A*). The hemispheroidal nature of the laminae is best seen in silicified beds (fig. 4*B*). The diameters of individuals commonly range from a few inches to 1 foot; however, during construction of the Melton Hill Dam, near Oak Ridge, Tenn., J. M. Kellberg (oral commun.) saw a silicified bed of LLH in which the diameter of individual hemispheroids was as much as 14 feet. The LLH structures occur throughout the Copper Ridge in zones of locally mud-cracked, olive-gray, silt-sized very finely crystalline argillaceous dolomite (figs. 2, 3).

The most abundant algal stromatolites occur in units from 5 feet to 140 feet thick and have as their basic structure element discrete, crudely column-shaped SH elements that exhibit paper-thin, vertically stacked hemispheroidal laminae (figs. 5*A*, *B*). The linkage of some discrete elements by laterally developed laminae

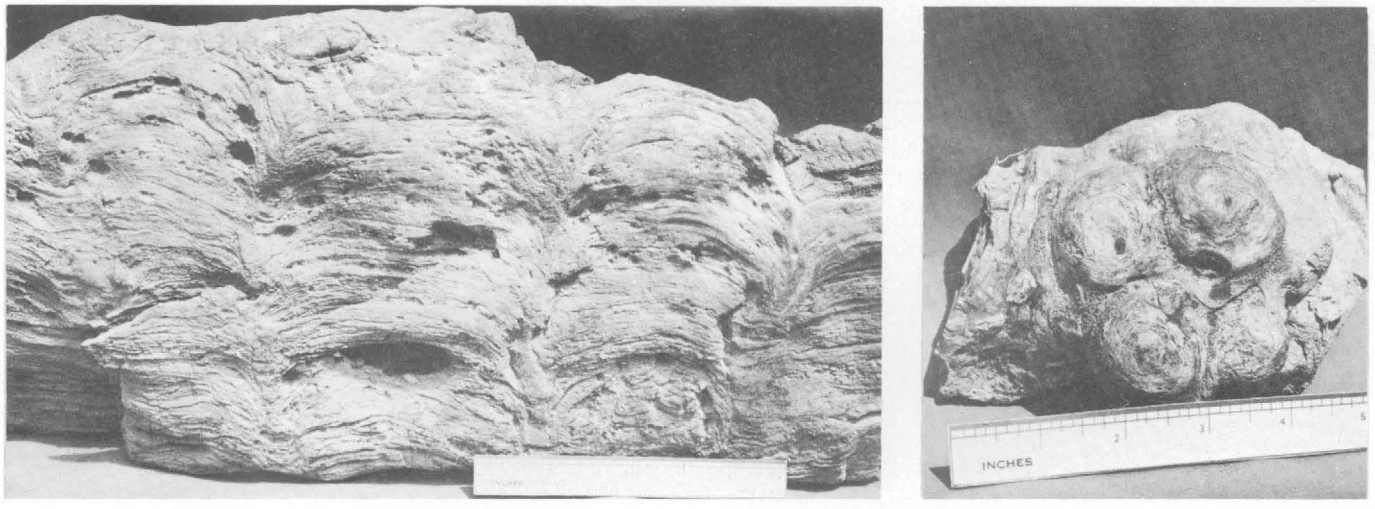


*A* *B*

FIGURE 4.—Closely spaced laterally linked hemispheroidal stromatolites (LLH-C). *A*, cross section; and *B*, plan view.

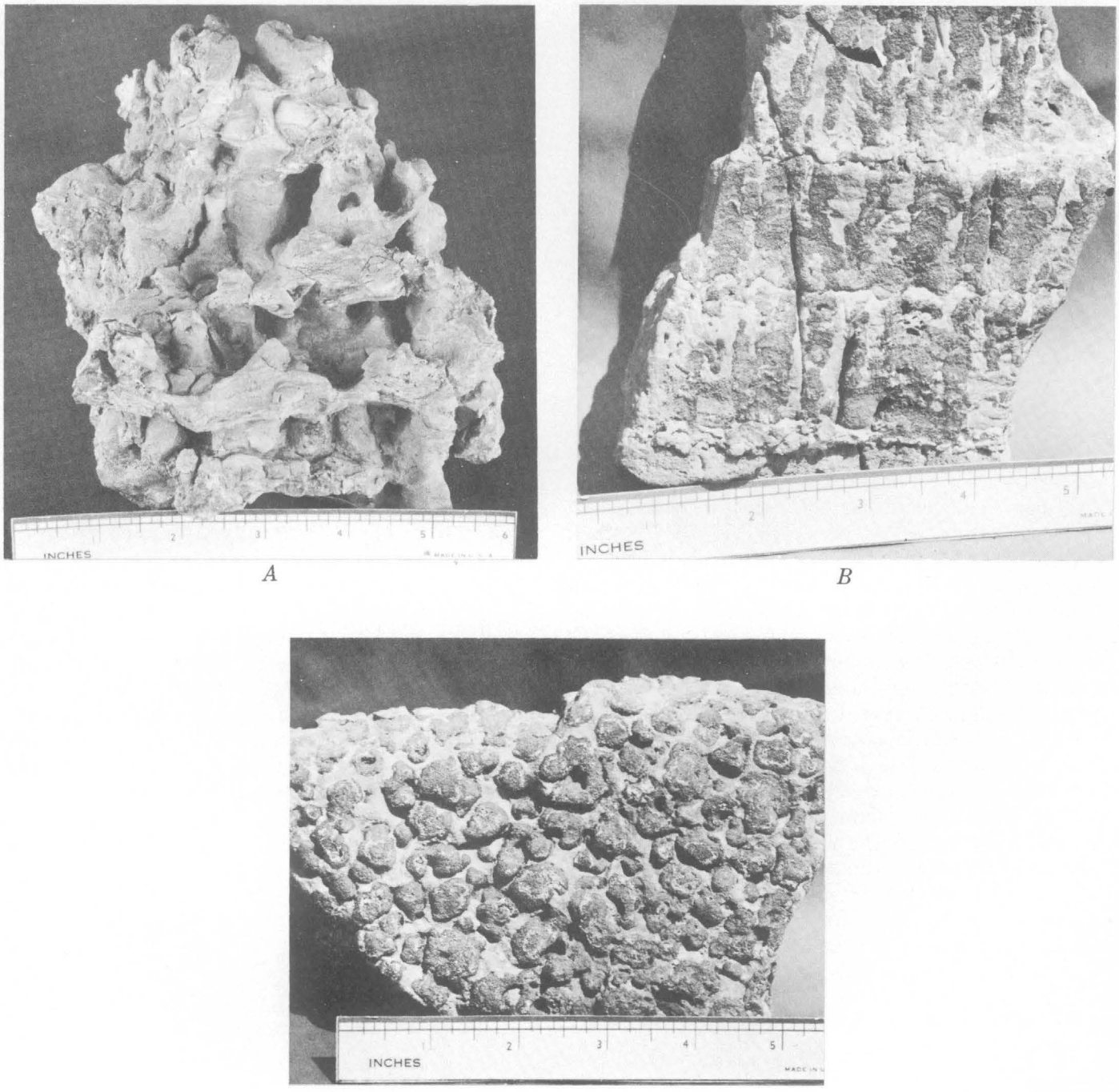


A B C

FIGURE 5.—Column-shaped discrete stromatolites with vertically stacked hemispheroidal laminae (SH). *A*, silicified mass showing columnal nature of the stromatolites; *B*, cross section; and *C*, plan view.

produces an alternation of SH–LLH–SH structures. The columnal bodies, which range from ¼ inch to 1 inch in diameter, are composed of brownish-gray, vuggy, finely to medium crystalline dolomite set in a groundmass of very finely to finely crystalline, olive-gray, slightly argillaceous dolomite (fig. 5*C*). This difference in grain size and clay content is readily apparent on freshly broken surfaces because it gives the rock a mottled appearance. Apparently the brown color of SH elements is imparted by residual organic matter, which was probably derived from breakdown of the original algal films.

Thousands of the basic SH elements occur in laterally continuous, stratum-like growth layers from 1 inch

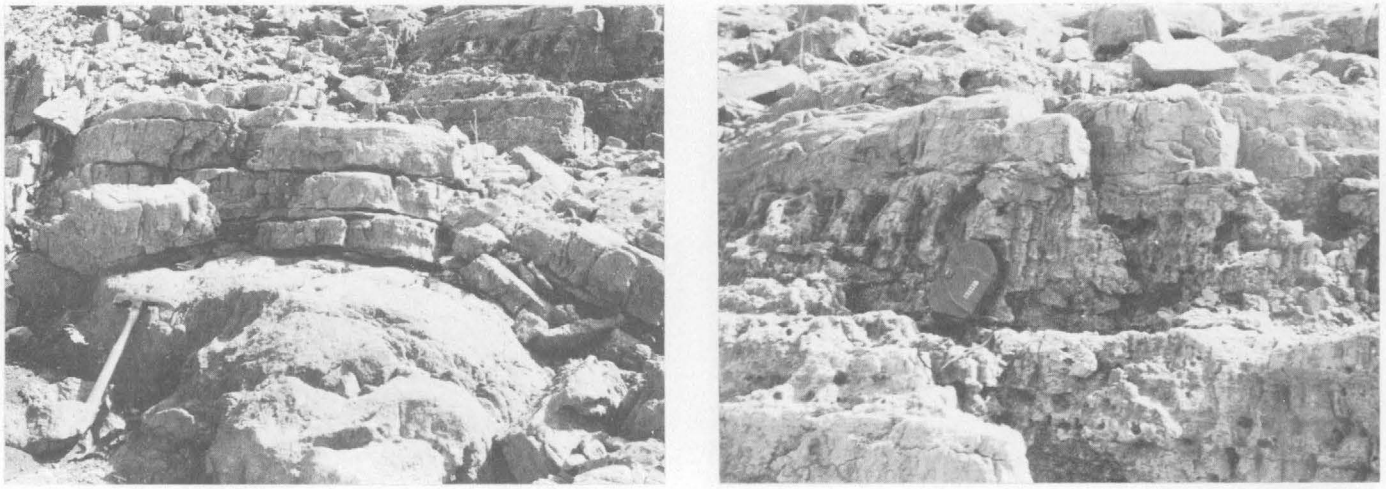

FIGURE 6.—Arrangement of growth layers of the SH stromatolite. *A*, hemispheroidal development, and *B*, planar development. All the rock in these photographs is stromatolitic.

to 3 feet thick. Silicified specimens, in which many primary structures are preserved in detail, suggest that the growth layers resulted from periodic interruptions in the upward growth of individual SH bodies. These interruptions are recorded as erosional breaks or as laterally continuous algal stromatolitic laminae, which form natural partings that present-day weathering tends to accentuate. When environmental conditions favored the development of a succession of growth layers, these layers accumulated as a series of widely spaced hemispheroids, from 1 to 15 feet in diameter, connected by planar layers (figs. 6*A*), *B*). The large-scale arrangement of growth layers is somewhat similar to the arrangement of small-scale laminae of the laterally linked hemispheroids (LLH–S) (fig. 7). The basic difference is partly in their scale, and partly in the fact that each large-scale growth layer is composed of thousands of SH columnals while each small-scale growth lamina of the LLH is not.

## ENVIRONMENTAL AND ECONOMIC SIGNIFICANCE

Logan and others (1964, p. 82) indicate that modern stromatolites similar to the stromatolites of the Copper Ridge Dolomite are for the most part restricted to intertidal zones. Specifically, the laterally linked hemispheroid (LLH) has been found to be characteristically developed in relatively low-energy environments on protected mud flats. A similar environment for the LLH stromatolites of the Copper Ridge Dolomite is suggested by their occurrence only in silt-sized to very finely crystalline laminated dolomite that locally exhibits mud cracks. The modern vertically stacked hemispheroidal stromatolites (SH) are best developed along exposed intertidal headlands (Logan and others, 1964, p. 82). In the Copper Ridge the occurrence of stromatolitic debris intimately associated with the massive SH units suggests a higher energy environment than that in which the LLH stromatolites existed (fig. 2).

Data from the four measured sections of the Copper Ridge Dolomite along Norris Reservoir indicate several important aspects of the SH stromatolite. First, SH stromatolites are distributed throughout the Copper Ridge, but they are more abundant in the lower two-thirds of the formation. The concentrations which are most laterally persistent occur at the base and near

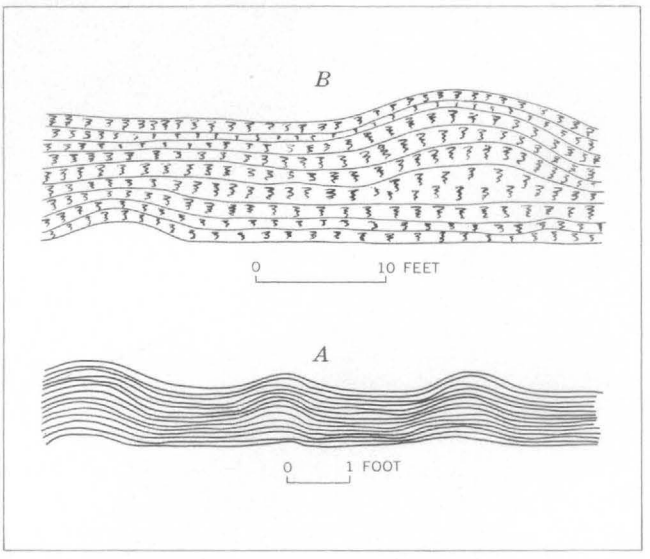


FIGURE 7.—Comparison of the structural similarity between arrangement of the small-scale laminae of the LLH–S stromatolite (*A*) and the large-scale bedding of the SH stromatolite (*B*). The main difference between the two types is in their relative scales.

the middle of the formation (fig. 3). Commonly, outcrops of stromatolite zones contain abundant vugs. The vugs are concentrated at the centers of large hemispheroids or are alined parallel to growth layers. This definite spacial alinement of vugs suggests that they were produced by processes operating prior to or shortly after burial; however, present-day weathering accentuates them.

The occurrence of laterally continuous porous zones is significant, because if these zones persist into the subsurface they may prove to be good reservoirs in which oil and gas have accumulated. Partial confirmation that the Copper Ridge may be porous in the subsurface is suggested by a study of the cuttings from a complete section of the Copper Ridge between 4,960 and 6,102 feet in Lee County, Va., in the Shell Oil Co. L. S. Bales No. 1 well, located about 26 miles northeast of the area of this report. In that well the author found small vugs and intercrystalline voids, on the order of 3 to 7 percent by volume, throughout what appear to be correlatives of the two laterally persistent stromatolite zones in the lower half of the Copper Ridge along Norris Reservoir (fig. 3). Fresh water was produced from the L. S. Bales No. 1 well at the rate of approximately 20 barrels per hour from a depth of 6,050 feet in the stromatolite zone at the base of the formation.

## REFERENCES

Black, Maurice, 1933, The algal sediments of Andros Island, Bahamas: Royal Soc. London Philos. Trans., ser. B, v. 222, p. 165–192.

Bridge, Josiah, 1956, Stratigraphy of the Mascot-Jefferson City zinc district, Tennessee: U.S. Geol. Survey Prof. Paper 277, 76 p.

Logan, B. W., Rezak, Richard, and Ginsburg, R. N., 1964, Classification and environmental significance of algal stromatolites: Jour. Geology, v. 72, p. 68–83.

Miller, R. L., and Fuller, J. O., 1954, Geology and oil resources of the Rose Hill district—the Fenster area of the Cumberland overthrust block—Lee County, Virginia: Virginia Geol. Survey Bull. 71, 383 p.

Rodgers, John, 1953, Geologic map of east Tennessee with explanatory text: Tennessee Div. Geology Bull. 58, pt. 2, 168 p.

# COMPARISON OF ORDOVICIAN EUGEOSYNCLINAL AND MIOGEOSYNCLINAL QUARTZITES OF THE CORDILLERAN GEOSYNCLINE

By KEITH B. KETNER, Denver, Colo.

*Abstract.*—Ordovician quartzite of the Cordilleran miogeosyncline is extremely pure, medium-grained quartz arenite whose grains are frosted, well rounded, and well sorted. Approximately correlative quartzites of the eugeosyncline are equally pure, and the grains are similarly frosted and equally well rounded, but they are more coarse and not quite so well sorted. The high degree of compositional and textural maturity of quartzites of both parts of the geosyncline indicates that they were derived from sedimentary terranes. Stratigraphic and textural relations show that quartzites of the eugeosyncline were derived from the west side of the geosyncline.

In Ordovician time, the Cordilleran geosyncline consisted of two parallel belts of contrasting sedimentation. The eastern belt, or miogeosyncline, was characterized by the deposition of carbonate sediments; the western belt, or eugeosyncline, was characterized by the deposition of siliceous sediments and the extrusion of lavas. An intermediate zone in the northern part of Nevada was later partly covered by rocks thrust eastward from the eugeosyncline (Roberts and others, 1958).

Throughout most of the miogeosyncline, quartzite beds—known in parts of Nevada, Utah, and California as the Eureka Quartzite (Kirk, 1933, p. 27), and in parts of Utah and Idaho as the Swan Peak Quartzite (R. J. Ross, 1953, p. 22)—are sandwiched between Lower and Upper Ordovician carbonate rocks (fig. 1). Because of their lithic similarity as indicated in this report, and because of stratigraphic relations to be brought out in another report, it seems certain that the Eureka and Swan Peak Quartzites are parts of one genetic unit whose basal beds are of somewhat different age from place to place, and whose deposition was interrupted in places by brief periods of carbonate deposition. A northward extension of this widespread unit is included in the type Kinnikinic Quartzite of central Idaho, described by C. P. Ross (1937, p. 17). In southern Nevada and California, tongues of the same unit wedge out among finer grained rocks in the intermediate zone between the miogeosyncline and eugeosyncline. These tongues form parts of the Toquima Formation (Ferguson, 1924, p. 22) in southern Nevada, the Johnson Spring Formation (D. C. Ross, 1965, p. 26) in the Inyo Range of California, and the Convict Lake Formation (Rinehart and Ross, 1964, p. 20) in the Sierra Nevada of California. Throughout its great extent, the Ordovician System of the Cordilleran miogeosyncline is extraordinarily simple and regular.

In contrast, the Ordovician System of the eugeosyncline is extremely complex and irregular. Quartzite units alternate with bedded chert, siliceous mudstone, and greenstone throughout the system, and individual lithic units and sequences in one exposure generally cannot be recognized in another exposure. The thickness of quartzite varies greatly, ranging from thousands of feet in the Valmy Formation to scores of feet in the Petes Summit Formation of Kay (Kay, 1960; Kay and Crawford, 1964) and a few feet in the Vinini Formation and the Basco Formation of Lovejoy (1959). However, the eugeosynclinal quartzite is lithically nearly as uniform as that of the miogeosyncline.

In this report, the lithologies of quartzites from the miogeosyncline are compared with those from the eugeosyncline, and conclusions drawn from this comparison are used in inference of the sources of sand in the quartzites.

## COMPARATIVE LITHIC DATA

Quartzite of the eugeosyncline is remarkably similar to that of the miogeosyncline in some respects but persistently, though subtly, different in others. In the

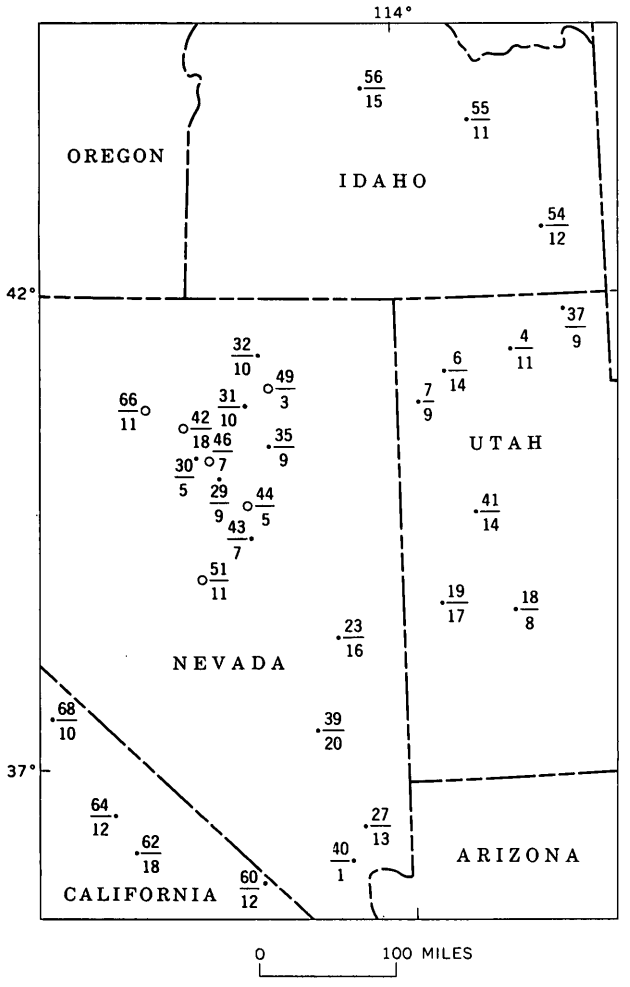


FIGURE 1.—Map showing sampled localities in the Cordilleran geosyncline. Upper number of each pair is the site designation; lower number is the number of samples from the site. ●, quartzite of miogeosynclinal and intermediate zones; ○, quartzite of eugeosyncline, thrust eastward.

following discussion, and especially in the table of chemical composition, similarities seem to outweigh differences, yet the subtle distinctions in grain size and sorting may be of critical importance in understanding the relationships between the two types of quartzite and between the parts of the geosyncline in which they were deposited. Comparative lithic and chemical data are discussed in detail in the following paragraphs. Comparative stratigraphic data, which will be discussed more fully in another report, are summarized in table 1.

### Light detrital minerals

More than 99 percent by weight of the detrital grains in both the eugeosynclinal and miogeosynclinal quartzites are quartz. (Some of the chemical analyses in table 1 show less than 99 percent $SiO_2$ because nonquartz inclusions within detrital quartz grains are included in the analyses.) All sand-size grains are monocrystalline, but a small proportion of the silt-size fraction in the eugeosynclinal quartzite is composed of detrital chert. Not a single grain of detrital feldspar was detected in 320 thin sections of quartzite.

### Heavy detrital minerals

In comparison with other notably pure sandstone, such as the St. Peter Sandstone (Thiel, 1935, p. 595), the quartzites of the Cordilleran geosyncline have an extremely low content of heavy minerals. Heavy min-

TABLE 1.—*Summary comparison of Ordovician quartzites of the Cordilleran geosyncline*

| | Eugeosyncline | Miogeosyncline and intermediate zone |
|---|---|---|
| Formations containing quartzite. | Valmy Formation<br>Vinini Formation<br>Basco Formation of Lovejoy (1959)<br>Petes Summit Formation of Kay (Kay, 1960; and Kay and Crawford, 1964). | Eureka Quartzite<br>Swan Peak Quartzite<br>Upper part of type Kinnikinic Quartzite<br>Toquima Formation<br>Johnson Spring Formation<br>Convict Lake Formation. |
| Extent of quartzite. | Several thousand square miles in thrust plates in Nevada. Site of deposition possibly in northwestern Nevada. | At least 125,000 square miles in an area extending from southern California to central Idaho. |
| Aggregate thickness of quartzite. | From a few feet in the Vinini and Basco Formations to thousands of feet in the Valmy Formation. | From a few feet to more than 1,200 feet. |
| Stratigraphic relations. | Numerous thick units alternating with siliceous mudstone, bedded chert, and greenstone. | Usually a single thick unit overlain with sharp contact by carbonate rocks and usually underlain by thin units of shale, siltstone, dolomite, and quartzite and by thick limestone. |
| Bedding | Internal bedding generally thick. Crossbeds rare. | Internal bedding generally thick. Crossbeds common but indistinct. |
| Fossils | None | Worm borings, fucoidal structures common. |
| Light detrital minerals. | More than 99 percent quartz, including less than 1 percent chert silt. | More than 99 percent quartz. |
| Heavy detrital minerals. | Zircon and tourmaline, both well rounded, about 0.002 percent of rock by weight. | Zircon and tourmaline, both well rounded, about 0.002 percent of rock by weight. |
| Nondetrital minerals. | Pyrite; amorphous carbon; quartz overgrowths on detrital quartz; dolomite. | Pyrite; quartz overgrowths on detrital quartz; dolomite; collophane; less than 1 percent authigenic feldspar silt. |

TABLE 1.—*Summary comparison of Ordovician quartzites of the Cordilleran geosyncline*—Continued

| | Eugeosyncline | Miogeosyncline and intermediate zone |
|---|---|---|
| Grain size | Very fine to coarse sand; grains larger than 0.5 mm abundant, and grains larger than 1 mm common. | Very fine to medium sand; grains larger than 0.5 mm rare, no grains larger than 1 mm. |
| Grain sorting | Well sorted | Very well sorted. |
| Grain roundness | Well rounded | Well rounded. |
| Grain surfaces | Frosted in the few samples which could be disaggregated for observation. | Frosted in the few samples which could be disaggregated for observation. |
| Cement | Silica, rarely carbonate. | Silica, rarely carbonate. |
| Metamorphism | None except for overgrowths on detrital quartz. | None except for overgrowths on detrital quartz and growth of authigenic feldspar. |

erals in quartzites of the eugeosyncline are microscopically indistinguishable from those of the miogeosyncline, and their abundance is nearly the same (table 2). Zircon and tourmaline constitute at least 95 percent by weight of the heavy detrital mineral observed in composite samples from 30 sites (fig. 1). Rutile, mica, and unidentified minerals make up the remaining few percent. In all but two samples (from sites 49 and 44), zircon outweighs tourmaline, usually by a wide margin. Spectrographic analyses (table 3) indicate higher percentages of zirconium than those calculated from the amounts of detrital zircon. Part of the discrepancy probably is due to zirconium contained in detrital quartz grains and part of it may be a result of the inherent inaccuracy of spectrographic analyses of concentrations so near the detection limit. Samples of quartzite from the eugeosyncline and from the southern part of the miogeosyncline commonly yield a few sand-size books and flakes of biotite and muscovite. Although the amounts are negligible, their presence is puzzling in view of the vulnerability of micas to comminution.

TABLE 2.—*Percentage of detrital zircon in Ordovician quartzite*

| Locality (fig. 1) | Zircon (weight percent) | Predominant constituent of heavy-mineral suite |
|---|---|---|
| **Miogeosyncline** | | |
| 55 | 0.001 | Zircon. |
| 54 | .005 | Do. |
| 32 | < .001 | Do. |
| 35 | .002 | Do. |
| 43 | .002 | Do. |
| 19 | .002 | Do. |
| 62 | .001 | Do. |
| 60 | < .001 | Do. |
| 40 | .002 | Do. |
| **Eugeosyncline** | | |
| 49 | <0.001 | Tourmaline. |
| 66 | < .001 | Zircon. |
| 42 | < .001 | Do. |
| 46 | .004 | Do. |
| 44 | < .001 | Tourmaline. |
| 51 | .001 | Zircon. |

## Nondetrital minerals

Pyrite cubes, many partially or wholly oxidized, are common in quartzites of both parts of the geosyncline. The small regional variation in iron content of the quartzites, shown by chemical analyses in table 3, suggests that the pyrite, in which most of the iron content of the rock is concentrated, is related to deposition of the quartzite rather than to random local epigenetic processes.

Amorphous carbon is a distinctive, though minor, constituent of the eugeosynclinal quartzite. It is responsible for the dark and dirty look of most outcrops of the eugeosynclinal quartzite, and is probably responsible for the misconception that quartzite of high purity is unusual in the eugeosynclinal environment.

Authigenic feldspar grains of silt size are detectable in some samples of quartzite from the miogeosyncline. The widespread but low content of potassium indicated by the chemical analyses may mean that authigenic feldspare is a common though sparse ingredient in most samples.

Dolomite cements quartz grains at a few places near the top and base of the quartzite in the miogeosyncline. It forms the cement in some thin sandstone units in the Vinini and Basco Formations but is totally absent as a cement in the quartzites of the Valmy Formation.

Quartz overgrowths are almost a universal feature of the miogeosynclinal quartzite and a common feature of that of the eugeosyncline. The most likely sources of the silica in these overgrowths are the pressure points, or original points of contact, between detrital grains.

Collophane constitutes about one percent of some beds of quartzite along the eastern edge of the miogeosyncline. Elsewhere it is extremely uncommon. Typically, the collophane is in the form of sand-sized curved plates with internal layering.

Mineral inclusions in detrital quartz grains have not yet been studied in detail, but routine inspection of thin sections indicates that inclusions in quartz of both the eugeosyncline and miogeosyncline are similar in kind and amount.

TABLE 3.—*Chemical and spectrographic analyses of quartzite from eugeosynclinal and miogeosynclinal deposits of the Cordilleran geosyncline*

[Chemical analyses by Paul Elmore, Samuel Botts, Gillison Chloe, Lowel Artis, and N. Smith, 1963–64; spectrographic analyses by J. C. Hamilton, 1963–64]

| Locality (fig. 1) | Sample No.[1] | Chemical analyses (weight percent) | | | | | | | | | | | | | | Spectrographic analyses (weight percent)[2] | | | | |
|---|---|---|---|---|---|---|---|---|---|---|---|---|---|---|---|---|---|---|---|---|
| | | $SiO_2$ | $Al_2O_3$ | $Fe_2O_3$ | FeO | MgO | CaO | $Na_2O$ | $K_2O$ | $H_2O^-$ | $H_2O^+$ | $TiO_2$ | $P_2O_5$ | MnO | $CO_2$ | Ba | Cr | Cu | Ni | Zr |
| **MIOGEOSYNCLINE** | | | | | | | | | | | | | | | | | | | | |
| **Kinnikinic Quartzite** | | | | | | | | | | | | | | | | | | | | |
| 56 | 1646–1650 | 98. 0 | 0. 24 | 0. 22 | 0. 12 | 0. 10 | 0. 14 | 0. 07 | 0. 06 | 0. 00 | 0. 33 | 0. 00 | 0. 00 | 0. 00 | <0. 05 | 0. 02 | 0. 0003 | 0. 001 | 0. 00 | 0. 007 |
| | 1641–1645 | 97. 6 | . 48 | . 20 | . 12 | . 71 | . 32 | . 04 | . 00 | . 12 | . 22 | . 00 | . 00 | . 00 | . 18 | . 01 | . 0003 | . 0005 | . 00 | . 002 |
| | 1636–1640 | 95. 8 | . 20 | . 07 | . 16 | . 67 | . 90 | . 04 | . 15 | . 00 | . 35 | . 00 | . 00 | . 00 | 1. 1 | . 003 | . 001 | . 003 | . 0005 | . 003 |
| **Swan Peak Quartzite** | | | | | | | | | | | | | | | | | | | | |
| 4 | 40 | 97. 0 | 0. 69 | 0. 10 | 1. 3 | 0. 76 | 0. 00 | 0. 05 | 0. 01 | 0. 29 | 0. 07 | 0. 01 | 0. 02 | 0. 03 | <0. 05 | 0. 0015 | 0. 0015 | 0. 005 | 0. 001 | 0. 002 |
| | 39 | 98. 3 | . 48 | . 05 | . 36 | . 71 | . 06 | . 04 | . 05 | . 25 | . 15 | . 02 | . 00 | . 03 | < . 05 | . 003 | . 0003 | . 005 | . 00 | . 003 |
| | 36 | 96. 4 | 1. 2 | . 51 | . 48 | . 41 | . 13 | . 06 | . 32 | . 38 | . 21 | . 05 | . 01 | . 02 | . 06 | . 002 | . 0007 | . 001 | . 00 | . 02 |
| | 32 | 97. 1 | . 63 | . 01 | . 84 | . 59 | . 01 | . 01 | . 30 | . 18 | . 23 | . 04 | . 00 | . 03 | . 09 | . 005 | . 0007 | . 002 | . 00 | . 01 |
| | 23 | 97. 2 | 1. 1 | . 33 | . 56 | . 25 | . 25 | . 03 | . 20 | . 26 | . 24 | . 02 | . 01 | . 02 | < . 05 | . 007 | . 0007 | . 0007 | . 00 | . 003 |
| **Eureka Quartzite** | | | | | | | | | | | | | | | | | | | | |
| 23 | 160 | 98. 7 | 0. 19 | 0. 00 | <0. 05 | 0. 00 | <0. 05 | 0. 03 | 0. 10 | 0. 04 | 0. 62 | 0. 02 | 0. 00 | 0. 00 | <0. 05 | 0. 002 | 0. 0005 | 0. 002 | 0. 00 | 0. 002 |
| | 152 | 99. 5 | . 21 | . 03 | . 08 | . 00 | < . 05 | . 00 | . 06 | . 02 | . 41 | . 00 | . 00 | . 00 | < . 05 | . 003 | . 0002 | . 003 | . 00 | . 0015 |
| | 150 | 99. 2 | . 19 | . 04 | . 04 | . 00 | . 10 | . 07 | . 06 | . 02 | . 32 | . 00 | . 00 | . 00 | < . 05 | . 003 | . 0002 | . 0015 | . 00 | . 002 |
| | 147 | 99. 2 | . 18 | . 05 | . 06 | . 00 | < . 05 | . 00 | . 06 | . 02 | . 40 | . 00 | . 00 | . 00 | < . 05 | . 003 | . 0003 | . 003 | . 00 | . 002 |
| | 144 | 98. 7 | . 05 | . 22 | . 10 | . 00 | < . 05 | . 04 | . 06 | . 04 | . 41 | . 02 | . 00 | . 01 | < . 05 | . 005 | . 0003 | . 002 | . 00 | . 003 |
| **EUGEOSYNCLINE** | | | | | | | | | | | | | | | | | | | | |
| **Valmy Formation** | | | | | | | | | | | | | | | | | | | | |
| 42 | 227–230 | 97. 5 | 0. 48 | 0. 29 | 0. 16 | 0. 18 | 0. 22 | 0. 08 | 0. 20 | 0. 20 | 0. 16 | 0. 00 | 0. 00 | 0. 00 | <0. 05 | 0. 03 | 0. 0007 | 0. 007 | 0. 001 | 0. 007 |
| | 223–226 | 97. 2 | . 44 | . 36 | . 08 | . 13 | . 19 | . 07 | . 17 | . 18 | . 23 | . 00 | . 00 | . 00 | < . 05 | . 02 | . 0005 | . 003 | . 0003 | . 005 |
| | 218–222 | 96. 7 | . 70 | . 26 | . 16 | . 68 | . 20 | . 04 | . 27 | . 15 | . 34 | . 00 | . 00 | . 00 | < . 05 | . 15 | . 0005 | . 003 | . 00 | . 003 |
| | 210–216 | 97. 0 | . 63 | . 05 | . 32 | . 54 | . 21 | . 02 | . 23 | . 21 | . 27 | . 02 | . 00 | . 00 | < . 05 | . 02 | . 0008 | . 001 | . 00 | . 005 |
| 46 | 244–246 | 96. 9 | . 63 | . 25 | . 12 | . 27 | . 20 | . 05 | . 23 | . 19 | . 26 | . 00 | . 00 | . 00 | < . 05 | . 015 | . 0007 | . 001 | . 00 | . 007 |
| | 240–243 | 97. 4 | . 48 | . 25 | . 08 | . 13 | . 23 | . 04 | . 18 | . 04 | . 41 | . 00 | . 00 | . 00 | < . 05 | . 01 | . 0005 | . 0015 | . 00 | . 007 |
| **Petes Summit Formation** | | | | | | | | | | | | | | | | | | | | |
| 51 | 367–370 | 97. 7 | 0. 35 | 0. 22 | 0. 12 | 0. 22 | 0. 20 | 0. 07 | 0. 08 | 0. 00 | 0. 54 | 0. 00 | 0. 00 | 0. 00 | <0. 05 | 0. 01 | 0. 0005 | 0. 001 | 0. 0003 | 0. 002 |
| | 363–366 | 96. 9 | . 44 | . 66 | . 12 | . 35 | . 58 | . 03 | . 17 | . 22 | . 28 | . 00 | . 00 | . 00 | . 25 | . 01 | . 0003 | . 0005 | . 0007 | . 007 |
| | 355–358 | 97. 6 | . 39 | . 35 | . 12 | . 35 | . 21 | . 05 | . 15 | . 20 | . 24 | . 00 | . 00 | . 00 | < . 05 | . 01 | . 0003 | . 001 | . 0005 | . 002 |

[1] For each formation, samples arranged in stratigraphic order, with youngest sample at top.

[2] Forty-six additional elements were looked for but were not detected or were found to occur sporadically in insignificant amounts.

### Grain size and sorting

Grain size and sorting were studied in four ways: (1) About 320 thin sections from 30 sites (fig. 1) were scanned and the maximum apparent diameter of the largest grain for each site was measured and recorded in figure 2. (2) The maximum diameter of the largest zircon in heavy-mineral concentrates of composite samples from each of the 30 sites was also measured and recorded in figure 2. (3) The size-frequency distribution of constituent grains was determined in two samples which, owing to their carbonate cement, could be completely disaggregated (fig. 3). (4) Photographic enlargements of all thin sections were made by projecting them on photographic paper through crossed Polaroid sheets. These prints were assembled in stratigraphic order and the columns arranged in geographic order to be scanned for stratigraphic and regional trends in grain size and sorting.

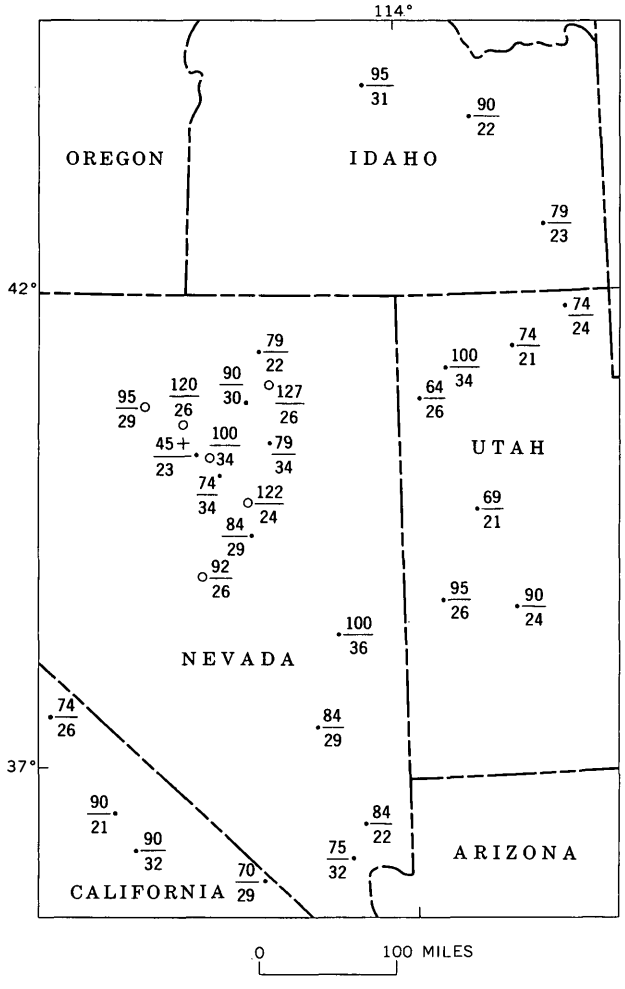


FIGURE 2.—Grain-size distribution in Ordovician quartzite of the Cordilleran geosyncline. Upper number of each pair is the maximum diameter of quartz grains, in hundredths of a millimeter, at the site; lower number is maximum zircon grain diameter. •, quartzite of the miogeosynclinal and intermediate zones; ○, quartzite of the eugeosyncline, thrust eastward.

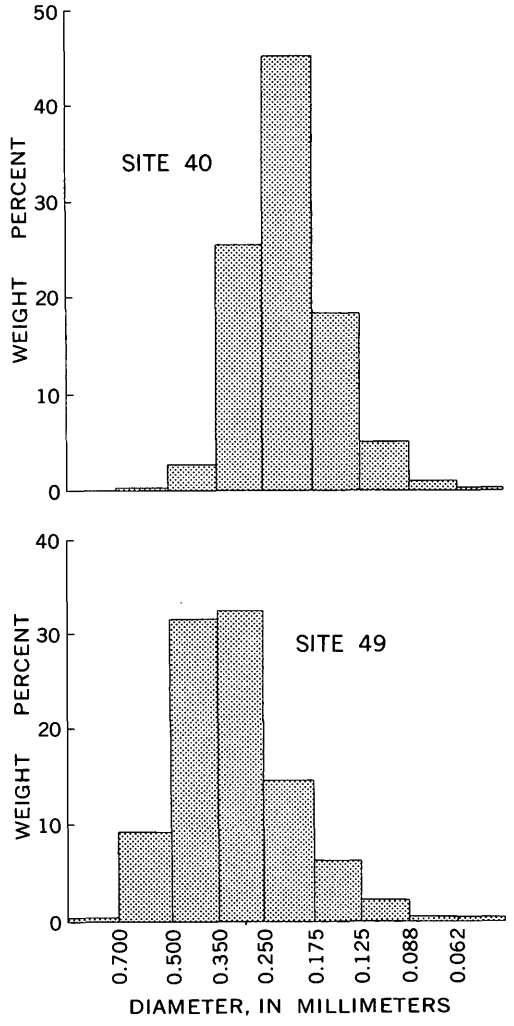


FIGURE 3.—Size-frequency distribution of detrital grains in two samples of quartzite from the Cordilleran geosyncline. Upper diagram, miogeosynclinal quartzite, same sample as that shown in figure 6; lower diagram, eugeosynclinal sandstone, same sample as that shown in figure 7.

These studies show that: (1) Quartzites of both the eugeosyncline and the miogeosyncline are composed of well-sorted sand, mostly of fine to medium size (fig. 4). (2) Quartzite of the eugeosyncline contains a higher proportion of coarse sand, and grains of larger maximum size, than does that of the miogeosyncline, and it is therefore somewhat less well sorted (fig. 5). (3) Regional variations in grain size and sorting within the eugeosyncline, and within the miogeosyncline, are small. Further study and additional data are required for interpretation of the genetic significance of these variations.

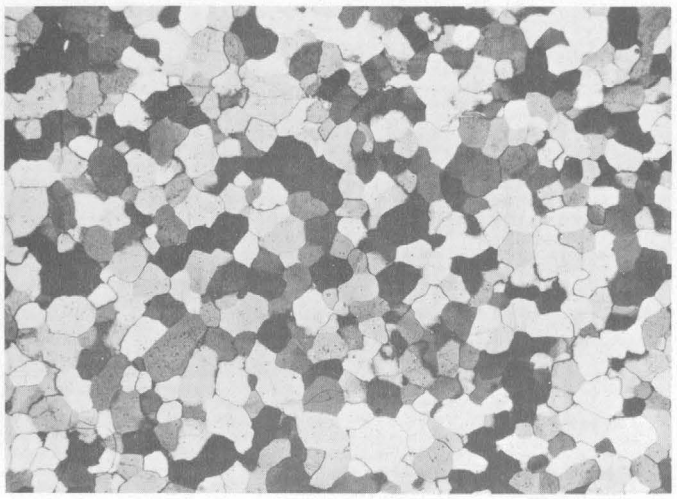

FIGURE 4.—Eureka Quartzite from the type section, Lone Mountain, Nev. (site 43), illustrating the even-grained texture and relatively fine grain size that are typical of Ordovician quartzite in the miogeosyncline. × 20. Crossed nicols.

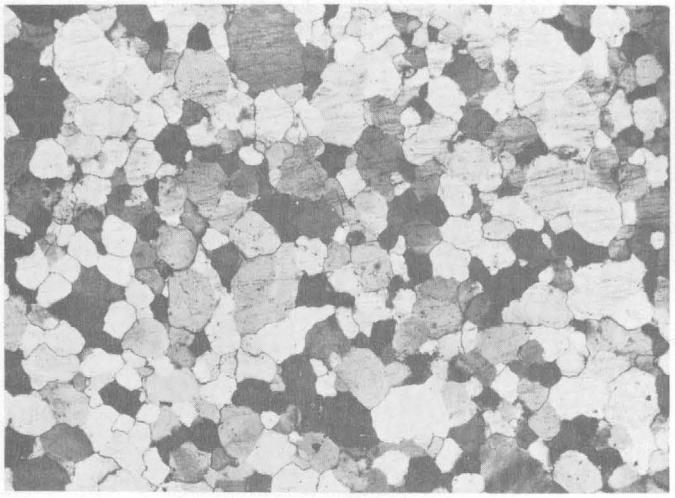

FIGURE 5.—Quartzite from the type section of the Valmy Formation, Battle Mountain, Nev. (site 42), illustrating the uneven-grained texture and relatively coarse size of some grains typical of Ordovician quartzite in the eugeosyncline. × 20. Crossed nicols.

### Grain roundness

The high degree of textural maturity indicated by the excellent grain sorting is confirmed by a high degree of roundness (figs. 6, 7). Quartz, zircon, and tourmaline in quartzite of both the eugeosyncline and the miogeosyncline are very well rounded, comparing almost perfectly with grains in the St. Peter Sandstone (Thiel, 1935, pls. 45, 46, and 48). Roundness is somewhat obscured by secondary overgrowths but can be seen in thin sections by using nonpolarized light.

211-690 O—66——5

### Grain surfaces

Only a few samples of Cordilleran Ordovician quartzite can be disaggregated to permit observation of original grain surfaces. However, certain strata from eugeosynclinal sites 44 and 49 and miogeosynclinal sites 60, 40, 19, 6, and 32 (fig. 1) contain enough carbonate cement to permit disaggregation with hydrochloric acid. The surfaces of all grains freed in this manner are frosted. When examined under high magnification the surfaces are seen to be roughened in a way that suggests corrosion by differential solution rather than pitting and scratching by abrasive action.

### Chemical composition

The chemical compositions of the eugeosynclinal and miogeosynclinal quartzites are virtually identical (table 3). The relative quantities of only two elements are consistently different by a significant amount. The barium content of the eugeosynclinal quartzites generally is several times that of the miogeosynclinal quartzites; and although it is not among the elements sought by analysis, elemental carbon commonly is visible in quartzites of the eugeosyncline, but not in those of the miogeosyncline. Much of the non-quartz material indicated by chemical analyses is due to mineral inclusions in quartz grains rather than to separate grains of other minerals.

## CONCLUSIONS

Constituent grains of Ordovician quartzites in both parts of the Cordilleran geosyncline were derived from sedimentary terranes composed, at least partly, of quartz sandstone. The high degree of composition-

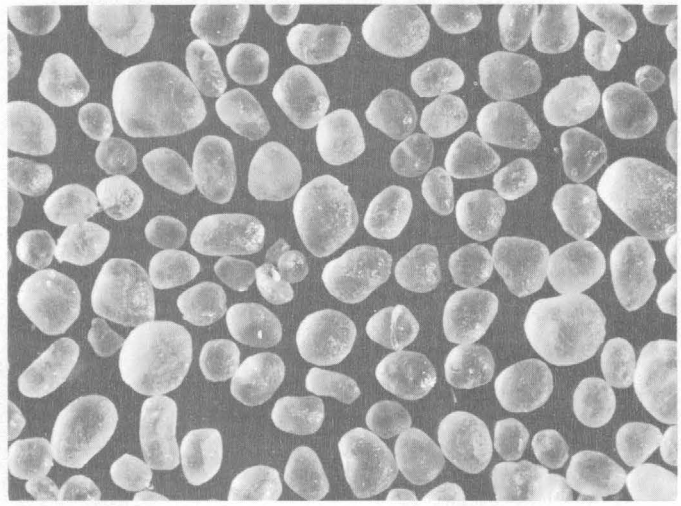

FIGURE 6.—Constituent grains of the Eureka Quartzite, southern Nevada (site 40), which illustrate the high degree of roundness typical of Ordovician quartzite in the miogeosyncline. × 20.

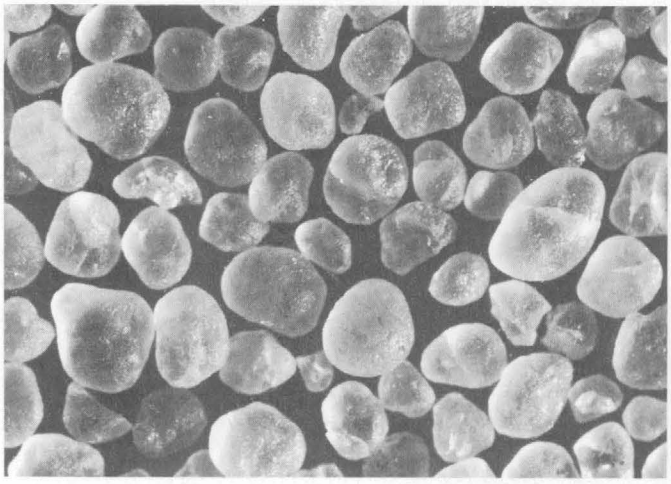

FIGURE 7.—Constituent grains of sandstone in the Basco Formation (site 49), which illustrate the high degree of roundness typical of Ordovician quartzite in the eugeosyncline. × 20.

al and textural maturity of these quartzites precludes a large contribution from igneous or metamorphic provenance terranes. The lack of compound quartz grains and metamorphic minerals further preclude metamorphic terranes.

Grains composing Middle Ordovician quartzite of the eugeosyncline must have been derived from the western side of the geosyncline. Their slightly coarser size and relatively poor sorting make it extremely unlikely that they could have been transported westward across the miogeosyncline where smaller and better sorted grains were being deposited. Moreover, as James Gilluly has pointed out (oral commun., 1954), the deposition of Early Ordovician eugeosynclinal quartzites was contemporaneous with the deposition of quartz-free carbonate rocks in the miogeosyncline.

In a realistic paleogeographic model of the Ordovician System, hypothetical volcanic islands bordering the geosyncline on the west (Kay, 1951, pl. 1) may have to be replaced by a land composed of unmetamorphosed quartz-rich sedimentary rocks, presumably of late Precambrian or Cambrian age.

## REFERENCES


Ferguson, H. G., 1924, Geology and ore deposits of the Manhattan district, Nevada: U.S. Geol. Survey Bull. 723, 163 p.

Kay, Marshall, 1951, North American geosynclines: Geol. Soc. America Mem. 48, 143 p.

——— 1960, Paleozoic continental margin in central Nevada, western United States: Internat. Geol. Cong., 21st, Copenhagen 1960, Rept., p. 12, p. 94–103.

Kay, Marshall, and Crawford, J. P., 1964, Paleozoic facies from the miogeosynclinal to the eugeosynclinal belt in thrust slices, central Nevada: Geol. Soc. America Bull., v. 75, p. 425–454.

Lovejoy, D. W., 1959, Overthrust Ordovician and the Nannie's Peak intrusive, Lone Mountain, Elko County, Nevada: Geol. Soc. America Bull., v. 70, no. 5, p. 539–563.

Kirk, Edwin, 1933, The Eureka Quartzite of the Great Basin region: Am. Jour. Sci., 5th ser., v. 26, p. 27–44.

Nolan, T. B., 1943, The Basin and Range province in Utah, Nevada, and California: U.S. Geol. Survey Prof. Paper 197–D, p. 141–196.

Rinehart, C. D., and Ross, D. C., 1964, Geology and mineral deposits of the Mount Morrison quadrange, Sierra Nevada, California: U.S. Geol. Survey Prof. Paper 385, 106 p.

Roberts, R. J., Hotz, P. E., Gilluly, James, and Ferguson, H. G., 1958, Paleozoic rocks of north-central Nevada: Am. Assoc. Petroleum Geologists Bull., v. 42, no. 12, p. 2813–2857.

Ross, C. P., 1937, Geology and ore deposits of the Bayhorse region, Custer County, Idaho: U.S. Geol. Survey Bull. 877, 161 p.

Ross, D. C., 1965, Geology of the Independence quadrangle, Inyo County, California: U.S. Geol. Survey Bull. 1181–O, 64 p.

Ross, R. J., Jr., 1953, The Ordovician system in northeastern Utah and southeastern Idaho, *in* Intermountain Assoc. Petroleum Geologists, 4th Ann. Field Conf., 1953: p. 22–26.

Thiel, G. A., 1935, Sedimentary and petrographic analysis of the St. Peter Sandstone: Geol. Soc. America Bull., v. 46, p. 559–614.

# EOCENE PALEOSOL IN THE NORTHERN GREAT PLAINS

By WAYNE A. PETTYJOHN, Bismarck, N. Dak.

*Abstract.*—A lateritic soil profile of probable late Eocene age crops out in widely separated localities in the northern Great Plains. Especially well developed in western South Dakota and northwestern Nebraska, it is characterized by vivid purple, yellow, and greenish-gray sediments directly underlying the Chadron Formation of the White River Group of Oligocene age. The stratigraphic units on which the soil profile formed range in age from Early or Late Cretaceous to late Eocene.

A soil profile of probable late Eocene age offers clues to the topography and areal distribution of stratigraphic units in the northern Great Plains region in late Eocene time. It is exposed at several widely separated localities in western North Dakota, western South Dakota, northwestern Nebraska, and eastern Wyoming (fig. 1), and several specific localities in South Dakota are described in detail by Pettyjohn (1964; in press).

The soil profile, recognized for many years, has been discussed by numerous authors, including Ward (1922, 1926), Toepelman (1922), Wanless (1923), Schultz and Stout (1955), Harvey (1956), and Dunham (1961). Ward (1922, p. 18-20) described variously colored weathered strata in the Badlands area of South Dakota, near the town of Interior, as the "Interior Phase" of the Pierre (Shale) but also suggested that these same strata may instead be equivalent to the Fox Hills Sandstone. Although Wanless (1923, p. 194) inclined toward including the "Interior Formation of Ward" as part of the Pierre, Ward (1926) concluded from his further observations that his "Interior Phase" is really Fox Hills. Most subsequent workers, however, have regarded the "Interior Phase" to be a weathered zone locally present on outcrops of the Pierre Shale (Upper Cretaceous) in southwestern South Dakota and northwestern Nebraska.

Schultz and Stout (1955) suggested the term "Interior Paleosol Complex" for these weathered sediments in northwestern Nebraska, and adjacent parts of Wyoming and South Dakota. They designated as the type locality of the paleosol the area originally defined by Ward (1922) as the type area of the "Interior Phase" of the Pierre. Schultz and Stout recognized the age of the soil profile as pre-Chadron (Oligocene) and post-Pierre Shale in Nebraska and South Dakota. In addition, they suggested that "Ward's interpretation (of the Interior) is now only of historical interest" (Schultz and Stout, 1955, p. 25).

Harvey (1956), in his paleoecological study of the White River Group faunas in Sioux County, Nebr., briefly discussed Ward's "Interior Formation." He noted (1956, p. 22) that "In later years most workers have agreed that this 'formation' is simply a weathered phase of the Pierre."

A major question remains—what is the "Interior Formation"? Most workers agree that (1) it is not a distinct formation, (2) it represents a weathered zone, (3) it was formed by chemical weathering of the Pierre Shale, (4) the period of weathering took place during post-Pierre and pre-Oligocene time, and (5) the term is of only historical interest. This writer has shown previously (Pettyjohn, 1964), however, that some of the above assumptions are probably incorrect, in that (1) the multicolored paleosol is definitely a stratigraphic unit that is mappable over wide areas, (2) it was formed by chemical weathering of rocks at least as old as the Skull Creek Shale of Early Cretaceous age and rocks as young as the Slim Buttes Formation of Bjork (1965) of latest Eocene age, and (3) the period of soil formation is probably late Eocene.

In view of the general confusion concerning the meaning and use of the terms "Interior Phase" of the Pierre, "Interior Formation," or "Interior" period of weathering, the writer is inclined to reject Schultz and Stout's term "Interior Paleosol Complex" because the name "Interior" is surrounded with confusion and contradiction. The term "Eocene paleosol" is sufficiently descriptive, and does not limit the paleosol to scattered outcrops near Interior, S. Dak.

U.S. GEOL. SURVEY PROF. PAPER 550–C, PAGES C61–C65

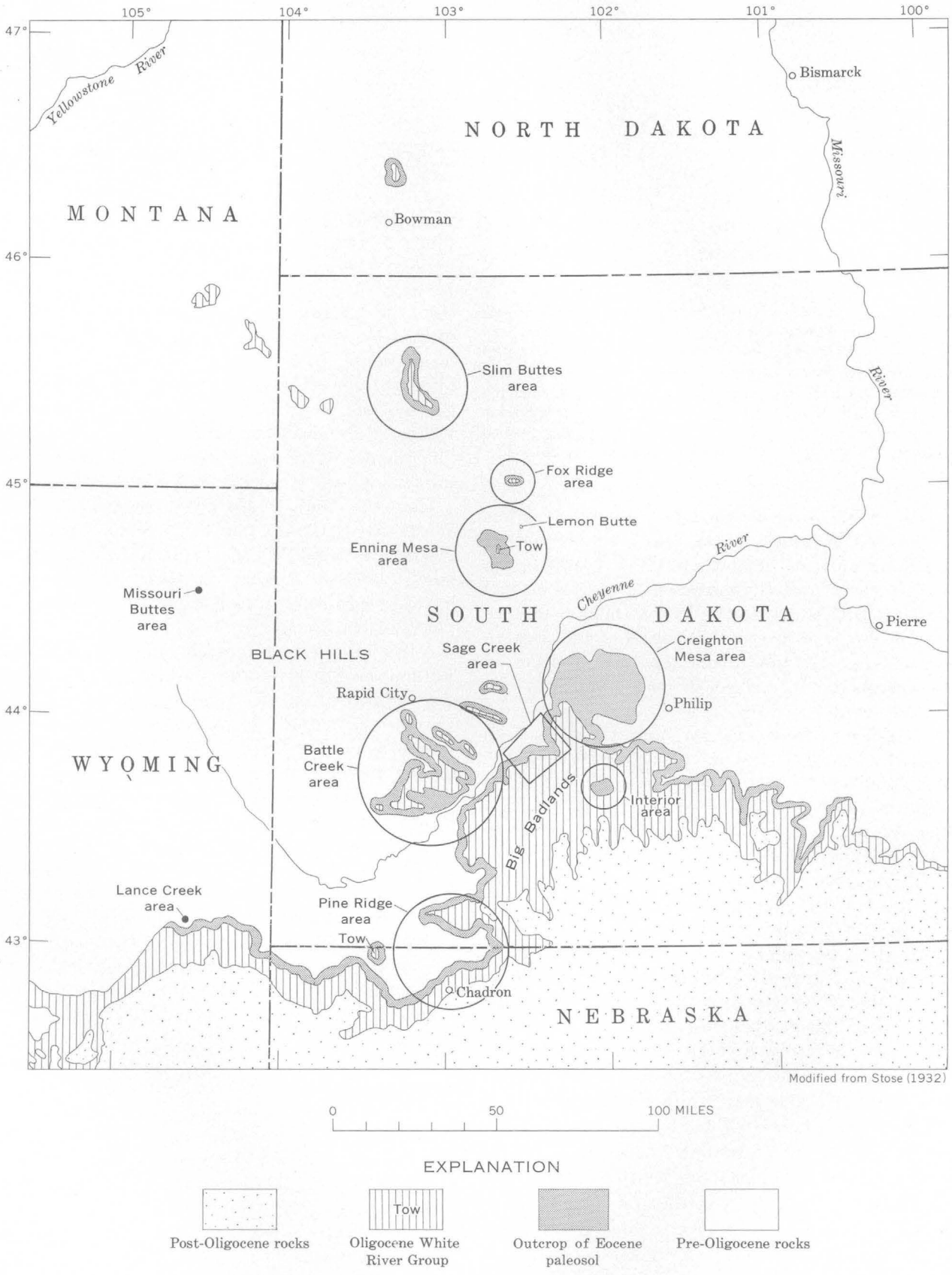


FIGURE 1.—Map showing generalized outcrops of Eocene paleosol in the northern Great Plains.

## THE SOIL PROFILE

The paleosol was formed by weathering of rocks probably exposed during late Eocene time. In addition to being characterized by vivid colors, these weathered deposits generally lack primary sedimentary features in the upper part and have chemical properties that differ from those of unweathered strata. Where the soil profile is buried beneath younger rocks, it is overlain disconformably by the White River Group of Oligocene age, or by Pleistocene gravel.

Dunham (1961, p. 55) apparently was the first to recognize the lateritic origin of the paleosol. He described its major features in the Chadron arch area in northwestern Nebraska and south-central South Dakota (Pine Ridge area, fig. 1) and assigned an Eocene(?) age to it. He divided the profile into three major zones which, in descending order, are the transformed zone, the oxidized zone, and the boundary zone. All three of these zones can be recognized in the vicinity of Chadron, Nebr., as well as in parts of the Big Badlands of South Dakota (fig. 1). Although not all the zones can be recognized in areas farther north in the Great Plains, one or two zones generally are present. Dunham's terminology is used in this report.

The transformed zone is as much as 25 feet thick near Interior, S. Dak., where the paleosol is developed on the Pierre Shale (Interior area, fig. 1). There the upper few feet of the transformed zone consists of purple or lilac noncalcareous clay, whereas the lower part is characterized by green and brownish-gray clay intercalated with thin layers of purple clay. The transformed zone is highly weathered, almost totally lacks effective porosity, and has a very low calcium carbonate content. Kaolinite, illite, and iron oxides are abundant; diffusion banding is locally present near iron concretions (Pettyjohn, 1964, p. 179).

The underlying oxidized zone generally consists of green or reddish-brown clay and is as much as 38 feet thick near Interior, S. Dak. Its calcium carbonate content is low in the upper part but increases with depth. Hematite and limonite commonly fill joints and cracks in concretions. Kaolinite and illite appear to be the dominant clays. Primary sedimentary features of the parent rock may be present. Because most unaltered Cretaceous and Tertiary rocks in the northern Great Plains contain limestone or siderite concretions, the general lack of these concretions within the oxidized zone suggests that they were either altered to limonite and hematite, or dissolved.

The boundary zone, which consists partly of weathered and partly of unweathered rocks, has a considerable range in thickness and in places is thicker than 60 feet. Although from a distance the contact between the boundary zone and unweathered rocks appears to be abrupt, it actually is quite indistinct and is gradational over several tens of feet.

The features of the paleosol just described are valid only where the weathered sediments consist predominantly of clay. In areas where the original sediments consist mainly of silt or sand, such as outcrops of the Fox Hills Sandstone, the soil profile may be difficult to recognize. Commonly the silt is greenish gray and the sand or sandstone is yellow or rusty brown; the calcium carbonate content generally is low. At a given place the percentage of calcium carbonate is related to the permeability of the strata and to the depth below the original soil surface. A distinguishing characteristic of the sand or silty deposits is the presence within the sandy strata of galls, or thin layers of clay, which are generally some shade of red.

Toepelman (1922, p. 65) suggested that the various shades of red, green, and yellow of the rocks here regarded as constituting a paleosol were derived from the overlying White River Group. For several reasons, however, this cannot be the case. If the color were carried down the faces of outcrops of the White River Group and stained the underlying sediments, the coloring would be merely superficial, which it is not. In addition, water percolating downward through the White River Group would be unlikely to stain the underlying sediments, because the transformed zone and the upper part of the oxidized zone are relatively impermeable. In fact, springs and seeps commonly issue at the base of the White River Group during the wet season, and thick layers of gypsum mark the contact locally. Finally, the White River Group is calcareous in many parts of the section, whereas the paleosol either lacks calcite or contains only minor amounts of it. Downward-percolating water would certainly have removed calcium carbonate from the White River Group and enriched the paleosol if the latter were permeable.

## LOCATION AND DESCRIPTION OF SPECIFIC OUTCROPS

The paleosol can be traced northward and westward from Interior, S. Dak., along the Cheyenne River and its tributaries. It is especially well exposed along the valleys of Sage, Spring, Bear, and Indian Creeks in Pennington County, S. Dak. (Sage Creek area, fig. 1). As in the vicinity of Interior, the paleosol was formed by weathering of the Pierre Shale; it is at least 30 feet thick.

In the Creighton Mesa area (fig. 1) nearly all of the upper part of the Fox Hills has been altered, but owing to later erosion the paleosol profile commonly is not complete. The effects of weathering are readily visible,

however, because the shale layers are commonly purple, the silt zones are light grayish green, and the sand and sandstone outcrops are shades of rusty brown and yellow. As much as 60 feet of the weathered rocks is exposed in this area.

Ward (1922, 1926) described the outcrops of the Fox Hills Sandstone in the Creighton Mesa area and used data on the high percentage of sand in those outcrops to support his view that the "Interior" is part of the Fox Hills. Toepelman (1922) and Wanless (1923) suggested that the "Interior" at its type locality is a part of the Pierre Shale. The writer believes that all these conclusions are valid: these workers were dealing with a soil profile that developed on several different formations. If Ward's observations had been given more attention by later workers, the true nature of the paleosol probably would have been recognized sooner.

The paleosol is especially well exposed in the drainage basins of Spring, Battle, and French Creeks (Battle Creek area, fig. 1), south of Rapid City. From an airplane the characteristic reddish purple of the soil profile appears to be quite widespread. Here the paleosol, at least 35 feet thick, was formed by weathering of the Pierre Shale and the Niobrara Formation. In this area it probably is present on older formations also.

In the Enning Mesa area (fig. 1), to the north across the Cheyenne River, the paleosol formed on the upper part of the Fox Hills Sandstone (Pettyjohn, 1964; in press). Here the paleosol is at least 88 feet thick. W. L. Russell [1] reported that the Hell Creek Formation on Lemon Butte in the drainage basin of Sulphur Creek, which forms the north boundary of Enning Mesa, is purple, green, and yellow. Probably these colored rocks represent the paleosol in that area.

Two particularly good exposures of the paleosol are on Fox Ridge and on the adjacent Signal Butte (Fox Ridge area, fig. 1). Here the paleosol was formed on the Fort Union Formation (Ludlow Member) of Paleocene age. The paleosol also is present on scattered outcrops of the Fort Union in areas farther north where the lowest part of the White River Group is present or was removed by recent erosion.

The Golden Valley Formation, where it crops out in west-central North Dakota, has been considerably altered by pre-Oligocene weathering. Jepsen (1963), on the basis of fossil vertebrates, has dated this formation as early Eocene. Bjork (1964, 1965), in a study of his Slim Buttes Formation of supposed late Eocene age in Harding County, S. Dak. (Slim Buttes area, fig. 1), reported sediments which, from their description, appear to represent the paleosol. The writer has not examined these exposures or exposures of similar variously colored sediments that form the upper part of the Ravenscrag Beds in southwestern Saskatchewan. The Ravenscrag is the Canadian equivalent of the Fort Union Formation.

Similar small exposures of the paleosol are present locally in the Lance Creek area, Wyoming (fig. 1). In these outcrops the soil profile is on the Lance Formation of Late Cretaceous age.

Robinson and others (1964, p. 105) described the disconformable contact of the White River Group and the Skull Creek Shale of Early Cretaceous age in an area about 4 miles north-northeast of Missouri Buttes in northeastern Wyoming (Missouri Buttes area, fig. 1). In this area, 11 to 15 miles south of Hulett, "the Skull Creek shale is bleached shades of light gray and pink for several feet below the contact." These bleached clay-shales probably represent the paleosol.

## AGE OF THE SOIL PROFILE

Everywhere that the writer examined rocks overlain by the oldest part of the White River Group, the paleosol is present immediately below the contact. In some areas where the White River Group has been removed recently by erosion, at least part of the paleosol is present. In areas where the oldest White River sediments are not present, either because of ancient erosion or nondeposition, the paleosol appears to be absent. In such places the paleosol and possibly the basal Oligocene rocks also were eroded prior to the deposition of younger sediments of the White River Group.

Nowhere has the paleosol been observed on or in the White River Group of Oligocene age. Thus the available evidence indicates that the period of soil formation was later than deposition of the Slim Buttes Formation in the Eocene Epoch and earlier than deposition of the White River Group in the Oligocene Epoch. Development of the paleosol is believed, therefore, to have occurred during the closing phase of the Eocene Epoch. Although the formation of the paleosol was probably time-transgressive, the stratigraphic relationships and available palentological data seem to indicate a relatively short period of time.

## PALEOGEOGRAPHY

### Topography

The Eocene paleosol was developed on a surface of considerable topographic relief. Along the flanks of the Black Hills, the land surface on which the soil formed sloped gently away from the central uplift. The region in the vicinity of Interior, S. Dak., appears

[1] W. L. Russell, no date, Stratigraphy and structure of western South Dakota: South Dakota Geol. Survey unpub. rept., 295 p.

to have been a large but relatively flat-floored basin. Because the soil profile lies at progressively lower altitudes in the upper valley of Sage Creek, that part of the channel in which Sage Creek now flows, roughly parallel to the northeast boundary of the Badlands National Monument, is believed to be a pre-Oligocene channel. It seems likely that much of the area in southwestern South Dakota, where Tertiary formations are present, represents a pre-Oligocene basin.

The Creighton Mesa area was probably only slightly higher than its present elevation, and was nearly flat. The paleosol in the Enning Mesa area probably was formed on a nearly level surface, because there the contact between the Fox Hills Sandstone and the White River Group does not vary more than 5 feet from a horizontal plane.

The writer is not familiar with the details of the late Eocene topography of the other areas, but a few isolated exposures of the Eocene paleosol suggest that the surface on which it developed was topographically higher, northward and westward from Enning Mesa.

The data suggest a relatively flat expanse of land that was drained by relatively wide, deep, and steep-walled valleys. Badland areas may have been locally present in the large valleys. The area was, no doubt, well drained, but the preservation of the altered sediments suggested that erosion was localized or of small extent. The coarse clastic material that locally forms the basal part of the White River Group, particularly in the Badlands areas, suggests a minor period of uplift in the central part of the Black Hills during latest Eocene or earliest Oligocene time. In some areas the eastward-flowing streams had sufficient discharge to erode channels into, but rarely through, the soil profile.

### Climate

The climate under which the soil profile was formed can be inferred from the sediments that were the end products. Spectrographic analyses of parts of the soil profile show relatively high concentrations of iron and alumina in the upper parts and a general lack of calcium (Dunham, 1961; Pettyjohn, 1964). Lack of calcium and carbonate and enrichment by iron and alumina indicate a pedalfer-type soil.

The ancient soil under consideration is characterized as a whole by alumina enrichment, moderate to high iron enrichment, red and yellow colors, kaolinization, poor vertical differentiation, and relatively great thickness. These features are those of a pedalfer, particularly of a laterite.

Modern deep lateritic soils are formed in hot, wet regions where leaching and eluviation are intensive. A constant supply of moisture in conjunction with high temperature is necessary for soil formation to continue throughout the year. In tropical rain forests, bacterial action prevents large accumulations of humus on and near the surface even though large quantities of vegetation are present. For complete leaching of soluble materials such as calcium carbonate, a soil must be well drained.

## SUMMARY

Although exposed in widely separated localities in the northern part of the Great Plains, the late Eocene paleosol is most conspicuous in western South Dakota. It probably was developed under hot and wet climatic conditions in relatively flat areas having deep and widely spaced drainage systems. Sedimentary and chemical features of the profile suggest a lateritic-type soil.

## REFERENCES

Bjork, P. R., 1964, Stratigraphy and paleontology of the Slim Buttes Formation in Harding County, S. Dak.: South Dakota School of Mines and Technology, unpub. M. S. thesis, 43 p.

——— 1965, Slim Buttes Formation of northwestern South Dakota [abs.]: Geol. Soc. America Spec. Paper 82, p. 319.

Dunham, R. J., 1961, Geology of uranium in the Chadron area, Nebraska and South Dakota: U.S. Geol. Survey open-file rept., 243 p.

Harvey, Cyril, 1956, A paleoecological interpretation of the White River faunas of Sioux County, Nebr.: Nebraska Univ., M.S. thesis, 135 p.

Jepsen, G. L., 1963, Eocene vertebrates, coprolites, and plants in the Golden Valley Formation of western North Dakota: Geol Soc. America Bull., v. 74, p. 673–684.

Pettyjohn, W. A., 1964, Geology of a part of west-central south Dakota: Boston Univ., unpub. Ph.D. thesis, 309 p.

——— in press, Geology of the Stoneville quadrangle: South Dakota Geol. Survey geol. quad. map and text.

Robinson, C. S., Mapel, W. J., and Bergendahl, M. H., 1964, Stratigraphy and structure of the northern and western flanks of the Black Hills uplift, Wyoming, Montana, and South Dakota: U.S. Geol. Survey Prof. Paper 404, 134 p.

Schultz, C. B., and Stout, T. M., 1955, Classification of Oligocene sediments in Nebraska: Nebraska Univ. State Museum Bull., v. 4, no. 2, p. 17–52.

Stose, G. W. (compiler), 1932, Geologic map of the United States: U.S. Geol. Survey, scale 1:2,500,000.

Toepelman, W. C., 1922, The paleontology of the [Badlands] area, *in* Ward, Freeman, Geology of a portion of the Badlands: South Dakota Geol. Nat. Hist. Survey Bull. 11, p. 61–73.

Wanless, H. R., 1923, The stratigraphy of the White River beds of South Dakota: Am. Philos. Soc. Proc., v. 62, p. 190–269.

Ward, Freeman, 1922; Geology of a portion of the Badlands: South Dakota Geol. Nat. Hist. Survey Bull. 11, 80 p.

——— 1926, The position of the Interior Formation: Am. Jour. Sci., 5th ser., v. 11, p. 350–352.

# CORRELATION OF LOWER CAMBRIAN AND SOME PRECAMBRIAN STRATA IN THE SOUTHERN GREAT BASIN, CALIFORNIA AND NEVADA

By JOHN H. STEWART, Menlo Park, Calif.

*Abstract.*—Lower Cambrian and some Precambrian strata of the Spring Mountains–Death Valley region of Nevada and California correlate with rocks of the White-Inyo Mountains region of California. The equivalent strata generally increase in thickness, are more calcareous, and become finer grained northwestward from the Spring Mountains–Death Valley facies to the White-Inyo Mountains facies. The Reed Dolomite, formerly correlated with the Noonday Dolomite, is here correlated with dolomite layers in the upper part of the Stirling Quartzite.

The Lower Cambrian and some of the conformably underlying Precambrian strata thicken and change facies from largely coarse clastic strata (Spring Mountains–Death Valley facies) in the Spring Mountains and Death Valley region of Nevada and California (fig. 1) to finer grained clastic rocks (White–Inyo Mountains facies) to the northwest in the White and Inyo Mountains region of California. The amount of limestone and dolomite increases to the northwest between these two regions. The present study was undertaken to determine the correlations of lithic units between these two facies. This report is part of a continuing study of the stratigraphy and sedimentary history of the Lower Cambrian and Precambrian strata in the southern Great Basin.

*Acknowledgments.*—The author is grateful for the use of unpublished stratigraphic sections kindly supplied by H. R. Cornwall, F. J. Kleinhampl, J. F. McAllister, and M. W. Reynolds, of the U.S. Geological Survey, and by C. A. Nelson, of the University of California at Los Angeles.

## STRATIGRAPHY AND CORRELATION

The formations recognized in the Spring Mountains–Death Valley facies are, in ascending order, the Noonday Dolomite, Johnnie Formation and Stirling Quartzite of Precambrian age, the Wood Canyon Formation of Cambrian and Precambrian age, the Zabriskie Quartzite of Early Cambrian age, the Carrara Formation of Early and Middle Cambrian age, and the Bonanza King Formation of Middle and Late Cambrian age (fig. 2). In the White–Inyo Mountains facies, which includes strata equivalent to the Spring Mountains–Death Valley facies, the following formations are recognized, in ascending order: the Wyman Formation, Reed Dolomite, and Deep Spring Formation of Precambrian age; Campito Formation of Cambrian and Precambrian age; the Poleta, Harkless, and Saline Valley Formations, and Mule Spring Limestone of Early Cambrian age; and the Monola Formation of Middle Cambrian age.

Correlations between the White–Inyo Mountains facies and the Spring Mountains–Death Valley facies have long been attempted. Geologists have in general considered the Noonday Dolomite to be equivalent to the Reed Dolomite, the Johnnie Formation equivalent to the Deep Spring Formation, and the Stirling Quartzite equivalent to the Campito Formation. The possibility of these correlations has been indicated by Nolan (1924, p. 34), Hazard (1937, p. 301), Nelson (1962a), and McKee and Moiola (1962, p. 533-536). The present study, however, indicates that the Noonday Dolomite, Johnnie Formation, and the lower part of the Stirling Quartzite correlate with strata below the Reed Dolomite, and that dolomite layers in the upper part of the Stirling Quartzite thicken to the northwest and form the Reed Dolomite. In addition, the study indicates that the lower part of the Wood Canyon Formation is largely equivalent to the Deep Spring Formation, and the middle part of the Wood Canyon Formation is equivalent to the Campito Formation. These correlations were largely suggested to me by J. F. McAllister before the present study was undertaken. Furthermore, C. A. Nelson and A. R. Palmer (written commun., 1962) indicated, on the basis of lithologic similarity and contained fossils, that

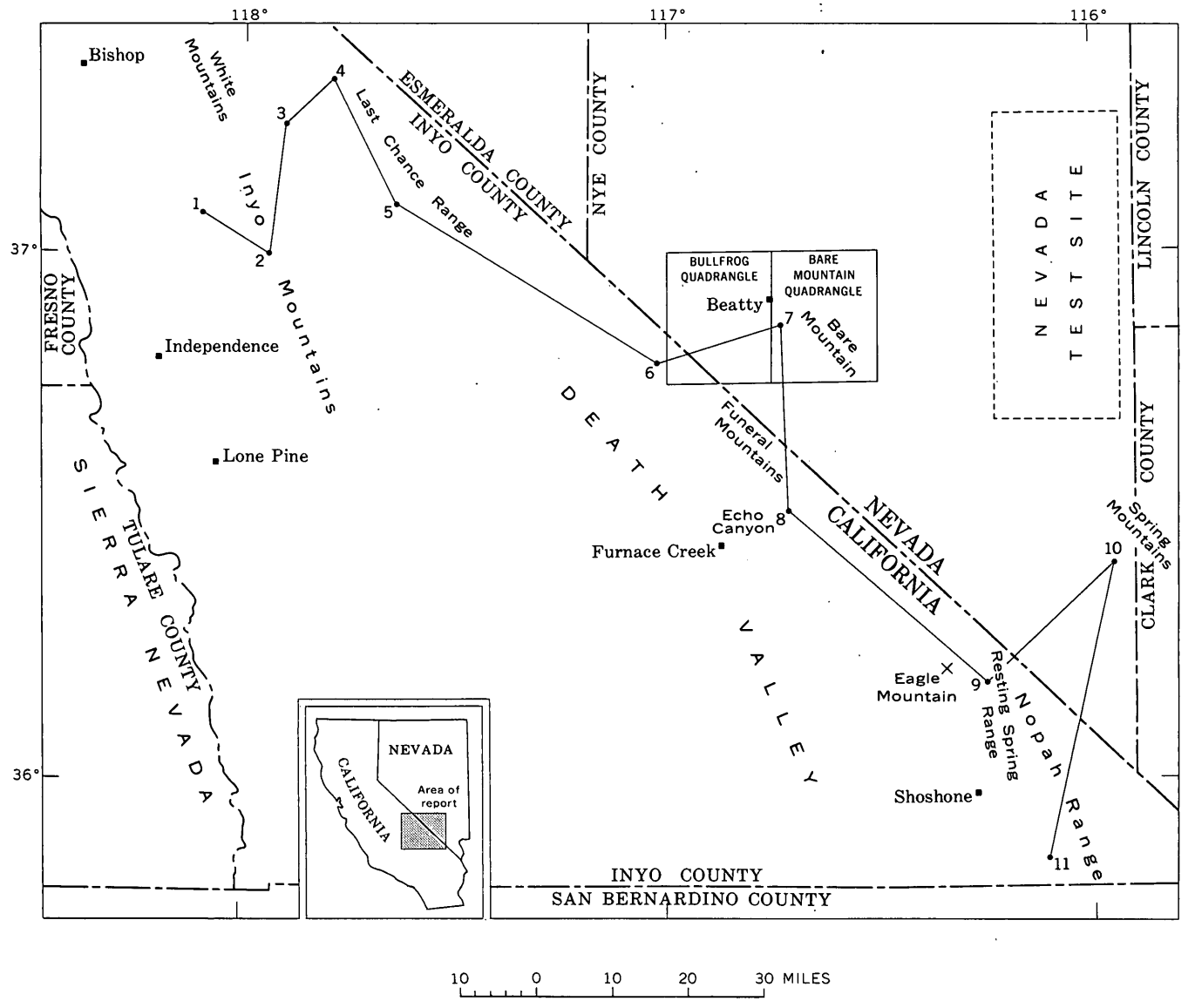


FIGURE 1.—Index map of part of southern Great Basin showing location of line of stratigraphic sections shown on figure 2.

the upper part of the Wood Canyon Formation correlated with the Poleta Formation, and that the Zabriskie Quartzite correlated with strata in the Harkless Formation. These correlations have been largely substantiated by the present study.

### Noonday Dolomite

The Noonday Dolomite (named by Hazzard, 1937, p.300–301) is a fairly homogeneous and massive, very pale orange, coarsely crystalline dolomite. It lies with marked unconformity (Hazzard, 1937, p. 301) on the underlying Precambrian strata. The Noonday Dolomite crops out widely in the southern part of the Death Valley region (sec 11, fig. 2), but it may not extend farther north, as it is apparently absent in the Funeral Mountains (L. A. Wright and B. W. Troxel, written commun., 1964). Perhaps, however, the absence of the Noonday Dolomite in the Funeral Mountains can be explained as a local feature, and the Noonday may grade laterally, with change of facies, into some part of the Wyman Formation or even lower unexposed rocks in the White–Inyo Mountains region. This latter correlation is speculative and is the subject of continuing study. The Wyman Formation (named by Maxson, 1935) consist of dark-gray phyllite and interbedded limestone, or marble, layers. Commonly calcsilicate hornfels are present. The Wyman Formation has a minimum thickness (Nelson, 1962b, p. 140) of 9,000 feet (shown only in part on fig. 2); no stratigraphic base is exposed.

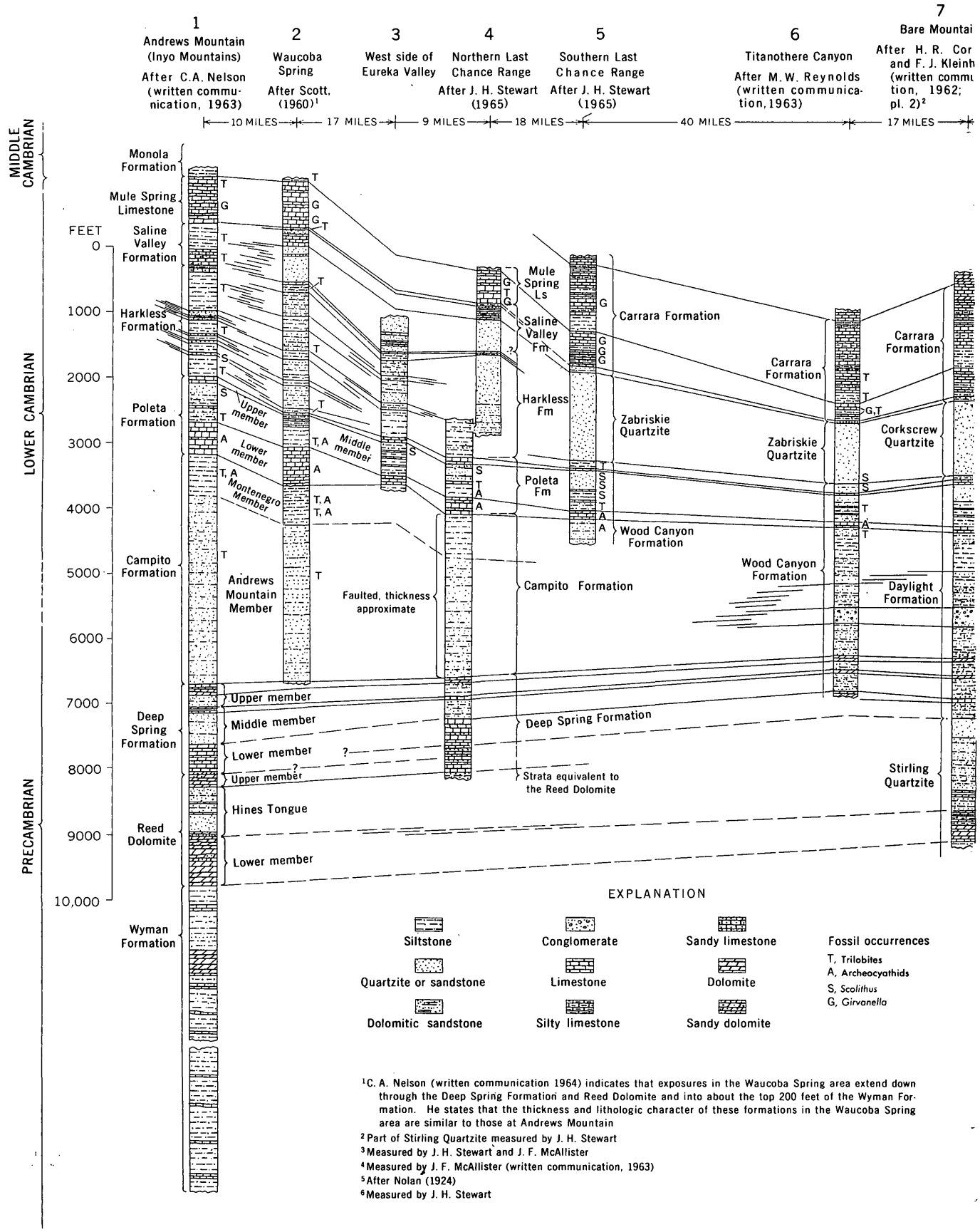


[1] C. A. Nelson (written communication 1964) indicates that exposures in the Waucoba Spring area extend down through the Deep Spring Formation and Reed Dolomite and into about the top 200 feet of the Wyman Formation. He states that the thickness and lithologic character of these formations in the Waucoba Spring area are similar to those at Andrews Mountain

[2] Part of Stirling Quartzite measured by J. H. Stewart

[3] Measured by J. H. Stewart and J. F. McAllister

[4] Measured by J. F. McAllister (written communication, 1963)

[5] After Nolan (1924)

[6] Measured by J. H. Stewart

FIGURE 2.—Correlation of Lower Cambrian and some Precambr

8
Echo Canyon
nnie and Wood anyon Formations d Stirling Quartz- e;[3] Zabriskie uartzite and Car- ra Formation[4]

9
Northern Resting Spring Range
(Carrara Formation measured on Eagle Mountain)

10
Spring Mountains
Johnnie and Carrara Formations and Zabriskie Quartz- ite;[5] Stirling Quartz- ite and Wood Canyon Formation[6]

11
Southern Nopah Range
After Hazzard (1937). Stirling Quartzite and part of Wood Canyon Formation measured by J. H. Stewart

ES — 34 MILES — 22 MILES — 39 MILES

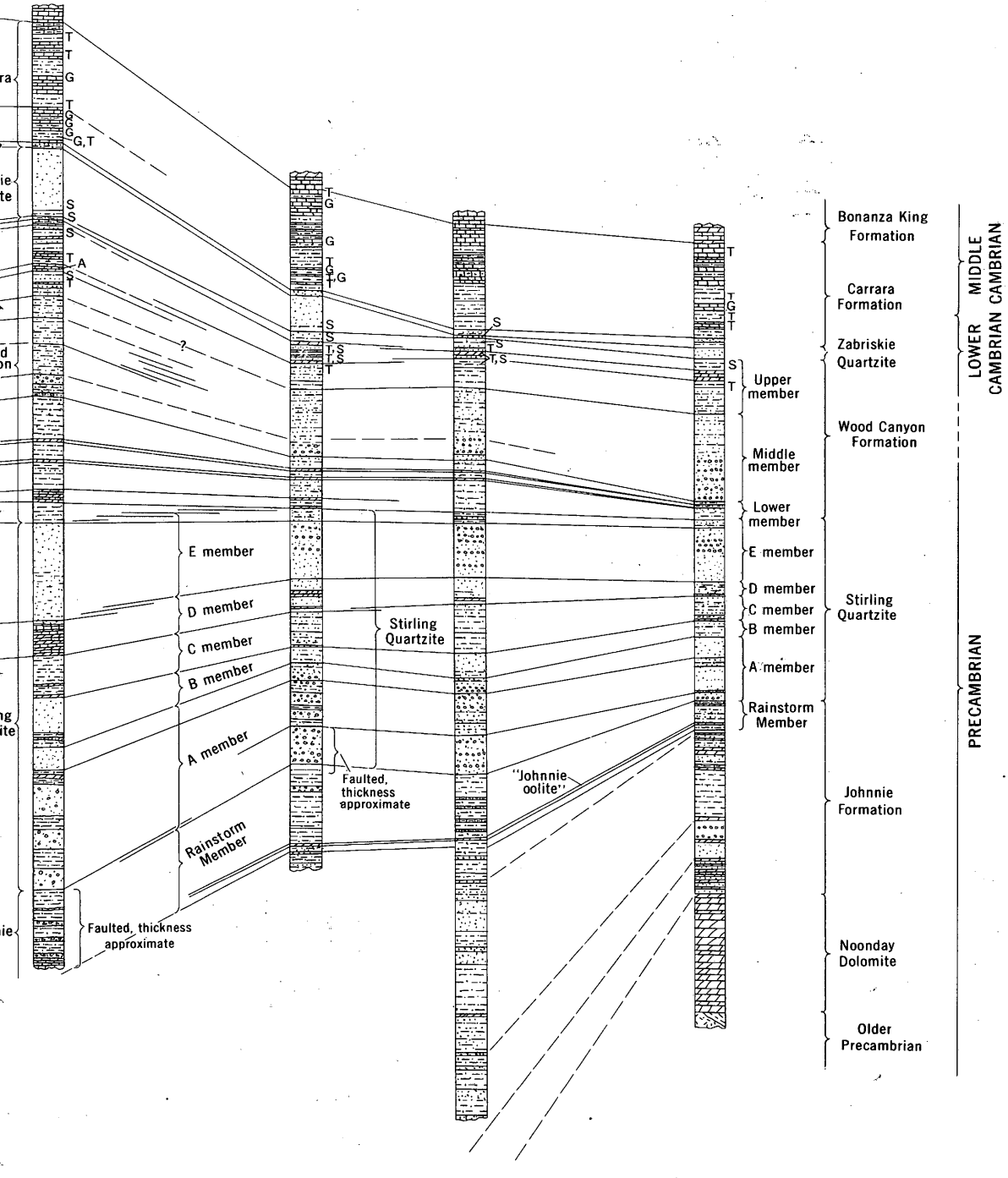


a in the southern Great Basin. Location of sections is shown on figure 1.

### Johnnie Formation

The Johnnie Formation (named by Nolan, 1929, p. 461-463) conformably overlies the Noonday Dolomite (sec. 11, fig. 2) and consists of a variety of lithologic types including green and brown phyllitic siltstone, light-colored very fine grained to coarse-grained quartzite, a few layers of conglomeratic quartzite, and minor amounts of yellowish-brown-weathering dolomite and reddish silty limestone and limy siltstone. The upper part of the Johnnie Formation consists dominantly of greenish siltstone and reddish limy siltstone or silty limestone, and has been designated the Rainstorm Member by Barnes and others (1965) for exposures in the northeast part of the Nevada Test Site (fig. 1). Locally, as in the Echo Canyon area (sec. 8, fig. 2), strata laterally equivalent to the Rainstorm Member contain minor amounts of granule conglomerate. A persistent and distinctive yellowish-brown-weathering oolitic dolomite (commonly referred to as the "Johnnie oolite") occurs near the base of the Rainstorm Member (fig. 2). This oolite is generally 6 to 12 feet thick. The Johnnie Formation may correlate with part of the Wyman Formation of the White–Inyo Mountains, but this correlation is uncertain.

### Stirling Quartzite

The Stirling Quartzite (named by Nolan, 1929, p. 463) is herein divisible into five members in the Spring Mountains–Death Valley area. These members are referred to informally as A, B, C, D, and E members, in ascending order (fig. 2). The A member consists of yellowish-gray quartzite and conglomeratic quartzite in the lower part and grayish-purple quartzite and minor amounts of purplish phyllitic siltstone in the upper part. The upper 100 feet or more of the A member is generally yellowish gray. In the Echo Canyon area (sec. 8, fig. 2), the A member contains three phyllitic siltstone units that range in thickness from about 175 to 250 feet. The uppermost phyllitic siltstone unit in Echo Canyon contains a prominent 45-foot-thick limestone and dolomite unit about 50 feet below the top.

The B member is a thin unit consisting of grayish-red-purple and grayish-purple coarse siltstone to very fine grained sandstone and minor amounts of coarse-grained quartzite. The amount of coarse-grained quartzite increases upward. Some brown-weathering sandy dolomite layers occur in the lower part of the member in the Funeral Mountains (sec. 8, fig. 2).

The C member consists of greenish-gray siltstone in the lower part and purplish siltstone and fine-grained quartzite in the upper part. The amount of purplish quartzite in the upper part of the member decreases markedly toward the northwest from the Nopah Range (sec. 11, fig. 2) and is largely replaced by green siltstone in the Echo Canyon area (sec. 8, fig. 2). Thin layers of light-brown-weathering dolomite are common in the lower 20 to 200 feet.

The D member consists, in the Echo Canyon and Bare Mountain areas (secs. 8 and 7, fig. 2), of very pale orange and light-gray dolomite and minor amounts of limestone. The upper part of the member in these areas contains some quartzite and siltstone and is transitional into the overlying E member. The D member to the south and southeast of Echo Canyon and Bare Mountain grades laterally into quartzite and dolomitic sandstone that are difficult to separate from the overlying quartzite of the E member.

The E member of the Stirling Quartzite is a thick homogeneous sequence of pale-red quartzite and conglomeratic quartzite. In Echo Canyon the lower half of the E member also contains minor amounts of siltstone and silty sandstone layers and a few brown-weathering dolomitic sandstone layers. On Bare Mountain the lower part of the E member consists of siltstone and quartzite; the siltstone constitutes about half of the lowermost part of the member, decreases in amount upward, and is absent from the top 300 feet of the member. The top 300 feet is a prominent yellowish-gray to white quartzite. Some dolomite layers also occur in the lower half of the E member on Bare Mountain.

The Stirling Quartzite thickens and contains a higher proportion of silty and carbonate strata to the northwest from the Nopah Range and Spring Mountains. In the Funeral Mountains (sec 8, fig. 2) and on Bare Mountain (sec. 7, fig. 2), silty strata and dolomite constitute a noticeable part of the Stirling, although over half of the formation is quartzite.

The A, B, and C members of the Stirling Quartzite may correlate with the upper part of the Wyman Formation, but this correlation is uncertain and is the subject of further study.

The D and E members of the Stirling Quartzite are correlated with the Reed Dolomite (named by Kirk, *in* Knopf, 1918, p. 24) of the White–Inyo Mountains region (secs. 1 and 2, fig. 2). The Reed Dolomite, which overlies the Wyman Formation, has been divided by Nelson (1962b, p. 141; 1963) into three members: a lower member composed of very pale orange dolomite; a middle member—the Hines Tongue—composed of yellowish-gray quartzite, brown-weathering dolomitic sandstone, and minor amounts of dolomite and sandy dolomite; and an upper member composed of very pale orange dolomite and local minor amounts of light-gray limestone. The D member of the Stirling Quartzite in the Funeral Mountains and

on Bare Mountain is lithologically similar to, if not identical with, the lower member of the Reed Dolomite, and these two members are considered to be correlative. The E member on Bare Mountain and the Hines Tongue in the White–Inyo Mountains area also have a similar lithology and are considered to be largely correlative. The upper member of the Reed Dolomite is apparently equivalent to the uppermost part of the E member and the lowermost part of the overlying Wood Canyon Formation, although at Bare Mountain this part of the Stirling Quartzite and Wood Canyon Formation contains only a few limestone or dolomite layers, whereas the upper member of the Reed Dolomite is predominantly dolomite.

#### Wood Canyon Formation

The Wood Canyon Formation (named by Nolan, 1929, p. 463–464) conformably overlies the Stirling Quartzite and is recognized throughout the Spring Mountains and Death Valley region. In the Bare Mountain and Bullfrog quadrangles (fig. 1), Cornwall and Kleinhampl (1964, p. J2–J3) have applied the name Daylight Formation to the rocks here considered to be the Wood Canyon Formation. Use of the name Daylight Formation is confined to these quadrangles.

The Wood Canyon Formation is herein divided into three members, referred to informally as lower, middle, and upper members. The lower member consists of grayish-olive siltstone, minor amounts of yellowish-gray quartzite, and three prominent brown-weathering layers of dolomite. The dolomite beds are quite persistent and may extend throughout much of the area of distribution of the lower member.

The lower member of the Wood Canyon Formation is correlated (fig. 2) largely with the Deep Spring Formation of the White–Inyo Mountains facies. The Deep Spring Formation (named by Kirk, *in* Knopf, 1918, p. 24) is a heterogeneous sequence of quartzite, siltstone, calcareous sandstone, limestone, and dolomite. Three members are recognized in the Deep Spring Formation (Nelson, 1962b, p. 141; 1963): a lower member consisting predominantly of limestone and dolomite; a middle member of quartzite with a limestone or dolomite unit at the top; and an upper member also of quartzite, with a limestone and dolomite unit at the top. The carbonate units at the top of the middle member and the top of the upper member of the Deep Spring Formation could be the same units as the upper two carbonate layers in the lower member of the Wood Canyon Formation (fig. 2). The Deep Spring Formation contains considerably more limestone and dolomite than the comparable part of the lower member of the Wood Canyon Formation.

The middle member of the Wood Canyon Formation consists of pale-red and grayish-red cross-stratified quartzite and minor amounts of siltstone. This member grades northwestward into finer clastic rocks that constitute the main part of the Campito Formation. The Campito Formation (named by Kirk, *in* Knopf, 1918, p. 27) consists of dark-greenish-gray to greenish-black, very fine grained quartzite and greenish-gray coarse siltstone, and is divided (Nelson, 1962b, p. 141) into a thick lower member—the Andrews Mountains Member—consisting dominantly of quartzite, and an upper member—the Montenegro Member—consisting dominantly of siltstone.

The upper member of the Wood Canyon Formation consists mostly of grayish-olive siltstone and yellowish-gray very fine grained quartzite. The quartzite commonly contains scraps of trilobites, and *Scolithus* tubes (worm borings) are common in both the quartzite and siltstone in the upper part of the member. The upper part also contains light-brown-weathering dolomite beds which are commonly oolitic and contain abundant plates of pelmatozoa. In the Echo Canyon, Bare Mountain, Titanothere Canyon, and southern Last Chance Range areas (secs. 8, 7, 6, and 5, fig. 2), limestone beds also are present in the upper part of the member; in these areas archeocyathids are found in the limestone near the base of the carbonate-bearing part of the member.

The lower part of the upper member of the Wood Canyon Formation is correlated (fig. 2) with the upper part of the Campito Formation (at least in part with the Montenegro Member of the Campito) of the White-Inyo Mountains facies. The upper part of the upper member of the Wood Canyon that contains limestone and dolomite is correlated largely with the Poleta Formation. The Poleta Formation (named by Nelson, 1962b, p. 141–142) is divided into three members (McKee and Moiola, 1962, p. 534-535; Stewart, 1965, p. A63): a lower member of archeocyathid-bearing limestone; a middle member of siltstone, quartzite, and minor amounts of limestone; and an upper member of limestone. Archeocyathids also occur, but are rare, in the upper member of the Poleta Formation. The archeocyathid-bearing limestone in the upper part of the Wood Canyon Formation in the Echo Canyon, Bare Mountain, Titanothere Canyon, and southern Last Chance Range areas appears to be a continuation of the archeocyathid-bearing limestone of the lower member of the Poleta Formation. The uppermost part of the upper member of the Wood Canyon Formation may be correlated with the basal part of the Harkless Formation (fig. 2).

### Zabriskie Quartzite

The Zabriskie Quartzite overlies the Wood Canyon Formation and is recognized throughout the Spring Mountains–Death Valley region. The Zabriskie Quartzite was described and named originally by Hazzard (1937, p. 309–310) as a member of the Wood Canyon Formation and has been raised to the rank of a formation by Wheeler (1948, p. 26) and Barnes and others (1965). In the Bare Mountain and Bullfrog quadrangles (fig. 1), Cornwall and Kleinhampl (1964, p. J3–J4) have applied the name Corkscrew Quartzite to the rocks here considered to be the Zabriskie Quartzite. Use of the name Corkscrew Quartzite is confined to these quadrangles.

The Zabriskie Quartzite is a homogeneous sequence of a pale-red fine- to coarse-grained quartzite. Some siltstone and micaceous quartzite transitional into the underlying Wood Canyon Formation are present at the base of the formation in some areas. The Zabriskie tongues out northwestward into the finer grained clastic rocks of the Harkless Formation and the lower part of the Saline Valley Formation. The Harkless Formation (named by Nelson, 1962b, p. 142) consists of grayish-olive siltstone interlayered with the fine- to coarse-grained quartzite tongues of the Zabriskie. The Saline Valley Formation (named by Nelson, 1962b, p. 142) is a laterally variable sequence of quartzite, sandstone, sandy limestone, limestone, and siltstone. The quartzite units in the lower part of the Saline Valley Formation are also considered to be tongues of the Zabriskie Quartzite. The amount of quartzite (tongues of the Zabriskie) in the Harkless and Saline Valley Formations decreased to the north in the White–Inyo Mountains area, and the Harkless and Saline Valley Formations may be almost entirely siltstone in the northwest part of the White–Inyo Mountains region (Nelson, written commun., 1962). The Harkless–Saline Valley equivalent in Esmeralda County, Nev. (Albers and Stewart, 1962, fig. 126.2), is also almost entirely siltstone.

### Carrara Formation

The Carrara Formation (named by Cornwall and Kleinhampl, 1961) of the Spring Mountains–Death Valley facies consists of gray limestone, light-brown-weathering silty limestone, and green siltstone. The lowermost part of this formation is correlative with the upper part of the Saline Valley Formation (fig. 2). Separate limestone units in the lower third of the Carrara Formation coalesce northwestward to form the Mule Spring Limestone (named by Nelson, 1962b, p. 142)—a uniform gray limestone unit commonly containing concretionary algal structures *(Girvanella)*. As recently described by Nelson (1965), the upper part of the Carrara Formation is correlative with the newly named Monola Formation of Middle Cambrian age of the White–Inyo Mountains area.

## REFERENCES


Albers, J. P., and Stewart, J. H., 1962, Precambrian(?) and Cambrian stratigraphy in Esmeralda County, Nevada: Art. 126 *in* U.S. Geol. Survey Prof. Paper 450–D, p. D24–D27.

Barnes, Harley, Christiansen, R. L., and Byers, F. M., Jr., 1965, Geologic map of Jangle Ridge, Nye County, Nevada: U.S. Geol. Survey Geol. Quad. Map GQ–363.

Cornwall, H. R., and Kleinhampl, F. J., 1961, Geology of the Bare Mountain quadrangle, Nevada: U.S. Geol. Survey Geol. Quad. Map GQ–157, scale 1:62,500 [1962].

——— 1964, Geology of Bullfrog quadrangle, and ore deposits related to Bullfrog Hills caldera, Nye County, Nevada, and Inyo County, California: U.S. Geol. Survey Prof. Paper 454–J, p. J1–J25.

Hazzard, J. C., 1937, Paleozoic section in the Nopah and Resting Springs Mountains, Inyo County, California: California Jour. Mines and Geology, v. 33, no. 4, p. 273–339.

Knopf, Adolph, 1918, A geologic reconnaissance of the Inyo Range and the eastern slope of the southern Sierra Nevada, California, with a section on the stratigraphy of the Inyo Range, by Edwin Kirk: U.S. Geol. Survey Prof. Paper 110, 130 p.

Maxson, J. H., 1935, Pre-Cambric stratigraphy of the Inyo Range [abs.]: Geol. Soc. America Proc. 1934, p. 314.

McKee, E. H., and Moiola, R. J., 1962, Precambrian and Cambrian rocks of south-central Esmerelda County, Nevada: Am. Jour. Sci., v. 260, no. 7, p. 530–538.

Nelson, C. A., 1962a, Age of the Johnnie Formation [abs.]: Geol. Soc. America Spec. Paper 68, p. 45–46.

——— 1962b, Lower Cambrian–Precambrian succession, White-Inyo Mountains, California: Geol. Soc. America Bull., v. 73, no. 1, p. 139–144.

——— 1963, Preliminary geologic map of the Blanco Mountain quadrangle, Inyo and Mono Counties, California: U.S. Geol. Survey Min. Inv. Field Studies Map MF–256, scale 1:48,000.

——— 1965, Monola Formation, *in* Cohee, G. V., and West, W. S., Changes in stratigraphic nomenclature by the U.S. Geological Survey, 1963: U.S. Geol. Survey Bull. 1194–A, p. 29–33.

Nolan, T. B., 1924, Geology of the northwest portion of the Spring Mountains, Nevada: Yale Univ., New Haven, Conn., Ph.D. thesis.

——— 1929, Notes on the stratigraphy and structure of the northwest portion of Spring Mountain, Nevada: Am. Jour. Sci., 5th ser., v. 17, p. 461–472.

Scott, K. M., 1960, Geology of the Waucoba Springs area, Inyo Mountains, California: California Univ. at Los Angeles, M.S. thesis, 109 p.

Stewart, J. H., 1965, Precambrian and Lower Cambrian strata in the Last Chance Range area, Inyo County, California, *in* Cohee, G. V., and West, W. S., Changes in stratigraphic nomenclature by the U.S. Geological Survey, 1964: U.S. Geol. Survey Bull. 1224–A, 77 p. [1966].

Wheeler, H. E., 1948, Late pre-Cambrian–Cambrian stratigraphic cross section through southern Nevada: Nevada Univ. Bull., v. 42, no. 3, Geology and Mining ser. no. 47, 61 p.

# LOCAL THICKENING OF BASALTS AND LATE TERTIARY SILICIC VOLCANISM IN THE CANYON CITY QUADRANGLE, NORTHEASTERN OREGON

By T. P. THAYER and C. ERVIN BROWN, Washington, D.C.

*Abstract.*—Thickening of basalts of the Columbia River Group to 6,000 feet along the Monument swarm of feeder dikes implies that the overlying Mascall Formation probably was at least 6,000–7,000 feet thick at Picture Gorge. Over much of the present Canyon City quadrangle the Columbia River Group and stratigraphically equivalent Strawberry Volcanics probably attained a thickness of 8,000 feet or more in early Pliocene time. The nature of the Mascall Formation reflects the former existence of a thick regional cover of silicic volcanic rocks, only relatively thin remnants of which are preserved in isolated structural basins.

The basalts of the Columbia Plateau and the volcanic rocks of Miocene and early Pliocene age in the adjacent part of the Basin and Range province have for some time been known in a general way to interfinger or intergrade. Only in recent years, however, has enough of the border zone been mapped in sufficient detail to reveal a rather close correlation within the two provinces between composition of the rocks, type of volcanism, and later deformation in the region around John Day, in northeastern Oregon (Thayer, 1957). The Mascall Formation was first recognized in 1957 as a derivative of dacitic and rhyolitic eruptions that were coeval, at least partly, with basaltic flows from a system of fissures now represented by the Monument dike swarm. Since 1957, detailed mapping by R. E. Wilcox and R. V. Fisher (in press), of the U.S. Geological Survey, and the authors (Brown and Thayer, in press; Thayer and Brown, 1966) has provided a basis for a much better understanding of the stratigraphy of the rocks and their relations to the eruptive sources. Local thickening of basalts along the dike swarm, while interesting in itself, has indirect regional implications of much greater import.

## COLUMBIA RIVER GROUP

The Columbia River Group in the Canyon City quadrangle (Brown and Thayer, in press) includes the Picture Gorge Basalt and the overlying Mascall Formation, which locally interfingers with the Picture Gorge. In the central and southern part of the area a rhyolitic marginal facies of the group comprises, in addition to basalts, interfingering rhyolitic flows and tuffs (fig. 1). The Strawberry Volcanics in the southeastern part of the quadrangle are equivalent in age to the Columbia River Group as a whole. The discussion here is concerned mainly with the units of the Columbia River Group (Brown and Thayer, in press) which occur within 20–25 miles of Picture Gorge (fig. 2). Some of the flows in the upper part of the thick basalt sections may be equivalent to the Yakima Basalt of the Columbia River Group in Washington. The petrology of the basalts has been described elsewhere (Waters, 1961, p. 594; Thayer and Brown, in press; Thayer, 1957), and is not of primary concern here. Likewise, the structural and stratigraphic relations of the Clarno and John Day Formations, which underlie the group, are not pertinent to the present problem except where specifically referred to; the two formations have therefore been omitted from figure 2 for simplicity.

### Picture Gorge Basalt and related flows

At the type locality (fig. 2) the Picture Gorge Basalt consists of 14 flows, nearly equal in thickness, which together are about 1,500 feet thick; they lie on the John Day Formation (fig. 3). In the valley of Flat Creek 10 miles southeast of Picture Gorge (fig. 2), a section that is 6,000 feet thick and comprises at least 50 basalt flows and 500 feet of intercalated bouldery gravels appears to be stratigraphically about equivalent to the Picture Gorge Basalt. The lower flows in the section appear identical with those at Picture Gorge, but the individual upper flows range from about 20 to 200 feet, the flows have a much larger proportion of top and bottom breccia, and they may be equivalent in part to the Yakima Basalt. The thick

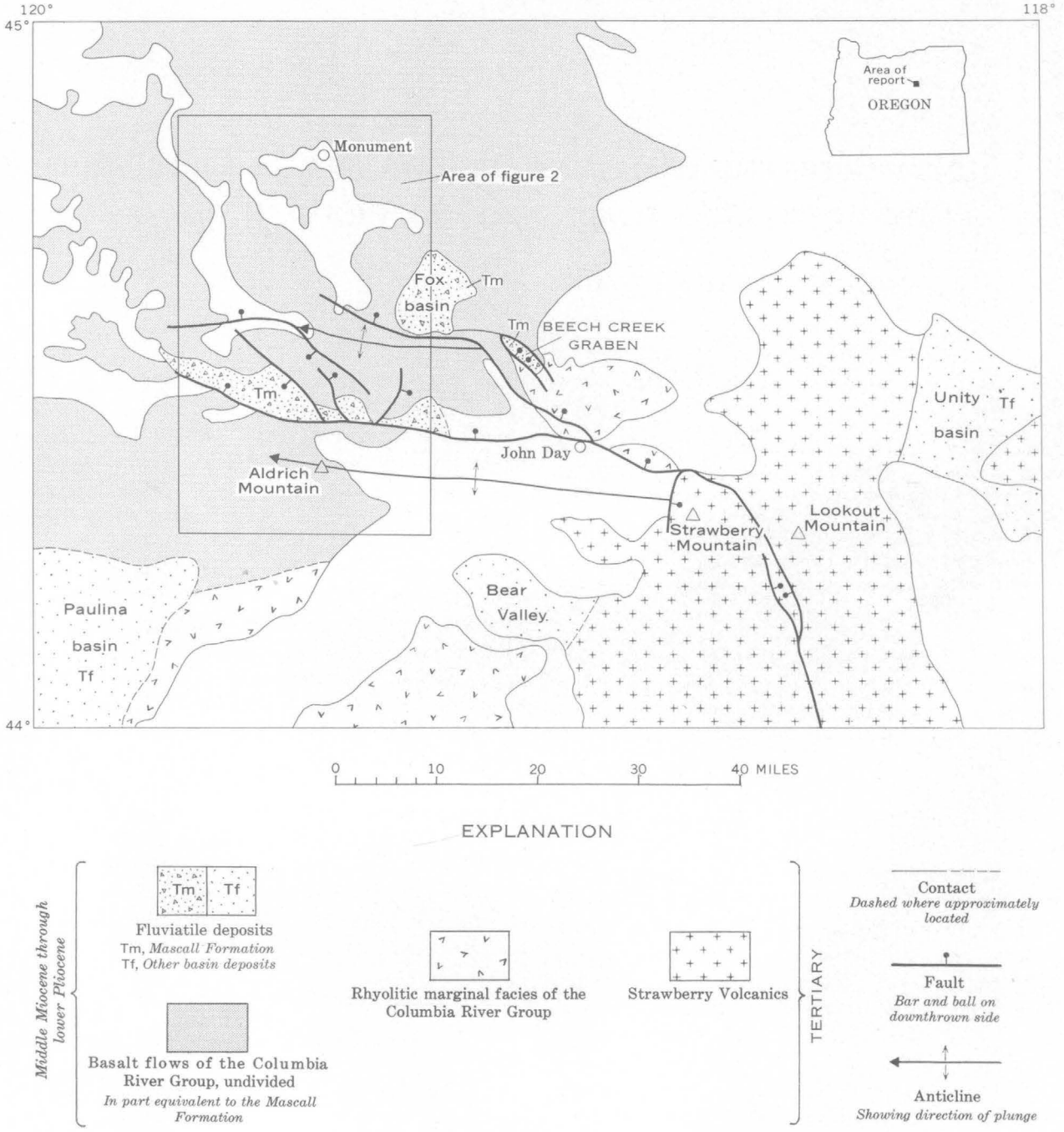


FIGURE 1.—Geologic index map of the Canyon City quadrangle, Oregon, showing distribution of the Columbia River Group and equivalent rocks.

section here dips vertically between the John Day fault and a fault to the south; it is a segment of the steep north limb of the strongly asymmetrical Aldrich Mountain anticline. Exposures nearby show that the flows lie unconformably on the Clarno Formation (Thayer and Brown, 1966) and are conformable with the overlying Mascall Formation. Good exposures and the variations in lithology preclude duplication of any parts of the section by faulting. Six miles east of Flat Creek the basalts are only 2,500 feet thick where they dip vertically between the Clarno and Mascall Formations. A conformable contact between the Mascall Formation and Picture Gorge Basalt is exposed south of the John Day fault 3 miles from the east edge of the map area (fig. 2), and north of the fault the contact appears to be conformable every-

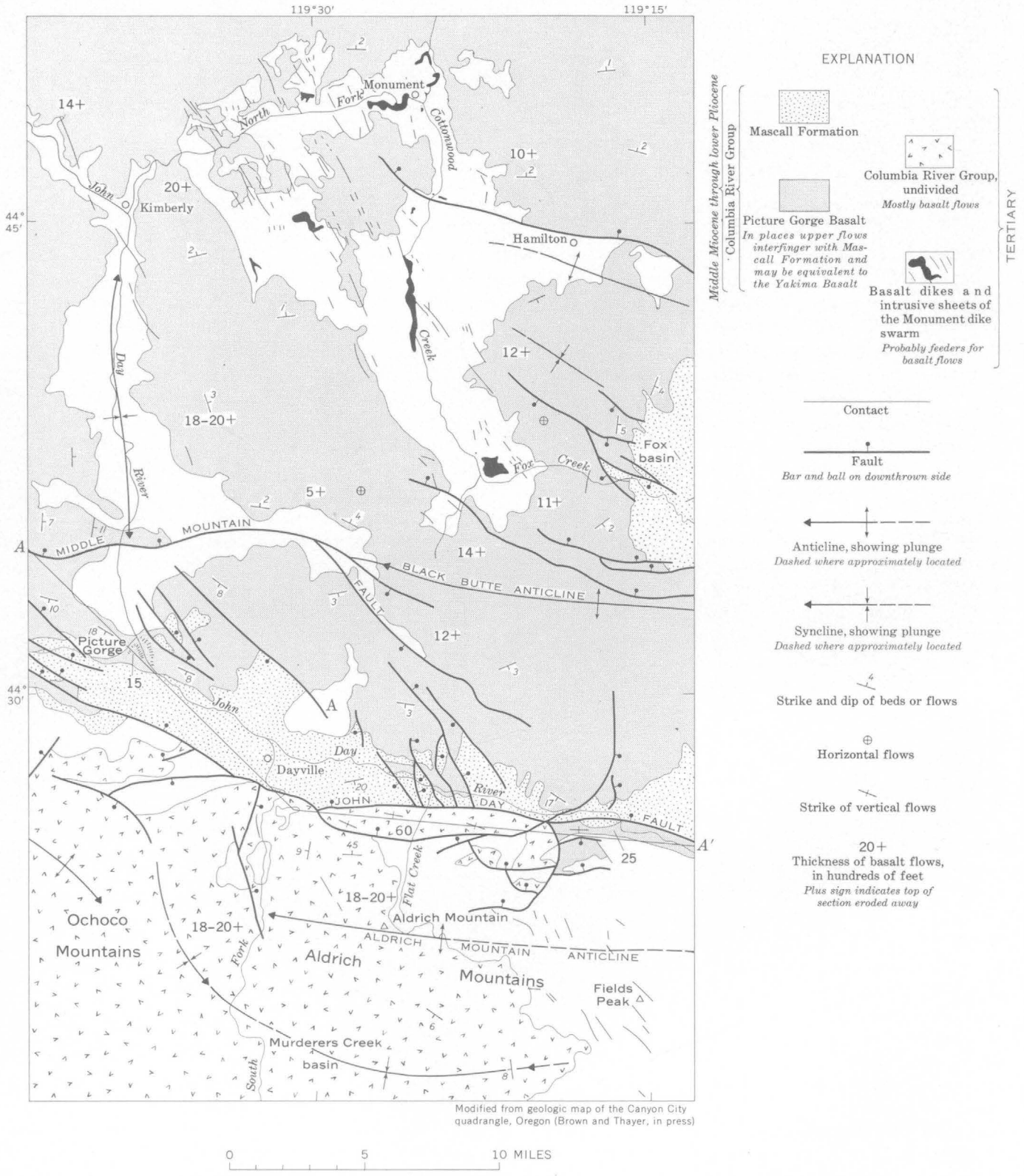


FIGURE 2.—Generalized geologic map of part of the Canyon City quadrangle, Oregon, showing rocks of the Columbia River Group, the Monument dike swarm, and thicknesses of basalt flows. Excepting a large unpatterned area (A) of Rattlesnake Formation (Pliocene) immediately northeast of Dayville, older and younger rocks are not shown.

211-690 O—66——6

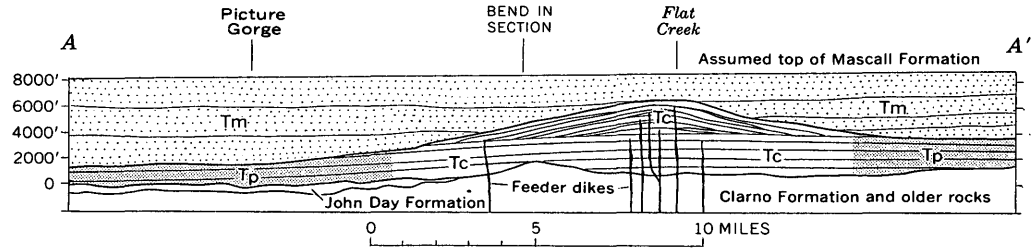


FIGURE 3.—Restored section along the John Day River valley (fig. 2, *A–A'*), showing inferred relations of the Mascall Formation (Tm) and basalts of the Columbia River Group (Tc) and Picture Gorge Basalt (Tp) in early Pliocene time. Datum is approximately the base of Picture Gorge Basalt at Picture Gorge; vertical exaggeration × 2.

where. Although the unconformable relations shown in figure 3 result from the vertical exaggeration of the section, such relationships should be expected where fine-grained water-laid sediments cover flows dipping away from the center of the ridge. Exposures, however, are not good enough to reveal angular discordances of the magnitude indicated.

Farther north, around the west side of Fox basin, the basalts of the group lie on the John Day Formation and dip gently eastward toward and under the basin filling of Mascall Formation. The total thickness of the basalt flows there probably is 1,200–1,500 feet. Near the northwest corner of the basin, where the rocks dip 4° (fig. 2), a 200-foot sequence of 4 basalt flows thins eastward within a mile to only 1 flow 15 feet thick, between water-laid tuffs. One or more thin basalt flows are interbedded with tuffs and gravels in the southwestern part of the basin, and along the southern margin basalts and interbedded bouldery conglomerates wedge out toward the center of the basin. The upper flows here may be equivalent to the Yakima Basalt.

### Mascall Formation

The Mascall Formation consists mostly of light-colored, water-laid, altered volcanic ash in which thin beds of well-rounded, polished pebble gravels are erratically distributed. Lignitic lenses as much as 5 feet thick have been exposed in roadcuts and in an old mine 4 to 5 miles east of Flat Creek. Most of the pebbles are of hard rocks such as chert, metavolcanic rocks, and intrusive rocks of pre-Tertiary age. The proportion of gravels and size of pebbles increase eastward, and some tuff probably of ash-flow origin is present near the east edge of the map area (fig. 2). The greatest known thickness of the Mascall Formation is 2,090 feet, measured south of Picture Gorge (Merriam and others, 1925, p. 52); equal or greater thicknesses very probably are preserved farther east, but are concealed or complexly faulted.

Although the Mascall Formation in the John Day River valley is separated by a gap of 10 miles from the nearest rocks of equivalent age to the east, their mutual relations can be traced by means of deposits in Fox basin and the Beech Creek graben (fig. 1). Lithologically, most of the deposits in the Fox basin are indistinguishable from those in the John Day Valley, although the conglomerates along the south side of the basin consist mostly of locally derived basaltic debris. In the Beech Creek graben 350 to 400 feet of pumice breccia and welded tuff with Mascall-like gravel at the base overlies basalt flows and interfingers southeastward with basalt. Where the graben dies out to the southeast, the flows and tuffs in it merge with the rhyolitic marginal facies of the Columbia River Group. This facies comprises basaltic and andesitic flows intercalated with rhyolitic water-laid debris, welded tuffs and thick lenticular rhyolite flows from local vents, and some conglomerate; it may be as much as 2,000 feet thick. The rhyolitic marginal facies, in turn, is separated from the Strawberry Volcanics (6,500 feet thick) by a 2-mile gap, but there is little doubt that the two units once interfingered (Thayer, 1957; Brown and Thayer, in press). The Mascall Formation, therefore, is believed to have accumulated as a flood plain or piedmont apron that extended to the north and west out over the basalt plateau many miles from volcanoes that rimmed it on the south and east.

## RATTLESNAKE FORMATION AND YOUNGER SEDIMENTARY DEPOSITS [1]

The Rattlesnake Formation, of middle to late Pliocene age in this area (Merriam and others, 1925, p. 53; Brown and Thayer, in press), consists of fanglomerate and poorly sorted finer sediments, deposited under semiarid conditions in structural lowlands formed by post-Mascall erosion and deformation. A welded rhyolite tuff in the middle of the formation

[1] Most of the Rattlesnake Formation and younger deposits have been left off the geologic map (fig. 2) to keep the map more readable at its present scale. The relationships of the Rattlesnake Formation are shown in Thayer and Brown (1966) and Brown and Thayer (in press).

forms prominent rimrocks along the John Day River valley. The maximum observed thickness of the Rattlesnake Formation in the John Day structural trough is about 700 feet at a section exposed just southeast of Dayville; the total thickness may be as much as 1,000 feet. The Rattlesnake lies unconformably across the Mascall Formation and Picture Gorge Basalt; in places it lies across the John Day fault, but elsewhere it is cut by the fault. Near the east edge of the map area (fig. 2) the Rattlesnake Formation appears to have been folded and faulted down about 1,000 feet below remnants of the welded tuff preserved on the rim of Picture Gorge. These relationships of the Rattlesnake Formation show that: (1) the Mascall Formation had been stripped completely from large areas by early middle Pliocene time, and (2) the basalts in the Black Butte and Aldrich Mountain anticlines have been exposed to erosion continuously since then.

## ORIGINAL THICKNESS OF THE COLUMBIA RIVER GROUP IN THE FLAT CREEK–PICTURE GORGE AREA

The thick section of basalt along Flat Creek and its relation to the Mascall Formation provide a unique measure for the minimum original thickness of the Mascall Formation and, consequently, of the Columbia River Group. The local variations in thickness of the basalts in the map area are believed to be related to the Monument dike swarm (Thayer, 1957, p. 234; Waters, 1961, p. 587) as their principal source. The thickest preserved section of the flows is directly on strike with the numerous feeder dikes in the Aldrich Mountains. The abundance of flow breccia and the thinness of the upper flows in Flat Creek indicate that a high ridge was built up along the present trend of the Monument dike swarm; the great thickness is not due to ponding of highly fluid flows in a low area. If the base of the basalts is assumed to have been horizontal, 4,500 feet of relief is indicated on their surface between Picture Gorge and Flat Creek, and 3,500 feet between Flat Creek and the area 6 miles to the east (fig. 3). The topographic relief of the ridge probably never exceeded a few hundred feet. The basalts, however, buried a surface that had a local relief of at least 2,000 feet, so their base may have been significantly higher on the Clarno Formation at Flat Creek than on the soft John Day Formation (Fisher, 1963) at Picture Gorge. Interfingering of basalts with the Mascall Formation in the Fox basin would result from eruptions near the dikes now exposed in the head of Cottonwood Creek. The 1,200–1,400 feet of basalt west of Fox basin suggests a sheet of uniform thickness from there at least as far as Picture Gorge, but this is misleading. As indicated previously, the basalts around the head of Cottonwood Creek have been exposed to erosion since early middle Pliocene time, so they represent only part of the original section. The marked local decrease in thickness from 1,400 feet to 500 feet north of the Black Butte anticline is due to a combination of relief on the prebasalt surface and erosion of the basalt. Farther north, in the Kimberly–Monument area, the original thickness of the basalt is not known, but about 2,000 feet of flows remains in a shallow syncline east of Kimberly.

The stratigraphic relations around Fox basin show that Mascall deposition began while fissure eruptions were still building up the ridge, but along the present line of the John Day River the lava ridge must have stood above the Mascall until basaltic eruptions ceased; this implies that the crest of the ridge sloped northward. The known thickness of Mascall immediately north of the John Day fault on a small horst in the vicinity of Flat Creek is 800–1,000 feet, and the thickness remaining in nearby grabens is probably at least twice as much. An assumed thickness of 1,500–2,000 feet of Mascall originally covering the basalts is believed to be conservative. It seems likely, therefore, that the Columbia River Group was 7,500–8,000 feet thick in the Flat Creek–Picture Gorge area, with the relative proportions of Mascall Formation and basalt reversed at the two localities (see fig. 3).

## MAGNITUDE OF LATE MIOCENE AND EARLY PLIOCENE SILICEOUS VOLCANISM

If our conceptions of the original volcanic topography of the Picture Gorge and Yakima Basalts are at all valid, and the estimates of the thickness of the Mascall Formation at Picture Gorge are anywhere near correct, the original volume of the Mascall must have been many hundreds of cubic miles. The Mascall Formation proper should be regarded as a mixture of some ash-fall material with the fluviatile debris carried away from centers of explosive volcanic activity around the margins of the basalt plateau. The remaining predominantly basaltic and andesitic flows in the Columbia River Group and Strawberry Volcanics are only the lower part of the original volcanic section, and therefore are not necessarily representative of the entire section, especially of the upper part which has vanished. Rhyolitic to dacitic flows and fragmental rocks form an important part of the marginal facies of the Columbia River Group, and are especially abundant in the Strawberry Volcanics between Strawberry Mountain and Bear Valley (Brown and Thayer, in press). One important center of

rhyolitic eruptions was located 1½–2 miles south-southwest of Strawberry Mountain.

Deposits preserved in Unity basin (fig. 1) imply that the Mascall Formation probably was even thicker than the Flat Creek section suggests. The bedded section in the Unity basin is several hundred to a few thousand feet thick, and has yielded several species of lower Pliocene vertebrate fossils (J. A. Shotwell, written commun., 1956). Along the western edge of the basin the beds interfinger with basalts of the Strawberry Volcanics, and obsidian flow breccia is interbedded along the southern margin. During the early Pliocene, while the eruptive centers in the vicinity of Strawberry and Lookout Mountains were shedding debris northeastward and northwestward, other centers south of the present Aldrich Mountains (fig. 2) were sources of materials that probably moved northward and westward. Absence of Pliocene fossils in the Mascall can be explained by removal of the higher parts of the original section, which may have substantially exceeded the estimated thickness of 6,000–6,500 feet.

There now remains little doubt that volcanic rocks equivalent in age to the Columbia River Group blanketed the entire Blue Mountain region to the northeast, and buried all the older rocks. Restoration of the early Pliocene surface by undoing all the post-Mascall deformation would reduce the pre-Columbia relief in the region well below the inferred thickness of the Columbia River Group. The region is envisioned, therefore, as having been a volcanic plateau above which rose eruptive centers, like the cluster in the vicinity of Strawberry and Lookout Mountains, (fig. 1) (Brown and Thayer, in press). The Mascall Formation and deposits of the same age in Bear Valley and in the Unity and Paulina basins, we believe, all merged in one extensive volcanic sheet. The upper deposits appear to have been stripped before the basins reached their ultimate depth, just as the Mascall was eroded before final sinking of the John Day valley structural trough. The stratigraphic relationships of the Mascall Formation to the upper basalt flows of the Columbia River Group are believed to have been like those described by Waters (1961, p. 606) between the Yakima Basalt and Ellensburg Formation, 150 miles northwest of the report area.

The relations postulated for the Canyon City quadrangle (fig. 2) in early Pliocene time are comparable to those now obtaining in the region around Crater Lake and Newberry crater in west-central Oregon (Wells and Peck, 1961). There, the extensive pumice blankets and dacitic products from Quaternary eruptions would be removed first by prolonged erosion, along with the higher silicic parts of the cones. The resistant rocks that remained would consist largely of the andesitic and basaltic flows of the High Cascades and the more massive flow sequences in the plateau to the east.

In conclusion, the fluviatile deposits similar to the Mascall Formation which are preserved in various structural basins in the Canyon City quadrangle might be compared to puddles left after a flood. The depth of a flood is measured, not by the depth of the puddles, but by high-water marks. Although it does not preserve the actual "high water" mark of the flood of debris that constituted the Mascall Formation, the 6,000-foot basalt section in Flat Creek, like a mud-covered boulder, provides information on the minimum height of the flood. The inferred original 6,000–7,000-foot thickness of the Mascall Formation at Picture Gorge implies a much more massive outpouring of silicic volcanic products in late Miocene and early Pliocene time around the southern edge of the Columbia Plateau than their present remnants would suggest. The northern limit of the original Mascall Formation can only be conjectured.

## REFERENCES


Brown, C. Ervin, and Thayer, T. P., in press, Geologic map of the Canyon City quadrangle, northeastern Oregon: U.S. Geol. Survey Misc. Inv. Map, I–447.

——— in press, Geologic map of the Mount Vernon quadrangle, Grant County, Oregon: U.S. Geol. Survey Geol. Quad. Map GQ–548.

Fisher, R. V., 1963, Zeolite-rich beds of the John Day Formation, Grant and Wheeler Counties, Oregon: Oregon State Dept. Geol. Mineral Industries, The Ore Bin, v. 25, p. 185–197.

Merriam, J. C., Stock, Chester, and Moody, C. L., 1925, The Pliocene Rattlesnake Formation and fauna of eastern Oregon, with notes on the geology of the Rattlesnake and Mascall deposits: Carnegie Inst. Washington Pub. 347, p. 43–92.

Thayer, T. P., 1957, Some relations of later Tertiary volcanology and structure in eastern Oregon, in v. 1 *of* Vulcanología del Cenozoico: Internat. Geol. Con., 20th, Mexico, D. F., 1956, [Trabajos], sec. 1, p. 231–245.

Thayer, T. P., and Brown, C. Ervin, 1966, Geologic map of the Aldrich Mountain quadrangle, Grant County, Oregon: U.S. Geol. Survey Geol. Quad. Map GQ–438.

Waters, A. C., 1961, Stratigraphic and lithologic variations in the Columbia River Basalt: Am. Jour. Sci., v. 259, p. 583–611.

Wells, F. G., and Peck, D. L., 1961, Geologic map of Oregon west of the 121st meridian: U.S. Geol. Survey Misc. Inv. Map, I–325.

Wilcox, R. E., and Fisher, R. V., in press, Geologic map of the Monument quadrangle, Grant County, Oregon: U.S. Geol. Survey Geol. Quad. Map GQ–541.

# FORAMINIFERA FROM THE ARCTIC OCEAN OFF THE EASTERN SIBERIAN COAST

By RUTH TODD and DORIS LOW, Washington, D.C.

*Abstract.*—A composite fauna of 56 species of Foraminifera is recorded from bottom sediments of the continental shelf along the Arctic coast of eastern Siberia. The fauna is impoverished, most of the specimens belonging in *Elphidium, Buccella, Cassidulina,* and various agglutinated genera, and there are many aberrant individuals. Nearly all the species are previously known Arctic inhabitants, and about half are also known in the Antarctic. The brackish-water species *Trochamminula fissuraperta* occurs off the mouths of large Siberian rivers.

Foraminifera from various coasts and islands of the Arctic Ocean have been studied in considerable detail and are fairly well known (Brady 1881; Norvang, 1945; Cushman, 1948; Phleger, 1952; Loeblich and Tappan, 1953; Jarke, 1960; Mayer, 1962; Stschedrina, 1962; Cooper, 1964; Nagy, 1965). However, since a 1901 expedition that collected 3 samples in the Laptev Sea and 3 from north of the New Siberian Islands (Awerinzew, 1911), nothing has been published on the Foraminifera of the shallow shelf along the eastern part of the Arctic coast of Siberia. To the west of this area, the Foraminifera in upper Tertiary and Quaternary sediments in some boreholes taken in the lower reaches of the Yenisey Valley, and in a few sea-bottom cores taken in the estuary of the Yenisey River and in the Kara Sea off the mouth of this river, are reported by Zagorskaya and others (1965, fig. 2, tables 9–21). The impoverished fauna resulting from subnormal marine conditions on the shallow shelf beneath the Laptev, East Siberian, and Chukchi Seas provides an interesting comparison with the better known Arctic Foraminifera.

## THE *NORTHWIND* TRAVERSE

In the late summer of 1963, the USCG cutter *Northwind* (WAGB–282) traversed the eastern part of the northern coast of Siberia as far west as long 115° E. Entering the Arctic Ocean through Bering Strait, the expedition sailed through the Chukchi Sea, the East Siberian Sea, behind the New Siberian Islands, around the delta of the Lena River, and into the Laptev Sea, nearly to the Taimur Peninsula which separates the Laptev Sea from the Kara Sea farther westward. The area traversed extends from about long 168° W. to long 115° E. between lat 65° and 76° N.

These offshore areas of eastern Siberia consist of a shallow shelf having less-than-normal marine salinity even in the bottom water (Zenkevitch, 1963, p. 255–269). In the western part of this area, water from the Arctic Ocean floods up onto the coastal shelf while the fresh-water discharge of the large Siberian rivers—the Khatanga, Lena, and Yana—spreads out over the Arctic bottom water for as much as several hundred miles. To the east, Pacific waters enter over the shallow threshold of Bering Strait and circulate within the Chukchi Sea (Zenkevitch, 1963, text fig. 111).

## ENVIRONMENTAL EFFECTS ON FORAMINIFERA

From data obtained by the *Northwind* and supplied by the National Oceanographic Data Center, we have summarized below certain environmental conditions that probably affect and may in part control the local distribution of Foraminifera over the region studied. The *Northwind* cruise corroborates by specific data the general statements of Zenkevitch (1963) regarding the dilution of the surface waters by river outflow.

Table 1 gives the observed range and mean of salinity and temperature of surface water and bottom water at the oceanographic stations from which our samples came.

We have grouped the samples into four categories on the basis of relative abundance (11 rich samples, 19 good to fair samples, 46 poor samples, and 26 barren samples) to facilitate seeking a correlation between richness or sparseness of the Foraminifera fauna and

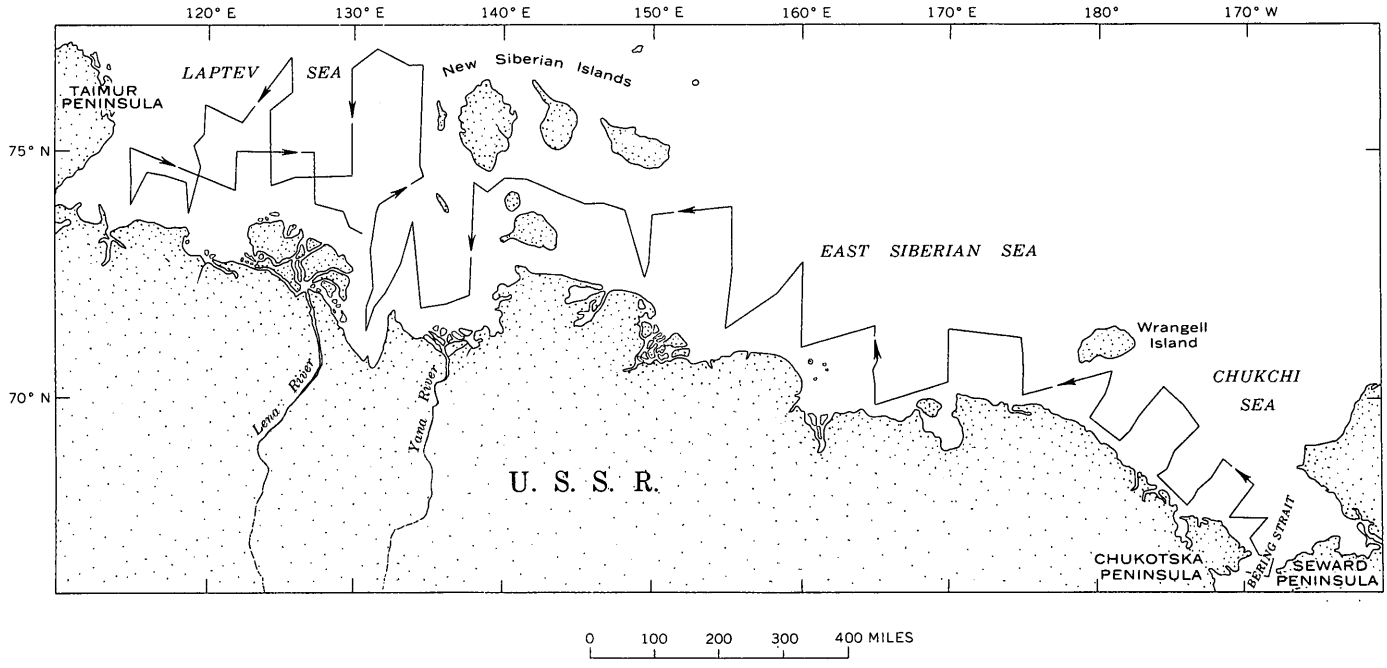


FIGURE 1.—Eastern Siberian coast of the Arctic Ocean and approximate route of the expedition.

TABLE 1.—*Salinity and temperature of surface and bottom waters*

| | Surface water | | | | | | Bottom water | | | | | |
|---|---|---|---|---|---|---|---|---|---|---|---|---|
| | Salinity (‰) | | | Temperature (°C) | | | Salinity (‰) | | | Temperature (°C) | | |
| | High | Low | Mean | High | Low | Mean | High | Low | Mean | High | Low | Mean |
| Chukchi Sea (20 stations) | 32. 74 | 2. 94 | 23. 41 | +6. 41 | −0. 06 | +3. 05 | 33. 35 | 31. 34 | 32. 58 | +4. 56 | −1. 80 | +1. 02 |
| East Siberian Sea (30 stations) | 29. 95 | 3. 64 | 15. 48 | +3. 76 | −1. 30 | −. 25 | 33. 00 | 9. 48 | 26. 89 | +3. 20 | −1. 72 | −1. 14 |
| Behind New Siberian Islands (8 stations) | 23. 54 | 14. 04 | 18. 70 | −. 47 | −. 99 | −. 83 | 32. 00 | 25. 25 | 28. 67 | −1. 20 | −1. 52 | −1. 35 |
| Laptev Sea (44 stations) | 32. 26 | 2. 56 | 14. 34 | +3. 75 | −1. 72 | +. 35 | 33. 86 | 11. 85 | 30. 04 | −. 36 | −1. 83 | −1. 51 |

TABLE 2.—*Observed range and mean of salinity and pH of bottom water for bottom samples grouped according to richness of their foraminiferal faunas*

| Sample groups | Salinity (‰) | | | pH | | |
|---|---|---|---|---|---|---|
| | High | Low | Mean | High | Low | Mean |
| Rich (11 samples) | 33. 86 | 31. 18 | 32. 51 | 8. 28 | 7. 78 | 8. 05 |
| Good to fair (19 samples) | 33. 75 | 22. 91 | 30. 56 | 8. 19 | 7. 25 | 7. 83 |
| Poor (46 samples) | 33. 72 | 11. 85 | 29. 21 | 8. 19 | 7. 26 | 7. 77 |
| Barren (26 samples) | 33. 72 | 9. 48 | 27. 96 | 8. 15 | 7. 27 | 7. 74 |

environmental factors. Table 2 gives the observed range and mean of salinity and pH of the bottom water (the deepest water samples that were obtained —usually within 1 or 2 meters of the bottom, and never more than 4 meters above the bottom) for these groups of samples.

We conclude that extremely low salinity inhibits the development of these Foraminifera faunas but that Foraminifera do not occur in all samples where the salinity is normal. Undoubtedly many factors other than salinity affect the local development of Foraminifera faunas along this shallow shelf sea; it may even be that distribution is haphazard, without controlling environmental influences.

## NATURE AND SIGNIFICANCE OF THE FAUNA

A small portion (about 20 ml) of each of 105 samples, from nearly 200 samples dredged by the *Northwind* between August 7 and September 11, was selected for examination for Foraminifera (table 3). In 26 of the 105 samples no identifiable Foraminifera were

observed. However, in some of these barren samples, as well as in most of the others, various kinds of organic remains were observed. Among these remains are diatoms, ostracodes, minute pelecypods and gastropods, bryozoans, indeterminate spicules, calcareous plates, worm tubes, fish teeth, arenaceous tubes of indeterminate origin, and possibly plant material.

The 79 Foraminifera-bearing samples yielded a composite fauna of 56 identified species (plus 5 or 6 additional indeterminate ones), but the maximum number of species present in any individual sample is 19. The mean number of species per sample is 4.6, as compared with the following mean numbers per sample at comparable depths in other Arctic regions: 27 around Point Barrow (Loeblich and Tappan, 1953, table 1), and 18 in the Canadian Arctic (Phleger, 1952, table 1). The range of depth at which the samples were taken is 10 to 55 meters, and the maximum distance from shore is about 175 miles.

The Foraminifera fauna is an impoverished one consisting of few specimens, fewer species than is normal for Arctic assemblages, and specimens mostly smaller and less well developed than normal for the species. Its elements consist chiefly of arenaceous genera and of species of the calcareous genus *Elphidium*. No planktonic Foraminifera were observed. In some samples, specimens are fragmentary as if their calcareous tests had been leached, although no pH readings were low enough to suggest acidic bottom water.

We noted no correlation between bottom type (sandy or muddy) and type of assemblage (predominantly arenaceous or calcareous). There seems to be no distinct pattern of richness or barrenness of samples, nor any preferred association of species with one another. In some samples the entire assemblage is composed of a single species or not more than three species. For example, sample 189 contained only *Ammotium cassis* (25 specimens), and sample 149 contained 51 specimens of *A. cassis* and 1 of *Adercotryma glomeratum*, but nothing else. Distribution appears to be haphazard for most species; possibly they exist in small transitory colonies.

Freak or aberrant specimens were observed with a frequency unexpectedly high for Foraminifera. High frequency of aberrant individuals is usually attributed to unfavorable habitats, such as low salinity, stagnant water, and large seasonal variation in water conditions. Arnal (1955), in seeking abnormal specimens, found high frequencies in Playa del Rey, a stagnant coastal lagoon, and in the Salton Sea around areas of fresh-water influx. On Martha's Vineyard we found a comparable high frequency of aberrant individuals of

TABLE 3.—*Locality and depth of bottom-sediment samples*

[Sample number is not identical with *Northwind* oceanographic station number because several samples were taken at some stations.]

| Date of collection (1963) | Sample | Latitude | Longitude | Depth (meters) |
|---|---|---|---|---|
| Aug. 7 | 1 | 65°36′ N. | 169°50′ W. | 42. 7 |
| 7 | 2 | 65°29.3′ | 169°21.5′ | 42. 7 |
| 7 | 3 | 65°26′ | 168°53′ | 51. 8 |
| 7 | 4 | 65°23.5′ | 168°27.5′ | 50 |
| 7 | 5 | 65°59.6′ | 168°27.3′ | 55 |
| 7 | 6 | 66°01.4′ | 168°42.5′ | 51 |
| 7 | 7 | 66°05.4′ | 169°02′ | 48 |
| 8 | 9 | 66°40.5′ | 169°26′ | 38 |
| 8 | 10 | 67°01′ | 168°35′ | 41 |
| 8 | 11 | 67°04′ | 169°53′ | 48 |
| 8 | 12 | 67°06.5′ | 171°11′ | 42 |
| 8 | 13 | 67°18.5′ | 170°46.5′ | 46 |
| 9 | 22 | 67°22′ | 173°55′ | 20 |
| 10 | 23 | 68°10.5′ | 176°00′ | 20 |
| 10 | 24 | 68°26′ | 175°23′ | 32 |
| 11 | 34 | 69°19.2′ | 177°35′ | 44 |
| 11 | 35 | 69°00′ | 178°30′ | 41 |
| 11 | 36 | 69°31.5′ | 179°30′ E. | 42 |
| 11 | 37 | 69°45′ | 179°48′ | 47 |
| 11 | 39 | 70°10.5′ | 179°34′ W. | 41 |
| 12 | 41 | 70°38′ | 179°00′ | 35 |
| 16 | 45 | 70°09′ | 175°00′ E. | 37 |
| 16 | 47 | 70°40′ | 175°00′ | 43 |
| 16 | 49 | 71°10′ | 175°00′ | 37 |
| 16 | 50 | 71°25′ | 174°57′ | 37 |
| 17 | 51 | 71°34′ | 170°00′ | 37 |
| 17 | 53 | 71°10′ | 170°00′ | 34 |
| 18 | 55 | 70°21′ | 170°00′ | 26 |
| 18 | 56 | 69°50′ | 165°01′ | 27 |
| 18 | 58 | 70°20.2′ | 165°00′ | 16 |
| 18 | 60 | 70°50′ | 165°04′ | 21 |
| 19 | 61 | 71°04′ | 165°02′ | 22 |
| 19 | 62 | 71°20′ | 165°00′ | 13 |
| 19 | 64 | 71°10′ | 159°57′ | 10 |
| 20 | 66 | 71°40′ | 160°00′ | 14 |
| 20 | 68 | 72°10′ | 160°00′ | 19 |
| 20 | 70 | 72°40′ | 160°07′ | 21 |
| 21 | 71 | 72°56′ | 160°15′ | 26 |
| 22 | 73 | 71°33′ | 154°58′ | 12 |
| 22 | 75 | 71°59′ | 155°08′ | 16 |
| 22 | 77 | 72°24′ | 155°14′ | 21 |
| 22 | 79 | 72°50′ | 155°20′ | 26 |
| 22 | 81 | 73°15′ | 155°24′ | 32 |
| 23 | 83 | 73°42′ | 155°24′ | 33 |
| 24 | 85 | 73°50′ | 149°50′ | 14 |
| 24 | 86 | 73°35′ | 149°40′ | 14 |
| 25 | 88 | 73°02′ | 149°38′ | 14 |
| 25 | 90 | 72°35′ | 149°30′ | 11 |
| 26 | 91 | 73°58′ | 148°05′ | 11 |
| 26 | 92 | 74°08′ | 146°40′ | 14 |
| 26 | 93 | 74°08′ | 145°20′ | 14 |
| 26 | 95 | 74°26.5′ | 142°43′ | 15 |
| 26 | 97 | 74°30′ | 140°26′ | 25 |
| 27 | 99 | 74°30′ | 138°00′ | 18 |
| 27 | 101 | 74°00′ | 138°02′ | 20 |
| 27 | 103 | 73°30′ | 138°00′ | 20 |
| 27 | 105 | 73°00′ | 137°50′ | 21 |
| 27 | 107 | 72°30′ | 137°40′ | 22 |
| 27 | 108 | 72°16′ | 137°36′ | 16 |
| 28 | 111 | 72°00′ | 134°30 | 15 |
| 28 | 113 | 72°30′ | 134°16′ | 20 |

TABLE 3.—*Locality and depth of bottom-sediment samples*—Con.

[Sample number is not identical with *Northwind* oceanographic station number because several samples were taken at some stations.]

| Date of collection (1963) | Sample | Latitude | Longitude | Depth (meters) |
|---|---|---|---|---|
| Aug. 28 | 116 | 73°15′ N. | 134°05′ E. | 16 |
| 28 | 118 | 73°45′ | 133°53′ | 14 |
| 28 | 119 | 72°48′ | 133°00′ | 14 |
| 28 | 122 | 71°30′ | 130°55′ | 14 |
| 28 | 123 | 71°45′ | 130°52′ | 16 |
| 29 | 124 | 72°00′ | 130°47′ | 14 |
| 29 | 126 | 72°31′ | 131°16′ | 22 |
| 30 | 128 | 73°02′ | 131°10′ | 22 |
| 30 | 130 | 73°34′ | 131°25′ | 22 |
| 30 | 132 | 74°08′ | 131°47′ | 14 |
| 30 | 134 | 74°46′ | 134°29′ | 22 |
| 30 | 135 | 75°00′ | 134°30′ | 20 |
| 31 | 137 | 75°28.5′ | 134°37′ | 37 |
| 31 | 139 | 76°01′ | 134°33′ | 35 |
| Sept. 2 | 143 | 76°26′ | 129°53′ | 54 |
| 2 | 145 | 75°47.5′ | 129°52′ | 42 |
| 2 | 147 | 75°20′ | 129°47′ | 41 |
| 2 | 149 | 74°47.5′ | 129°46′ | 31 |
| 2 | 150 | 74°32.5′ | 129°45′ | 19 |
| 2 | 152 | 74°32′ | 127°05′ | 34 |
| 3 | 154 | 74°23′ | 124°24′ | 16 |
| 3 | 156 | 74°55′ | 124°22′ | 43 |
| 3 | 158 | 75°26′ | 124°25′ | 41 |
| 3 | 161 | 76°02′ | 125°58′ | 46 |
| 3 | 163 | 76°34′ | 125°53′ | 53 |
| 4 | 165 | 75°45′ | 120°00′ | 53 |
| 5 | 167 | 75°19′ | 119°45′ | 30 |
| 5 | 169 | 74°46′ | 119°33′ | 17 |
| 5 | 170 | 73°52′ | 119°00′ | 10 |
| 6 | 172 | 74°15′ | 118°54′ | 17 |
| 6 | 174 | 74°35′ | 117°10′ | 19 |
| 6 | 175 | 74°38′ | 116°00′ | 19 |
| 6 | 176 | 74°00′ | 115°00′ | 18 |
| 7 | 178 | 74°29.5′ | 114°55′ | 30 |
| 7 | 179 | 74°46′ | 114°57′ | 28 |
| 8 | 180 | 75°04′ | 115°01′ | 29 |
| 9 | 181 | 74°20′ | 122°00′ | 14 |
| 10 | 183 | 74°59′ | 122°00′ | 27 |
| 10 | 187 | 74°57′ | 126°02′ | 32 |
| 10 | 188 | 74°56′ | 127°18′ | 38 |
| 10 | 189 | 74°45.5′ | 127°18′ | 31 |
| 10 | 190 | 74°31′ | 127°18′ | 29 |
| 11 | 194 | 73°50′ | 129°20′ | 12 |
| 11 | 195 | 73°36′ | 129°43′ | 15 |

*Elphidium gunteri* in a pond, under conditions of restricted circulation where the temperature was higher and the salinity lower than normal (Todd and Low, 1961, p. 19). In a Miocene brackish-water deposit in the Mainz basin of Germany, aberrant individuals of a species of *Nonion* and of a species of *Bolivina* are interpreted as a response to a habitat that was becoming progressively fresher (Bik, 1964, p. 72).

The following species were found as major constituents in the three seas (Chukchi, East Siberian, and Laptev) traversed by the *Northwind*. (In this analysis we have included the samples from behind the New Siberian Islands with those from the East Siberian Sea.):

*Ammotium cassis* (Parker)
*Eggerella advena* (Cushman)
*Elphidium clavatum* Cushman
*E. incertum* (Williamson)
*E. orbiculare* (Brady)
*Reophax curtus* Cushman
*R. scorpiurus* Montfort

Also present in all three seas, but more rarely and with more scattered records, are:

*Buccella frigida* (Cushman)
*Cassidulina islandica* Norvang
*Pseudopolymorphina novangliae* (Cushman)
*Quinqueloculina agglutinata* Cushman
*Rhabdammina* aff. *R. discreta* Brady

The following species were found as significant though not abundant elements, restricted to the Chukchi Sea and absent from the other two seas:

*Buccella inusitata* Andersen
*Cibicides lobatulus* (Walker and Jacob)
*Elphidium bartletti* Cushman
*Eponides wrightii* (Brady)
*Oolina borealis* Loeblich and Tappan
*Pseudononion auricula* (Heron-Allen and Earland)
*Reophax arcticus* Brady
*Trochammina squamata* Parker and Jones

Four additional species are also significant components of the Chukchi Sea fauna, but each has 1, 2, or 3 rare occurrences in the Laptev Sea:

*Elphidiella arctica* (Parker and Jones)
*Elphidium frigidum* Cushman
*Recurvoides turbinatus* (Brady)
*Spiroplectammina biformis* (Parker and Jones)

No significant species appear to be restricted to the East Siberian Sea, but several species were found only in the East Siberian and Laptev Seas together:

*Elphidiella groenlandica* (Cushman)
*Saccammina longicollis* (Wiesner)
*Textularia torquata* Parker
*Trochammina nana* (Brady)
*T. rotaliformis* Wright
*Trochamminula fissuraperta* Stschedrina

Two species, both rare, were found in the Laptev Sea but not elsewhere in the present collections.

*Cassidulina teretis* Tappan
*Hippocrepina indivisa* Parker

The remaining 28 species, about half of the composite fauna, fail to show any significant distribution patterns or are too rare to be of significance.

Most of the species are known elsewhere from near-shore and cold environments. Table 4 (p. C84–C85) lists the identified species and includes the record of occurrence and estimate of abundance for each species and each sample. It also includes information regarding other reported occurrences. Starred species in this table are those considered to have been living when collected, as determined by rose bengal stain in six selected samples (Walton, 1952).

Only four of the identified species have not already been reported from the Arctic regions. Two of them, *Saccammina longicollis* and *Nouria polymorphinoides*, have been reported from the Antarctic. The other two, *Marginulina glabra* and *Rosalina ornatissima*, are cold-water species that have not previously been reported in the Arctic.

The present fauna falls into Stschedrina's sublittoral group of species, which she describes as characteristic of depths that are less than 50 meters, have seasonal temperature fluctuations, and within which salinity is reduced by influx of fresh water (Stschedrina, 1959). The major species in this cold water sublittoral group are reported by her to be *Hippocrepina indivisa*, *Reophax curtus*, *Spiroplectammina biformis*, and *Trochamminula fissuraperta*.

The most interesting of these species is *Trochamminula fissuraperta*. The genus was described as being distributed in shallow depths, along the Siberian coast from the Barents Sea to the Chukchi Sea, and in the Okhotsk and Bering Seas. In our material it is found only off the mouths of the Lena and Yana Rivers, which empty into the eastern part of the Laptev Sea. In its morphology the genus seems only questionably distinguishable from *Arenoparrella*. *Arenoparrella mexicana* occurs widely under equivalent ecological conditions, except for temperature, at numerous marsh and brackish localities along the Gulf Coast of the United States, around Trinidad, on the south shore of Cape Cod, off southern California and Baja California, and even off the Asiatic coast in the southwestern Yellow Sea.

## REFERENCES


Arnal, R. E., 1955, Some occurrences of abnormal Foraminifera: The Compass of Sigma Gamma Epsilon, v. 32, no. 3, p. 185–194, pl. 1, figs. 1–3.

Awerinzew, S., 1911, Zur Foraminiferen-Fauna des Sibirischen Eismeeres [On the Foraminifera fauna of the Siberian Eismeer]: Mem. Acad. Imp. Sci. St. Pétersbourg, ser. 8, v. 29, no. 3, p. 1–27, 1 pl.

Bik, E. Th. A., 1964, An aberrant nonionid from the Miocene of the Mayence basin: Hessischen Landesamtes für Bodenforschung Notizblatt, Wiesbaden, v. 92, p. 68–74, pl. 5, figs. 1–3.

Brady, H. B., 1881, On some Arctic Foraminifera from soundings obtained on the Austro-Hungarian North-Polar Expedition of 1872–1874: Annals Mag. Nat. History, ser 5, v. 8, p. 393–418, table.

Cooper, S. C., 1964, Benthonic Foraminifera of the Chukchi Sea: Cushman Found. Foram. Research Contr., v. 15, p. 79–104, pls. 5, 6, figs. 1–17.

Cushman, J. A., 1948, Arctic Foraminifera: Cushman Lab. Foram. Research Spec. Pub. 23, 79 p., 8 pls.

Jarke, Joachim, 1960, Beitrag zur Kenntnis der Foraminiferenfauna der mittleren und westlichen Barents-See [Contribution to the knowledge of the Foraminifera fauna of the middle and western Barents Sea]: Internat. Rev. Gesamten Hydrobiologie, v. 45, no. 4, p. 581–654, pls. 1–13, figs. 1–25, tables 1–4.

Loeblich, A. R., Jr., and Tappan, Helen, 1953, Studies of Arctic Foraminifera: Smithsonian Misc. Colln., v. 121, no. 7 p. 1–150, pls. 1–24, fig. 1.

Mayer, E. M., 1962, Novye vidy Foraminifer melkovodiy Kandalakshskogo Zaliva [New species of Foraminifera of the Kandalaksha Bay in the vicinity of the White Sea Biological Station], *in* L. A. Zenkewitch, ed., Biology of the White Sea: Repts. White Sea Biol. Station of State Univ. Moscow, v. 1, 1961, p. 70–87, text figs. (pls.) 1–3.

Nagy, Jenö, 1965, Foraminifera in some bottom samples from shallow waters in Vestspitsbergen: Norsk Polarinst. Arbok 1963, Oslo, p. 109–128, pls. 1, 2.

Norvang, Aksel, 1945, The zoology of Iceland, v. 2, pt. 2, Foraminifera: Copenhagen and Reykjavik, Ejnar Munksgaard, p. 1–79, figs. 1–14.

Phleger, F. B., 1952, Foraminifera distribution in some sediment samples from the Canadian and Greenland Arctic: Cushman Found. Foram. Research Contr., v. 3, p. 80–89, pls. 13, 14, fig. 1, table 1.

Stschedrina, Z. G., 1959, The dependence of the distribution of Foraminifera in the seas of the U.S.S.R. on the environmental factors: Internat. Cong. Zoology, 15th, London 1958, Proc., sec. 3, paper 30, p. 218–221.

——— 1962, Foraminifery Zalivov Belogo Morya [Foraminifera of the White Sea bays], *in* L. A. Zenkewitch, ed., Biology of the White Sea: Repts. White Sea Biol. Station of State Univ. Moscow, v. 1. 1961, p. 51–69, text figs. 1–10.

Todd, Ruth, and Low, Doris, 1961, Near-shore Foraminifera of Martha's Vineyard Island, Massachusetts: Cushman Found. Foram. Research Contr., v. 12, p. 5–21, pls. 1, 2, figs. 1, 2, table 1.

Walton, W. R., 1952, Techniques for recognition of living Foraminifera: Cushman Found. Foram. Research Contr., v. 3, p. 56–60.

Zagorskaya, N. G., Jashina, Z. I., Slobodin, V. Ja., Levina, F. M., and Belevich, A. M., 1965, Morskiye Neogen(?)–Chetvertichnye Otlozheniya Nizhnego Techeniya Reki Yeniseya [Marine Neogene(?)–Quaternary deposits of the lower course of the Yenisey River]: Nauchno-issl. inst. geol. arktiki gosud. geol. Komitet SSSR, Trudy, v. 144, p. 1–91, figs. 1–28, tables 1–21.

Zenkevitch, L. A., 1963, Biology of the seas of the U.S.S.R. (translation by S. Botcharskaya): New York, Interscience Publishers, 955 p., 427 figs.

TABLE 4.—*Distribution and abundance of Foraminifera off*

[Samples are listed approximately in order from east to west. A, abundant;

| Species | Chukchi Sea | | | | | | | | | | | | | | | East Siberian Sea | | | | | | | | | | | | | | | | | | | | | |
|---|---|---|---|---|---|---|---|---|---|---|---|---|---|---|---|---|---|---|---|---|---|---|---|---|---|---|---|---|---|---|---|---|---|---|---|---|---|
| | 4 | 5 | 10 | 6 | 3 | 7 | 2 | 1 | 9 | 11 | 13 | 12 | 22 | 23 | 34 | 36 | 37 | 45 | 47 | 49 | 53 | 51 | 56 | 58 | 60 | 61 | 66 | 68 | 71 | 83 | 81 | 79 | 77 | 85 | 88 | 90 | 91 | 92 | 93 |
| **Adercotryma glomeratum* (Brady) | | | R | | | | R | R | | | | | | | | | | | | | | | | | | | | | | | | | | | | | |
| *Ammodiscus gullmarensis* Hoglund | | | | | | | | | | | | | | | | | | | | | | | | | | | | | | R | | | | | | | | | |
| **Ammotium cassis* (Parker) | C | | C | | | | | | | | | | R | R | | R | | R | | A | | R | R | | R | R | | | | | | | | | | | | |
| **Buccella frigida* (Cushman) | | C | A | R | R | | C | | R | R | | | | | | | | R | | | | | | | | | | | R | | | | | | | | | |
| *inusitata* Andersen | | A | | A | | R | | | | | | | | | | | | | | | | | | | | | | | | | | | | | | | | | |
| *Bulimina exilis* Brady | | | | | | | | | | | | | | | | | | | | | | | | | | | | | | | | | | | | | | | |
| **Cassidulina islandica* Nørvang | | R | | R | | R | | | | | | | | | | | | | | | | | | | | | | | | R | | | | | | | | | |
| *teretis* Tappan | | | | | | | | | | | | | | | | | | | | | | | | | | | | | | | | | | | | | | | |
| **Cibicides lobatulus* (Walker and Jacob) | | R | | R | | R | | | | | | | | | | | | | | | | | | | | | | | | | | | | | | | | | |
| *Cornuspira involvens* (Reuss) | | | | | | | | | | | | | | | | | | | | | | | | | | | | | | R | | | | | | | | | |
| *Dentalina frobisherensis* Loeblich and Tappan | | | | | | | | | | | | | | | | | | | | | | | | | | | | | | | | | | | | | | | |
| **Eggerella advena* (Cushman) | R | C | A | R | C | R | C | A | R | A | C | C | | R | | | | | | | | | R | | R | | | | | | | | | | | | | | |
| **Elphidiella arctica* (Parker and Jones) | | C | | R | | A | R | | | | | | | | | | | | | | | | | | | | | | | | | | | | | | | | |
| *groenlandica* (Cushman) | | | | | | | | | | | | | | | | | | | | | | | | | | | | | | | | R | | | R | | | | |
| *Elphidium bartletti* Cushman | | C | | R | | | | | | | | | | | | | | | | | | | | | | | | | | | | | | | | | | | |
| **clavatum* Cushman | R | C | C | C | | C | C | | R | R | R | | | | | | | C | | | | | | | | | R | R | R | C | R | | | | | | | | |
| **frigidum* Cushman | | A | R | A | | R | R | | R | | | | | | | | | | | | | | | | | | | | | | | | | | | | | | |
| *incertum* (Williamson) | | | | | R | R | | | | | | | | | | | | | | | | | | | | | | | | R | R | | | | | | | | |
| *orbiculare* (Brady) | | R | R | R | | R | | | | R | | | | | | | | R | | | | | | | | | | | | | C | C | R | | | | | | |
| **Eponides wrightii* (Brady) | | C | | C | | C | | | | | | | | | | | | | | | | | | | | | | | | | | | | | | | | | |
| *Esosyrinx curta* (Cushman and Ozawa) | | R | | | | | | | | | | | | | | | | | | | | | | | | | | | | | | | | | | | | | |
| *Gordiospira arctica* Cushman | | | | | | | | | | | | | | | | | | | | | | | | | | | | | | | | | | | | | | | |
| *Haplophragmoides crassimargo* (Norman) | | | | | | | | | | | | | | | | | | | | | | | | | | | | | | R | | | | | | | | | |
| *jeffreysii* (Williamson) | | | | | | R | | | | | | | | | | | | | | | | | | | | | | | | | | | | | | | | | |
| *Hippocrepina indivisa* Parker | | | | | | | | | | | | | | | | | | | | | | | | | | | | | | | | | | | | | | | |
| *Lagena gracillima* (Seguenza) | | | | | | | | | | | | | | | | | | | | | | | | | | | | | | R | R | | | | | | | | |
| *laevis* (Montagu) | | | | | | | | | | | | | | | | | | | | | | | | | | | | | | | | | | | | | | | |
| *Laryngosigma hyalascidia* Loeblich and Tappan | | | | R | | | | | | | | | | | | | | | | | | | | | | | | | | | | | | | | | | | |
| *williamsoni* (Terquem) | | | | | | | | | | | | | | | | | | | | | | | | | | | | | | R | | | | | | | | | |
| *Marginulina glabra* d'Orbigny | | | | | | | | | | | | | | | | | | R | | | R | | | | | | | | | | | | | | | | | | |
| *Nonion labradoricum* (Dawson) | | | | | | | | | | | | | | | | | | | | | | | | | | | | | | | | | | | | | | | |
| **Nouria polymorphinoides* Heron-Allen and Earland | | | | | ? | | | | R | | | | | | | | | | | | | | | | | | | | | | | | | | | | | | |
| *Oolina borealis* Loeblich and Tappan | | C | | C | | | R | | | | | | | | | | | | | | | | | | | | | | | | | | | | | | | | |
| *melo* d'Orbigny | | | | R | | | | | | | | | | | | | | | | | | | | | | | | | | | | | | | | | | | |
| *Protoschista findens* (Parker) | | | | | R | | | | | | | | | | | | | | | | | | | | | | | | | | | | | | | | | | |
| *Psammatodendron arborescens* Norman | | | | | | | | | | | | | | | | | | R | | | | | | | | | | | | | | | | | | | | | |
| **Pseudononion auricula* (Heron-Allen and Earland) | R | R | | R | | | R | | R | R | | | | | | | | | | | | | | | | | | | | | | | | | | | | | |
| *Pseudopolymorphina novangliae* (Cushman) | | | R | R | | | | | | | | | | R | | | | R | | | | | | | | | | | | | | | | | | | | | |
| *Pyrgo williamsoni* (Silvestri) | | | | | | | | | | | | | | | | | | | | | | | | | | | | | | R | | | | | | | | | |
| *Quinqueloculina agglutinata* Cushman | R | | | | | | | | | R | | | | | | | | | | | | | | | | | | | | | | | | | | | | | |
| *arctica* Cushman | | | | | | | | | | | | | | | | | | | | | | | | | | | | | | | | | | | | | | | |
| *Recurvoides turbinatus* (Brady) | | | | | | | | | | C | | | | | | | | | | | | | | | | | | | | | | | | | | | | | |
| **Reophax arcticus* Brady | | | C | | R | | R | R | | R | | | | | | | | | | | | | | | | | | | | | | | | | | | | | |
| *curtus* Cushman | A | R | R | | R | | C | R | | R | C | R | | R | R | R | | R | | R | | | R | R | | R | | | | R | R | | | R | | | R | | |
| *scorpiurus* Montfort | R | | R | | | | R | | | | | | | | | | | R | | | | | | | | | R | R | | C | R | | R | R | | | R | | R |
| *Rhabdammina* aff. *R. discreta* Brady | | | R | | | | R | | | | | | | | R | | R | | | | | | | | | | | | | R | | | | | | | | | R |
| *Rhizammina*? aff. *R. indivisa* Brady | | | | | | | R | | | | | | | | | | | | | | | | | | | | | | | | | | | | | | | | |
| *Rosalina ornatissima* (Cushman)? | | | | | | | R | | | | | | | | | | | | | | | | | | | | | | | | | | | | | | | | |
| **Saccammina longicollis* (Wiesner) | | | | | | | | | | | | | | | | | | | | | | | | | | | R | C | | C | R | | C | | R | | R | | R |
| **Spiroplectammina biformis* (Parker and Jones) | | | R | R | | | R | R | | C | | R | | | | | | | | | | | | | | | | | | | | | | | | | | | |
| **Textularia torquata* Parker | | | | | | | | | | | | | | | | | | | R | R | | | R | | | | | | | A | | | | | | | | | |
| *Triloculina tricarinata* d'Orbigny | | | | | | | | | | | | | | | | | | | | | | | | | | | | | | | | | | | | | | | |
| *Trochammina nana* (Brady) | | | | | | | | | | | | | | | | | | | | | | | | | | | R | | | | | | | C | | R | | | R |
| *rotaliformis* Wright | | | | | | | | | | | | | | | | | | | | | | | | | | | | | | | | | | C | | R | R | | R |
| **squamata* Parker and Jones | | | | R | | R | | R | | | | | | | | | | | | | | | | | | | | | | | | | | | | | | | |
| *Trochamminula fissuraperta* Stschedrina | | | | | | | | | | | | | | | | | | | | | | | | | | | | | | | | | | | | | | | |

*the eastern Siberian coast and recorded occurrences elsewhere*

C, common; R, rare; × recorded elsewhere; *, living when collected]

| Species | Behind New Siberian Islands | | | | | | | Laptev Sea | | | | | | | | | | | | | | | | | | | | | | | | | | | | | | Recorded occurrences | | |
|---|---|---|---|---|---|---|---|---|---|---|---|---|---|---|---|---|---|---|---|---|---|---|---|---|---|---|---|---|---|---|---|---|---|---|---|---|---|---|---|---|
| | 95 | 97 | 99 | 101 | 103 | 105 | 108 | 139 | 137 | 135 | 134 | 111 | 116 | 118 | 119 | 132 | 128 | 123 | 149 | 147 | 145 | 143 | 190 | 189 | 188 | 152 | 187 | 161 | 154 | 156 | 183 | 165 | 167 | 170 | 172 | 174 | 180 | 176 | 179 | 178 | Arctic | Antarctic | Widespread |
| **Adercotryma glomeratum* (Brady) | | | | | | | | | | | | | | | | | | | R | | | | | | | | | | | | | | | | | | | | | | × | × | × |
| *Ammodiscus gullmarensis* Hoglund | | | | | | R | | | | | | | | | | | | | | | | | | | | | | | | | | R | | | | | | | | | × | | |
| **Ammotium cassis* (Parker) | | | | R | R | R | | C | R | | R | | | | R | | | | A | R | | R | | A | C | | | | C | R | | R | | | A | R | | | | | × | | × |
| **Buccella frigida* (Cushman) | | | | | | R | | | R | | R | | | | | | | | | | | | | | | | | | | | | R | | | | | | | | | | × | × | × |
| *inusitata* Andersen | | | | | | | | | | | | | | | | | | | | | | | | | | | | | | | | | | | | | | | | | × | | |
| *Bulimina exilis* Brady | | | | | | | | | R | | R | | | | | | | | | | | R | | | | | | | | | | C | | | | | | | | | × | ---- | × |
| **Cassidulina islandica* Nørvang | | | | | | | | | | | | | | | | | | | | | | R | | | | | | | | | | R | | | | | | | | | × | | |
| *teretis* Tappan | | | | | | | | | | | | | | | | | | | | | | C | | | | | | | | | | R | | | | | | | | | × | | |
| **Cibicides lobatulus* (Walker and Jacob) | | | | | | | | | | | | | | | | | | | | | | | | | | | | | | | | | | | | | | | | | × | × | × |
| *Cornuspira involvens* (Reuss) | | | | | | | | | | | R | | | | | | | R | | | | | | | | | | | | | | | | | R | | | | | | × | × | × |
| *Dentalina frobisherensis* Loeblich and Tappan | | | | | | | | | | | R | | | | | | | | | | | | | | | | | | | | | R | | | | | | | | | × | | |
| **Eggerella advena* (Cushman) | | | | | | | | R | R | R | R | | | | | | | | | | | | R | | | | R | | | | | R | R | | C | R | C | | | | × | × | × |
| **Elphidiella arctica* (Parker and Jones) | | | | | | | | | | | | | | | | | | | | | R | | | | | | | | | | | | | | | | | | | | | × | | |
| *groenlandica* (Cushman) | | | | | | | | R | | | R | | | | | | | | | | | | | | R | | | | | | | R | | | | | | | | R | × | | |
| *Elphidium bartletti* Cushman | | | | | | | | | | | | | | | | | | | | | | | | | | | | | | | | | | | | | | | | | × | | |
| **clavatum* Cushman | | | ? | | | C | | R | R | | C | | | | | | | R | | | R | R | R | | A | R | | | | | C | R | R | | R | | R | R | R | × | ---- | × |
| **frigidum* Cushman | | | | | | | | | | | | | | | | | | | | | | | | | | | | | | | | R | | | R | | | | | R | × | | |
| *incertum* (Williamson) | | | | | | | | | | | R | | | | | | | | | | | A | | | R | | | | | | | C | | | | | | | | | × | × | × |
| *orbiculare* (Brady) | R | | | | | | | | | | | | | | | | | R | | | R | C | | | | | | | | | | R | | | | | | | | | × | × | |
| **Eponides wrightii* (Brady) | | | | | | | | | | | | | | | | | | | | | | | | | | | | | | | | | | | | | | | | | × | | |
| *Esosyrinx curta* (Cushman and Ozawa) | | | | | | | | | | | | | | | | | R | | | | | | | | | | | | | | | | | | | | | | | | | × | × | |
| *Gordiospira arctica* Cushman | | | | | | R | | | | | | | | | | | | | | | | | | | | | | | | | | | | | | | | | | | × | | |
| *Haplophragmoides crassimargo* (Norman) | | | | | | | | | R | | | | | | | | | | | | | R | | | | | | R | | | | | | | | | | | | | × | × | |
| *jeffreysii* (Williamson) | | | | | | | | | | | | | | | | | | | | | | | | | | | | | | | | | | | | | | | | | × | | |
| *Hippocrepina indivisa* Parker | | | | | | | | | | | | | | | | | | | | | | | | | | | | | R | | | | R | | R | | | | | | × | × | |
| *Lagena gracillima* (Seguenza) | | | | | | | | | | | | | | | | | | | | | | R | | | | | | | | | | | | | | | | | | | × | × | × |
| *laevis* (Montagu) | | | | | | | | | | | R | | | | | | | | | | | | | | | | | | | | | | | | | | | | | | R | × | × | × |
| *Laryngosigma hyalascidia* Loeblich and Tappan | | | | | | | | | | | | | | | | | | | | | | | | | | | | | | | | | | | | | | | | | × | × | |
| *williamsoni* (Terquem) | | | | | | | | | | | R | | | | | | | | | | | | | | | | | | | | | | | | | | | | | | × | × | × |
| *Marginulina glabra* d'Orbigny | | | | | | R | | | | | | | | | | | | | | | | | | | | | | | | | | | | | | | | | | | | | × |
| *Nonion labradoricum* (Dawson) | | | | | | | | | | | | | | | | | | | | | | R | | | | | | | | | | | | | | | | | | | × | | |
| **Noturia polymorphinoides* Heron-Allen and Earland | | | | | | | | | | | | | | | | | | | | | | | | | | | | | | | | | | | | | | | | | | × | × |
| *Oolina borealis* Loeblich and Tappan | | | | | | | | | | | | | | | | | | | | | | | | | | | | | | | | | | | | | | | | | × | | × |
| *melo* d'Orbigny | | | | | | | | | | | R | | | | | | | | | | | | | | | | | | | | | | | | | | | | | | × | × | × |
| *Protoschista findens* (Parker) | | | | | | | | | | | | | | | | | | | | | | | | | | | | | | | | | | | | | | | | | × | | |
| *Psammatodendron arborescens* Norman | | | | | | | | | | | | | | | | | | | | | | | | | | | | | | | | | | | | | | | | | × | × | |
| **Pseudononion auricula* (Heron-Allen and Earland) | | | | | | | | | | | | | | | | | | | | | | | | | | | | | | | | | | | | | | | | | × | | × |
| *Pseudopolymorphina novangliae* (Cushman) | | | | | | | | | | | R | | | | | | | | | | R | R | | | R | R | | | | | | R | | | | | | | | | × | | |
| *Pyrgo williamsoni* (Silvestri) | | | | | | | | | | | | | | | | | | | | | | R | | | | | | | | | | | | | | | | | | | × | | |
| *Quinqueloculina agglutinata* Cushman | | | | | | | | | | R | | | | | | | | | | | | | | | | | | | | | R | | | | | R | | | | | × | ---- | × |
| *arctica* Cushman | | | | | | | | | | | R | | | | | | | | | | | | | | | | | | | | | | | | | | | | | | × | | |
| *Recurvoides turbinatus* (Brady) | | | | | | | | | | | | | | | | | | | | | | R | | | | | | | | | | R | | | | | | | | | × | ---- | × |
| **Reophax arcticus* Brady | | | | | | | | | | | | | | | | | | | | | | | | | | | | | | | | | | | | | | | | | × | | |
| *curtus* Cushman | | | R | | | | | | | | A | | R | R | R | | R | | | | R | R | C | | | | | R | A | | | R | A | | C | R | | | | × | × | × |
| *scorpiurus* Montfort | C | | | R | | | R | | | | R | | | R | R | C | | | | | | | | | | | | C | | | R | | R | C | | | | | | × | ---- | × |
| *Rhabdammina* aff. *R. discreta* Brady | | | | | | | | | | R | | | | | R | R | | | | | | | | | | | | | | | | | | | | | | | | | | | |
| *Rhizammina*? aff. *R. indivisa* Brady | | | | | | | | | | | | | | | | | | | | | | | | | | | | | | | | | | | | | | | | | | | | |
| *Rosalina ornatissima* (Cushman)? | | | | | | | | | | | | | | | | | | | | | | | | | | | | | | | | | | | | | | | | R | | | |
| **Saccammina longicollis* (Wiesner) | A | | | | R | | | | | | | C | R | C | | | | | | | | | | | | | | | | | | | | | | | | | | | | × | × |
| **Spiroplectammina biformis* (Parker and Jones) | | | | | | | | | | | | | | | | | | | | | | | | | | | | | | | | R | | | | | | | | | × | × | × |
| **Textularia torquata* Parker | | | | | | R | | | R | | R | | | | | | | | | | | | | | | | | | | | | R | | | | | | | | | × | | |
| *Triloculina tricarinata* d'Orbigny | | | | | | | | | | | R | | | | | | | | | | | | | | | | | | | | | | | | | | | | | | × | × | × |
| *Trochammina nana* (Brady) | C | | | | | | | | | | | | | | | | | | | | | | | | | | | | | | | C | | | | | | | | | × | × | |
| *rotaliformis* Wright | C | R | | | | | | | | | | | | | | R | | | | | | | | | | | | | | | | | R | | | | | | | | | × | × | × |
| **squamata* Parker and Jones | | | | | | | | | | | | | | | | | | | | | | | | | | | | | | | | | | | | | | | | | × | × | × |
| *Trochamminula fissuraperta* Stschedrina | | | | | | | R | | | | | R | R | R | R | C | | | | | | | | | | | | | C | | | | | | R | R | | | | | × | | |

# AGE OF THE UNCOMPAHGRE UPLIFT AND UNAWEEP CANYON, WEST-CENTRAL COLORADO

By FRED W. CATER, Denver, Colo.

*Abstract.*—Unaweep Canyon, a wind gap that crosses the Uncompahgre Plateau, is an uplifted and deserted channel that ancient river gravels and physiographic relations indicate was occupied by the Gunnison River, rather than the Colorado River as believed by some earlier investigators. Tentative dating of fanglomerates overlying the ancient river gravels indicates the Gunnison River probably abandoned Unaweep Canyon in early Pleistocene or latest Pliocene time. Uplift of the Uncompahgre Plateau totals more than 2,000 feet, of which about 1,300 to 1,400 feet occurred after Unaweep Canyon was abandoned. Uplift probably started no earlier than mid-Pliocene. Since Unaweep Canyon has been abandoned the trunk streams in the area have downcut no more than about 100 feet.

The Uncompahgre uplift and the remarkable wind-gap of Unaweep Canyon that crosses it have excited the interest of geologists since the features were first described by Peale (1877) nearly 90 years ago. The northwest-trending uplift, one of the large monoclinal upwarps that characterize the Colorado Plateaus province, is 25 to 30 miles wide and more than 100 miles long. Throughout most of its length the uplift is a northeasterly tilted block bounded on the southwest by a sharply flexed, faulted monocline and on the northeast by a similar but smaller monocline that southeastward passes into a rather gently dipping, simple monocline. To the northwest, the uplift plunges into the Uinta Basin; to the southeast, it is interrupted by structures of the San Juan Mountains.

The southwest front of the Uncompahgre uplift approximately coincides with that of the ancestral Uncompahgre highland that rose in late Paleozoic time; the old highland, however, was much larger and extended many miles east of the present uplift. During late Paleozoic and early Mesozoic times the old highland shed vast quantities of debris into the bordering lowlands. The Permian Cutler Formation, consisting of arkosic detritus derived from the highland, attains a thickness of perhaps 14,000 feet a few miles southwest of the Uncompahgre Plateau, but about 4 miles northeast of Gateway along the southwest flank of the uplift the formation abruptly pinches out between the unconformably overlying Triassic Chinle Formation and underlying Precambrian crystalline rocks. It is for this reason that the bottom of Unaweep Canyon is mostly carved in Precambrian rocks, whereas the almost equally deep Dolores River canyon at Gateway bottoms in the upper part of the Cutler Formation (fig. 1).

Unaweep Canyon, one of the most unusual and spectacular physiographic features of western Colorado, cuts northeasterly for 25 miles across the Uncompahgre uplift from a point about 4 miles northeast of Gateway to Cactus Park, about 9 miles southwest of Whitewater. The canyon reaches a depth of more than 3,000 feet where it crosses the crest of the uplift, and its floor is nearly a mile wide, a size far out of proportion to that of the two small streams, East Creek and West Creek, which presently drain it. Both creeks head in the flat bottom of the canyon and are separated by a nearly imperceptible divide.

Both Peale (1877, p. 64–69) and Gannett (1882) recognized that the canyon once had been occupied by a far larger stream which Peale believed to have been the Gunnison River and Gannett the Colorado. Most later authors have agreed with Gannett (Stokes, 1948, p. 38; Shoemaker, 1954; Cater, 1955; Lohman, 1961, 1965). Hunt (1956), however, suggested that Unaweep Canyon might have been cut by either the Dolores or Gunnison River.

## PREVIOUS WORK

Uncertainty as to the identity of the stream that cut Unaweep Canyon is accompanied by uncertainty as to when the canyon was abandoned, when uplift of the Uncompahgre Plateau started, and how much differential uplift has occurred. Lohman (1961;

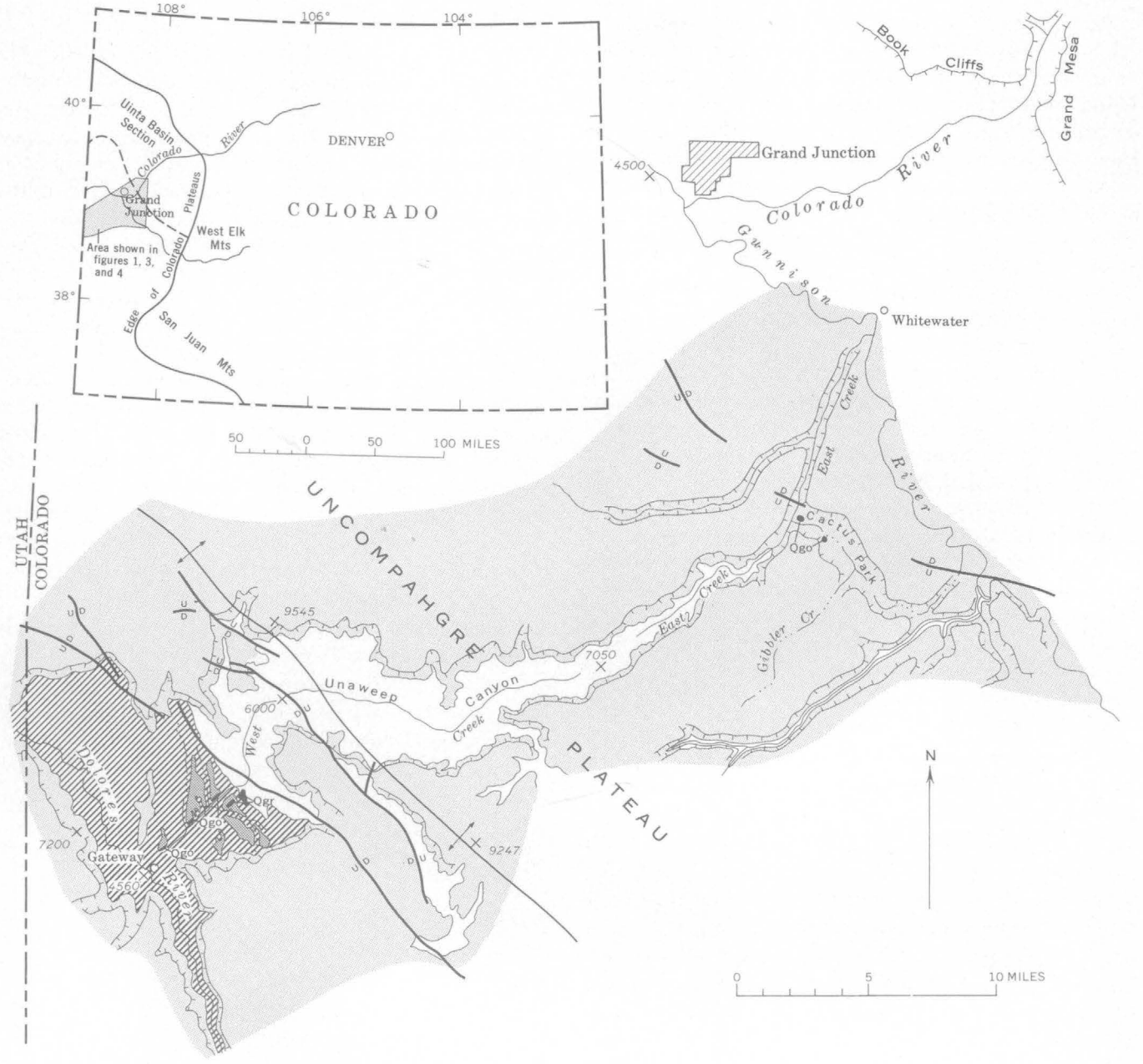


EXPLANATION

Pleistocene fanglomerate

Pleistocene gravel
Qgo, *old river gravel*
Qgr, *reworked gravel*

Mesozoic sedimentary rocks

Permian Cutler Formation

Precambrian crystalline rocks

Contact

Fault
U, *upthrown side;*
D, *downthrown side*

Asymmetric anticline
*Short arrow indicates steeper limb*

Rim of canyon

FIGURE 1.—Geologic sketch map of Unaweep Canyon and part of the Uncompahgre Plateau, Colorado. Geology after F. W. Cater (1955) and P. L. Williams (1964).

1965, p. 72–74) has dealt most comprehensively with these problems, but since completion of his studies, new occurrences of ancient river gravels have been found and certain fanglomerates have been tentatively dated. Although the new evidence confirms many of Lohman's conclusions, the conclusions herein presented differ from both his and my earlier conclusions (Cater, 1955), principally in denying that the Colorado River carved Unaweep Canyon and in recognizing a greater amount of uplift of the Uncompahgre Plateau since the abandonment of Unaweep Canyon. Of greater geologic significance, however, is a difference in viewpoint concerning the timing of uplift. In both Lohman's (1965, p. 91) and Hunt's (1956, p. 73–85) view the Uncompahgre uplift started near the beginning of Tertiary time, and renewed uplift has occurred periodically since then, including a late pulse of uplift after Unaweep Canyon was abandoned. In my view, the Uncompahgre uplift became a distinct structural feature only in late Tertiary time, when it rose on the northeast side of the Colorado Plateaus province which to the southwest was structurally much higher. Probably uplift occurred as a more or less continuous, single event; during the earlier stages of uplift Unaweep Canyon was deepened, and later, after the downcutting river abandoned it, the canyon was elevated. It is the purpose, then, of this paper to reexamine the history of the canyon and the uplift in the light of the new evidence, and to present the following conclusions: (1) Unaweep Canyon was carved by the Gunnison River, and the Colorado River never flowed through it; (2) Unaweep Canyon was abandoned in late Pliocene time; (3) the rise of the modern Uncompahgre uplift probably began in mid- or late Pliocene time; and (4) almost all the difference in altitude between the Dolores River at Gateway and the floor of Unaweep Canyon is the result of uplift.

The assumption that Unaweep Canyon is the abandoned channel of the Colorado River has been based largely on the alinement of the canyon with the course of the Colorado River above Grand Junction. Reasons for believing otherwise are based on the following lines of evidence: (1) The composition of the gravels deposited by the stream that cut the canyon; (2) the small size and different topographic characteristics of the valley of East Creek north of Cactus Peak as compared with Unaweep Canyon and the old channel of the Gunnison in and southeast of Cactus Park; and (3) the rerouted post-Unaweep course of the Gunnison River, which is inconsistent with a Colorado River that formerly flowed through Unaweep Canyon.

### Gravels

The best indication of the identity of a stream that cut a now-deserted channel is the composition of the gravels left behind. The Colorado and Gunnison Rivers drain areas of strongly contrasting rock types, and this contrast is reflected by the difference in composition of their gravels. The Gunnison River drains a considerable part of the San Juan Mountains and the West Elk Mountains volcanic fields, and as a consequence its gravels consist predominantly of pebbles of intermediate and silicic volcanic and porphyritic intrusive rocks, and they also contain a wide variety of Precambrian, Paleozoic, and Mesozoic rocks. Basalt pebbles, particularly vesicular varieties, are not abundant. Gravels of the Dolores River are similar to those of the Gunnison except for a lack of basalt pebbles. Colorado River gravels, on the other hand, are characterized by abundant basalt pebbles of which many are vesicular. Only the most durable of Precambrian and Paleozoic rocks have survived as pebbles, and pebbles of volcanic and porphyritic intrusive rocks other than basalt are rare.

Ancient river gravels newly exposed in roadcuts (fig. 2) along State Highway 141, 1 to 4 miles northeast of Gateway, and gravels from Unaweep Canyon later reworked and deposited by West Creek contain numerous pebbles of intermediate and silicic volcanic and porphyritic intrusive rocks but only a few of basalt, a composition that strongly suggests a Gunnison River rather than a combined Colorado–Gunnison River source.

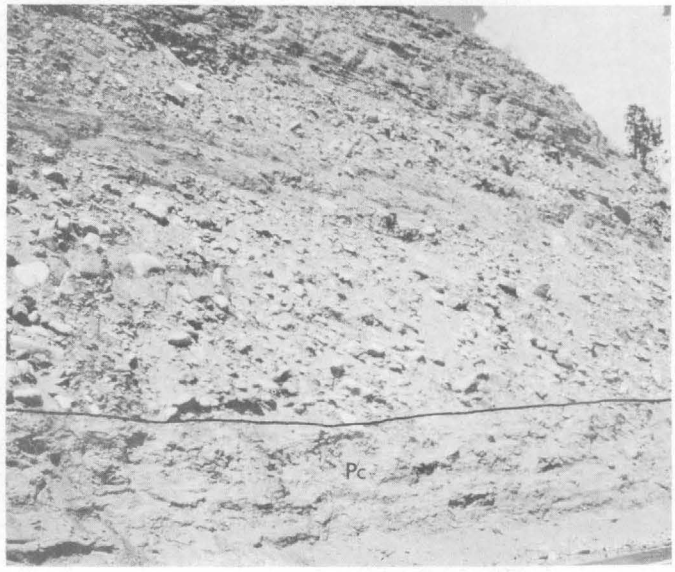


FIGURE 2.—Ancient river gravels resting on the Permian Cutler Formation (Pc) in roadcut about 1½ miles northeast of Gateway, Colo. Shrub at upper right corner is about 4 feet high.

It could be argued, of course, that gravels deposited by the Colorado River had been swept from the canyon after the Colorado was captured and before the Gunnison was diverted. Such a possibility seems unlikely, however, because in Cactus Park river gravels are preserved in a terrace more than 100 feet above the bed of the ancient river, and, as will be explained later, capture of the Colorado River should have been followed almost immediately by diversion of the Gunnison down the abandoned channel.

### Topographic features

The second reason for believing that the Colorado River never flowed through Unaweep Canyon is that the valley of East Creek becomes much smaller and topographically different once it leaves Unaweep Canyon below Cactus Park. In Cactus Park and Unaweep Canyon the floor of the ancient channel is broad and flat; below Cactus Park the valley of East Creek is relatively narrow and the floor slopes rather steeply and irregularly to the creek. A topographic break, therefore, occurs in the valley of East Creek below Cactus Park; the valley above preserves the appearance of a relatively unmodified channel of a large river and that below preserves the appearance of a canyon cut by a minor stream and never occupied by a large river. No residual river gravels have been found on the slopes and shoulders of this segment of East Creek valley; their presumed absence supports this argument.

### Present course of Gunnison River

The third reason, in part corollary to the second, is the present course of the Gunnison River southeast of Whitewater. Had the Colorado River entered Unaweep Canyon from East Creek valley at Cactus Park, then the Gunnison should have been captured through this same channel shortly after it had been abandoned by the Colorado (fig. 3). Reversal of drainage down this abandoned channel, which was aided, incidentally, by northeasterly tilting of the channel on the rising Uncompahgre uplift, would have required far less cutting through a shorter distance by a capturing stream than by any other route. The modern course of the Gunnison River above Whitewater would have required the river's capture by a stream that not only had to cut headward much farther in order to tap the Gunnison at its point of eventual capture more than 10 miles southeast of Cactus Park, but also in the process had to cross a very considerable spur ridge that separated the two streams. As a matter of fact, the stream that captured the Gunnison cut headward from Grand Junction for about 25 miles along the northeast flank of the Uncompahgre Plateau before tapping the Gunnison; it then crossed the presumed abandoned course of the Colorado River (fig. 4). A stream capable of cutting an unwavering course head-

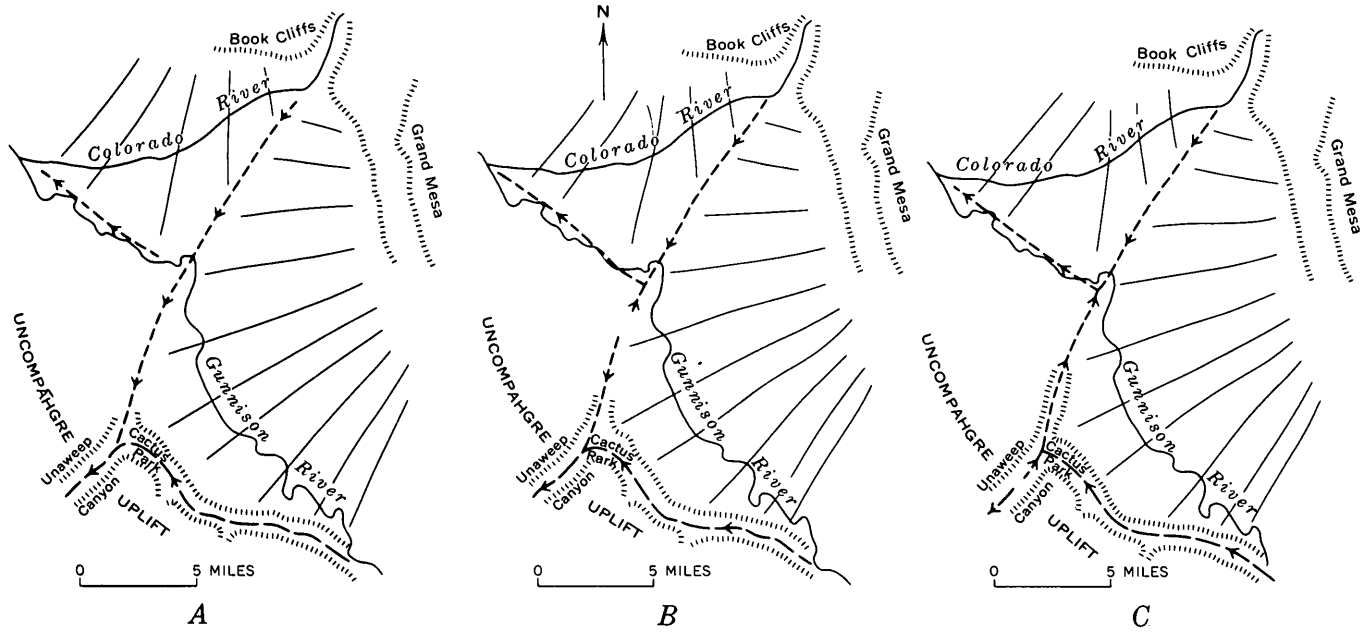


FIGURE 3.—Sketch maps showing stages in stream captures and diversions that probably would have occurred had the Colorado River flowed through Unaweep Canyon. Hypothetical course of Colorado River, capturing stream, and diversions that should have occurred shown by short dashes; ancestral course of Gunnison River shown by long dashes; and modern streams by solid lines. Arrows show direction of flow. *A*, immediately preceding assumed piracy of Colorado River; *B*, immediately after assumed piracy of Colorado River; *C*, after diversion of Gunnison River.

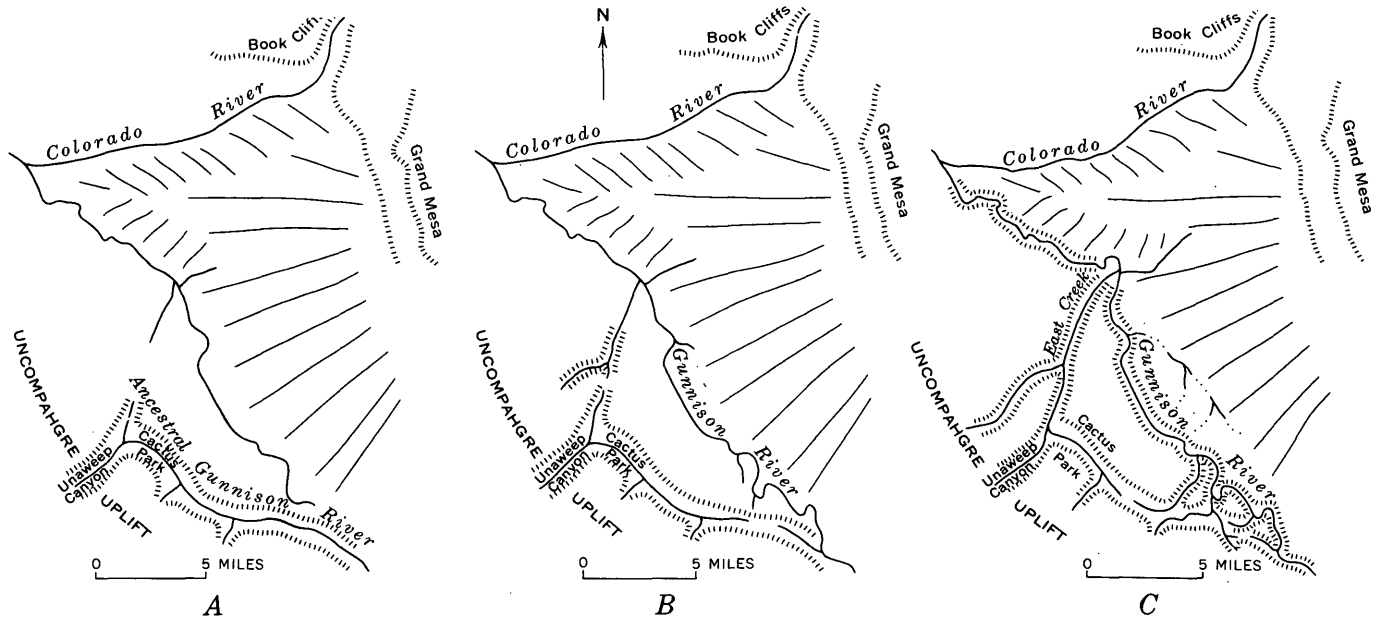


FIGURE 4.—Sketch maps showing stages in capture of Gunnison River and related drainage changes. *A*, immediately preceding capture of the Gunnison River; *B*, immediately after capture of the Gunnison River; *C*, present drainage pattern.

ward across the abandoned channel of a far larger stream without turning either up or down the old channel must at least be credited with an unusual degree of enterprise and singleness of purpose. Furthermore, as will be shown later, the Dolores River at Gateway has downcut only about 100 feet since the Gunnison River deserted Unaweep Canyon. Inasmuch as the Uncompahgre uplift, cored by granite, was rising across the courses of both the Colorado and Gunnison Rivers northeast of the uplift it is unlikely that they have downcut farther than the Dolores. Because the Gunnison River is trapped on the rising flank of the uplift, however, it has carved a deeper canyon. Both the Gunnison and Colorado Rivers are 300 to 500 feet below the dissected pediment that any possible channel of the Colorado River must have crossed north of Whitewater had it once flowed through Unaweep Canyon, and no trace of such a channel exists. Therefore, it is concluded that the Colorado River never occupied Unaweep Canyon.

## AGE OF ABANDONMENT OF UNAWEEP CANYON

Dating the abandonment of Unaweep Canyon is still subject to some uncertainty, but sediments that overlie the ancient river gravels northeast of Gateway permit establishing a minimum age. The open valley of West Creek between Gateway and the lower end of Unaweep Canyon at the southwest front of the Uncompahgre Plateau has been blanketed by two sequences of fanglomerates. Both fanglomerates cap low ridges sloping toward the creek, but where they are in mutual contact an erosional unconformity separates the two. The older fanglomerate attains a maximum thickness of more than 200 feet. It consists of a light-red to buff unsorted mixture of silt, sand, gravel, and angular cobbles and boulders derived almost entirely from the Mesozoic formations that rim the valley. The material is fairly well consolidated and where cut by rapidly eroding gullies it stands as nearly vertical bluffs approaching 100 feet in height. This fanglomerate overlies the old river gravels northeast of Gateway, and hence was deposited after the Gunnison River abandoned Unaweep Canyon. The younger fanglomerate is similar to the older in all respects except that it is unconsolidated and contains large quantities of material derived from Precambrian rocks and the Permian Cutler Formation in the canyon walls.

These fanglomerates in lower West Creek valley are believed to correlate with the Pleistocene Harpole Mesa Formation described by Richmond (1962) in the nearby La Sal Mountains in Utah. Richmond divided this formation into three members which he tentatively correlated with the Nebraskan, Kansan, and Illinoian Glaciations of the Midwestern States. The middle member of this formation contains an ash bed that Wilcox and Powers (*in* Richmond, 1962, p. 34–35) classed as a probable correlative of the Kansas Pearlette Ash Member of the Sappa Formation of the Great Plains. The fanglomerates in the lower valley of West Creek mark a period of extensive and vigorous aggradation similar to that of the lower member of

the Harpole Mesa, and they have a similar topographic setting. For these reasons the older fanglomerate is correlated with the lower member of the Harpole Mesa; hence, it is probably pre-Wisconsin and probably older than Nebraskan. The younger fanglomerate may correlate with either the middle or the upper member of the Harphole Mesa or perhaps with both.

If these correlations are correct then the Gunnison River had deserted Unaweep Canyon by early Pleistocene time, but how much earlier is impossible to say with accuracy. Sufficient time had elapsed after diversion for most of the river gravels to have been stripped from the lower valley before the oldest fanglomerate was deposited. This process may not have taken long, but if the rate of removal of the gravel was no faster than has been the rate of removal of the fanglomerate, then diversion of the Gunnison could have occurred before the beginning of the Pleistocene, perhaps in late Pliocene time if not earlier. Lohman (1961; 1965, p. 72–73), reasoning from other evidence from the northeast side of the plateau, reached the same conclusion for the general time of diversion.

## AGE OF UNCOMPAHGRE UPLIFT

Diversion of the Gunnison River from Unaweep Canyon happened early in the history of the present Uncompahgre uplift; dating the diversion therefore fixes roughly the beginning of uplift. Some earlier efforts at dating the beginning of uplift have placed it too far back. Hunt (1956, p. 73, 75) and Lohman (1965, p. 91), for example, suggest that uplift may have started in the Paleocene. Early dates probably were inferred because the faulted monocline marking the northeast front of the uplift coincides with the upper part of the great homocline that separates the Piceance Basin from the structurally much higher region to the southwest. The basin began forming, and consequently also the homocline, in earliest Tertiary time (J. R. Donnell, oral commun., 1965), and the homocline has been tilted periodically since then. Early tilting of the homocline, accordingly, has been confused with early rise of the Uncompahgre uplift. The southwest flank of the uplift, however, indicates the uplift is a separate structural feature rising from the crestal part of the most northeasterly of a series of broad, relatively gentle anticlines, the rest of which are localized along much older salt structures (Cater and Elston, 1963; Williams, 1964). These anticlines formed in post-Cretaceous time, possibly concomitantly with tilting of the homocline bordering the Piceance Basin.

Later, following epeirogenic uplift of the Colorado Plateaus, the cycle of vigorous canyon cutting began, and both Unaweep Canyon and the Dolores River canyon were entrenched to depths of more than 2,000 feet prior to beginning of the Uncompahgre uplift.

The Uncompahgre uplift probably started forming not long before the Gunnison River deserted Unaweep Canyon. Only about 600 to 700 feet of differential uplift had occurred along the faulted monocline forming the southwest flank of the uplift by the time the river had left the canyon. This is indicated by the greater depth beneath the Triassic Wingate Sandstone to which Unaweep Canyon was carved on the uplifted side of the monocline. An additional 1,300 to 1,400 feet of differential uplift occurred along this monocline after the canyon was abandoned. The amount of this uplift is measurable between the ancient stream gravels immediately below the mouth of Unaweep Canyon and the canyon floor on the uplifted side of the monocline. Unless the rate of prediversion uplift was considerably slower than the rate of postdiversion uplift, it seems unlikely that uplift started before mid-Pliocene time. Uplift, as a matter of fact, could not greatly predate abandonment of the canyon because structural and topographic displacement of the Uncompahgre Plateau coincide; that is, the plateau surface is eroded to only about the same stratigraphic level as the mesa lands to the southwest, which are more than 2,000 feet lower. This condition would not be likely to exist had uplift occurred in the distant past, particularly so because the sedimentary rocks capping the plateau in the vicinity of Unaweep Canyon are relatively soft. It is concluded that uplift began no earlier than the mid-Pliocene and probably continued into the Pleistocene.

Another problem solved by the exposure of the ancient river gravels northeast of Gateway is the amount of downcutting by the Dolores River since Unaweep Canyon was abandoned. Prior to the uncovering of these gravels in a roadcut, it was a question of how much of the difference in elevation between the floor of Unaweep Canyon and the Dolores River at Gateway was the result of uplift and how much the result of downcutting by the river. Indirect although fairly convincing evidence indicated downcutting had been minor, but the gravels indicate it could not exceed 200 feet, the height of the lowermost Gunnison River gravels above the present river level at Gateway. Moreover, close to 100 feet of this altitude difference is probably due to lifting of the gravels because of slight uptilting of the more gently dipping rocks below the sharply flexed and faulted monocline marking the southwest flank of the Uncompahgre uplift. The ancient gravels in the roadcuts presently have a gradient toward the Dolores River of about

211-690 O—66——7

100 feet per mile, a gradient that seems unreasonably steep for the river that formerly occupied Unaweep Canyon. Thus it seems that although there has been vigorous local tectonic activity—as indicated by the Uncompahgre uplift—as late as early Pleistocene time, the major trunk streams in this part of the Colorado Plateaus have not greatly deepened their canyons for some time.

## REFERENCES


Cater, F. W., 1955, Geology of the Gateway quadrangle, Colorado: U.S. Geol. Survey Geol. Quad. Map GQ–55.

Cater, F. W., and Elston, D. P., 1963, Structural development of the salt anticlines of Colorado and Utah, *in* The backbone of the America—tectonic history from pole to pole, a symposium: Am. Assoc. Petroleum Geologist Mem. 2, p. 152–159.

Gannet, Henry, 1882, The Unaweep Canyon [Colorado]: Pop. Sci. Monthly, v. 20, p. 781–786.

Hunt, C. B., 1956, Geology of the Taylor site, Unaweep Canyon, Colorado, in Archaeological investigations on the Uncompahgre Plateau in west central Colorado: Denver Mus. Nat. History Proc., no. 2, p. 64–69.

Lohman, S. W., 1961, Abandonment of Unaweep Canyon, Mesa County, Colorado, by capture of the Colorado and Gunnison Rivers: Art. 60 *in* U.S. Geol. Survey Prof. Paper 424–B, p. B144–B146.

——— 1965, Geology and artesian water supply of the Grand Junction area, Colorado: U.S. Geol. Survey Prof. Paper 451, 149 p.

Peale, A. C., 1877, Report on the Grand River district Colorado: U.S. Geol. and Geog. Survey Terr. 9th Ann. Rept.: p. 31–101.

Richmond, G. M., 1962, Quaternary stratigraphy of the LaSal Mountains, Utah: U.S. Geol. Survey Prof. Paper 324, 135 p.

Shoemaker, E. M., 1954, Structural features of southeastern Utah and adjacent parts of Colorado, New Mexico, and Arizona: Utah Geol. Soc. Guidebook, no. 9, p. 48–69.

Stokes, W. L., 1948, Geology of the Utah-Colorado salt dome region with emphasis on Gypsum Valley, Colorado: Utah Geol. Soc. Guidebook, no. 3, 50 p.

Williams, P. L., 1964, Geology, structure, and uranium deposits of the Moab quadrangle, Colorado and Utah: U.S. Geol. Survey Misc. Geol. Inv. Map I–360.

# PARÍCUTIN, 1965—AFTERMATH OF ERUPTION

By KENNETH SEGERSTROM, Denver, Colo.

*Work done in cooperation with the Instituto de Geologia, Universidad Nacional Autónoma de México*

*Abstract.*—In contrast to their earlier catastrophic history, Parícutin volcano and its surroundings were approaching stability in 1965. The pattern and extent of lapilli fans on the outer slopes of the cone and the arrangement of fissures and slump blocks on inner (crater) slopes changed little during 1957–65. Most fumaroles still active in 1965 were in fissures on the crater rim, although the lava field outside the cone still had local hot spots. Increase in the vegetal cover was evident in the crater and on the rim but small on the outer slopes. Llanos along the edge of the lava field produced better crops than previously, or produced for the first time. Discharge of springs outside the lava field declined during 1957–65, reversing an earlier trend. Except on very steep slopes, devastated areas outside the lava field recovered spectacularly, chiefly through revegetation. Human population of the devastated zone was nearly constant during 1957–65.

Parícutin still provides an advantageous natural laboratory for studying the recovery of land devastated by lava and ash. Continued studies of this volcano and its surroundings are particularly appropriate because observations and records since the end of the eruption in 1952 have been exceptionally complete. In 1960, Parícutin and its surroundings were still strongly out of adjustment with the erosional and vegetal environment of the region (Beaman, 1961; Eggler, 1963; Segerstrom, 1961). By 1965, however, an approach toward stability was evident in all the devastated area: the cinder cone, the lava field with its associated ponded areas, and the surrounding ash-covered terrain (fig. 1). This progress toward recovery is described here in the light of earlier conditions.

*Acknowledgments.*—Celedonio Gutiérrez, formerly of San Juan Parangaricutiro and now of San Juan Nuevo, was the field companion of the author during the 1965 studies of the volcano region. G. P. Salas, Director of the Instituto de Geología of the Universidad Nacional Autónoma de México, kindly supplied a jeep for use during the study. J. H. Beaman, of the Department of Botany and Plant Pathology, Michigan State University, identified plants of the 1965 collection; the plants were deposited in the Michigan State University Herbarium.

## CINDER CONE

On the volcano, observations were made of the slopes and crater, of fumaroles, and of the status of vegetation. In June 1965, as in February 1957, narrow, fingerlike lapilli fans extended from near the crater rim down the southern and northwestern slopes toward the base of the Parícutin cone. Those on the southern slope (figs. 1 and 2) were similar in 1965 and 1957; on the northwestern slope, the fans extended lower in 1965 than they did in 1957. A wide area without lapilli fans existed on the southwestern and northern sides in 1957 and 1965. The persistence of fans and of fan-free areas suggests that the cone has been relatively stable in the past 8 years; in contrast, fans had been highly ephemeral when the volcano was active in 1946 (Segerstrom, 1950, p. 28–30).

An ascent of the crater on June 11, 1965, revealed little change in its various features since February 24, 1957 (Segerstrom, 1960, p. 3). The rim of the cone still had an east peak and a slightly higher west peak. The lowest part of the interior, about 40–50 meters below the southwest rim, was separated from a more shallow depression to the northeast by a saddle about 20 m high. Large blocks of agglomerate that rested in apparently unstable positions on the north and east inner walls in 1957 had not moved much by 1965 (compare fig. 3 *top* with fig. 3 *bottom*). One difference was noted: rock slides moved almost continuously on the rubbly west inner wall on the day of

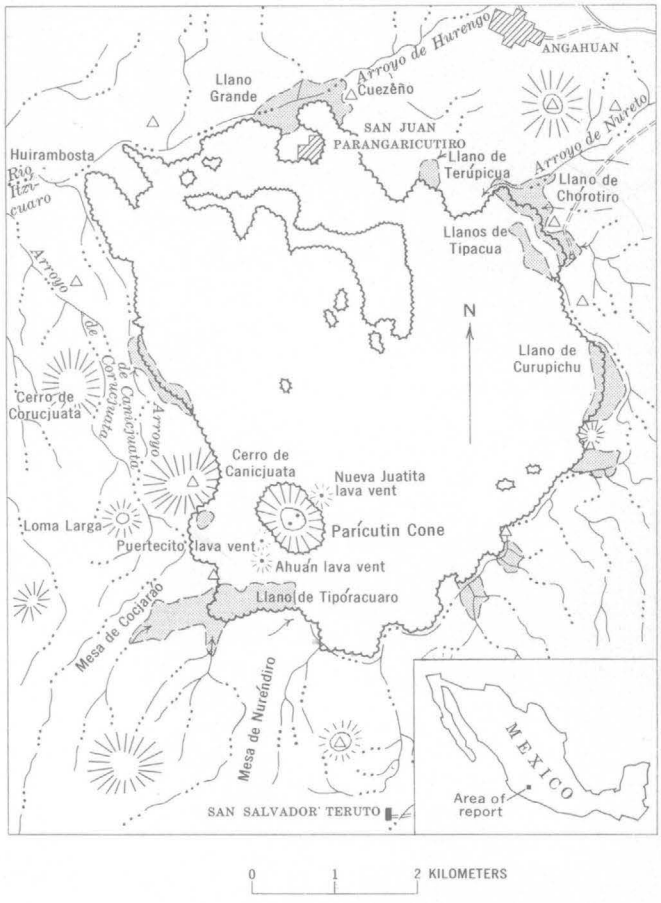


FIGURE 1.—Map of area around Parícutin volcano, State of Michoacán, Mexico. Scalloped lines show limits of lava field which surrounds the volcano. Stippled areas are llanos where clastic sediments were deposited in lava-blocked arroyos.

the 1957 ascent, but they were not observed on the day of the 1965 ascent.

Dissection of the Parícutin cone has not yet begun, and comparison of its form and surface with those of nearby cinder cones of greater age suggests that erosion will not be apparent for at least another century. Rill erosion had not started on the sides of the cone by 1965; the pyroclastic material of the cone is still too coarse and too permeable to permit surface flow of rainwater. With the passage of time, however, as soil which is less permeable than this material accumulates, the outer slopes of Parícutin will eventually become furrowed like those of the 200-year old Jorullo cinder cone, approximately 100 kilometers to the southeast. Inasmuch as the inner slopes of the crater of Parícutin are comparatively coarse, it is unlikely that water erosion will be evident there even after 200 years. Such is the situation at Jorullo (Segerstrom, 1950, p. 140). However, Cutzato crater (6½ km east-northeast of Parícutin) which is perhaps a thousand

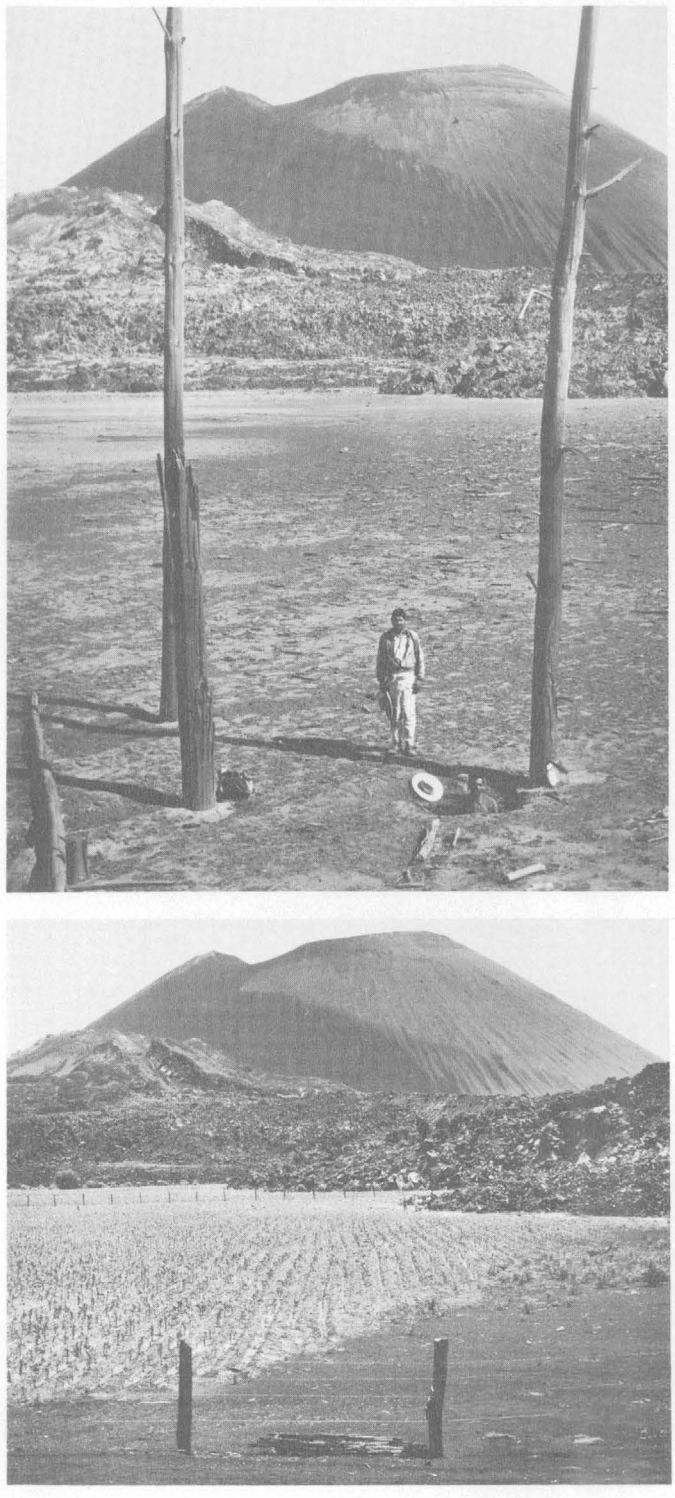

FIGURE 2.—Parícutin volcano from the southwest. Light-toned streaks on the cone are lapilli fans. *Top*, February 1957. Broken ground (middle distance) is part of lava field. Plain is lower end of Llano de Tipóracuaro, covered by litter from flash floods. Sinkhole (foreground, with man inside) disappeared before the 1965 photograph, below, was taken. *Bottom*, June 1965. Cornfield covers lower end of Llano de Tipóracuaro. Bushes at apparent edge of lava field, to the left, border depression through which floodwaters sink into underlying lava.

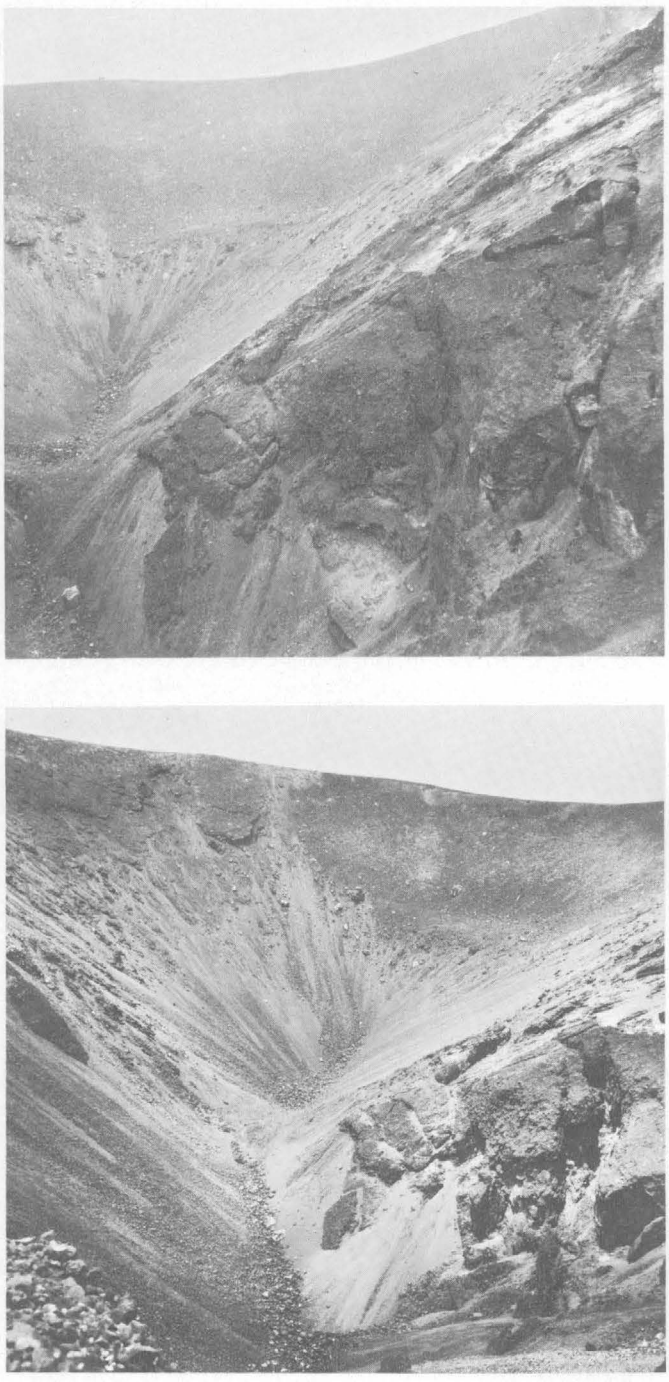

FIGURE 3.—Interior of Parícutin crater from southwest rim, showing two vents (lower left and middle left). *Top,* February 1957; *bottom,* June 1965.

years old (Williams, 1950, p. 199), is gullied on both outer and inner slopes (Segerstrom, 1950, p. 129 and pl. 6).

Small amounts of nearly invisible, nearly odorless vapor rose from cracks on the south and east inner crater walls during the sunny afternoon of June 11, 1965. Crusts of white and pale-yellow sublimate were found in the crater, particularly at fissures on the east and south walls. In a few places the sublimate had a reddish tinge, particularly on the south inner wall. The sublimates are probably ammonium chloride with variable amounts of iron chloride (Fries and Gutiérrez, 1954, p. 492).

Vegetation on the cone was much better established in some places in 1965 than it had been in 1960 (Beaman, 1961); in other places little change was noted. A large area within the crater, about 20 m below the north rim, was almost completely covered with grass on June 11, 1965. Plants collected along the south rim by the author that day included a small shrub, *Pernettya mexicana* Camp, which had not been previously collected at Parícutin by Beaman[1] nor mentioned by Eggler (1963). Other signs of life seen on the rim in 1965 included an oak leaf (windborne), spiders, and moths. A few mosses, but no vascular plants, grew on the south outer slope of the cone in 1965—the only slope that was examined closely.

## VEGETATION AND FUMAROLES ON THE LAVA FIELD

On the lava field, observations were made of the increase of plant life between 1960 and 1965, and of surviving fumaroles. Overlapping lavas of several ages had flowed from Parícutin, partly concurrently with eruptions of ash, and the development of a cover of vegetation in various parts of the lava field is to some extent dependent on local differences in amounts of superimposed ash from direct fall and time available for invasion by plants.[2]

Considerable ash fell on early flows, and very little on late flows. Because the late flows are near the cone and cover most of the early flows, very little of the exposed lava field has a heavy blanket of ash. Most of the Parícutin lava is of the aa, or blocky, type, and it forms a jagged surface (fig. 2.) The establishing of vegetation on such a surface depends on the presence of crevices and of ash which has partly or wholly filled them. Erosion and sedimentation by floods, caused by rapid drainage of water impounded by lava, are other factors affecting recovery.

Progressive establishment of vegetation of the lava field has been described by W. A. Eggler, who in 1950 found that "algae and mosses had become well established on the aa flows of Parícutin in 3 years and ferns were established in 4 years" (1959, p. 273). By

[1] J. H. Beaman, written commun., July 1965. The collection from this area included a fern, *Pityrogramma tartarea* (Cav.) Maxon, and the following herbs: *Aegopodon cenchroides* H. and B. ex. Willd., *Phytolacca icosandra* L., *Eupatorium malecolepis* Robins, *Gnaphalium semiamplexicaule* DC., and *Calamagrostis mcvaughii* Sohns?

[2] See Eggler (1963), fig. 1) for a convenient composite map indicating the relative ages of lava-flow exposures. Fries and Gutiérrez, (1954, p. 493) computed the total area of lava as 24.8 sq. km.

1960, Eggler was able to compile a list of 33 species of plants that were present on the 1944, 1945, and 1950 flows. This list included 2 gymnosperms, 9 angiosperm shrubs or small trees, 6 angiosperm herbs, 12 ferns, and 4 mosses (Eggler, 1963, table 4). According to Eggler, plants on the flows were usually in crevices and depressions, with a greater number of kinds of plants on the 1944 flow, in the northern part of the lava field. "Crevices were farther apart on the 1944 flow and hence collected more water and more ash" (Eggler, 1963, p. 55–57).

By 1965, most rock crevices in the north part of the lava field had mosses, many had ferns, and a few had shrubs and even pine trees. The largest pines were 2½–3 m high. Crevices in the south part of the field were still very sparsely vegetated; however, both the north and south parts had a few scattered shrubs and pines on ash-covered areas at that time. Plants already established by 1960 continued to survive. Since 1960, at least two new ferns had appeared in the north part of the lava field (1944 flow): *Polypodium plebejum* Schlect. and Cham., and *Polypodium thyssanolepis* A. Br.

Residual heat in the lava inhibited plant growth at some places. In June 1965, hot spots still existed at the surface of flows, even near the outer edges of the lava field; they were especially evident near the Llano de Tipóracuaro. During times of cool and humid atmospheric conditions, vapor columns rose from fumaroles in the lava. The largest and most persistent of these were on the Nueva Juatita lava-vent mound, on the northeast side of the cone, and on the Puertecito and Ahuán lava-vent mounds on the southwest side (fig. 1).

## PONDED AREAS ASSOCIATED WITH LAVA FIELD

Ponded areas that border the lava field and extend into some of its lowest parts have been the first ones near the volcano to become productive again. They were formed when lava flows filled the main valley at the head of the west-flowing Río Itzícuaro, causing the blocking of preexisting drainage and redeposition of ash and eroded soil. The principal lava-blocked areas of deposition, called "playas" by Eggler (1948, 1959), are the Llanos de Tipóracuaro, Curupichu, Tipacua, Chórotiro and Terúpicua, and Llano Grande (fig. 1).

The lakelike Llano de Tipóracuaro (pictured in Segerstrom, 1960, fig. 8, but not by name) is floored with a basin-fill deposit washed in from the south and dammed by the lava field. A relatively small alluvial fan at the east end formed a low divide, about 3 m high in 1957 and 1965, and prevented drainage into a barranca that closely follows the eastern edge of the lava field. As recently as 1960 the northern end of the flat plain was flooded during each heavy rain. In 1965 the floodwater escaped through a depression that was 12 m across and 3½ m deep and had caving sides, into underlying lava from Parícutin (fig. 2, *bottom*). A new gully from the west cut through the fill deposit to the depression. The depression did not exist in 1957, but at that time a hole 1 m deep in a different part of the basin allowed some floodwater to filter into the lava (fig. 2, *top*). This hole had disappeared by 1965. The basin fill has a large component of preexisting soil and has been a suitable site for plants since before 1957. Because of the periodic flooding, agriculture was unsuccessful until 1962, when the subterranean drainage system became more efficient. In June 1965 a cornfield on the plain extended over an area of 2 hectares (about 5 acres) (fig. 2, *bottom*).

The Llano de Curupichu lies along the barranca at the eastern edge of the lava field. (fig. 1). Floods that supplied most of its sediment were finally stopped in 1953 by a manmade bypass (Segerstrom 1960, p. 10). Since then, Curupichu has been successfully cultivated.

There are two Llanos de Tipicua, on and near the northeast edge of the lava field. One of them, inside the lava field, was filled as a result of manmade diversion of sediment-laden floods that bypassed Curupichu. Its fill covers a lava surface of 9 hectares (about 22 acres) with an average thickness of about 3 m. The other llano lies nearby but outside the lava field. Enriched by an admixture of eroded preexisting soil, largely brought in by ash-laden floods, these two areas have been cultivated since 1959 and 1953, respectively, mostly in corn but also in beans, squash, and chilicayote. Up to 1965, the western llano had been invaded by water on an average of about 30 times each summer, but only 5 or 6 times by sizable flash floods. In 1965 and for several years previously, the water quickly drained away into surrounding rock of the 1944 lava flow without drowning much of the crop. Before that, an efficient drainage system had not been developed on the western llano, and most of the plants were killed by flooding. On the eastern llano, equilibrium between runoff and infiltration of water into the lava field was established much earlier, and cultivation there was profitable as early as 1957.

The Llano de Chórotiro, just north of the Llanos de Tipacua, is floored with sediment washed in chiefly from the Arroyo de Nureto, to the northeast, and dammed by the lava field. In 1965 a small depression, about 1 m in diameter and 1 m deep, provided underground drainage of excess floodwater into lava near

the south edge of the plain. Agriculture has been possible at Chórotiro since 1946. A luxuriant growth of the large shrub, *Baccharis heterophylla* H.B.K., and of pine trees, grasses, and smaller plants, bordered the cornfield at Chórotiro in 1965.

The relatively small Llano de Terúpicua, which was produced by lava damming of an arroyo from the north, has an area of about 3 hectares (about 7½ acres). A 6-centimeter increase in the depth of fill at the edge of the lava field was observed over the period 1957–60 (Segerstrom, 1961, p. D225), and a gully that formerly directed floodwater into the lava had been filled. A comparable increase seems to have taken place over the period 1960–65. Corn was first planted at Terúpicua in 1959 and has done well ever since.

The large Llano Grande, farther to the west, was formed chiefly by flooding from the Arroyo de Hurengo, where it was blocked by the 1944 lava flow. At some time during the period 1947–57 the basin overflowed westward toward Huirambosta (Segerstrom, 1960, p. 11). In January and February 1965, a rock dam 1½ m high and 80 m long was built at the place of overflow, and by June of that year the dam had caused considerable sedimentation upstream (fig. 4). Cultivation of older parts of the Llano Grande basin fill began in 1953 and progressed slowly for 7 or 8 years. In June 1965, the cultivated area was about 10 times greater than in 1960.

The springs of Sipicha, which rise in a meadow near the Río Itzícuaro (west of area shown on fig. 1), several kilometers downstream from Huirambosta, are probably fed by ground water from the lava field of Parícutin. The flow of these springs increased more than 50 percent during the period 1946–57. This change was attributed to increase of effectiveness of the lava field as a recharge area (Segerstrom, 1960, p. 15). Surprisingly enough, by 1965 there had been a marked decline of average flow of these springs, although this decline seems not to have been accompanied by a marked lessening of mean annual rainfall.

In summary, the ponded areas dramatically illustrate recovery of the zone devastated by the volcano. Slopes along preexisting valleys, unsuited for agriculture because of topographic relief, have been buried. In their stead, the overlying new fields, flat as a floor and enriched by flood sediment, have already become productive.

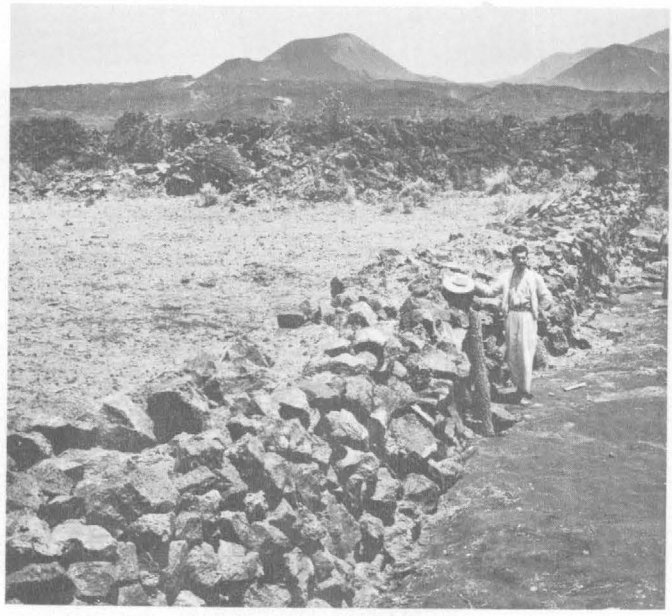

FIGURE 4.—Dam built in January–February 1965 at west end of Llano Grande–Cuezeño area, showing fill (to left) that had already accumulated there by June 1965.

## ASH-COVERED TERRAIN AWAY FROM THE LAVA FIELD

Much of the region around Parícutin is densely wooded, largely with pines. One of the first effects of the eruption, especially to the west of Parícutin, was the killing of the forest. In 1944 the thickly ash-covered area of Cerro de Canicjuata, Loma Larga, and Cerro de Corucjuata bristled with dead trees. The ash-covered floor of the dead forest was intricately dissected with rills and gullies, even on interfluves (fig. 5 *top*). Many of these rills and gullies were initiated by rainwater running down the tree trunks. Two decades later, the landscape just west of the lava field had a very different aspect; almost all the old tree trunks had fallen and had reached an advanced state of decay. Windborne seeds had taken root, preferentially in the old forest litter (fig. 5, *bottom*) (compare with Eggler, 1959, fig. 3), and together with other seedlings that had sprouted in preexisting soil exposed on the floors of deep gullies they gave rise to a vigorous stand of high grasses and shrubs. Most of the high grasses are in the genus *Eupatorium* (at least 6 species). The shrubs include *Baccharis* (2 species), and *Senecio* (3 species). Some specimens of *Eupatorium* that were growing in ash had attained heights as great as 4 m in 1965. Also becoming increasingly important was the genus *Buddleia*, with two species present as shrubs or small trees. These two species were first observed by W. A. Eggler, who visited the area in 1963 (written commun., Oct. 1965). A factor that favorably influences growth in these areas is animal droppings, because these further fertilize the ash.

Most of the forest north and east of the lava field was not killed by the ashfall. New trees are growing

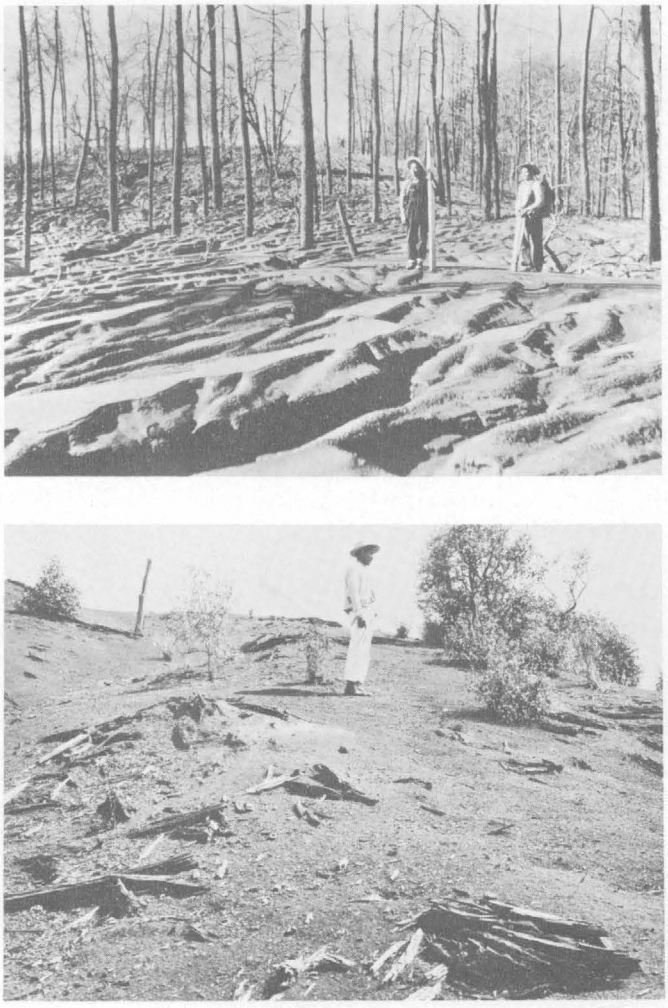

FIGURE 5.—Parts of the ridge between Arroyo de Corucjuata and Arroyo de Canicjuata. *Top,* January 1946, showing ash-killed forest and rills in the ash cover. *Bottom,* June 1965, showing rotten logs of ash-killed forest and new vegetation that has taken place. Note absence of rills.

in two environments: under older trees, and on exposed patches of the original soil. The many surviving trees shed guinumo (pine needles and similar litter) on the ash and provided fertile ground for seedlings, as was noted in 1957 and 1959 (Segerstrom, 1960, p. 16; Eggler, 1963, p. 48). By 1965 some of the seedlings in ash had grown to trees 2–3 m tall. The underlying soil was exposed over broad areas where the ashfall had been less than 25 cm and where the slope is more than 15° or 20°, and it was also exposed in relatively narrow, steeply sloping areas where the ash cover was thicker. These stripped areas provided optimum conditions for revegetation, and they are now well covered by plants except on nearly vertical walls of some gullies, and even there mosses coat much of the surface.

There has been much less revegetation of open fields which once formed clearings in the forest. The fields were generally in the flattest areas, where there has been little or no rill erosion since the ashfall. The factors that encouraged revegetation in the dead forest (presence of decaying tree trunks and admixture of eroded and redeposited soil) were thus absent in the fields, and significant numbers of new plants were growing only around the scattered trees that dotted these open spaces (Segerstrom, 1960, p. 16–17; Eggler, 1963, p. 50–52) or near the edges of the bordering forest. By 1965, much of the vicinity of Zirosto, about 8 km west-northwest of Parícutin (Segerstrom, 1961, fig. 370.2), as well as the areas of Huirambosta, 5 km north-northwest of the cone, Nureto, 6½ km northeast of the cone, and San Salvador Teruto, 4 km south-southeast of the cone (fig. 1), were still virtually barren.

Redeposition of ash by the wind has had two principal effects. Fields in the Zirosto area and toward the east, where some grass continued to grow during and since volcanic activity, had a hummocky surface in 1965. The hummocks, which are composed of thickly matted, creeping Bermuda grass, *Cynodon* (Eggler, 1963, p. 52), and wind-driven ash, did not exist in the region immediately before the eruption. By June 1965, however, they had grown to mounds as much as 7–8 m long and 1½ m high (fig. 6) (compare with Eggler, 1963, fig. 8). Another effect of eolian action—this one in the ash-killed forest—has been the filling in of rill heads with loose ash during successive dry seasons (November to May).

The following cycle of development has resulted from water erosion of the ash-killed forest terrain: (1) Incision of rills and gullies. (2) Their lateral (and in part longitudinal) growth, partly through

FIGURE 6.—Hummocks of creeping Bermuda grass (*Cynodon*) and wind-driven ash in western outskirts of Zirosto, June 1965.

capture of tributary and neighboring channels. In 1946, single storms produced capture of Arroyo de Canicjuata drainage by tributaries of the deeper Arroyo de Corucjuata (Segerstrom, 1950, p. 90.) Surveys along the narrow divide between the two arroyos have indicated, however, that no such drainage changes took place between 1957 and 1965. (3) The overall "softening" of the landscape as the gully divides become rounded. This sequence is illustrated by photographs taken in 1946, 1957, and 1965 of a knoll north of Loma Larga (fig. 7).

Runoff and rill erosion on the formerly wooded ridges and slopes are now inhibited by the dead tree trunks which have fallen (fig. 5, *bottom*) and by the new shrubs and trees which are springing up. This is exemplified by an area on the lower slopes of the Arroyo de Canicjuata where kill by the eruption was nearly 100 percent and gullying was intense (fig. 8). The recovery here occurred without marked additional stripping of the ash mantle, in 8 years.

On a few very steep ridges and slopes, however, continuance of the stripping of ash and soil during the period 1957–65 was evident. Headwalls of major gullies on old cones of the area, and the fronts of old lava flows where ash from Parícutin was deposited on slopes steeper than about 30° to 35°, were still being eroded. Continued stripping of areas that already had been partly freed of the ash by 1957 was particularly evident, in 1965, in a dozen or so headwalls on the Canicjuata and Corucjuata cones and at the lower edges of the Cocjaráo and Nuréndiro lava mesas (fig. 1). Nevertheless, the newly exposed original soil already supported heavy vegetation in such places, and so little ash remained in 1965 that there is little immediate likelihood of much further erosion.

Where the forest was not killed by the eruption, stabilization of the ash mantle has been even more rapid. In 1957 it was noted that the floor of a crater of the Curitzerán cinder cones, 2½ northwest of Llano Grande, had not been raised by redeposition of ash washed down from the inner slopes since 1946, indicating that erosion was unimportant. At that place, where 34 cm of ash had been deposited by direct fall, "forest growth had inhibited, if not stopped erosion and redeposition" (Segerstrom, 1960, p. 13–14). By 1965 there had still been no measurable increase of the crater deposit at Curitzerán. There, and in other areas of surviving forest where stripping of slopes had not been completed by 1946, the ash mantle from Parícutin is probably firmly established as part of the stratigraphic column.

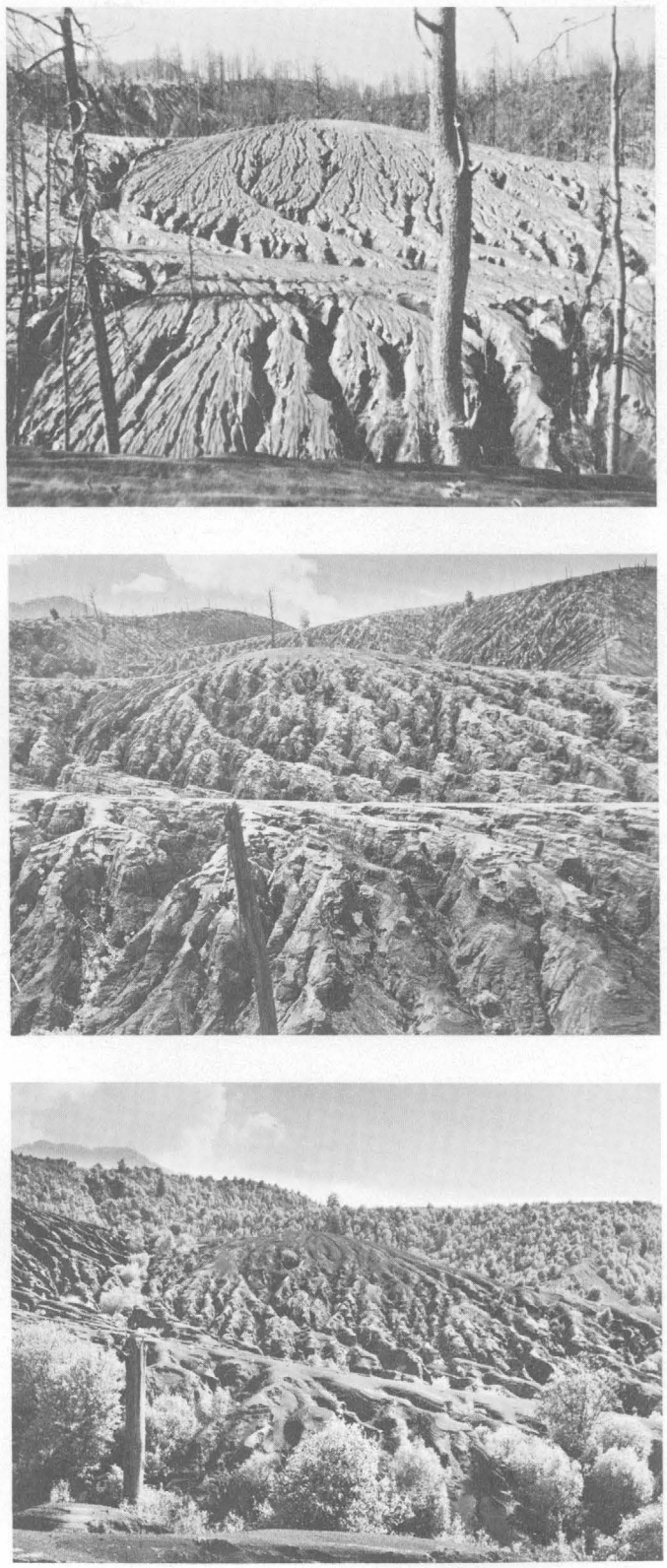

FIGURE 7.—Knoll north of Loma Larga, showing changes in erosion and vegetation over a 19-year period. *Top*, 1946; *middle*, 1957; *bottom*, 1965.

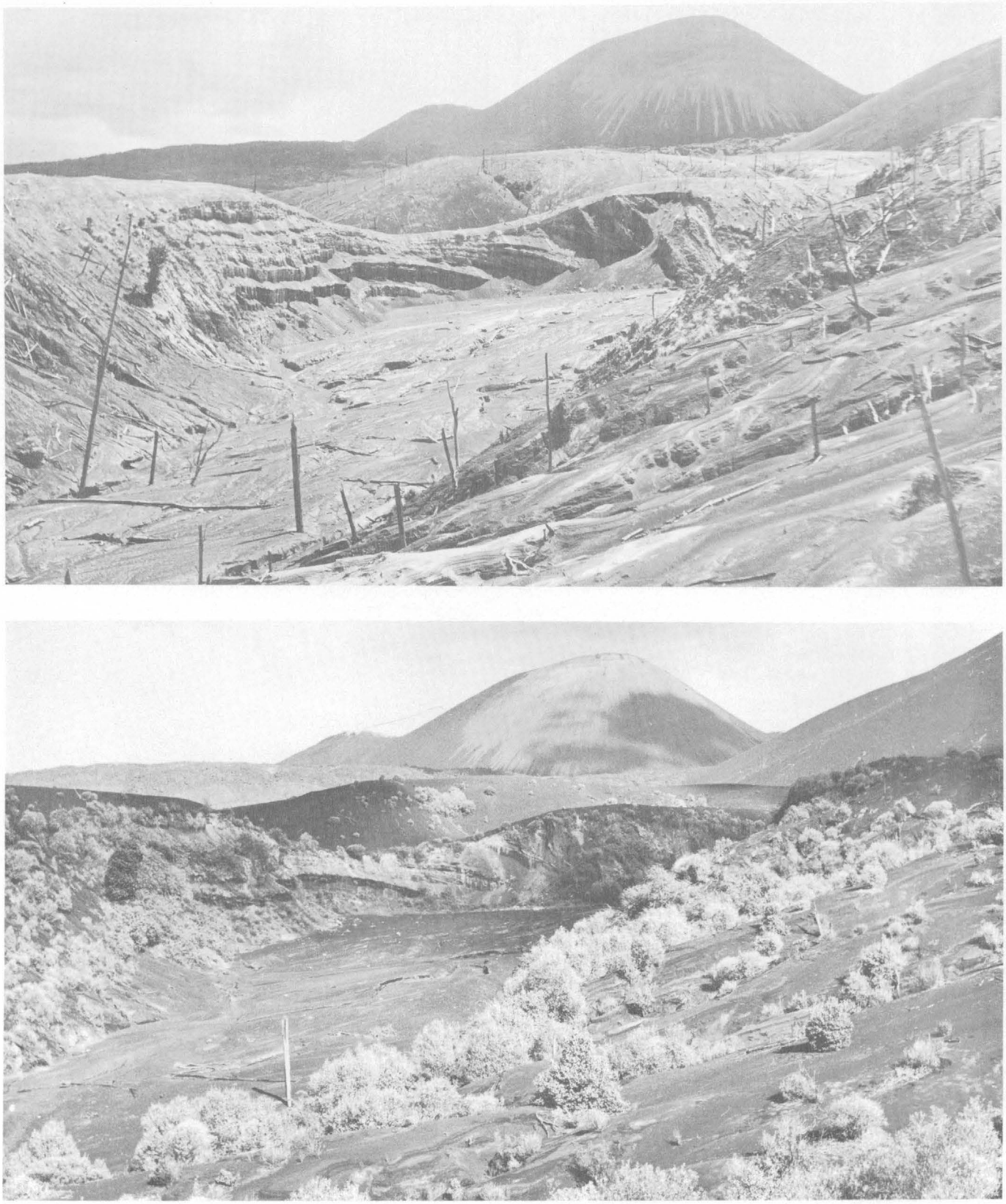

FIGURE 8.—Parícutin volcano from the northwest. Lower end of Arroyo de Canicjuata in left foreground. *Top*, February 1957; *bottom*, June 1965.

## REPOPULATION

Animals in the region made a strong and rapid recovery from a low in 1944, when most forms of life were exterminated to distances of 5–8 km from the cone. The first creatures to return included insects, field mice, crows, and foxes (Foshag and González, 1956, p. 480). By 1947, cottontails, tree squirrels, rock squirrels, gophers, bats, coyotes, and about 40 kinds of birds were reported in the vicinity of the volcano (Burt, 1961, p. 9–10). By 1965, most forms of the preexisting animal life had reappeared, except tusas (pack rats), guacamayos (macaws), and honey bees (Celedonio Gutiérrez, written commun., Nov. 1965).

The prospect of increased human resettlement of the area devastated by Parícutin volcano did not materialize during the period 1960–65. In 1965, the town of San Salvador Teruto, 3 km south of the cone, had 130 people, as compared with about 200 in 1960. San Juan Parangaricutiro, or San Juan Viejo, had 16 people in 1965, as compared with about 35 in 1960. In 1965 about 130 people lived at La Capilla, also known as "Capilla de San Isidro", a new town approximately 5 km south of San Salvador Teruto, whereas the older La Escondida settlement, between those two places, is now abandoned (see Segerstrom, 1960, p. 18).

## REFERENCES


Beaman, J. H., 1961, Vascular plants on the cinder cone of Parícutin volcano in 1960: Rhodora, v. 63, p. 340–344.

Burt, W. H., 1961, Some effects of Volcán Parícutin on vertebrates: Univ. Michigan Occasional Papers Mus. Zool. no. 620, 24 p.

Eggler, W. A., 1948, Plant communities in the vicinity of the volcano El Parícutin, Mexico, after two and a half years of eruption: Ecology, v. 29, p. 415–436.

——— 1959, Manner of invasion of volcanic deposits by plants with further evidence from Parícutin and Jorullo: Ecol. Monographs, v. 29, p. 267–284.

——— 1963, Plant life of Parícutin volcano, Mexico, eight years after activity ceased: Am. Midland Naturalist, v. 69, p. 38–68.

Foshag, W. F., and González, R., Jenaro, 1956, Birth and development of Parícutin volcano, Mexico: U.S. Geol. Survey Bull. 965–D, p. 355–489.

Fries, Carl, Jr., and Gutíerrez, Celedonio, 1954, Activity of Parícutin volcano during the year 1952: Am. Geophys. Union Trans., v. 35, p. 486–494.

Segerstrom, Kenneth, 1950, Erosion studies at Parícutin, State of Michoacán, Mexico: U.S. Geol. Survey Bull. 965–A, p. 1–164.

——— 1960, Erosion and related phenomena at Parícutin in 1957: U.S. Geol. Survey Bull. 1104–A, p. 1–18.

Segerstrom, Kenneth, 1961, Deceleration of erosion at Parícutin, Mexico: Art. 370 *in* U.S. Geol. Survey Prof. Paper 424–D, p. D225–D227.

Williams, Howel, 1950, Volcanoes of the Parícutin region, Mexico: U.S. Geol. Survey Bull. 965–B, p. 165–279.

# ORGANIC GEOCHEMISTRY OF THREE NORTH PACIFIC DEEP-SEA SEDIMENT SAMPLES

By JAMES G. PALACAS, VERNON E. SWANSON, and GEORGE W. MOORE,
Denver, Colo.; Menlo Park, Calif.

*Work done in cooperation with the U.S. Coast and Geodetic Survey*

*Abstract.*—Analyses of two samples, one taken about 150 miles northwest of Hawaii, and the other about halfway between the Aleutian Islands and the Hawaiian Islands, showed a nearly identical organic and inorganic composition, indicating a similar environment of deposition and history of diagenesis. The third sample, taken from the Aleutian Trench, south of the Aleutian Islands, showed significant differences and was characterized by the largest amount of organic carbon (0.34 percent), humic acids (1,145 ppm), and amino acids (180 ppm).

As part of a broader program to study organic matter in modern environments of deposition, three deep-sea core samples from the North Pacific were obtained for studies. Analyses were made for organic carbon, carbonate carbon, amino acids, humic acids, and bitumens. Emission spectrographic, X-ray, and microscopic analyses were also conducted, and moisture content determined.

Small segments about 15 centimeters in length were taken from 3 of some 15 cores collected during the 1963 cruise of the U.S. Coast and Geodetic Survey ship *Pioneer*. These cores were collected by personnel of the U.S. Coast and Geodetic Survey and turned over to the U.S. Geological Survey for geological and geochemical studies. The core sections were taken about 40 cm from the top of the 3 cores, which range from 1.2–2.5 meters in length and are 10 cm in diameter. To prevent bacterial decay, the cores were frozen immediately after they were collected, and the cores and samples from them were kept frozen until they were analyzed.

The nautical positions where the cores were taken are shown on figure 1. Measurements of temperature, salinity, and oxygen content of the ocean water above two of the sediment samples are given in table 1.

## PROCEDURE

The frozen core sections were removed from their plastic liners and all possible precautions to eliminate contamination were taken. Small representative fractions were examined for grain size, texture, mineralogy, fossil content, and color. No significant lithologic differences, from top to bottom, were noted within any of the core sections, and each section was designated as one sample.

Moisture content was determined by drying small portions of the samples for 48 hours at 100°C. The bulk of the core material was dried in a nitrogen atmosphere under vacuum at 40°C, and the dried sediment was ground in a porcelain mortar to less than 115 mesh. The powdered samples were stored in a freezer at —20°C until analyzed.

Carbon analyses were made following the procedures described by Rader and Grimaldi (1961, p. 33–39). Total carbon was determined in an induction-furnace carbon analyzer by burning a sample at 1350°C and converting the volume of evolved carbon dioxide to percentage of carbon by weight. Carbonate carbon was determined by a gasometric method. Organic carbon was calculated as the difference between total carbon and carbonate carbon.

The organic matter soluble in benzene, herein referred to as the bitumen fraction, was obtained by extracting 50 grams of sample with 150 milliliters of benzene for 5–10 minutes in an ultrasonic agitator at room temperature. After three successive ultrasonic treatments, the mixtures were centrifuged. The supernatant solutions were decanted and combined, evaporated to dryness, and weighed. A control (with no sample added) was also run simultaneously with the

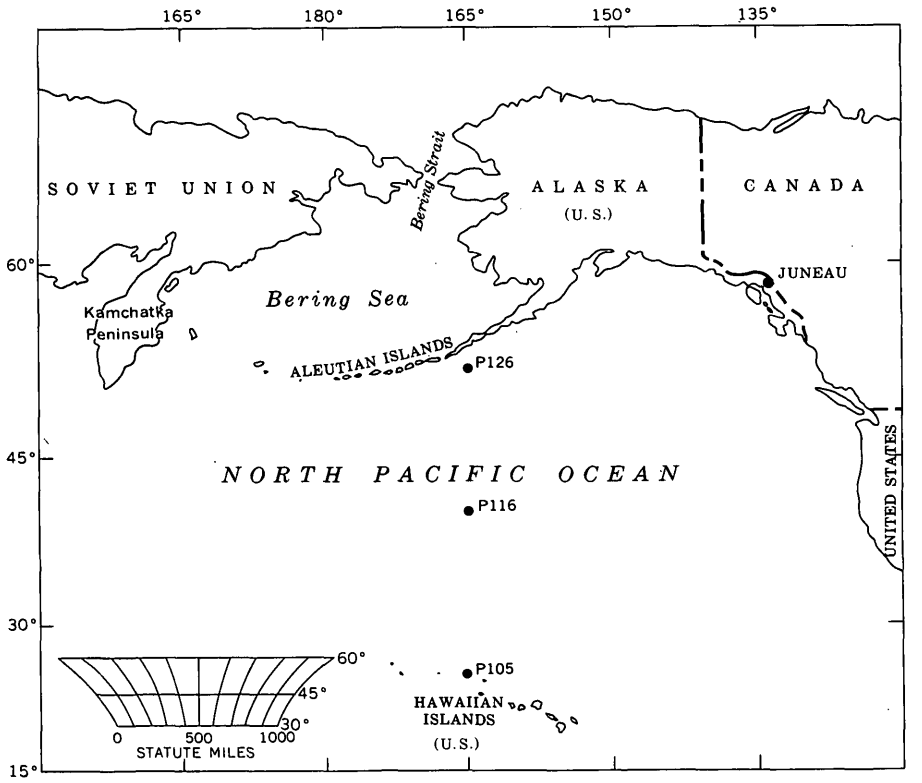


FIGURE 1.—Nautical positions of cores P105, P116, and P126.

TABLE 1.—*Geographic position of cores and measurements taken at each sample site*

[Samples and data collected in 1963 by Capt. Edward B. Brown, Comdr. Glenn Moore, Lt. Comdr. W. D. Barbee, and CBM W. V. Lavery, of the U.S. Coast and Geodetic Survey ship *Pioneer*]

| Core | Position | | Depth to bottom (m) | Length of core (m) | Measurements taken during sampling | | | |
|---|---|---|---|---|---|---|---|---|
| | Latitude | Longitude | | | At depth (m) | Temperature (°C) | Salinity (‰) | Oxygen (ml/l) |
| P105 | 25°01′ N. | 165°01′ W. | 4, 960 | 2. 5 | 4, 910 | 1. 50 | 34. 69 | 3. 58 |
| P116 | 40°00′ N. | 165°00′ W. | 5, 440 | 1. 2 | | | | |
| P126 | 52°15′ N. | 165°25′ W. | 6, 850 | 2. 1 | 4, 995 | 1. 55 | 34. 69 | 3. 59 |

three core samples, and no appreciable contamination was detected. No attempt was made to remove any free sulfur that might have been present, nor to fractionate the bitumen extract into its respective saturated hydrocarbon, aromatic hydrocarbon, and asphaltic fractions.

The alkaline-soluble humic fraction was obtained by suspending the bitumen-free sediment from the above treatment in 150 ml of 0.1*N* NaOH and shaking vigorously on a mechanical shaker for 8–10 hours at room temperature. The brown-colored extract was separated from the sediment by centrifugation and filtration. Additional extractions of the humic fraction were run at ultrasonic frequencies for 5–10-minute intervals with occasional shaking until color was no longer detected in the solvent. After the additional extracts were centrifuged and filtered, they were combined with the first extract and then acidified with HCl to pH 1. The resulting flocculate, which contains the humic acid, was separated by centrifugation from the supernatant or fulvic-acid fraction, washed with 0.001*N* HCl, and dried to constant weight. Due to varying amounts of inorganic matter, particularly silica, in the humic-acid flocculate, carbon and ash analyses were run on the dried extract. The actual humic-acid fraction was then calculated to an ash-free basis and is reported as such in table 2.

The amino acids were released by refluxing 20 g of sediment with 60 ml of 6*N* HCl for 24 hours. After treatment with strongly acidic ion-exchange resins to remove inorganic salts, the amino-acid extract was fractionated into individual amino acids by two-dimen-

sional, ascending paper chromatography (Block and others, 1958, p. 35, 118). Identification was accomplished by reacting the amino acids with a 0.25-percent solution of ninhydrin in acetone to which 1 percent lutidene was added. Semiquantitative estimates of the content of each amino acid were made by visually comparing the intensity and size of the unknown amino-acid spots to known standard amino-acid spots. The accuracy of this method is estimated to be about ±15 percent.

## RESULTS AND DISCUSSION

The samples for this study were deliberately taken at a uniform depth below the sea floor. However, additional studies, to be reported elsewhere, indicate that the geologic age of the samples is not uniform. The sample from core P126 is probably Pleistocene, and those from P105 and P116, pre-Pleistocene.

### Sediment analyses

Microscopic examination showed that samples P105 and P116 are generally similar in grain size, mineral composition, and color (table 2). Sample P116, however, contains a richer assemblage of radiolaria and diatoms. The Aleutian Trench sample (P126) differs from the pale-yellowish-brown clay sediment of P105 and P116 in its higher silt content and in its light-gray to greenish-gray color.

X-ray analyses of three samples, made by L. G. Schultz, of the U.S. Geological Survey, show that the major mineralogic components are potassium mica and chlorite, with lesser amounts of montmorillonite, quartz, and plagioclase. Cores P105 and P116 appear to be almost identical in mineral composition, whereas core P126 differs in having less mica and quartz and more montmorillonite and plagioclase.

Emission spectrographic analysis of the samples showed little difference in the value of most elements (table 3). Sample P126, however, does contain considerably more Ca than either P105 or P116, and P105 shows significantly higher values for Mn, Ba, La, and Ni than does P126. The concentration of the elements of each core sample compares closely with the average value for deep-sea clay as compiled by Turekian and Wedepohl (1961, table 1).

### Organic carbon content

The data show a nearly similar composition for the various fractions of organic matter in samples P105 and P116, which were collected, respectively, at a station about 150 miles northwest of Hawaii, and at a station near the middle of the North Pacific. The calculated organic matter content in both these samples (0.24 and 0.25 percent) is comparable to the average organic content of 0.27 percent in tropical siliceous diatomaceous mud of the Western Pacific Ocean as reported by Romankevich (1961). In contrast, the Aleutian Trench sample (P126) contains more than twice as much organic matter (0.58 percent) as either P105 or P116; yet even this amount is relatively low compared to some other North Pacific deep-sea sediment. Romankevich (1961, p. 384) found the greatest amount of organic matter in the high-latitude diatomaceous mud of the Western Pacific Ocean, which averages 0.85 percent organic carbon; and Bordovskii (1957, p. 2) found the following high contents of organic carbon in Recent sediments of the

TABLE 2.—*Description and analytical data of the three North Pacific core sections*

[Carbon analyses by I. C. Frost. Values on dry-weight basis except moisture content, which is on wet weight]

| Core | Description of dry sediment [1] | Moisture content (percent) | Total carbon (percent) | Carbonate carbon (percent) | Organic carbon (percent) | Total organic matter (percent organic carbon×1.7) | Humic-acid fraction (ppm) | Bitumen fraction (ppm) | Amino-acid fraction (ppm) |
|---|---|---|---|---|---|---|---|---|---|
| P105 | Clay, siliceous, pale-yellowish-brown (10YR6/2); microfossils rare except for few siliceous spicules. | 41 | 0.23 | 0.09 | 0.14 | 0.24 | 20 | 55 | 75 |
| P116 | Clay, siliceous, pale-yellowish-brown (10YR7/2); abundant radiolaria and diatoms. | 56 | .17 | .02 | .15 | .25 | 100 | 70 | 50 |
| P126 | Clay, silty, siliceous, light-gray (N7) to greenish-gray (5GY6/1); abundant diatom platelets and some spicules, with scattered dark grains, mainly magnetite, and some glass shards. | 49 | .34 | <.01 | .34 | .58 | 1,145 | 40 | 180 |

[1] Color ter ms and number designations are taken from Rock-Color Chart, Geological Society of America, 1951.

TABLE 3.—*Emission spectrographic analysis of core samples from the North Pacific Ocean*

[Barbara Tobin and H. G. Neiman, analysts]

| Element | Core | | |
|---|---|---|---|
| | P105 | P116 | P126 |
| Si | >10. | >10. | >10. |
| Al | >10. | >10. | >10. |
| Fe | 5. | 3. | 7. |
| Mg | 3. | 3. | 3. |
| Ca | .7 | .7 | 3. |
| Na | 2. | 3. | 2. |
| K | 5. | 5. | 2. |
| Ti | .7 | .3 | .7 |
| Mn | 1. | .5 | .07 |
| Ag | .0002 | ---- | ---- |
| B | .02 | .01 | .01 |
| Ba | 1. | .3 | .1 |
| Be | .0003 | .0003 | ---- |
| Ce | .02 | .015 | ---- |
| Co | .005 | .003 | .002 |
| Cr | .02 | .01 | .01 |
| Cu | .02 | .02 | .01 |
| Ga | .005 | .003 | .002 |
| La | .01 | .007 | .003 |
| Mo | ---- | ---- | .0007 |
| Nb | .003 | .0015 | .002 |
| Nd | .015 | .007 | ---- |
| Ni | .01 | .007 | .003 |
| Pb | .007 | .005 | .002 |
| Sc | .005 | .005 | .005 |
| Sn | .0015 | ---- | ---- |
| Sr | .03 | .05 | .05 |
| V | .02 | .02 | .02 |
| Y | .01 | .005 | .005 |
| Yb | .001 | .0007 | .0007 |
| Zr | .015 | .02 | .015 |

Results are reported in percent to the nearest number in a six-step series, for example 0.1, 0.15, 0.2, 0.3, 0.5, 0.7, 1, which represent approximate midpoints of group data on a geometric scale.

Note: Thirty-one other elements were looked for but not reported because the amounts of each were below the limit of detection.

Bering Sea: 1.46 percent in silty clays, 1.08 percent in fine silts, and 0.92 percent in clay sediments.

### Humic acids

The humic-acid content ranges from 20 to 100 ppm of dry sediment in samples P105 and P116, respectively, to as much as 1,145 ppm in sample P126. The humic-acid content of these three samples, particularly P105 and P116, is relatively low when compared to some of the values obtained for other deep-sea sediment of the North Pacific. For example, the average values of the alkaline-soluble humic matter in the fine-grained sediments of the Bering Sea were reported as 4,800 ppm for clays, 5,100 ppm for fine silts, and 7,800 ppm for silty clays (Bordovskii, 1957).

In these three deep sea samples, the humic acids account for nearly the entire humic fraction extractable with 0.1*N* NaOH, with the possible exception of P126, in which a small amount of fulvic acid was observed but not measured because of the large amount of salt associated with it.

It is noteworthy that in the Aleutian Trench sample (P126) the humic-acid fraction accounts for a relatively high proportion (20 percent) of the total organic matter (table 4). Degens and others (1964, p. 61), however, also reported high humic-acid contents ranging from 30 to 60 percent of the total organic matter in offshore sediment of California, and Romankevich (1957, p. 4) showed a range of 27–47 percent in the bottom sediment east of the Kamchatka Peninsula in the northwestern part of the Pacific Ocean. The humic-acid content of P116, however, is only 4 percent of the total organic matter, and in P105 humic acids make up less than 1 percent. The very low value in P105 resembles the values (less than 2 percent) reported for the red abyssal clays of the Western Pacific Ocean (Romankevich, 1961).

TABLE 4.—*Ratio of extracted organic matter to total organic matter (organic carbon × 1.7)*

[In percent]

| Sample | Humic acids | Bitumens | Amino acids |
|---|---|---|---|
| P105 | 0.8 | 2.3 | 3.1 |
| P116 | 4.0 | 2.8 | 2.0 |
| P126 | 20.0 | .7 | 3.1 |

### Bitumens

The bitumen content of the three core samples ranges from 40 to 70 ppm (table 2) and accounts for 0.7–2.8 percent of the total organic matter (table 4). The amount of bitumen in these samples compares closely with the amount of bitumen in other similar deep-sea sediment of the North Pacific Ocean. For example, Romankevich (1957, p. 2) reported, in another core sample, bitumen content (extracted with benzene and alcohol) of 100 ppm for diatomaceous clay at a core depth of 10–32 cm and 40 ppm for clay at a depth of 245–253 cm.

The bitumen values of these North Pacific deep-sea sediments, however, seem relatively very low when compared to the bitumen values of other marine sediments. In some of the basins off the California coast, such as the Santa Barbara Basin, Catalina Basin, and Santa Cruz Basin, the sediment obtained from cores at depths of 0.5–5 m below the sediment surface yielded a much higher content of bitumen—an average of 1,930, 925, and 1,500 ppm, respectively (Orr and Emery, 1956, p. 1251); and the surface sediment of these same 3 cores contained higher amounts, namely 3,010, 1,410, and 1,840 ppm respectively. Although the

bitumen values of these offshore basin sediments are relatively high, their ratios of extractable bitumens to total organic matter (range of 1.55–4.75 percent) are nearly similar to the ratios obtained for the North Pacific sediment samples. It should be pointed out that Orr and Emery, in their extraction procedure, used a solvent system of 70 percent benzene, 15 percent methanol, and 15 percent acetone; a mixed solvent generally extracts a larger fraction of organic matter, especially the more polar organic compounds, than benzene alone.

### Amino acids

The amino-acid content, including both combined and free amino acids, ranges from 50 to 180 ppm. Despite the range in amino-acid content the ratio of extractable amino acid to total organic matter is quite similar in all three, ranging from 2 to 3.1 percent and averaging about 2.7 percent (table 4). It is interesting to note that the amino-acid fraction of P105 exceeds both the humic-acid and bitumen fractions (table 4) and that the amino-acid content in all three samples is generally similar to the bitumen content.

A rather high content of an unknown amino-acid-like compound was noted in all three samples (table 5). This unknown compound, which may be an artificial substance produced during the treatment with strong acid, has a distinctive color similar to that of aspartic acid when reacted with ninhydrin and lutidine on a paper chromatogram.

In all three samples the combined content of the basic amino acids, arginine and lysine, is greater than the content of the acidic amino acids, aspartic and glutamic acid. Similar relations of basic amino acids predominating over acidic amino acids in marine sediments, particularly those sediments buried below the sediment surface to a depth of 0.5 m or more, were also indicated in the sediment studies of the Santa Barbara Basin (Degens and others, 1961, p. 418), in the experimental Mohole off Guadalupe Island, Mexico (Rittenberg and others, 1963, p. 162), and in the San Diego Basin (Degens and others, 1964, p. 62).

Alanine appeared to be the most abundant of the neutral amino acids. The aromatic acids, tyrosine and phenylalanine, were not detected except for a very small amount, 3 ppm, of phenylalanine in sample P126. Tryptophane may have been present but was not looked for because it would have been destroyed during acid hydrolysis.

## CONCLUSIONS

Samples from cores P105 and P116 are more similar to each other in organic and mineral composition, content if microfossils, environment of deposition, and history of diagenesis than to the sample from core P126 (the Aleutian Trench sample).

Although the humic acids, bitumens, and amino acids were selected to characterize the kind of organic matter present in the core samples, the combined total of the 3 fractions constitutes less than 10 percent of the total organic matter in samples P105 and P116. In P126, however, these 3 fractions make up about 24 percent of the total organic matter, of which 20 percent is represented by the humic-acid fraction. The remainder of the organic matter in all three samples is believed to be made largely of complex organic matter that has high molecular weight, is in part polymerized, and is not extracted by organic solvents or dilute acids and bases.

The large alkaline-soluble humic fraction of sample P126 and the proximity to land indicate that much of the organic matter was probably derived from the nearby Aleutian Islands and other parts of southern Alaska. Support for this conclusion is that lignin, a constituent of woody plants, is considered by many scientists as one of the major sources of this humic fraction, and that woody plant fragments have been observed in other core samples from near the Aleutian Trench (Smith, 1963, p. C77).

TABLE 5.—*Extractable amino-acid content of three North Pacific cores*

[In parts per million; N.D., not determined; Tr., trace]

| Core | Basic | | Acidic | | Neutral | | | | | | | Aromatic | | Unknown | Total |
|---|---|---|---|---|---|---|---|---|---|---|---|---|---|---|---|
| | Arginine | Lysine | Aspartic acid | Glutamic acid | Glycine | Alanine | Serine | Proline | Valine | Threonine | Isoleucine and leucine | Tyrosine | Phenylalanine | | |
| P105 | 10 | 10 | 2 | 1 | 4 | 18 | 0.7 | N.D. | 0.2 | Tr. | 0.6 | N.D. | N.D. | 28 | 75 |
| P116 | 7 | 6 | 2 | 1 | 4 | 6 | 1 | N.D. | .3 | Tr. | .4 | N.D. | N.D. | 22 | 50 |
| P126 | 33 | 19 | 16 | 10 | 12 | 20 | 15 | Tr. | 8 | 12 | 5 | N.D. | 3 | 27 | 180 |

## REFERENCES

Block, R. J., Durrum, E. L., and Zweig, G., 1958, Paper chromatography and paper electrophoresis: New York, Academic Press Inc., 710 p.

Bordovskii, O. K., 1957, Composition of the organic matter of Recent sediments in the Bering Sea: Doklady Akad. Nauk SSSR, v. 116, no. 3, p. 443–446 [translation by Associated Technical Services, Inc., 5 p.].

Degens, E. T., Prashnowsky, A., Emery, K. O., and Pimenta, J., 1961, Organic materials in Recent and ancient sediments, pt. II. Amino acids in marine sediments of Santa Barbara Basin, California: Neues Jahrb. Geol. u. Paläontologic Monatsh., v. 8, p. 413–426.

Degens, E. T., Reuter, J. H., and Shaw, K. N. F., 1964, Biochemical compounds in offshore California sediments and sea waters: Geochim. et Cosmochim. Acta, v. 28, p. 45–66.

Orr, W. L., and Emery, K. O., 1956, Composition of organic matter in marine sediments—Preliminary data on hydrocarbon distribution in basins off southern California: Geol. Soc. America Bull., v. 67, p. 1247–1258.

Rader, L. F., and Grimaldi, F. S., 1961, Chemical analyses for selected minor elements in Pierre Shale: U.S. Geol. Survey Prof. Paper 391–A, 45 p.

Rittenberg, S. C., Emery, K. O., Hűlsemann, Jobst, Degens, E. T., Fay, R. C., Reuter, J. H., Grady, J. R., Richardson, S. H., and Bray, E. E., 1963, Biogeochemistry of sediments in experimental Mohole: Jour. Sed. Petrology, v. 33, no. 1, p. 140–172.

Romankevich, E. A., 1957, The organic matter in core-samples of bottom sediments in the northwestern part of the Pacific Ocean (East of Kamchatka): Doklady Akad. Nauk SSSR, v. 116, no. 3, p. 447–450 (translation by Associated Technical Services, Inc. 5 p.).

——— 1961, Organic substance in the surface layer of bottom sediments in the western Pacific Ocean: Abstracts, 10th Pacific Sci. Cong., Honolulu, Hawaii, p. 384–385.

Smith, P. B., 1963, Possible Pleistocene–Recent boundary in the Gulf of Alaska, based on benthonic Foraminifera: Art. 79 *in* U.S. Geol. Survey Prof. Paper 475–C, p. C73–C77.

Turekian, K. K., and Wedepohl, K. H., 1961, Distribution of the elements in some major units of the Earth's crust: Geol. Soc. America Bull., v. 72, no. 2, p. 175–192.

211–690 O—66——8

# HEAVY MINERALS IN STREAM SEDIMENTS OF THE CONNORS PASS QUADRANGLE, WHITE PINE COUNTY, NEVADA

By E. J. YOUNG, Denver, Colo.

*Abstract.*—A comparative study of the heavy minerals in the sands being transported from Paleozoic sedimentary and Tertiary volcanic source rocks in the Connors Pass quadrangle in the central part of the Schell Creek Range shows that (1) the abundance of heavy minerals varies directly as their sorting, and (2) the abundance of the opaque minerals varies directly as the median size of the heavy minerals. The first empirical result confirms the theoretical relationship described by Rubey in 1933. Zircon/sphene ratios in 230–325-mesh stream sands derived from limestone are generally 1 or less; those from clastic-rock areas are greater. Higher content of allanite and sphene is found where source rocks are volcanic; higher content of zircon, rutile, and tourmaline where they are clastic.

The purpose of this study is to relate heavy-mineral suites in stream sediments to source areas drained by the major creeks in the Connors Pass quadrangle, Schell Creek Range, White Pine County, Nev. Drainage areas, generalized lithology, and sample sites for the seven creeks studied are shown in figure 1. Drainage areas rise to a maximum elevation of about 10,400 feet, and sample sites range in elevation from 6,200 to 7,300 feet. From north to south the four creeks that drain eastward are Cleve Creek, Bastian Creek, Cooper Creek, and an unnamed stream 1 mile south of Majors Place, which is at the junction of U.S. Highways 6, 50, and 93. The sampled streams draining westward are Taylor Creek in the south and Steptoe Creek and its tributary, Cave Creek, in the north.

*Acknowledgment.*—Appreciation is expressed to Harald Drewes, of the U.S. Geological Survey, for lithologic information.

## METHODS

At each sample site about a pound of sediment was taken from just below the surface of the streambed or adjacent bank in order to sample the youngest material unaffected by winnowing action of the wind. Carbonaceous matter was removed using a 10-percent solution of $H_2O_2$, and limestone fragments were dissolved with cold 1:4 HCl. After elutriation to remove clay and the finest silt, the samples were dried and screened at 35 mesh (0.50 mm). The undersize material was separated with bromoform, weighed, and sieved for 20 minutes on a shaking machine to obtain eight size grades. Magnetite was removed from each of these with a hand magnet.

The recommendations of Rubey (1933) were followed in selecting the 2 size grades to be used for study, 230–325 mesh (0.062–0.044 mm) size grade and the size grade containing the median of the heavy minerals. These two size grades for each sample were run through a microsplitter and then mounted in Aroclor ($n$=1.66), after which at least 325 grains were counted in each mount. Size grades containing the median for each sample are:

| *Sample No.* | *Mesh* | *Opening (mm)* |
|---|---|---|
| 1 | 80–120 | 0. 177–0. 125 |
| 2 | 170–230 | . 088– . 062 |
| 3 | 45–60 | . 35 – . 25 |
| 4 | 80–120 | . 177– . 125 |
| 5 | 45–60 | . 35 – . 25 |
| 6 | 80–120 | . 177– . 125 |
| 7 | 120–170 | . 125– . 088 |

## SIZE DISTRIBUTION

Size distribution of all the heavy minerals is shown in the histograms of figure 1. The heavy-mineral fraction of finest grain size (sample 2, Bastian Creek) contains the least amount of opaque minerals, while the coarsest fraction (sample 5, Taylor Creek) contains the greatest amount of opaque minerals. For the seven samples studied the amount of opaque minerals increases directly with the median grain size of the heavy-mineral fraction (fig. 2). The Bastian Creek sample also is strongly (negatively) skewed towards the coarse fraction and is thus distinguished

from the Steptoe Creek sample, with zero skewness, and from the other five samples, which are positively skewed. Finally, the best sorted sands contain the greatest amount of heavy minerals (fig. 3) in accordance with Rubey's (1933) theoretical results.

## MINERALOGY

The mineral content of the average of the two size grades of each sample is shown on figure 1. Thus, for example, in sample 1 the number frequency (expressed as percent) of mica in the 230–325-mesh size grade was 6.0; in the 80–120-mesh size grade, 3.3. Hence the average is 4.7, which has been plotted on the pie diagram of figure 1.

Of the opaque minerals found, the black ores are mostly hematite with minor amounts of ilmenite and unidentified minerals. The red opaque minerals are earthy hematite. X-ray powder patterns of yellow-orange opaque minerals show peaks of geothite, muscovite (sericite), and rutile (leucoxene). White opaque minerals were found by X-ray study to be mixtures of muscovite (sericite) and rutile (leucoxene).

Rock-forming minerals in the sand include hypersthene, monoclinic pyroxene, and several different types of amphibole. The most common type of amphibole is pleochroic from olive drab to green or brown and has refractive indices slightly greater than 1.66. Muscovite is abundant only in sample 2. Chlorite is scarce in all samples. Brown biotite is common. A less common red-brown biotite was tentatively identified as lepidomelane (iron-titanium biotite) in samples 4 and 6. This identification is based on the following optical properties noted: 2 $V \approx 32°$ (—); strong dispersion, $r < v$; $\beta > 1.66$; and yellow-brown to red-brown pleochroic colors on the basal plates.

Of the nonopaque accessory minerals, zircon is mostly colorless to pale pink, but a yellow variety was found in sample 2. Sphene occurs as mostly colorless anhedral grains; infrequently the grains are pale yellow and slightly pleochroic. Six varieties of tourmaline with slight differences in color were noted. The most common variety is pleochroic from colorless to shades of brown. Allanite is present as prismatic crystals; some grains are metamict and isotropic. It is possible that undetected chevkinite is present; it is sometimes difficult to distinguish between allanite and chevkinite on the basis of optical properties alone. Garnet, epidote, and yellow to yellow-brown rutile are persistent but scarce. Apatite is found in two samples, and only in small amounts, but it is probable that this mineral has been removed from the samples by the acid leaching. Sillimanite was found only in sample 2.

## PROVENANCE

The drainage area of Cleve Creek is underlain mostly by Cambrian quartzite and by Cambrian and Ordovician limestone and shale. The heavy minerals are dominantly opaque. The zircon/sphene ratio in the 230–325- mesh material is 2.35. Subsequent ratios are also given for this size fraction.

The small drainage area of Bastian Creek is underlain almost entirely by Cambrian and Ordovician limestone and shale. As noted earlier, this is the only stream where size distributions of the heavy minerals were found to show a negative skewness. The zircon/sphene ratio is 0.78. Sillimanite indicates metamorphism of some of the source rocks.

Cooper Creek drains Cambrian and Ordovician limestone, Mississippian shale, Pennsylvanian and Permian calcareous clastic rocks, and Tertiary latite and dacite. The rather large amount of opaque minerals in the heavy-mineral fraction probably came from the Mississippian Chainman Shale. Allanite is contributed by the Tertiary volcanic rocks, and the rather high zircon/sphene ratio of 2.67 is attributed to the clastic Permian Arcturus and Rib Hill Formations.

The drainage area of the unnamed creek south of Majors Place is underlain mostly by Permian calcareous clastic rocks and by Pennsylvanian and Permian limestone. The clastic rocks are probably the source of the large amounts of zircon, tourmaline, and rutile found in the sediments of this stream and result in the high, 14.50, zircon/sphene ratio. The strongest bimodal (poorest sorting) size distribution of heavy minerals occurs here, the coarse mode stemming from the opaque minerals and the fine mode from the unusually large amount of accessory minerals.

Taylor Creek drains mostly Mississippian shale, smaller areas of Permian clastic rocks, and Mississippian, Pennsylvanian, and Permian limestone. The large amount of opaque minerals in sediments of the creek are obviously derived from the Mississippian Chainman Shale, as the source rocks are almost entirely of that formation. The high zircon/sphene ratio, 7.33, is due to the clastic rocks. Strong positive skewness results from the large amounts of opaque minerals which tend to be coarse.

Source rocks in the Cave Creek drainage area are mostly Devonian limestone and dolomite and Tertiary conglomerate and quartz latite. There are smaller areas of lower to middle Paleozoic limestone, dolomite, and shale. Sphene and allanite are derived from the volcanic rocks, and the zircon/sphene ratio of 1.00 approaches that of a pure limestone terrane, owing to the absence of sand-size clastic source material in the drainage area.

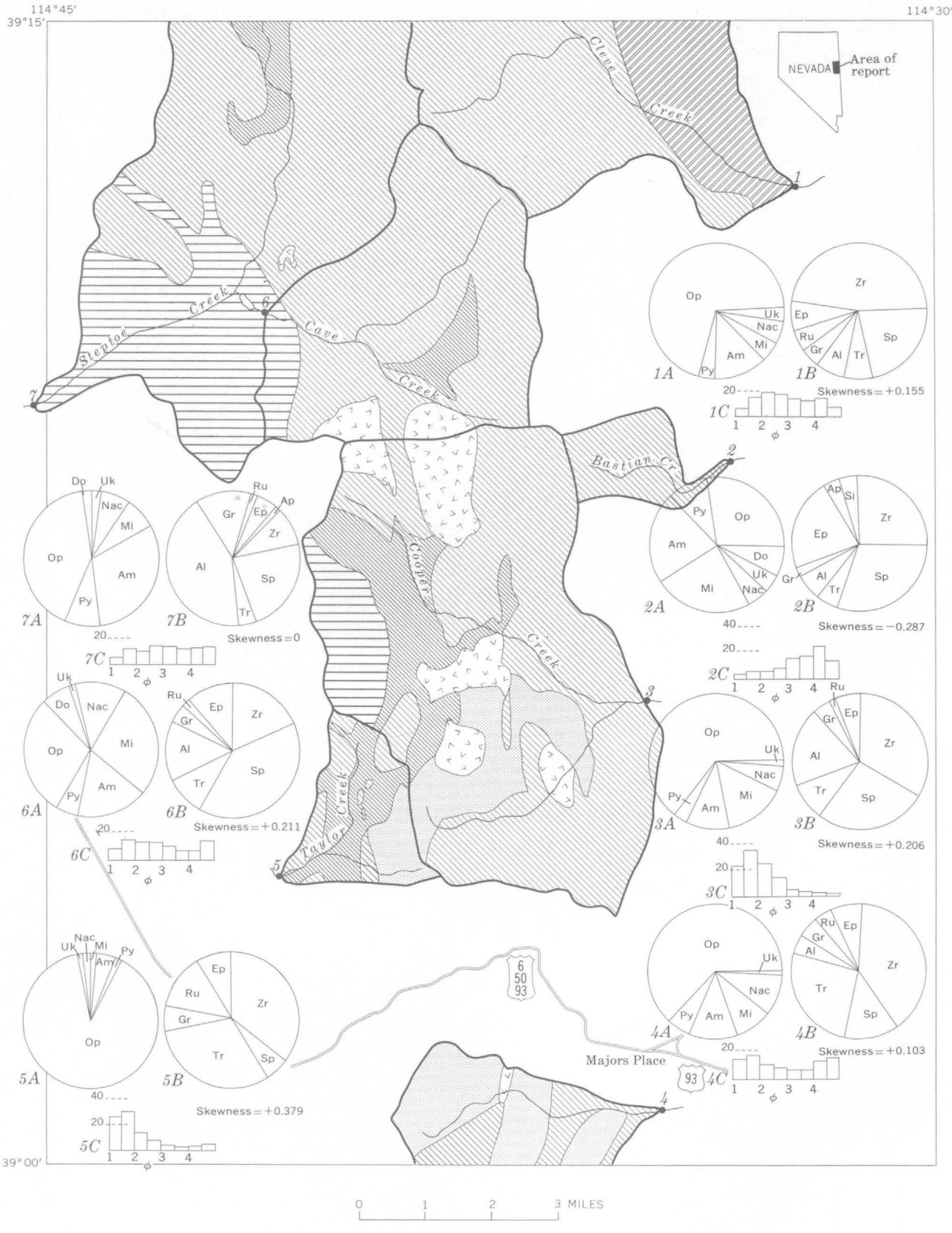


FIGURE 1.—Map of the Connors Pass quadrangle, Nevada, showing sample locations, drainage areas (heavy outlines), generalized lithology, and heavy-mineral data.

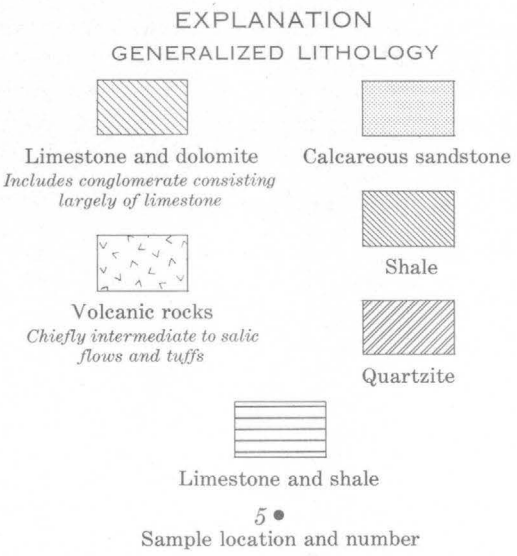


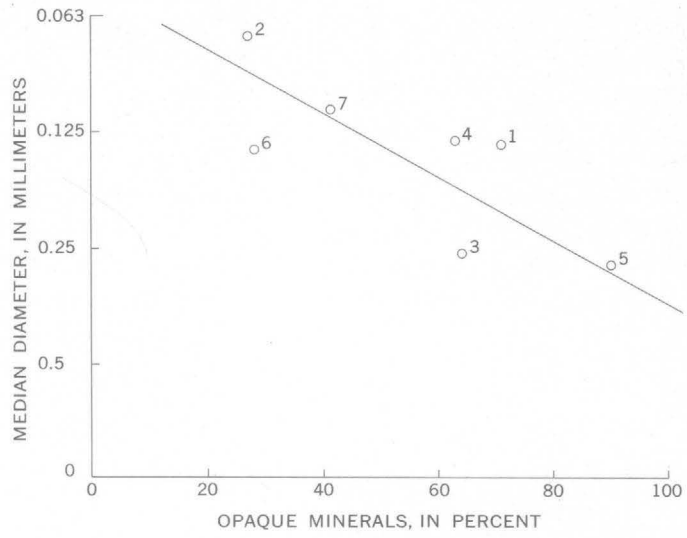


FIGURE 2.—Relation of median diameter of heavy minerals to the percentage of opaque minerals in the heavy fraction (number percent for the average of two size grades). Numbers identify samples described in text and referred to on figure 1.

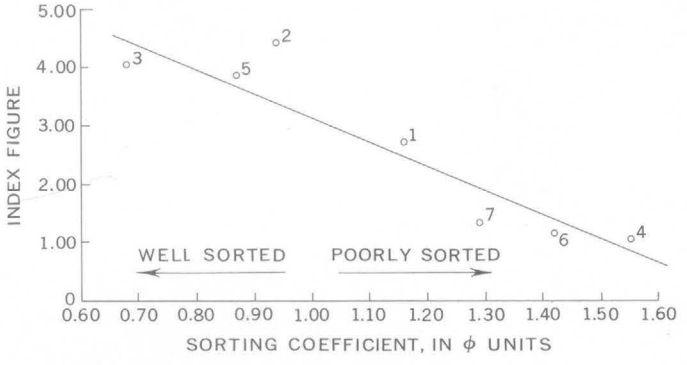


FIGURE 3.—Relation of the index figure (bromoform heavy minerals in −35-mesh sand, in weight percent) to sorting in the heavy minerals. Numbers identify samples described in text and referred to on figure 1.

Steptoe and Cave Creeks drain mostly Cambrian and Ordovician limestone, Mississippian shale, and Pennsylvanian and Permian limestone. There are also smaller areas of lower to middle Paleozoic limestone, dolomite, and shale, and Tertiary volcanic rocks and conglomerate. Opaque minerals come from the shale, and amphibole and allanite from the volcanic rocks; the low zircon/sphene ratio, 0.50, results from the lack of sand-size clastic source material in the drainage area.

## CONCLUSIONS

Large amounts of allanite and sphene, which together contribute about 50 percent of the nonopaque

accessory minerals, are characteristic of volcanic terrane in this area. In sediments of Steptoe Creek the relatively high (1 percent) garnet content, along with large amounts of allanite and sphene, suggests that garnet, too, is derived from volcanic rocks.

Zircon/sphene ratios of 1.00 or less seem to result from limestone terranes and lack of clastic source rocks. Ratios greater than 1.00 indicate the presence of clastic source rocks. The reason for low zircon/sphene ratios in limestone is not known. It may either result from authigenic sphene in the limestone, or it may result from an originally greater amount of sphene than zircon being deposited during formation of the limestone.

## REFERENCE

Rubey, W. W., 1933, The size-distribution of heavy minerals within a water-laid sandstone: Jour. Sed. Petrology, v. 3, p. 3–29.

# GENERAL FEATURES OF THE BOUGUER GRAVITY FIELD IN SOUTHWESTERN OREGON

By H. RICHARD BLANK, JR., Menlo Park, Calif.

*Abstract.*—A contoured Bouguer anomaly map of a region 75 miles wide and 130 miles long shows an average west-to-east negative gradient that corresponds qualitatively to an inland thickening of the continental crust. Gravity highs in the Coast Range may reflect ultramafic bodies at depth as well as near-surface accumulations of lower Eocene basalt. Anomalous northeast trends in the Cascade Range are attributed to a concealed extension of the Klamath Mountains upwarp. A negative anomaly not exceeding 10 mgals is associated with the Crater Lake caldera, and a negative anomaly of 20 to 30 mgals coincides with the northern end of the Klamath graben.

In the summers of 1962 and 1963 a reconnaissance gravity survey was made of a rectangular region some 75 miles wide and 130 miles long, or about 10,000 square miles in area, that extends across southwestern Oregon from the upper Klamath basin to the Pacific Ocean (fig. 1). The region embraces portions of the Great Basin, Middle Cascade Mountains, Klamath Mountains, and Oregon Coast Range physiographic sections of Fenneman (1931). The gravity survey has the dual purpose of supplementing recent geologic mapping in the region and investigating major crustal elements in a zone transitional from a continental interior to an oceanic environment.

## GRAVITY DATA

A base net was established with reference to the Eugene and Medford airport gravity stations of Woollard (1958). A value of 980,236.5 milligals was assumed for the observed gravity at Medford, based on a closed-loop tie to U.S. Geological Survey base station "A" at Menlo Park, Calif. This value is 1.0 mgal lower than Woollard's most recently published value for Medford (Woollard and Rose, 1963) but results in a value identical to his for the observed gravity at Eugene. The location of primary and secondary base stations and nearly all points of observation (a total of about 2,250 stations) is shown in figure 2 (see also Blank, 1965). Two gravimeters were used in the survey, and the base network was later checked with another gravimeter. With a few exceptions, where altimetry was used, elevations at gravity stations are published values obtained from U.S. Geological Survey 15-minute and 30-minute topographic maps. The meter readings were reduced with the aid of an electronic computer to Bouguer anomaly values based on the international ellipsoid, using a reduction density of 2.67 grams per cubic centimeter. Contoured Bouguer values are superimposed on a geologic map of the region in figure 3; representative gravity profiles taken from the contours, together with interpretative geologic sections, are presented in the same figure.

Partial terrain corrections are incorporated in the data for the eastern third of the map area, but none have been applied elsewhere. Stations with obviously large terrain effects have been ignored in drawing the contours; the contours have been smoothed by inspection. Although the resulting representation of the

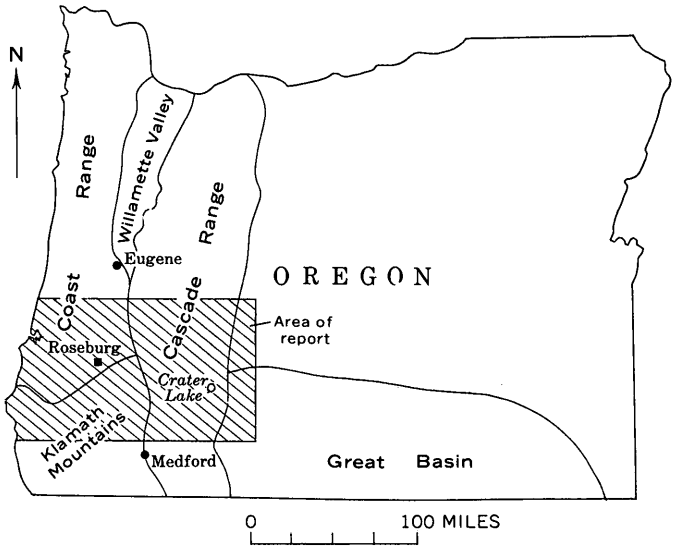


FIGURE 1.—Index map of Oregon, showing major physiographic boundaries and location of report area.

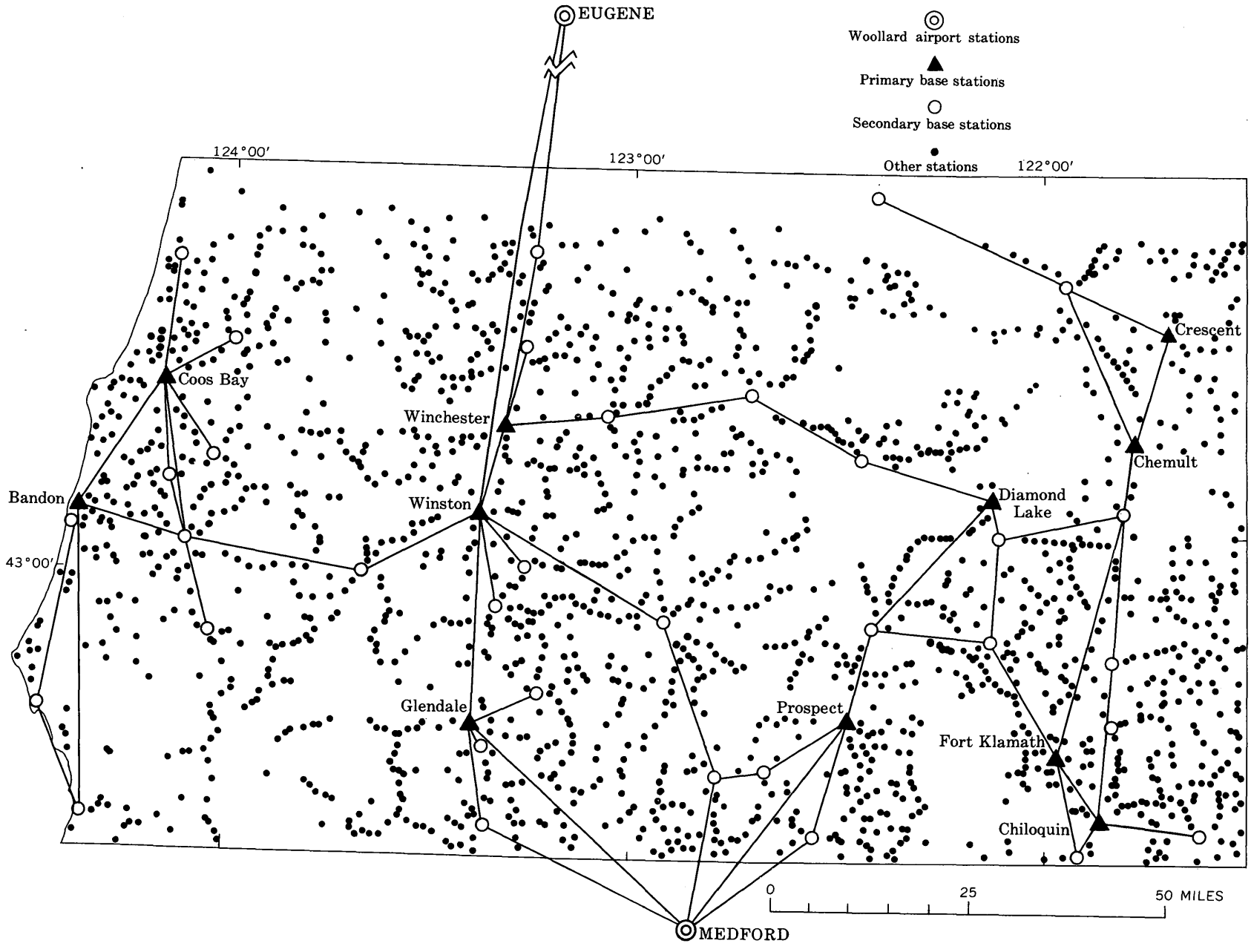


FIGURE 2.—Gravity-station location map of report area. Lines show tie routes between base stations.

Bouguer gravity field differs in detail from a complete Bouguer gravity map of the region, the larger gravity features are delineated with an accuracy compatible with the 10-mgal contour interval, and their spatial relation to regional geologic features is adequately shown.

## GENERAL GEOLOGY

Rock units shown on the geologic map are grouped for convenience into three main divisions, on the basis of age and physiographic location—the Klamath Mountains and Coast Range pre-Tertiary sequence, the Coast Range sequence of Cretaceous and early Tertiary age, and the Cascades and Great Basin sequence of Tertiary and Quaternary age.

A structural synthesis for the ultramafic belts of northwestern California and southwestern Oregon, which include the Klamath Mountains region, has recently been published by Irwin (1964). Rocks involved in the Late Jurassic Nevadan orogeny in the region are distinguished from all younger rocks in Irwin's analysis by the terms "subjacent" and "superjacent." In figure 3, pre-Nevadan rocks, Nevadan intrusive rocks, and some of the ultramafic bodies constitute "subjacent" terrane of Irwin. The pre-Nevadan rocks are a eugeosynclinal suite of weakly to strongly metamorphosed sedimentary and volcanic rocks that occur in the eastern part of the northern Klamath Mountains and also near the Pacific Ocean. Their age is chiefly Triassic and Late Jurassic; locally some Paleozoic rocks may be present. The associated Nevadan plutons range from felsic to mafic.

Eugeosynclinal rocks assigned to the Dothan Formation (Diller, 1907) consist of sandstone, mudstone, shale, and conglomerate, with interbedded lava and chert (Wells and Walker, 1953). They form a broad northeast-trending belt on the northwest flank of the known pre-Nevadan portion of the Klamath Mountains. The age and stratigraphic position of the Dothan are controversial, owing both to a lack of fossils and to the steep and faulted marginal contacts. The formation is regarded as post-Nevadan ("superjacent") by Irwin (1964, p. C3) and as being in thrust contact with older rocks to the southeast. Dott (1965, p. 4690), among others, believes that the Dothan is pre-Nevadan, and probably older than the pre-Nevadan (Galice Formation) adjacent on the southeast. A critical review of the problem is not in order here, nor is either interpretation ruled out by the gravity data.

Stratigraphically above the Nevadan and older rocks are formations comprising the Myrtle Group (Imlay, 1959), which consists predominantly of interlayered beds of graywacke, mudstone, and conglomerate. These rocks have been dated as post-Nevadan and pre-Upper Cretaceous. According to Irwin (1964), the "superjacent" Myrtle Group is the youngest unit involved in a second orogeny which occurred in Late Cretaceous time and produced westward or northwestward thrusting over a broad region. Thin plates and irregular masses of ultramafic rocks were intruded mainly along thrust planes during both orogenies. The "subjacent" pre-Nevadan rocks and Nevadan intrusives west of the Dothan belt are possibly upper plate rocks of a Late Cretaceous thrust whose root zone lies east of the belt of Dothan. This concept is adopted in section *C–C′* of figure 3 for purposes of illustration.

The area surveyed includes the southern end of the so-called Coast Range early Tertiary eugeosyncline that is inferred to have occupied a generally linear region extending from Vancouver Island, British Columbia, to the Klamath Mountains (Snavely and Wagner, 1963; 1964). Although the lateral extent of this feature is poorly known, the eastern margin probably lay within the site of the present Cascade Range, and a western margin may have existed a considerable distance west of the present Pacific coastline. To a first approximation the eugeosyncline is considered to include the terrane of the Coast Range sequence in the present report (see figs. 1 and 3).

Four rock units are distinguished in the Coast Range sequence: (1) Upper Cretaceous and lower and middle Eocene sedimentary rocks (chiefly alternating mudstone and sandstone of the Umpqua and Tyee Formations), (2) lower to middle Eocene volcanic rocks (basaltic flows and pillow lavas intercalated with sedimentary rocks of the Umpqua Formation and equivalent to the Siletz River Volcanic Series in the central part of the Oregon Coast Range), (3) upper Eocene volcanic rocks (chiefly andesitic pyroclastic rocks of the Colestin and Calapooya Formations), and (4) upper Eocene and younger sedimentary rocks (sandstone, siltstone, and shale, with subordinate coal). The upper Eocene volcanic rocks are exposed only along the western margin of the Cascade Range in the region studied and could be equally well regarded as formations of the Cascades sequence.

Volcanic rocks of the Cascades and Great Basin sequence occupy the eastern half of the report area. They consist predominantly of the following: east-dipping Oligocene- and Miocene-age lavas and pyroclastic rocks of the Western Cascades; Pliocene and Pleistocene basalt flows of the High Cascades; and late Quaternary plugs, cinder cones, and valley-filling lava flows (see Peck and others, 1964; Williams, 1957). The lavas of the High Cascades extend east-

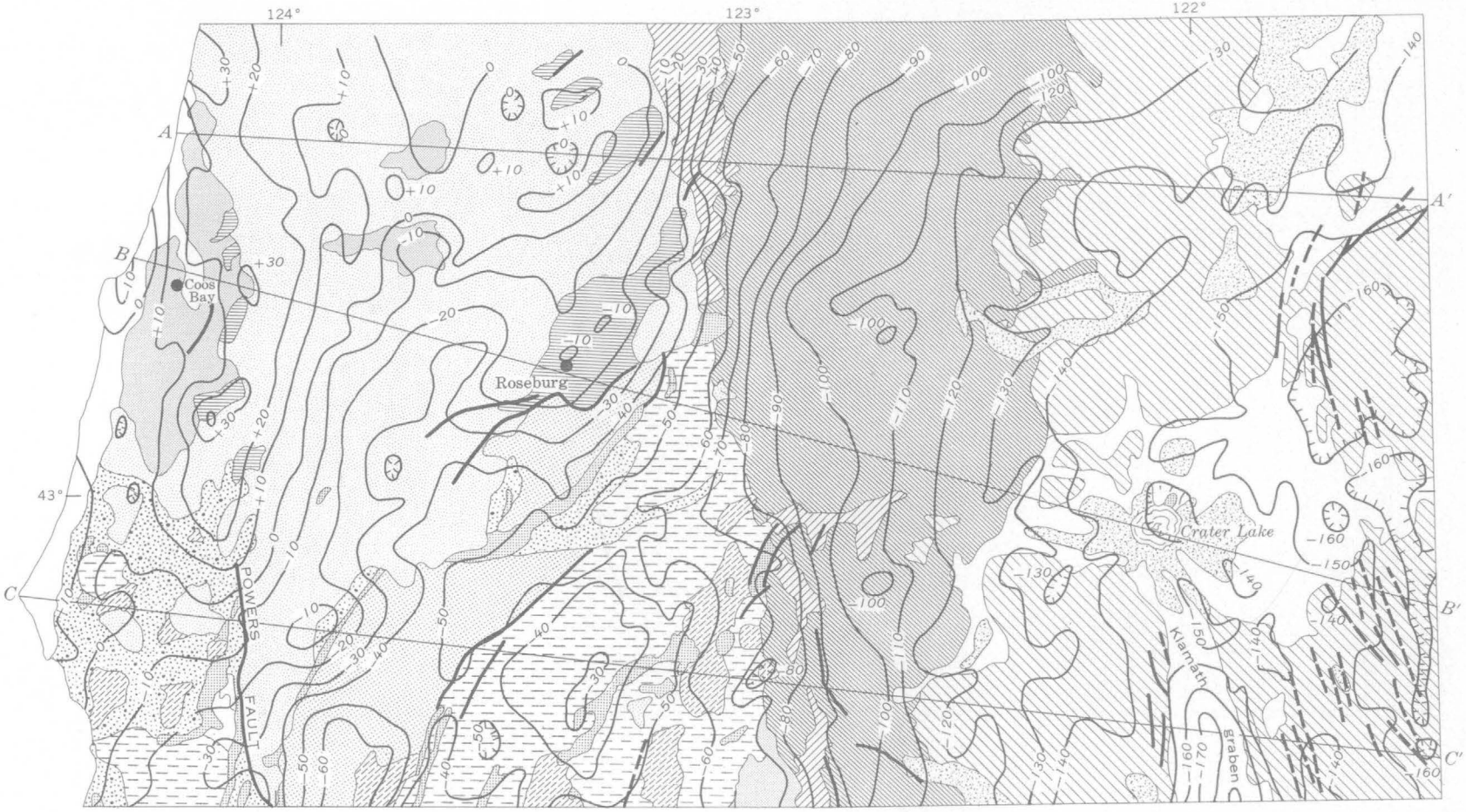


EXPLANATION

KLAMATH MOUNTAINS AND COAST RANGE

PRE-TERTIARY

- Myrtle Group
- Dothan Formation
- Ultramafic intrusive rocks
- Nevadan felsic and mafic intrusive rocks
- Pre-Nevadan rocks

COAST RANGE

TERTIARY

CRETACEOUS

- *Upper Eocene and younger* — Sedimentary rocks
- *Upper Eocene* — Volcanic rocks
- *Lower to middle Eocene* — Volcanic rocks
- *Upper Cretaceous and lower and middle Eocene* — Sedimentary rocks

CASCADES AND GREAT BASIN

TERTIARY AND QUATERNARY

- *Recent* — Unconsolidated deposits
  *Includes ash and alluvial deposits; also dune sand and marine terrace deposits of Pacific coastal area*
- *Upper Pleistocene and Recent* — Volcanic rocks
  *Includes rock of cinder cones, plugs, and lava flows*
- *Pliocene and Pleistocene* — Volcanic rocks
- *Oligocene and Miocene* — Volcanic rocks

Contact

Fault
*Dashed where approximately located*

-50

Gravity contour with simple Bouguer anomaly value in milligals
*Contour interval 10 milligals; hachured contours enclose gravity lows*

0 25 MILES

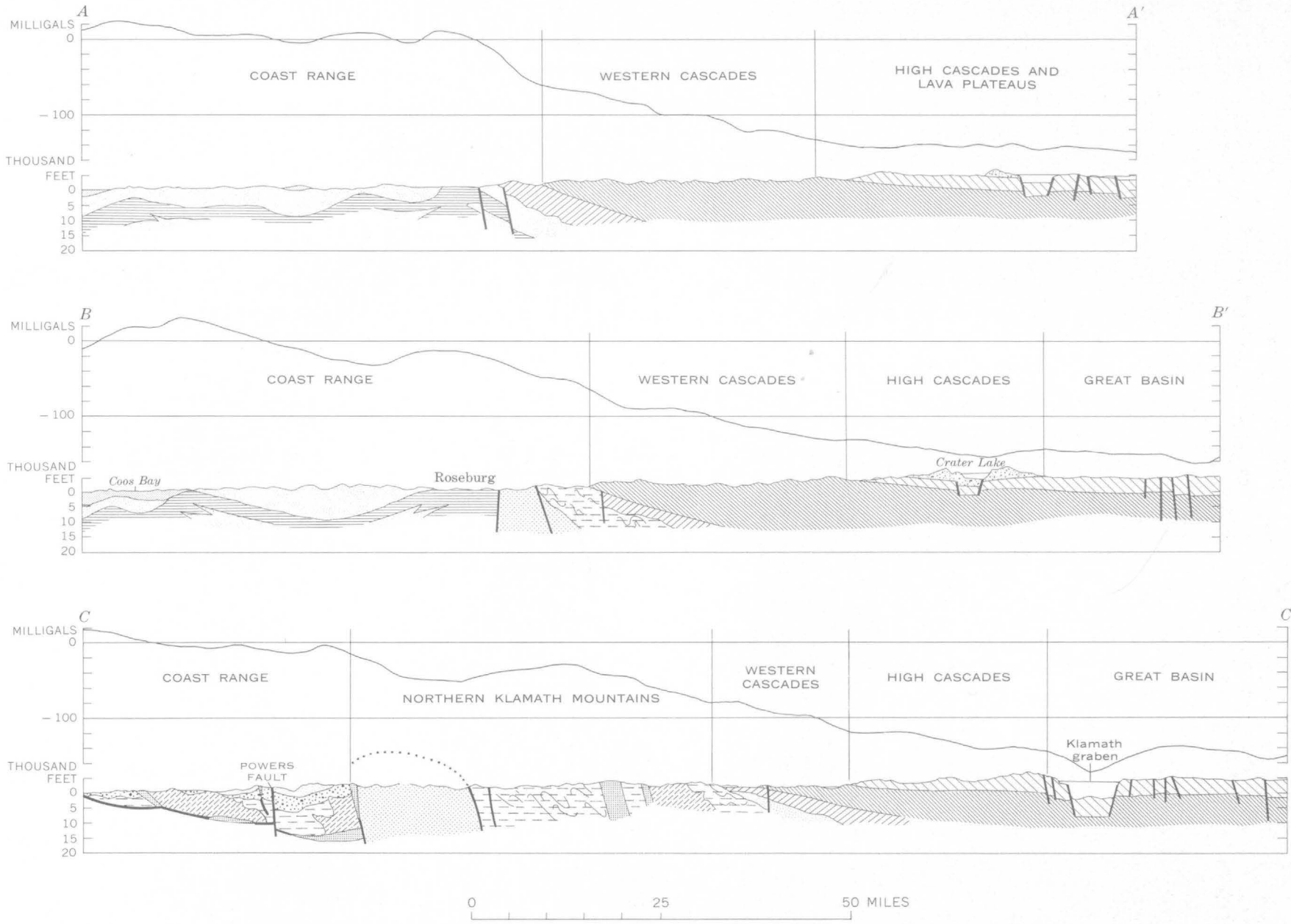


FIGURE 3.—Generalized geologic and Bouguer gravity map, and gravity profiles, of southwestern Oregon. Geology generalized from Wells and Peck (1961). Gravity profiles are shown along interpretive geologic sections on which the veneer of Recent sediments has been omitted, except where such sediments are thick, as in the Klamath graben.

BLANK

ward into the Great Basin and there interfinger with volcanic-type sedimentary rocks and pyroclastic rocks.

## QUALITATIVE INTERPRETATIONS

Total gravity relief shown by the map is about 210 mgals. There is an overall decrease in average Bouguer values from west to east of about 1 mgal per mile. This corresponds qualitatively to an increase in average regional elevation progressing inland from the continental margin, which is compatible with an isostatic condition of the Airy type and an inland thickening of the continental crust. Various isostatic models for the region are currently being tested.

The highest Bouguer values, as much as +40 mgals, occur on an elongate north-trending gravity high whose axis passes just east of Coos Bay on the west side of the map area (fig. 3). Lower Eocene olivine basalts are exposed at several places near the crest of this anomaly where they have been tectonically elevated. The local structures are roughly en echelon and trend north-northeasterly, but the overall patterns of basalt outcrop and linear gravity feature coincide. Other gravity highs are associated with lower to middle Eocene basalt cropping out at, and north of, Roseburg.

It might be assumed that these positive gravity anomalies are expressions of thick partially concealed accumulations of dense submarine lavas, in accordance with interpretations of gravity surveys of the Coast Range in northwestern Oregon (Bromery and Snavely, 1964) and western Washington (Stuart, 1961). The high near Coos Bay, however, extends southward 10–15 miles into pre-Tertiary terrane, and westward as far as the axial portion of the structural embayment at Coos Bay (shown by the pattern of upper Eocene and younger sedimentary rocks on fig. 3), where a gravity minimum might have been predicted. Moreover, inspection of the gradients suggests a depth to the surface of the anomalous mass of several miles or more. It therefore seems unlikely that this anomaly can be attributed wholly to the basalts of the Coast Range sequence. Instead, the main source of the anomaly may be a high-density mass within the pre-Tertiary basement, such as a gabbroic or ultramafic intrusive body. The basalts would be responsible for local accentuations of the general gravity high, in this interpretation. They may have been extruded through a fissure system genetically related to emplacement of the deeper anomalous mass; geographically, at least, the system could be considered a northern extension of the Powers fault zone. Alinement of Eocene submarine vents along north-trending fissures is common in the central part of the Oregon Coast Range (Snavely and others, 1965), though the reason for this is unclear.

Similar considerations apply to interpretation of the positive anomaly at Roseburg. In this case the anomalous mass may underlie Dothan as well as younger rocks, and if so, it is difficult to equate with Eocene volcanic rocks. The presence of ultramafic rocks and serpentinites in tectonic zones associated with the basalts both here and near Coos Bay may support the hypothesis of an ultramafic body at depth.

The gravity high indicated by closure of the —10-mgal contour about 40 miles southwest of Roseburg is not associated with any known occurrence of Eocene volcanic rocks and is probably also best explained by density contrasts within the pre-Tertiary basement. An interpretation attributing the anomaly to an ultramafic mass intruded along a Late Cretaceous thrust plane is depicted in section *C–C′* of figure 3.

The detailed configuration of the gravity field of the Coast Range is determined by depth of cover of the Eocene volcanic rocks and by variations in their thickness. Local gravity depressions such as those associated with upper Eocene sedimentary rocks 20 to 30 miles northwest of Roseburg may represent local depositional basins. The linear low with an amplitude of 10 to 20 mgals located west of the Coos Bay structural embayment may reflect a local lower to middle Eocene structure concealed by younger deposits.

The Cascade Range is, in general, a region of a pronounced negative easterly gravity gradient. The gradient decreases from the Western Cascades to the High Cascades, and is weak or absent in the Great Basin (east and southeast of Crater Lake). A portion of this gradient is the overall west-to-east decrease in gravity associated with inland thickening of the continental crust, but upon removal of that trend the Cascades will almost certainly have an associated negative residual anomaly. LaFehr (1965) computed the mass deficiency represented by the negative residual anomaly of the Cascade Range in northern California by the use of Gauss′ theorem, and showed that the deficiency was approximately equal to the topographic mass excess of the range, thereby implying that the range is in a state of isostatic equilibrium. He further demonstrated that the negative residual anomaly could be accounted for by a near-surface prism of low-density material and that it was not necessary to invoke thickening of the crust beneath the range to achieve isostatic compensation. In the Cascades of southwestern Oregon such a negative density contrast should be readily provided by the thick sequence of pyroclastic rocks and lava flows that make up the Western Cascades and are presumed to underlie the region to the east.

The western margin of the Cascade Range, if one includes the upper Eocene volcanic formations, is remarkably linear and trends slightly west of north, nearly parallel to the trend of the Powers fault zone and its possible northern extension (fig. 3). Locally, this lineament generally coincides with a sharp gravity discontinuity, which suggests that the structural boundary of the province is a concealed fault or fault zone (profile *A–A′* and *B–B′*, fig. 3). Elsewhere, particularly east of the Klamath Mountains, the gravity gradient is more nearly continuous, and the structural transition might be interpreted as a monocline or gentle downwarp of the pre-Tertiary surface (profile *C–C′*).

Gravity contours in the Western Cascades 20 to 25 miles east-northeast of Roseburg swing to the northeast and diverge to form a pattern that possibly reflects the progressively more deeply buried northwest margin of the Klamath Mountains pre-Tertiary province. Weaker northeasterly trends are present elsewhere in the Cascades and provinces to the east. Thus the gravity data appear to support the contention of Peck and others (1964) that the Klamath Mountains "upwarp" is continuous beneath the cover of Cenozoic volcanic rocks of the Cascades and central Oregon.

Low-amplitude gravity depressions are associated with Crater Lake and other areas of andesitic volcanism in the High Cascades. The Crater Lake complex produces an anomaly of as much as about —10 mgals (closure of the —150-mgal contour); the anomaly appears to be centered somewhat to the northeast of the center of the caldera, although no observations were made on the lake floor. Gravity surveys of similar calderas of the Krakatoa type in Japan (Yokoyama, 1963) have shown negative anomalies of 10 to 46 mgals coincident with the calderas. The rather small amplitude of the anomaly in this case is probably due to a low-density contrast between fragmental material occupying the caldera and the "basement" of ancestral Mount Mazama, and to the small thickness of such fragmental deposits.

The most conspicuous gravity feature in the eastern portion of the map area is a low of 20 to 30 mgals. This low is produced by low-density fill in the northern end of the Klamath graben to the south of Crater Lake (see section *C–C′* of fig. 3). Anomalous trends east of the Cascade Range generally follow the basin-range structural grain and indicate local variations in the thickness of unconsolidated material and sedimentary or pyroclastic rocks intercalated with the lavas.

## REFERENCES


Blank, H. R., Jr., 1965, Southwest Oregon gravity data: U.S. Geol. Survey open-file report, 63 computer print-out sheets, 1 p., 1 map, scale 1:250,000.

Bromery, R. W., and Snavely, P. D., Jr., 1964, Geologic interpretation of reconnaissance gravity and aeromagnetic surveys in northwestern Oregon: U.S. Geol. Survey Bull. 1181–N, p. N1–N13.

Diller, J. S., 1907, The Mesozoic sediments of southwestern Oregon: Am. Jour. Sci., 4th ser., v. 23, p. 401–421.

Dott, R. H., Jr., 1965, Mesozoic–Cenozoic tectonic history of the southwestern Oregon coast in relation to Cordilleran orogenesis: Jour., Geophys. Research, v. 70, no. 18, p. 4687–4705.

Fenneman, N. M., 1931, Physiography of western United States: New York, McGraw-Hill Book Co., 534 p.

Imlay, R. W., and other, 1959, Relations of certain Upper Jurassic and Lower Cretaceous formations in southwestern Oregon: Am. Assoc. Petroleum Geologists Bull., v. 43, no. 12, p. 2770–2785.

Irwin, W. P., 1964, Late Mesozoic orogenies in the ultramafic belts of northwestern California and southwestern Oregon, *in* Geological Survey Research 1964: U.S. Geol. Survey Prof. Paper 501–C, p. C1–C9.

LaFehr, T. R., 1965, Gravity, isostasy, and crustal structure in the southern Cascade Range: Jour. Geophys. Research, v. 70, no. 22, p. 5581–5597.

Peck, D. L., Griggs, A. B., Schlicker, H. G., Wells, F. G., and Dole, H. M., 1964, Geology of the central and northern parts of the Western Cascade Range in Oregon: U.S. Geol. Survey Prof. Paper 449, 56 p.

Snavely, P. D., Jr., and Wagner, H. C., 1963, Tertiary geologic history of western Oregon and Washington: Washington Div. Mines and Geology Rept. Inv. 22.

——— 1964, Geologic sketch of northwestern Oregon: U.S. Geol. Survey Bull. 1181–M, p. M1–M17.

Snavely, P. D., Jr., Wagner, H. C., and MacLeod, N. S., 1965, Preliminary data on compositional variations of Tertiary volcanic rocks in the central part of the Oregon Coast Range: The Ore Bin, v. 27, no. 6.

Stuart, D. J., 1961, Gravity study of crustal structure in western Washington: Art. 248, *in* U.S. Geol. Survey Prof. Paper 424–C, p. C273–C276.

Wells, F. G., and Peck, D. L., 1961, Geologic map of Oregon west of the 121st Meridian: U.S. Geol. Survey Misc. Geol. Inv. Map I–325, scale 1:500,000.

Wells, F. G., and Walker, G. W., 1953, Geology of the Galice quadrangle, Oregon: U.S. Geol. Survey Geol. Quad. Map GQ 25, scale 1:62,500.

Williams, Howel, 1957, A geologic map of the Bend quadrangle, Oregon, and a reconnaissance geologic map of the central portion of the High Cascade Mountains: Oregon Dept. Geology and Mineral Industries, in coop. with U.S. Geol. Survey, scale 1:125,000.

Woollard, G. P., 1958, Results for a gravity control network at airports in the United States: Geophysics, v. 23, no. 3, p. 520–535.

Woollard, G. P., and Rose, J. C., 1963, International gravity measurements: Tulsa, Okla., Soc. Explor. Geophysicists, 544 p.

Yokoyama, Izumi, 1963, Structure of caldera and gravity anomaly: Bull. volcanol. [Italy], v. 26, p. 67–72.

# REGIONAL GRAVITY SURVEY, WIND RIVER BASIN, WYOMING

By J. E. CASE and W. R. KEEFER, Denver, Colo.

*Abstract.*—Bouguer anomaly values range from about —235 milligals in the Wind River and Great Divide Basins, Wyo., to about —170 mgal over the bordering mountains. The gravity profiles reflect generally the configuration of the upper surface of the Precambrian basement complex and the relative thickness of the basin fill of upper Mesozoic and Cenozoic sedimentary rocks, which have low density. The amplitude and gradient of the gravity anomalies show that the fault zone between the Wind River Basin and the Owl Creek Mountains is high angle, and gravity anomalies and drill-hole data show that the fault zone between the Granite Mountains and the Great Divide Basin is low angle.

A regional gravity survey of the Wind River Basin in central Wyoming (fig. 1) was conducted to provide data regarding the deep-seated configuration of the basin, the attitudes of some of the major faults that border the basin, and the relations between the gravitational field of the basin and the adjacent ranges (figs. 2 and 3). About 355 gravity stations were established along several widely separated traverses; Worden portable gravity meters with constants of about 0.5 mgal per scale division were used. The survey was tied to a base at the Casper, Wyo., airport where the value of gravity is 979.9562 gals (Behrendt, 1962, p. 890). Subsidiary bases were established at intervals along the main highways within the Wind River Basin. Bouguer anomalies were computed with a reduction factor corresponding to a density of 2.67 grams per cubic centimeter, and terrain corrections were made through zone "J" of Hammer's (1939) tables. Principal facts for the gravity stations have been placed on open file (Case, 1965). Gravity data in the vicinity of Jeffrey City are after Healey (1965). Although the lines of traverse were widely separated, the station spacing along individual traverses was relatively close, ranging from ½ to 3 miles. Thus the survey outlines the major gravitational features of the basin and provides information on gravity gradients along the lines of traverse. It, however, does not detect small anomalies that are undoubtedly associated with many of the smaller structural features in the basin except in the area of Healey's detailed survey near Jeffrey City.

## GENERAL GEOLOGY

The Wind River Basin, about 8,500 square miles in area, exemplifies the type of large sedimentary and structural basin that developed in the Rocky Mountain region during Laramide deformation. It is completely surrounded by broad belts of folded and faulted Paleozoic and Mesozoic strata which form the flanks of the adjacent mountains and anticlinal uplifts (fig. 2). Along the south and west margins these strata dip 10° to 20° toward the center of the basin, whereas along the north and east margins, dips are commonly vertical to overturned. The basin thus is markedly asymmetrical with the structurally deepest parts close to the Owl Creek Mountains and the Casper arch. Flat-lying lower Eocene rocks cover the central part

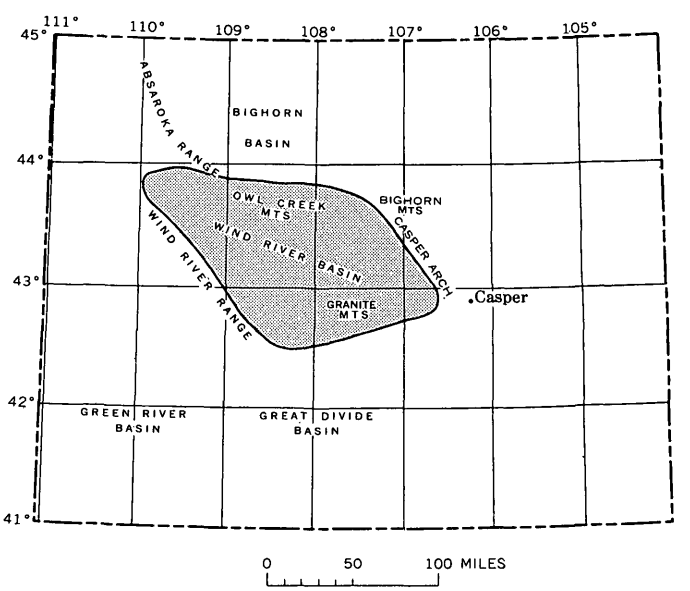


FIGURE 1.—Index map of Wyoming, showing area (stippled) of figures 2 and 3.

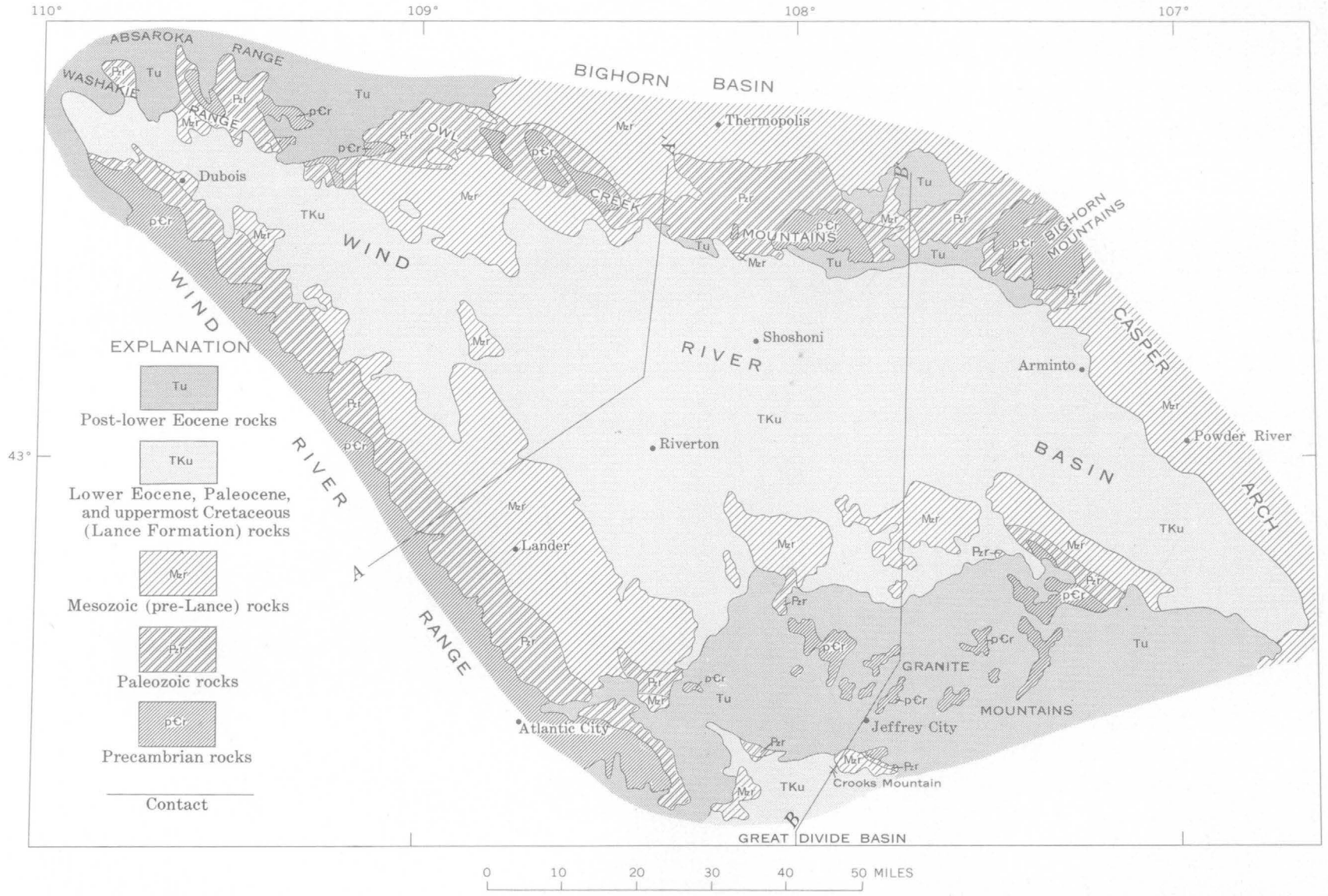


FIGURE 2.—Generalized geologic map of the Wind River Basin and adjacent areas, central Wyoming. Adapted from Love and others (1955). Sections $A'$–$A'$ and $B'$–$B'$ shown on figure 4.

of the basin, and overlap all older strata along the margins.

The Granite Mountains are formed from a large anticlinal uplift that extends along the south edge of the Wind River Basin, for about 75 miles. The south and southwest flanks of the uplift are steeper than the north and northeast flanks; the major boundary fault between the range and the Great Divide Basin to the south is the Emigrant Trail thrust fault (Stephens, 1964, p. F31, pl. 1), which dips about 20° NE. The Granite Mountains were uplifted and deeply eroded during Laramide deformation, but later were almost completely buried by middle and upper Tertiary sediments (Love, 1960, p. 208–212). At present, the range is visible only as a series of prominent granite knobs projecting as much as 1,000 feet above a nearly level plain of flat-lying Miocene and Pliocene rocks. The south edge of this plain terminates abruptly against the normal-fault system along the south margin of the Granite Mountains. Several large subsidiary anticlines project northwestward into the Wind River Basin along the north edge of the Granite Mountains.

The Wind River Range trends northwest through west-central Wyoming for about 100 miles. The rocks on its west flank, bordering on the Green River Basin, are steep to overturned and broken by northeastward-dipping reverse faults (Berg, 1961; 1962, p. 2020–2022). In contrast, the rocks on its east flank have gentle dips. The structural continuity of the east flank is interrupted in a few places by high-angle reverse and normal faults, with displacements commonly less than 1,000 feet, and by sharply folded monoclines and anticlines (Love and others, 1955). Precambrian crystalline rocks, chiefly massive granite and granite gneiss, form the core of the range.

The Washakie Range, at the northwest corner of the Wind River Basin, consists of several large en echelon anticlines that were completely buried by Eocene and Oligocene pyroclastic rocks of the Absaroka Mountains, and which have now been partly exhumed (Keefer, 1957, p. 205–206). The rocks along the south flank of the range generally dip steeply and are broken by northward-dipping reverse faults in several areas. Precambrian crystalline rocks exposed in some of the larger folds may be part of the central core of the fold belt. The Absaroka Mountains to the north are carved from a thick sequence of essentially undeformed volcanic sedimentary rocks.

The Owl Creek Mountains rise abruptly along the north edge of the Wind River Basin. This large anticlinal uplift, separating the Wind River Basin from the Bighorn Basin to the north, extends nearly eastwest across central Wyoming from the southeastern edge of the Absaroka Mountains to the south end of the Bighorn Mountains, a distance of about 80 miles. Rocks on the south flank of the range are steep to overturned, and have overridden the north margin of the Wind River Basin along an extensive system of Laramide reverse faults (Keefer and Love, 1963, p. 50; Wise, 1963). A younger set of normal faults, with the north block downdropped, is present along the south side of the range (Tourtelot, 1953; Tourtelot and Thompson, 1948). Strata on the north side of the Owl Creek Mountains dip gently northward into the Bighorn Basin. Precambrian granitic rocks and mafic dikes, as well as metasedimentary rocks, are exposed locally; the most extensive exposures are in the eastern part of the range.

The southwest end of the Bighorn Mountains forms the northeast margin of the Wind River Basin. This part of the range has an extensive core of Precambrian crystalline rocks flanked on the south by moderately southward-dipping (15°) Paleozoic and lower Mesozoic strata (Tourtelot, 1953). These have likewise been thrust over the deep part of the Wind River Basin. The Bighorn Mountains are separated structurally from the Owl Creek Mountains to the west by a broad shallow syncline underlain chiefly by flat-lying Eocene rocks.

The Casper arch is a major but not deeply eroded Laramide structural upwarp with a steep to overturned and faulted west flank that coincides with the east margin of the Wind River Basin (Keefer and Love, 1963, p. 50). The Casper arch is underlain mostly by Upper Cretaceous and Paleocene rocks.

Paleozoic strata in the Wind River Basin consist chiefly of resistant limestone, dolomite, and sandstone; thicknesses range from 1,200 feet in the southeastern part of the basin to more than 3,200 feet in the northwestern part. Mesozoic strata, on the other hand, are predominantly shale, siltstone, and sandstone and, exclusive of the uppermost Cretaceous Lance Formation, thicken from 8,500 feet along the east margin to an estimated 11,500 feet along the west margin. During Laramide deformation in latest Cretaceous, Paleocene, and early Eocene times, more than 15,000 feet of fluviatile and lacustrine sediments accumulated in the central, downwarped areas of the basin. The sedimentary and structural history of the region has been summarized by Keefer (1965).

## GENERAL FEATURES OF THE GRAVITY MAP

The gravity map (fig. 3) shows a large negative anomaly over the central part of the Wind River Basin and positive anomalies over the surrounding mountain ranges. Bouguer anomaly values decrease

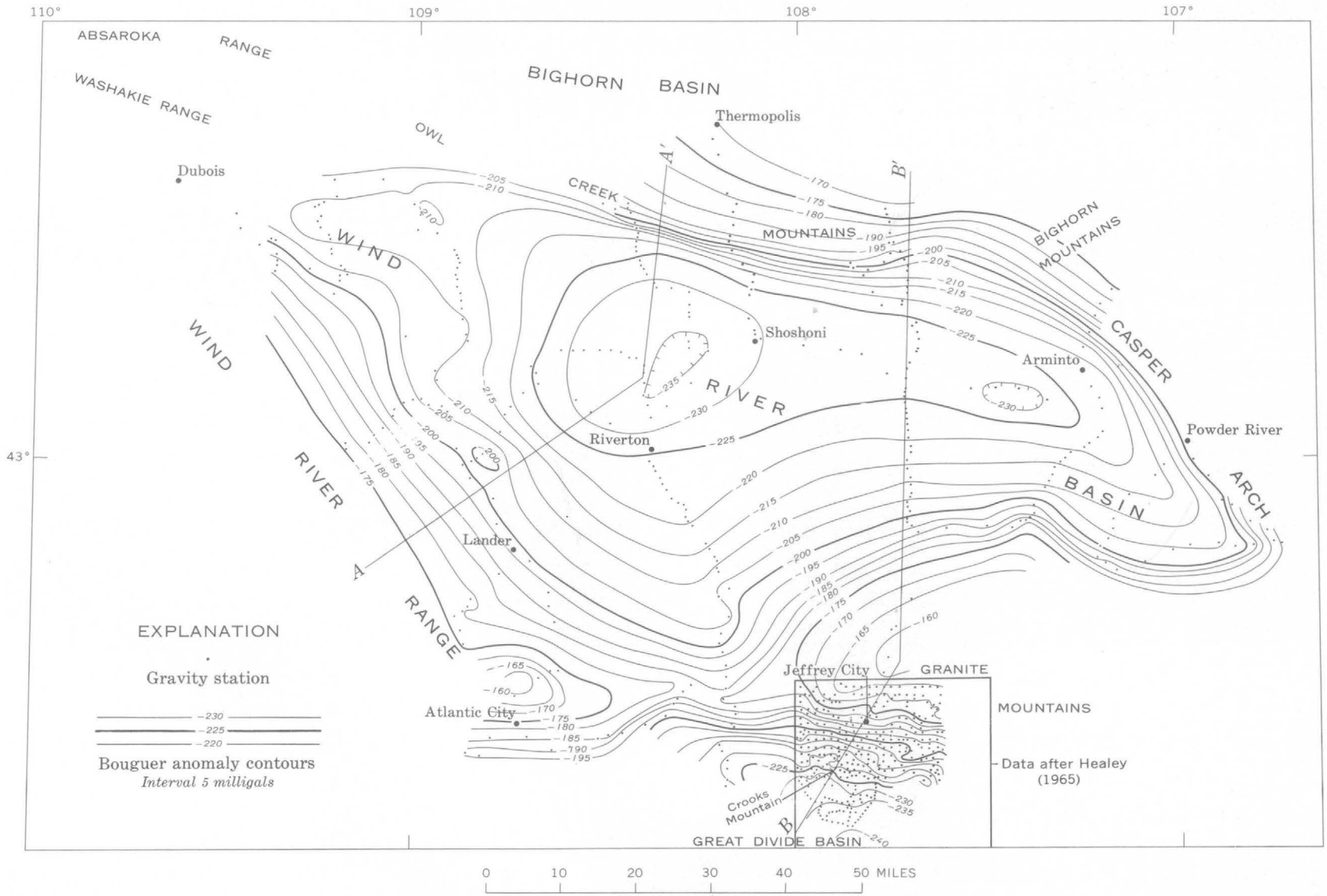


FIGURE 3.—Bouguer gravity anomaly map of the Wind River Basin and adjacent areas, central Wyoming. Bouguer anomaly values were computed with a reduction factor corresponding to a density of 2.67 grams per cubic centimeter.

from —160 and —170 mgal over the Wind River Range and Granite Mountains to —230 and —235 mgal in the basin. Values range from —170 to —190 mgal over the Owl Creek Mountains. From incomplete data, values as high as —180 mgal have been measured over the western edge of the Casper arch, southeast of Powder River. The lowest gravity values occur along the north and northeast sides of the basin in an elongate pattern. This generally coincides with the region containing maximum thicknesses of uppermost Cretaceous and lower Tertiary rocks. The available drill-hole data, however, suggest that the deepest part of the basin, above the top of the Precambrian crystalline basement, lies even closer to the Owl Creek Mountains and the Casper arch than does the trough of the gravity low.

The gravity map of the United States (Woollard, 1964) indicates that the regional gravity field becomes more negative westward and southward across Wyoming. This relation may be the result of increasing crustal thickness, of decreasing density of the crust and upper mantle materials, or of some combination of these two factors, westward and southward across the State. It should be pointed out that because of scarcity of data, gravity contours over the Wind River Range and part of the Wind River Basin were shown by Woollard as trending diagonally across the structural grain of the region. More detailed work, however, now shows that a closed gravity high with Bouguer anomaly values as great as —160 to —170 mgal closely follows the present physiographic and structural outline of the Wind River Range.

Relations between geology and Bouguer anomalies across the Wind River Basin are shown in detail in the two profiles on figure 4. On profile *A–A′*, variations in Bouguer anomaly values are generally consistent with the configuration of the Precambrian surface. The relatively uniform northward dip of the Precambrian surface on the northeast flank of the Wind River Range is indicated by the uniformly smooth, northeastward-sloping gravity gradient. The small anticline that interrupts the dip slope is indicated by a small positive nose in the gravity contours. The lowest Bouguer anomaly values, reflecting thick sections of low-density rocks of latest Cretaceous and early Tertiary age, are located a few miles south of the structurally deepest part of the basin, but this discrepancy may be attributed in part to the gravitational "masking" effect of the large mass of higher density rocks of Precambrian and Paleozoic age at the surface in the nearby Owl Mountains. Bouguer anomaly values increase abruptly at the southern front of the Owl Creek Mountains, and then flatten markedly over the crest of the range. However, the values continue to increase northeastward toward Thermopolis even though the surface of the Precambrian basement complex slopes downward into the Bighorn Basin. This discrepancy between the configuration of the Precambrian surface and the behavior of the gravitational field on the north flank of the Owl Creek Mountains may be caused in part by density variations within the basement complex. Precambrian rocks exposed in Wind River canyon, just south of Thermopolis, for example, include a high proportion of amphibolites and biotite gneisses which are denser than the granitic rocks found in adjacent areas of the range. Variations in crustal thickness or density may also cause the apparent discrepancy (Malahoff, 1964, fig. 8).

Along profile *B–B′* the Bouguer anomaly values and the configuration of the Precambrian surface correlate less closely than in profile *A–A′*. Here again, the axis of the gravity low in the basin is displaced south of the structurally deepest part as inferred from well data. Bouguer anomaly values are higher over the Granite Mountains than over the Owl Creek Mountains, possibly indicating that the Precambrian rocks are more dense in the Granite Mountains. South of the Granite Mountains the Bouguer anomaly values decrease to about —235 or —240 mgal in the Great Divide Basin. The steepest gravity gradient between the central part of the Granite Mountains and the Great Divide Basin is located several miles north of the southern faulted front of the Precambrian core of the mountains, indicating that the Emigrant Trail and related thrust faults dip relatively gently northward beneath the mountains.

The steepened gravity gradient along the southern margin of the Granite Mountains is continuous with the steep gradient along the southeastern end of the Wind River Range (fig. 2). Thus, gravitationally at least, the southern margins of the two uplifts appear to have the same or similar structural relations to the Great Divide Basin.

The relations between small gravity anomalies and the local near-surface structure in the vicinity of Jeffrey City have been discussed by D. L. Healey (*in* Stephens, 1964, p. F70-F78).

Although coverage is incomplete, a local gravity high is apparently present at the southeastern end of the Wind River Range, near the Atlantic City iron mining district. Precambrian rocks in the area include serpentinite, greenstone, iron-formation, and various amphibole and mica schists (Bayley, 1963), and these are probably more dense than the granites and granitic gneisses found elsewhere in the Wind River Range. A local but very conspicuous positive magnetic anom-

DRILL HOLES USED FOR CONTROL

| No. | Company and well | Location | | |
|---|---|---|---|---|
| | | Sec. | T. | R. |
| 1 | Phillips Petroleum Co. Missouri 1 | 28 | 2 N. | 4 E. |
| 2 | Pan American Petroleum Corp. Shoshone - Arapahoe Tribal 1 | 11 | 5 N. | 4 E. |
| 3 | General Petroleum Corp. 45-25-G | 25 | 27 N. | 94 W. |
| 4 | Sinclair Oil Co. core hole 5-A | 21 | 29 N. | 92 W. |
| 5 | Continental Oil Co. Love Ranch 1 | 11 | 35 N. | 91 W. |
| 6 | Continental Oil Co. Squaw Butte 14-4 | 14 | 36 N. | 91 W. |
| 7 | Continental Oil Co. Moneta Hills 11-1 | 11 | 37 N. | 91 W. |
| 8 | Sinclair - Wyoming Oil Co. Lysite 1 | 25 | 39 N. | 91 W. |
| 9 | Gulf Oil Co. Lysite-Federal 1 | 23 | 39 N. | 91 W. |

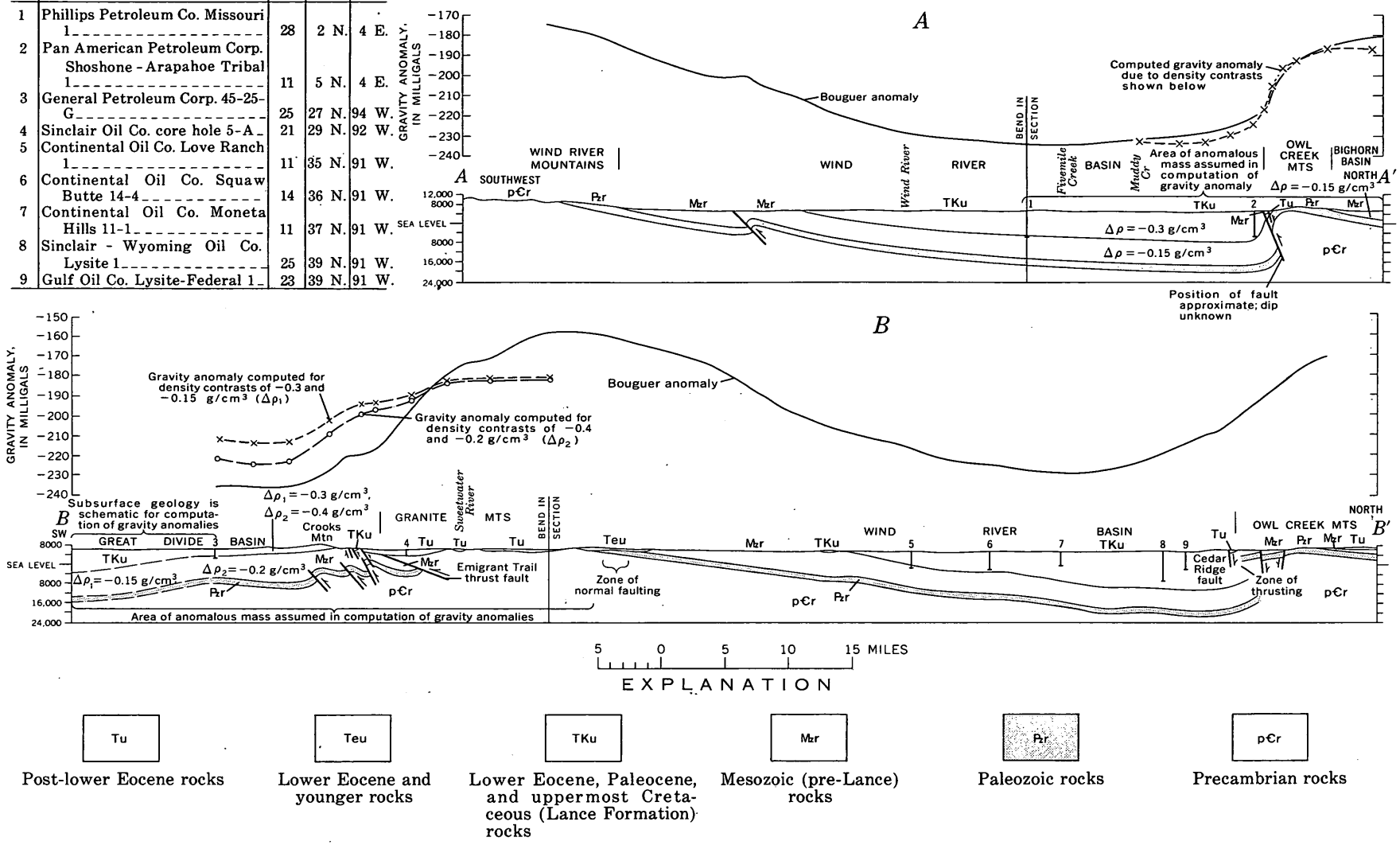


FIGURE 4.—Geologic sections and Bouguer anomaly profiles across the Wind River Basin. Location of profiles shown on figures 2 and 3. *A*, Geologic section and Bouguer anomaly profile from the Wind River Range, across the Wind River Basin and Owl Creek Mountains, to the Bighorn Basin. *B*, Geologic section and Bouguer anomaly profile from the Great Divide Basin, across the Granite Mountains and Wind River Basin, to the Owl Creek Mountains. Data in the Granite Mountains and Great Divide Basin from J. D. Love (written commun., 1965) and Stephens (1964).

aly, probably also related to concealed iron-formation, was outlined by an aeromagnetic survey (Dempsey and others, 1962) several miles northeast of the Atlantic City district, along the southwest margin of the Wind River Basin, but coverage during the present gravity survey was not sufficiently detailed in that area for comparable detection of this feature.

## COMPARISON OF COMPUTED AND OBSERVED GRAVITY ANOMALIES

Because of burial by lower Eocene and younger rocks and a lack of subsurface data in many areas, the character and inclination of the major fault zones separating mountain and basin structural provinces in central Wyoming are problematic. Data are especially meager regarding the configuration of these faults as they extend downward into the Precambrian crystalline basement. Were tectonic movements predominantly horizontal along "submountain" thrust faults, or were they predominantly vertical along high-angle faults? These questions are partially answered by an analysis of the gravity profiles acquired during the present investigation.

Structure cross sections provide a two-dimensional model for use in computing the gravitational effects of the various rock types comprising the stratigraphic column across the southern fault zones bordering the Owl Creek and Granite Mountains (fig. 4). For purposes of computation of the anomaly along profile *A–A′* (fig. 4) the following densities have been assumed: Precambrian and Paleozoic rocks, 2.7 grams per cubic centimeter; pre-Lance Mesozoic rocks, 2.55 g per $cm^3$; uppermost Cretaceous (Lance Formation) and Tertiary rocks, 2.4 per $cm^3$. The true distribution of density is undoubtedly much more complex, but these assumed values seem to be geologically plausible, and result in a computed gravity relief of 45 to 50 mgal between the trough line of the Wind River Basin and the crestline of the Owl Creek Mountains. A Precambrian surface at a depth of about 20,000 feet below sea level in the deep part of the basin is also consistent with the gravity data. From analysis of the gravity low in the basin, a substantial fraction of this negative anomaly is caused by the thick section of uppermost Cretaceous and Tertiary sedimentary rocks, as pointed out by Malahoff and others (1964). The steep gravity gradient across the mountain front can be satisfactorily produced by relatively near-surface density contrasts, and evaluation of the influence of the northward-increasing regional gravity field was not required in the analysis.

The computed gravity profile across the south flank of the Owl Creek Mountains and the north margin of the Wind River Basin, based on the structural relations shown in figure 4, closely parallels the steep gradient of the observed gravity profile; however, the slight discrepancies between observed and computed profile indicate that the inclination of the fault zone may be even steeper than that shown on the cross section. In other words, a better fit between the observed and computed gravity profiles would be obtained if the wedge of low-density sedimentary rocks beneath the fault were smaller. It should be noted that the true dip of the fault plane cannot be determined from the available surface or subsurface data. On the basis of regional stratigraphic studies of the uppermost Cretaceous and lower Tertiary rocks, Keefer and Love (1963) have suggested that it is high rather than low angle.

The structure section across the southern Granite Mountains and northern Great Divide Basin for two sets of density contrasts yields computed gravity profiles which fail to match the observed gravity profile, either in amplitude or gradient (*B–B′*, fig. 4). The computed profile does not trend at right angles to the gravity contours, but the small angular difference is insignificant in view of the extreme discrepancies between the observed and computed profiles. A closer fit could be obtained if: (1) the depth to the Precambrian surface near Crooks Mountain were greater; (2) the wedge of low density Mesozoic rocks extended farther north beneath the Granite Mountains; (3) the density contrast between the older (Precambrian and Paleozoic) and younger (Mesozoic and Tertiary) rock units were substantially greater in this region than in the Wind River Basin farther north; (4) the density of Precambrian rocks in the Granite Mountains structural block is considerably greater than the density of Precambrian rocks of the Great Divide Basin structural block; or (5) another major reverse fault zone were present in the Great Divide Basin farther south than those shown on figure 4, possibly extending northward at depth beneath Crooks Mountain.

The stratigraphic and structural relations along the south margin of the Granite Mountains and north margin of the Great Divide Basin are sufficiently well known from drill-hole data to partially discount the first three items listed above. Although no data are available to properly evaluate the fourth item, it seems highly unlikely that density variations within the basement complex would be great enough to cause the discrepancy. The fifth item, however, remains a possibility. If a buried thrust extends northward beneath Crooks Mountain, with Cenozoic and Mesozoic rocks present at depth, the gravitational discrepancies could be partly resolved (fig. 5). Stephens (1964, p.

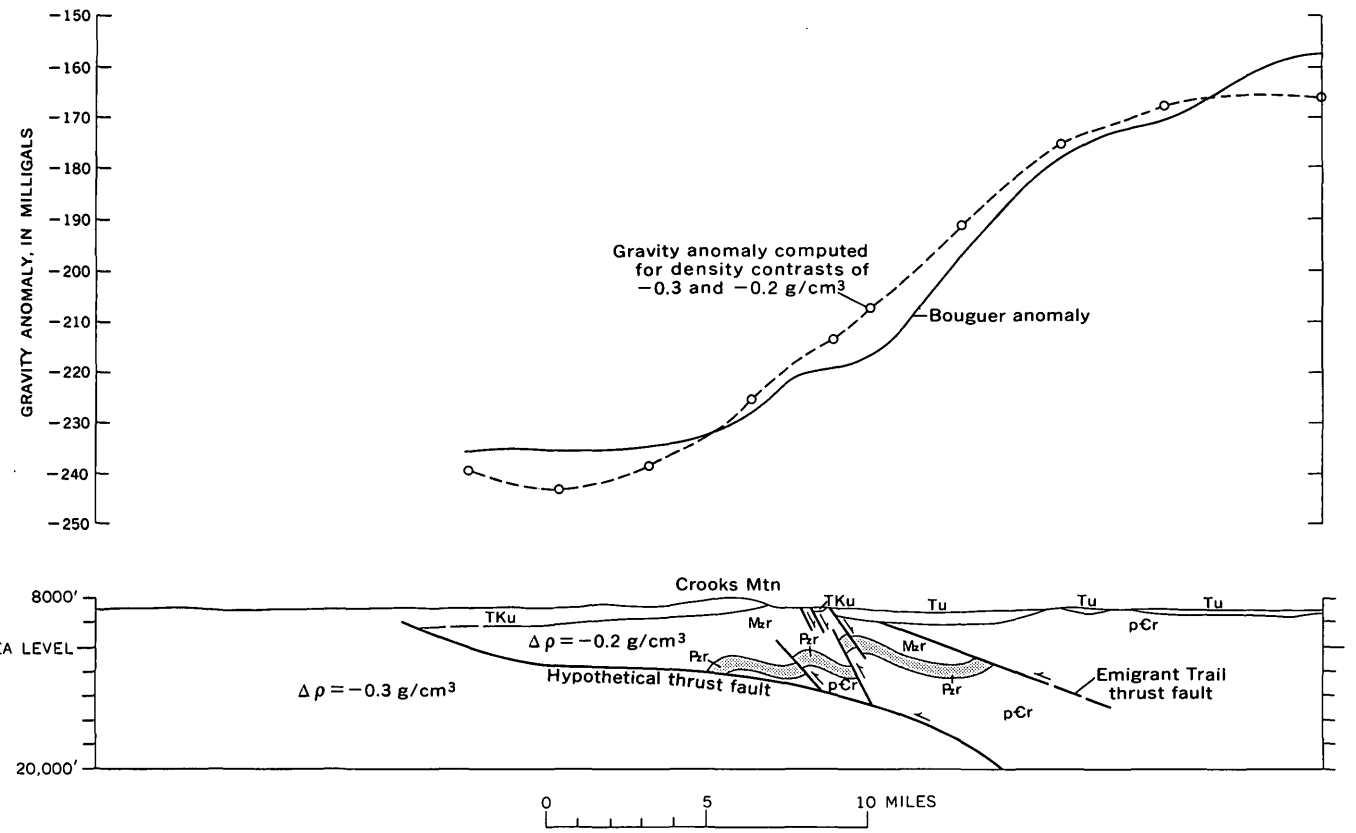


FIGURE 5.—Gravitational effects of a thrust fault at depth beneath Crooks Mountain. See figure 4 for explanation of rock units.

F26–F28), for example, believes that a buried thrust fault trending east-west across the Great Divide Basin, several miles south of the deformed belt shown on figures 4 and 5, can best explain some of the anomalous structural relations in the region. J. D. Love (oral commun., 1965), during investigations of the subsurface of a large part of the northern Great Divide Basin, on the other hand, has observed no compelling evidence for a thrust fault that far south in the basin. More data are needed before the true relations can be worked out.

From analysis of the gravity data, it appears that the major flanking faults along the southern margins of the Owl Creek and Granite Mountains are fundamentally different: the fault zone along the Owl Creek Mountains, locally at least, is high angle, whereas that along the Granite Mountains is low angle.

## REFERENCES


Bayley, R. W., 1963, A preliminary report on the Precambrian iron deposits near Atlantic City, Wyoming: U.S. Geol. Survey Bull. 1142-C, 23 p.

Behrendt, J. C., 1962, A statistical comparison of five geodetic gravimeters: Geophysics, v. 26, no. 6, pt. 1, p. 889–891.

Berg, R. R., 1961, Laramide tectonics of the Wind River Mountains *in* Symposium on Late Cretaceous rocks, Wyoming and adjacent areas, Wyoming Geol. Assoc. Guidebook 16th Ann. Field Conf., 1961: p. 70–80.

——— 1962, Mountain flank thrusting in Rocky Mountain foreland, Wyoming and Colorado: Am. Assoc. Petroleum Geologists Bull., v. 46, no. 11, p. 2019–2032.

Case, J. E., 1965, Principal facts for gravity stations in the Wind River Basin area, Wyoming: U.S. Geol. Survey open-file report, 9 pages of tables.

Dempsey, W. J., and others, 1962, Aeromagnetic map of south central Fremont County, Wyoming: U.S. Geol. Survey Geophys. Inv. Map GP-393.

Hammer, S. I., 1939, Terrain corrections for gravimeter stations: Geophysics, v. 4, p. 184–194.

Healey, D. L., 1965, Principal facts for gravity stations in the Crooks Gap area, Fremont County, Wyoming: U.S. Geol. Survey open-file report.

Keefer, W. R., 1957, Geology of the DuNoir area, Fremont County, Wyoming: U.S. Geol. Survey Prof. Paper 294–E, p. 155–221.

——— 1965, Geologic history of Wind River Basin, central Wyoming: American Assoc. Petroleum Geologist Bull., v. 49, p. 1878–1892.

Keefer, W. R., and Love, J. D., 1963, Laramide vertical movements in central Wyoming: Univ. Wyoming Contr. to Geology, v. 2, p. 47–54.

Love, J. D., 1960, Cenozoic sedimentation and crustal movement in Wyoming: Am. Jour. Sci., v. 258–A, p. 204–214.

Love, J. D., Wzitz, J. L., and Hose, R. K., 1955, Geologic map of Wyoming: U.S. Geol. Survey.

Malahoff, A., 1964, A detailed study, *in* Strange, W. E., and Woollard, G. P., The use of geologic and geophysical parameters in the evaluation, interpolation, and prediction of gravity: Hawaii Institute of Geophysics rept. HIG–64–17.

Malahoff, A., Malahoff, B., and Strange, W. E., 1964, A study of the gravity field of Wyoming [abs.]: Am. Geophys. Union Trans., v. 45, no. 4, p. 593.

Stephens, J. G., 1964, Geology and uranium deposits at Crooks Gap, Fremont County, Wyoming: U.S. Geol. Survey Bull. 1147–F, 82 p.

Tourtelot, H. A., 1953, Geology of the Badwater area, central Wyoming: U.S. Geol. Survey Oil and Gas Inv. Map OM124.

Tourtelot, H. A., and Thompson, R. M., 1948, Geology of the Boysen area, central Wyoming: U.S. Geol. Survey Oil and Gas Inv. Map 91.

Wise, D. U., 1963, Keystone faulting and gravity sliding driven by basement uplift of Owl Creek Mountains, Wyoming: Am. Assoc. Petroleum Geologists Bull., v. 47, p. 586–598.

Woollard, G. P., chm. 1964, Bouguer gravity anomaly map of the United States: U.S. Geol. Survey.

# HAWAIIAN SEISMIC EVENTS DURING 1964

By ROBERT Y. KOYANAGI and ARNOLD T. OKAMURA,
Hawaiian Volcano Observatory

*Abstract.*—During 1964, 30,285 earthquakes were detected by seismographs in Hawaii. Of these, 481 of magnitude 2.0 to 5.5 were located and plotted along the Hawaiian Ridge. One hundred and seven earthquakes were reported felt by residents of Hawaii, and 3 were felt as far as Maui and Oahu islands. The Kilauea summit region and the Kaoiki fault region, on the island of Hawaii, were the areas of highest earthquake concentration.

This report, which summarizes and illustrates the earthquake locations compiled in 1964 in U.S. Geological Survey Hawaiian Volcano Observatory Summaries 33, 34, 35, and 36 (Koyanagi, Okamura, and Powers, 1965; Okamura and others, 1965; Kinoshita and others, 1965; Koyanagi and others, 1965), is the third of a series (Koyanagi, 1964; Koyanagi and Endo, 1965) presenting the locations of Hawaiian earthquakes in this form.

Five volcanoes, two of which (Kilauea and Mauna Loa) are active, cap the island of Hawaii (fig. 1). Most of the earthquakes noted in this report occurred beneath the island, but a few were beneath other islands on the Hawaiian Ridge, and many were beneath the adjacent sea floor. Determinations of earthquake location and magnitude were based on Hawaiian seismic-wave traveltimes and procedures compiled and applied by J. P. Eaton since 1956 at the Hawaiian Volcano Observatory. As was noted in the two earlier reports, for 1962 and 1963, earthquakes of magnitude 2.5 or greater which occur beneath the island of Hawaii are located with fair confidence within a 5-kilometer sphere of error. Offshore earthquakes may be subject to errors in location of as much as 10 km.

The local earthquakes plotted (figs. 2, 3, and 4) are those of magnitude 2.0 or greater detected on the HVO seismic net and located along the Hawaiian Ridge, within the geographic coordinates lat 18° to 23° N. and long 154° to 161° W.

## 1964 SEISMIC CHRONOLOGY

The first and second quarters of 1964 showed a low level of seismic activity. One of the few events of interest was an earthquake of magnitude 3.7 which occurred along the southeast flank of Kilauea at $01^h06^m$ [1] on January 7. Residents in the southeastern parts of the island felt the quake strongly. About 44

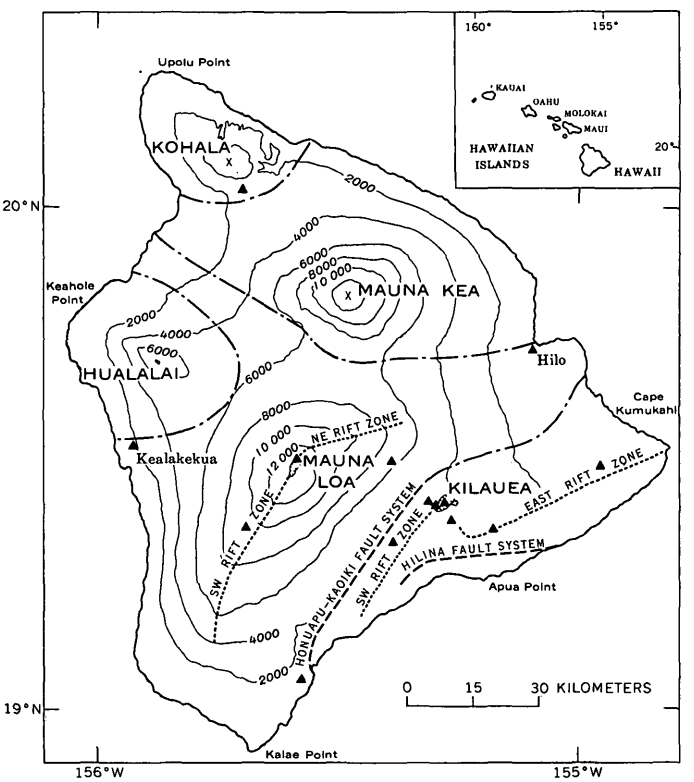


FIGURE 1.—Map of the island of Hawaii, the five volcanoes, and their principal structural features. Dot-and-dash lines are boundaries of volcanic systems. Locations of seismograph stations are indicated by closed triangles. Contour interval is 2,000 feet, and datum is mean sea level.

[1] All times given are in hours and minutes, Hawaiian standard time.

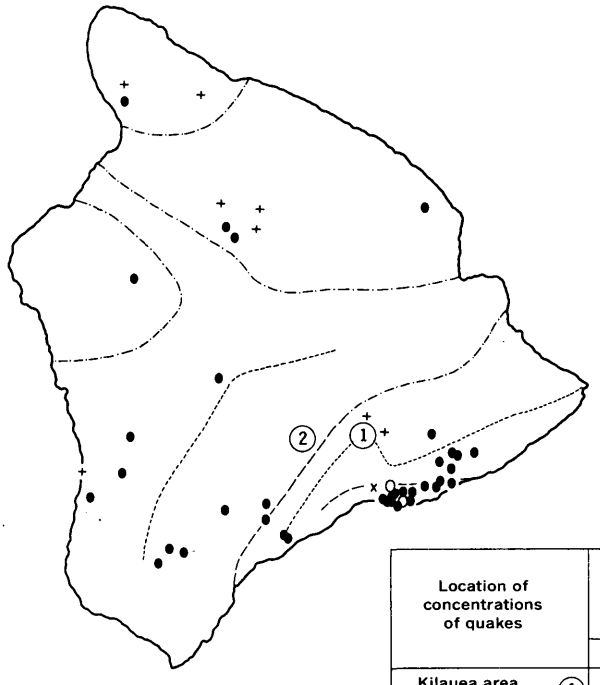


| Location of concentrations of quakes | Number of quakes of magnitude 2.0 to 3.5 (first figure) and >3.5 (second figure) | |
|---|---|---|
| | 1st quarter | 2nd quarter |
| Kilauea area (30-km depth) (1) | 11, 0 | 21, 0 |
| Kaoiki fault system (2) | 22, 0 | 14, 1 |

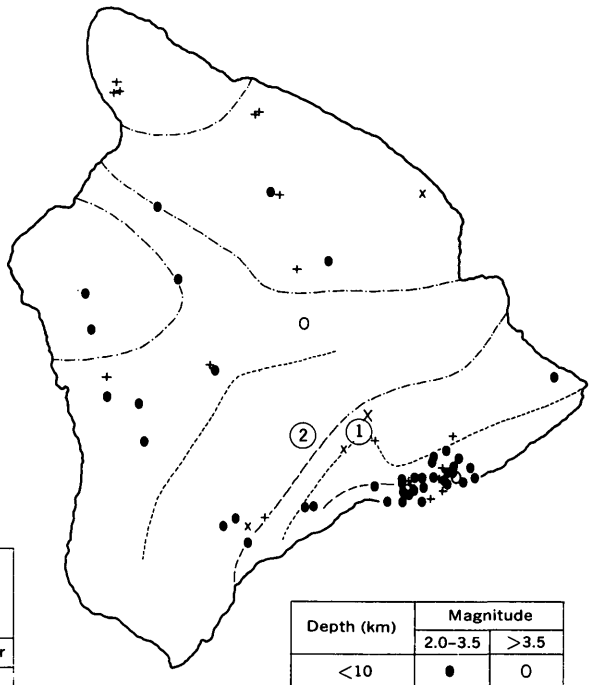


| Depth (km) | Magnitude | |
|---|---|---|
| | 2.0–3.5 | >3.5 |
| <10 | ● | O |
| 10–20 | + | |
| 20–60 | x | X |

FIGURE 2.—Epicenters of earthquakes of magnitude 2.0 or greater beneath the island of Hawaii during the first and second quarters of 1964. The circled numerals indicate areas with too many earthquakes to plot individually: (1) Kilauea area (30-km depth), and (2) Kaoiki fault system. Dot-and-dash lines are boundaries of volcanic systems, long-dashed lines are fault systems, and short-dashed lines are rift zones. Geographic names are shown on figure 1.

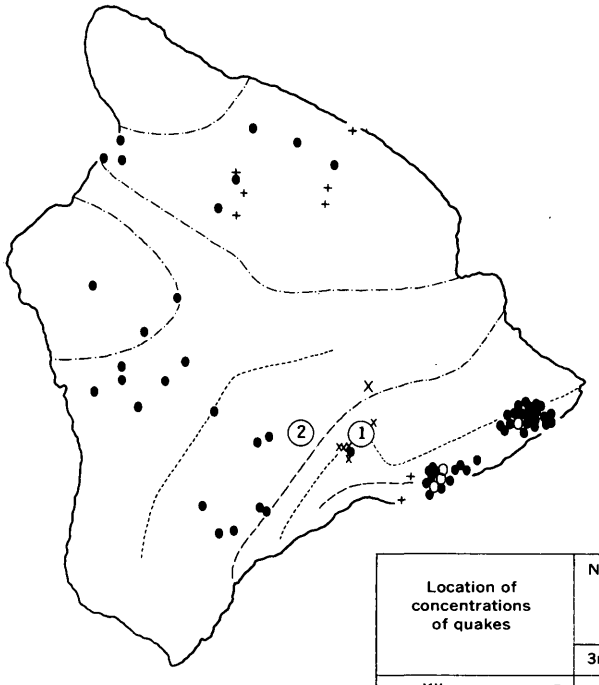


| Location of concentrations of quakes | Number of quakes of magnitude 2.0 to 3.5 (first figure) and >3.5 (second figure) | |
|---|---|---|
| | 3rd quarter | 4th quarter |
| Kilauea area (30-km depth) (1) | 10, 0 | 39, 3 |
| Kaoiki fault system (2) | 17, 0 | 11, 0 |

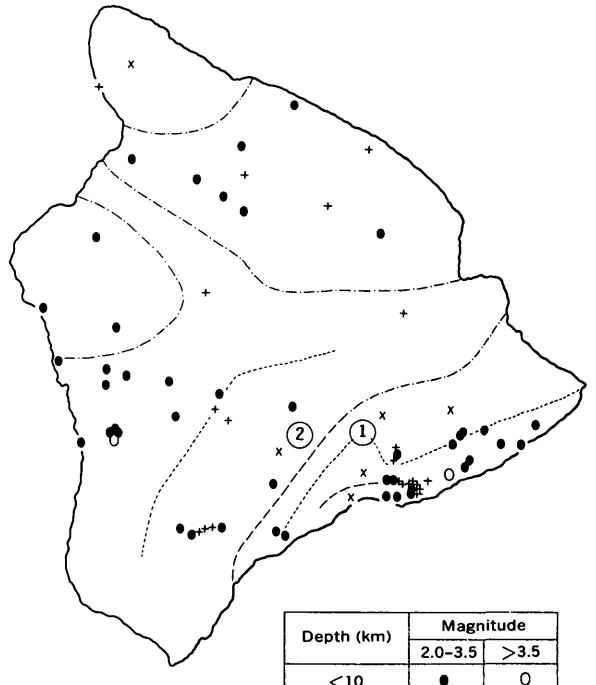


| Depth (km) | Magnitude | |
|---|---|---|
| | 2.0–3.5 | >3.5 |
| <10 | ● | O |
| 10–20 | + | |
| 20–60 | x | X |

FIGURE 3.—Epicenters of earthquakes of magnitude 2.0 or greater beneath the island of Hawaii during the third and fourth quarters of 1964. The circled numerals indicate areas with too many earthquakes to plot individually: (1) Kilauea area (30-km depth), and (2) Kaoiki fault system. Dot-and-dash lines are boundaries of volcanic systems, long-dashed lines are fault systems, and short-dashed lines are rift zones. Geographic names are shown on figure 1.

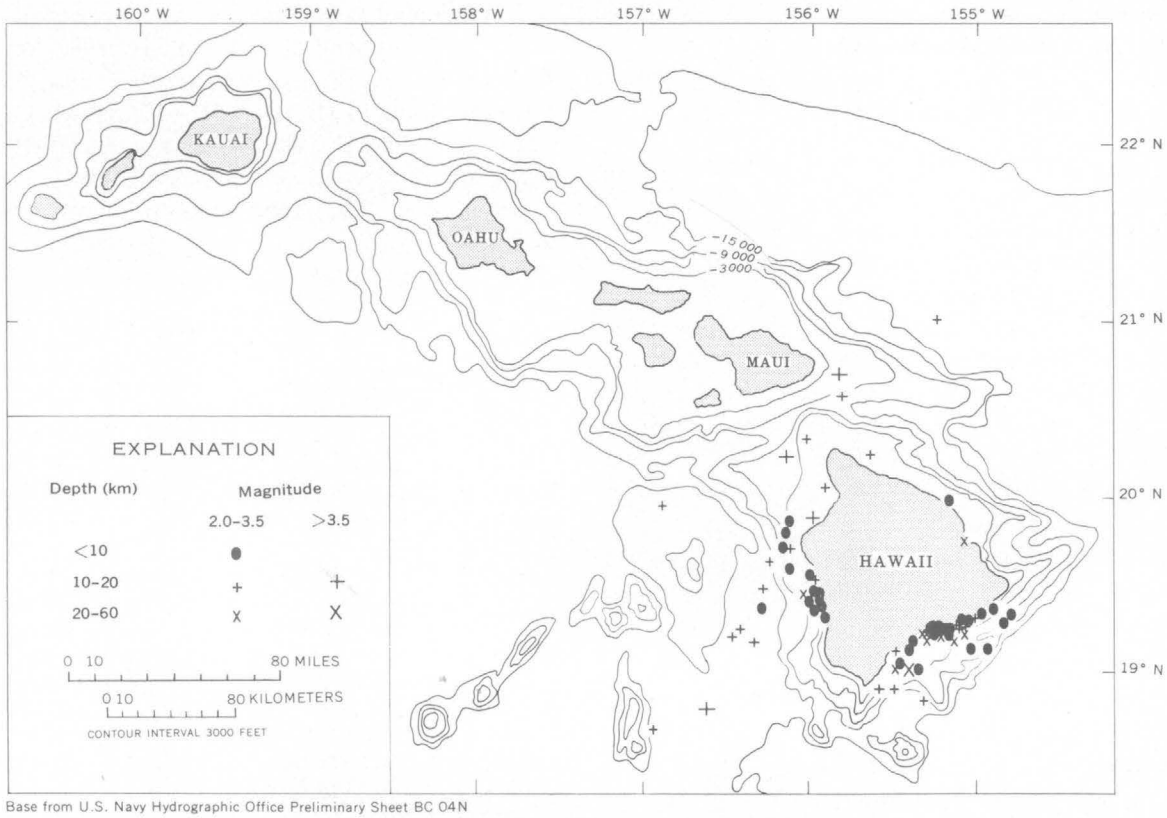


FIGURE 4.—Map of the Hawaiian Islands, showing epicenters of earthquakes with magnitudes of 2.0 or greater that occurred off the island of Hawaii during 1964.

small aftershocks were recorded that day. An earthquake of magnitude 4.3 occurred off the east shore of Maui at $22^h32^m$ on February 20 and was felt by residents of Maui and northern Hawaii.

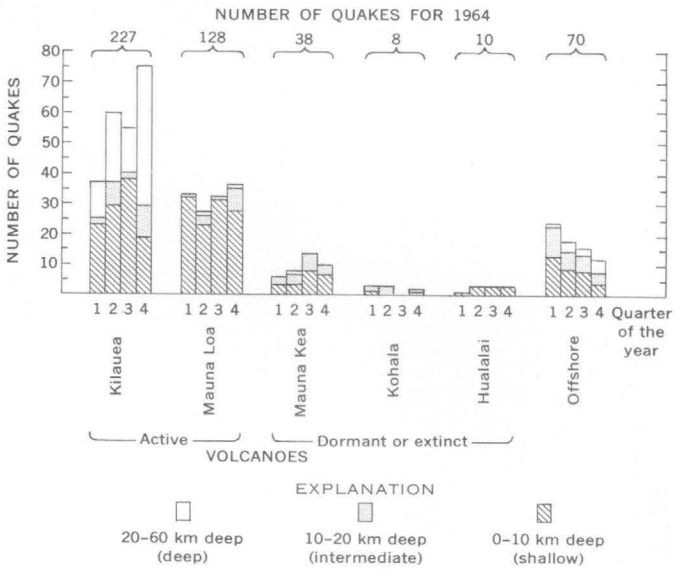


FIGURE 5.—Bar graph showing the geographic location and the distribution, with depth, of earthquakes of magnitude 2.0 and greater which occurred in the Hawaiian Islands during 1964.

Earthquake activity along the eastern part of Kilauea's east rift zone increased in late August and September. This area, accessible from the town of Pahoa, was occasionally monitored with a portable seismic unit. A total of 596 local quakes of magnitudes ranging from 0.5 to 3.8 were recorded at HVO's Pahoa seismograph station from August 27 to September 25. In addition, 5 local earthquakes with magnitudes ranging from 4.4 to 4.9 were strongly felt on the island during the third quarter. The quake of magnitude 4.9 occurred at $00^h25^m$ on September 18, under the southeast flank of Kilauea. Nearly a hundred aftershocks were recorded in the initial two days of activity.

The largest earthquake during the fourth quarter occurred at $00^h07^m$ on October 11 and had a magnitude of 5.5. It was located off the southwest shore of Hawaii and was felt on Hawaii, Maui, and Oahu islands. Also, 2 small flurries of earthquakes were noted in the Kilauea region during October and November: about 60 deep Kilauea shocks during October 28–29, and about 100 shocks from the eastern east rift zone during November 10–17. On December 2, at $22^h29^m$, a deep Kilauea earthquake of magnitude 4.7 was felt on Hawaii, Maui, and Oahu. Several hundred deep Ki-

lauea earthquakes with magnitudes of 0.5 to 4.0 occurred in the week that followed.

## STATISTICAL SUMMARY

As in earlier years, Kilauea remained the most seismic region along the Hawaiian Ridge (fig. 5). During 1964, 481 earthquakes of magnitude 2.0 or greater were recorded and located. Of this total, 227 (47 percent) were located beneath Kilauea, 128 (27 percent) were located beneath Mauna Loa, 38 (8 percent) were located beneath Mauna Kea, 8 (2 percent) were located beneath Kohala, 10 (2 percent) were located beneath Hualalai, and the remaining 70 (14 percent) were located offshore. Nearly three-fourths of the total number occurred beneath the active volcanic systems of Kilauea and Mauna Loa.

One hundred seven earthquakes were reported felt during 1964. Generally, shocks with magnitude near 3 were felt slightly; those with magnitudes of 4 to 5 were felt throughout the island of Hawaii, and 3 of them were felt on Maui and Oahu islands as well.

Including very small seismic events, 30,285 earthquakes were detected on the HVO seismic net. A large part of the low-intensity earthquake activity was concentrated in the Kilauea caldera region at depths ranging from near surface to about 5 km. There were commonly 50 to 100 shallow earthquakes of magnitudes 0.5 to 1.5 daily in the Kilauea caldera region.

Earthquake focal depths were relatively shallow, ranging from near surface to about 60 km. Of the 481 earthquakes located and plotted, 289 (60 percent) were less than 10 km deep, 81 (17 percent) were 10–20 km deep, and 111 (23 percent) were 20–60 km deep. Most of the deeper shocks were beneath the Kilauea summit area. The large numbers of quakes along the Kaoiki fault system and the southeast flank of Kilauea strongly augmented the count in the shallower categories.

## REFERENCES

Kinoshita, W. T., Okamura, A. T., Powers, H. A., 1965, Hawaiian Volcano Obesrvatory summary: U.S. Geol. Survey Hawaiian Volcano Observatory Summary 35 (July, Aug., and Sept. 1964).

Koyanagi, R. Y., 1964, Hawaiian seismic events during 1962: Art. 144 *in* U.S. Geol. Survey Prof. Paper 475–D, p. D112–D117.

Koyanagi, R. Y., and Endo, E. T., 1965, Hawaiian seismic events during 1963, *in* Geological Survey Research 1965: U.S. Geol. Survey Prof. Paper 525–B, p. B13–B16.

Koyanagi, R. Y., Okamura, A. T., Kinoshita, W. T., and Powers, H. A., 1965, Hawaiian Volcano Observatory summary: U.S. Geol. Survey Hawaiian Volcano Observatory Summary 36 (Oct., Nov., and Dec. 1964).

Koyanagi, R. Y., Okamura, A. T., and Powers, H. A., 1965, Hawaiian Volcano Observatory summary: U.S. Geol. Survey Hawaiian Volcano Observatory Summary 33 (Jan., Feb., and Mar. 1964).

Okamura, A. T., Koyanagi, R. Y., Kinoshita, W. T., and Powers, H. A., 1965, Hawaiian Volcano Observatory summary: U.S. Geol. Survey Hawaiian Volcano Observatory Summary 34 (April, May and June 1964).

# FERROSELITE IN A ROLL-TYPE URANIUM DEPOSIT, POWDER RIVER BASIN, WYOMING

By H. C. GRANGER, Denver, Colo.

*Abstract.*—Delicate, stellate penetration twins of ferroselite occur in sandstone on the concave side of a roll-type uranium ore body in the Powder River basin, Wyoming. Comparison with occurrences in the Ambrosia Lake uranium district, New Mexico, suggests that the margins of altered rock may contain selenium concentrations irrespective of the presence of uranium.

Ferroselite ($FeSe_2$), a fairly common mineral associated with sandstone-type uranium deposits, has been recognized as unusual twinned crystals in the Mrak No. 2 uranium mine in the southern part of the Powder River basin, Wyoming (fig. 1).

The Mrak No. 2 mine is one of several open-pit uranium mines in the vicinity which are developed on deposits in the Wasatch Formation of Eocene age. Descriptions of the host rocks and deposits are given by Sharp and Gibbons (1964), Sharp and others (1964), and Rosholt and others (1965). The Wasatch Formation here consists of several hundred feet of interbedded continental claystone, siltstone, and lenticular sandstone. Sharp and Gibbons (1964) have described the dull shades of gray, yellow, and brown which characterize the outcrops of most of the sandstones as drab and imply that such colors are caused by hydrated iron oxides. A large elongate zone in sandstones of the central and southern parts of the basin, however, is marked by the dominance of red stains caused by hematite. Sharp and Gibbons (1964) described the contact between red and drab sandstone lenses as being "sharp but irregular in plan and cross section; lobes and long arms of red color commonly extend into drab sandstone." Most of the uranium deposits and all of the larger ore bodies are along the boundary between the dominantly red sandstone and the drab-colored sandstone. In detail the ore bodies are generally in the drab-colored sandstone bordering the convex margin of roll-like or tonguelike extensions of dominantly red sandstone.

The Mrak No. 2 deposit and several other nearby deposits form sinuous roll-type bodies in light-gray sandstone just beyond a tongue of nearly white, bleached-appearing sandstone hereafter called altered sandstone. Rosholt and others (1965) point out that the Mrak No. 2 deposit, although above the water table, has been partly protected from weathering by an overlying mudstone 20 to 25 feet thick. Possibly the white sandstone in the pit is either the unweathered equivalent of the red sandstones as described by Sharp and Gibbons (1964, p. D9), or is a leached zone between the red and drab-colored sandstone zones. Its relation to the widespread white sandstone mapped on the surface by Sharp and Gibbons (1964) is not known. Both white sandstones are clay rich.

The sample containing ferroselite described in this report is from the pit wall of the Mrak No. 2 mine. It occurs in nearly white altered sandstone between the upper and lower limbs of the roll-type ore body and near the front of the ore-rimmed, altered tongue.

A reexamination of samples BMK–4 and BMK–7, described by Rosholt and others (1965) and previously collected on the concave side of a roll adjacent to ore in the altered sandstone at the Mrak No. 2 pit, also disclosed the presence of ferroselite (A. P. Butler, oral commun., June 1965). Also seleniferous samples from a similar position relative to ore and altered rock in the Petrotomics mine, Shirley basin, Wyoming, contain twinned crystals of ferroselite of finer grain size than the Powder River basin samples (E. N. Harshman, oral commun., June 1965).

## SAMPLE DESCRIPTION

The sample of altered sandstone in which the ferroselite was found is friable, nearly white, and poorly sorted. Although most of the grains range in size from medium to coarse, a few scattered granules are

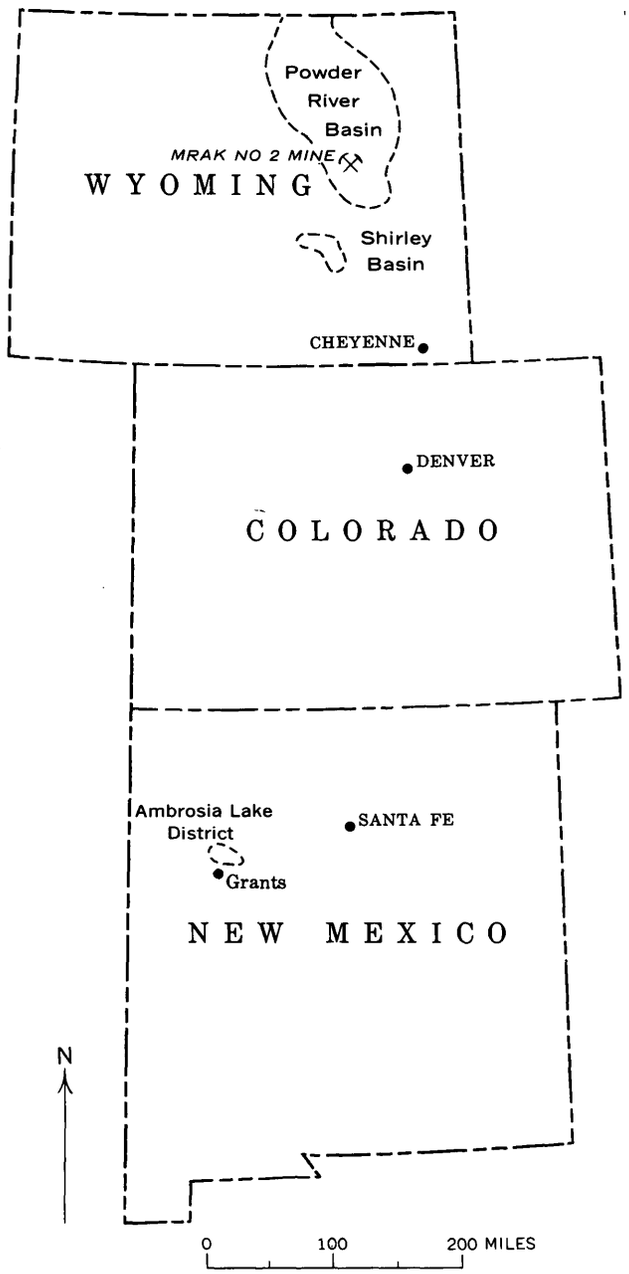


FIGURE 1.—Index map showing location of the Powder River basin (report area) and Shirley basin, Wyoming, and the Ambrosia Lake district, New Mexico.

present and interstices contain abundant clay. Most sand grains are subangular.

The petrography of the sandstone was not studied in detail. However, the sandstone is composed mostly of quartz, feldspar, and interstitial montmorillonite and has scattered greenish altered flakes of mica and less abundant rounded green grains that may be glauconite. Among the heavy minerals recognized are small amounts of pale-green epidote, red garnet, zircon, pyrite, and ilmenite. Pyrite is very sparse.

Minute stellate twin clusters of ferroselite are perched on the sand grains and clay in interstitial openings. None of the ferroselite appears to be enclosed by clay.

## SEPARATION AND IDENTIFICATION OF FERROSELITE

A separate of the ferroselite for X-ray and optical studies was made by first gently disaggregating about 50 grams of the friable sandstone and screening. The $< 200$-mesh fraction, which contained most of the dislodged ferroselite, was centrifuged in bromoform, and the heavy fraction was washed in acetone. Most of the nonmetallic minerals were removed from the heavy fraction by a flotation process involving n-hexanol and water followed by washing in acetone. Finally, a nearly pure separate of ferroselite was collected in the residue by panning the metallic fraction in either acetone or water on a large watch glass. By this procedure the number and severity of steps were kept to a minimum, and it was possible to get a separation without destroying the delicate twin clusters.

The separate was mixed and ground with a small amount of silicon, which served as an internal X-ray standard. The mixture was mounted on a collodion membrane in an aluminum holder as described by Gude and Hathaway (1962). A chart pattern was run on an X-ray diffractometer with attached monochromatic filter to eliminate all beta radiation and extraneous radiations caused by the high iron content of the mineral. The measurements from the chart pattern were refined, and cell dimensions were calculated by computer by D. E. Appleman, of the U.S. Geological Survey. The results are shown in table 1. The cell dimensions are nearly identical with those published by Kullerud and Donnay (1958) for a sample of ferroselite collected by R. G. Coleman, of the U.S. Geological Survey, at Temple Mountain, Utah.

Several handpicked sand grains with unusual concentrations of ferroselite twin clusters were mounted on gelatin-coated plates for photomicrographs of the twins in place (fig. 2).

## DESCRIPTION OF FERROSELITE

Ferroselite twin clusters are perched only on those sand grains and montmorillonite which border open spaces. Many sand grains, however, are completely enclosed by the clay and other sand grains and are not associated with ferroselite. The number of ferroselite clusters perched on individual sand grains is variable but locally more than a dozen minute clusters are discretely distributed about the surface of very coarse grains.

TABLE 1.—*X-ray data for ferroselite from the Mrak No. 2 mine, Powder River basin, Wyoming*

[Calculations programmed on a computer by D. E. Appleman, U.S. Geological Survey]

| hkl | Calculated | Observed | | hkl | Calculated | Observed | | hkl | Calculated | Observed | |
|---|---|---|---|---|---|---|---|---|---|---|---|
| | $d_{hkl}$ | $d_{hkl}$ | $I$ | | $d_{hkl}$ | $d_{hkl}$ | $I$ | | $d_{hkl}$ | $d_{hkl}$ | $I$ |
| 110 | 3.692 | 3.686 | 25 | 330 | 1.2307 | 1.2309 | 5 | 060 | .96274 | | |
| 011 | 3.046 | 3.053 | 15 | 400 | 1.2001 | 1.2004 | 10 | 303 | .95748 | | |
| 020 | 2.888 | 2.894 | 10 | 410 | 1.1750 | | | 152 | .95179 | | |
| 101 | 2.872 | 2.871 | 50 | 013 | 1.1702 | | | 510 | .94715 | | |
| 111 | 2.572 | 2.568 | 100 | 241 | 1.1697 | | | 313 | .94459 | .94471 | 5 |
| 120 | 2.474 | 2.474 | 100 | 312 | 1.1690 | 1.1686 | 15 | 160 | .94395 | | |
| 200 | 2.400 | 2.400 | 35 | 331 | 1.1640 | 1.1647 | 10 | 422 | .94266 | | |
| 210 | 2.216 | 2.218 | 20 | 103 | 1.1596 | | | 350 | .93669 | | |
| 121 | 2.036 | 2.037 | 20 | 232 | 1.1512 | | | 233 | .93512 | | |
| 211 | 1.8853 | 1.8853 | 70 | 113 | 1.1369 | 1.1364 | 10 | 501 | .92746 | .92745 | 5 |
| 220 | 1.8460 | 1.8465 | 20 | 042 | 1.1245 | 1.1241 | 5 | 440 | .92302 | .92300 | 5 |
| 031 | 1.6962 | 1.6951 | 40 | 150 | 1.1232 | | | 342 | .92008 | | |
| 221 | 1.6412 | | | 411 | 1.1166 | | | 511 | .91573 | | |
| 112 | 1.6124 | | | 420 | 1.1083 | | | 161 | .91283 | | |
| 131 | 1.5993 | 1.5985 | 20 | 322 | 1.1032 | 1.1035 | 15 | 520 | .91112 | | |
| 310 | 1.5421 | 1.5414 | 35 | 051 | 1.0996 | | | 323 | .90884 | | |
| 022 | 1.5230 | | | 142 | 1.0949 | | | 351 | .90627 | | |
| 230 | 1.5019 | | | 123 | 1.0761 | | | 143 | .90418 | | |
| 301 | 1.4612 | | | 151 | 1.0718 | | | 252 | .90019 | | |
| 122 | 1.4517 | 1.4512 | 30 | 421 | 1.0588 | 1.0590 | 15 | 004 | .89624 | .89630 | <5 |
| 040 | 1.4441 | | | 213 | 1.0518 | 1.0513 | 10 | 411 | .89387 | | |
| 202 | 1.4362 | 1.4371 | 5 | 250 | 1.0409 | | | 260 | .89355 | | |
| 311 | 1.4166 | 1.4165 | 15 | 341 | 1.0271 | 1.0275 | 10 | 432 | .88555 | | |
| 320 | 1.3997 | 1.3992 | 15 | 242 | 1.0183 | | | 521 | .88305 | | |
| 212 | 1.3937 | 1.3941 | 5 | 033 | 1.0153 | 1.0158 | 10 | 114 | .87095 | | |
| 231 | 1.3853 | 1.3858 | 5 | 332 | 1.0145 | | | 261 | .86702 | | |
| 140 | 1.3829 | | | 223 | 1.0031 | 1.0036 | <5 | 243 | .85959 | | |
| 321 | 1.3038 | 1.3027 | 5 | 251 | .99970 | | | 530 | .85924 | | |
| 141 | 1.2902 | | | 402 | .99728 | .99715 | 5 | 333 | .85733 | | |
| 222 | 1.2860 | 1.2848 | 5 | 133 | .99337 | .99352 | <5 | 024 | .85597 | | |
| 132 | 1.2655 | 1.2659 | 5 | 412 | .98274 | .98312 | 5 | 062 | .84815 | | |
| 240 | 1.2374 | 1.2390 | 20 | | | | | | | | |

Radiation: $\lambda = 1.5418$ A below $2\theta = 50°$
$\lambda = 1.54050$ A above $2\theta = 50°$

Unit cell: $a$ (A) = $4.8007 \pm 0.0007$
$b$ (A) = $5.776 \pm 0.002$
$c$ (A) = $3.5850 \pm 0.0005$
$V$ (A$^3$) = $99.42 \pm 0.03$

The X-ray pattern also showed weak, but well-defined peaks at $d$ (A) = 2.36, 1.742, 1.073, 1.019, and 0.9806. These represent some unidentified impurity.

Stellate twin clusters of ferroselite range from about 0.035 mm to 0.08 mm in diameter. Individual crystals or rays of the stellate clusters range from about 0.004 mm to 0.015 mm in width. In many clusters there seems to be a larger central crystal from which smaller crystals branch (fig. 3).

Details of the twinning scheme and crystallography could not be resolved because of the extremely small size and complexity of the twins. Many of the faces are rough, and under high magnification the edges and terminations commonly appear to be rounded as if the surfaces were corroded. Attempts were made to study the twins on a universal stage using both oblique and vertical illumination but were not successful.

Individual crystals in the twin clusters are orthorhombic and have recognizable crystal faces similar to marcasite. If they follow the same pattern as marcasite crystals, the ferroselite crystals are elongate in the direction of the $a$ axis. In cross section most of the crystals are diamond shaped, consisting of the four $(0kl)$ prism faces (fig. 3). Some crystals appear to be terminated by a (100) face; most, however, are terminated by a macrodome or prism made up of $(hkO)$ faces.

The twinning scheme appears to be based on a penetration trilling with angles of about 60°; one member of the trilling is commonly a little larger than the others. From the plane of trilling, which may be only partly developed, other crystals emerge, all originating near the center of the trilling. Although the angles

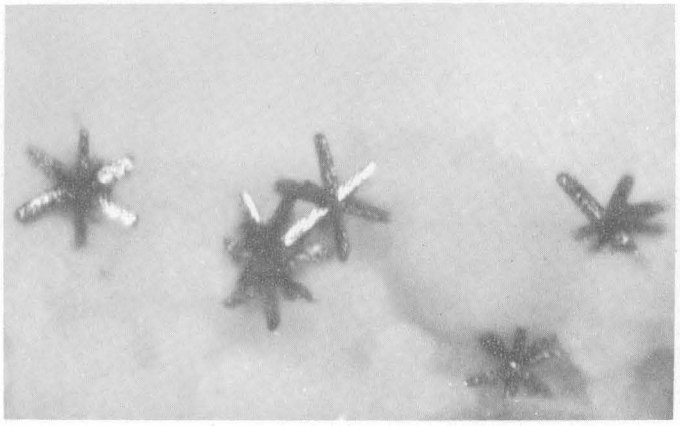

FIGURE 2.—Photomicrograph of natural occurrence of ferroselite twins perched on montmorillonite which coats a sand grain. × 350. Photomicrograph by W. N. Sharp.

between these extra crystal rays were not accurately measured because of the small crystal size, it appears that they have no regular angular relations either one to the other or to the plane of the trilling. Minute, stubby crystals no more than one-tenth the length of the trilling twins commonly project from the center but are overshadowed by the larger crystals. At least 10 crystals project from the centers of most twin clusters, and perhaps 20 or more crystals are present in the more completely developed stellate aggregates.

## DISCUSSION

The sizes and shapes of ferroselite twin clusters in the Powder River basin, Wyoming, are similar to those of clusters recently found in the Shirley basin, Wyoming, and in the Ambrosia Lake district, New Mexico. Although other varieties have been reported (Granger, 1963), descriptions of the Wyoming and New Mexico ferroselite clusters have not yet been published. A brief description of the Ambrosia Lake occurrence is given below.

Deep oxidation in the Ambrosia Lake district locally has affected the uranium deposits and host rocks to as much as several hundred feet below the present water table. In many places the interface between oxidized sandstone and unoxidized pyritic sandstone is quite sharp. The oxidized sandstone is either yellow stained and goethitic or red stained and hematic(?). Stellate twins of ferroselite were found in the Section 22 mine (Granger and others, 1961) in a narrow goethitic zone between unoxidized barren sandstone and red oxidized sandstone. Each twin cluster is enclosed by a goethite-rich bleb or pseudomorph after pyrite. Pyrite in the unoxidized sandstone generally contains a small amount of selenium, but the red hematitic(?) sandstone has virtually none. The ferroselite twin clusters were evidently destroyed by the strongly oxidizing conditions imposed during development of the hematitic(?) environment.

The relations at Ambrosia Lake suggest that this particular ferroselite was formed near the front of an expanding oxidation environment. Presumably, selenium held in solid solution in pyrite was made available to form a seed crystal of ferroselite early in the sequence of events as the pyrite was destroyed, but more complete oxidation destroyed the ferroselite. Consequently, the ferroselite was formed and only was stable just behind the oxidation front in goethitic sandstone.

The ferroselite in the Mrak No. 2 mine also seems to occur just behind a "front" that has encroached on the unaltered sandstone. In this case the "front" gives no obvious evidence of having been produced by an oxidizing environment because of the lack of oxidized iron minerals. In fact, samples BMK–4 and BMK–7 collected from behind this "front" (Rosholt and others, 1965, p. 204) contained considerable pyrite as well as ferroselite (A. P. Butler, oral commun., June 1965). In this contradictory situation, the pyrite may be later than the ferroselite; there is no evidence to dispute this. In other deposits in the basin, however, the altered sandstone does contain oxidized iron minerals presumably from original pyrite (Sharp and Gibbons, 1964). The presence of gray, reduced(?) uranium ore

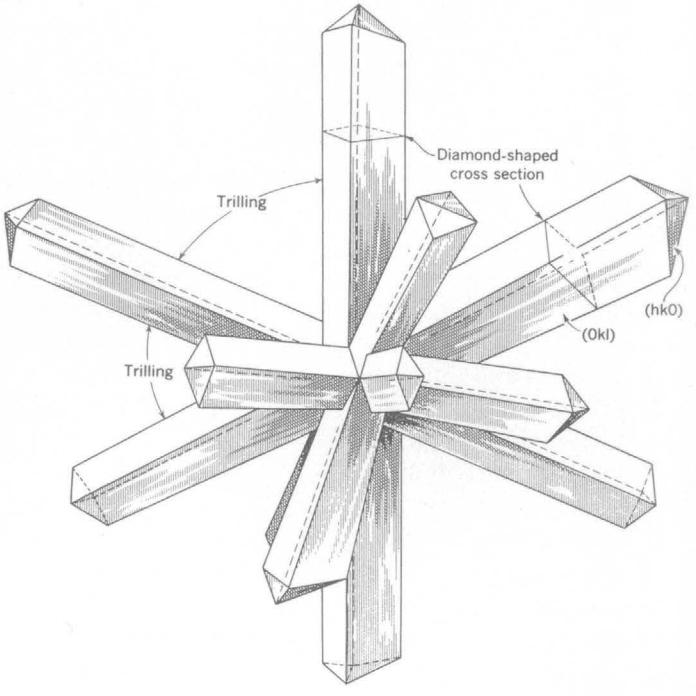


FIGURE 3.—Schematic illustration of a stellate penetration-twin cluster of ferroselite.

(Rosholt and others, 1965, p. 201) in a roll form in advance of the altered zone suggests that the altered zone may represent an environment that was oxidizing relative to uranium at the time of uranium deposition.

Experience gained at Ambrosia Lake (Granger and others, 1961; Granger, 1963) indicates that some of the selenium there was carried ahead of the oxidized zone and was precipitated as native selenium. Sharp and others (1964, p. 576 and 597) and Sharp and Gibbons (1964, p. D41) found native selenium and selenium concentrated in unidentified form in close association with some of the uranium deposits throughout the Powder River basin. These interfaces between altered and unaltered seleniferous sandstones may, therefore, be found consistently to mark abnormal selenium concentrations dominantly in the forms of ferroselite immediately behind, and (or) native selenium immediately in front of, the interface. In the course of exploration for uranium deposits, it might be desirable to make at least qualitative analyses for selenium at any alteration interface regardless of the presence or absence of abnormal radioactivity.

It has been pointed out by D. F. Davidson and H. W. Lakin (oral commun., 1965) that the field observations and interpretations of selenium in relation to the oxidation interface do not seem to be compatible with the known chemical behavior of selenium. Selenides, such as ferroselite, represent a more reduced form of selenium than does native selenium, and it would seem more reasonable if their positions were reversed on opposite sides of the oxidation interface. This is an important point to consider in interpreting conditions under which some roll-type uranium deposits have formed, and it must be reconciled to complete the picture.

## REFERENCES

Granger, H. C., 1963, Mineralogy, *in* Geology and technology of the Grants [New Mexico] uranium region: New Mexico Bur. Mines and Mineral Resources, Mem. 15, *prepared by* Soc. of Econ. Geologists, V. C. Kelley, Chm., Uranium Field Conference, p. 21–37.

Granger, H. C., Santos, E. S., Dean, B. G., and Moore, F. B., 1961, Sandstone-type uranium deposits at Ambrosia Lake, New Mexico—an interim report: Econ. Geology, v. 56, no. 7, p. 1179–1210.

Gude, A. J. 3d, and Hathaway, J. C., 1962, A diffractometer mount for small samples: Norelco Reporter, v. 9, no. 1, p. 10–11.

Kullerud, G., and Donnay, G., 1958, Natural and synthetic ferroselite. A roentgenographic mimesis of rammelsbergite: Geochim. et Cosmochim. Acta, v. 15, nos. 1 and 2, p. 73–79.

Rosholt, J. N., Butler, A. P., Garner, E. L., and Shields, W. R., 1965, Isotopic fractionation of uranium in sandstone, Powder River basin, Wyoming, and Slick Rock district, Colorado: Econ. Geology, v. 60, no. 2, p. 199–213.

Sharp, W. N., and Gibbons, A. B., 1964, Geology and uranium deposits of the southern part of the Powder River Basin, Wyoming: U.S. Geol. Survey Bull. 1147–D, p. D1–D60.

Sharp, W. N., Mackay, E. J., McKeown, F. A., and White, A. M., 1964, Geology and uranium deposits of Pumpkin Buttes area of the Powder River Basin, Wyoming: U.S. Geol. Survey Bull. 1107–H, p. 541–638.

# GEOLOGIC AND GEOCHEMICAL FEATURES OF THE REDSKIN GRANITE AND ASSOCIATED ROCKS, LAKE GEORGE BERYLLIUM AREA, COLORADO

By C. C. HAWLEY, CLAUDE HUFFMAN, JR., J. C. HAMILTON, and L. F. RADER, JR., Denver, Colo.

*Abstract.*—Precambrian igneous rocks northwest of Lake George, Colo., consist of (1) catazonal Boulder Creek(?) Granodiorite, (2) mesozonal Silver Plume(?) Granite, and (3) epizonal rocks that include gabbro and monzonite, the Pikes Peak Granite, and the Redskin Granite, which is a late intrusive of the Pikes Peak Granite magma series. The Pikes Peak Granite of the area is an alkali granite that contains more than normal amounts of F, Sn, Li, Rb, and Be—a suite of trace elements generally found in greisen ore deposits. The somewhat younger Redskin Granite, which is herein named, has associated beryllium-bearing greisen. It is also an alkali granite that is enriched in F and contains more Sn, Li, Rb, and Be than the Pikes Peak Granite.

The Lake George beryllium area is on the west side of the Front Range, a few miles northwest of Lake George (fig. 1), and is mainly in eastern Park County, Colo. This is a Precambrian terrane whose matrix and oldest element is paragneiss of the Idaho Springs Formation. Younger rocks, including granitic orthogneiss, granite, and more mafic igneous rocks, occur in plutons of different ages that can be grouped into catazonal, mesozonal, and epizonal types, following the usage of Buddington (1959). Because the paragneiss of the Lake George area belongs to the almandine-amphibolite facies of regional metamorphism, Buddington's correlation between the metamorphic rank of the host rocks and the zone of emplacement of plutons does not necessarily apply.

## GEOLOGY OF THE INTRUSIVE ROCKS

The igneous rocks of the Lake George area are of Precambrian age and were emplaced in three main episodes, each probably of long duration. The threefold sequence probably corresponds to that of the north-central Front Range exemplified by the Boulder Creek Granodiorite, Silver Plume Granite, and Pikes Peak Granite (Tweto, 1965).

### Catazonal intrusive rocks

The oldest rocks of undoubted igneous origin are mesocratic biotite-quartz diorite gneiss and lighter colored orthogneiss which varies from granodiorite to granite in composition. These rocks crop out in the southern part of the Lake George area, where they form concordant sheetlike and phacolithic bodies

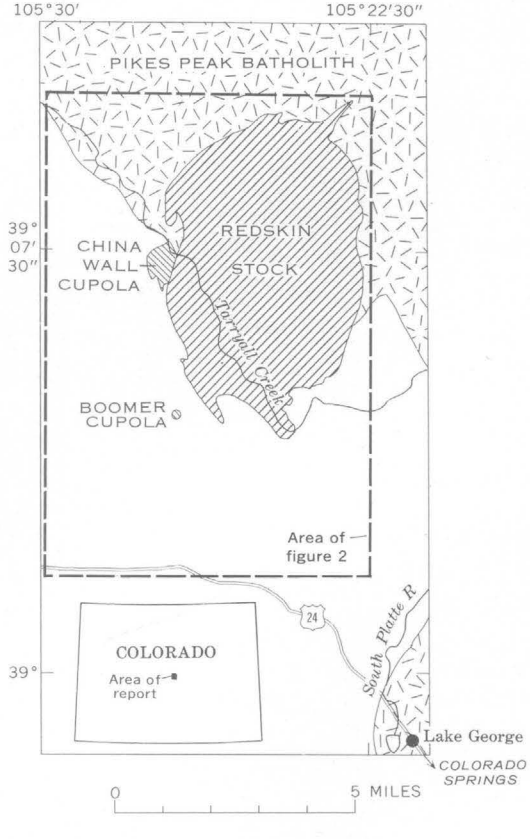


FIGURE 1.—Geologic index map of the Lake George beryllium area (dashed lines), Colorado.

(fig. 2). Although crosscutting relations show that the lighter colored gneiss is younger than the quartz diorite gneiss, both types are intimately mixed in the conformable plutons and thus are assigned to the same magmatic episode. They are tentatively correlated with the Boulder Creek Granodiorite of the central Front Range which contains rocks with a similar range in composition, and like them, is of syntectonic origin.

A syntectonic origin is indicated by the concordance of planar and linear structures in the Boulder Creek(?) Granodiorite and the host paragneiss and by the locally phacolithic form of the granodiorite. Similar criteria have been used to demonstrate syntectonic emplacement of granodiorite in the central Front Range close to the type Boulder Creek Granodiorite pluton (Harrison and Wells, 1959, p. 12–15; Moench and others, 1962, p. 38). The Boulder Creek(?) Granodiorite of the Lake George area is classed as catazonal because of its marked foliation, concordant form, and high metamorphic grade of the country rock; Buddington (1959, p. 730), however, classed the type Boulder Creek Granodiorite as transition mesozone-catazone.

The age of the Boulder Creek-like rocks of the Front Range is uncertain. Possibly the Boulder Creek is as old as 1,730 million years, as is indicated by the $Pb^{207}/Pb^{206}$ ratio in zircon from the Boulder Creek batholith (T. W. Stern, George Phair, and David Gottfried *in* U.S. Geol. Survey, 1964, p. A95). Almost certainly it is at least 1,600 or 1,650 m.y. old, the oldest ages found on Front Range rocks by the Rb-Sr and K-Ar methods (Wetherill and Bickford, 1965; Houston and others, 1965).

### Mesozonal intrusive rocks

The next youngest igneous rocks in the Lake George area are fine- to coarse-grained nearly massive to well-foliated granites in sheets, dikes, and crudely oval shaped plutons (fig. 2). These are tentatively correlated with the Silver Plume Granite as well as with the lithologically similar granite of the Kenosha batholith and the Cripple Creek Granite. Contacts between the Silver Plume(?) Granite of the Lake George area and adjacent rocks commonly are concordant, but are discordant locally. Emplacement of the granite apparently followed one period of movement on the Badger Flats fault, as shown by a partly disconformable pluton in the south-central part of the area, which has a dikelike extension along the fault.

The Silver Plume(?) Granite varies from tan to light gray and has a wide variation in grain size. The most abundant type is medium-grained biotite or biotite-muscovite granite with an equigranular to seriate porphyritic texture. It has nearly equal amounts of quartz, oligoclase, and poorly twinned microcline, and is a quartz monzonite by some modal classifications. In thin section, minute crosscutting fractures filmed with muscovite sillimanite cut this granite, indicating formation under metamorphic conditions, possibly during a regional cataclastic event such as the younger deformation described by Moench and others (1962). The larger Silver Plume(?) plutons recrystallized parts of the Idaho Springs Formation, and caused a new foliation to develop in it. This late foliation is particularly well developed around the two oval-shaped plutons in the southeastern part of the area (fig. 2).

The age of the type Silver Plume is not closely known at present, but the granite probably is somewhat older than 1,350 m.y. Aldrich and others (1958) reported a range in 2 samples from the type area by the Rb-Sr method of 1,350-1,360 m.y., K-Ar analyses of the same samples indicated ages of about 1,200 m.y., but recalculation using a revised K-Ar constant indicates an age of 1,250 m.y. (R. L. Pearson, oral commun., 1965). The closely related St. Kevin Granite has been dated at 1,390 m.y. by a whole-rock Rb-Sr method (Pearson and others, in press). A 1,080-m.y. date on the Cripple Creek (Hutchinson, 1964) probably reflects thermal changes induced by the nearby Pikes Peak batholith more than the true age of this granite.

### Epizonal intrusive rocks

The late igneous rocks are gabbro and monzonite, Pikes Peak Granite, and Redskin Granite.

*Gabbro and monzonite.* — Gabbro and monzonite (which includes quartz monzonite) occur together in a small pluton near the south end of the Redskin stock, and monzonite forms a small body nearly surrounded by Pikes Peak Granite in the northeastern part of the area. The gabbro, which forms the outer zone of a small funnel-shaped pluton that was invaded by the Redskin Granite, is a coarse-grained rock composed mainly of labradorite, dark silicates, and ilmenite. At one place the dark silicates are olivine and hypersthene, but at most places the original mafic silicates have been altered to green biotite. The inner part of the pluton is quartz monzonite which varies from a coarse-grained granular hornblende-biotite quartz monzonite to a fine-grained biotite quartz monzonite porphyry.

Relatively shallow emplacement of gabbro and quartz monzonite is indicated by the discordant contacts and the funnel-like form of the pluton. The pluton can only be dated by crosscutting relations as post-Silver Plume(?) and pre-Redskin Granites, but its manner of occurrence suggests that it is but slightly

211-690 O—66——10

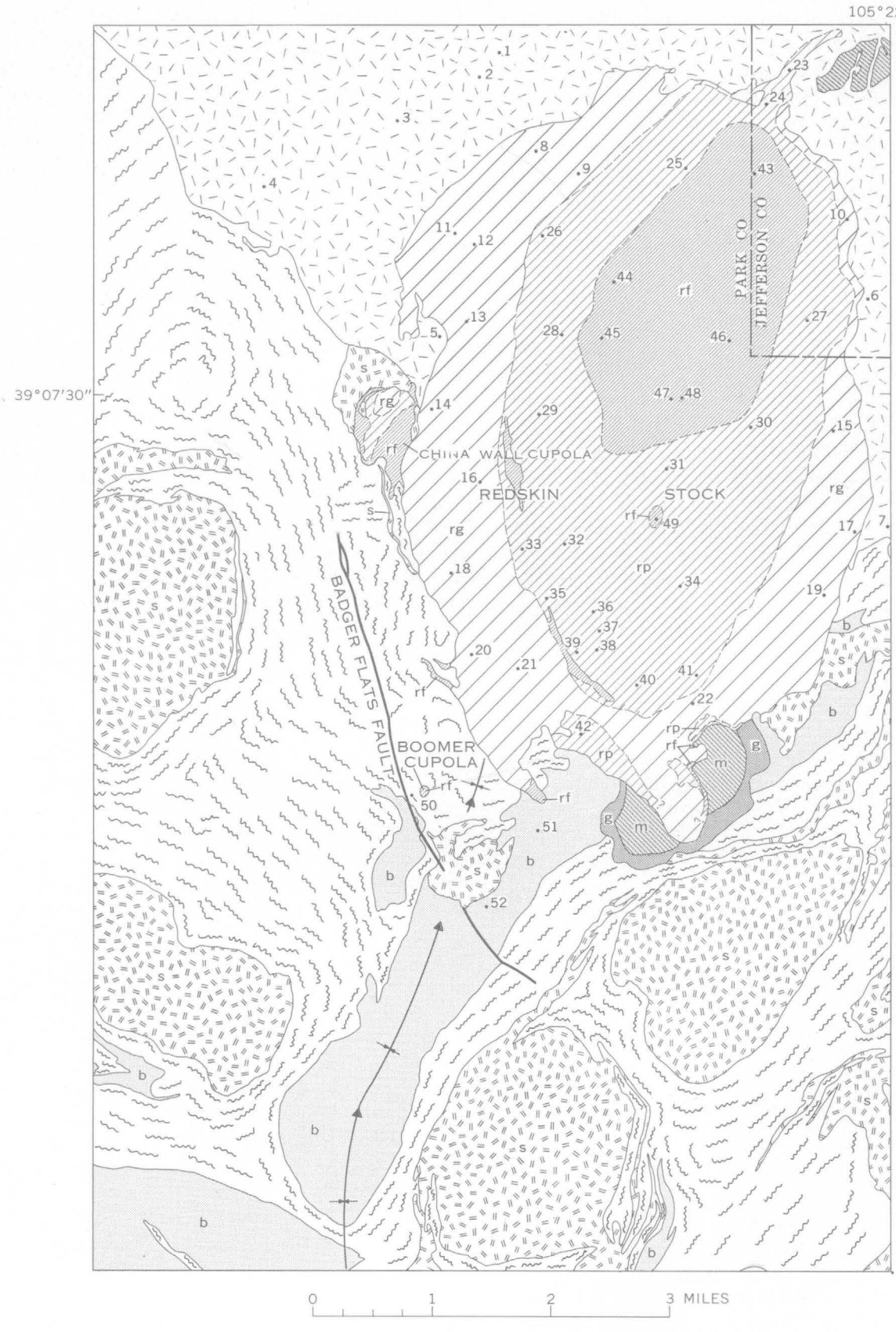


FIGURE 2.—Generalized geologic map of the Lake George beryllium area.

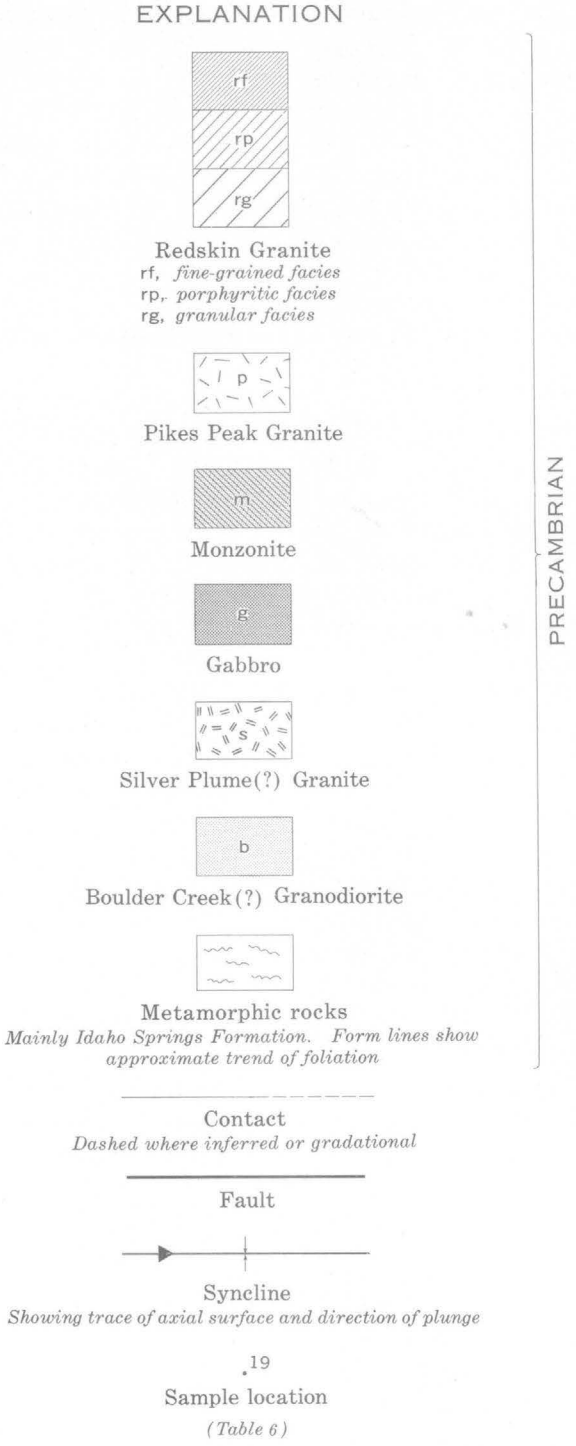


older than the Redskin. The only other occurrence of gabbro nearby is in a composite pluton in the Cripple Creek district (Graton, 1906, p. 53–65). The gabbro and associated rocks of the Cripple Creek district can be judged to be relatively young because they are not metamorphosed. They are cut by dikes of the Spring Creek Granite, which forms a local border zone of the Pikes Peak batholith west of Cripple Creek, but were regarded by Graton as older than the Pikes Peak Granite.

*Pikes Peak Granite.*—The Pikes Peak Granite occurs in the north and northeast parts of the Lake George beryllium area, which lies along the western flank of the Pikes Peak batholith of the Colorado Front Range. The granite is coarse grained and subequigranular to porphyritic. At most places, it is massive to very faintly foliated, but in some porphyritic facies potassic feldspars are markedly alined in a primary foliation. Locally, the coarse-grained granite is cut by dikes or irregular masses of pegmatite, aplite-pegmatite, and fine-grained granite, and granite porphyry. The aplite-pegmatite is a miarolitic rock which contains abundant nearly euhedral crystals of smoky quartz, perthitic microcline, and albite and rare crystals of topaz and fluorite—minerals characteristic of the Pikes Peak Granite.

The granite is classed as epizonal because of its clearly discordant contacts, generally massive structure, and local miarolitic nature. Neither the structural trends nor the mineralogy of the country rocks were apparently affected by the emplacement of this granite.

The age of the Pikes Peak Granite is approximately 1,000 m.y. Hutchinson (1960) reported values of 1,050 and 1,080 m.y. for the northern part of the Pikes Peak batholith, and Aldrich and others (1958) and Giffin and Kulp (1960) found a range of about 980 to 1,060 m.y. in the Pikes Peak and the nearly synchronous Windy Point and Mount Rosa Granites, in the southern part of the batholith. Hutchinson (1964) also reported an age of 995 m.y. for a porphyritic aplite facies of the granite.

*Redskin Granite.*—The Redskin Granite previously was termed a late facies of the Pikes Peak Granite (Hawley, 1963, 1964), and the Redskin stock was called the Tarryall lobe (Hawley, 1963). The granite is now named the Redskin Granite for Redskin Gulch, in the northern part of the Tarryall 7½-minute quadrangle, and its type area is the area occupied by the Redskin stock. The Redskin stock of this report was called the Redskin Gulch granite stock by Hutchinson (1964).

The Redskin Granite crops out in the northern part of the Lake George area, in the Redskin stock and in the China Wall and Boomer cupolas (figs. 1 and 2). It is fine to medium grained, white to pink, and mostly a massive granite. Its aplitic and pegmatitic facies are locally miarolitic. The porphyritic facies and the fine-grained aplitic granite of the stock and cupolas have associated beryllium-bearing greisen deposits.

The Redskin stock is concentrically zoned. The central zone or core consists of fine-grained equi-

granular granite that is named the fine-grained facies (fig. 2). Surrounding the core is the porphyritic facies, a medium-grained seriate porphyritic rock. The rocks of the outer zone, named the granular facies, consist of medium-grained equigranular granite. All three facies are composed of microcline that is variably perthitic, quartz, albite ($An_{5-10}$), and mica. The granular facies is biotitic and contains quartz, microcline perthite, and albite in the proportions 33:43:24. Both the fine-grained and porphyritic types in the stock are 2-mica granites and contain quartz, microcline, and albite in nearly equal proportions; the weighted modal average of all 3 facies in the stock also approaches this ratio (table 1). A fine-grained aplitic granite that forms the Boomer cupola (fig. 2) is a quartzose muscovitic two-alkali-feldspar granite (see table 1). Rocks of similar composition form outer parts of the China Wall cupola and local border zones of the Redskin stock (fig. 2).

Like the Pikes Peak Granite, the Redskin Granite is considered epizonal because of its occurrence in discordant plutons, its generally massive structure, and local miarolitic facies.

TABLE 1.—*Modal (volume percent) composition of the Redskin Granite*

| | Average composition of Redskin stock [1] | Average composition of Boomer cupola [2] |
|---|---|---|
| Quartz | 30.4 | 37.1 |
| Albite | 29.9 | 32.2 |
| Microcline, variably perthitic | 34.8 | 24.0 |
| Biotite | 3.0 | .1 |
| Muscovite | 1.3 | 6.0 |
| Fluorite | .5 | .15 |
| Opaque minerals | .1 | .15 |
| Topaz, zircon, and others | Trace | .3 |

[1] Weighted average of 118 modal analyses.
[2] Average of 12 modal analyses.

The age of the granite and the associated greisen of the Redskin stock and Boomer cupola is about 1,000 m.y. (table 2). The lead-isotope ratios have also been determined on the same samples of microcline from the granite, and these ratios are consistent with 1,000-m.y.-old lead (B. R. Doe, written commun., 1964), as is the lead-isotope composition of galena from greisen at the Boomer cupola determined by Antweiler (1965) to be about 1.42, 24.04, 22.13, and 52.41 atom percent of $Pb^{204}$, $Pb^{206}$, $Pb^{207}$, and $Pb^{208}$.

## CHEMISTRY OF THE PIKES PEAK AND REDSKIN GRANITES

### Major elements

Chemical analyses made for this study (table 3) and the analyses reported by Hutchinson (1960) show that most of the Pikes Peak Granite is peraluminous alkali granite. The composition is, however, not uniform, and variants as mafic as granodiorite have been found by Hutchinson (1960) in its northern part and by Gotthard Kraus (written commun., 1960) in its southwestern part.

The granular facies of the Redskin Granite is very similar chemically to the nearby Pikes Peak Granite. The porphyritic and fine-grained facies of the Redskin Granite are more sodic and less potassic than the Pikes Peak Granite (table 3). Fine-grained aplitic granite in local borders to the stock, in the outer part of the China Wall cupola, and in the Boomer cupola, is much more siliceous than the bulk of Redskin Granite, as exemplified by an analysis of granite from the Boomer cupola.

### Trace elements

Samples of granite from the Redskin stock, the Pikes Peak batholith, and from representative older igneous and metamorphic rocks were analyzed for Sn, Li, Rb,

TABLE 2.—*K-Ar and Rb-Sr ages of the Redskin Granite and associated greisen*

[Analysts: Carl Hedge, H. H. Thomas, Richard Marvin, and Frank Walthall]

| Field No. | Lab. No. | Description and location | Mineral | $K_2O$ (percent) | $Ar^{40}$ (ppm) | $Ar^{40}/K^{40}$ | Age (m.y.) |
|---|---|---|---|---|---|---|---|
| Pprs-1b | 307-61 | Porphyritic facies of Redskin Granite in Redskin stock. | Biotite | 9.18 | 0.696 | 0.0757 | 980 |
| Pprs-lmg | 306-61 | Greisen in Redskin stock | Muscovite | 10.64 | .853 | .0800 | 1,020 |
| Ppb-lm | 309-61 | Granite-aplite facies in Boomer cupola | do | 10.17 | .785 | .0770 | 990 |
| Ppb-lmg | 308-61 | Greisen in Boomer cupola | do | 10.70 | .835 | .0779 | 1,000 |

| Field No. | Lab. No. | Description and location | Mineral | $Rb^{87}$ (ppm) | Normal Sr (ppm) | $Sr^{87}$ (ppm) | $Sr^{87}/Rb^{87}$ | Age (m.y.) |
|---|---|---|---|---|---|---|---|---|
| Pprs-1K | 100-62 | Porphyritic facies of Redskin Granite of Redskin stock. | Microcline | 219 | 9.1 | 3.31 | 0.0136 | 915±50 |
| Ppb-1K | 101-62 | Granite-aplite facies in the Boomer cupola. | do | 285 | 38.1 | 4.01 | .0141 | 950±50 |

TABLE 3.—*Chemical composition of representative rocks of the Pikes Peak and Redskin Granites*

[Standard rock analyses by Paula M. Buschmann, Ellen S. Daniels, and Elaine L. Munson]

| | Pikes Peak Granite | | Redskin Granite | | | | Average alkali granite of Nockolds (1954) |
|---|---|---|---|---|---|---|---|
| | | | Redskin stock | | | Boomer cupola | |
| | | | Granular facies | Porphyritic facies | Fine-grained facies | Aplitic granite | |
| Sample No. (fig. 2) | (1) | 2 | 21 | 37 | 47 | (2) | |
| Field No. | TR-74 | M3-156 | BA-657 | BA-687 | T1-172 | B2-7-5 | |
| Lab. No. | H3247 | D100 428 | H3601 | H3604 | D100 389 | H3246 | |
| $SiO_2$ | 72. 39 | 74. 38 | 74. 47 | 74. 03 | 74. 12 | 77. 07 | 73. 86 |
| $Al_2O_3$ | 13. 20 | 12. 79 | 12. 93 | 13. 44 | 13. 70 | 12. 18 | 13. 75 |
| $Fe_2O_3$ | . 74 | . 51 | . 60 | . 48 | 1. 23 | . 79 | . 78 |
| FeO | 1. 98 | 1. 60 | 1. 26 | 1. 17 | . 29 | . 69 | 1. 13 |
| MgO | . 10 | . 06 | . 05 | . 06 | . 07 | . 03 | . 26 |
| CaO | 1. 20 | . 88 | . 76 | . 80 | . 50 | . 38 | . 72 |
| $Na_2O$ | 3. 38 | 3. 29 | 3. 72 | 4. 18 | 4. 20 | 3. 31 | 3. 51 |
| $K_2O$ | 5. 30 | 5. 27 | 5. 22 | 4. 82 | 4. 91 | 4. 03 | 5. 13 |
| $H_2O^+$ | . 34 | . 39 | . 20 | . 17 | . 45 | . 42 | . 47 |
| $H_2O^-$ | . 09 | . 06 | . 04 | . 06 | . 14 | . 21 | ---------- |
| $TiO_2$ | . 26 | . 17 | . 13 | . 11 | . 12 | . 02 | . 20 |
| $P_2O_5$ | . 03 | . 03 | . 00 | . 02 | . 01 | . 01 | . 14 |
| MnO | . 06 | . 04 | . 04 | . 05 | . 01 | . 02 | . 05 |
| $CO_2$ | . 02 | . 01 | . 01 | . 01 | . 00 | . 02 | ---------- |
| Cl | . 05 | . 03 | . 02 | . 02 | . 02 | . 01 | ---------- |
| F | . 49 | . 67 | . 45 | . 52 | . 24 | . 27 | ---------- |
| Subtotal | 99. 63 | 100. 18 | 99. 90 | 99. 94 | 100. 01 | 99. 46 | Not given |
| Less O for F | . 22 | . 29 | . 19 | . 22 | . 10 | . 11 | ---------- |
| Total | 99. 41 | 99. 89 | 99. 71 | 99. 72 | 99. 91 | 99. 35 | ---------- |

[1] Three miles northwest of locality of sample 2.
[2] Boomer mine, Boomer cupola.

and Be. The granular, porphyritic, and fine-grained facies of the Redskin Granite in the stock are each represented, respectively, by 15, 19, and 7 samples (see fig. 2)—the number of samples is approximately proportional to the areal extent of each of these rock types. Granite from the Pikes Peak batholith is represented by 7 samples, and the older igneous and metamorphic rocks by 3 samples.

*Analytical methods.*—Tin was determined by the method described by Huffman and Bartel (1964). Acid decomposition of the sample was followed by separation of the tin by anion-exchange resin in dilute (1.4*M*) hydrochloric acid containing sufficient oxalic acid to make the solution 0.05*M* in oxalic acid. The tin was then concentrated into a small volume by a carbamate-chloroform extraction and measured as the flavanol complex using a fluorimeter.

Lithium and rubidium were determined on about 50 percent of the samples by a quantitative spectrographic method using an alkali buffer to enhance the intensity of the low-energy spectral lines (Ahrens and Taylor, 1961). Subsequently, the rest of the samples were analyzed by the quantitative spectrographic procedure of Annell (1964). In this procedure, the sample is mixed with potassium carbonate and burned in a 16-amp d-c arc. Selective filtering at the focal plane permits measurable line intensities for the two exposure conditions required. A comparison of 3 analyses determined by using an alkali buffer with those made by the spectrographic procedure of Annell indicates that the results are in substantial agreement (table 4).

Beryllium was determined by a semiquantitative spectrographic method (Myers and others, 1961); the results of analyses were, however, reported in a 6-step geometric interval of each power of 10, that is as 1, 1.5, 2, 3, 5, 7, 10 parts per million, rather than the 3-step interval shown by Myers and others (1961). The re-

TABLE 4.—*Comparison of analyses for lithium and rubidium by two quantitative spectrographic methods*

[Results given in percent. Analyst: Joseph Haffty]

| Field No. | Lab. No. | Li | | Rb | |
|---|---|---|---|---|---|
| | | 1 | 2 | 1 | 2 |
| BA-821 | H3608 | 0. 0051 | 0. 0052 | 0. 078 | 0. 082 |
| BA-822 | H3602 | . 011 | . 012 | . 075 | . 082 |
| BA-872 | H3606 | . 0089 | . 010 | . 067 | . 076 |

1. Analysis made using an alkali buffer to enhance intensity of low-energy spectral lines (Ahrens and Taylor, 1961).
2. Analysis made by the method of Annell (1964).

sults thus obtained compare favorably with check analyses obtained on six representative samples by a morin-fluorescence method and also by a quantitative spectrographic method (Bastron and others, 1960) as shown in table 5.

*Results of analyses.*—Partial spectrographic or fluorimetric analyses of rocks from the Lake George beryllium area are given in table 6. The range in content of selected minor elements found in the Redskin Granite of the stock is from 7 to 26 ppm of Sn, 16 to 160 ppm of Li, 540 to 1,500 ppm of Rb, and 3 to 20 ppm of Be. The corresponding ranges of values in the nearby coarse-grained granite of the Pikes Peak batholith are from 7 to 13 ppm of Sn, 41 to 100 pm of Li, 400 to 860 ppm of Rb, and 3 to 7 ppm of Be.

Arithmetic and geometric means of individual analyses, according to rock type, are given in table 7. The arithmetic mean (or abundance) can be compared with similar averages generally reported in the geologic literature. The geometric mean, however, is probably a more representative measure of central tendency for a relatively small number of samples.

The Sn, Li, Rb, and Be content of the Redskin Granite is clearly greater than that of the Pikes Peak Granite of the nearby part of the Pikes Peak batholith (table 7). The Redskin Granite is richer in these elements than many other granite bodies of similar bulk composition, but it has about the same amount of these elements as some of the late granite differentiates termed the "tin-granites" by Westerveld (1936). According to Westerveld, the tin granites are similar in bulk composition to their parent rocks, but are distinguished from them by a higher content of rare elements, including Sn, Li, W, Bi, Cu, Co, and U. The name "tin granite" of course comes from the fact that many tin-granite bodies do have associated tin deposits, examples being the granite in Cornwall, Saxony, Pitkaranta, the Transvaal, and the Malayan tin belt, all

TABLE 5.—*Comparison of analyses for beryllium by three methods*

[Results given in parts per million]

| Field No. | Lab. No. | Spectrographic | | Morin fluorescence |
|---|---|---|---|---|
| | | Semiquantitative | Quantitative | |
| M4–145 | D114 206 | 20 | 19 | 16 |
| BA–1002 | D114 190 | 10 | 10 | 8 |
| T1–172 | D100 389 | 7 | 7 | 6 |
| M3–293 | D114 198 | 5 | 8 | 7 |
| T1–127 | D114 193 | 5 | 6 | 6 |
| M3–156 | D100 428 | 3 | 5 | 8 |

TABLE 6.—*Selected minor-element data, Lake George beryllium area*

[Results in parts per million. Analysts: Claude Huffman, Jr., J. C. Hamilton, L. F. Rader, Harriet Neiman, and Joseph Haffty. N.D., not determined]

| Sample No. (fig. 2) | Field No. | Lab. No. | Sn | Li | Rb | Be |
|---|---|---|---|---|---|---|
| **PIKES PEAK GRANITE (COARSE-GRAINED)** | | | | | | |
| 1 | TR–96 | D114 330 | 13 | 66 | 700 | 5 |
| 2 | M3–156 | D100 428 | N.D. | 100 | 860 | 3 |
| 3 | M3–227 | D114 195 | 9 | 41 | 460 | 7 |
| 4 | M3–232 | D114 196 | 12 | 52 | 400 | 3 |
| 5 | M3–108 | D100 429 | 10 | 71 | 620 | 3 |
| 6 | M4–179 | D114 329 | 11 | 42 | 480 | 7 |
| 7 | T1–98 | D114 192 | 7 | 68 | 480 | 7 |
| **REDSKIN GRANITE** | | | | | | |
| **Granular facies** | | | | | | |
| 8 | M4–15 | D100 431 | 26 | 120 | 1, 100 | 3 |
| 9 | M4–161 | D114 208 | 16 | 88 | 620 | 5 |
| 10 | M4–119 | D114 204 | 19 | 120 | 610 | 7 |
| 11 | M3–258 | D114 197 | 11 | 86 | 540 | 15 |
| 12 | M3–279 | D100 430 | 17 | 96 | 1, 200 | 3 |
| 13 | M3–293 | D114 198 | 14 | 82 | 670 | 5 |
| 14 | BA–944 | H 3 603 | N.D. | 93 | 720 | 5 |
| 15 | T1–107 | D114 203 | 18 | 120 | 560 | 7 |
| 16 | TR–42 | 278 774 | 16 | 45 | 740 | 7 |
| 17 | T1–66 | D114 191 | 10 | 100 | 580 | 7 |
| 18 | BA–589 | 293 643 | 11 | 96 | 660 | 7 |
| 19 | BA–822 | H 3 602 | 12 | 110 | 750 | 5 |
| 20 | BA–637 | 293 644 | 16 | 80 | 620 | 7 |
| 21 | BA–657 | H 3 601 | N.D. | 95 | 650 | 7 |
| 22 | TR–100 | 293 642 | 15 | 61 | 660 | 5 |
| **Porphyritic facies** | | | | | | |
| 23 | M4–20 | D114 199 | 16 | 120 | 820 | 5 |
| 24 | M4–48 | D114 200 | 20 | 140 | 540 | 5 |
| 25 | M4–153 | D100 432 | 17 | 110 | 920 | 7 |
| 26 | M4–92 | D114 202 | 18 | 160 | 1, 500 | 7 |
| 27 | M4–148 | D114 207 | 20 | 110 | 580 | 7 |
| 28 | M4–85 | D114 201 | 23 | 120 | 870 | 7 |
| 29 | BA–1002 | D114 190 | 17 | 94 | 600 | 10 |
| 30 | T1–127 | D114 193 | 19 | 120 | 1, 100 | 5 |
| 31 | T1–23 | 293 645 | 14 | 81 | 650 | 5 |
| 32 | BA–642 | 293 647 | 19 | 110 | 790 | 5 |
| 33 | BA–889 | H 3 607 | 12 | 120 | 720 | 7 |
| 34 | BA–737 | 293 650 | 15 | 95 | 710 | 5 |
| 35 | BA–578 | 293 646 | 18 | 73 | 730 | 5 |
| 36 | BA–670 | 293 648 | 18 | 71 | 680 | 7 |
| 37 | BA–687 | H 3 604 | 18 | 140 | 810 | 10 |
| 38 | BA–682 | 293 649 | 16 | 100 | 760 | 5 |
| 39 | TR–83 | H 3 248 | N.D. | N.D. | N.D. | 15 |
| 40 | BA–719 | H 3 605 | 23 | 130 | 880 | 10 |
| 41 | BA–872 | H 3 606 | 12 | 89 | 670 | [1] 500 |
| 42 | BA–556 | 293 651 | N.D. | N.D. | N.D. | 5 |
| **Fine-grained facies** | | | | | | |
| 43 | M4–139 | D114 205 | 17 | 110 | 640 | 3 |
| 44 | MR–5 | 304 818 | N.D. | N.D. | N.D. | 7 |
| 45 | M4–87 | D100 390 | 15 | 100 | 700 | 15 |
| 46 | M4–145 | D114 206 | 14 | 110 | 620 | 20 |
| 47 | T1–172 | D100 389 | 7 | 16 | 620 | 7 |
| 48 | T1–37 | 293 653 | 14 | 62 | 620 | 5 |
| 49 | T1–19 | 293 652 | 18 | 130 | 780 | 5 |
| **METAMORPHIC ROCKS NEAR THE REDSKIN STOCK** | | | | | | |
| 50 | O2A–4 | G 2 956 | <3 | 70 | 180 | 1.5 |
| 51 | BA–337 | D114 328 | 12 | 32 | 320 | N.D. |
| 52 | BA–107 | D114 331 | <3 | 28 | 140 | <3 |

[1] Not included in average.

TABLE 7.—*Summary of analytical results—tin, lithium, rubidium, and beryllium in the Redskin Granite of the Redskin stock and in nearby rocks*

[Results in parts per million. Analysts: Claude Huffman, Jr., J. C. Hamilton, L. F. Rader, Ardith Bartel, Harriet Neiman, and Joseph Haffty]

| | Sn | | Li | | Rb | | Be | |
|---|---|---|---|---|---|---|---|---|
| | A.M. | G.M. | A.M. | G.M. | A.M. | G.M. | A.M. | G.M. |
| **Redskin Granite of the Redskin stock** | | | | | | | | |
| Granular facies | [1] 16 | [1] 15 | [2] 93 | [2] 90 | [2] 712 | [2] 693 | [2] 6 | [2] 6 |
| Porphyritic facies | [3] 18 | [3] 17 | [4] 110 | [4] 106 | [4] 796 | [4] 763 | [4] 7 | [4] 7 |
| Fine-grained facies | [5] 14 | [5] 14 | [6] 102 | [6] 99 | [6] 663 | [6] 661 | [6] 9 | [6] 7 |
| Average (weighted by area occupied by granular, porphyritic, and fine-grained facies in the Redskin stock) | 16 | 16 | 101 | 98 | 736 | 715 | 7 | 7 |
| **Coarse-grained Pikes Peak Granite of the Pikes Peak batholith** | | | | | | | | |
| Near the Redskin stock | [5] 10 | [5] 10 | [6] 63 | [6] 60 | [6] 571 | [6] 553 | [6] 5 | [6] 4 |
| Batholith and satellitic plutons (W. N. Sharp, unpub. data, 1965) | N.D. | N.D. | N.D. | N.D. | N.D. | N.D. | [7] 5. 6 | N.D. |
| **Metamorphic rocks** | | | | | | | | |
| Granitic gneiss of the Boulder Creek (?) granodiorite | 12 | N.D. | 32 | N.D. | 320 | ---- | N.D. | N.D. |
| Quartz diorite gneiss of the Boulder Creek(?) granodiorite | <3 | N.D. | 28 | N.D. | 140 | ---- | <3 | N.D. |
| Biotite-quartz-plagioclase gneiss of the Idaho-Springs Formation | <3 | N.D. | 70 | N.D. | 180 | ---- | 1. 5 | N.D. |

A.M., arithmetic mean (or single analysis of metamorphic rocks).
G.M., geometric mean.
N.D., not determined.

NOTE: Results are averages for the number of analyses indicated in footnotes.
[1] 13. [2] 15. [3] 18. [4] 19. [5] 6. [6] 7. [7] 72.

listed by Westerveld, and the Australian tin belt (Rattigan, 1960, p. 1278–1279), and Seward Peninsula, Alaska (Sainsbury, 1964). In this report granite bodies with abnormally high amounts of tin are described as "tin granites" although other names might be more appropriate. They are compared with other granites with lesser trace-element content which, in a relative sense, are average or barren granites (table 8).

Onishi and Sandell (1957) proposed that average granite probably contains about 3 ppm of Sn. Further studies tend to confirm their work, thus Hamaguchi and others (1964) found 3.6 ppm of Sn in acidic rocks and Barsukov and Pavlenko (1955) found 3-5 ppm of Sn in Russian granite that does not differ "substantially in age or composition from 'tin-bearing granites'." In contrast, the tin content of the Redskin stock (about 16 ppm) is similar to the Seward Peninsula tin granite and possibly to the Cornwall tin granite (table 8). It is slightly less than that of unaltered Russian tin granite which contains from 16 to 30 ppm of Sn (Barsukov, 1957) and Australian tin granite which averages 21 ppm of Sn (geometric mean) calculated from data of Rattigan (1963). The tin content of the Pikes Peak

TABLE 8.—*Comparison of average trace-element content of the Redskin stock with selected average or composite analyses of granite of similar bulk composition from other localities*

[Results in parts per million. The results are either geometric means of multiple samples or single analyses of composite samples. ND, not determined]

| Type and location of rock analyzed | Type of sample and number of analyses, in parentheses | Sn | Li | Rb | Be |
|---|---|---|---|---|---|
| 1. Redskin stock | Multiple (37–41) [1] | 16 | 98 | 715 | 7 |
| 2. Granite, United States and Canada (average $SiO_2$, 77.0 percent). | Composite (8) | 2. 5 | 14 | 130 | 3 |
| 3. Granitic rocks, California (average $SiO_2$, 74.1 percent). | Composite (9) | 2 | 29 | 190 | 2. 4 |
| 4. Granite, Llano region, Texas (average $SiO_2$, about 73 percent). | Composite (6) | 4 | 39 | 210 | [2] 5. 5 |
| 5. Granite and acid adamellite, Cornwall. | Multiple (5) | [3] <23 | 180 | 180 | 14 |
| 6. Porphyritic biotite granite, Seward Peninsula, Alaska. | Multiple (4) | 17 | 193 | 536 | 14 |
| 7. Granite, rapakivi, eastern Fennoscandia (average $SiO_2$, 72.58 percent). | Composite (54) | N.D. | 23 | 1, 500 | 4 |

1. This paper.
2–4. A suite of composite samples analyzed for Sn by Onishi and Sandell (1957), Li and Rb by Horstmann (1957), and Be by Sandell (1952).
5. Butler (1953).
6. Sainsbury (1964 and written commun.).
7. Sahama (1945).

[1] See table 7 for numbers of samples.
[2] Based on 5 samples.
[3] Two samples contained <15 ppm, and 3 samples contained 20, 25, and 45 ppm Sn.

Granite near the Redskin stock (about 10 ppm) is apparently intermediate between average or barren granites and the lower level of the range of Sn in the tin granites.

The Redskin Granite of the Redskin stock and tin granite from Cornwall and the Seward Peninsula (table 8) are also enriched in Be, Li, and Rb relative to most rocks of similar bulk composition. Most granites contain from 2 to 5 ppm of Be (Sandell, 1952; Beus, 1962), but in many places late granite differentiates contain 7 ppm or more of Be. Besides the examples of table 8 (samples 1, 5, and 6) other Be-enriched granite includes the beryllium granite of Mt. Antero, Colorado (7.7 ppm of Be; W. N. Sharp, unpub. data, 1965), and, possibly, Russian 2-mica and muscovite granite (9 ppm of Be; Beus, 1962).

Data on Li and Rb are somewhat less abundant, but Horstman (1957) estimated from many analyses that average granite contains about 40 ppm of Li and 170 ppm of Rb; Horstman's analyses include the North American composite samples shown on table 8 (samples 2, 3, and 4). New England calc-alkaline granite (Ahrens and others, 1952) contains more Rb (about 510 ppm) than Horstman's average, but slightly less than the Seward Peninsula tin granite and appreciably less than the Redskin Granite. A still higher Rb content in a rock of similar bulk composition was found in Fennoscandian rapakivi granite (Sahama, 1945, table 8, sample 8).

## CONCLUSIONS

Three distinct periods of igneous activity are recognized in the Precambrian terrane of the Lake George area. The oldest igneous rocks, those of the Boulder Creek type, are syntectonic and were emplaced at greath depth under regional metamorphic conditions. Next, granite of the Silver Plume type was emplaced at intermediate depth under less intense metamorphic conditions. Finally, post-tectonic gabbro and monzonite, Pikes Peak Granite, and Redskin Granite, were emplaced epizonally.

When compared with most granites, the Pikes Peak Granite is moderately enriched and the Redskin Granite noticeably enriched in a suite of trace elements shared with greisen ore deposits. This suite which includes Sn, Li, Rb, Be, and F is characteristic of the tin granites of the world. The Redskin Granite has associated berylliferous greisens, and it seems likely that the processes which caused trace-element enrichment in the Pikes Peak magma series ultimately contributed beryllium and other trace elements to the greisen-forming fluids.

## REFERENCES


Ahrens, L. H., Pinson, W. H., and Kearns, M. M., 1952, Association of rubidium and potassium and their abundance in common igneous rocks and meteorites: Geochim. et Cosmochim. Acta, v. 2, p. 229–242.

Ahrens, L. H., and Taylor, S. R., 1961, Spectrochemical analysis, 2nd ed.: Reading, Mass., Addison-Wesley Publishing Co., Inc. 454 p.

Aldrich, L. T., and others, 1958, Radioactive ages of micas from granitic rocks by Rb-Sr and K-A methods: Am. Geophys. Union Trans., v. 39, p. 1124–1134.

Annell, Charles, 1964, A spectrographic method for the determination of cesium, rubidium, and lithium in tektites, *in* Geological Survey Research 1964: U.S. Geol. Survey Prof. Paper 501–B, p. B148–B151.

Antweiler, J. C., 1965, Isotopic evidence of Precambrian episodes of mineralization in Colorado [abs.]: Geol. Soc. America, Rocky Mtn. Sec., 18th Mtg., Ft. Collins, Colo., Program, p. 18–19.

Barsukov, V. L., 1957, The geochemistry of tin: Geochemistry, a translation of Geokhimiya, no. 1, 1957, p. 41–52, pub. by the Geochem. Soc., 1960.

Barsukov, V. L., and Pavlenko, L. I., 1955, Distribution of tin in granitoid rocks: Academy of Sci. of the USSR Proc. (1956), v. 109, nos. 1–6. [English translation.]

Bastron, Harry, Barnett, P. R., and Murata, K. J., 1960, Method for the quantitative spectrochemical analysis of rocks, minerals, ores, and other materials by a powder d-c arc technique: U.S. Geol. Survey Bull. 1084–G, p. 165–182.

Beus, A. A., 1962, Beryllium: San Francisco, W. H. Freeman Co., 161 p.

Buddington, A. F., 1959, Granite emplacement with special reference to North America: Geol. Soc. America Bull., v. 70, p. 671–747.

Butler, J. R., 1953, The geochemistry and mineralogy of rock weathering; 1. The Lizard area, Cornwall: Geochim. et Cosmochim. Acta, v. 4, p. 157–178.

Giffin, C. E., and Kulp, J. L., 1960, Potassium-argon ages in the Precambrian basement of Colorado: Geol. Soc. America Bull., v. 71, p. 219–222.

Graton, L. C., 1906, Description and petrology of the metamorphic and igneous rocks, *in* Lindgren, Waldemar, and Ransome, F. L., Geology and gold deposits of the Cripple Creek district, Colorado: U.S. Geol. Survey Prof. Paper 54, p. 41–113.

Hamaguchi, Hiroshi, and others, 1964, The geochemistry of tin: Geochim. et Cosmochim. Acta, v. 28, p. 1039–1053.

Harrison, J. E., and Wells, J. D., 1959, Geology and ore deposits of the Chicago Creek area, Clear Creek County, Colorado: U.S. Geol. Survey Prof. Paper 319, 92 p.

Hawley, C. C., 1963, Geology of the Pikes Peak Granite and associated ore deposits, Lake George beryllium area, Park County, Colorado: U.S. Geol. Survey open-file report 692, 287 p.

——— 1964, Genetic relation of Pikes Peak Granite and beryllium-bearing greisens, Lake George area, Park County, Colorado [abs.]: Geol. Soc. America Spec. Paper 76, p. 276.

Horstman, E. L., 1957, The distribution of lithium, rubidium, and caesium in igneous and sedimentary rocks: Geochim. et Cosmochim. Acta, v. 12, p. 1–28.

Houston, R. S., Hills, Alan, and Gast, P. W., 1965, Regional aspects of structure and age of rocks of the Medicine Bow Mountains, Wyoming [abs.]: Geol. Soc. America, Rocky Mtn. Sec., 18th Mtg., Ft. Collins, Colo., Program, p. 35–36.

Huffman, Claude, Jr., and Bartel, A. J., 1964, Ion-exchange separation of tin from silicate rocks, *in* U.S. Geological Survey Research 1964: U.S. Geol. Survey Prof. Paper 501–D, p. D131–D133.

Hutchinson, R. M., 1960, Structure and petrology of north end of Pikes Peak batholith, Colorado, *in* Weimer, R. J., and Haun, J. D., Guide to the geology of Colorado: Rocky Mtn. Assoc. Geologists, p. 170–180.

——— 1964, Time span and field-time relations of Pikes Peak batholith and its wall rocks, Colorado [abs.]: Geol. Soc. America Spec. Paper 76, p. 277.

Moench, R. H., Harrison, J. E., and Sims, P. K., 1962, Precambrian folding in the Idaho Springs–Central City area, Front Range, Colorado: Geol. Soc. America Bull., v. 73, p. 35–58.

Myers, A. T., Havens, R. G., and Dunton, P. G., 1961, A spectrochemical method for the semiquantitative analysis of rocks, minerals, and ores: U.S. Geol. Survey Bull. 1084–I, p. 207–229.

Nockolds, S. R., 1954, Average chemical composition of some igneous rocks: Geol. Soc. America Bull., v. 65, p. 1007–1032.

Onishi, Hiroshi, and Sandell, E. B., 1957, Meteoritic and terrestrial abundance of tin: Geochim. et Cosmochim. Acta, v. 12, p. 262–270.

Pearson, R. L., Hedge, C. E., Thomas, H. H., and Stern, T. W., in press, Geochronology of the St. Kevin Granite and neighboring Precambrian rocks, northern Sawatch Range, Colorado: Geol. Soc. America Bull.

Rattigan, J. H., 1960, Residual characteristics of crystallates genetically associated with ore deposits: Econ. Geology, v. 55, p. 1272–1284.

——— 1963, Geochemical ore guides and techniques in exploration for tin: Australian Inst. Mining and Metallurgy, Proc. no. 207, p. 137–151.

Sahama, T. G., 1945, On the chemistry of the East Fennoscandian rapakivi granites: Comm. Geol. Finlande Bull. 136, p. 15–67, 86 p.

Sainsbury, C. L., 1964, Association of beryllium with tin deposits rich in fluorite: Econ. Geology, v. 59, p. 920–926.

Sandell, E. B., 1952, The beryllium content of igneous rocks: Geochim. et Cosmochim. Acta, v. 2, p. 211–216.

Tweto, Ogden, 1965, Regional features of Precambrian rocks in north-central Colorado [abs.]: Geol. Soc. America, Rocky Mtn. Sec., 18th Ann. Mtg., Ft. Collins, Colo., Program, p. 52.

U.S. Geological Survey, 1964, Geological Survey Research 1964: U.S. Geol. Survey Prof. Paper 501–A, 367 p.

Westerveld, J., 1936, The granites of the Malayan tin-belt compared with tin-granites from other regions: K. Akad. v. Wetenschappen, T. Amsterdam Proc., v. 39, p. 1199–1209.

Wetherill, G. W., and Bickford, M. E., 1965, Primary and metamorphic Rb-Sr chronology in central Colorado: Jour. Geophys. Research, v. 70, no. 18, p. 4669–4686.

# A TWO-AMPHIBOLE GLAUCOPHANE SCHIST IN THE FRANCISCAN FORMATION, CAZADERO AREA, SONOMA COUNTY, CALIFORNIA

By DONALD E. LEE,[1] ROBERT G. COLEMAN,[2] HARRY BASTRON,[2] and VERTIE C. SMITH,[1]
[1] Denver, Colo., [2] Menlo Park, Calif.

*Abstract.*—A detailed study of a large glaucophane schist tectonic block has shown that the primary assemblage actinolite-glaucophane-garnet-epidote has been partly replaced by retrograde chlorite and pumpellyite. The whole rock and each of the major mineral phases have been analyzed for major and minor elements. Results of this study are consistent with the hypothesis that the primary metamorphic assemblage represents a high-grade schist that has been dislocated from its bedrock location by upward tectonic movement. The retrograde assemblage may have formed during the period of tectonic dislocation.

Intensive petrologic study of glaucophane schists in the Cazadero area (fig. 1) has shown that metamorphic rocks in this area can be divided into three types: II, III, and IV, in order of increasing metamorphic rank (type-I rocks are unmetamorphosed) (Coleman and Lee, 1963). This division into types was made so that variations in mineralogy and degree of metamorphism could be mapped in the field.

The purpose of this paper is to present, in detail, the mineralogy and petrology of an unusual two-amphibole rock belonging to the high-grade type-IV group. This coarsely crystalline schist occurs as a large rounded exotic block, about 600 feet in diameter, resting on bedrock of type-III schist. It occupies the north bank of Ward Creek in the NE1/4 sec. 17, T. 8 N., R. 11 W., Cazadero quadrangle, Sonoma County, Calif. (see Coleman and Lee, 1963, fig. 1, or Lee and others, 1963b, fig. 1).

In the Cazadero area, schists of type IV are concentrated in a broad layer parallel to serpentinites and major faults. These isolated coarsely crystalline rocks (including eclogites) have been interpreted as tectonically displaced blocks from an unexposed part of a glaucophane schist terrane. The general problem of these blocks, as related to the Franciscan metamorphism, has recently been discussed by Bailey and others (1964). The mineral assemblages and coarse-grained nature of the type-IV schists indicate that they form under higher pressure-temperature conditions than the type-III bedrock schists on which they rest. Potassium-argon age determinations on muscovite and glaucophane from the type-IV and bedrock schists (types II and II) indicate that these minerals probably formed during the same metamorphic period (Lee and others, 1963b), about 130 to 150 million years ago.

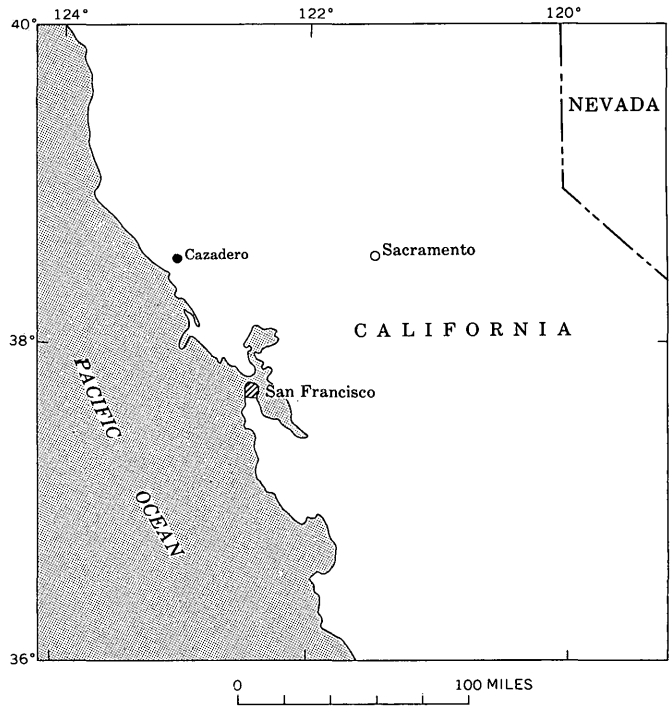


FIGURE 1.—Index map showing the location of the Cazadero area, California.

## ROCK DESCRIPTION

The material used for this investigation was collected from the center of the tectonic block. The block as a whole shows irregular compositional layering cut by veins with retrograde minerals, and it was not possible to obtain a sample representative of the whole mass. A nearly continuous cover of moss and other vegetation obscures the internal structure of this block; there is, however, evidence in the hand specimen of at least two periods of deformation.

In hand specimen, the rock is greenish-blue with the platy or micaceous minerals locally concentrated into layers. Reddish garnet (up to 1.5 mm in diameter) is visible and occurs randomly, except in a few layers that are garnet rich. Shears and fractures cutting the rock are filled with pumpellyite and chlorite.

### Primary metamorphic-mineral assemblages

In thin section, porphyroblastic garnet occurs in a nematoblastic groundmass of actinolite, glaucophane, and muscovite. Epidote forms irregular anhedral grains intimately associated with the other minerals. Small subhedral grains of sphene (<0.1 mm in length) are ubiquitous. A few irregularly shaped grains of sphene, up to 1.0 mm in length, contain rutile cores. Apatite porphyroblasts up to 1.0 mm in length are scattered throughout the groundmass.

Actinolite and glaucophane are present as distinct individual grains, but more often a single amphibole grain may consist of both actinolite and glaucophane. Such relations suggest replacement of one by the other but, as shown in the accompanying drawings, there is no clear evidence that one is earlier than the other (fig. 2). Because the rock does have strong local compositional variations, it is likely that the distribution of the two amphiboles could be controlled by local variations of bulk composition.

Modal analyses of four thin sections taken from the same rock used for chemical analysis and cut at different angles to the schistosity are listed in table 1. The following assemblages are representative of the various compositional layers from different parts of the block:

1. Garnet, muscovite, glaucophane, actinolite.
2. Actinolite, glaucophane, epidote.
3. Actinolite, glaucophane, muscovite, epidote.
4. Actinolite, glaucophane, garnet, epidote, muscovite.

### Retrograde-mineral assemblages

The distribution of chlorite and pumpellyite is variable, and they are found concentrated within shears and fractures. Commonly these two minerals invade beyond the vein walls and replace the wallrock minerals. Other retrograde areas, unrelated to late fractures and veins, are replaced by pumpellyite and chlorite. Garnet near the fractures is replaced by chlorite whereas, in other parts of the rock, pumpellyite and minor stilpnomelane may replace garnet. Chlorite selectively replaces actinolite, leaving the intergrown glaucophane unaltered (fig. 2). The epidote, in areas of retrograde alteration near veins, is pseudomorphosed by pumpellyite. Thus garnet, actinolite,

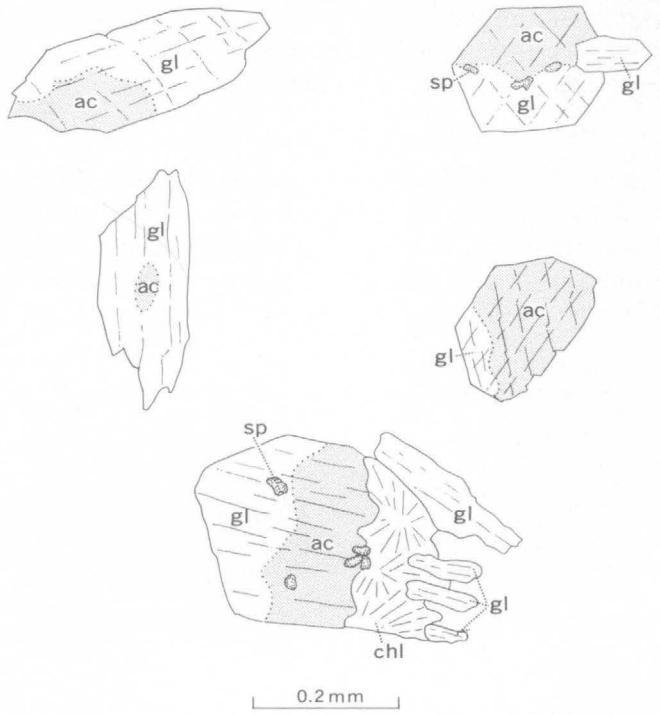


FIGURE 2.—Sketches of glaucophane (gl) -actinolite (ac) crystals, illustrating their mutual relations within a single grain. The lower larger grain shows preferential replacement of actinolite by chlorite (chl). Small amounts of sphene (sp) are also present in two of the crystals.

TABLE 1.—*Norm and mode of type IV schist*

[USGS lab. No. H-3393, field No. 50-CZ-60]

| Norm (molecular percent) [1] | | Mode (volume percent) [2] | | | | |
|---|---|---|---|---|---|---|
| | | 1 | 2 | 3 | 4 | Average |
| Q 0.06 | Glaucophane | 20.0 | 17.3 | 10.8 | 19.0 | 16.7 |
| Ab 8.20 | Actinolite | 19.6 | 25.2 | 18.9 | 18.5 | 20.7 |
| An 42.12 | Epidote | 17.7 | 28.6 | 15.3 | 18.0 | 19.9 |
| Or 1.65 | Muscovite | 17.1 | 9.1 | 22.0 | 17.0 | 16.3 |
| Wo 15.08 | Garnet | 10.7 | 6.8 | 15.4 | 12.2 | 11.2 |
| En 12.81 | Chlorite | 7.8 | 5.6 | 8.8 | 7.5 | 7.4 |
| Fs 3.67 | Sphene | 6.1 | 7.2 | 8.1 | 6.9 | 7.1 |
| Ap .54 | Apatite | .9 | .2 | .5 | .2 | .5 |
| Il 4.12 | Rutile | .1 | | | .3 | .1 |
| Mt 9.71 | Pumpellyite | | | .2 | .4 | .1 |
| Fr .02 | | 100.00 | 100.00 | 100.00 | 100.00 | 100.00 |
| Cc .05 | | | | | | |
| 98.03 | | | | | | |

[1] CIPW norm calculated after normalizing to 100 percent.
[2] Each column represents 1,000 points counted.

and epidote tend to be unstable in the presence of chlorite and pumpellyite, while glaucophane and muscovite remain stable or metastable.

### Significance of assemblages

Recalling the earlier mention of sphene replacing rutile, along with those replacement relations just discussed, primary metamorphic and retrograde mineral assemblages must be present and are summarized as follows:

| *Stable primary assemblage* | | *Stable retrograde assemblage* | |
|---|---|---|---|
| Actinolite, Epidote, Garnet, Rutile | replaced by → | Pumpellyite, Chlorite | deposited in veins |
| | | Sphene | |
| Glaucophane, Muscovite, Sphene, Apatite | remain stable or metastable → | Glaucophane, Muscovite, Sphene, Apatite | |

These observed primary metamorphic and retrograde assemblages indicate that this particular tectonic block has undergone a change following its original metamorphism. We have earlier postulated that the type-IV rocks have been transported tectonically upward along major fault zones (Coleman and Lee, 1963) and therefore the retrogression observed in this case may relate, in part, to this period of tectonic movement.

## GENERAL DISTRIBUTION OF ELEMENTS

In the discussion on systematic mineralogy to follow, calculation of ionic ratios is based on oxide weights that combine the results of chemical and spectrographic analyses. The major elements in the rock and in each of the constituent minerals are presented in table 2 and the minor elements in table 3.

Certain of the metamorphic-mineral structures may be more receptive to a given minor element than for other minor elements of nearly equal ionic radii under the pressure-temperature conditions of original metamorphism when contrasted with conditions of retrogression. $Pb^{+2}$ (ionic radius 1.20A) is concentrated in the calcium-rich minerals (ionic radius of $Ca^{+2}$ is 0.99A) epidote and sphene, but was not detected in pumpellyite (retrograde), garnet, apatite, or actinolite. Also $Sr^{+2}$ (ionic radius 1.12A) is present in much larger amounts in epidote and apatite than in other calcium minerals. Regarding pumpellyite, a calcium-rich mineral, the comparisons drawn are qualified by the fact that it is retrograde and formed under different pressure–temperature conditions characterizing the primary metamorphic assemblage. Zircon is not present in this rock; except for its greater concentration in rutile and sphene, zirconium is fairly evenly distributed among the various minerals.

The bulk composition of the rock is considered basaltic (Coleman and Lee, 1963, p. 288); however, the rock does have some characteristics that set it apart from the typical basalts in the Franciscan Formation (table 2). The $Na_2O$ content (0.97 percent $Na_2O$) is considerably below the average (3.5 percent $Na_2O$) found in the Franciscan metabasalts (unpublished USGS analyses) and the alumina content (17.36 percent $Al_2O_3$) is considerably above the average (14.2 percent $Al_2O_3$). This, combined with a low silica content (42.16 percent $SiO_2$), gives a very peculiar norm (table 1) that shows minor quartz with abundant hypersthene and wollastonite. Such a composition suggests that some metasomatism prevailed during metamorphism, and that these factors are largely responsible for the formation of a two-amphibole rock.

The distribution of minor elements is probably controlled by the ionic radii of the major elements. $Ga^{+3}$(0.62A) is confined to the aluminum-rich minerals ($A^{+3}$, 0.51A), $Cr^{+3}$(0.63A) follows $Fe^{+3}$(0.64A), $Ba^{+2}$(1.34A) substitutes for $K^{+1}$(1.33A) in muscovite, and $Cu^{+2}$(0.72A) takes the place of $Mg^{+2}$(0.66A) in chlorite and $Ti^{+3}$(0.76A) in sphene and rutile.

## MINERALOGY

### Method of study

A 5-kilogram sample (USGS lab. No. H–3393, field No. 50–CZ–60) was obtained from the block and approximately 2 kilograms was crushed for chemical analysis and recovery of individual minerals. The final purification of the minerals was accomplished with minus-200 mesh material, using an isodynamic separator and centrifuging in heavy liquids. Specific-gravity determinations were made by measuring the liquid used for centrifuging; for the range below 3.32, specific gravity of the bromoform-methylene iodide mixtures was determined by using a specific-gravity balance. For those gravities above 3.32, clerici solution was used and specific gravities were determined by index of refraction measurements on the liquid. Optical constants were determined using sodium light and angular values measured on a 4-axis universal stage. Unit-cell determinations were made using X-ray powder spacings and the least-squares method. The chemical analyses of the rock and minerals were performed

TABLE 2.—*Major elements in type-IV schist*

[N.D., not determined. USGS lab. No. H-3393, field No. 50-CZ-60.]

| | Whole rock [1] | Amphibole [1] | | Apatite [2] | Chlorite [1] | Epidote [1] | Garnet [2] | Muscovite [1] | Pumpellyite [1] | Sphene [2] |
|---|---|---|---|---|---|---|---|---|---|---|
| | | Actinolite | Glaucophane | | | | | | | |
| $SiO_2$ | 42.16 | 54.04 | 55.04 | N.D. | 27.54 | 38.11 | 37.6 | 50.24 | 37.48 | 31.0 |
| $Al_2O_3$ | 17.36 | 2.85 | 9.06 | N.D. | 19.03 | 25.75 | 20.3 | 25.85 | 25.43 | N.D. |
| $Fe_2O_3$ | 6.71 | 2.10 | 2.83 | N.D. | 1.22 | 9.66 | 1.4 | .27 | 1.29 | [3].48 |
| FeO | 6.64 | 11.79 | 11.62 | N.D. | 24.36 | .64 | [4] 25.3 | 3.07 | 3.16 | N.D. |
| MgO | 5.15 | 14.62 | 9.64 | N.D. | 15.93 | .14 | 2.1 | 3.69 | 2.94 | N.D. |
| CaO | 16.14 | 10.36 | 3.58 | 55.5 | .08 | 23.41 | 11.1 | .00 | 22.14 | 26.9 |
| MnO | .33 | N.D. | N.D. | N.D. | N.D. | .10 | 1.6 | N.D. | [5].83 | N.D. |
| $TiO_2$ | 2.17 | .11 | .22 | .08 | .09 | .50 | .25 | .27 | .20 | 39.2 |
| $Na_2O$ | .97 | 1.52 | 5.50 | N.D. | [5].14 | .00 | N.D. | .45 | [5].32 | [5].06 |
| $K_2O$ | .28 | .09 | .05 | N.D. | [5].08 | .00 | N.D. | 10.39 | [5].02 | [5].01 |
| $P_2O_5$ | .23 | N.D. | N.D. | 41.5 | N.D. | N.D. | N.D. | N.D. | N.D. | .05 |
| $CO_2$ | .02 | N.D. | N.D. | N.D. | N.D. | N.D. | N.D. | N.D. | N.D. | N.D. |
| $SO_3$ | .00 | N.D. | N.D. | N.D. | N.D. | N.D. | N.D. | N.D. | N.D. | N.D. |
| $H_2O+$ | 1.94 | 2.02 | 1.99 | N.D. | 11.20 | 1.78 | N.D. | 4.44 | 6.36 | N.D. |
| $H_2O-$ | .04 | .04 | .00 | N.D. | .06 | .00 | N.D. | .02 | .02 | N.D. |
| Cl | .00 | N.D. | N.D. | N.D. | N.D. | N.D. | N.D. | N.D. | N.D. | N.D. |
| F | .02 | N.D. | .01 | 1.8 | N.D. | .00 | N.D. | .00 | .04 | N.D. |
| Subtotal | 100.16 | | 99.54 | | | 100.09 | | [6] 98.69 | 100.23 | |
| Less O | .01 | | .00 | | | .00 | | .00 | .02 | |
| Total | 100.15 | 99.54 | 99.54 | 98.9 | 99.73 | 100.09 | 99.7 | 98.69 | 100.21 | 97.7 |
| Powder density | 3.39 | N.D. | N.D. | N.D. | N.D. | N.D. | N.D. | N.D. | N.D. | N.D. |
| Weight of sample submitted for analysis (grams) | 100.0 | 2.3 | 4.9 | 1.6 | 1.8 | 5.0 | 6.5 | 2.5 | 4.0 | 5.0 |

[1] Vertie C. Smith, analyst.
[2] Paul Elmore, Ivan Barlow, Samuel Botts, and Gillison Chloe, analysts. Samples were analyzed by methods similar to those described by Shapiro and Brannock (1956).
[3] Total iron determined as $Fe_2O_3$.
[4] FeO determination by Robert Meyrowitz.
[5] MnO (spectrophotometric) and $Na_2O$ and $K_2O$ (flame photometric) determinations by A. C. Bettiga and W. W. Brannock.
[6] Analyst notes: "A preliminary spectrographic analysis indicates that the barium content of this sample is high."

TABLE 3.—*Minor elements in type-IV schist* [1]

[Quantitative spectrographic analyses by Harry Bastron. N.D., not determined. USGS lab. No. H-3393, field No. 50-CZ-60]

| | Whole rock | Amphibole | | Apatite | Chlorite | Epidote | Garnet | Muscovite | Pumpellyite | Sphene | Rutile |
|---|---|---|---|---|---|---|---|---|---|---|---|
| | | Actinolite | Glaucophane | | | | | | | | |
| Cu | 0.0052 | 0.0072 | 0.0036 | 0.0029 | 0.034 | 0.0030 | 0.0007 | 0.0054 | 0.0024 | 0.021 | 0.036 |
| Pb | <.002 | <.002 | <.002 | <.002 | <.002 | .013 | <.002 | <.002 | <.002 | .005 | <.002 |
| Zn | <.04 | <.04 | <.04 | <.04 | .07 | <.04 | <.04 | <.04 | <.04 | <.04 | <.04 |
| Mn | N.D. | .16 | .090 | .022 | N.D. | N.D. | N.D. | .0077 | N.D. | .015 | .025 |
| Co | .0039 | .0063 | .0064 | <.0004 | .011 | <.0004 | 0.021 | .0013 | .0022 | <.0004 | <.0004 |
| Ni | .0096 | .016 | .014 | <.0004 | .027 | <.0004 | <.0004 | .0036 | .0071 | <.0004 | <.0004 |
| Fe | N.D. | N.D. | N.D. | .067 | N.D. | N.D. | N.D. | N.D. | N.D. | .030 | .26 |
| Cr | .054 | .018 | .020 | <.0002 | .026 | .060 | .023 | .025 | .032 | .017 | .091 |
| V | .062 | .040 | .056 | <.001 | .022 | .11 | .018 | .062 | .11 | .092 | .16 |
| Ga | .0027 | .0004 | .0005 | <.0004 | .0020 | .0045 | .0005 | .0020 | .0019 | <.0004 | <.0004 |
| Sc | .0056 | .0067 | .0059 | <.0004 | <.0004 | .0085 | .0072 | <.0004 | <.0004 | <.0004 | <.0004 |
| Y | .008 | <.002 | <.002 | .006 | <.002 | .014 | .009 | <.002 | .009 | .029 | .025 |
| Yb | .0007 | <.0002 | <.0002 | .0004 | .0002 | .0008 | .0020 | <.0002 | .0014 | .0016 | <.0002 |
| Zr | .015 | .0083 | .011 | .0072 | .0070 | .014 | .0079 | .0072 | .0076 | .070 | .11 |
| Be | <.0002 | <.0002 | <.0002 | <.0002 | <.0002 | <.0002 | <.0002 | .0002 | <.0002 | <.0002 | <.0002 |
| Mg | N.D. | N.D. | N.D. | .015 | N.D. | .060 | N.D. | N.D. | N.D. | .040 | .0028 |
| Sr | .20 | .0021 | .0042 | .13 | .0002 | .26 | <.0004 | .0024 | .0008 | .0080 | .0076 |
| Ba | .029 | .0054 | .0018 | .0019 | .0075 | .0029 | <.0004 | 1.3 | .0021 | .0008 | .48 |
| B | <.002 | <.002 | <.002 | <.002 | <.002 | <.002 | <.002 | .006 | <.002 | <.002 | <.002 |

Looked for but not found: Ag, Au, Hg, Ru, Rh, Pd, Ir, Pt, Re, Ge, Sn, As, Sb, Bi, Cd, In, La, Ce, Nd, Hf, Th, Nb, Ta, U, Li.
Phosphorus present only in apatite.
[1] Overall accuracy of ±15 percent except near limits of detection, where only one digit is reported

by standard gravimetric methods and emission spectrography.

Each of the analyzed minerals represents an average composition within a narrow gravity range controlled during separation. All of the physical properties given represent the average values for these mineral separates. None of these fractions were checked by electron microprobe for homogeneity, but for the purposes of this discussion all analyzed phases are considered to be homogenous and unzoned. The aggregate color of each anaylzed fraction (−200 mesh) is given for plain incident light (table 4).

TABLE 4.—*Color of minerals in −200 mesh fractions*

[USGS lab. No. H-3393, field No. 50-CZ-60]

| | Color | |
|---|---|---|
| | Reflected light | Munsell designation [1] |
| Amphibole: | | |
| Actinolite | Grayish green | 5*G* 5/2 |
| Glaucophane | Dusky blue | 5*PB* 3/2 |
| Apatite | Yellowish gray | 5*Y* 8/1 |
| Chlorite | Dusky yellowish green | 5*GY* 5/2 |
| Epidote | Grayish yellow | 5*Y* 8/4 |
| Garnet | Light brown | 5*YR* 6/4 |
| Muscovite | Light greenish gray | 5*GY* 8/1 |
| Pumpellyite | Grayish green | 5*GY* 5/2 |
| Sphene | Pale greenish yellow | 10*Y* 8/2 |
| Rutile | Moderate red | 5*R* 4/6 |

[1] Munsell (1929).

## Primary metamorphic minerals

### Essential minerals

*Amphiboles.*—Coexisting actinolite and glaucophane are unusual in the glaucophane schists, and their respective compositions are important to the petrology of this rock. These two amphiboles have a specific-gravity range of from less than 3.13 to more than 3.19. In order to investigate the corresponding compositional range, two fractions were prepared for analysis by careful and repeated centrifuging. The entire heavier fraction (glaucophane) analyzed was in suspension along the length of the tube after centrifuging in a liquid with a specific gravity of 3.184. Since the liquid was checked before and after this operation, 3.184 not only is the bulk specific gravity of this mineral fraction, but applies also to each of the individual mineral grains. The lighter fraction (actinolite) analyzed was centrifuged at 3.131 and 3.143 during final purification; these figures represent the specific gravity limits of the actinolite.

The chemical analysis and physical properties (tables 5, 6) illustrate the distinct nature of the coexisting amphiboles. Even though the glaucophane contains 26 molecular percent of the actinolite molecule, the X-ray and optical examinations show it to consist of only 1 phase. On the basis of this work, we conclude that the 2 coexisting amphiboles do not grade one into the other or replace one another, but represent 2 distinct amphibole compositions in stable coexistence.

*Epidote.*—In the type-IV rocks, epidote takes the place of lawsonite and pumpellyite. In general, the ferric iron content of the epidote is higher with increasing grade of metamorphism, both in the greenschist and glaucophane schist facies (Deer and others, 1962, p. 207). The epidote in sample 50–CZ–60 has approximately 19 mol percent $Ca_2{}^{+3}Fe^{+3}Si_3O_{12}(OH)$, somewhat less than the average of 25 mol percent characteristic of the epidotes from type-IV schists (table 7). Epidotes from the blueschist facies from the Sanbagawa belt Shikoku, Japan, also average approximately 25 mol percent of iron component (Banno, 1964, and Iwasaki, 1963). No perceptible zoning could be seen in thin section, but the concentrate used for analysis contained numerous minute inclusions of sphene. The 0.50 percent $TiO_2$ reported in the analysis represents approximately 1 percent sphene impurity. The unit-cell data were obtained from G. H. Myer, Yale University, (written commun., 1963) and the same epidote (GM-14) is plotted on the X-ray determinative curve constructed by Myer (1965, fig. 2, p. 85) to determine the ferric iron content of epidotes.

*Mica.*—The primary metamorphic mica from this assemblage is similar in composition to those phengitic micas described by Ernst (1963b) from other glaucophane schist terranes (table 8). The composition of the phengites from glaucophane schists is intermediate between muscovite and MgAl celadonite. The range in composition of these phengites can best be expressed by the amount of aluminum in six-fold coordination

$$\frac{(Al^{IV} \times 100)}{(Al^{IV}+Fe^{+3}+Fe^{+2}+Mg)}$$

and it has been pointed out by Velde (1964, P–143) that the substitution of $Al^{IV}$ is a function of pressure. Analyzed phengites from glaucophane schists reveal that the amount of $Al^{IV}$ ranges from 59 to 75 percent; sample 50–CZ–60 has 72 percent. Further work is needed before this parameter can be correlated with the grade of metamorphism.

Another feature of the phengitic micas from glaucophane schists is the strong concentration of barium. Ernst (1963b, p. 1300, table 1) has reported 2 phengites containing 1.89 and 1.64 percent BaO similar to the value of 1.45 percent for this material; such high barium contents have not been reported from muscovites from other metamorphic facies.

TABLE 5.—*Chemical analyses and physical properties of amphiboles in type-IV schist* [1]

[Weight percent of oxides based on tables 2 and 3. USGS lab. No. H-3393, field No. 50-CZ-60]

| Actinolite | | | | Glaucophane | | | |
|---|---|---|---|---|---|---|---|
| **CHEMICAL ANALYSES** | | | | | | | |
| Chemical composition (weight percent) | | Number of ions on the basis of 24(O,OH,F) | | Chemical composition (weight percent) | | Number of ions on the basis of 24(O,OH,F) | |
| $SiO_2$ | 54.04 | Si 7.787 | 8.00 | $SiO_2$ | 55.04 | Si 7.796 | 8.00 |
| | | Al 0.473 (.213 + .260) | | | | Al 1.498 (.204 + 1.294) | |
| $Al_2O_3$ | [2] 2.79 | | | $Al_2O_3$ | [2] 8.98 | | |
| $TiO_2$ | .11 | Ti .012 | 0.51 | $TiO_2$ | .22 | Ti .024 | 1.63 |
| $V_2O_3$ | [3] .06 | V .007 | 5.06 | $V_2O_3$ | [3] .08 | V .009 | 5.04 |
| $Fe_2O_3$ | 2.10 | $Fe^{+3}$ .228 | | $Fe_2O_3$ | 2.83 | $Fe^{+3}$ .301 | |
| FeO | 11.79 | $Fe^{+2}$ 1.420 | | FeO | 11.62 | $Fe^{+2}$ 1.375 | |
| MgO | [4] 14.46 | Mg 3.105 | 4.55 | MgO | [4] 9.55 | Mg 2.017 | 3.41 |
| MnO | [3] .21 | Mn .026 | | MnO | [3] .12 | Mn .013 | |
| CaO | 10.36 | Ca 1.598 | | CaO | 3.58 | Ca .545 | |
| $Na_2O$ | 1.52 | Na .424 | 2.04 | $Na_2O$ | 5.50 | Na 1.506 | 2.06 |
| $K_2O$ | .09 | K .017 | | $K_2O$ | .05 | K .008 | |
| $H_2O+$ | 2.02 | OH 1.940 | 1.94 | F | .01 | F .004 | 1.88 |
| $H_2O-$ | .04 | | | $H_2O+$ | 1.99 | OH 1.880 | |
| | | | | $H_2O-$ | .00 | | |
| Total | 99.59 | | | Total | 99.57 | | |
| **PHYSICAL PROPERTIES** | | | | | | | |
| Specific gravity [5] | | 3.137 ± 0.006 | | Specific gravity [5] | | 3.184 ± 0.003 | |
| Calculated density [6] | | 3.131 g/cm³ | | Calculated density [6] | | 3.218 g/cm³ | |
| **Optical properties** | | | | | | | |
| $\alpha$ | | 1.623 ± 0.003 | | $\alpha$ | | 1.625 ± 0.003 | |
| $\beta$ | | 1.640 | | $\beta$ | | 1.645 | |
| $\gamma$ | | 1.646 | | $\gamma$ | | 1.650 | |
| $\gamma-\alpha$ | | 0.023 | | $\gamma-\alpha$ | | 0.025 | |
| $2V$ | | 66° ± 4° (−) | | $2V$ | | 39° ± 5° (−) | |
| $X$ | | Colorless. | | $X$ | | Colorless. | |
| $Y$ | | Pale green. | | $Y$ | | Violet. | |
| $Z$ | | Green. | | $Z$ | | Pale blue. | |
| $Z \wedge C$ | | 13° | | $Z \wedge C$ | | 3°–5° | |

[1] See table 6 for cell dimensions.
[2] Corrected from table 2 for $V_2O_3$, assuming the 2 metals were weighed together as oxides.
[3] Calculated from table 3.
[4] Corrected from table 2 for MnO, assuming the 2 metals were weighed together as pyrophosphates.
[5] See text for explanation.
[6] Based upon cell volumes listed in table 6.

*Garnet.*—The garnet from this rock has been described in a previously published report on garnets from the Cazadero area (Lee and others, 1963a). The garnet has a composition (almandine 56.3, grossular 26.7, pyrope 8.3, andradite 5.0, and spessartine 3.7) that is quite similar to that of garnet in other coarse-grained type-IV rocks, including the garnets from the associated eclogites (Coleman and others, 1965). These garnets are characterized by a fairly low pyrope content (<15 percent) and a large amount of ugrandite moles mixed with pyralspites, a distinguishing feature of the garnets characterizing type-IV glaucophane schists.

## Accessory minerals

Enough material was concentrated during the mineral separation to obtain chemical information on most of the accessory minerals.

*Rutile.*—Rutile is ubiquitous in type-IV rocks (Coleman and Lee, 1963) and in this rock 60 mg was recovered. Spectrographic analysis (table 3) shows that the rutile contains noteworthy amounts of V, Zr, Cr, and Ba. The barium (0.48 percent) is puzzling as it is difficult to place a large cation such as this in the rutile structure. Barite is often present in these schists and may well have been present as a minor contaminant

TABLE 6.—*2θ measurements and cell dimensions of amphiboles in type-IV schist* [1]

[Determinations by W. G. Ernst, Univ. of California at Los Angeles. USGS lab. No. H-3393, field No. 50-CZ-60]

| | Actinolite | Glaucophane |
|---|---|---|
| **2θ (degrees)** | | |
| (*hkl*) | | |
| 040 | 24.748 | 25.123 |
| 131 | 33.202 | 33.278 |
| 240 | 34.314 | 35.073 |
| 201 | | 36.238 |
| 310 | 36.060 | 36.970 |
| 151 | 41.838 | 42.146 |
| 202 | 44.837 | |
| **Unit-cell data** | | |
| *a* | 9.86A | 9.55A |
| *b* | 18.10A | 17.81A |
| *c* | 5.29A | 5.27A |
| *β* | 104.7° | 103.0° |
| Cell volume | 913.A[3] | 873.4A[3] |

[1] $FeK_\alpha$ radiation, indexed on space group *C2/m*. See table 5 for chemical analyses of these amphiboles.

TABLE 7.—*Chemical analysis and physical properties of epidote in type-IV schist*

[Weight percent of oxides based on tables 2 and 3. USGS lab. No. H-3393, field No. 50-CZ-60]

| CHEMICAL PROPERTIES | | | | PHYSICAL PROPERTIES | |
|---|---|---|---|---|---|
| Chemical composition (weight percent) | | Number of ions on the basis of 13(O,OH) | | Specific gravity | 3.404±0.01 |
| | | | | **Optical properties** | |
| $SiO_2$ | [1] 38.02 | Si | 3.019 3.02 | | |
| $Al_2O_3$ | [2] 25.50 | Al | 2.385 | *α* | 1.725±0.003 |
| $Fe_2O_3$ | 9.66 | $Fe^{+3}$ | .572 2.97 | *β* | 1.738 |
| $Cr_2O_3$ | [3] .088 | Cr | .006 | *γ* | 1.747 |
| $V_2O_3$ | [3] .16 | V | .009 | *γ*−*α* | 0.022 |
| FeO | [1] .64 | $Fe^{+2}$ | .043 | 2*V* | 72(−) |
| CaO | [4] 22.93 | Ca | 1.950 | *X*=*Y*=*Z* | Colorless. |
| MgO | .14 | Mg | .014 2.03 | Dispersion | *r*>*v*, slight. |
| SrO | [3] .31 | Sr | .014 | **Unit-cell data** | |
| MnO | .10 | Mn | .005 | | |
| $Na_2O$ | .00 | | | *a* | 8.886±0.002A |
| $K_2O$ | .00 | | | *b* | 5.620±0.001A |
| $H_2O^+$ | 1.78 | OH | .944 .94 | *c* | 10.159±0.003A |
| $H_2O^-$ | .00 | | | *β* | 115°26.5′±1.5′ |
| F | .00 | | | Cell volume [5] | 458.15±0.35A[3] |
| Total | 99.33 | | | | |

[1] Corrected for sphene impurity, 0.5 weight percent $TiO_2$.

[2] Corrected from table 2 for $Cr_2O_3$ and $V_2O_3$, assuming the 3 metals were weighed together as oxides.

[3] Calculated from table 3.

[4] Corrected from table 2 for SrO, assuming the 2 metals were weighed together as oxides.

[5] Determined by G. H. Myer, Yale University.

even though optical examination did not reveal its presence in the concentrate.

*Sphene.*—Sphene is the most abundant accessory mineral and commonly replaces the rutile. It is well known that sphene may contain appreciable amounts

TABLE 8.—*Chemical analysis and physical properties of muscovite in type-IV schist*

[Weight percent of oxides based on tables 2 and 3. USGS lab. No. H-3393, field No. 50-CZ-60]

| CHEMICAL PROPERTIES | | | | PHYSICAL PROPERTIES | |
|---|---|---|---|---|---|
| Chemical composition (weight percent) | | Number of ions on the basis of 12(O, OH, F) | | Specific gravity | 2.885±0.003 |
| | | | | **Optical properties** | |
| $SiO_2$ | 50.24 | Si | 3.398 | *β* | 1.600±0.003 |
| $B_2O_3$ | [1] .019 | B | .002 4.00 | 2*V* | 35°(−) |
| | | | .600 | *X*=*Y*=*Z* | Colorless. |
| $Al_2O_3$ | [2] 25.72 | Al | 2.051 | | |
| | | | 1.451 | | |
| $Fe_2O_3$ | .27 | $Fe^{+3}$ | .014 | | |
| $TiO_2$ | .27 | Ti | .014 | | |
| $V_2O_3$ | [1] .091 | V | .005 2.03 | | |
| $Cr_2O_3$ | [1] .036 | Cr | .002 | | |
| FeO | 3.07 | $Fe^{+2}$ | .173 | | |
| MgO | 3.69 | Mg | .372 | | |
| CaO | .00 | | | | |
| BaO | [1] 1.45 | Ba | .039 | | |
| $Na_2O$ | .45 | Na | .059 1.00 | | |
| $K_2O$ | 10.39 | K | .898 | | |
| F | .00 | | | | |
| $H_2O^+$ | 4.44 | OH | 2.004 2.00 | | |
| $H_2O^-$ | .02 | | | | |
| Total | 100.16 | | | | |

[1] Calculated from table 3.

[2] Corrected from table 2 for $Cr_2O_3$ and $V_2O_3$, assuming the 3 metals were weighed together as oxides.

of many elements besides those appearing in the idealized formula $CaTiSiO_5$ (see, for example, Deer and others, 1962, p. 70–73) and this sphene is not unusual in that respect (tables 3, 9).

*Apatite.*—The apatite analysis is not complete, as determinations were not made for chlorine or water; therefore, it is difficult to state exactly the end-member components that are represented (table 10). The bulk specific gravity 3.18, and optical properties combined with the chemical analysis suggest that it its a mixture of fluorapatite and chlorapatite.

*Pyrite.*—A few scattered grains of very fresh-looking pyrite were present in the mineral separation; however, there was not enough for analytical work.

## Retrograde minerals

*Chlorite.*—Chlorite of the type-IV schist is similar in composition (table 11) to those reported from basic schists in the Sanbagawa metamorphic belt of central Sikoku, Japan (Banno, 1964). According to Banno, the $Fe^{+2}/Fe^{+2}+Mg$) ratio varies from 0.29 to 0.47, and the Cazadero chlorite has a ratio of 0.47. Chlorites have not been found as a primary and (or) stable mineral in the type-IV schists; therefore, this chlorite must form under conditions distinct from those giving rise to the primary metamorphic assemblage. The chlorite

TABLE 9.—*Chemical analysis and physical properties of sphene in type-IV schist*

[Weight percent of oxides based on tables 2 and 3. USGS lab. No. H-3393, field No. 50-CZ-60]

| CHEMICAL PROPERTIES | | | | | PHYSICAL PROPERTIES | |
|---|---|---|---|---|---|---|
| Composition (weight percent) | | Number of ions on the basis of 20 (O) | | | Specific gravity--3.50±0.01 | |
| | | | | | Optical properties | |
| $SiO_2$ | 31.0 | Si | 4.11 | 4.12 | α | 1.91±0.005 |
| $P_2O_5$ | .05 | P | .006 | | 2V | 25°±2°(+) |
| $TiO_2$ | 39.2 | Ti | 3.91 | | X=Y=Z | Colorless. |
| $Fe_2O_3$ | [1] .48 | $Fe^{+3}$ | .048 | | | |
| MgO | [2] .066 | Mg | .012 | 3.99 | | |
| CuO | [2] .026 | Cu | .003 | | | |
| $V_2O_3$ | [2] .135 | V | .014 | | | |
| $ZrO_2$ | [2] .082 | Zr | .005 | | | |
| $Y_2O_3$ | [2] .037 | Y | .003 | | | |
| MnO | [2] .019 | Mn | .002 | | | |
| CaO | 26.9 | Ca | 3.82 | 3.84 | | |
| $Na_2O$ | .06 | Na | .016 | | | |
| $K_2O$ | .01 | K | .002 | | | |
| Total | 98.1 | | | | | |

[1] Assuming all iron is present as $Fe^{+3}$.
[2] Calculated from table 3.

TABLE 10.—*Chemical analysis and physical properties of apatite in type-IV schist*

[Weight percent of oxides based on tables 1 and 2. USGS lab. No. H-3393, field No. 50-CZ-60]

| CHEMICAL PROPERTIES | | | | | PHYSICAL PROPERTIES | |
|---|---|---|---|---|---|---|
| Chemical composition (weight percent) | | Number of ions on the basis of 26(O, OH, F) | | | Specific gravity--3.19±0.01 | |
| | | | | | Optical dimensions | |
| CaO | [1] 54.8 | Ca | 10.19 | | Uniaxial | (−) |
| SrO | [2] .15 | Sr | .018 | | ε | 1.639±0.003 |
| MnO | [2] .028 | Mn | .004 | 10.25 | ω | 1.643 |
| FeO | [2] .086 | $Fe^{+3}$ | .013 | | ε−ω | .004 |
| MgO | [2] .025 | My | .006 | | | |
| $TiO_2$ | .08 | Ti | .021 | | | |
| $P_2O_5$ | 41.5 | P | 6.10 | | | |
| F | 1.8 | F | .99 | | | |
| Total | 98.5 | | | | | |

[1] SrO and MgO subtracted from original value as the 2 oxides were not separated from calcium during analysis.
[2] Calculated from spectrographic analysis, table 3.

analysis is calculated by the method of Foster (1962) and, following her nomenclature, the mineral could be called a pychnochlorite. It is interesting to note here that Zn, Co, and Ni are somewhat concentrated in the retrograde chlorite, similar to the 0.13 percent NiO found by Hutton (1940, p. 18) in a chlorite from a New Zealand albite-chlorite schist.

*Pumpellyite.*—The pumpellyite has a relatively low $Fe'''/R'''$ ratio (table 12) characteristic of the glaucophane schists as shown by Seki (1961). The analysis was calculated according to the method of Coombs

TABLE 11.—*Chemical analysis and physical properties of chlorite in type-IV schist*

[Weight percent oxides based on tables 2 and 3. USGS lab. No. H-3393, field No. 50-CZ-60]

| CHEMICAL PROPERTIES | | | | | PHYSICAL PROPERTIES | |
|---|---|---|---|---|---|---|
| Chemical composition (weight percent) | | Number of ions on the basis of 36(O, OH) | | | Specific gravity--2.98±0.01 | |
| | | | | | Optical properties | |
| $SiO_2$ | 27.54 | Si | 5.727 | 8.00 | β | ≈1.627±0.003 |
| $Al_2O_3$ | [1] 18.96 | Al | 4.644 [2.273 / 2.371] | | γ−α | ≈0.001 |
| $TiO_2$ | .09 | Ti | .019 | | 2V | 0°(+) |
| $V_2O_3$ | [2] .032 | V | .005 | 2.59 | X=Y | Pale green. |
| $Cr_2O_3$ | [2] .038 | Cr | .006 | | Z | Colorless. |
| $Fe_2O_3$ | 1.22 | $Fe^{+3}$ | .191 | | | |
| FeO | 24.36 | $Fe^{+2}$ | 4.232 | | | |
| MgO | [3] 15.62 | Mg | 4.857 | | | |
| MnO | [2] .43 | Mn | .075 | | | |
| CaO | .08 | Ca | .018 | | | |
| NiO | [2] .034 | Ni | .006 | 9.29 | | |
| CuO | [2] .043 | Cu | .007 | | | |
| CoO | [2] .014 | Co | .003 | | | |
| ZnO | [2] .087 | Zn | .013 | | | |
| $Na_2O$ | .14 | Na | .056 | | | |
| $K_2O$ | .08 | K | .021 | | | |
| $H_2O+$ | 11.20 | OH | 15.616 | 15.62 | | |
| $H_2O-$ | .06 | | | | | |
| Total | 100.12 | | | | | |

[1] Corrected from table 2 for $V_2O_3$ and $Cr_2O_3$, assuming the 3 metals were weighed together as oxides.
[2] Calculated from table 3.
[3] Corrected from table 2 for MnO, assuming the 2 metals were weighed together as pyrophosphates.

(1953) and although none of the collected analyses listed in Deer and others (1962, p. 229) shows $Mn^{+2}$ replacing $Ca^{+2}$ in the structure, our calculation presents this possibility. The $TiO_2$ (0.20 percent) and $K_2O$ (0.02 percent) probably represent impurities.

## CHEMICAL PETROLOGY

The presence of coexisting actinolite and glaucophane does not appear unusual when the bulk composition of the rock is considered. Even though chemical analyses indicate that the actinolite contains some sodium (1.52 percent $Na_2O$) and the glaucophane contains calcium (3.58 percent CaO), it is clear that we are dealing with two amphiboles of distinct composition. If one amphibole replaced the other, gross chemical adjustments in sodium and calcium would have been necessary; however, there is no mineralogic evidence supporting this concept. Further-more, the garnet-epidote-glaucophane-actinolite assemblage is permissible for a rock of this bulk composition (fig. 3).

It is difficult to suggest a reaction for the retrograde alteration even though we know the composition of each mineral, for there is no way to estimate the amounts of reactants and products involved in the process. Modal analyses of the rock (table 1) suggest

TABLE 12.—*Chemical analysis and physical properties of pumpellyite in type–IV schist*

[Weight percent of oxides based on tables 2 and 3. USGS lab. No. H-3363, field No. 50-CZ 60]

| CHEMICAL PROPERTIES | | | | | PHYSICAL PROPERTIES |
|---|---|---|---|---|---|
| Chemical composition (weight percent) | | Number of ions on the basis of 28(O, OH, F) | | | Specific gravity 3.25±0.01 |
| | | | | | **Optical properties** |
| $SiO_2$ | 37.48 | Si | 6.041 | 6.04 | $\alpha$ 1.684±0.003 |
| $Al_2O_3$ | [1] 25.22 | Al | 4.791 | | $\gamma$ 1.699 |
| $TiO_2$ | .20 | Ti | .024 | | $\gamma-\alpha$ 0.015 |
| $V_2O_3$ | [2] .16 | V | .019 | 5.00 | $2V$ 44(+) |
| $Cr_2O_3$ | [2] .047 | Cr | .006 | | $X$ Colorless. |
| $Fe_2O_3$ | 1.29 | $Fe^{+3}$ | .155 | | $Y$ Pale green. |
| FeO | 3.16 | $Fe^{+2}$ | .426 | | $Z$ Colorless. |
| MgO | [3] 2.34 | Mg | .562 | 1.03 | Dispersion $r>v$, strong. |
| MnO | .83 | Mn 0.112 | .044 | | |
| | | | .068 | | |
| CaO | 22.14 | Ca | 3.831 | 4.00 | |
| $Na_2O$ | .32 | Na | .097 | | |
| $K_2O$ | .02 | K | .004 | | |
| F | .04 | F | .019 | 3.00 | |
| $H_2O^+$ | 6.36 | OH | 2.981 | | |
| $H_2O^-$ | .02 | $H_2O$ | 1.929 | 1.93 | |
| Total | 99.63 | | | | |
| Less O | .02 | | | | |
| | 99.61 | | | | |

[1] Corrected from table 2 for $V_2O_3$ and $Cr_2O_3$, assuming the 3 metals were weighed together as oxides.

[2] Calculated from table 3.

[3] Corrected from table 2 for MnO, assuming the 2 metals were weighed together as pyrophosphates.

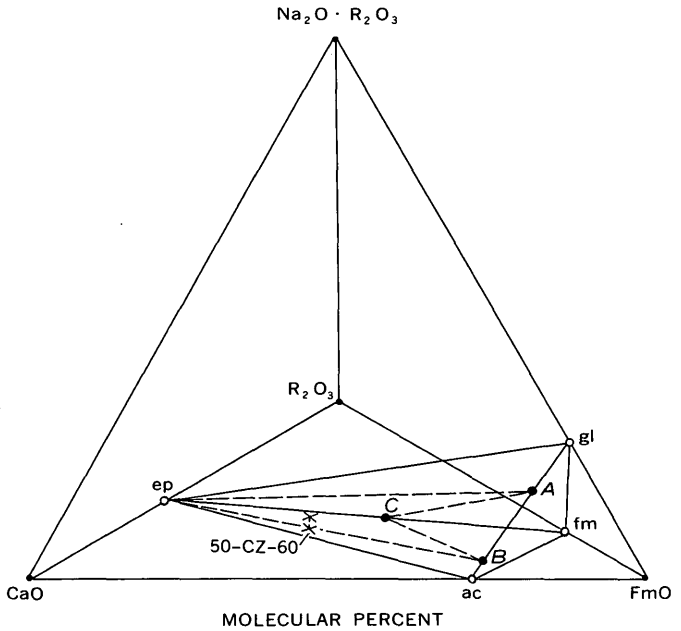


FIGURE 3.—Ernst tetrahedron showing the primary-mineral assemblage of sample 50–CZ–60. Four critical end members are glaucophane [gl, $Na_2Mg_3Al_2Si_8O_{22}(OH)_2$], actinolite [ac, $Ca_2(Fe^{+2}Mg)_5Si_8O_{22}(OH)_2$], epidote [ep, $Ca_2Fe^{+3}Al_2O \cdot OH(Si_2O_7)(SiO_4)$], and ferromagnesian silicate (fm, garnet, chlorite, stilpnomelane) as shown by Ernst (1963). The actual chemical compositions of the minerals from the sample are shown by the following approximate positions on the diagram: *A*, glaucophane; *B*, actinolite; *C*, garnet, epidote (coincides with end member ep) and the bulk composition of the sample. The molecular proportions for the 4 components shown on the tetrahedron are recalculated to 100 percent for each mineral and the rock, and are plotted directly on the diagram.

that almost any equation would involve disproportionate amounts of one phase or another. The irregular distribution of chlorite and pumpellyite do not allow us to estimate the bulk composition of the retrograde assemblage so that it could realistically be compared with the primary metamorphic assemblage.

The relation between the primary metamorphic minerals and the retrograde products is best illustrated using the Ernst (1963a, p. 20, 21) "assemblage tetrahedra." This representation allows 13 components of glaucophane schists to be considered as 4 compositional variables. Such a simplification, of course, involves a number of assumptions, some of which are admittedly tenuous but carefully qualified by Ernst. The advantage of the Ernst tetrahedron over the usual ACF diagram is that it makes possible the representation of the albite molecule in the sodium-bearing silicates glaucophane, jadeite, and paragonite. One of the special disadvantages of this chemographic treatment results from the fact that muscovite (table 8) contains 3.69 percent MgO, but $K_2O$ is treated as an indifferent component and this does not allow phengitic muscovite to be represented. Bearing in mind this limitation as well as those outlined by Ernst (1963a), we will consider a graphic analysis of the assemblages.

The theoretical end members upon which Ernst bases his treatment are shown in figure 3 along with the actual compositions established for minerals in sample 50–CZ–60. Because hydrous minerals are present in both the original and retrograde assemblages, it is assumed the $P_{H_2O}$ was equal to or slightly less than the total pressure during the initial metamorphism and later retrogression. The absence of carbonate minerals indicates that the chemical potential of $CO_2$ was extremely low at all times.

The compositions of the original metamorphic minerals are divergent from the theoretical end members (fig. 3). This is particularly true for garnet because of its high grossular content. As noted earlier, the coexisting amphiboles seem anomalous, but when plotted, the degree of "mixing" is seen clearly and the assemblage glaucophane-actinolite-garnet-epidote is permissible with this bulk composition.

To illustrate the relations between the retrograde and initial metamorphic assemblages, the triangular plane $CaO–R_2O_3–FmO$ from the tetrahedron has chlorite and pumpellyite plotted on the projection (fig. 4). The chlorite-pumpellyite tie line cuts the epidote-garnet and epidote-actinolite tie lines, illustrating that

garnet and epidote are unstable during retrogression and were replaced by chlorite and pumpellyite. If the bulk composition remains the same during retrogression, then actinolite could remain as a stable or metastable phase. The assemblage pumpellyte-chlorite-glaucophane is typical of the lower grade type-III metabasalt bedrock schists of the Cazadero area. It would appear then that the bulk composition has changed during retrogression because actinolite is being replaced by chlorite. However, we are not able to estimate the possible bulk composition of the retrograded rock against that of the original because of the patchy retrogressive replacement. The possibility exists that retrogression was accompanied by metasomatism. The presence of nearly pure pumpellyite veins replacing the rock suggests that calcium was introduced. Assuming an original basaltic composition, the presence of wollastonite in the norm is further indication of possible calcium metasomatism during retrogression.

The geologic position of this exotic high-grade metamorphic tectonic block resting on a lower grade metamorphic bedrock can be explained, in part, by the observed petrologic relations. The two-amphibole high-grade assemblage represents a period of recrystallization under high pressures and temperatures. Retrogression and perhaps metasomatism developed along fractures as illustrated by the formation of chlorite and pumpellyite, both characteristic of a lower grade of metamorphism. Such retrogression and metasomatism could have transpired during upward tectonic transport.

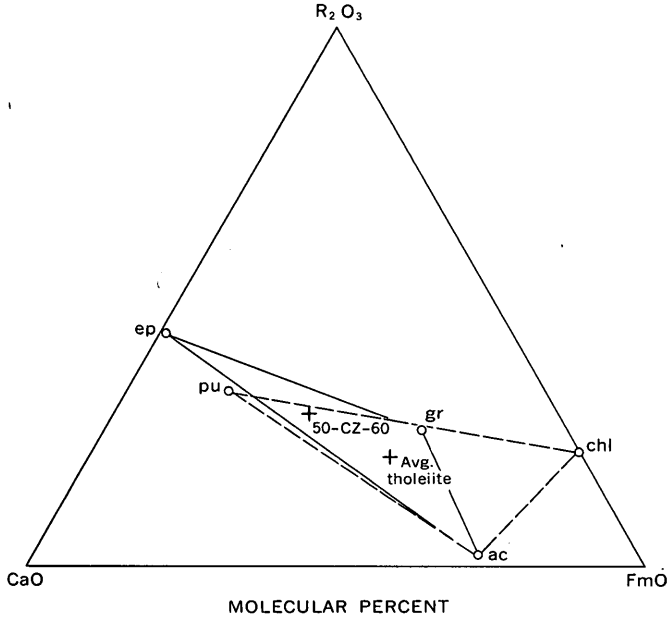


FIGURE 4.—FmO–CaO–$R_2O_3$ triangular base of the Ernst tetrahedron, showing the primary and retrograde three-phase mineral assemblages. In this section, epidote (ep), garnet (gr), actinolite (ac), pumpellyite (pu), and chlorite (chl) compositions are plotted in molecular precents of the three components. Bulk compositions of sample 50–CZ–60 and an average tholeiitic basalt (Nockolds, 1954, p. 1021) are plotted in a similar fashion. Solid lines connect the primary metamorphic assemblage ep+gr+ac and dashed lines connect the possible retrograde assemblage pu+chl+ac.

## REFERENCES

Bailey, E. H., Irwin, W. P., and Jones, D. L., 1964, Franciscan and related rocks, and their significance in the geology of western California: California Div. Mines and Geology Bull. 183, p. 177.

Banno, Shohei, 1964, Petrologic studies on Sanbagawa crystalline schists in the Bessi-Ino district, central Sikoku, Japan: Tokyo Univ. Fac. Sci. Jour., sec. 2, v. 15, pt. 3, p. 203–319.

Coleman, R. G., and Lee, D. E., 1963, Glaucophane-bearing metamorphic rock types of the Cazadero area, California: Jour. Petrology [Oxford], v. 4, no. 2, p. 260–301.

Coleman, R. G., Lee, D. E., Beatty, L. B., and Brannock, W. W., 1965, Eclogites and eclogites—their differences and similarities: Geol. Soc. America Bull. v. 76, no. 5, p. 483–508.

Coombs, D. S., 1953, The pumpellyite mineral series: Mining Mag. [London], v. 30, p. 113–135.

Deer, W. A., Howie, R. A., and Zussman, J., 1962, Ortho- and ring silicates, v. 1 *of* Rock-forming minerals: New York, John Wiley and Sons, Inc., 333 p.

Ernest, W. G., 1963a, Petrogenesis of glaucophane schists: Jour. Petrology [Oxford], v. 4, no. 1, p. 1–30.

——— 1963b, Significance of phengitic micas from low-grade schists: Am. Mineralogist, v. 48, p. 1357–1373.

Foster, M. D., 1962, Interpretation of the composition and a classification of the chlorites: U.S. Geol. Survey Prof. Paper 414–A, p. A1–A33.

Hutton, C. O., 1940, Metamorphism in the Lake Wakatipu region, Western Otago, New Zealand: New Zealand Geol. Survey Geol. Mem. no. 5, 84 p.

Iwasaki, Masso, 1963, Metamorphic rocks of the Kotu-Bizan area, eastern Sikoku: Tokyo Univ. Fac. Sci. Jour., sec. 2, v. 15, pt. 1, p. 1–90.

Lee, D. E., Coleman, R. G., and Erd, R. C., 1963a, Garnet types from the Cazadero area, California: Jour. Petrology [Oxford], v. 4, no. 3, p. 460–492.

Lee, D. E., Thomas, H. H., Marvin, R. F., and Coleman, R. G., 1963b, Isotopic ages of glaucophane schists from Cazadero, California: Art. 142 *in* U.S. Geol. Survey Prof. Paper 475–D, p. D105–D107.

Munsell, A. H., 1929, Munsell book of color [abridged edition]: Baltimore, Md., Munsell Color Co., Inc.

Myer, G. H., 1965, X-ray determinative curve for epidote: Am. Jour. Sci., v. 263, no. 1, p. 78–86.

Nockolds, S. R., 1954, Average chemical compositions of some igneous rocks: Geol. Soc. America Bull., v. 65, no. 10, p. 1007–1032.

Seki, Yotaro, 1961, Pumpellyite in low-grade metamorphism: Jour. Petrology [Oxford], v. 2, no. 3, p. 407–423.

Shapiro, Leonard, and Brannock, W. W., 1956, Rapid analysis of silicate rocks: U.S. Geol. Survey Bull. 1036–C, p. 19–56.

Velde, B., 1964, Low-grade metamorphism of micas in pelitic rocks: Carnegie Inst., Washington, Yearbook 63, 1963–64, p. 143–147.

# STRONTIUM-BEARING TODOROKITE FROM SOGANLIYÜRÜK, TURKEY

By ARTHUR S. RADTKE and LOIS M. JONES, Menlo Park, Calif.

*Abstract.*—A variety of todorokite with a significant amount of strontium has been recognized in volcanic-sedimentary manganese ores from Soganliyürük, Turkey. Optical, physical, chemical, and X-ray powder data are given. Chemical analysis shows the approximate formula of the todorokite to be

$(Ca, Sr, Mn^{+2}, Mg, Ba, Na_2)\ (Mn^{+4})_6O_{12}\cdot 3H_2O$.

Manganese ore containing todorokite from Soganliyürük, Turkey (fig. 1), is found in deposits similar in geologic occurrence to the deposits of the Charco Redondo-Taratana district, Cuba. However the todorokite from the Soganliyürük deposits contains significant amounts of strontium and is distinct in chemical composition from that found in Cuba. This paper describes the physical, optical, chemical, and X-ray characteristics of the strontium-rich Soganliyürük todorokite.

*Acknowledgments.*—In October 1964, specimens of manganese ores from Soganliyürük, Turkey, collected in the field by Mr. G. Van Der Kaaden of the Mineral Research and Exploration Institute, Ankara, Turkey, were sent to the U.S. Geological Survey by Clarence A. Wendel, Regional Minerals Attaché of the American Embasy in Ankara. These specimens were studied under the direction of D. F. Hewett, of the U.S. Geological Survey, in conjunction with a Geological Survey research project dealing with mineralogy and geochemistry of stratified manganese deposits. Thanks are due to Charles M. Taylor of Materials Analysis Co., Palo Alto, Calif., for advice and assistance in sample preparation.

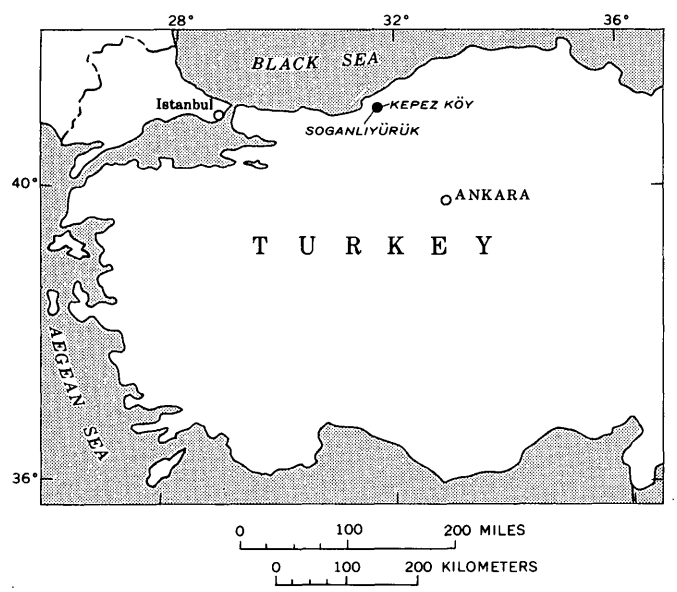


FIGURE 1.—Index map of Turkey, showing location of the Soganliyürük and Kepez Köy manganese deposits.

## OCCURRENCE AND ORIGIN

Todorokite has been identified in manganese ores from two mines, the Soganliyürük and Kepez Koy, located in Eregli County of northwest Turkey. Todorokite is the dominant manganese oxide mineral in these ores; pyrolusite is a very minor constituent in both deposits. Minerals associated with todorokite at Soganliyürük include pyrolusite, calcite, quartz, montmorillonite, and maghemite. A sample of todorokite ore from Soganliyürük is shown in figure 2.

In contrast, samples of ore from four other manganese deposits in the same area are massive pyrolusite without associated todorokite. Nahai (1958) states that pyrolusite is the dominant ore mineral in these deposits. In addition to todorokite and pyrolusite, Helke (1955) reports psilomelane, cryptomelane, hausmannite, and manganite.

Manganese ores from deposits near the Black Sea coast of northern Turkey form persistent beds and lenses in marl, tuff, and volcanic flows and breccias. Foraminifera identified in the marls indicate that the rocks are of Late Cretaceous age. The close association of the manganese ores of northern Turkey with volcanic material indicates deposition in shallow marine basins during extensive vulcanism. The ores are classified as volcanic-sedimentary.

The distribution of strontium in deposits of man-

ganese oxides is discussed by Hewett and others (1963). The concentration range of the element, according to Hewett's data, is rather uniform in all types of deposits—hypogene veins, hot-spring aprons, and beds.

## PHYSICAL PROPERTIES

Todorokite from Soganliyürük occurs chiefly as massive bladed or columnar aggregates and, to a lesser extent, as irregularly shaped compact botryoidal masses. The fine-grained todorokite is colloform banded and porous, resembling zincian todorokite from Philipsburg, Mont., described by Larson (1962). The mineral is brownish black in color and streak, and has a submetallic luster. Both the bladed and compact todorokite feel greasy and readily smudge the fingers. The Mohs hardness of Soganliyürük todorokite is less than 2, based on comparison with calcite in polished section. Two measurements by Michael Sheridan, Stanford University, of the specific gravity of bladed todorokite by means of a Berman balance gave 3.94 and 3.98; the samples were soaked in $CCl_4$ for 7 days to remove air bubbles. A sample of fine-grained todorokite treated in the same manner gave 3.86, the lower value probably being due to entrapped air and minor calcite within the compact manganese oxide.

## OPTICAL AND X-RAY PROPERTIES

The optical properties of todorokite were studied in polished and thin sections. Owing to its softness and lack of cohesion, todorokite is difficult to polish satisfactorily, but by trial and error, one method was developed that gave good results. Before the sample was mounted in either cold-setting plastic or bakelite, a flat-sawed surface was impregnated with epoxy resin. The surface was then ground on 2/0 followed by 3/0 emery paper, reimpregnated with diallyl phthalate resin dissolved in acetone, and reground lightly with 3/0 and 4/0 wax-coated emery papers. The surface was then polished with a 3-micron diamond abrasive on nylon cloth lubricated with Metadi fluid. For the final polish the surface was buffed in a slurry of 0.3-micron $Al_2O_3$ and water-soluble oil on microcloth.

In well-polished sections under reflected light, the mineral is yellowish brown to light brown and faintly bireflectant. Todorokite is strongly anisotropic, with polarization colors of light reddish brown to midnight blue, and is opaque except in very thin fragments. Attempts to prepare sections sufficiently thin to transmit light for optical study were unsuccessful because the mineral is so poorly cohesive. The indices of refraction are greater than 2.00, and the phase difference is positive.

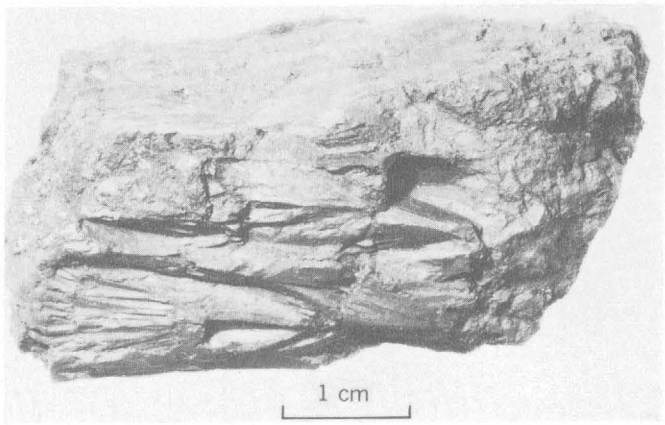


FIGURE 2.—Photograph of small hand specimen of manganese ore from Soganliyürük, Turkey. Massive bladed todorokite is in the center of the specimen, and fine-grained todorokite, pyrolusite, plus minor amounts of montmorillonite and calcite are at both ends.

X-ray powder data for strontium-bearing todorokite are given in table 1 and compared with data for other types of todorokite.

## CHEMICAL ANALYSIS

A chemical analysis of strontium-bearing todorokite from Soganliyürük is given in table 2. A semiquantitative spectrographic analysis of the mineral is presented in table 3.

The methods used in the chemical analysis are outlined below: The todorokite was dissolved in a mixture of HF–HCl–$H_2SO_4$ and evaporated to fumes of $SO_3$; the total manganese was then determined using sodium bismuthate. The same solution was used for the analysis of sodium by flame photometry, and total iron was determined spectrophotometrically using o-phenanthroline. The interfering manganese was removed by extraction with diethyldithiocarbamate and chloroform, and aluminum was determined as the Alizarin Red S complex, and magnesium as the Titan Yellow complex.

The alkaline earths were determined by flame photometry on a separate portion of sample, which was dissolved in HF-HCl-$HClO_4$ and evaporated to fumes of $HClO_4$. Following double precipitation with $NH_4OH$, destruction of ammonium ion with $HNO_3$, and evaporation almost to dryness, the slurry was then diluted to a suitable volume that was approximately 1.0*M* $HClO_4$. Strontium was determined at 460.8 m$\mu$; no interference from Ca or Ba was detected in the composition range of the sample. Calcium was determined at 423.3 m$\mu$ with no interference from Sr or Ba. The most satisfactory wave length for deter-

TABLE 1.—*X-ray powder diffraction data for strontium-bearing todorokite from Soganliyürük, Turkey, compared with those of todorokite from Cuba and zinc-bearing todorokite from Philipsburg, Mont.*

| Soganliyürük, Turkey | | Oriente Province, Cuba (Straczek and others, 1960) | | | | Philipsburg, Mont. (Larson, 1962) | |
|---|---|---|---|---|---|---|---|
| Observed [1] | | Observed [2] | | Calculated [3] | | Observed [4] | |
| $d_{hkl}$ (A) | $I$ | $d_{hkl}$ (A) | $I$ [5] | $d_{hkl}$ (A) | $hkl$ | $d_{hkl}$ (A) | $I$ |
| | | | | 9.747 | 100 | | |
| 9.65 | 10 | 9.6 | s | 9.592 | 001 | 9.6 | 10 |
| 7.03 | 4 | | | | | 7.0 | ½ |
| | | | | 6.837 | 101 | | |
| | | | | 4.873 | 200 | | |
| 4.83 | 8 | 4.77 | s | 4.796 | 002 | 4.8 | 6 |
| 4.41 | 2 | | | | | 4.45 | 1½ |
| | | | | 4.345 | 201 | | |
| | | | | 4.303 | 102 | | |
| | | | | 3.418 | 202 | | |
| | | | | 3.256 | 300 | | |
| 3.22 | 3 | 3.19 | w | 3.185 | 003 | 3.20 | 1 |
| 3.13 [6] | 3 | 3.11–2.95 | Band | 3.077 | 301 | | |
| | | | | 3.038 | 103 | | |
| | | | | 2.849 | 010 | | |
| | | | | 2.734 | 110 | | |
| 2.75 | <1 | 2.7 | Band | 2.731 | 011 | | |
| | | | | 2.690 | 302 | | |
| | | | | 2.673 | 203 | | |
| | | | | 2.630 | 111 | | |
| | | | | 2.460 | 210 | | |
| 2.46 | 2 | 2.448 | m | 2.449 | 012 | 2.46 | 2 |
| | | | | 2.437 | 400 | | |
| | | | | 2.398 | 004 | | |
| 2.41 | 4 | 2.398 | s | 2.382 | 211 | 2.405 | 4 |
| | | | | 2.376 | 112 | | |
| | | | | 2.362 | 401 | | |
| 2.36 | 2 | 2.34 | m | 2.329 | 104 | 2.34 | 1 |
| | | | | 2.279 | 303 | | |
| 2.22 | 1 | 2.21 | m | 2.189 | 212 | 2.22 | 2 |
| | | | | 2.172 | 402 | | |
| 2.17 | 1 | 2.16 | f-b | 2.152 | 204 | | |
| | | | | 2.142 | 310 | | |
| | | | | 2.127 | 013 | | |
| 2.11 [6] | <1 | 2.11 | f-b | 2.091 | 311 | | |
| | | | | 2.078 | 113 | | |
| | | | | 1.956 | 312 | | |
| 1.980 | 1 | 1.98 | m | 1.950 | 500, 213 | 1.99 | 2 |
| | | | | 1.938 | 403 | | |
| 1.935 | <1 | | | 1.930 | 304 | | |
| | | 1.92 | w | 1.918 | 005 | | |
| | | | | 1.910 | 501 | | |
| | | | | 1.882 | 105 | | |
| | | | | 1.852 | 410 | | |
| | | | | 1.834 | 014 | | |
| | | | | 1.818 | 411 | | |
| | | | | 1.806 | 502 | | |
| | | | | 1.803 | 114 | | |
| | | | | 1.785 | 205 | | |
| | | | | 1.780 | 313 | | |
| 1.743 | 1 | 1.74 | wm | 1.728 | 412 | 1.75 | ½ |
| | | | | 1.717 | 214 | | |
| | | 1.69 | f-b | 1.709 | 404 | | |
| | | | | 1.664 | 503 | | |
| | | | | 1.652 | 305 | | |
| 1.630 | 1 | | | 1.623 | 600 | | |
| | | | | 1.612 | 510 | | |
| | | | | 1.605 | 601 | | |
| | | | | 1.602 | 413 | | |
| | | | | 1.599 | 006 | | |
| | | | | 1.597 | 314 | | |
| | | | | 1.591 | 015 | | |
| | | | | 1.587 | 511 | | |
| | | | | 1.578 | 106 | | |
| 1.563 | 1 | | | 1.570 | 115 | | |
| 1.541 | 1 | | | 1.543 | 512 | 1.54 | 1 |
| | | 1.53 | w | 1.539 | 602 | | |
| | | | | 1.519 | 206 | | |
| | | | | 1.513 | 215, 504 | | |
| | | | | 1.507 | 405 | | |
| | | | | 1.466 | 414 | | |
| | | | | 1.448 | 603 | | |
| 1.440 | 1 | | | 1.437 | 513 | | |
| | | | | 1.434 | 306 | | |
| | | | | 1.429 | 315 | | |
| 1.423 | 1 | 1.423 | m | 1.424 | 020 | 1.42 | 3 |

[1] Film 314 (prepared by R. C. Erd). Fe/Mn radiation, λ=1.9373A. Camera diameter 114.6 mm.
[2] Fe/Mn radiation, λ=1.9373A. Camera diameter 114 mm.
[3] Indexing of Straczek and others (1960, p. 1182).
[4] Fe/Mn radiation, λ=1.9373A. Camera diameter 114.6 mm.
[5] Abbreviations: s, strong; m, medium; wm, weak to medium; w, weak; f-b, faint to broad.
[6] May possibly also be due to admixed pyrolusite.

TABLE 2.—*Chemical analysis of todorokite from Soganliyürük, Turkey*

[Analyst: Lois M. Jones]

| | Weight percent | Recalculated [1] | Molecular proportions | |
|---|---|---|---|---|
| $MnO_2$ | 78. 79 | 81. 41 | 0. 9364 | |
| MnO | 1. 88 | 1. 94 | . 0273 | |
| CaO | 4. 46 | 3. 23 | . 0576 | |
| SrO | 2. 30 | 2. 38 | . 0230 | |
| BaO | . 17 | . 18 | . 0012 | 0. 1428 |
| MgO | . 63 | . 65 | . 0161 | |
| $Na_2O$ | 1. 05 | 1. 09 | . 0176 | |
| $Al_2O_3$ | . 32 | | | |
| $Fe_2O_3$ | . 08 | | | |
| $SiO_2$ | . 46 | | | |
| $CO_2$ | 1. 04 | | | |
| $H_2O^+$ | 7. 66 | 7. 91 | . 5061 | |
| $H_2O^-$ | 1. 17 | 1. 21 | | |
| Others [2] | . 16 | | | |
| Total | 100. 17 | 100. 00 | | |

[1] Recalculated to 100 percent after subtracting $CO_2$ and CaO present as calcite and $Al_2O_3$, $Fe_2O_3$, and $SiO_2$.
[2] Includes other elements detected by spectrographic analysis given in table 3.

TABLE 3.—*Semiquantitative spectrophraphic analysis of todorokite from Soganliyürük, Turkey*

[In percent. Analyst: Chris Heropoulos]

| Element | Amount | Element | Amount | Element | Amount |
|---|---|---|---|---|---|
| Si | 0. 5 | B | 0. 015 | Nb | 0. 003 |
| Al | . 2 | Ba | . 3 | Ni | . 003 |
| Fe | . 1 | Co | . 0015 | Tl | . 02 |
| Mg | . 7 | Cu | . 005 | V | . 015 |
| Na | . 7 | Mo | . 02 | W | . 015 |
| Ti | . 005 | | | | |

Looked for but not found: K, P, Ag, As, Au Be, Bi, Cd, Ce, Cr, Ga, Ge, Hf, Hg, In, La, Li, Pb, Pd, Pt, Re, Sb, Sc, Sn, Ta, Te, Th, U, Y, Yb, Zn, Zr. For limits of detection see Bastron and others (1960).
Amounts of major elements reported in table 2.

mining Ba was 488.0 mμ. The transmission was enhanced by Ca and Sr, but once their concentrations were known, a correction was applied to the Ba value.

Silica was determined as the Molybdenum Blue complex following fusion of the sample with NaOH. Carbon dioxide was determined gravimetrically by absorption on ascarite after liberation from the sample by $H_2SO_4$. Available oxygen was determined following a procedure described by Fleischer (1943). Total water was determined by the Penfield method using a PbO-$PbCrO_4$ flux, and $H_2O^-$ found by heating the sample at 110°C.

The analysis (table 2) was recalculated after subtracting $CO_2$ and an equivalent part of the CaO for calcite. Other minor constituents, including $Al_2O_3$,

$SiO_2$, and $Fe_2O_3$, were considered to be present in associated montmorillonite. Straczek and others (1960), however, thought it possible that $SiO_2$, $Al_2O_3$, and $Fe_2O_3$ are constituents of todorokite.

The empirical formula for strontium-bearing todorokite derived from the chemical analysis is

$$(Ca,Sr,Mn^{+2},Mg,Ba,Na_2)_2(Mn^{+4})_{13}O_{28}\cdot 7H_2O.$$

Assuming 12 oxygen atoms per unit cell (excluding $H_2O$) as reported by Ross (Straczek and others, 1960), the formula may be written as

$$(Ca,Sr,Mn^{+2},Mg,Ba,Na_2)\ (Mn^{+4})_6O_{12}\cdot 3H_2O.$$

The $Mn^{+2}$ and Mg may also be included with $Mn^{+4}$ in the second group. The relatively high $Mn^{+4}$ content in Soganliyürük todorokite may be due to a small amount of admixed pyrolusite.

## REFERENCES


Bastron, Harry, Barnett, P. R., and Murata, K. J., 1960, Method for the quantitative spectrochemical analysis of rocks, minerals, ores, and other materials by a powder d-c arc technique: U.S. Geol. Survey Bull. 1084–G, p. 165–182.

Fleischer, Michael, 1943, Determination of active oxygen in the presence of barium and lead: Indus. and Eng. Chemistry, anal. ed. v. 15, p. 31–32.

Helke, Adolf, 1955, Beobachtungen an türkischen Minerallagerstätten: Neues. Jahrb. Mineralogie Abh., v. 88, p. 55–224.

Hewett, D. F., Fleischer, Michael, and Conklin, N. M., 1963, Deposits of the manganese oxides—Supplement: Econ. Geology, v. 58, no. 1, p. 1–51.

Larson, L. T., 1962, Zinc-bearing todorokite from Philipsburg, Montana: Am. Mineralogist, v. 47, p. 59–66.

Nahai, Lotfollah, 1958, The mineral industry of Turkey: U.S. Bur. Mines Inf. Circ. 7855, 140 p.

Straczek, J. A., Horen, Arthur, Ross, Malcolm, and Warshaw, C. M., 1960, Studies of the manganese oxides, [pt. ]4, Todorokite: Am. Mineralogist, v. 45, p. 1174–1184.

# OCCURRENCE OF PYROPHYLLITE IN THE KEKIKTUK CONGLOMERATE, BROOKS RANGE, NORTHEASTERN ALASKA

By BRUCE L. REED and J. J. HEMLEY, Menlo Park, Calif.

*Abstract.*—Pyrophyllite occurs in the matrix of the Upper(?) Devonian or Mississippian Kekiktuk Conglomerate. Pyrophyllite may have formed from the alteration of kaolinite or other high-alumina clay minerals during low-grade metamorphism.

The Kekiktuk Conglomerate is a thin, locally absent Upper(?) Devonian or Mississippian conglomerate in the northeastern Brooks Range (Brosgé and others, 1962). It underlies the Upper Mississippian Kayak(?) Shale and overlies with angular unconformity the Neruokpuk Formation of Devonian or older age. Although the pyrophyllite described here is from the vicinity of Lake Peters (fig. 1), a sample of lithologically similar Kekiktuk Conglomerate (made available by W. P. Brosgé) from the Kongakut River also contains considerable pyrophyllite. This sample locality is 80 miles east of Lake Peters and indicates that the occurrence of pyrophyllite in the Kekiktuk Conglomerate is not restricted to the Lake Peters area. Other pre-Kayak(?) quartzite on the south side of the eastern Brooks Range is also known to locally contain pyrophyllite (W. P. Brosgé, oral communication, 1965). From the description the pyrophyllite in the Sioux Quartzite (Berg, 1938) appears to be somewhat similar to the pyrophyllite in the Kekiktuk Conglomerate. In the Yakkabag Mountains, in the Soviet Union, Shumara (1965) has described pyrophyllite related to secondary quartzites which are found among volcanogenic rocks. However, the pyrophyllitization is restricted to the volcanogenic rocks; the associated sedimentary rocks underwent silicification.

## STRATIGRAPHY

### Neruokpuk Formation

In the Lake Peters area (fig. 1) the Neruokpuk Formation consists of interbedded quartz wacke, quartz semischist and phyllite with lesser amounts of chert and conglomerate. Detrital feldspar and rock fragments in the quartz semischist and quartz wacke are each less than 10 percent of the total rock. Mineral assemblages of the wackes, semischists and phyllites commonly include quartz, albite ($<An_5$), muscovite, and chlorite. Chloritoid is locally present and epidote is rare. The rocks of the Neruokpuk Formation have been regionally metamorphosed to the quartz-albite-muscovite-chlorite subfacies of the greenschist facies (Turner and Verhoogen, 1960, p. 534–537). The rocks in general possess a well-developed metamorphic fabric, but no evidence of a polymetamorphic history was seen. Uplift occurred subsequent to regional metamorphism and folding, and more than 10,000 feet of Neruokpuk rocks was eroded off prior to Kekiktuk deposition. The contact, where exposed, between the Neruokpuk Formation and the Kekiktuk Conglomerate is sharply defined. Any regolith that may have developed on the erosion surface of the Neruokpuk Formation would have subsequently been removed during the depositional regime of the Kekiktuk Conglomerate.

### Kekiktuk Conglomerate

The Kekiktuk Conglomerate is composed of 0 to 350 feet of resistant generally massive irregularly bedded units of quartzite and varying amounts of medium to thick, lenticular beds of pebble and cobble conglomerate. Thin lenses of siltstone are locally present. The siltstone is light to dark gray and weathers light gray and pale yellowish brown to reddish brown. The quartzite consists of medium-grained to granule size angular to subrounded strained and unstrained quartz grains with a few dark-gray chert grains in a matrix of quartz, pyrophyllite, and minor sericite (sericite as used in this paper refers to a very fine-grained 2M muscovite). Secondary quartz overgrowths are locally abundant, but welding and interpenetration of detrital quartz grains are more com-

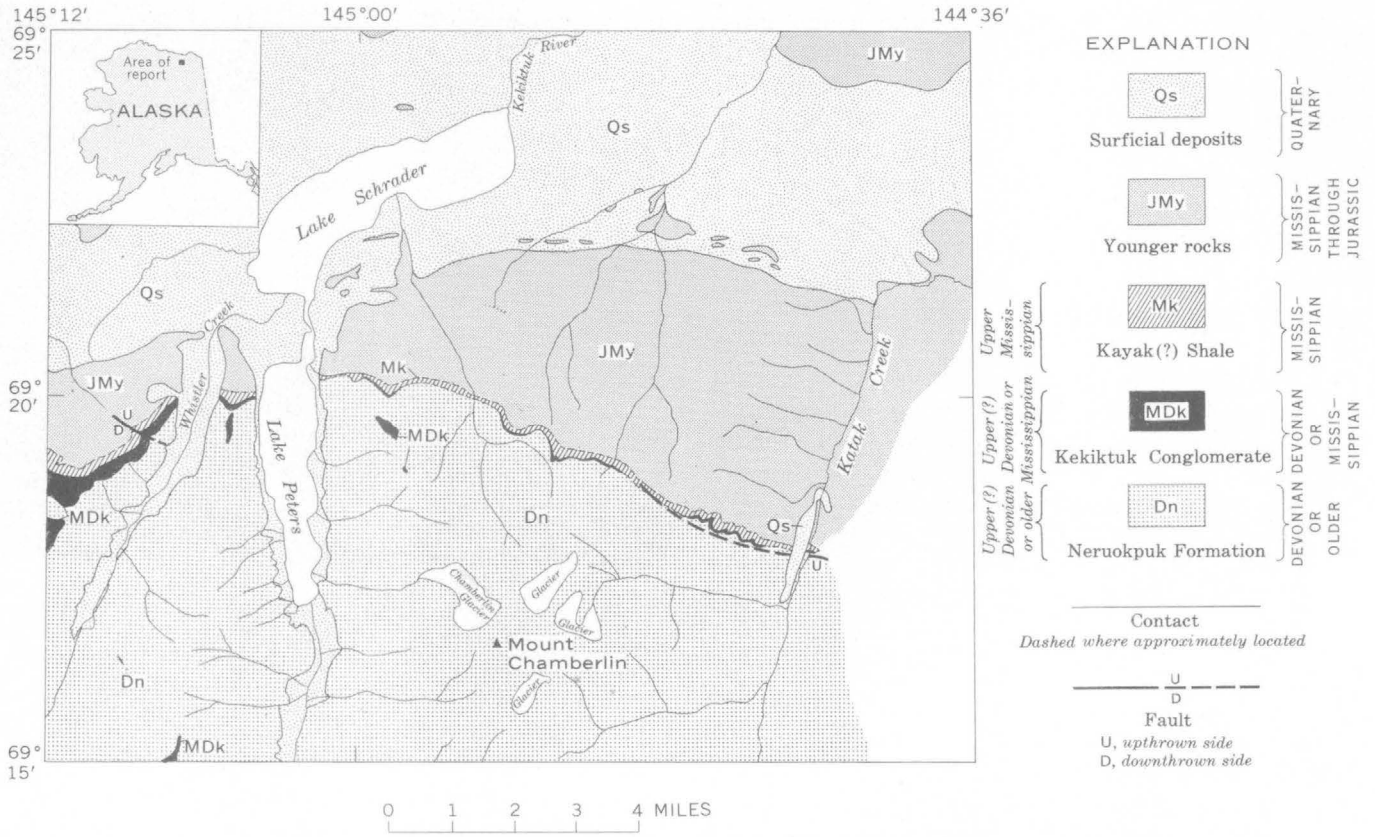


FIGURE 1.—Generalized geologic map of the Lake Peters area, northeastern Alaska, showing distribution of the Kekiktuk Conglomerate.

mon. Interstitial quartz is present as microcrystalline anhedral grains and as clear secondary quartz adjacent to welded grains. At a few places twinned detrital plagioclase grains occur in the specimens collected. Heavy minerals include tourmaline, ilmenite, magnetite, cassiterite, and rutile. Pebbles and cobbles in the conglomerate consist of quartz, metachert, and a few clasts of phyllite and quartzite. The conglomerate commonly occurs at the base of the formation, although discontinuous beds and lenses are found at higher levels. The general appearance of the formation suggests rapid deposition of gravel as sheets or channels, probably as an ancient fluvial deposit of a piedmont or flood-plain type.

### Kayak(?) Shale and younger rocks

The Kayak(?) Shale consists of argillite and siltstone with limestone occurring near the top of the formation. Mississippian through Jurassic limestone, sandstone, and shale overlie the Kayak(?) Shale (fig. 1); these rocks do not contain pyrophyllite. They are metamorphosed however, and slaty cleavage is locally developed. Igneous rocks are not present in the Lake Peters area.

## OCCURRENCE OF PYROPHYLLITE

Pyrophyllite occurs as a matrix mineral in the quartzite and conglomerate of the Kekiktuk Conglomerate. Of 22 samples examined (collected throughout the map area) 20 contain pyrophyllite. It also occurs in minor amounts in the underlying Neruokpuk Formation and the overlying Kayak(?) Shale. It is restricted, however, to within a few feet of both contacts with the Kekiktuk Conglomerate. Pyrophyllite in quartzite is easily overlooked in the field. A thin yellowish-gray film of pyrophyllite fills the interstices between quartz grains, and the characteristic soapy feel of pyrophyllite is absent even in specimens containing as much as 30 percent (by weight) pyrophyllite. Because pyrophyllite is difficult to distinguish from sericite in thin section, positive identification was made by X-ray diffraction.

The pyrophyllite occurs as fine compact feltlike aggregates of small clear crystals that range from 0.02 to 0.1 mm in length. It occurs in slightly broader platy crystals than does the less common sericite. The larger crystals of pyrophyllite occasionally form poorly developed radiating rosettes. Its birefringence is high, and 2V is greater than 45°.

Pyrophyllite fills interstices between quartz grains and replaces the original matrix, quartz overgrowths, and detrital quartz grains (fig. 2). In places pyrophyllitization is so complete that it is difficult to identify the original texture of the replaced matrix. Small irregular patches of unreplaced quartz are locally present within the pyrophyllite; in extreme cases of pyrophyllitization there is an absence of original detrital quartz outlines, and only isolated, embayed fragments of the original quartz grains remain (fig. 3). Strained quartz grains show a greater tendency for replacement than do unstrained grains. As much as 40 percent (by weight) of pyrophyllite may be present in some samples, but in general it makes up less than 20 percent of the rock. X-ray diffraction patterns show 2M muscovite as a minor constituent in 11 of the samples.

## STABILITY FIELD OF PYROPHYLLITE

The upper stability limit of kaolinite and of kaolinite in equilibrium with quartz has been the subject of considerable experimental work (Roy and Osborn, 1954; Carr and Fyfe, 1960). Unfortunately the results of these studies, although sometimes quoted in literature, cannot be taken as the thermodynamic stability limit of kaolinite. They are based either upon gel crystallizations or upon short-term unreversed thermal decomposition runs. The true limit of stability is therefore lower, and perhaps considerably lower, than these findings would indicate.

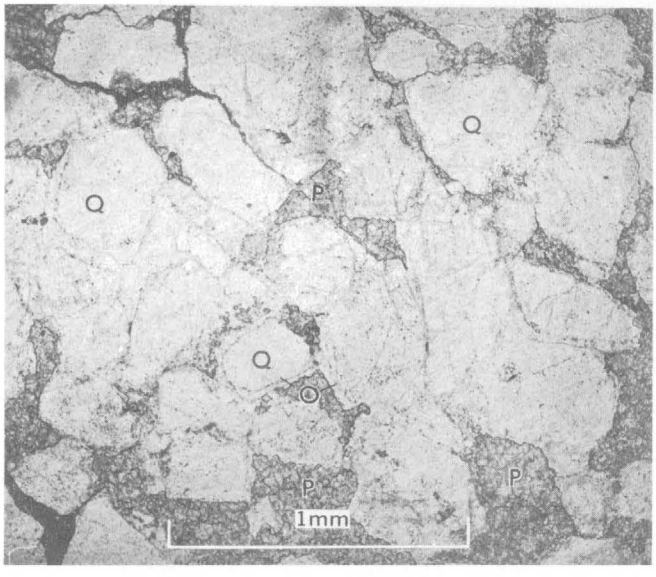


FIGURE 2.—Photomicrograph showing quartz overgrowths (O), detrital quartz grains (Q) and pyrophyllite (P). Most of the contacts among adjacent grains are between authigenic overgrowths, but the number of detrital grain contacts is high. Plane light.

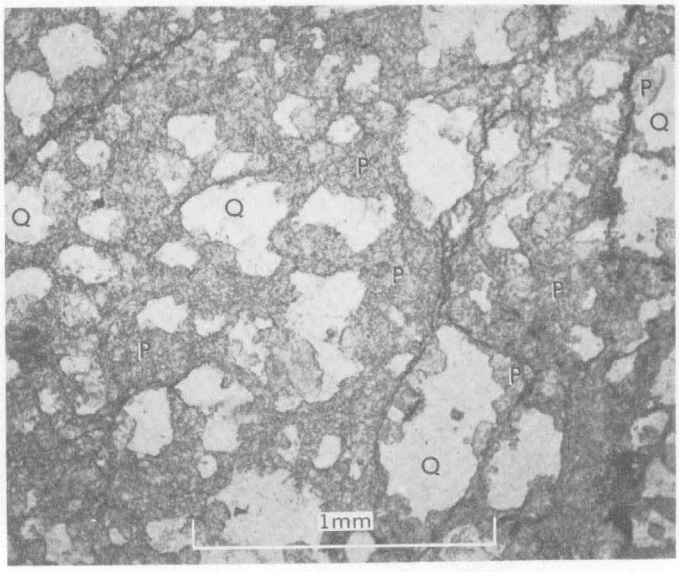


FIGURE 3.—Photomicrograph showing extreme case of pyrophyllitization in quartzite of the Kekiktuk Conglomerate. In most of the photomicrograph there is a lack of detrital grain outlines, and only embayed fragments of the original grains remain. (Q) quartz, (P) pyrophyllite. Plane light.

In a pure water environment Hemley and Jones (1965) observed the reaction kaolinite + quartz to pyrophyllite in the region of 380°C, 1,000 bars $P_{H_2O}$ (partial pressure of water), in runs of moderate (several weeks) duration. The reaction is:

$$Al_2Si_2O_5(OH)_4 + 2SiO_2 \rightarrow Al_2Si_4O_{10}(OH)_2 + H_2O.$$

In earlier work (Hemley, 1959), decomposition temperatures 20° to 30°C lower than this were realized in a dilute electrolyte environment (water activity still very close to that of pure water at the given pressure and temperature). More important, however, is the result of a run of long duration (1 year) in which pyrophyllite was produced from kaolinite plus quartz (Hemley, unpublished data) at 300°C and 1,000 bars $P_{H_2O}$. A stability limit no higher than about 300°C at 1,000 bars is thus indicated. This observation has been further corroborated by extensive solubility work on kaolinite and pyrophyllite by Hemley in the same experimental program, the results of which are being compiled for publication. Finally, it is apparent that at lower water pressures and higher silica activities the upper stability limit of kaolinite would be further depressed. These controls have important implications to the present geological discussion.

A possible origin for the pyrophyllite that is consistent with the quartz-pyrophyllite-sericite assemblage is summarized below. Extensive weathering of the Neruokpuk Formation, and the depositional regime associated with the profound unconformity at the base

of the Kekiktuk Conglomerate, produced a quartzite containing minor clay minerals, particularly kaolinite-type clays, but relatively free of feldspar or other mineral contaminants. During folding and low-grade metamorphism, pyrophyllite was formed by reaction of kaolinite with associated quartz.[1]

Lenses of siltstone within the quartzite, which probably had a high content of clay minerals originally, contain considerably more pyrophyllite than does the quartzite. This suggests that clay minerals were the source of the alumina required to form pyrophyllite. The temperatures and pressures at which pyrophyllite formed are uncertain. Temperatures may have been as much as 300°C, but most likely were much lower. The preserved thickness of rocks overlying the Kekiktuk Conglomerate is about 5,000 feet. However, there may have been an additional 5,000 feet or more of younger sedimentary rocks (post-Jurassic) that have been eroded off. In any event a lithostatic pressure of from 400 to 900 bars is indicated. Water pressure, on the other hand, may have been much lower than this lithostatic pressure. Also, the kaolinite to pyrophyllite transition should be favored not only by low $P_{H_2O}$, but also by a large differential between total pressure (including some possible tectonic overpressure) and in itself favors the phase of higher density and lower the $P_{H_2O}$, in the rock inasmuch as confining pressure hydration and entropy (Fyfe and others, 1958).

Because quartz is present as a major constituent, aqueous silica concentration was probably at least equivalent to quartz saturation in the pore fluid phase, but supersaturation may also have developed at least locally during metamorphism. Lithostatic stress on contacts between quartz grains would increase their solubility, causing solution and redeposition of silica. This increase in aqueous silica concentration would favor the reaction between silica and clay minerals. Strained quartz grains would tend to show preferential replacement by pyrophyllite inasmuch as grains in such a state have a decreased thermodynamic stability. That the fabric of the rock points to the operation of these processes is evidenced by petrographic features described in a previous paragraph.

Thus, there is no apparent inconsistency between known experimental relations in the alumina-silica-water system and the occurrence of pyrophyllite in this geologic setting. The most important requisite for pyrophyllite formation under the pressure and temperature conditions of low-grade metamorphism is a bulk composition relatively pure in alumina-silica. Where such conditions are not met, chlorite, muscovite, and other typical greenschist minerals are produced. For example, the overlying Kayak argillite contains predominantly 2M muscovite and chlorite. Although pyrophyllite is confined essentially to the Kekiktuk Conglomerate, it does occur in the overlying Kayak(?) Shale and underlying Neruokpuk Formation. It is confined in these rocks, however, to within a few feet of the contacts. This limited distribution apparently reflects the influence of the conglomerate as the source of the silica during metamorphism, which locally migrated into the overlying and underlying rocks and reacted with pockets of aluminous clay minerals to form pyrophyllite. Minor potassium is also present in Kekiktuk quartzite, reflected by the occurrence of minor sericite.

Low-grade metamorphism (greenschist facies) can yield pyrophyllite from the appropriate bulk composition with or without the presence of water as a phase. On the basis of the similarity of pyrophyllite to sericite in thin section, the apparent scarcity of pyrophyllite in low-grade metamorphic rocks may be more apparent than real. More X-ray work in the future will resolve this question. Furthermore, sediments, soils and weathering products rich in Al and Si and low in associated cations (kaolinitic-type materials) are not rare geologically. Therefore if pyrophyllite is indeed a rare mineral in quartzose metamorphic sections, it would imply that metasomatic processes (such as K introduction to form sericite) apparently accompany low-grade metamorphic processes in most instances.

[1] Montmorillonite, of course, may also have been present and involved in the metamorphic event, but montmorillonite reactions and stability relations are not quite as well understood as those of kaolinite, and the fact that montmorillonite contains minor base cations would require some leaching as well as simple reaction with silica in the metamorphic process.

## REFERENCES

Berg, E. L., 1938, Notes on catlinite and the Sioux quartzite: Am. Mineralogist, v. 23, p. 258–268.

Brosgé, W. P., Dutro, J. T., Jr., Mangus, M. D., and Reiser, H. N., 1962, Paleozoic sequence in eastern Brooks Range, Alaska: Am. Assoc. Petroleum Geologists Bull., v. 46, no. 12, p. 2174–2198.

Carr, R. W., and Fyfe, W. S., 1960, Synthesis fields of some aluminum silicates: Geoch. et Cosmoch. Acta, v. 21, p. 99–109.

Fyfe, W. S., Turner, F. J., and Verhoogen, J., 1958, Metamorphic reactions and metamorphic facies: Geol. Soc. America Mem. 73, 259 p.

Hemley, J. J., 1959, Some mineralogical equilibria in the system $K_2O$-$Al_2O_3$-$SiO_2$-$H_2O$: Am. Jour. Sci., v. 257, p. 241–270.

Hemley, J. J., and Jones, W. R., 1964, Chemical aspects of hydrothermal alteration with emphasis on hydrogen metasomatism: Econ. Geology, v. 59, p. 538–569.

Roy, R., and Osborne, E. F., 1954, The system $Al_2O_3$-$SiO_2$-$H_2O$: Am. Mineralogist, v. 39, p. 853–885.

Shumara, O. A., 1965, Pirofillit iz vtorichnykh kvartsitov yakkabagskikh gor (yuzhnyy Uzbekistan) [Pyrophyllite from secondary quartzites of the Yakkabagsk Mountains (South Uzbekistan)]: Izvest. Vyssh. Uchebn. Zavedemiy, Geol. i Razved., Izv., no. 1, 1965, p. 55–57 [in Russian].

Turner, F. J., and Verhoogen, J., 1960, Igneous and metamorphic petrology: 2d ed., New York, McGraw-Hill Book Co., Inc., 694 p.

# GENETIC IMPLICATIONS OF SOME ELEMENTS ASSOCIATED WITH URANIUM DEPOSITS, SHIRLEY BASIN, WYOMING

By E. N. HARSHMAN, Denver, Colo.

*Abstract.*—A systematic distribution of uranium, selenium, ferrous and ferric iron, carbon, beryllium, and sulfate sulfur is shown by analytical data on samples of unaltered sandstone, ore, and altered sandstone from a roll-type uranium deposit in the lower Eocene Wind River Formation of the Shirley basin. Transportation of uranium and other elements in a neutral to slightly alkaline, oxidizing solution and deposition by changes in the Eh and pH of that solution are suggested by the geochemistry of these elements at low temperatures and pressures.

Field and laboratory investigations of unoxidized uranium deposits in sandstone have resulted in considerable data on the possible sources of uranium and the geochemistry of its solution, transportation, and deposition. In spite of these data, and perhaps because uranium is a widely distributed element, easily dissolved and transported by solutions of diverse character, there is little agreement on the genesis of the deposits.

It is improbable that any one genetic concept can be applied to all uranium deposits in sandstone, for each has its own peculiarities of detail. On the other hand, most deposits have similarities that suggest that certain broad geochemical proceses may have been responsible for their origin.

C. F. Davidson (1964) suggests that "in geological theorizing it is wise to extrapolate from the known to the unknown, from the young to the old, from the simple to the complex." The Shirley basin uranium deposits are young, simple in form, and since their formation, apparently unaffected by significant redistribution of uranium or by weathering. In this paper certain physical and chemical data, and genetic concepts interpreted from these data, are presented. Extrapolation of the concepts to older and more complex deposits is not attempted.

## GEOLOGY AND ORE DEPOSITS

The major uranium deposits in the Shirley basin (fig. 1) are in a well-defined belt coincident with the lowest part of a basin filled with clastic and tuffaceous rocks of fluviatile and lacustrine origin. The basin was eroded in rocks of Cretaceous and older age, and was filled with rocks ranging in age from Eocene to Miocene that aggregated at least 1,500 feet in thickness. The ore deposits are in sandy beds of the Wind River Formation of early Eocene age which rests unconformably on the Cretaceous and older rocks.

Near the deposits, the Wind River Formation ranges from 300 to 500 feet in thickness. It is composed of clayey siltstone, arkosic sandstone, and conglomerate, all interbedded and poorly cemented. The sediments for the most part were derived from granitic rocks to the west. Regional dips are about 1° northward. Plant and vertebrate fossils indicate that the early Eocene environment was subtropical. Carbonaceous trash is abundant in the fine-grained rocks in the lower part of the basin and common in the sandstones interbedded with them.

The present ground-water table is at depths of a few feet to more than 300 feet below the ground surface. Ground water is tributary to the present surface drainage system and flows southward at gradients of 10 to 30 feet per mile.

The principal anions in the Shirley basin ground water are bicarbonate (210 parts per million) and sulfate (110 ppm) as shown by analyses of 25 water samples collected by the writer from the Wind River Formation. Radioelements include uranium (20 parts per billion), radium (10 picocuries per liter), and radon (as much as 200,000 pc/liter). The pH of the ground water ranges from 6.6 to 8.3; the median pH is about 7.8.

U.S. GEOL. SURVEY PROF. PAPER 550-C, PAGES C167-C173

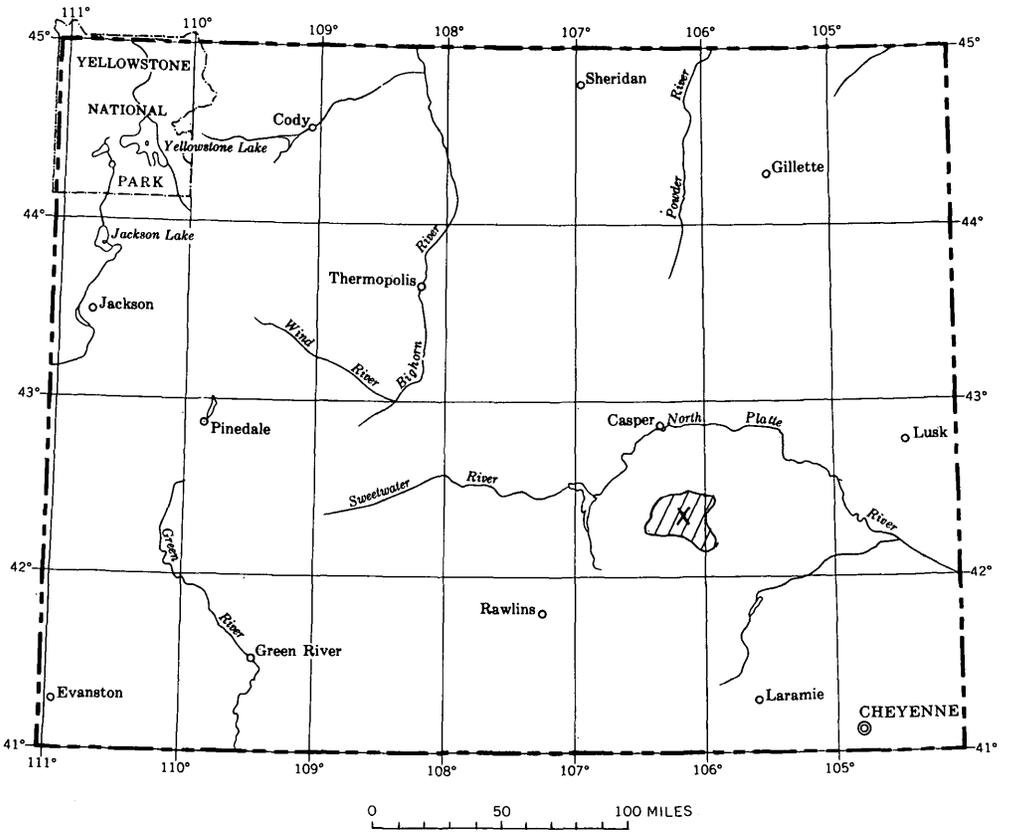


FIGURE 1.—Index map of Wyoming, showing location of Shirley basin (diagonal lines) and the Petrotomics Co. pit (×). The Utah Construction and Mining Co. mine is 2½ miles north of the Petrotomics Co. pit.

Large tongues of altered [1] sandstone, formed in the most transmissive parts of thick sandstone beds, were the loci for ore deposition. Two such tongues at different stratigraphic levels have been delineated by exploration and development drilling, and the upper tongue has been partly exposed by mining operations in the Petrotomics Co. open pit and in the Utah Construction and Mining Co. mine 2½ miles to the north. A third tongue, possibly a split from the upper tongue, may be present locally. Data on it are meager, and it is not discussed in this report. The upper tongue is 5 miles long in a northwesterly direction and has a maximum width of 3 miles. It is at depths of 100 to 450 feet below the ground surface and is as much as 200 feet above the base of the Wind River Formation. The upper tongue ranges in thickness from a few feet near its edge to about 70 feet, several thousand feet back from the edge.

The lower tongue is separated from the upper one by 50 to 70 feet of silty claystone. It has not been exposed by mining operations, but drilling data suggest that it is similar to the upper tongue. In part, the two tongues are superimposed, although the upper tongue extends farther to the north and west than does the lower one.

The major ore bodies in the Shirley basin are at the margins of tongues of altered sandstone in a curved zone between altered and unaltered sandstone. An ore body in its most simple form is crescent shaped in cross section, has a sharp contact with altered sandstone on the concave side, and grades into unaltered sandstone on the convex side. Ore bodies are elongate parallel to the margins of the altered sandstone tongues. Ore bodies of this configuration are commonly known as rolls.

Epigenetic minerals in the ore are uraninite, pyrite, marcasite, calcite, hematite, native(?) selenium, and an unidentified sulfate mineral; in altered sandstone they are goethite, limonite, and ferroselite.

The geology and ore deposits of the Shirley basin are discussed in more detail in papers by Harshman (1961, 1962), Melin (1964), and Rosholt and others (1964). Similar deposits in Russia have been described, most recently by Kashirtseva (1964).

[1] In this report the term "altered" is used in a restricted sense to refer to those physical and chemical changes, excluding mineralization, effected by the ore-bearing solution on the medium through which it passed. "Unaltered" denotes a lack of such changes.

## SAMPLES AND ANALYSES

A portion of the western edge of the upper altered sandstone tongue was well exposed by mining operations in the northwestern part of the Petrotomics Co. open pit. The exposure was sampled in vertical channels spaced horizontally 5, 10, and 50 feet apart. The samples in the channels were broken at each observed change in mineral composition; they ranged from 2 inches to 10 feet in length. Fifty-six samples were collected, consisting, from west to east, of (1) unaltered and unmineralized sandstone, (2) ore, and (3) altered sandstone. All samples were analyzed for U, eU, mineral carbon, organic carbon, sulfide sulfur, sulfate sulfur, total iron, ferrous iron (corrected for iron in $FeS_2$), ferric iron (by difference), selenium, and arsenic. Semiquantitative spectrographic analyses for 51 elements were made on all samples, and mercury determinations, by the atomic absorption method sensitive to 5 ppb, were made on a suite of 24 samples.

Figure 2*A* is a scale drawing of the exposure in the Petrotomics pit. It is a vertical section, normal to the trend of the edge of the altered sandstone tongue, and it shows the relation of ore to altered and unaltered sandstone, the configuration of the edge of the tongue at this location, and the position and length of 20 samples discussed in this report. The 20 samples shown on figure 2*A* constitute a suite extending horizontally across altered sandstone, ore, and unaltered sandstone. Data from analyses on the 20 selected samples shown on figure 2*A* are compatible with similar data from the 36 samples not shown on the figure.

## ANALYTICAL DATA

A systematic distribution of uranium, selenium, ferrous and ferric iron, carbon, beryllium, and sulfate sulfur, with respect to the contact between altered sandstone and ore, is shown by analyses of the 20 selected samples (fig. 2*A*) as well as by analyses of several hundred other samples from the Petrotomics Co. open pit and the Utah Construction and Mining Co. underground mine.

Figure 2*B* shows graphically the selenium content of the sample suite. Of particular interest are the low selenium content of unaltered sandstone, less than 0.5 ppm, the moderate selenium content of most of the ore, 2 to 15 ppm, and the moderate selenium content of most of the altered sandstone, 10 to 60 ppm. The presence of a high concentration of selenium in altered sandstone near the contact with ore is shown also by the analyses plotted on figure 2*B*, but not shown, because of sample locations, is the large amount of selenium known to be present in ore near the contact. Analyses of close spaced samples from ore bodies in the Petrotomics pit and the Utah mine show that selenium in amounts of as much as 1,200 ppm occurs in a zone about 1 foot wide parallel to, and extending about 6 inches each way from, the contact between altered sandstone and ore.

The distribution of ferrous and ferric iron as well as the amounts of ferrous iron in pyrite are shown on figures 2*C* and *D*. Of interest are: (1) a ferrous/ferric ratio of about 2 to 1 in the samples of unaltered sandstone most distant from ore and therefore least affected by ore deposition, in contrast to a ferrous/ferric ratio of about 1 to 1 in the samples of altered sandstone most distant from ore; (2) the nearly equal amounts of total iron in both altered and unaltered sandstone samples distant from ore; (3) the decrease in the ferric iron content of altered sandstone samples with increasing proximity to ore; (4) the high ferrous iron, high total iron, and low ferric iron contents of ore; and (5) the absence of pyritic ferrous iron (pyrite) in altered sandstone except for minor amounts near the contact with ore. Similar iron distributions are shown by analyses of sample suites from the Utah mine.

Analyses for carbon are shown on figure 2*E*. They confirm observations made in the open pit that: (1) moderate but erratic amounts of carbonized fossil plant debris are contained in ore and unaltered sandstone, (2) very minor amounts of such debris are present in the outer few feet of the altered sandstone tongues, and (3) no carbonized debris is present in the altered sandstone from the interior of the tongues.

Minor amounts of beryllium are associated with uranium in the Shirley basin deposits. Of the 20 samples shown on figure 2*A*, ore samples 312 and 319 contain 0.00015 percent Be, all other samples contain less than 0.0001 percent, the lower limit of detectability. The following Be distribution is shown when the analyses of these 20 samples are combined with the analyses of 145 samples from the Utah mine and the Petrotomics open pit:

*Number of samples*

| *Material* | *Total* | Be *detectable* | Be *not detectable* |
|---|---|---|---|
| Ore | 77 | 30 | 47 |
| Altered sandstone | 46 | 2[1] | 44 |
| Unaltered sandstone | 42 | 0 | 42 |

[1] Samples adjacent to ore.

Statistically there is no doubt that the uranium ore is enriched in beryllium, although the amounts of Be present in the highest grade ore are generally 0.0003 percent or less.

The high sulfate content shown in figure 2*B* is characteristic of some but not all of the Shirley basin uranium ore bodies. Sulfate-bearing ore placed in

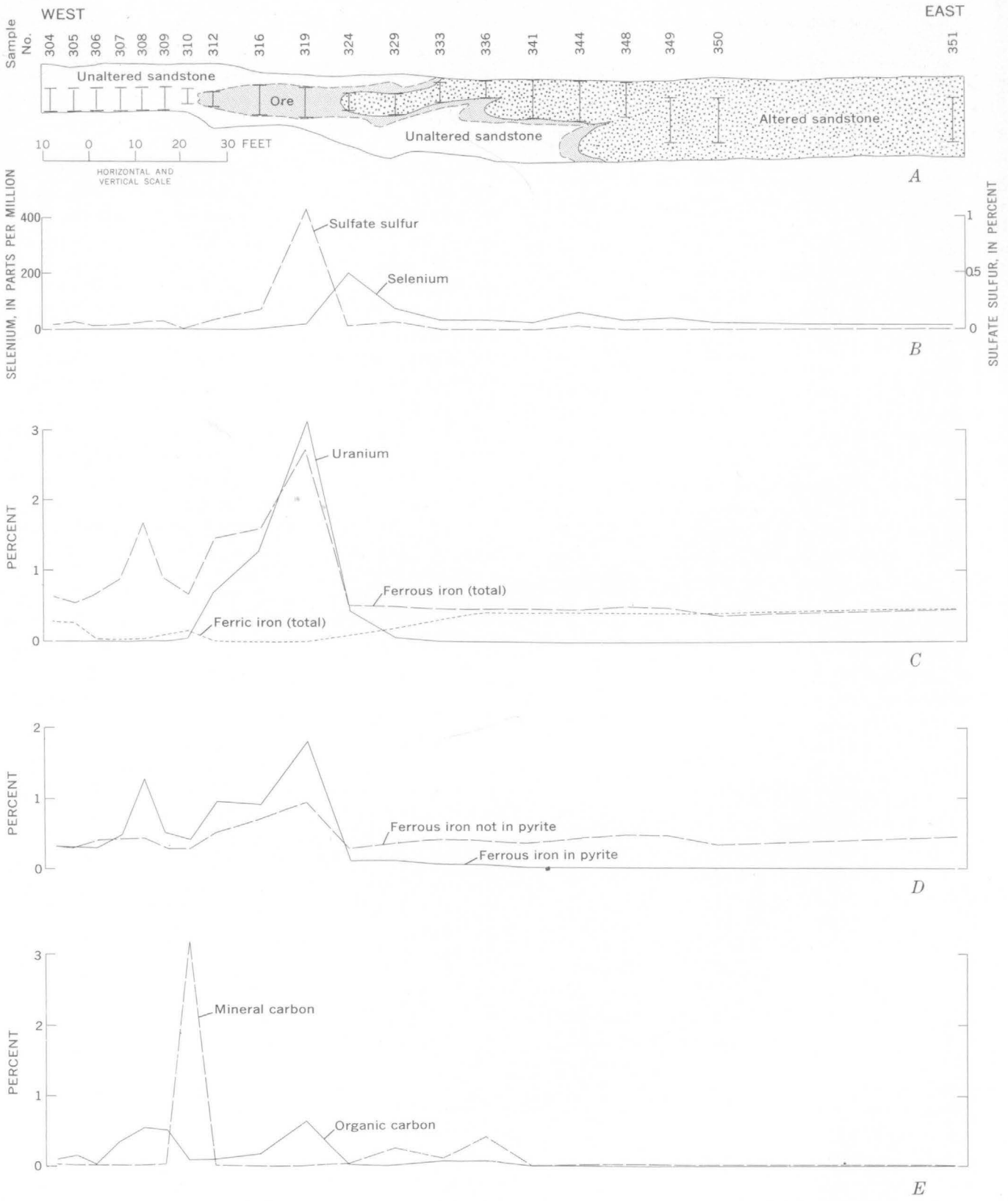


FIGURE 2.—Vertical section (*A*) through uranium ore body, showing sample locations and analytical data (*B–E*) from Petrotomics Co. pit, Shirley basin, Wyoming.

distilled water and heated on a steam bath for 10 hours yielded a solution saturated in calcium sulfate and enriched in iron. Analytical data on the high-sulfate-bearing samples are inconclusive regarding elements possibly combined with the sulfate, and no sulfate-bearing mineral has been recognized in polished sections of the ore.

## GENETIC IMPLICATIONS OF ANALYTICAL DATA

Certain genetic implications regarding the character of the solutions that transported uranium and other elements to the site of deposition may be drawn from the distribution of some of the elements in the deposits and their geochemistry at low temperatures and pressures.

Selenium, one of the more diagnostic elements with respect to the character of the transporting medium, is intimately associated with ore and altered sandstone, and undoubtedly was transported with uranium in the ore-bearing solutions. According to Lakin (1961), the selenite ion ($(Se_2O_3)^{-2}$) is readily formed at moderate oxidation potentials in mildly acid or alkaline solutions. However, the selenite is almost immediately immobilized by reacting with ferric ions present in most ground water to form an insoluble precipitate, probably a basic ferric selenite.

Selenate ion ($(SeO_4)^{-2}$) is soluble in most natural waters, but it is formed only under restricted Eh and pH conditions. In acid solutions, oxidation potentials far higher than can be reasonably expected in the most rigorous natural environments are required to oxidize selenium to selenate. However, in solutions of about pH 7 and greater the moderate oxidation potentials common in near-surface ground waters will oxidize selenium as selenate and it is probable that solutions of this character dissolved and transported selenium in the Shirley basin.

The geochemistry of beryllium, particularly in a low-temperature–low-pressure environment, is poorly known. Beus (1962) refers to transportation of beryllium as a complex with chlorine, fluorine, or carbonate in alkaline solutions. Govorov and Stunzhas (1963) have demonstrated that alkalic carbonatoberyllate complexes are stable in the pH range 6.8 to 11.8 at temperatures of about 80° to 210°C and that the complexes are decomposed with the precipitation of beryllium compounds as a result of a decrease in alkalinity. Available data therefore suggest that beryllium, intimately associated with uranium in the Shirley basin deposits, was transported in low-temperature alkaline solutions, but the data do not preclude transportation in solutions of other character.

211-690 O—66——12

Pyrite and carbonized plant debris, not present in altered sandstone except in small amounts near the margins of the altered tongues, are ubiquitous components of unaltered sandstone throughout the Shirley basin. The dispersed pyrite bears no relation to ore deposition, and its absence in altered sandstone implies destruction by the ore-bearing solutions. Similarly, the absence of carbonized plant debris in the altered sandstone tongues implies its destruction by chemical reactions, for the presence or absence of such debris is related spacially to the altered-unaltered sandstone contact and not to primary sedimentary features. The destruction of pyrite and of carbonized plant debris by the ore-bearing solution clearly implies that the solution was oxidizing.

The ferrous/ferric iron ratios of 2/1 in unaltered sandstone and 1/1 in altered sandstone reflect the destruction of pyrite in the latter by the ore-bearing solution and a redistribution of the iron so released, in part as ferric iron in geothite and (or) limonite and in part as ferrous iron in the clay minerals. This redistribution and conversion of at least a part of the iron from the ferrous to the ferric state implies an oxidizing ore-bearing solution.

Deposition of uranium and the elements associated with it in the Shirley basin deposits appears to have resulted principally from a decrease in the Eh of the ore-bearing solution, although a moderate drop in its pH may have been a contributing factor. Strongly reducing conditions in the zone of deposition are indicated by: (1) the decrease in ferric iron content of samples of altered sandstone taken progressively closer to ore, (2) the low ferric and high ferrous iron content of ore, (3) the high pyrite content of ore, and (4) the high selenium content of a narrow zone near the contact of ore and altered sandstone. Although the exact nature of the reducing agent for the Shirley basin deposits is not known, it may have been $H_2S$ of biogenic origin as suggested by Lindgren and others (1910) for the agent that reduced copper in "red-bed" deposits of New Mexico, and as suggested by Jensen (1958) as a possible reducing agent for uranium deposits in the Gas Hills area of Wyoming and the Colorado Plateau area of Colorado, Utah, and New Mexico.

There is some evidence to support the conjecture that the Shirley basin uranium deposits, as we now see them, are the final stage of a continuing process of solution and redeposition, "frozen" by a disruptive change in the conditions under which the ore elements were being dissolved and transported or by a change in the reducing environment responsible for ore deposition. Minor amounts of pyrite, carbonized plant

debris, uranium, and selenium found in altered sandstone near the contact with ore are believed to represent the leached remnants of former ore bodies. Particularly indicative of leaching are the corroded pyrite grains seen in heavy-mineral separates from altered sandstone in the Petrotomics pit, and described by Melin (1964) from altered sandstone in the Utah mine. These corroded grains contrast with the euhedral pyrite grains characteristic of ore and unaltered sandstone.

## CONCLUSIONS

The geochemistry of certain elements associated with uranium in the Shirley basin ore deposits suggests that the ore-bearing solution was neutral to weakly alkaline and oxidizing ground water. It probably dissolved uranium and other elements from tuffaceous and arkosic sedimentary rocks that once filled the basin. The solution migrated through the porous sandy members of the Wind River Formation and moved from the flank of the basin down the hydraulic gradient toward the lower part of the basin. As the solution moved basinward its oxidation potential was lowered by reaction with the minerals in the sandstone, particularly pyrite, and by intermixing with reducing solutions buffered by $H_2S$ of biogenic origin. Ore deposition is known to have occurred at depths of as much as 500 feet below the ground surface, a depth at which deposits are now found, and it may have occurred at depths of as much as 1,500 feet, the estimated thickness of Tertiary rocks that once filled the basin. Deposits formed in a narrow zone where the oxidation potential of the solution was reduced below that required for continued transportation of uranium and the associated elements. The spent ore-bearing solution, considerably changed chemically, passed beyond the zone of the ore deposition and eventually was discharged from the basin.

The zone of deposition is considered to have been a dynamic feature migrating basinward by oxidation and solution of ore on the updip side of the zone and by reduction and redeposition on the downdip side. Oxidation of pyrite on the updip side probably resulted in a sharp drop in the pH of the ore-bearing solution, but as these solutions passed through and beyond the zone of deposition, normal alkalinity would be restored by reaction with arkoses in the Wind River formation. Approximations of Eh and pH values believed to have been controlling factors in the solution, transportation, and deposition of uranium and associated elements in the Shirley basin deposits are shown on figure 3.

The processes described in this report as responsible for the genesis of the Shirley basin uranium deposits are similar to genetic processes by which secondary sulfide deposits are formed. In the formation of both types of deposits there are: (1) oxidation and solution of selected elements on the updip side of a mineralized zone, (2) a rather sharp drop in the pH of the water due to oxidation of pyrite, (3) downward migration of the water and its dissolved elements, and (4) reduction and redeposition of the dissolved elements. In addition, the gossans characteristic of many secondary sulfide deposits and the altered sandstone characteristic of the Shirley basin uranium deposits are similar chemically and in their position relative to ore. The concept of deep secondary enrichment may have application, along with other ore guides, in exploration for uranium deposits.

## REFERENCES

Beus, A. A., 1962, Beryllium: San Francisco, W. H. Freeman and Co. [English translation of Russian edition of 1956].

Davidson, C. F., 1964, Uranium in ancient conglomerates—a review: Econ. Geology, v. 59, p. 168–176.

Govorov, I. N., and Stunzhas, A. A., 1963, Mode of transport

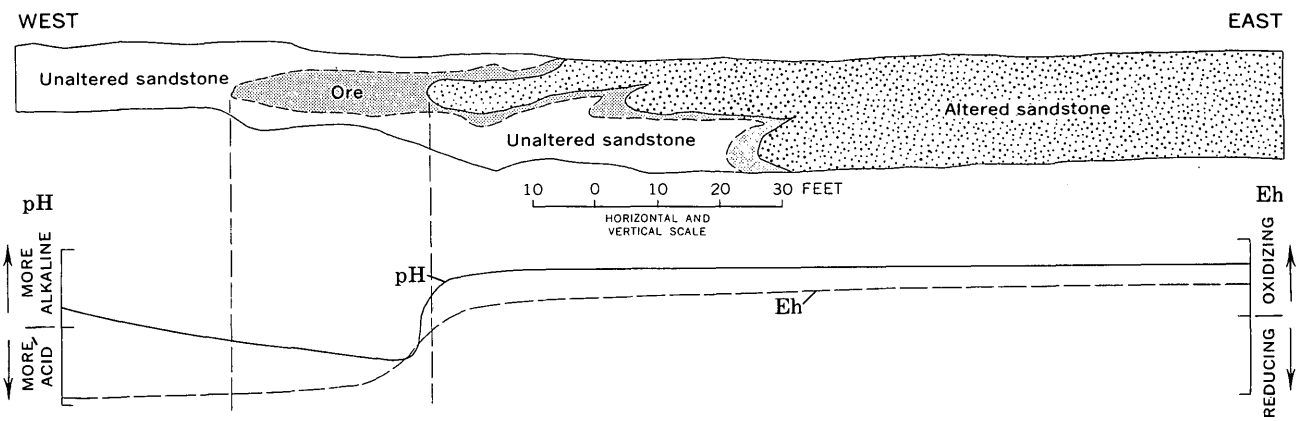


FIGURE 3.—Postulated Eh and pH conditions during transportation and deposition of uranium and other elements, Shirley basin, Wyoming.

of beryllium in alkalic metasomatism: Geochemistry [English translation], no. 4, p. 402–409.

Harshman, E. N., 1961, Paleotopographic control of a uranium mineral belt, Shirley Basin, Wyoming: Art. 148 *in* U.S. Geol. Survey Prof. Paper 424–C, p. C4–C6.

——— 1962, Alteration as a guide to uranium ore, Shirley Basin, Wyoming: Art. 122 *in* U,S. Geol. Survey Prof. Paper 450–D, p. D8–D10.

Jensen, M. L., 1958, Sulfur isotopes and the origin of sandstone-type uranium deposits: Econ. Geology, v. 53, p. 598–616.

Kashirtseva, M. F., 1964, Mineralic and chemical zonality in uranium infiltration ore occurrences: Sovetskaya Geologiya, no. 10, p. 51–65 [in Russian].

Lakin, W. H., 1961, Geochemistry of selenium in relation to agriculture, *in* Anderson, M. S., and others, Selenium in agriculture: U.S. Dept. Agriculture, Handb. 200, p. 3–12.

Lindgren, Waldemar, Graton, L. C., and Gordon, C. H., 1910, The ore deposits of New Mexico: U.S. Geol. Survey Prof. Paper 68, 361 p.

Melin, R. E., 1964, Description and origin of uranium deposits in Shirley Basin, Wyoming: Econ. Geology, v. 59, p. 835–849.

Rosholt, J. N., Harshman, E. N., Shields, W. R., and Garner, E. L., 1964, Isotopic fractionation of uranium related to roll features in sandstone, Shirley Basin, Wyoming: Econ. Geology, v. 59, p. 570–585.

# METAL SORPTION BY NORTHWEST FLORIDA HUMATE

By VERNON E. SWANSON, IRVING C. FROST, LEWIS F. RADER, JR., and CLAUDE HUFFMAN, JR., Denver, Colo.

*Abstract.*—Experiments with both natural and chemically extracted humate indicate that this water-soluble organic material from Florida can sorb between 1 and 17 percent by dry weight of cobalt, copper, iron, lead, manganese, molybdenum, nickel, silver, vanadium, and zinc. The enrichment of metals in ancient carbonaceous sedimentary rocks may be due in part to humate that acted as a scavenger or sponge for metals during exposure to metal-bearing natural water before, during, or shortly after deposition. Because of its metal-sorptive properties, large tonnages, and thin, easily removed overburden of loose sand, the Florida humate may find use in the chemical and fertilizer industries.

The metal content of carbonaceous rocks is commonly high, but the kinds and amounts of the metals are highly variable. Reasons for this variability are many and undoubtedly complex, and at present are very poorly understood. Krauskopf (1955, p. 456) ended his very thorough review of the geology and geochemistry of the distribution and enrichment of metals in sedimentary rocks with this succinct summary:

> The principal stumbling block [in understanding the enrichment of metals in sedimentary rocks] is usually the organic matter; it has become abundantly clear that certain metals are preferentially associated with particular kinds of organic matter, and that these different kinds represent different depositional environments, yet the differences are not apparent to field observation or even to some laboratory tests. Research aimed at setting up tests for the significant varieties of organic matter . . . would help immensely not only in building up a theory of . . . metal deposition but also in the practical problem of prospecting.

Investigations are now underway to decipher the genesis and geologic role of one of these kinds of organic matter—humate, a water-soluble, coal-like material found in sediments (Swanson and Palacas, 1965, p. B2–B3). The solubility characteristics of humate, and its distinctive capacity to sorb[1] and retain large amounts of many different metals, are believed to explain, at least in part, the concentration of metals in many carbonaceous rocks.

The humate discussed here is soluble organic material deposited in the past and also accumulating today in the dune and beach sands along the Gulf of Mexico in northwest Florida (fig. 1). The distribution, chemical composition, and probable origin of this humate have been described by Swanson and Palacas (1965). The preliminary results of experiments to determine the sorption capacity of the humate for 10 metals are reported here.

## SAMPLE MATERIAL

Two types of samples were used in the laboratory tests: (1) humate-impregnated sand, just as collected in the field, which was used to test the sorption of six metals, and (2) humate extracted from the sand by

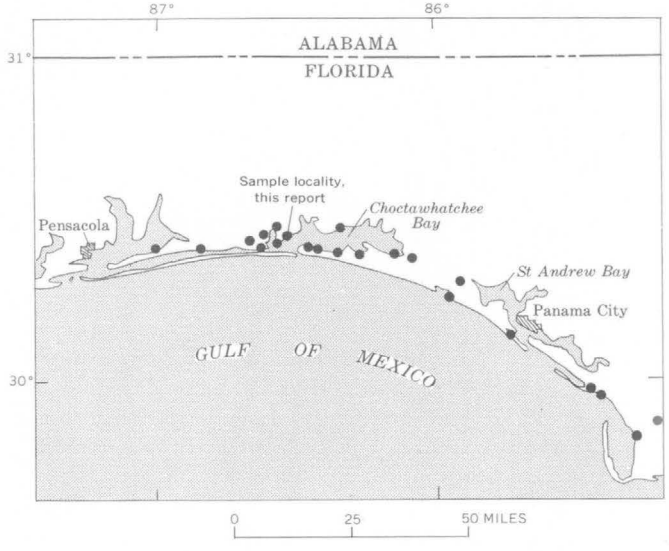


FIGURE 1.—Localities of humate-cemented beach and dune sands near the coast of the Gulf of Mexico, in the Florida panhandle.

[1] The exact type of bonding between the humate and metal ions is not known. The bonding may be one of adsorption, ion-exchange, or chelation, but for the purposes of this report it is hereafter termed sorption.

alkaline solution and which was used to test the sorption of 10 metals. This latter material, when extracted by alkaline solution and precipitated with dilute acid, is commonly designated as humic acids. However, when this material is precipitated as a salt of humic acids, whether by calcium, magnesium, or iron, as is common in nature, or when combined with metals as described here, the term humate is applicable (Horner and others, 1934) and is so used in this report.

The humate-impregnated sand was collected on the shore of the northwestern part of Choctawhatchee Bay, Fla. (near center sec. 4, T. 2 S., R. 23 W.). The sand, which is dark brownish black when wet and brown when dry, contained 9.0 percent humate and 5.4 percent organic carbon. The 5.4 percent carbon is equivalent to an estimated 9.2 percent total organic matter. The medium- to fine-grained sand is mainly composed of quartz grains, with less than 5 percent clay.

When dried, the humate extracted from the sand by alkaline solution is a jet-black lustrous coal-like material with a conchoidal fracture. It contains 45.0 percent organic carbon and 7.12 percent ash. Ultimate analysis of this humate was not obtained, but the carbon determination of 45.0 percent and the ultimate analyses of very similar material (Swanson and Palacas, 1965, table 2) suggest that the humate had an approximate moisture- and ash-free content of 48.5 percent carbon, 4.5 percent hydrogen, 45.5 percent oxygen, 1.0 percent nitrogen, and 0.5 percent sulfur.

## PROCEDURES AND RESULTS

The 10 metals used in the sorption tests were silver, cobalt, copper, iron, manganese, molybdenum, nickel, lead, vanadium, and zinc. These metals were dissolved in triply distilled water in their salt form as $AgNO_3$, $CoCl_2.6H_2O$, $CuSO_4.5H_2O$, $FeCl_3.6H_2O$, $MnCl_2.4H_2O$, $(NH_4)_6Mo_7O_{24}.4H_2O$, $NiSO_4.6H_2O$, $Pb(NO_3)_2$, $NH_4VO_3$, and $ZnCl_2$, respectively. The amount of metal ions added in solution in each test was sufficient to permit the humate to sorb as much as 20 percent metal by dry weight.

The tests to determine the metal-sorption capacity of the humate-impregnated sand were run by simply adding the metal-containing solution to a 10-gram sample of lightly crushed sand. The samples were stirred intermittently for 24 hours, then were centrifuged, thoroughly washed twice with distilled water, dried, and analyzed for metals by the spectrographic method. A control sample without any metal added was run with each set of samples. The results for the six metals tested are shown in table 1. On the basis of these semiquantitative values and the fact that the sand contained 9 percent humate, the metal-sorption capacity of the humate is on the order of 1 to 10 percent.

TABLE 1.—*Capacity of humate-impregnated sand to sorb metal ions, in percent by dry weight, as determined by semiquantitative spectrographic analysis*

[Analysts: R. G. Havens and Nancy Conklin]

| Metal | Control sample (no metals added) (Lab. No. D116543) | Metals added individually (Lab. Nos. D116546-551) | Mixed Ag-Cu-Fe-Ni-Pb-Zn solution added (Lab. No. D116544) |
|---|---|---|---|
| Ag | <0.0001 | 0.5 | 0.07 |
| Cu | .001 | .3 | .05 |
| Fe | .03 | .2 | .03 |
| Ni | <.0003 | .07 | .003 |
| Pb | <.001 | .7 | .15 |
| Zn | <.05 | .2 | <.05 |

The tests to determine the metal-sorption capacity of the isolated humate were run in a similar manner, except that the metal solution was added while the humate was in solution. This humate was obtained by extraction from sand with 0.1*N* NaOH, followed by centrifuging and filtering twice to remove clay and particulate organic material from the humate solution. Precipitation of the humate, with its sorbed metal, was accomplished either by addition of the metal solution, or by lowering the pH of the solution to about 2.5 with 6*N* MCl. After centrifuging and thorough washing twice, the black humate gel was dried and analyzed by methods indicated in table 2. The simplified experimental procedure that was used did not preclude the possible inclusion of a small but unknown amount of metal hydroxide that may

TABLE 2.—*Capacity of extracted humate to sorb metal ions, in percent by dry weight.*

[All Ag, Cu, Fe, Mn, Ni, Pb, and Zn analyses by atomic absorption method by Claude Huffman, Jr., and J. D. Mensik; Co and Mo by colorimetric method by L. F. Rader, Jr., and J. D. Mensik; and V by volumetric method by H. H. Lipp. Laboratory numbers of samples analyzed are D116577–D116588 and D117294–D117299]

| Metal | Control sample (no metals added) | Metals added individually | Mixed Ag-Cu-Fe-Ni-Pb-Zn solution added | Mixed Co-Mn-Mo-V solution added |
|---|---|---|---|---|
| Ag | 0.0068 | 17.4 | 1.65 | ---------- |
| Co | .0008 | 4.5 | ---------- | 1.9 |
| Cu | .0093 | 12.0 | 6.3 | ---------- |
| Fe | .089 | 10.1 | .11 | ---------- |
| Mn | .0014 | 4.3 | ---------- | .27 |
| Mo | .028 | 5.3 | ---------- | 1.9 |
| Ni | <.001 | 11.0 | 3.28 | ---------- |
| Pb | <.001 | 10.2 | .058 | ---------- |
| V | .019 | 3.9 | ---------- | 2.1 |
| Zn | .0008 | 11.2 | .012 | ---------- |
| Total | 0.1561 | (avg 8.9) | 11.410 | 6.17 |

have been sorbed by, or coprecipitated with, the humate.

A comparison between the chemically extracted humate and natural or untreated humate shows that the two are very similar, in appearance and also chemically (table 3), particularly in carbon and sulfur content, though some of the major ions, such as calcium, magnesium, and iron, are apparently stripped from the humate during chemical extraction. The natural humate sample was taken from the cast of a *Pecten*-type shell in humate-cemented sand (Swanson and Palacas, 1965, p. B10, B17). The original calcareous shell had been dissolved by subsurface water and completely replaced by black humate.

The large metal-sorption capacity of the Florida humate, whether dispersed in sand or chemically extracted from the sand, is generally from 1 to 17 percent, as shown in tables 1 and 2, though the values shown should be considered as approximate because of the simplified experimental procedures used.

The results shown are comparable to the results of other workers who tested the metal-sorption capacities or metal content of different kinds of organic matter. Some of these other studies involved peat, dopplerite, lignite, soil humus, humic acids, and humate (Aschan, 1932; Horner and others, 1934, p. 665, 668; Hewitt, 1952, p. 106-107; Rozhkova and Shcherbak, 1956; Szalay, 1957; Vine and others, 1958; Martin, 1960; Kashirtseva, 1960; Fraser, 1961; Mortensen, 1963), which can sorb from a few percent to 20 percent metal by dry weight.

## ECONOMIC CONSIDERATIONS

The main result of this study of metal sorption by the Florida humate is that a probable geochemical process is indicated whereby metals could have been concentrated in an ancient organic-rich sandstone that was deposited in a similar coastal environment. Also, it is suggested that the metal-sorption property of the Florida humate may be of economic use. In northwest Florida, surprisingly large tonnages of humate that could be extracted simply and cheaply were discovered during this study and may potentially be suitable for use in the chemical and fertilizer industries. Six of the metals used in this study, cobalt, copper, iron, manganese, molybdenum, and zinc, are known to be essential micronutrients for plant and animal metabolism (Mitchell, 1964, p. 320), and are widely used in fertilizer and animal-feed additives. The biochemical function or importance of the other four metals tested, silver, nickel, lead, and vanadium, is not known, though these metals are commonly concentrated in plants, in the humus of soils, in aquatic organisms, and in organic-rich sediments.

TABLE 3.—*Partial chemical composition, in percent by dry weight, of natural humate and of chemically extracted humate.*

[C and S analyses by induction-furnace and gasometric method by I. C. Frost; other determinations by semiquantitative spectrographic method by R. G. Havens. Laboratory numbers of samples analyzed are D116685, D116687, D116689, D116691 and D117090]

| Element | Natural humate [1] | Chemically extracted humate [2] |
|---|---|---|
| Organic C | 43.6 | 44.2 |
| S | .39 | .41 |
| Al | 2.0 | 1.0 |
| Fe | .5 | .07 |
| Mg | .3 | .015 |
| Ca | .5 | .005 |
| Na | .7 | .7 |
| Ti | .15 | .15 |
| Ba | .003 | .002 |
| Cr | .002 | .003 |
| Cu | .0015 | .003 |

[1] From replaced *Pecten*-type fossil.
[2] Average of four samples of the same type and from the same locality as humate used in metal-sorption experiments.

An ever-present problem in the biologic use of micronutrient-metal additives has been to find a substance or form that permits the required kinds and amounts of metals to be easily assimilated by plants and animals. Additional requirements of the micronutrient compound are that it will be nontoxic, that it will not break down or chemically combine with other constituents to result in an "unavailable" form, that it is easy to apply, and that it is inexpensive. Synthetically prepared metal chelates (Wallace, 1956) have been proven to meet most of these requirements, particularly for iron, manganese, and zinc additives, though these chelates, such as EDTA (ethylenediamine tetraacetic acid), are relatively expensive. The composition, solubility, and metal-sorption properties of the Florida humate strongly suggest that it may find a use as a natural or processed chelating agent, though extensive biologic and agronomic tests will be necessary to establish its usefulness.

It seems probable that the Florida humate could be easily and cheaply mined and processed. The humate-rich sand, which in itself is soft or semifriable, is concentrated at a depth of generally less than 35 feet from the surface, suggesting easy removal by shallow open-pit mining methods. It is estimated that 100,000 to 1,000,000 tons of humate are present per square mile in discontinuous beds at a depth of less than 35 feet over an area of 300–500 square miles along the northern coast of the Gulf of Mexico (Swanson and Palacas, 1965, p. B11, fig. 1). Simple drying, light crushing, and sieving of the humate-rich sand produces a powder that is 60 to 75 percent humate. Another seemingly attractive aspect of the humate is its almost

instantaneous solubility, for example, in ammonia. Ammonia is widely applied in liquid form to soils as a nitrogen fertilizer. Humate is also soluble in a potassium phosphate ($K_3PO_4$) solution, and might also provide the other 2 of the 3 major constituents of fertilizers—potassium and phosphorous.

Other possible, but untested, uses of the physically separated or chemically extracted humate are as a water purifying compound, as an additive in well-drilling fluids, as a wood stain or paint pigment, and as a metal scavenger in a variety of commercial processes.

## REFERENCES


Aschan, Ossian, 1932, Water humus and its role in the formation of marine iron ore: Arkiv. Kemi Mineral Geol., v. 10A, no. 15, p. 1–143.

Fraser, D. C., 1961, Organic sequestration of copper: Econ. Geology, v. 56, no. 6, p. 1063–1078.

Hewitt, E. J., 1952, Sand and water culture methods used in the study of plant nutrition: [British] Commonwealth Bur. Horticulture and Plantation Crops, Tech. Commun. 22, 241 p.

Horner, C. K. Burk, Dean, and Hoover, S. R., 1934. Preparation of humate iron and other humate metals: Plant Physiology, v. 9, p. 663–669.

Kashirtseva, M. F., 1960, Experimental data on sorption of copper by various minerals and sorbing agents: Internat. Geol. Rev., v. 2, no. 1, p. 52–59.

Krauskopf, K. B., 1955, Sedimentary deposits of rare metals: Econ. Geology, 50th Anniversary Volume, pt. 1, p. 411-463.

Martin, A. E., 1960, Chemical studies of podzolic illuvial horizons; V, Flocculation of humus by ferric and ferrous iron and nickel: Jour. Soil Sci., v. 11, p. 382–393.

Mitchell, R. L., 1964, Trace elements in soils, *in* Bear, F. E., ed., Chemistry of the soil: New York, Reinhold Publishing Corp., p. 320–368.

Mortensen, J. L., 1963, Complexing of metals by soil organic matter: Soil Sci. Soc. America Proc., v. 27, no. 2, p. 179–186.

Rozhkova, E. V., and Shcherbak, O. V., 1956, Sorption of lead on various rocks and its possible role in the formation of ore deposits: Izvest. Akad. Nauk SSSR, ser. Geol., no. 2, p. 13–24. English translation by Assoc. Tech. Services, East Orange, N.J., 1956.

Swanson, V. E., and Palacas, J. G., 1965, Humate in coastal sands of northwest Florida: U.S. Geol. Survey Bull. 1214–B, p. B1–B29.

Szalay, A., 1957, The role of humus in the geochemical enrichment of U in coal and other bioliths: Acad. Sci. Hungaricae, Acta Physica, v. 8, p. 25–35.

Vine, J. D., Swanson, V. E., and Bell, K. G., 1958, The role of humic acids in the geochemistry of uranium: Second Internat. Conf. on Peaceful Uses of Atomic Energy Proc., Geneva, v. 2, p. 187–191.

Wallace, Arthur, ed., 1956, Symposium on the use of metal chelates in plant nutrition: Palo Alto, Calif., The National Press, 80 p.

# NEW ISOTOPIC MEASUREMENTS OF COLORADO ORE LEADS

By M. H. DELEVAUX, A. P. PIERCE, and J. C. ANTWEILER,
Denver, Colo.

*Abstract.*—Seventy-six mass spectrometric analyses were made by electron bombardment of $PbI_2$, during which 36 runs on a lead reference sample, GS/4, showed standard deviations from the mean for isotopic ratios of 206/204, 206/207, and 206/208 of 0.21 percent, 0.09 percent, and 0.11 percent, respectively. Ten samples were mass spectrometrically analyzed by thermal emission of PbS, during which 18 runs on the same reference sample showed percent standard deviations in the three ratios of 0.12 percent, 0.06 percent, and 0.12 percent, respectively. In contrast, the range in natural variations was many times greater: from the Yule marble quarry, Gunnison County, the isotopic ratios were 206/204=24.15, 207/204=16.24, and 208/204=41.62, compared to 15.76, 15.35, and 35.42 in a sample from the High Lonesome mine in Grand County.

The present study was undertaken to extend knowledge of isotopic variations in lead minerals of ore deposits in central Colorado. A previous study of isotopic compositions of galena from 12 deposits in this region was made by Phair and Mela (1956), and isotopic analyses of galena from several other deposits are listed by Bate and others (1960). Their early data showed significant isotopic variations in $Pb^{206}$, $Pb^{207}$, and $Pb^{208}$ among the samples analyzed. However, analytical uncertainty in measurements of $Pb^{204}$ was large and was a limiting factor in interpretation of the data. In the present study a reference sample, GS/4, was analyzed repeatedly along with the unknowns to establish the degree of precision. Interlaboratory reference samples that have been analyzed (Delevaux, 1963) also permit the data to be compared with results of other laboratories.

## SAMPLE INFORMATION

The samples analyzed in this study were in part collected by us, in collaboration with R. S. Cannon, Jr., and K. L. Buck, of the U.S. Geological Survey. The remainder were donated by colleagues in the Geological Survey or in the mining industry. Our principal objective in sampling was to ascertain the isotopic varieties and range in isotopic composition of Colorado ore lead. This objective was met by sampling (1) deposits inside and outside the Colorado mineral belt, (2) deposits of presumed Precambrian age and presumed Tertiary age, and (3) deposits in diverse—sedimentary, igneous, and metamorphic—geologic settings. Sample locations are plotted in a general way on the sample locality map (fig. 1), and are given more specifically, by longitude and latitude, in table 1.

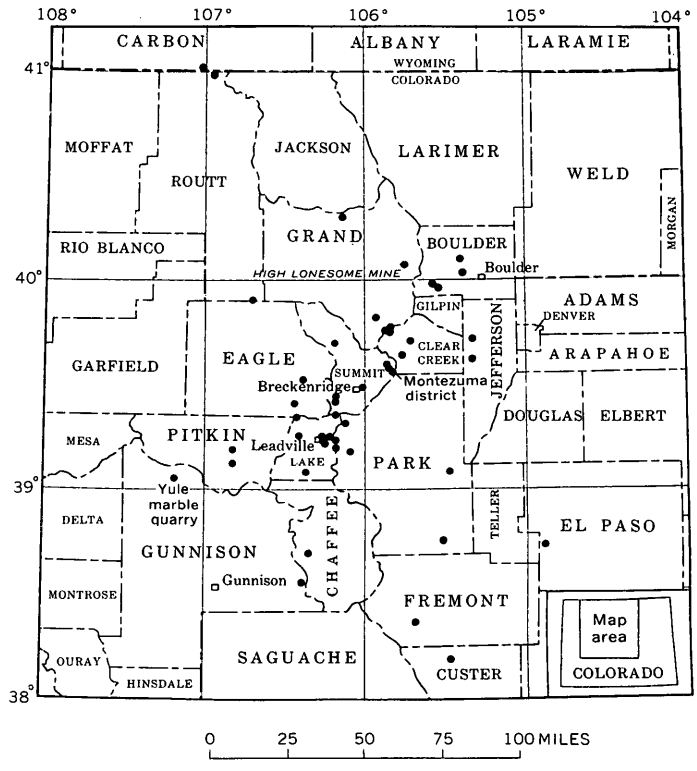


FIGURE 1.—Map of part of Colorado, showing location of mining centers or districts (dots) from which samples were collected for isotopic analysis of lead in ore minerals.

TABLE 1.—*New isotopic measurements of Colorado ore leads*

[First six samples prepared by George Phair; sample descriptions given in Phair and Mela (1956). All other samples prepared by J. C. Antweiler, A. P. Pierce, R. S. Cannon, Jr., and K. L. Buck]

| Sample No. | Date | County (in Colorado, except as noted) | District or mine | Location | | $\frac{Pb^{206}}{Pb^{204}}$ | $\frac{Pb^{207}}{Pb^{204}}$ | $\frac{Pb^{208}}{Pb^{204}}$ | $\frac{Pb^{206}}{Pb^{207}}$ | $\frac{Pb^{206}}{Pb^{208}}$ |
|---|---|---|---|---|---|---|---|---|---|---|
| | | | | N. lat. | W. long. | | | | | |
| **A. Electron bombardment method, using $PbI_2$** | | | | | | | | | | |
| GS/3 | 7/25/62 | Boulder | Caribou | 39°59′ | 105°34′ | 17. 53 | 15. 64 | 38. 56 | 1. 121 | 0. 4547 |
| GS/266 | 7/27/62 | Clear Creek | Silver Plume | 39°42′ | 105°44′ | 17. 86 | 15. 65 | 39. 31 | 1. 141 | . 4545 |
| GS/268 | 1/14/63 | Fremont | Cotopaxi | 38°22′ | 105°42′ | 15. 83 | 15. 38 | 35. 61 | 1. 029 | . 4444 |
| GS/269 | 2/ 4/63 | Park | Guffey | 38°45′ | 105°31′ | 15. 93 | 15. 44 | 35. 62 | 1. 032 | . 4472 |
| GS/274 | 7/26/62 | Clear Creek | Waldorf | 39°39′ | 105°46′ | 18. 66 | 15. 66 | 39. 42 | 1. 191 | . 4732 |
| GS/277 | 1/30/63 | El Paso | Stove Mountain | 38°45′ | 104°55′ | 16. 90 | 15. 56 | 36. 77 | 1. 086 | . 4596 |
| DSw205 | 3/29/62 | Lake | Homestake | 39°21′ | 106°26′ | 18. 79 | 15. 79 | 38. 75 | 1. 190 | . 4849 |
| 206 | 3/30/62 | Jefferson | Augusta lode | 39°37′ | 105°19′ | 17. 76 | 15. 70 | 38. 94 | 1. 131 | . 4561 |
| 208 | 4/ 3/62 | Park | Boomer | 39°05′ | 105°27′ | 16. 91 | 15. 57 | 36. 87 | 1. 086 | . 4586 |
| 210 | 4/ 5/62 | Summit | Kokomo | 39°25′ | 106°11′ | 18. 19 | 15. 71 | 38. 72 | 1. 158 | . 4698 |
| 211 | 4/ 6/62 | Grand | St. Louis | 39°50′ | 105°56′ | 15. 88 | 15. 41 | 35. 55 | 1. 031 | . 4466 |
| 212 | 4/ 9/62 | do | do | 39°50′ | 105°56′ | 15. 93 | 15. 44 | 35. 63 | 1. 032 | . 4472 |
| 213 | 4/10/62 | Chaffee | Mary Murphy | 38°42′ | 106°21′ | 17. 93 | 15. 66 | 38. 41 | 1. 145 | . 4669 |
| 215 | 4/12/62 | Custer | Bull Domingo | 38°11′ | 105°28′ | 17. 55 | 15. 59 | 37. 32 | 1. 126 | . 4703 |
| 216 | 4/13/62 | Eagle | Morning | 39°24′ | 106°26′ | 17. 38 | 15. 60 | 38. 24 | 1. 114 | . 4543 |
| 217 | 4/16/62 | do | Gold Park claims | 39°24′ | 106°26′ | 17. 51 | 15. 66 | 38. 42 | 1. 118 | . 4558 |
| 218 | 4/17/62 | do | do | 39°24′ | 106°26′ | 17. 50 | 15. 65 | 38. 40 | 1. 118 | . 4556 |
| 220 | 5/21/62 | do | do | 39°24′ | 106°26′ | 17. 52 | 15. 65 | 38. 44 | 1. 119 | . 4556 |
| 221 | 5/22/62 | do | Yarmony | 39°55′ | 106°41′ | 21. 97 | 16. 12 | 40. 02 | 1. 363 | . 5490 |
| 223 | 5/24/62 | Lake | Homestake | 39°21′ | 106°26′ | 18. 87 | 15. 82 | 38. 83 | 1. 193 | . 4861 |
| 224 | 5/25/62 | Custer | Bull Domingo | 38°11′ | 105°28′ | 17. 63 | 15. 68 | 37. 56 | 1. 124 | . 4694 |
| 225 | 5/28/62 | Park | Boomer | 39°05′ | 105°27′ | 17. 00 | 15. 63 | 37. 08 | 1. 088 | . 4585 |
| 226 | 5/29/62 | Clear Creek | Urad | 39°45′ | 105°50′ | 17. 85 | 15. 70 | 40. 00 | 1. 138 | . 4464 |
| 228 | 6/ 1/62 | Eagle | Gilman | 39°32′ | 106°24′ | 17. 80 | 15. 65 | 38. 75 | 1. 137 | . 4593 |
| 229 | 6/ 4/62 | do | do | 39°32′ | 106°24′ | 17. 92 | 15. 66 | 38. 75 | 1. 144 | . 4624 |
| 230 | 6/ 5/62 | Lake | Climax | 39°22′ | 106°10′ | 17. 96 | 15. 68 | 38. 69 | 1. 145 | . 4644 |
| 231 | 6/ 6/62 | do | do | 39°22′ | 106°10′ | 18. 12 | 15. 65 | 38. 85 | 1. 157 | . 4663 |
| 233 | 6/20/62 | do | Leadville | 39°13′ | 106°14′ | 18. 18 | 15. 71 | 38. 89 | 1. 157 | . 4673 |
| 234 | 6/21/62 | do | do | 39°13′ | 106°14′ | 18. 00 | 15. 66 | 38. 71 | 1. 150 | . 4650 |
| 235 | 6/25/62 | do | do | 39°13′ | 106°14′ | 18. 29 | 15. 67 | 38. 82 | 1. 167 | . 4711 |
| 236 | 6/26/62 | do | Sugarloaf | 39°15′ | 106°24′ | 17. 84 | 15. 65 | 38. 80 | 1. 139 | . 4597 |
| 238 | 6/28/62 | Summit | Roberts Tunnel | 39°36′ | 105°52′ | 18. 13 | 15. 71 | 38. 82 | 1. 154 | . 4670 |
| 239 | 6/29/62 | do | do | 39°35′ | 105°51′ | 18. 14 | 15. 70 | 38. 90 | 1. 156 | . 4664 |
| 240 | 7/ 2/62 | do | do | 39°35′ | 105°51′ | 18. 08 | 15. 63 | 38. 73 | 1. 157 | . 4668 |
| 241 | 7/ 3/62 | do | do | 39°34′ | 105°51′ | 18. 11 | 15. 67 | 38. 78 | 1. 156 | . 4671 |
| 243 | 7/ 6/62 | do | do | 39°34′ | 105°50′ | 18. 08 | 15. 66 | 38. 74 | 1. 155 | . 4666 |
| 244 | 7/ 9/62 | Lake | Climax | 39°22′ | 106°10′ | 18. 08 | 15. 63 | 38. 67 | 1. 157 | . 4676 |
| 245 | 7/10/62 | Routt | Elkhorn | 40°59′ | 106°57′ | 16. 20 | 15. 44 | 35. 63 | 1. 049 | . 4545 |
| 246 | 7/11/62 | Lake | Leadville | 39°14′ | 106°16′ | 18. 00 | 15. 65 | 38. 72 | 1. 150 | . 4649 |
| 248 | 7/30/62 | do | do | 39°15′ | 106°16′ | 18. 00 | 15. 66 | 38. 68 | 1. 150 | . 4653 |
| 249 | 7/31/62 | do | do | 39°15′ | 106°14′ | 18. 10 | 15. 68 | 38. 71 | 1. 154 | . 4676 |
| 250 | 8/ 1/62 | do | do | 39°15′ | 106°16′ | 17. 99 | 15. 65 | 38. 76 | 1. 149 | . 4642 |
| 251 | 8/ 2/62 | do | do | 39°16′ | 106°13′ | 18. 36 | 15. 69 | 38. 88 | 1. 170 | . 4723 |
| 253 | 8/20/62 | Park | Hilltop | 39°13′ | 106°10′ | 20. 45 | 15. 86 | 39. 97 | 1. 290 | . 5116 |
| 254 | 8/21/62 | do | do | 39°13′ | 106°10′ | 20. 69 | 15. 87 | 40. 09 | 1. 304 | . 5162 |
| 255 | 8/22/62 | Carbon (Wyo.) | Three Forks prospect. | 41°01′ | 107°01′ | 16. 36 | 15. 44 | 35. 65 | 1. 059 | . 4588 |
| | 1/10/63 | do | do | 41°01′ | 107°01′ | 16. 37 | 15. 45 | 35. 64 | 1. 059 | . 4592 |
| 258 | 11/16/62 | Boulder | Nederland | 39°58′ | 105°32′ | 17. 65 | 15. 58 | 38. 79 | 1. 133 | . 4549 |
| 259 | 11/19/62 | Lake | Climax | 39°22′ | 106°10′ | 17. 76 | 15. 64 | 38. 59 | 1. 135 | . 4602 |
| 260 | 11/20/62 | do | do | 39°22′ | 106°10′ | 18. 14 | 15. 65 | 38. 71 | 1. 159 | . 4686 |
| 261 | 11/21/62 | Boulder | Caribou | 39°59′ | 105°34′ | 17. 53 | 15. 60 | 38. 51 | 1. 124 | . 4553 |
| 263 | 11/30/62 | do | do | 39°59′ | 105°34′ | 17. 53 | 15. 60 | 38. 46 | 1. 124 | . 4557 |
| 264 | 12/ 3/62 | do | do | 39°59′ | 105°34′ | 17. 59 | 15. 60 | 38. 61 | 1. 127 | . 4555 |
| 265 | 12/ 4/62 | do | do | 39°59′ | 105°34′ | 17. 57 | 15. 62 | 38. 54 | 1. 125 | . 4559 |
| 266 | 12/ 5/62 | do | do | 39°59′ | 105°34′ | 17. 53 | 15. 61 | 38. 54 | 1. 122 | . 4548 |
| 269 | 12/28/62 | Clear Creek | Urad | 39°45′ | 105°50′ | 17. 80 | 15. 64 | 40. 06 | 1. 138 | . 4442 |
| 270 | 12/27/62 | El Paso | Valjean claim | 38°45′ | 104°53′ | 16. 80 | 15. 49 | 36. 62 | 1. 084 | . 4587 |
| 271 | 1/ 2/63 | Summit | Breckenridge | 39°29′ | 106°02′ | 18. 38 | 15. 69 | 38. 65 | 1. 171 | . 4755 |
| 273 | 1/ 3/63 | do | do | 39°29′ | 106°02′ | 18. 37 | 15. 65 | 38. 52 | 1. 174 | . 4770 |
| 274 | 1/ 7/63 | do | do | 39°29′ | 106°02′ | 18. 35 | 15. 65 | 38. 52 | 1. 173 | . 4764 |

TABLE 1.—*New isotopic measurements of Colorado ore leads*—Continued

[First six samples prepared by George Phair; sample descriptions given in Phair and Mela (1956). All other samples prepared by J. C. Antweiler, A. P. Pierce, R. S. Cannon, Jr., and K. L. Buck]

| Sample No. | Date | County (in Colorado, except as noted) | District or mine | Location | | $\frac{Pb^{206}}{Pb^{204}}$ | $\frac{Pb^{207}}{Pb^{204}}$ | $\frac{Pb^{208}}{Pb^{204}}$ | $\frac{Pb^{206}}{Pb^{207}}$ | $\frac{Pb^{206}}{Pb^{208}}$ |
|---|---|---|---|---|---|---|---|---|---|---|
| | | | | N. lat. | W. long. | | | | | |
| **A. Electron bombardment method, using $PbI_2$—Continued** | | | | | | | | | | |
| 275 | 1/ 8/63 | do | do | 39°29′ | 106°02′ | 18.38 | 15.65 | 38.54 | 1.175 | .4768 |
| 307 | 2/ 8/63 | do | Montezuma | 39°34′ | 105°50′ | 18.15 | 15.69 | 38.82 | 1.157 | .4676 |
| 308 | 2/ 9/63 | do | do | 39°34′ | 105°52′ | 18.10 | 15.68 | 38.73 | 1.154 | .4672 |
| 309 | 2/11/63 | Jefferson | Hosa Lodge prospect. | 39°43′ | 105°19′ | 15.96 | 15.45 | 35.69 | 1.033 | .4471 |
| 310 | 2/12/63 | Grand | High Lonesome | 40°04′ | 105°44′ | 15.76 | 15.35 | 35.42 | 1.027 | .4450 |
| 312 | 2/13/63 | Summit | Boss | 39°42′ | 106°11′ | 18.51 | 15.71 | 38.69 | 1.178 | .4784 |
| 313 | 2/14/63 | Clear Creek | Jean | 39°45′ | 105°52′ | 17.78 | 15.62 | 40.83 | 1.138 | .4354 |
| 314 | 2/18/63 | do | Woods Creek adit | 39°46′ | 105°50′ | 18.49 | 15.78 | 40.98 | 1.172 | .4513 |
| 315 | 2/19/63 | Park | Hilltop | 39°13′ | 106°10′ | 20.81 | 15.95 | 40.43 | 1.305 | .5148 |
| 317 | 2/20/63 | do | Sheep Mountain | 39°12′ | 106°05′ | 20.62 | 15.92 | 40.15 | 1.295 | .5136 |
| 318 | 2/21/63 | Lake | Leadville | 39°14′ | 106°10′ | 19.10 | 15.79 | 39.45 | 1.210 | .4843 |
| 319 | 2/28/63 | Boulder | Nederland | 40°02′ | 105°23′ | 18.71 | 15.72 | 39.09 | 1.190 | .4787 |
| 320 | 3/ 2/63 | Gunnison | Tomichi | 38°33′ | 106°23′ | 18.32 | 15.65 | 38.61 | 1.170 | .4744 |
| 322 | 3/ 3/63 | do | Yule | 39°03′ | 107°11′ | 24.15 | 16.24 | 41.62 | 1.487 | .5803 |
| 323 | 3/ 4/63 | Pitkin | Aspen | 39°08′ | 106°49′ | 18.00 | 15.65 | 38.24 | 1.150 | .4707 |
| 333 | 2/25/63 | Lake | Homestake | 39°21′ | 106°26′ | 18.86 | 15.81 | 38.84 | 1.193 | .4856 |
| 334 | 2/26/63 | Jefferson | Augusta Lode | 39°37′ | 105°19′ | 17.76 | 15.70 | 38.93 | 1.131 | .4562 |
| **B. Thermal emission method, using PbS** | | | | | | | | | | |
| DSw319 | 8/19/63 | Boulder | Nederland | 40°02′ | 105°23′ | 18.67 | 15.71 | 39.13 | 1.188 | .4772 |
| | 9/ 5/63 | | | | | 18.64 | 15.66 | 38.97 | 1.190 | .4783 |
| 320 | 9/ 6/63 | Gunnison | Tomichi | 38°33′ | 106°23′ | 18.22 | 15.58 | 38.44 | 1.169 | .4739 |
| | 9/21/63 | | | | | 18.33 | 15.73 | 38.85 | 1.165 | .4717 |
| | 9/26/63 | | | | | 18.28 | 15.67 | 38.66 | 1.167 | .4728 |
| 322 | 8/21/63 | do | Yule Marble | 39°03′ | 107°11′ | 24.09 | 16.21 | 41.65 | 1.486 | .5784 |
| | 9/ 6/63 | | | | | 24.09 | 16.22 | 41.66 | 1.485 | .5784 |
| 323 | 8/22/63 | Pitkin | Aspen | 39°08′ | 106°49′ | 17.98 | 15.66 | 38.40 | 1.148 | .4682 |
| | 9/ 9/63 | | | | | 17.98 | 15.65 | 38.35 | 1.148 | .4687 |
| 324 | 8/ 7/63 | Summit | Kokomo | 39°26′ | 106°11′ | 18.17 | 15.65 | 38.73 | 1.161 | .4692 |
| | 9/10/63 | | | | | 18.19 | 15.65 | 38.67 | 1.162 | .4705 |
| 325 | 8/ 8/63 | Pitkin | Aspen | 39°12′ | 106°49′ | 18.25 | 15.63 | 38.45 | 1.167 | .4745 |
| | 9/24/63 | | | | | 18.28 | 15.68 | 38.55 | 1.166 | .4741 |
| 327 | 9/12/63 | Park | Alma | 39°19′ | 106°07′ | 17.82 | 15.58 | 38.47 | 1.144 | .4632 |
| | 9/23/63 | | | | | 17.90 | 15.68 | 38.80 | 1.142 | .4614 |
| 328 | 8/14/63 | Boulder | Jamestown | 40°06′ | 105°24′ | 17.71 | 15.68 | 39.00 | 1.130 | .4540 |
| | 9/13/63 | | | | | 17.66 | 15.62 | 38.84 | 1.131 | .4548 |
| 329 | 8/15/63 | Lake | Twin Lakes | 39°05′ | 106°23′ | 17.72 | 15.57 | 38.15 | 1.138 | .4643 |
| | 9/18/63 | | | | | 17.74 | 15.59 | 38.27 | 1.137 | .4635 |
| 330 | 9/19/63 | Grand | Parkview Mountain prospect. | 40°19′ | 106°08′ | 17.92 | 15.67 | 37.84 | 1.144 | .4735 |
| | 9/25/63 | | | | | 17.91 | 15.66 | 37.79 | 1.144 | .4740 |

Detailed descriptions of the samples are reserved for subsequent publications which will deal with geologic interpretations. All the samples are galena, with or without other primary sulfides, excepting samples DSw254 (anglesite) and DSw319 (trace lead concentrated by acid extraction of a tungsten ore specimen).

## PREPARATION OF SAMPLES

Galena concentrates or other lead minerals of high mineralogic purity were obtained from all samples where possible; a limited amount of material containing sparse or trace amounts of lead minerals is all that was available for a few samples. A mineralogically pure lead mineral was obtained from some samples by handpicking, drilling, or sawing. In many of the samples, however, the galena was too fine grained for handpicking and was separated by a two-step procedure that consisted of removing light minerals by floating in bromoform, followed by heavy-liquid superpanning of the heavy minerals in a closed tube. A few samples were purified by other techniques such as electromagnetic separation, or selective solution of impurities—as, for example, dissolving away carbonate impurities with 10-percent formic acid.

Some galena concentrates were cleaned with 10-percent potassium hydroxide to remove cerussite or other oxidation products.

Mineralogically pure lead minerals were further purified chemically by the method described by Antweiler (1963). That method consists of dissolution of the lead mineral in hot dilute (1:1 v/v) nitric acid followed by four precipitations of lead nitrate in very strong (sp gr 1.42 or higher) nitric acid, and conversion of the purified lead nitrate to iodide or to sulfide for isotopic analysis. The lead compound analyzed was lead iodide in samples DSw205 through DSw318 and in DSw333 and DSw334 (table 1*A*). Lead sulfide was analyzed in samples DSw324 through DSw330 (table 1*B*). Both compounds were analyzed for samples DSw319 through 323.

The effects of impurities on lead-isotope analyses are not definitely known, but were minimized in the present work by the combination of mineralogic and chemical purification techniques that resulted in ore-lead samples of exceptionally high purity. A few analyses were made on samples of somewhat lesser purity. The first four samples, DSw205 through DSw210, were prepared before the nitrate method (Antweiler, 1963) was developed. The quantity of lead available in two samples, DSw246 and DSw319, was so small that only 1 precipitation in nitric acid rather than the usual 4 was made.

## MASS SPECTROMETRY

All the samples in this study were analyzed by M. H. Delevaux in the Washington laboratory of the U.S. Geological Survey. Most of the samples (table 1) were analyzed from March 1962 to February 1963 on the mass spectrometer previously described by Delevaux (1963). This was a 12-inch radius, 60° sector Nier-type mass spectrometer using electron bombardment of $PbI_2$. The data were taken from a strip-chart recorder, and each ratio represents the average of four measurements of the $PbI^+$ signal. All measurements were taken using magnetic scanning and accelerating potential of 4,500 volts and at pressures below $10^{-6}$ mm of mercury. Ion currents, measured by a vibrating-reed electrometer, were usually of the order of magnitude of $2 \times 10^{-11}$ amperes. For each analysis four double scans of the $PbI^+$ spectrum were made. Resolution in terms of the ratio of $Pb^{207}$ peak to $Pb^{208}$ -$Pb^{207}$ valley was usually in the range of 250 to 300.

Ten samples were analyzed later (table 1*B*), in August and September 1963, on a mass spectrometer newly assembled for the Geological Survey in Washington by W. R. Shields of the National Bureau of Standards. This instrument is a 12-inch radius, 68° sector, solid-source mass spectrometer which uses thermal emission of $Pb^+$ ions from a single tantalum filament on which samples were loaded as PbS. The data were taken from a strip-chart recorder, and each ratio represents an average of six measurements. All measurements were taken using the peak-hopping method at an accelerating potential of 10,000 volts and a pressure below $2 \times 10^{-7}$ mm of mercury. Ion currents were usually of the order of magnitude of $8 \times 10^{-12}$ amperes, as measured by a vibrating-reed electrometer. Resolution in terms of the ratio of $Pb^{207}$ peak to $Pb^{208}$ -$Pb^{207}$ valley was greater than 5,000.

## PRECISION AND PROBLEMS IN MEASUREMENT

### Reproducibility of reference sample GS/4

The Geological Survey reference sample GS/4 was analyzed repeatedly during the course of the study in order to control the quality of the measurements. The reference sample was analyzed 36 times as $PbI_2$, from March 15, 1962 to February 27, 1963 (table 2*A*), and 18 times as PbS, from August 22, 1963 to January 16, 1964 (table 2*B*).

The variations in the measurement of GS/4 reference sample as observed within individual runs are less than variations observed between runs. Therefore the quality of the data is best tested in terms of variations observed between runs. The mean and the standard deviations (table 3) for 36 $PbI_2$ measurements were $16.27 \pm 0.03_4$, $1.0487 \pm 0.0009_6$, and $0.4507 \pm 0.0004_9$ for $Pb^{206}/Pb^{204}$, $Pb^{206}/Pb^{207}$, and $Pb^{206}/Pb^{208}$ ratios, respectively. For the 18 PbS runs the corresponding means and standard deviations were $16.21 \pm 0.01_9$, $1.0472 \pm 0.0006_6$, and $0.4496 \pm 0.0005_2$, respectively. Maximum deviations observed in each of these two sets of data are about plus or minus two standard deviations. The probability that an error this large will occur between single analyses of 2 unknowns analyzed under the same conditions is less than 1 percent.

The mean values for GS/4 (table 3) by electron bombardment and by thermal emission on Ta filament are in reasonably good agreement. Mean values for the sulfide runs, however, are lower than the mean values for the iodide runs for these ratios by the following amounts: for $Pb^{206}/Pb^{204}$ by 0.056; for $Pb^{206}/Pb^{207}$ by 0.0015; and for $Pb^{206}/^{208}$ by 0.00118. Therefore, the two sets of analytical data presumably can be made more comparable by empirically changing one or the other set of analyses by these amounts.

Long-term variations in the data for GS/4 by the lead iodide method show evidence of broad cyclical changes with time, particularly in the ratio $Pb^{206}/Pb^{204}$ (fig. 2). As a result, variations within short periods of time are less than those over the total

TABLE 2.—*Isotopic analyses of USGS lead iodide reference sample GS/4*

| Date of analysis | Isotope ratios | | | Date of analysis | Isotope ratios | | |
|---|---|---|---|---|---|---|---|
| | 206/204 | 206/207 | 206/208 | | 206/204 | 206/207 | 206/208 |
| **A. Electron bombardment method, using $PbI_2$** | | | | | | | |
| 3/15/62 | 16. 26 | 1. 048 | 0. 4504 | 8/28/62 | 16. 24 | 1. 048 | 0. 4504 |
| 3/21/62 | 16. 26 | 1. 048 | . 4506 | 9/7/62 | 16. 26 | 1. 050 | . 4514 |
| 3/28/62 | 16. 28 | 1. 052 | . 4518 | 9/21/62 | 16. 25 | 1. 049 | . 4503 |
| 4/4/62 | 16. 28 | 1. 049 | . 4510 | 10/5/62 | 16. 27 | 1. 047 | . 4508 |
| 4/11/62 | 16. 31 | 1. 049 | . 4506 | 10/16/62 | 16. 26 | 1. 049 | . 4517 |
| 4/18/62 | 16. 30 | 1. 048 | . 4504 | 10/24/62 | 16. 27 | 1. 051 | . 4520 |
| 5/1/62 | 16. 31 | 1. 049 | . 4507 | 11/2/62 | 16. 28 | 1. 050 | . 4513 |
| 5/11/62 | 16. 32 | 1. 049 | . 4504 | 11/3/62 | 16. 24 | 1. 049 | . 4508 |
| 5/18/62 | 16. 29 | 1. 047 | . 4507 | 11/23/62 | 16. 23 | 1. 050 | . 4510 |
| 5/23/62 | 16. 31 | 1. 048 | . 4502 | 12/6/62 | 16. 26 | 1. 050 | . 4513 |
| 5/31/62 | 16. 32 | 1. 048 | . 4510 | 12/14/62 | 16. 20 | 1. 049 | . 4511 |
| 6/7/62 | 16. 28 | 1. 048 | . 4500 | 12/26/62 | 16. 27 | 1. 048 | . 4508 |
| 6/19/62 | 16. 28 | 1. 049 | . 4507 | 1/4/63 | 16. 18 | 1. 049 | . 4505 |
| 6/27/62 | 16. 29 | 1. 048 | . 4506 | 1/15/63 | 16. 25 | 1. 049 | . 4505 |
| 7/5/62 | 16. 24 | 1. 048 | . 4498 | 1/24/63 | 16. 28 | 1. 048 | . 4511 |
| 7/12/62 | 16. 25 | 1. 049 | . 4510 | 2/7/63 | 16. 28 | 1. 049 | . 4504 |
| 7/24/62 | 16. 22 | 1. 049 | . 4507 | 2/15/63 | 16. 31 | 1. 048 | . 4504 |
| 8/17/62 | 16. 19 | 1. 049 | . 4504 | 2/27/63 | 16. 27 | 1. 048 | . 4503 |
| **B. Thermal emission method, using PbS** | | | | | | | |
| 8/22/63 | 16. 20 | 1. 048 | 0. 4499 | 9/3/63 | 16. 19 | 1. 047 | 0. 4500 |
| 8/23/63 | 16. 24 | 1. 046 | . 4488 | 9/16/63 | 16. 22 | 1. 047 | . 4494 |
| 8/26/63 | 16. 22 | 1. 047 | . 4496 | 9/27/63 | 16. 21 | 1. 048 | . 4498 |
| 8/26/63 | 16. 21 | 1. 047 | . 4490 | 10/25/63 | 16. 19 | 1. 048 | . 4495 |
| 8/27/63 | 16. 20 | 1. 048 | . 4498 | 11/7/63 | 16. 17 | 1. 048 | . 4504 |
| 8/28/63 | 16. 21 | 1. 048 | . 4500 | 12/5/63 | 16. 19 | 1. 048 | . 4499 |
| 8/29/63 | 16. 25 | 1. 047 | . 4492 | 1/10/64 | 16. 22 | 1. 046 | . 4486 |
| 8/29/63 | 16. 22 | 1. 046 | . 4490 | 1/13/64 | 16. 20 | 1. 047 | . 4495 |
| 8/30/63 | 16. 21 | 1. 048 | . 4504 | 1/16/64 | 16. 22 | 1. 046 | . 4491 |

TABLE 3.—*Standard deviation on GS/4 lead reference and sample pairs and mean values for GS/4*

| | 206/204 | 207/204 | 208/204 | 206/207 | 206/208 | 204 | 206 | 207 | 208 |
|---|---|---|---|---|---|---|---|---|---|
| **STANDARD DEVIATION Electron bombardment method** | | | | | | | | | |
| $PbI_2$ (avg 36 runs) | $\pm 0.03_4$ | $\pm 0.03_7$ | $\pm 0.08_5$ | $\pm 0.0009_6$ | $\pm 0.0004_9$ | $\pm 0.003_2$ | $\pm 0.01_7$ | $\pm 0.01_3$ | $\pm 0.02_2$ |
| $PbI_2$ (4 pairs) | $\pm .02_5$ | $\pm .01_9$ | $\pm .06_4$ | $\pm .0003_8$ | $\pm .0004_4$ | $\pm .001_7$ | $\pm .01_1$ | $\pm .01_4$ | $\pm .02_8$ |
| **Thermal emission method** | | | | | | | | | |
| PbS Ta filament (avg 18 runs) | $\pm 0.01_9$ | $\pm 0.02_6$ | $\pm 0.07_6$ | $\pm 0.0006_6$ | $\pm 0.0005_2$ | $\pm 0.002_5$ | $\pm 0.01_7$ | $\pm 0.00_6$ | $\pm 0.02_3$ |
| PbS Ta filament (10 pairs) | $\pm .03_2$ | $\pm .04_3$ | $\pm .13$ | $\pm .0012$ | $\pm .007_8$ | $\pm .003_7$ | $\pm .03_1$ | $\pm .00_8$ | $\pm .03_3$ |
| **MEAN VALUES FOR GS/4** | | | | | | | | | |
| $PbI_2$ (avg 36 runs) | 16. 27 | 15. 51 | 36. 09 | 1. 0487 | 0. 4507 | 1. 452 | 23. 62 | 22. 52 | 52. 40 |
| PbS Ta filament (avg 18 runs) | 16. 21 | 15. 48 | 36. 06 | 1. 0472 | 4496 | 1. 455 | 23. 58 | 22. 52 | 52. 45 |

NOTE.—Formula for standard deviation: $s = \pm \sqrt{\frac{\Sigma\, dx^2}{n-1}}$

period of time. The total variation in $Pb^{206}/Pb^{204}$ ratios during the course of this study was about 0.8 percent, but within intervals of 1 month the total variations were about 0.4 percent or less.

Measurement errors for reference sample GS/4 can be examined in terms of coefficients of variation, that is, standard deviations expressed as percent of the average values of measured atom ratios or abundances. In figure 3 such coefficients of variation are plotted against mass of the ions measured by the two analytical methods. The analytical uncertainties for ratio measurements by the thermal emission method correlate with difference in mass (fig. 3*A*) and evidently reflect mass-dependent fractionation in the ion source. No such correlation is observed for the $PbI_2$ data (fig. 3A). Analytical uncertainties for abundance measurements by the two methods (fig. 3*B*) are nearly comparable. Each method shows a more or less similar decrease in measurement error with increasing ion mass. This decrease we attribute primarily to corresponding differences in atom abundance—there is a general tendency for the relative error to be greatest in measuring the latest abundant isotope, $Pb^{204}$, and smallest in measuring the most abundant isotope, $Pb^{208}$.

### Use of replicate analyses in checking precision of measurements

Another test of the quality of data obtained in the course of this study is provided by replicate analyses of splits of a given chemical preparation of an ore-lead sample. All 10 ore-lead samples analyzed by thermal emission of PbS were run in duplicate on different days, starting from the prepared $PbI_2$; one sample was run in triplicate. Ten sets of replicate analyses of PbS samples (table 3) have standard deviations of $\pm 0.03_2$, $\pm 0.001_2$, and $\pm 0.0007_8$, for the $Pb^{206}/Pb^{204}$, $Pb^{206}/Pb^{207}$, and $Pb^{206}/Pb^{208}$ ratios, re-

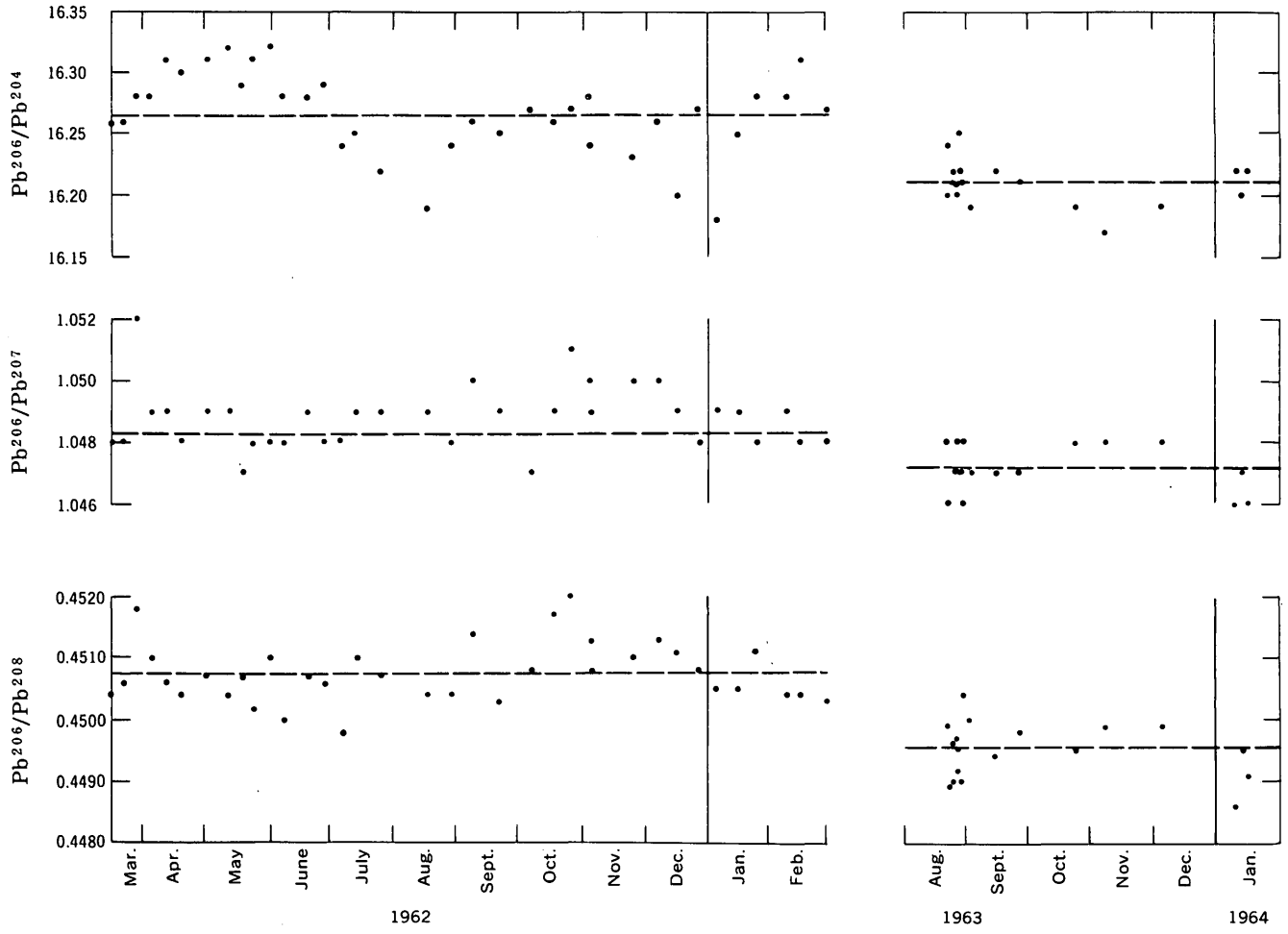


FIGURE 2.—Variations of $Pb^{206}/Pb^{204}$, $Pb^{206}/Pb^{207}$, and $Pb^{206}/Pb^{208}$ ratios of reference sample GS/4 with time.

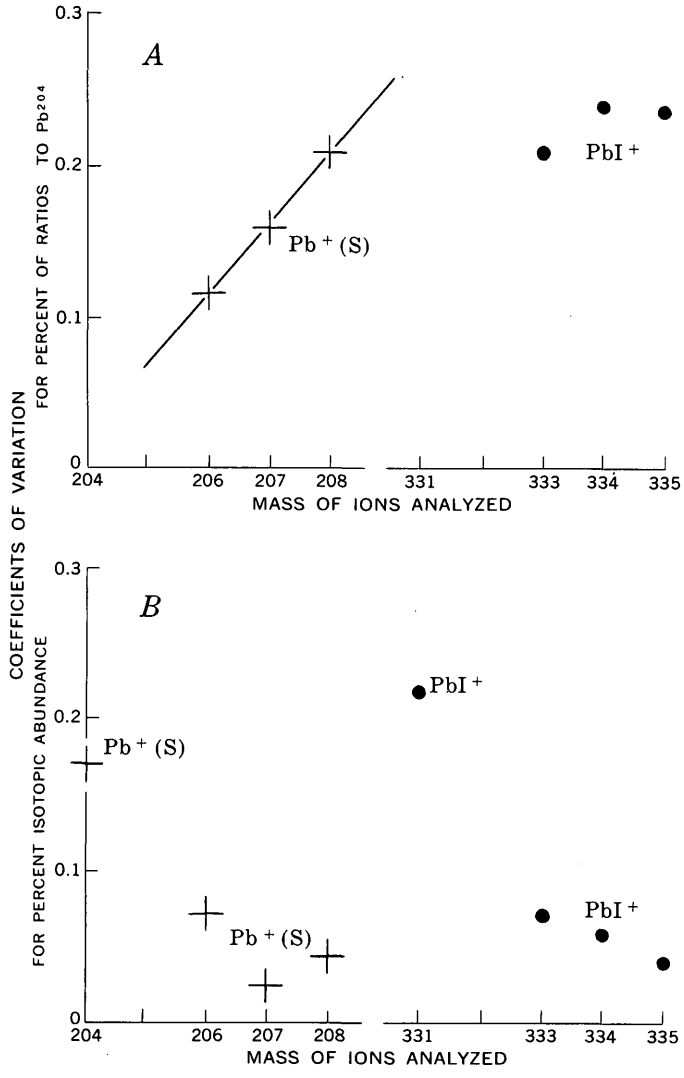


FIGURE 3.—Analytical uncertainty for reference sample GS/4 in terms of coefficients of variation (that is, standard deviations expressed as mean values of quantity measured) correlated for the thermal emission ($PbS$) and electron bombardment ($PbI_2$) methods. *A*, coefficient of variation for percent of ratios to $Pb^{204}$ plotted against ion mass; *B*, coefficient of variation for percent isotopic abundance plotted against ion mass.

spectively. By the electron bombardment method, however, only four iodides were analyzed in duplicate or triplicate. Deviations for four sets of replicate analyses of $PbI_2$ samples are within limits equivalent to the standard deviations for GS/4.

### Effects of chemical impurities and nonrepresentative sampling on measurements

In addition to the kinds of measurement errors described above, other variations may result from chemical impurities passed on from the sample or from nonrepresentative sampling of a given mineral concentrate due to unsuspected inhomogeneities. Only a few tests have been made of the possible effects of chemical impurities. Two pairs of samples (DSw205, and 333; DSw206 and 334) represent analyses of iodides that were of different chemical purity. They were prepared by different chemical methods from splits of one vial of galena concentrate. The variations in their isotopic analyses are equal to or less than standard deviations for GS/4. This inconclusive evidence does not imply that variations due to chemical impurities are unlikely—more experiments are necessary to reach a valid conclusion.

Two pairs of analyses (DSw215 and 224; DSw205 and 223) represent attempts to obtain representative samples by two different sampling procedures. These pairs of iodides were prepared from different galena concentrates made from a single hand specimen by handpicking and by superpanning. Differences within pairs were measured ranging from less than 1 to about 3 times the standard deviation for GS/4. The largest differences appear to be real, at the 95-percent confidence level. These observations indicate a probability that real isotopic variations existed within the hand specimen, and they point out the need for greater attention to the problems of sampling a hand specimen, including the need for preparing multiple samples from each specimen tested.

In our investigation of Colorado ore leads we devised three experiments to test for natural variations in a single hand specimen. Small variations were found in two of these experiments, and larger variations were found in the third. The first experiment was made with analyses DSw264, 265 and 266 of three samples of galena taken progressively within an interval of 0 to 2 cm from a pitchblende layer in an ore specimen from the Caribou mine. The observed $Pb^{206}/Pb^{204}$ ratios decrease away from the pitchblende layer, but the magnitude of this effect is less than two standard deviations. On the other hand, variations in $Pb^{206}/Pb^{207}$ ratios equal four standard deviations. The latter difference is an indication of real variations, at the 99-percent confidence level. In the second experiment, a similar analytical result arose from our attempt to sample a single galena crystal, 2 × 1.5 × 1 in., from Breckenridge, Colo. Four samples of this crystal, 2 from the interior (DSw275, 273) and 2 from the outermost "skin" (DSw271, 274) show no analytically significant variation in $Pb^{206}/Pb^{204}$ ratios. However, the $Pb^{206}/Pb^{207}$ ratios from the outer skin samples are lower than those of samples from the interior of the crystal. This suggests that $Pb^{206}$ was less abundant in the latest lead to deposit on this crystal. The difference between the average of the skin samples and the average of the interior samples indicates that the variations are real,

at the 95-percent confidence level. The third experiment showed larger variations. Analyses of a galena core (DSw253) and of anglesite (DSw254) in concentric shells replacing galena differ in ratios of $Pb^{206}/Pb^{204}$ and $Pb^{206}/Pb^{207}$ by about 6 and 12 standard deviations respectively, showing that the anglesite is richer in $Pb^{206}$ (by about $1.0 \pm 0.2$ percent).

In a previous study made on a large galena crystal from Picher, Okla., we found variations ranging up to 11 times the comparable standard deviations for GS/4 between growth zones (Cannon, Pierce, and Delevaux, 1963; Cannon, Buck, and Pierce, 1963).

The above experiments demonstrate that significant isotopic variations may exist even in hand specimens of ores. The magnitude of such variations must be assessed before variations within a mine, district, or region can be correctly interpreted. Improvement in sampling procedures is needed to profit fully from these variations, and further profit can be realized through improvement in analytical techniques.

## RESULTS

Measurable isotopic differences were found in samples from nearly every district sampled in the present study. These range from differences in $Pb^{206}/Pb^{204}$ ratios as large as 15 percent in 13 samples in and near the Leadville district to differences less than analytical error in 7 samples from the Montezuma district. In the latter example, the 7 samples from the vicinity of the Montezuma quartz monzonite stock differed in $Pb^{206}/Pb^{204}$ ratios from the average by less than the standard deviation for GS/4. Five of these samples (DSw238, 239, 240, 241, and 243, table 1) were taken at intervals through a 2-mile traverse in a water tunnel penetrating a Tertiary stock, and two samples (DSw307 and 308) are from ore deposits located in Precambrian gneiss 2,000 and 4,000 feet, respectively, above the tunnel. A statistical test of tunnel samples versus mine samples indicates that the two mean compositions are the same at the 60– to 80-percent confidence level.

Analytical results obtained in the investigation (table 1) are plotted in figure 4 (p. C186), which shows the variations in abundance of $Pb^{206}$, $Pb^{207}$, and $Pb^{208}$, relative to $Pb^{204}$, owing to additions of radiogenic lead to preexisting lead in geological sources where the ore lead originated. Curves that approximate isotopic variations observed in "ordinary" ore lead (Cannon and others, 1962) are shown for comparison.

The magnitude of the isotopic variations found in the investigation is unusually large. Perhaps the most fundamental contribution that these data provide is the demonstration that ore leads within a limited portion of a single geologic province can vary this widely in isotopic composition. Such isotopic variations imply significant differences in geologic and geochemical history. These relationships will be examined in more detail and interpretations will be attempted in subsequent reports.

## REFERENCES

Antweiler, J. C., 1963, Chemical preparation of samples for lead isotope analysis: Art. 102 *in* U.S. Geol. Survey Prof. Paper 475–C, p. C166–C170.

Bate, G. L., Gast, P. W., Kulp, J. L., and Miller, D. S., *in* Russell, R. D., and Farquhar, R. M., 1960, Lead isotopes in geology: New York and London, Interscience Publishers Inc., 243 p.

Cannon, R. S., Jr., Buck, K. L., and Pierce, A. P., 1963, Sampling a zoned galena crystal for lead isotope study: Art. 199 *in* U.S. Geol. Survey Prof. Paper 450–E, p. E73–E77.

Cannon, R. S., Jr., Pierce, A. P., Antweiler, J. C., and Buck, K. L., 1962, Lead-isotope studies in the Northern Rockies, U.S.A., *in* Engel, A. E. J., James, H. L., and Leonard B. F. (eds.) Petrologic studies—a volume in honor of A. F. Buddington: Geol. Soc. America, p. 115–131.

Cannon, R. S., Jr., Pierce, A. P., and Delevaux, M. H., 1963, Lead isotope variations with growth in a galena crystal: Science, v. 142, p. 574–576.

Delevaux, M. H., 1963, Lead reference sample for isotopic abundance ratios: Art. 42 *in* U.S. Geol. Survey Prof. Paper 475–B, p. B160–B161.

Phair, George, and Mela, Henry, Jr., 1956, The isotopic variation of lead in Front Range galenas and its geological significance: Am. Jour. Sci., v. 254, p. 420–428.

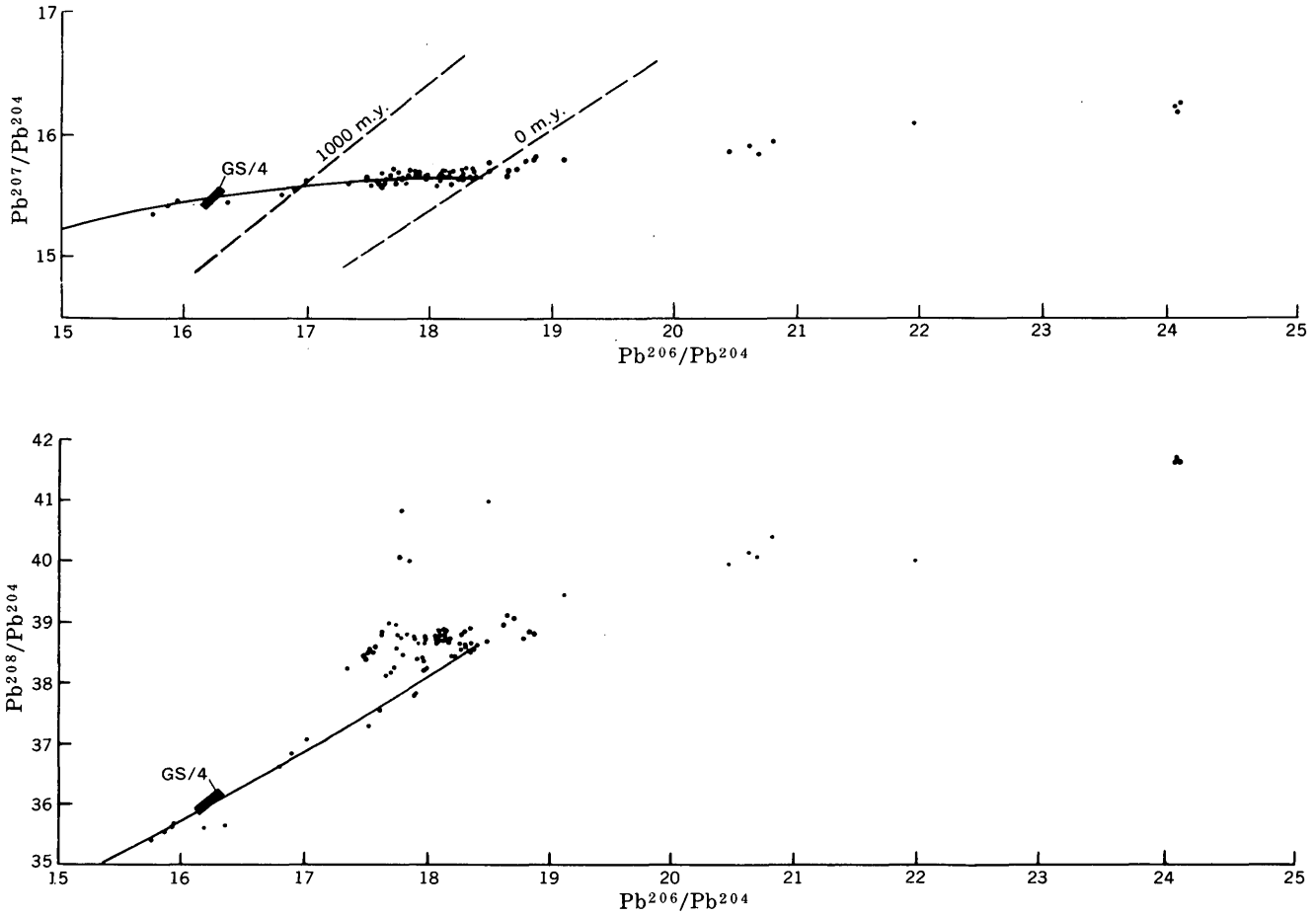


FIGURE 4.—Isotopic variations shown by analyses of Colorado ore lead and the reference sample GS/4. The solid lines are the growth curves derived from the evolutionary model of ordinary ore lead (Cannon and others, 1962). The dashed lines are isochrons, in millions of years.

# ANOMALOUS METAL CONCENTRATIONS IN JASPEROID FROM HYPOGENE BARITE VEINS NEAR RABIGH, KINGDOM OF SAUDI ARABIA

By DONALD A. BROBST, Denver, Colo.

*Work done in cooperation with the Ministry of Petroleum and Mineral Resources, Kingdom of Saudi Arabia*

*Abstract.*—An unusual dark-brown jasperoid was found in pods in the thicker parts of barite veins in fractures of the Red Sea rift system near Rabigh, about 150 km north of Jiddah, Saudi Arabia. The suite of trace elements in the jasperoid includes Be, Pb, Y, B, Mn, and Fe in anomalous amounts. Petrographic and spectrographic data suggest that the jasperoid is of hypogene origin. It is suggested that the area of the barite deposits be checked for further indications of potentially valuable hydrothermal ore deposits.

## GEOLOGY

About 20 kilometers N. 50° E. of Rabigh on the Red Sea coast 150 km north of Jiddah, Saudi Arabia (fig. 1), barite veins from a few centimeters to 3 meters wide fill fractures in the Red Sea rift system of Tertiary age. The geology of the area is complex: country rocks consist principally of granite, granodiorite, quartz diorite, and diorite of Precambrian(?) age cut by dikes of andesite, rhyolite, and aplite. The barite veins are well exposed, chiefly with northerly, northwesterly, and northeasterly trends. The veins dip steeply, generally 60° or more, and the dip commonly changes or is even reversed in direction along the strike. The veins pinch and swell along the strike and down the dip.

Most of the barite veins near Rabigh are clustered in an area of several square kilometers along the base of a low range of northerly trending hills. The lower flanks of the hills are much more fractured than the higher core of the range. Some of the barite veins in the hills extend outward beneath the sand that covers the surrounding valleys, and isolated patches of bedrock containing barite veins crop out through the sandy valley fill. Thus the area of barite mineralization might be much more extensive than that exposed in the foothills.

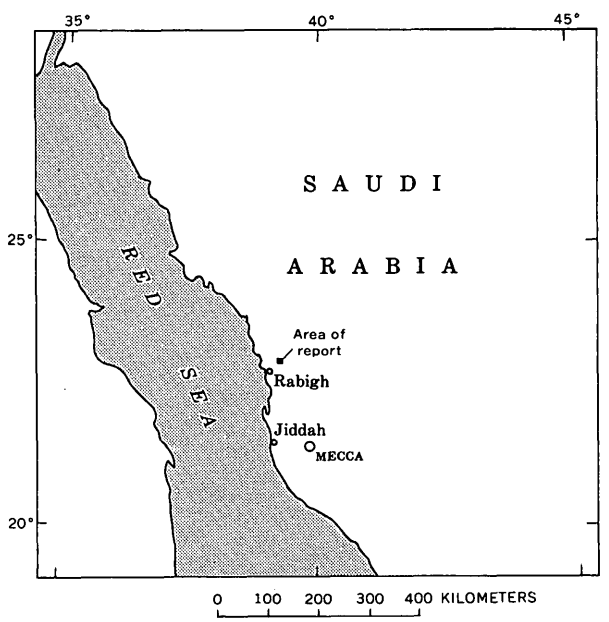


FIGURE 1.—Index map of west-central Arabia, showing the location of the barite deposits near Rabigh.

The veins chiefly are filled with white to pink crystalline masses of barite that contain scattered crystals of chalcopyrite (commonly altered to malachite) and galena. The thicker parts of the veins also contain pods of dark-golden-brown jasperoid with black oxides of manganese.



211-690 O - 66 - 13

## JASPEROID

A sample of jasperoid, described below, is considered typical of the jasperoid occurrences in the area. The jasperoid was taken from a pod about 2 feet wide and 6 feet long in the middle of an 8-foot-wide barite vein. The jasperoid appears to have been deposited in an opening in the earlier baritic vein material. In hand specimen, it is dense, fine grained, and has swarms of tiny black specks. In thin section, the quartz grains are about 0.3 mm across, and many are interlocking. Many specks of brown limonite and dark oxides of iron and manganese are disseminated through the quartz. Local segregations of tiny particles of iron oxide (±0.01 mm) and chalcedonic silica that probably precipitated from a colloidal gel are interstitial to isolated grains and groups of interlocking grains of quartz. The grains of quartz do not appear to have been formed from a gel but rather by direct crystallization from solution. They contain disseminated inclusions of iron oxide, however, that seem to have been precipitated in colloidal form. T. G. Lovering (oral commun. Feb. 1965) regards these features as unusual in jasperoid. He points out that normally, quartz derived from the crystallization of a mixed colloidal precipitate of hydrous iron oxides and silica is extremely fine grained and cherty in appearance and contains the disseminated hydrous iron oxides. Also, coarse-grained quartz that is precipitated directly from solution is normally free of such hydrous iron inclusions.

Three semiquantitative spectrographic analyses of the Arabian jasperoid are shown in table 1. According to chemical criteria established by Lovering and Hamilton (1962) for the recognition of jasperoid associated with sulfide ore, the content of iron and lead in the Arabian jasperoid respectively would be regarded as "significant" and "highly significant." The copper content is at the threshold of their "highly significant" category. The values obtained for the beryllium, boron, and yttrium content of the Arabian jasperoid are highly anomalous compared to the median values for these elements, in jasperoid, namely, Be, 0.2 ppm; B, 5 ppm; and Y, 4 ppm (T. G. Lovering, written commun. Feb., 1965). These elements were spectrographically detected in only about 60 of the 210 jasperoid samples from many localities studied by T. G. Lovering. Molybdenum and mercury were detected in the Arabian jasperoid, but not in amounts that may be regarded as anomalous.

TABLE 1.—*Semiquantitative spectrographic analyses of the trace-element content of selected samples from barite deposits near Rabigh, Saudi Arabia*

[Determined by emission spectroscope and reported in parts per million, except as noted. Analysts: G. A. Curtin, samples 1, 2, 4, 5, and 6; Barbara Tobin, sample 3]

| Element | Jasperoid | | | Barite | Wall-rock [1] | Fresh granodiorite [2] |
|---|---|---|---|---|---|---|
| | 1 | 2 | 3 | 4 | 5 | 6 |
| Be | 20 | 15 | 15 | <1 | 2 | 1 |
| Cr | <5 | <5 | 2 | <5 | <5 | 150 |
| Ba | 1,000 | 1,500 | 700 | >1 percent | 1,500 | 300 |
| Sr | <50 | <50 | ---- | >1 percent | 150 | 500 |
| Ti | <50 | <50 | 7 | <50 | 1,000 | 2,000 |
| Mn | 3,000 | 3,000 | ---- | <20 | 150 | 1,500 |
| V | 70 | 50 | 50 | <10 | 15 | 300 |
| Ni | <2 | <2 | 3 | <2 | 5 | 5 |
| Cu | 20 | 50 | 100 | <2 | 15 | <2 |
| Pb | 1,500 | 300 | 500 | 150 | <2 | <2 |
| B | 50 | 20 | 30 | <10 | <10 | <10 |
| Y | 50 | 20 | 50 | <5 | 7 | 7 |
| Mo | 3 | 2 | ---- | <2 | <2 | <2 |
| Fe (percent) | 15 | 7 | >1 | <.1 | .2 | 15 |
| Mg (percent) | .01 | <.01 | .05 | <.01 | .7 | .3 |
| Ca (percent) | .1 | .2 | .3 | <.1 | .2 | 7 |
| Hg (ppb) [3] | 150 | 120 | ---- | 20 | 80 | 20 |

Other elements sought, but not found: Bi, Ga, As, Sb, W, Zn, Sc, Zr, La, Cd, and Sn, except as given in footnotes 1 and 2.

Results are reported to the nearest number in the series 1, 0.7, 0.5, 0.3, 0.2, 0.15, 0.1, and so forth, which represent approximate midpoints of groups of data on a geometric scale. Assigned group for semiquantitative results will include the quantitative value about 30 percent of the time.

[1] Also contains Zr, 70 ppm; La, 30 ppm; and Ag, 2 ppm.

[2] Also contains Sc, 70 ppm; and Co, 30 ppm.

[3] Determined by absorption spectroscope; J. H. McCarthy, analyst.

## INTERPRETATION

The unusual textural and chemical characteristics of the Arabian jasperoid suggest a hypogene origin. Barite veins commonly are associated with the outer parts of zoned hypogene mineral deposits, and the suite of trace elements is one commonly found in deposits of hydrothermal origin. The jasperoid appears to be late in the paragenetic sequence of the barite veins; therefore, the composition of the jasperoid may reflect the residual composition of the ore-forming solution. If so, greater concentrations of these elements might have been deposited in the vicinity.

In many mining districts, barite deposits are above or laterally outward from mineralized centers containing valuable concentrations of fluorite and base and precious metals. Hewett (1964) has synthesized data on the relations of manganese oxides, barite, and fluorite to occurrences of base and precious metals, and the paragenetic and spatial relations he has found may apply to these barite deposits in Saudi Arabia.

In the Arabian deposits, the mineralizing solutions followed the fracture system closely, and the wall and country rocks were little altered by hydrothermal solutions. Spectographic analyses of a sample of wallrock and one of the granodioritic country rock, near the vein from which the jasperoid sample was collected, are shown in table 1. The wallrock sample is not enriched in the elements abundant in the jasperoid and the barite, although some silver was de-

tected. The trace-element content of the granodiorite appears normal compared to other reported analyses of granodiorite. The trace-element analyses of table 1 support the field observations that there was little, if any, leakage of the mineralizing solutions from the fracture system in which they moved and that, at least in this area, the vein deposits are structurally controlled.

## CONCLUSIONS

The occurrence of barite veins northeast of Rabigh, Saudi Arabia, that contain an unusual jasperoid with anomalous amounts of metallic trace elements may indicate hydrothermal activity in this general area. The veins were deposited along fractures belonging to the Red Sea rift system, which is extensive and deep rooted and offers a wide target in which to search for potential ore deposits. The area of barite veins is only about 20 km inland from the Red Sea across easily accessible terrain, and further exploration for other possible local centers of mineralization seems both practical and desirable.

## ACKNOWLEDGMENTS

Fieldwork on which this report is based was sponsored during September 1964 by Dr. Fadil Kabbani, Deputy Minister for Mineral Resources, Directorate General of Mineral Resources, Ministry of Petroleum and Mineral Resources, Royal Saudi Arabian Government. The writer wishes to express his appreciation to Mr. Ahmed Shanti, geologist with the Directorate General, for introducing him to the geology of the Rabigh area.

## REFERENCES

Hewett, D. F., 1964, Veins of hypogene manganese oxide minerals in the southwestern United States: Econ. Geology, v. 59, no. 8, p. 1429–1472.

Lovering, T. G., and Hamilton, J. C., 1962, Criteria for the recognition of jasperoid associated with sulfide ore: Art. 63 *in* U.S. Geol. Survey Prof. Paper 450–C, p. C9–C11.

# A GEOCHEMICAL INVESTIGATION OF THE CARAÍBA COPPER DEPOSIT, BAHIA, BRAZIL

By RICHARD W. LEWIS, JR., Rio de Janeiro, Brazil

*Work done in cooperation with the Departmento Nacional da Produção Mineral and the University of Bahia (Salvador, Brazil), under the auspices of the Agency for International Development, U.S. Department of State*

*Abstract.*—Norite and cupriferous pyroxenite intrude closely folded Precambrian biotite-quartz-plagioclase gneiss, amphibolite, and migmatite at Caraíba. Geochemical soil analyses revealed close correlation of copper, cobalt, and nickel anomalies with the mineralized area and of cobalt and nickel values with rock types. Copper in leguminous vegetation had fair coincidence with mineralization.

The Caraíba copper deposit lies in the north-central part of the State of Bahia, Brizil, about 360 kilometers northwest of the port of Salvador and 80 km south of the São Francisco River (fig. 1).

Copper at Caraíba has been known for about 100 years; this deposit has been studied off and on by both government and private groups for the past 30 years. The present owners, the Grupo Industrial Pignatari, are continuing an extensive exploration program, while awaiting essential hydroelectric energy and water from the São Francisco River.

## GEOLOGY

The Caraíba region lies in a belt of gneiss, migmatite, and granite of early Precambrian age which forms the eastern flank of the Brazilian shield. Medium-grained biotite-quartz-plagioclase banded or streaky gneiss containing concentrations and intercalations of amphibole-rich rock (amphibole gneiss and amphibolite) underlies much of the Caraíba area. Along major folds, the gneiss has been converted to migmatite. The migmatite consists of medium- to coarse-grained biotite (or hornblende)-quartz-plagioclase gneiss which shows a veined or small-fold texture. Migmatite is cut by, or mixed with fine-grained homogeneous gneiss, granite, and small pegmatitelike veins of coarse-grained quartz and microcline. The coarse-grained gneiss, which may contain almandine garnet, makes up the older part of the migmatite. It is highly contorted and shows marked separation into mafic and nonmafic bands. The granite, or younger part of the migmatite, penetrates the coarser gneiss in northward-trending dikes and elongated bodies that are generally concordant and have sharp boundaries with the enclosing gneiss. The granite is equigranular and shows only a vague foliation, which is parallel to regional foliation.

At Caraíba the gneiss and migmatite have been intruded by an ultramafic complex that is in part localized along the crests of small anticlinal folds (fig. 1). The ultramafic complex is composed of barren norite and serpentinite, together with the cupriferous pyroxenite that constitutes the ore bodies at Caraíba. These ultramafic rocks are surrounded by a series of intermediate rocks, which are progressively more feldspathic and quartzose and less mafic away from the ultramafic masses. These intermediate rocks, in order of increasing feldspar and quartz content, are: pyroxene granulite, garnetiferous hornblende granulite, hornblende-plagioclase-biotite amphibolite, biotite-hornblende-plagioclase amphibolite, and biotite-plagioclase gneiss. The distribution of these rocks suggests that they were formed by reaction of the ultramafic rocks with the gneissic country rock at the time of intrusion.

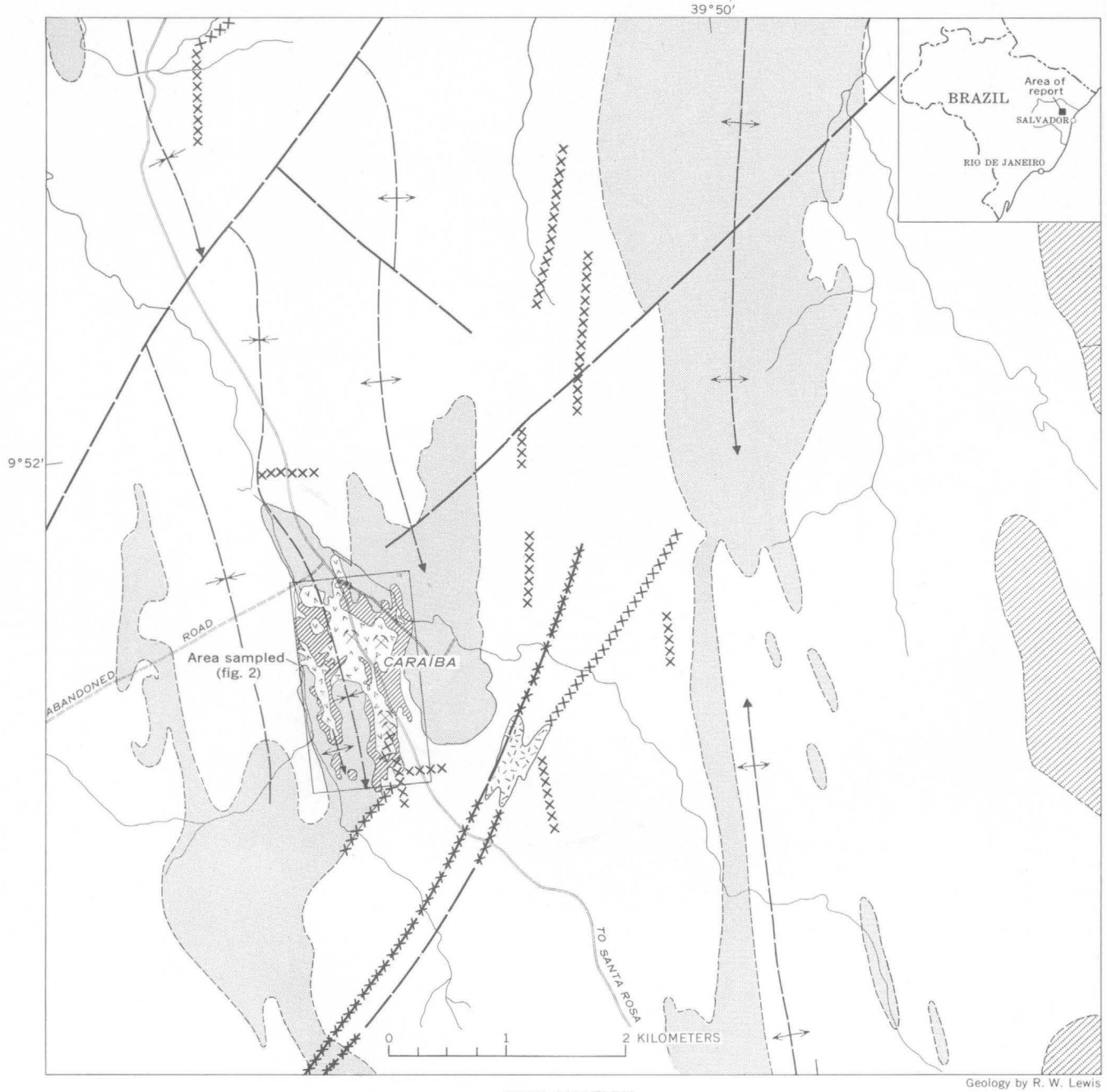


FIGURE 1.—Generalized geologic map of the Caraíba region, Bahia, Brazil. Mapped units not in chronologic order.

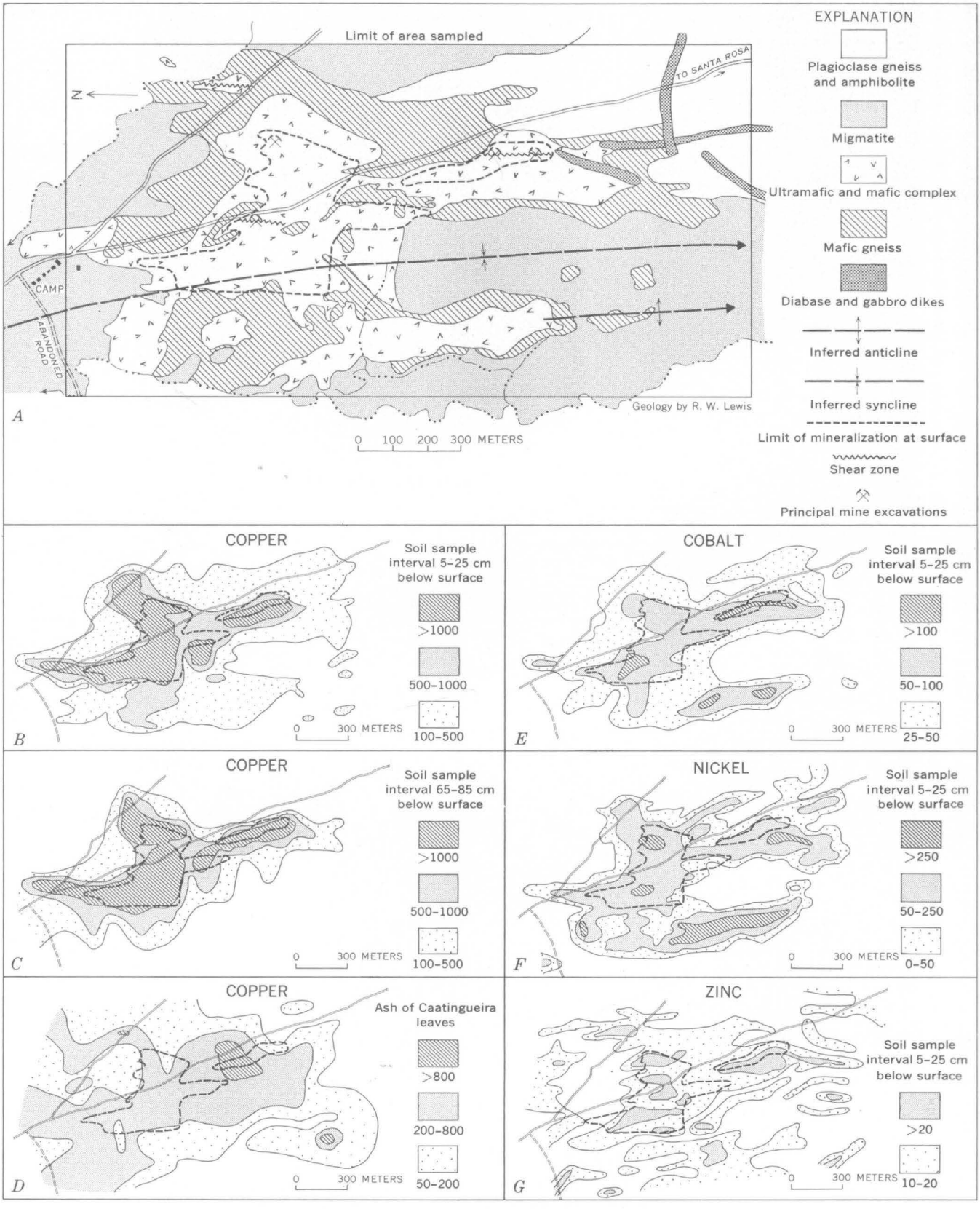


FIGURE 2.—Geologic map and metal dispersion patterns of the Caraíba copper deposit. *A*, mineralized area and the area sampled geochemically; mapped units not in chronologic order. *B–G*, dispersion patterns, in parts per million, for copper, cobalt, nickel, and zinc.

East of Caraíba a coarse-grained syenitic augen gneiss crops out in a series of northward-trending hills (fig. 1), which are from 50 to 200 meters higher than the surrounding plain. These rocks are considered to be orthogneiss and younger than the other metamorphic rocks.

Throughout the area, and notably south of the Caraíba mine, dikes of diabase and gabbro crop out. They trend north to northeast and are from 2 to 10 m wide. These rocks are younger than all the other rocks of the area and have no relation to the mineralization.

Rocks of the area have been affected by strong regional metamorphism. In general they belong to the almandine-amphibolite facies and were probably formed at considerable depth, comparable to the catazone of Grubenmann. Around the ultramafic complex, however, rocks belonging to the granulite facies have formed.

The gneissic rocks at Caraíba are folded into steeply dipping isoclinal folds which strike approximately north. These folds appear to be part of a north-trending anticlinorium that lies on the west flank of a stable area, called the Uaua dome by F. L. Humphrey and G. O. Allard (written commun., 1962).

Original bedding in these rocks is not discernible. Foliation and banding are nearly always parallel, trending northward and dipping at high angles either east or west.

Major faults of the area fall into a northeast, north, and northwest pattern. The northeasterly faults appear to be younger, and most are filled with quartz or diabase. Surface exploratory work at Caraíba has uncovered near-surface pockets of oxide ore concentrated in north-trending shear zones that are characterized by intense hydrothermal alteration (fig. 2*A*).

## MINERALIZATION

Primary mineralization probably formed contemporaneously with the pyroxenite and consists of disseminations and irregular veinlets of chalcopyrite, bornite, and pyrrhotite in the pyroxenite. Small amounts of sulfide are concentrated in knots of mafic minerals in adjacent rocks of intermediate composition. Minor amounts of nickel and cobalt sulfides, sphalerite, bismuthinite, and tetrahedrite were reported to be in these rocks by Schneider (1957).

Secondary copper minerals include covellite, tenorite, chalcocite, malachite, azurite, brocanthite, and chrysocolla. Secondary mineralization reaches depths of 30 m or more and is best developed in fracture zones that cut across the ore body. The best concentrations of secondary sulfide minerals are found above the present ground-water table, at fracture junctions at depths of 5 to 20 m below the surface. Copper sulfates and secondary sulfides rather than copper carbonates tend to appear at depth. Both silicates and carbonates are commonly precipitated in minor amounts in wallrock as much as 5 to 10 m from the protore body, and concentrations of secondary copper minerals are found in major fracture zones as far as a 100 m from the nearest protore body.

The ore reserves of the Caraíba deposit were estimated by Lino de Mello, Jr., (Mello and others, 1962) of the Departamento Nacional da Produção Mineral to be 3,900,000 metric tons of oxidized ore. This figure was calculated for reserves to a depth of 16 m and averaging 1.2 percent copper. About 35,400,000 metric tons of measured, indicated, and inferred sulfide ore averaging 0.9 percent copper was calculated to a depth of 60 m.

## CLIMATE, SOILS, AND VEGETATION

The climate of north-central Bahia is subtropical and semiarid. Rainfall ranges from 200 to 700 millimeters per year, most of which falls between December and April. Rains are usually torrential, and runoff is as much as 80 percent. Low relief, shallow soil cover, and low permeability of underlying rocks impede the circulation of ground water, permitting a high accumulation of salts.

The soils at Caraíba are slightly alkaline and mostly residual, reflecting the underlying rock in their texture and composition. Soils developed from rocks composed mainly of quartz and feldspar (gneiss and granite) are sandy clays and sandy clay loams that are usually thin (from 30 to 40 centimeters thick). They vary from pale orange to light gray. Soils formed from rocks of intermediate composition are brown to brownish-gray clayey to sandy clay loams. Soils developed from the mafic and ultramafic rocks are desert or alkaline clays and clay loams (gumbos). These rocks are dark gray, black, or dark chestnut brown; range from 60 to 120 cm in depth; are very sticky and plastic; show a prismatic structure; and characteristically develop gaping cracks upon drying. Nonresidual, alluvial soils are found only close to stream courses. They consist of silty to coarse-grained, buff to yellow-brown sands.

Seven types of soils were recognized on the basis of color and texture. They were extensively used for defining geologic contacts because of the sparsity of outcrops. The validity of this procedure is confirmed

by the close correlation of the cobalt, copper, and nickel content with soil type.

Low trees, spiny bushes, and cacti are the typical vegetation of the semiarid "sertao" region of northeastern Brazil. Plants are typically xerophytic and show special adaptations to the sporadic rains and prolonged dry periods. These plants have urticarial or spiny leaves as protection against foraging animals, composite leaves with reduced surface area, tubers for water storage, leaf droppage during the dry periods, and modification of stem and leaves into fleshy tissue. Low brushy or succulent plants predominate, and trees seldom grow more than 4 m high except along stream courses, because of the climate and a deep and saline phreatic zone. Plants of the Cactaceae, Brumeliaceae, Euphorbiaceae, and Leguminosae families are most common. Certain plants showed a marked tendency to prefer particular soil types. Caatingueira (*Caesalpina* sp.), pinhão (*Jatropha curcas*), matapasto (*Cassia* sp.), and a small unidentified flower locally called Saint Lucia herb (Erva de Santa Luzia) are characteristic plants of the heavy clays developed over mafic and ultramafic rocks. Calumbí (*Mimosa asperata*), cansansão (*Jatropha urens*), carqueja (*Calliandra* sp.), corôa de frade (*Melocactus bahiensis*), jurema (*Mimosa nigra*), and xique-xique (*Pilocereus gounellei*) grow in sandy soils developed from siliceous rocks.

## GEOCHEMICAL INVESTIGATIONS

Geochemical investigations at Caraíba were made of (1) soils over the ore bodies, (2) stream sediments bordering the mineralized area, (3) soils over principal rock types of the region, (4) parts of common plants of the area, and (5) caatingueira leaves in the mineralized area. The geology, including soil types, was mapped in detail, and a magnetic survey of the mineralized area was made.

Soils were sampled over the ore bodies on a rectangular grid, 2 km long from north to south and 1 km wide from east to west. East-to-west sample lines were spaced 100 m apart, and soil samples were taken at 50-m intervals along these lines. At each sample location, profile soil samples were taken at 20-cm intervals from a depth of 5 cm down to altered rock or saprolitic material which was reached in most places at a depth of 80 cm. The first sample interval was between 5 and 25 cm, the second between 25 and 45 cm, the third between 45 and 65 cm, and the fourth between 65 and 85 cm, and so on.

Stream sediments were sampled every 100 m for about 3 km along the intermittent stream that borders the western edge of the area. Samples were taken from the surface to depths of 45 cm in the middle of the streambed.

To obtain normal background values, soils over different regional rock types were sampled along roads for a distance of 20 km north and south of the deposit and 5 km to the west.

The leaves, stem wood, bark, and roots of the 12 commonest plants of the area were sampled. Two samples of each plant part were taken, one sample in an area with less than 200 parts per million of copper and the other sample where the copper content was over 1,000 ppm.

Caatingueira leaves were sampled over the mineralized area at 100-m intervals along the grid used for soil sampling. This plant was used for systematic geobotanical sampling because of its widespread abundance, its preference for soils developed from mafic rocks, and its relatively deep root system.

To minimize contamination of samples, analytical error, and variations in the results imposed by a rustic field laboratory with no electricity or water and with constant dust, all samples, except stream sediments, were prepared and analyzed in the geochemical laboratory of the University of Bahia in Salvador. Rapid trace-element analytical techniques, described by Ward and others (1963), were used throughout; these visual comparison standards were employed for determination of metal content.

The range and mean average background values of six metals in soils covering the principal rock types of the Caraíba area shown in table 1 fall within the ranges expected for soils developed from these diverse rock types (Green, 1959).

The local threshold for anomalous copper values outlining the mineralization at Caraíba was determined to be 1,000 ppm, which is 5 times the upper limit of normal regional background fluctuation and about 40 times the mean average copper value for the region. The highest copper values were in the center of the mineralized area over shear zones containing concentrations of secondary copper. The values range from 5,000 to 30,000 ppm (figs. 2*B* and 2*C*), which are from 5 to 30 times the local threshold value and more than 200 times the regional background values. High values for cobalt range from 75 to 150 ppm (5 to 10 times regional background) and values for nickel range from 250 to 800 ppm (10 to 32 times regional background). The highest values for nickel and cobalt were found over unmineralized ultramafic rocks in the western part of the area (figs. 2*E* and 2*F*). High values for zinc range from 20 to 50 ppm and generally correspond to areas of high copper mineralization (fig. 2*G*).

TABLE 1.—*Estimated range and mean average background values, in parts per million, for selected metals in soils above different rock types in the Caraíba region*

[Analyst: Adelaide M. Santos, Laboratório de Geoquímica University of Bahia, Salvador, Brazil]

| Metal | Amphibolite | | Gabbroic dike rocks | | Gneiss | | Granite | | Migmatite | | Ultramafic rocks | | Ultramafic rocks at Caraíba deposit | |
|---|---|---|---|---|---|---|---|---|---|---|---|---|---|---|
| | Mean average | Range | Mean average | Range | Mean average | Range | Mean average | Range | Mean average | Range | Mean average | Range | Mean average | Range |
| Copper | 50 | 0–200 | 25 | 10–100 | 17 | 5–100 | 17 | 5–50 | 10 | 0–25 | 25 | 17–200 | 1, 500 | 75–30, 000 |
| Chromium | 100 | 0–400 | 20 | 0–200 | 0 | 0–200 | 0 | 0–150 | 0 | 0–50 | 50 | 0–4, 000 | 200 | 0–1, 000 |
| Cobalt | 20 | 10–50 | 20 | 10–40 | 10 | 0–50 | 15 | 0–75 | 10 | 10–20 | 20 | 20–40 | 50 | 20–150 |
| Lead | 20 | 0–40 | 8 | 0–20 | 8 | 0–40 | 8 | 0–40 | 8 | 0–20 | 8 | 0–20 | 0 | 0–10 |
| Nickel | 25 | 0–200 | 25 | 0–50 | 10 | 0–50 | 0 | 0–75 | 0 | 0–25 | 25 | 0–1, 500 | 300 | 150–900 |
| Zinc | 5 | 0–30 | 10 | 0–20 | 5 | 0–30 | 5 | 0–20 | 5 | 0–10 | 5 | 0–20 | 20 | 5–35 |

The dispersion pattern for copper (fig. 2*B*) determined from soil samples collected from 5 to 25 cm below the surface shows good correlation with mineralization. Most of the known mineralized area, as deduced from copper mineralization in pits, trenches, and diamond drill holes, is enclosed by the 1,000-ppm contour line (fig. 2*B*). The dispersion pattern coincides with the geology only in delimiting the area of migmatites, which contain less than 100 ppm of copper, and in outlining the mineralized pyroxenites. The dispersion pattern of copper tends to shrink with depth over the mineralized areas. The isopleths for the saprolitic soil samples taken from 65 to 85 cm below the surface are tight and relatively uniform around the 1,000-ppm isopleth (fig. 2*C*). The area outlined by the 1,000-ppm isopleth does not change notably with depth and is believed to represent the actual outline of the underlying ore body.

The dispersion patterns for cobalt and nickel, determined from analytical data of soil samples collected from a depth of 5 to 25 cm, show exceptionally good correlation with the geology. The patterns outline both the ultramafic complex and the halo of regional gneiss affected by the ultramafic intrusions (figs. 2*E* and 2*F*). The area with more than 50 ppm of cobalt and 100 ppm of nickel outlines the ultramafic and mafic rocks and includes the unmineralized pyroxenite and serpentinite along the west flank of the area. The dispersion pattern of cobalt tends to shrink with depth. However, the dispersion pattern for samples collected from 65 to 85 cm below the surface is large and uniform, and the 30 ppm of cobalt isopleth encloses a large oval area 250 m north-south by 750 m which contains a few isolated highs of 50 ppm or more. This pattern is thought to be caused by the precipitation of cobalt on top of the less permeable saprolitic rocks during the annual dry spells. The nickel dispersion pattern tends to spread out and become erratic with depth.

The dispersion pattern for zinc is erratic and shows little relation to rock or soil types (fig. 2*G*). The locations of high zinc values, however, do correspond with comparable high values of copper.

The dispersion pattern for chromium follows, in general, the patterns of nickel and cobalt, but it does not have the range in values nor does it spread out at depth. The dispersion pattern for lead shows little correlation with rock type or mineralization.

The geochemical sampling of sediments in the intermittent streams on the west flank of the Caraíba deposit (fig. 2*A*) showed a concentration of high copper and nickel values north and downstream from the junction with the only stream that drains the mineralized area. High copper values were 50 ppm and only twice a normal background of 25 ppm of copper, and high nickel values were 40 to 80 ppm as compared with a background value of less than 5 ppm. Analyses were made of the minus 10-mesh fraction, without attempting to concentrate the heavy minerals which were scarce. This may account for the low values obtained. No significant concentration in chromium, cobalt, lead or zinc was found below the stream junction.

Systematic samples of caatingueira leaves at about 170 different sites were taken on a 100×100-meter grid over the Caraíba deposit. The values of copper in leaf ash ranged from 35 to 2,400 ppm. The distribution pattern for copper in the leaf ashes showed a general similarity to the pattern for copper in the soil (fig. 2*D*). Outside the mineralized area little similarity in patterns was found. Local drainage characteristics are probably the dominant factor in copper accumulation in vegetation.

Analyses of zinc and cobalt in the ashes of the caatingueira leaves showed the highest values from areas of copper mineralization. Zinc values were 300 ppm compared to a background of 100 ppm, and co-

balt showed high values of 40 ppm relative to a background of 10 ppm.

The pattern for lead in caatingueira leaves was erratic and showed no correlation with the lead dispersion pattern in soil.

Nickel was generally not present in detectable quantities in the leaf ash.

Preliminary results of the geobotanical sampling of plant parts showed that the bark of roots contains the highest accumulations of copper and the greatest differences over background. The average value for copper in ashes of root bark from the mineralized area is 20 times the value found in unmineralized areas. Leaves and trunk bark were found to be about equally sensitive to an increase of copper in the soils, showing an average increase of 10 times over background. The woody parts of the plants were the least sensitive. The plants that showed consistently the highest increases of copper over mineralized areas were the leguminous trees, caatingueira, calumbí, and jurema.

A preliminary geomagnetic survey with a portable magnetometer was made of the Caraíba deposit. Measurements were made along the geochemical soil-sampling grid. The results were not satisfactory; magnetic highs and lows over the granitic and gneissic rocks were found to be erratically distributed.

## CONCLUSIONS

From the studies at Caraíba the following conclusions were reached:

(1) Geochemical copper values in soils sampled from a depth of 5 to 25 cm show good correlation with subjacent geology and mineralization and obviate time-consuming deep sampling for outlining ore bodies.

(2) Cobalt and nickel values obtained from soil samples collected from a depth of 5 to 25 cm show better correlation with the known geology than they do in deep samples.

(3) High nickel and cobalt values obtained from soils that overlie the ultramafic rocks at Caraíba strongly suggest an igneous origin for these rocks and serve to distinguish them from mafic-rich metamorphic rocks which may form similar dark gumbo soils.

(4) The very low regional background values for copper and the complete encirclement of the Caraíba deposit by a 100-ppm isopleth for copper suggest that on a regional basis, soil samples containing 100 ppm or more of copper could represent a secondary dispersion halo caused by mineralization. If so, they can be used to outline areas of potential copper mineralization.

(5) Geochemical anomalies defined by copper values of 250 ppm or more in this region denote places definitely worthy of further investigation.

(6) Copper content of 1,000 ppm, together with nickel values of 100 ppm or more, probably outline cupriferous pyroxenite bodies that are near the surface and indicate places that should be explored in more detail by trenching and drilling.

## REFERENCES

Green, Jack, 1959, Geochemical table of the elements for 1959: Geol. Soc. America Bull., v. 70, p. 1127–1184.

Leinz, Viktor, 1946, Gênese da jazida de cobre de Caraíba, Bahia: Eng. Min. e Met., v. 11, no. 65, p. 277–278.

Mello, J. L. de, Jr., Pouchain, E. B., and Castiel, Nassim, 1962, Relatório sôbre a jazida de Caraíba, Estado de Bahia: Div. Fom. Prod. Min., D.N.P.M., Bol. 117.

Schneider, André, 1957, Rejuvenescimento hidrotermal dos minérios cuproniquelíferos secundários de Caraíba, Bahia: Eng. Min. e Met., v. 25, no. 149, p. 251–254.

Ward, F. N., Lakin, H. W., Canney, F. C., and others, 1963, Analytical methods used in geochemical exploration by the U.S. Geological Survey: U.S. Geol. Survey Bull. 1152, 100 p.

# DISTRIBUTION OF SELECTED METALS IN THE STOCKTON DISTRICT, UTAH

By WILLIAM J. MOORE [1], G. C. CURTIN [2], R. J. ROBERTS [1], and E. W. TOOKER [3],
[1] Menlo Park, Calif., [2] Denver, Colo., [3] Washington, D.C.

*Abstract.*—Spectrographic analyses of bedrock and oxidized surficial materials from the Stockton district in northeastern Utah indicate a zonal distribution of metals spatially related to an intrusive center of Tertiary age. Largely coextensive areas of locally high bismuth-copper-molybdenum concentrations define a central zone; lead-zinc areas of greater lateral extent partly overlap the central zone; locally high arsenic-antimony (and boron?) concentrations characterize the outer zone, with boron extending beyond the limits of significant known mineralization. Silver is erratically distributed in the area studied. The present distribution of metals at Stockton apparently reflects hypogene environmental controls.

The Stockton district lies in the western foothills of the Oquirrh Mountains about 1¼ miles east of Stockton, Utah (fig. 1), and 30 miles southwest of Salt Lake City. A study of the metal distribution in surficial materials was undertaken to supplement a geologic investigation in the Bingham district, approximately 12 miles to the northeast.

*Acknowledgments.*—During the fieldwork at Stockton, E. H. Snyder and I. S. Droubay of the Combined Metals Reduction Co. generously made available many district maps and reports. Sahng Yup Kim of the Korean Geological Survey assisted with magnetic studies.

## GENERAL GEOLOGY

The geology and ore deposits of the Stockton district have been studied by Butler and others (1920) and Gilluly (1932). The district is underlain by an interbedded sequence of quartzite and limestone of the Pennsylvanian and Permian Oquirrh Formation; the exposed part of the Oquirrh Formation includes rocks that lie between about 4,000 and 9,000 feet above its basal contact with the Manning Canyon Shale of Mississippian and Pennsylvanian age. The limestone layers, rarely more than 50 feet thick, are medium to dark gray, arenaceous, and thin bedded. Dense, buff to gray quartzites and cherty, calcareous sandstones separate the limestone beds. The outcrop map (fig. 1), prepared in the course of geochemical sampling, shows the distribution of the most persistent calcareous units in the area. Many of the thin limestone beds are obscured or concealed by a cover of scrub oak and quartzite slopewash.

The beds form part of the northeast limb of the northwest-plunging Ophir anticline (Gilluly, 1932, pl.I), generally strike about N. 70°–80° W., and dip 60°–80° N. The beds in the northern part of the map area are overturned locally and dip about 70° S. Minor drag folds are associated with some of the larger faults in the northern and central portions of the district.

Gilluly (1932, p. 88–90) recognizes several periods of faulting in the Stockton district. The earliest faults are bedding faults of minor displacement that presumably accompanied folding. These were followed by north-trending faults that dip steeply to the west and may have controlled, in part, the emplacement of quartz monzonitic intrusive rocks. Ore bodies are localized principally along the north-trending and bedding faults. Sheared sulfides occur locally in the underground workings, suggesting continuing postore faulting. The horizontal displacement on the faults rarely exceeds 100 feet; an exception is the Continental fault, which displaces the beds horizontally about 1,000 feet.

Intrusive rocks ranging in composition from diorite to quartz monzonite cut the Oquirrh Formation. Most of these are dikes of quartz monzonite porphyry. The stocklike bodies shown near the southern limits of the map (fig. 1) include several small masses of quartz diorite. The igneous rocks in the vicinity of Stockton are part of an intrusive center which includes the large

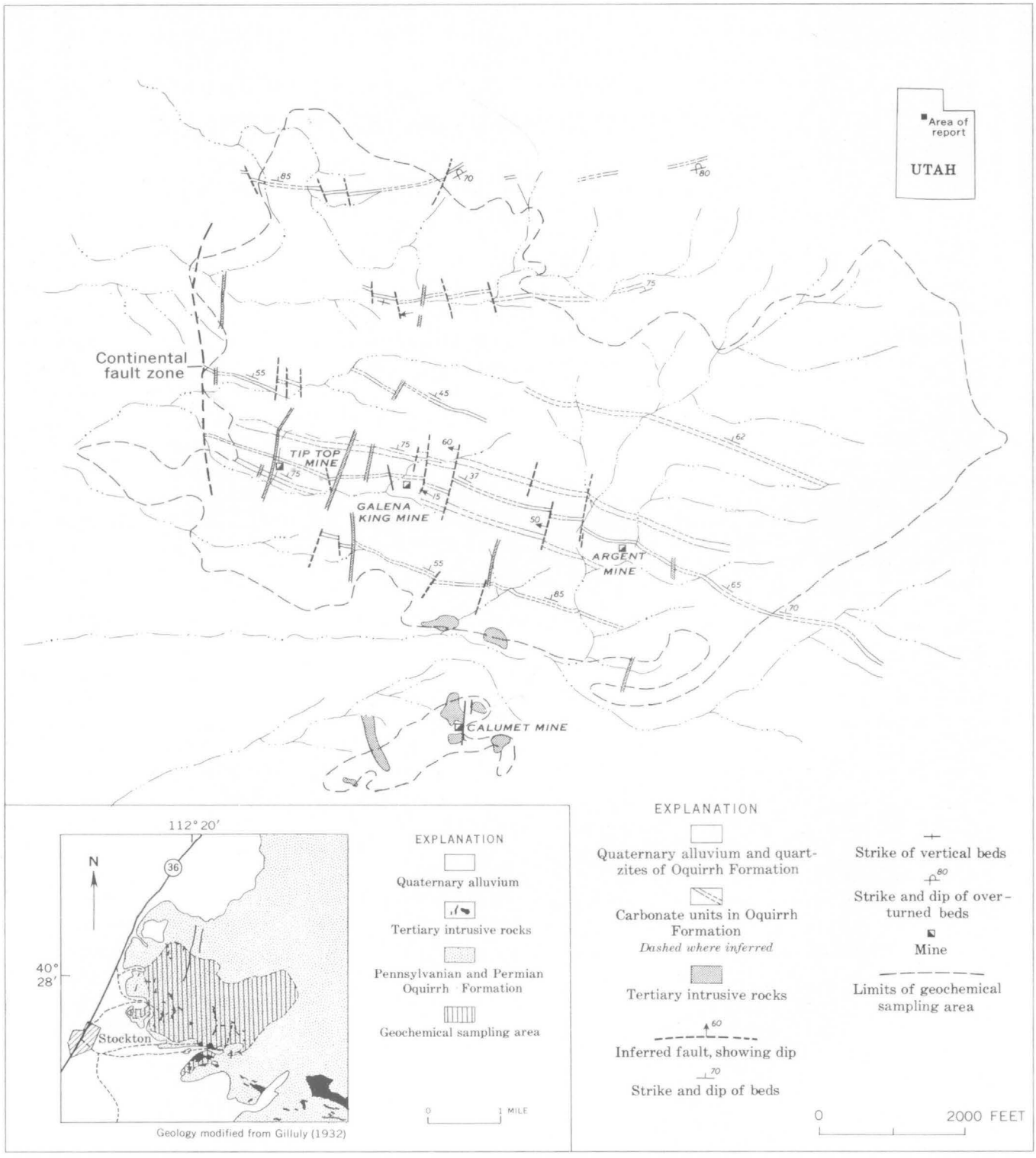


FIGURE 1.—Outcrop map of the Stockton district, Utah.

stock and numerous sills exposed 2 miles to the southeast in Soldier Canyon.

A northwest-trending aeromagnetic anomaly, presumably related to intrusive rocks at depth, was found in this area (Mabey and others, 1964) (fig. 2, insert). Its presence has been confirmed by additional traverses at the surface over portions of the Stockton district, by means of a portable flux-gate magnetometer. A local magnetic high also occurs northwest of the Calumet mine over the alluviated area surrounded by stocklike intrusives (fig. 2). This suggests the presence of a major extension from the larger, northwest-trending intrusive mass.

Limestone beds near intrusive contacts are normally bleached and recrystallized; recrystallized limestone is common within the area defined approximately by the 600-gamma contour line in figure 2. Small bodies of lime silicate minerals including diopside, epidote, andradite, idocrase, and wollastonite are found in this area but also occur locally in narrow zones along dikes and fissures throughout the district. The more siliceous clastic rocks in the southern portion of the district have been metamorphosed to spotted or layered hornfelses. Gilluly (1932, p. 94) found that the calcareous cement in these rocks is partly replaced by diopside, epidote, orthoclase, and garnet.

Propylitization is the dominant type of intrusive-rock alteration at Stockton (Gilluly, 1932, p. 93). Weathering has obscured the effects of this process at the surface, but several dikes have a matrix composed, in part, of a soft, pale-green material, presumably chlorite. Sericitic alteration is common in gouge zones and in the plagioclase phenocrysts of the intrusive rocks.

## ORE DEPOSITS

Ore deposits were first discovered in the Stockton district in 1864 and have since yielded metals valued at more than $30 million from about 1,200,000 short tons of ore (E. H. Snyder, written commun., 1965). Production values through 1927 were divided among the following metals: lead, 75 percent; silver, 16 percent; zinc, 5 percent; gold, 3 percent; and copper, 1 percent. The major properties have been owned by the Combined Metals Reduction Co. since 1924. At the present time the underground workings are inaccessible.

The major ore deposits are pipelike or blanketlike replacement bodies that plunge steeply to the north; they are chiefly localized at the intersections of north-trending fault and breccia zones with favorable limestone units. The strike length of the ore shoots seldom exceeds 100 feet, although several have been followed downplunge from the surface for more than 1,800 feet (Gilluly, 1932, p. 162). Weak mineralization was observed along some north-trending fissures cutting quartzite beds and along the brecciated margins of quartz monzonite dikes.

Hypogene ore minerals include galena and argentite with minor amounts of sphalerite and chalcopyrite in a gangue composed of pyrite, calcite, and quartz. Oxidation of the ore bodies is practically complete to depths of 600 to 800 feet (Gilluly, 1932, p. 160). Cerussite, plumbojarosite, and anglesite are the major ore minerals in the zone of oxidation; minor amounts of cerargyrite, pyromorphite, smithsonite, hemimorphite, and malachite are also present in some ores. Gangue minerals in the oxidized zone include quartz and hydrated iron oxides and, locally, manganese oxides, barite, and gypsum.

## GEOCHEMICAL STUDIES

About 1,000 bedrock samples were collected for semiquantitative spectrographic analysis within the areas outlined by dashed lines in figure 3*A*. The southern and western boundaries of the sample area approximate the outcrop limits of the Oquirrh Formation; boundaries on the north and east were selected along or near prominent drainage divides. Nearly 70 percent of the samples were taken from gossans or breccia zones that showed variable amounts of iron staining; the remainder represent "background" sample sites where no ore mineralization was visible.

The sample distribution is shown in figure 3*A*. No attempt was made to sample at regular intervals on a grid system, as the ore metals are chiefly concentrated along north-trending fissures and fractures.

All analytical work was done by G. C. Curtin, A. P. Marranzino, and Uteana Oda of the Branch of Exploration Research, U.S. Geological Survey. Each sample was analyzed for calcium, magnesium, iron, and 27 minor elements.

The distribution of locally high concentration areas for bismuth, molybdenum, copper, lead, zinc, arsenic, antimony, silver, and boron is shown in figures 3–5. Threshold concentrations were arbitrarily chosen after studying the analyses of the visibly unmineralized samples; they are greater than local background by at least a factor of five for all elements except bismuth and boron. Background concentrations of bismuth and boron are less than, or similar to, the 10 parts per million lower sensitivity limit of the spectrographic method used. The directional trend of individual areas is not significant, since most areas contain

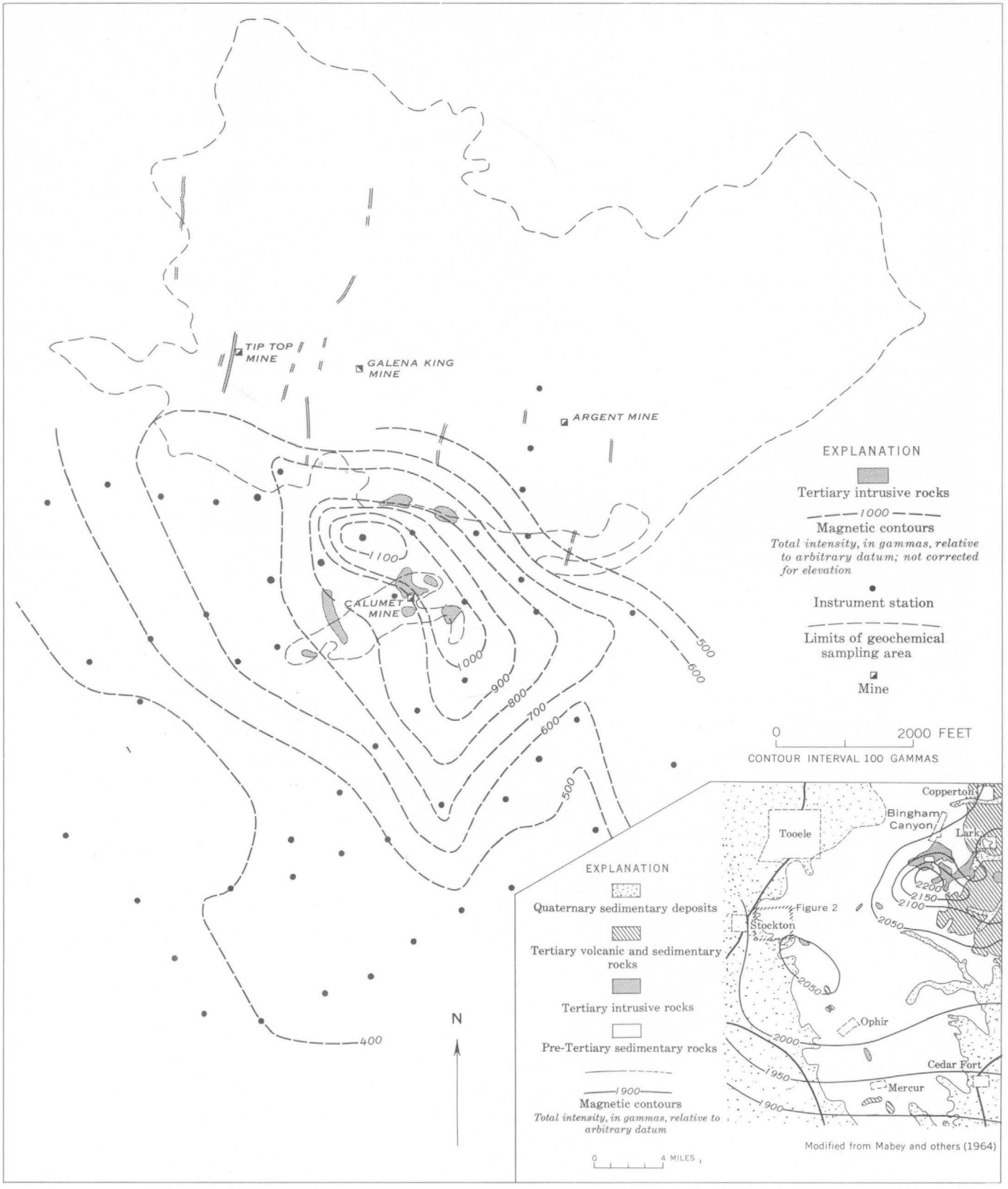


FIGURE 2.—Map showing magnetic contours and distribution of Tertiary intrusive rocks in the Stockton district, Utah.

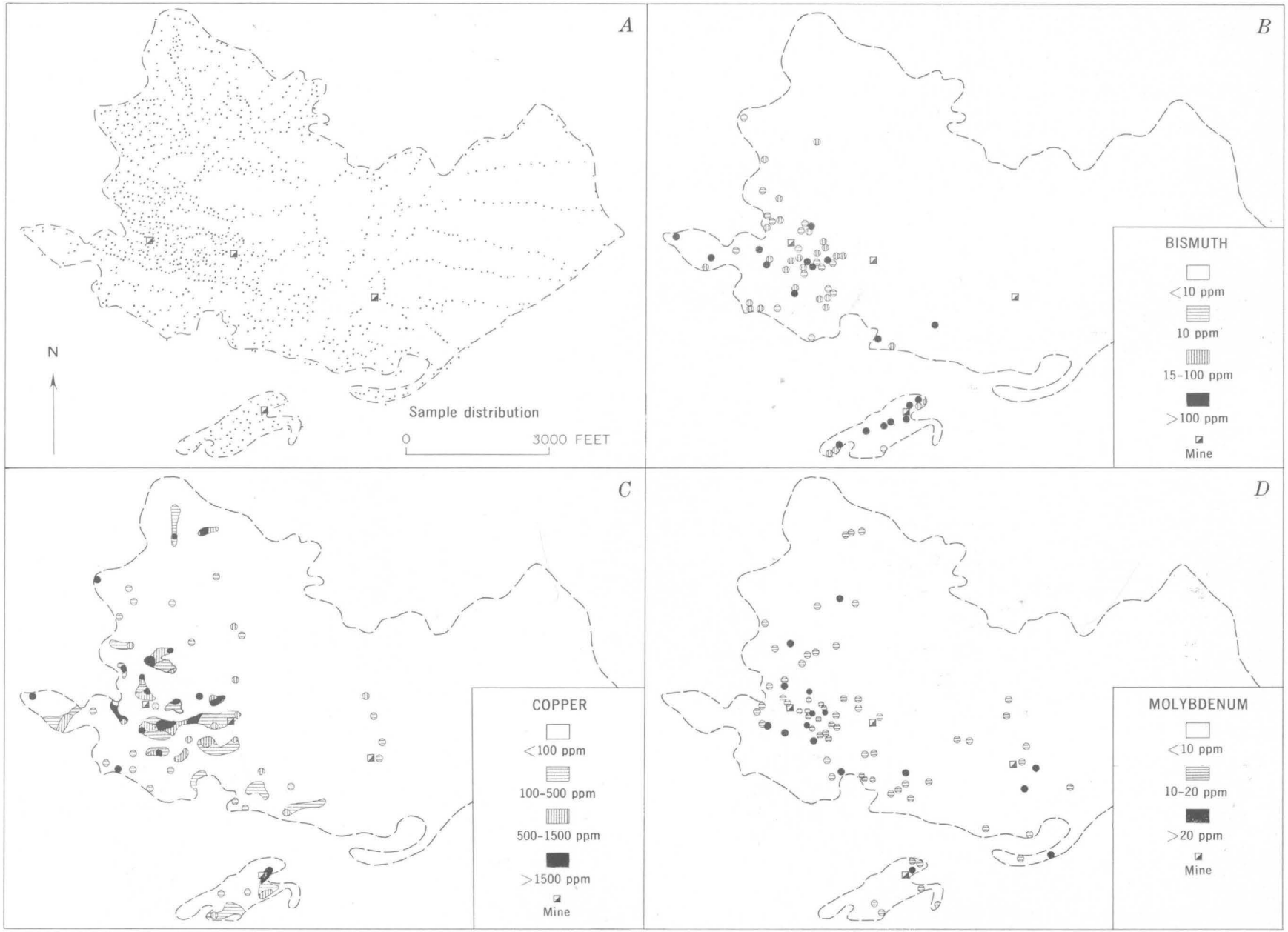


FIGURE 3.—Sample distribution and distribution of bismuth, copper, and molybdenum in the Stockton district, Utah. Mines shown on the maps, from west to east in the larger sampling area, are the Tip Top, Galena King, and Argent; and in the smaller area, the Calumet.

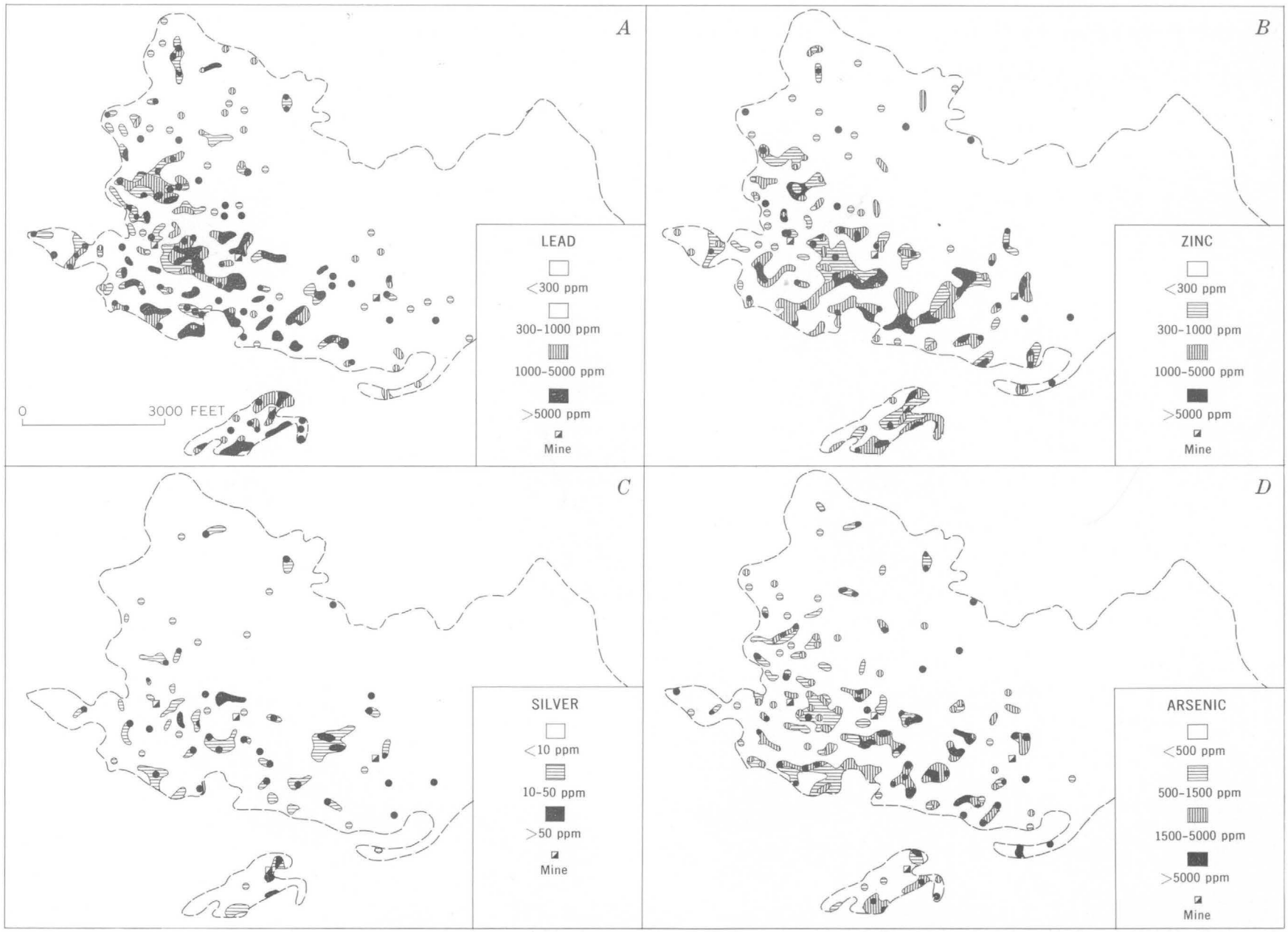


FIGURE 4.—Distribution of lead, zinc, silver, and arsenic in the Stockton district, Utah. Mines shown on the maps, from west to east in the larger sampling area, are the Tip Top, Galena King, and Argent; and in the smaller area, the Calumet.

211-690 O - 66 - 14

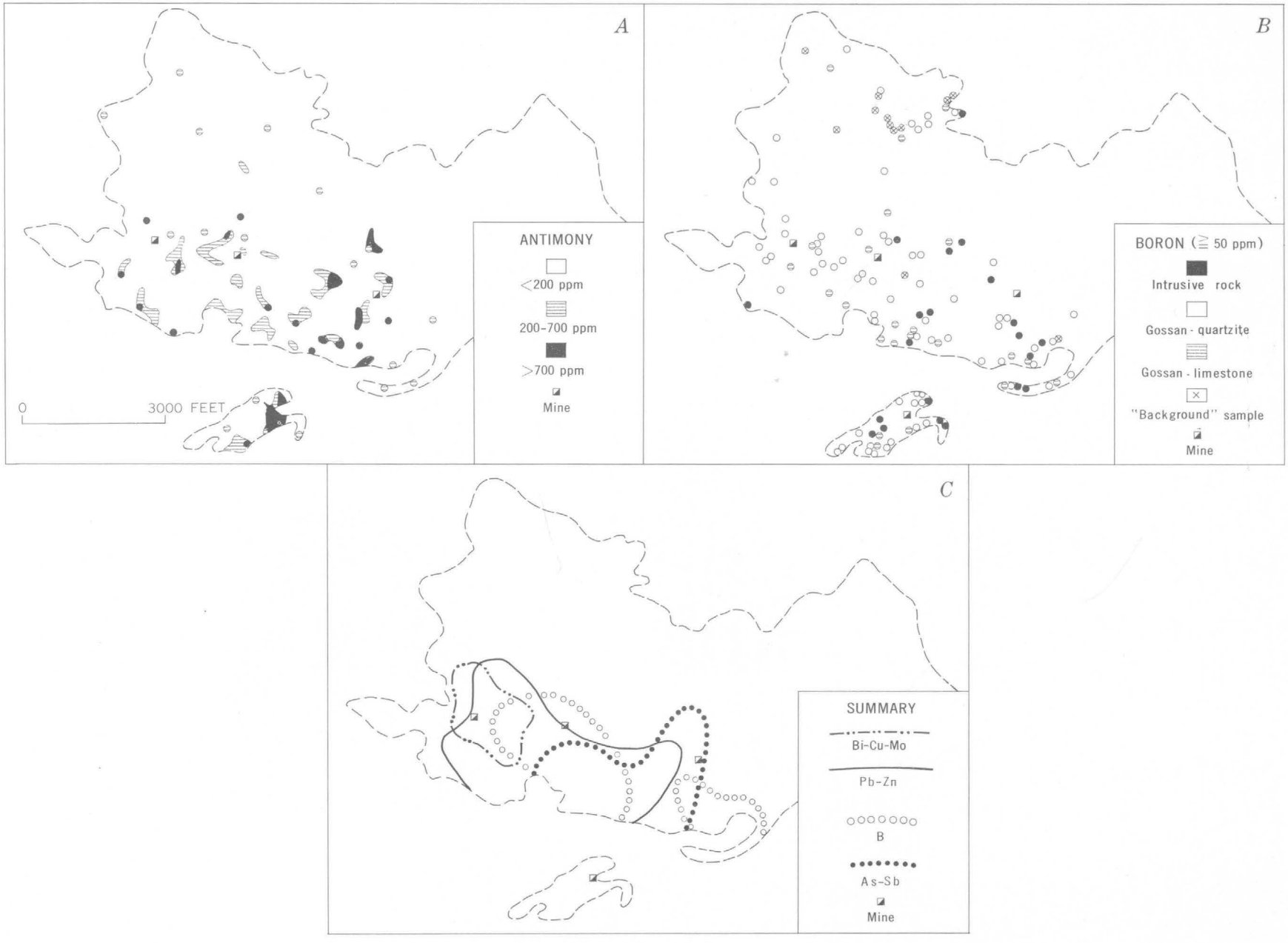


FIGURE 5.—Distribution of antimony and boron, and generalized summary of metal distribution in the Stockton district, Utah. Mines shown on the maps, from west to east in the larger sampling area, are the Tip Top, Galena King, and Argent; and in the smaller area, the Calumet.

diversely oriented fissures; however, their aggregate distribution may be significant.

In the sample area north of the Calumet mine, locally high concentrations of bismuth, copper, and molybdenum are clustered in gossan samples near the Tip Top shaft (fig. 3*B*, *C*, *D*); several narrow dikes have been mapped in this area (fig. 2). The first dike east of the Tip Top mine is locally termed the Raddatz porphyry and, according to Gilluly (1932, p. 52), "widens considerably at depth and where cut on the 1,200-foot level of the Honorine mine is 300 feet wide."

The areas of locally high lead and zinc concentrations partly overlap the bismuth-copper-molybdenum zone and extend appreciably farther to the north and east; silver is erratically distributed in the lead-zinc zone (figs. 3–5). The highest reported arsenic and antimony concentrations occur largely in and beyond the eastern part of the lead-zinc zone. Boron concentrations equal to or greater than 50 ppm extend beyond the eastern limits of significant known mineralization but are common throughout the lead-zinc zone.

A generalized summary of the distribution of metals in the main sample area at Stockton is shown in figure 5*C*; the overall pattern appears to reflect hypogene environmental controls. The areas of locally high bismuth-copper-molybdenum concentrations are inferred to have formed in relatively high temperature zones near the source of the metal-bearing solutions (Goldschmidt, 1954, p. 483; Erickson and others, 1961, p, D317). The intermediate lead-zinc zone would indicate lower temperatures of sulfide deposition.

Arsenic and antimony are most noticeably concentrated in the eastern (lower temperature?) part of the mineralized area, an occurrence consistent with the relatively high volatilities predicted for these metals in hydrothermal ore fluids (Krauskopf, 1964, p. 44). The distribution of boron may be a result of preore magmatic processes.

Each of the metals considered in the main sample area, except molybdenum, is concentrated in the smaller area surrounding the Calumet mine (figs. 3–5). The features of this distribution may be unrelated to the postulated center of mineralization near the Tip Top shaft.

The hypogene minerals which supplied certain metals now found in the gossan samples at Stockton are largely a matter of speculation. Galena, sphalerite, chalcopyrite, and argentite are likely sources for the lead, zinc, copper, and silver; small amounts of tetrahedrite and arsenopyrite reported by Butler and others (1920, p. 372) may account for the presence of antimony and arsenic. Hypogene tourmaline occurs in the metamorphosed limestones of the Ophir and Mercur districts southeast of Stockton (Gilluly, 1932, p. 129), but no minerals having boron as an essential constituent were identified in the Stockton area itself. Similarly, hypogene molybdenum and bismuth minerals remain unknown; molybdenum may be present as the trace mineral molybdenite, whereas bismuth may occur as microscopic inclusions of bismuthinite or matildite in galena (Fleischer, 1955, p. 979–980).

## EXPLORATION POSSIBILITIES

Geochemical studies in the areas of known mineralization at Stockton indicate a distribution of metals characterized by a central bismuth-copper-molybdenum, a medial lead-zinc, and an outer antimony-arsenic-(boron?) zone. The western and southwestern portions of the district are covered by alluvium and have been only partly explored; on the basis of the zonal interpretation, further exploration is suggested in these areas. Geophysical methods and geochemical analysis may isolate target areas in the alluvium-covered limestones marginal to the intrusive center shown in figure 2. Recent work by Erickson and Marranzino (1960, p. B98) and by Erickson and his coworkers (1964, p. 17) suggests that copper and possibly silver are concentrated in caliche coatings on clasts in alluvial sediments overlying buried ore deposits; a reconnaissance study of caliche and soil samples based on traverses extended from the bedrock control areas may be worthwhile.

Geophysical anomalies have been reported in Rush Valley, 2 miles south of Stockton (anonymous oral commun., 1965); these anomalies have been confirmed by the writers. This area lies along the projected axial zone of the Ophir anticline, the locus of ore bodies in the Ophir district (Gilluly, 1932, pl. I), and may be a favorable area for additional geophysical and geochemical exploration.

## REFERENCES

Butler, B. S., Loughlin, G. F., Heikes, V. C., and others, 1920, The ore deposits of Utah: U.S. Geol. Survey Prof. Paper 111, 672 p.

Erickson, R. L., and Marranzino, A. P., 1960, Geochemical prospecting for copper in the Rocky Range, Beaver County, Utah: Art. 47 *in* U.S. Geol. Survey Prof. Paper 400–B, p. B98–B101.

Erickson, R. L., Marranzino, A. P., Oda, Uteana, and Janes, W. W., 1964, Geochemical exploration near the Getchell mine, Humboldt County, Nevada: U.S. Geol. Survey Bull. 1198–A, 26 p.

Erickson, R. L., Masursky, Harold, Marranzino, A. P., and Oda, Uteana, 1961, Geochemical anomalies in the upper

plate of the Roberts thrust near Cortez, Nevada: Art. 401 *in* Geol. Survey Prof. Paper 424–D, p. D316–D320.

Fleischer, Michael, 1955, Minor elements in some sulfide minerals: Econ. Geology, 50th Anniversary Volume, 1905–1955, p. 970–1024.

Gilluly, James, 1932, Geology and ore deposits of the Stockton and Fairfield quadrangles: U.S. Geol. Survey Prof. Paper 173, 171 p.

Goldschmidt, V. M. (Muir, Alex, ed.), 1954, Geochemistry: Oxford, Clarendon Press, 730 p.

Krauskopf, K. B., 1964, The possible role of volatile metal compounds in ore genesis: Econ. Geology, v. 59, p. 22–45.

Mabey, D. R., Crittenden, M. D., Jr., Morris, H. T., Roberts, R. J., and Tooker, E. W., 1964, Aeromagnetic and generalized geologic map of part of north-central Utah: U.S. Geol. Survey Geophys. Inv. Map GP–422 scale 1:250,000.

# ARIZONA–NEW MEXICO AND NEVADA–UTAH BERYLLIUM BELTS

By D. R. SHAWE, Denver, Colo.

*Abstract.*—Beryllium occurrences of several types in southern Arizona and New Mexico are found in a belt characterized by fluorspar deposits and beryllium- and fluorine-rich igneous rocks. The Arizona–New Mexico area is geologically similar to the Nevada–Utah belt that contains the world's largest beryllium deposits at Spor Mountain, Utah.

Numerous occurrences of beryllium minerals in an east-northeast-trending belt in southeastern Arizona and southwestern New Mexico mark a province in which exploration may lead to the discovery of nonpegmatitic beryllium deposits of commercial value. The belt is discernible on maps published by Warner and others (1959) and Griffitts and others (1962). The belt has geologic similarities to a known beryllium belt in east-central Nevada and west-central Utah centered at Spor Mountain, Thomas Range, Utah, which has the world's largest known beryllium deposits (Griffitts, 1964a). The Nevada–Utah belt, which also has a northeasterly trend, is discernible on the map of Griffitts and others (1962), and part of it has been described briefly by Cohenour (1963a).

The Spor Mountain beryllium deposits are large semiconcordant tabular bodies in a thick, carbonate-rich tuffaceous assemblage of sedimentary rocks, and they are closely associated with fluorspar deposits and rhyolitic rocks of unusually high fluorine and beryllium content (Staatz, 1963). Because this association seems to be genetically significant (Staatz, 1963, p. M33–35), the search for new beryllium deposits may profitably be directed to localities containing fluorspar deposits together with fluorine- and beryllium-rich rhyolitic rocks. On a larger scale, areas with beryllium deposits, fluorspar deposits, and fluorine- and beryllium-rich rhyolites may be outlined as beryllium-fluorine provinces. Coats and others (1962, p. 967) suggested that areas where volcanic rocks with a high beryllium content are found in the Western United States are favorable for the occurrence of deposits of the Spor Mountain type.

The purpose of this article is to compare the Arizona–New Mexico province with the Nevada–Utah belt to evaluate the likelihood that deposits of the Spor Mountain type may be found in Arizona and New Mexico.

## DESCRIPTION OF BERYLLIUM BELTS

The Arizona–New Mexico and Nevada–Utah belts and also other areas of numerous beryllium occurrences in these States are outlined in figure 1. Individual beryllium localities in east-central Nevada and west-central Utah are shown on figure 2, and those in southeastern Arizona and southwestern New Mexico are shown on figure 3; further data are in table 1. Most of these beryllium deposits are probably Tertiary in age (Cohenour, 1963a; Jahns, 1944); others are older, as at Wheeler Peak in eastern Nevada, where

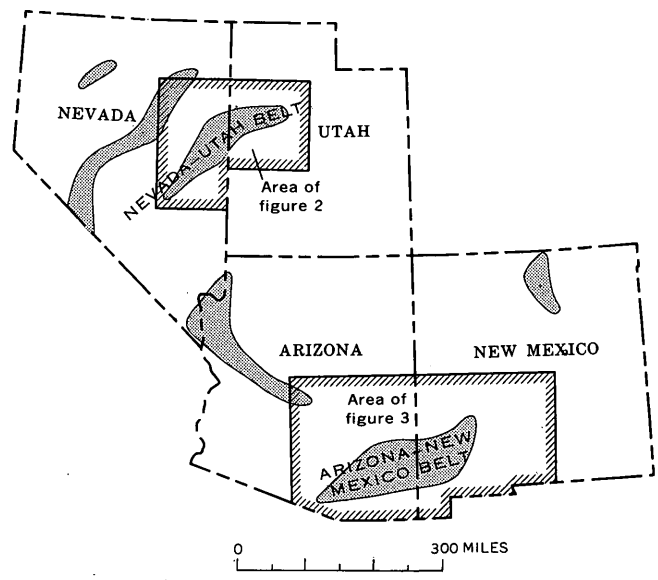


FIGURE 1.—Index map of Nevada, Utah, Arizona, and New Mexico, showing areas (shaded) of numerous beryllium occurrences (after Griffitts and others, 1962; Griffitts, 1964a, 1964b; and other sources).

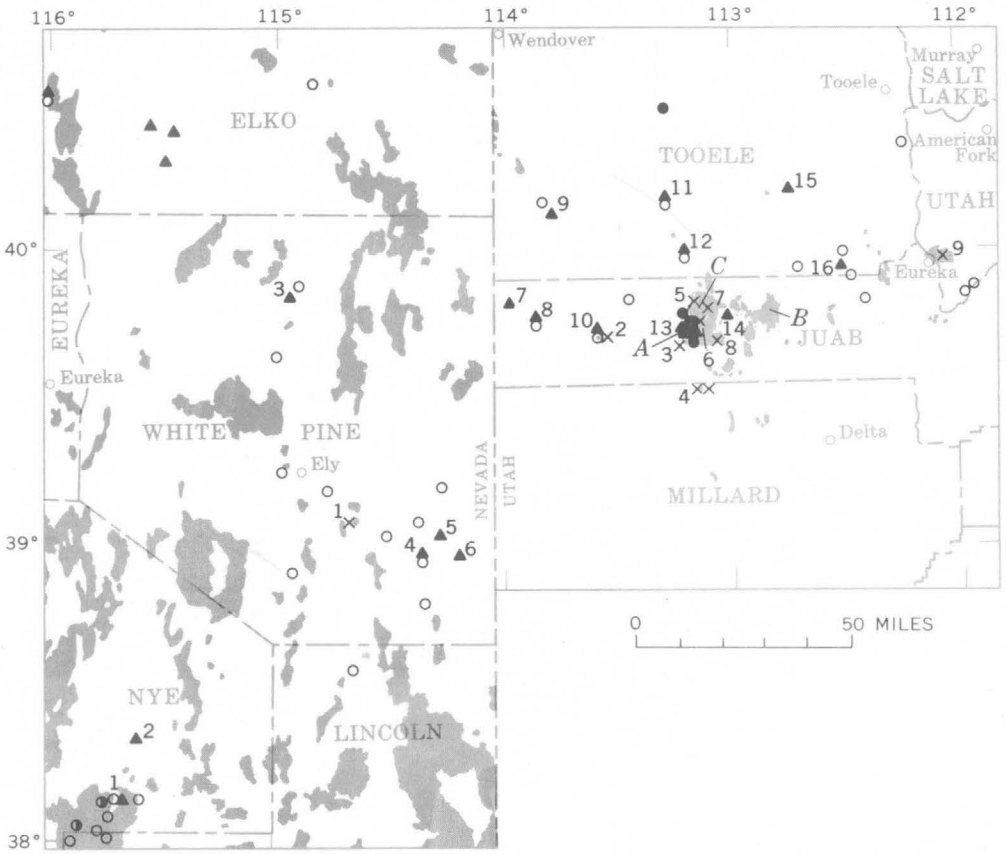


FIGURE 2.—Beryllium and fluorite occurrences in east-central Nevada and west-central Utah. Dark-gray areas: Nevada, volcanic rocks (chiefly silicic), based on geologic map of Nevada (Tagg and others, 1964); Utah, rhyolitic rocks, modified from geologic maps of northwestern and southwestern parts of Utah (Stokes, 1963; Hintze, 1963). Beryllium occurrence: ▲; based on Griffitts (1964a, 1964b) and other sources; numbers refer to occurrences described in table 1. Fluorite occurrence: ●, more than 1,000 tons fluorspar production; ◑, less than 1,000 tons fluorspar production; ○, fluorite mineral occurrence; based on Horton (1961), Dasch (1964), and other sources. Fluorine- or beryllium-rich rhyolite or quartz latite: ×; based on Staatz and Carr (1964), other sources, and this report; numbers refer to localities described in table 2. *A*, Spor Mountain; *B*, Keg Mountains; *C*, Thomas Range.

their age is probably Mesozoic (Whitebread and Lee, 1961).

Fluorite deposits shown on figures 2 and 3 tend to be larger and more numerous in the vicinity of beryllium occurrences. This same relation also is apparent in comparing figure 1 with the map showing fluorspar occurrences in the Western United States published by Peters (1958, p. 664). Probably most of these fluorite deposits are Tertiary in age, although Peters (1958, p. 667, 683–684) emphasizes recurrent mobilization of fluorine from older deposits in fluorine-rich regions.

Numerous silicic igneous rocks near the beryllium belts, particularly volcanic rocks of Tertiary age, have unusually high beryllium and fluorine contents (figs. 2 and 3, and table 2). Beryllium- and fluorine-rich volcanic rocks from the Nevada–Utah and Arizona–New Mexico belts (table 3) are similar in composition to the average alkali rhyolite given by Nockolds (1954), but contain slightly more MgO and CaO, slightly less total Fe oxides and $Na_2O$, and appreciably less $TiO_2$ and $P_2O_5$ than average alkali rhyolite. They ordinarily contain 6–20 parts per million Be and 0.12 to 0.79 percent F, yet the average rhyolitic flow rock (74–78 percent $SiO_2$) contains only 5–6 ppm Be (Shawe and Bernold, 1966, table 3) and 0.10 percent F (calculated from plate 5, *B*, Shawe and Bernold, 1966).

The rhyolitic welded tuff in the Cenozoic Rhyolite Canyon Formation of Enlows (1951) from Chiricahua National Monument, Ariz., is unusual in that the two samples contain 0.14 and 0.49 percent F (loc. 11, tables 2 and 3) which is much greater than the 0.05 percent F found in the average tuff with this silica content (Shawe and Bernold, 1966, pl. 5, *A*). There may be

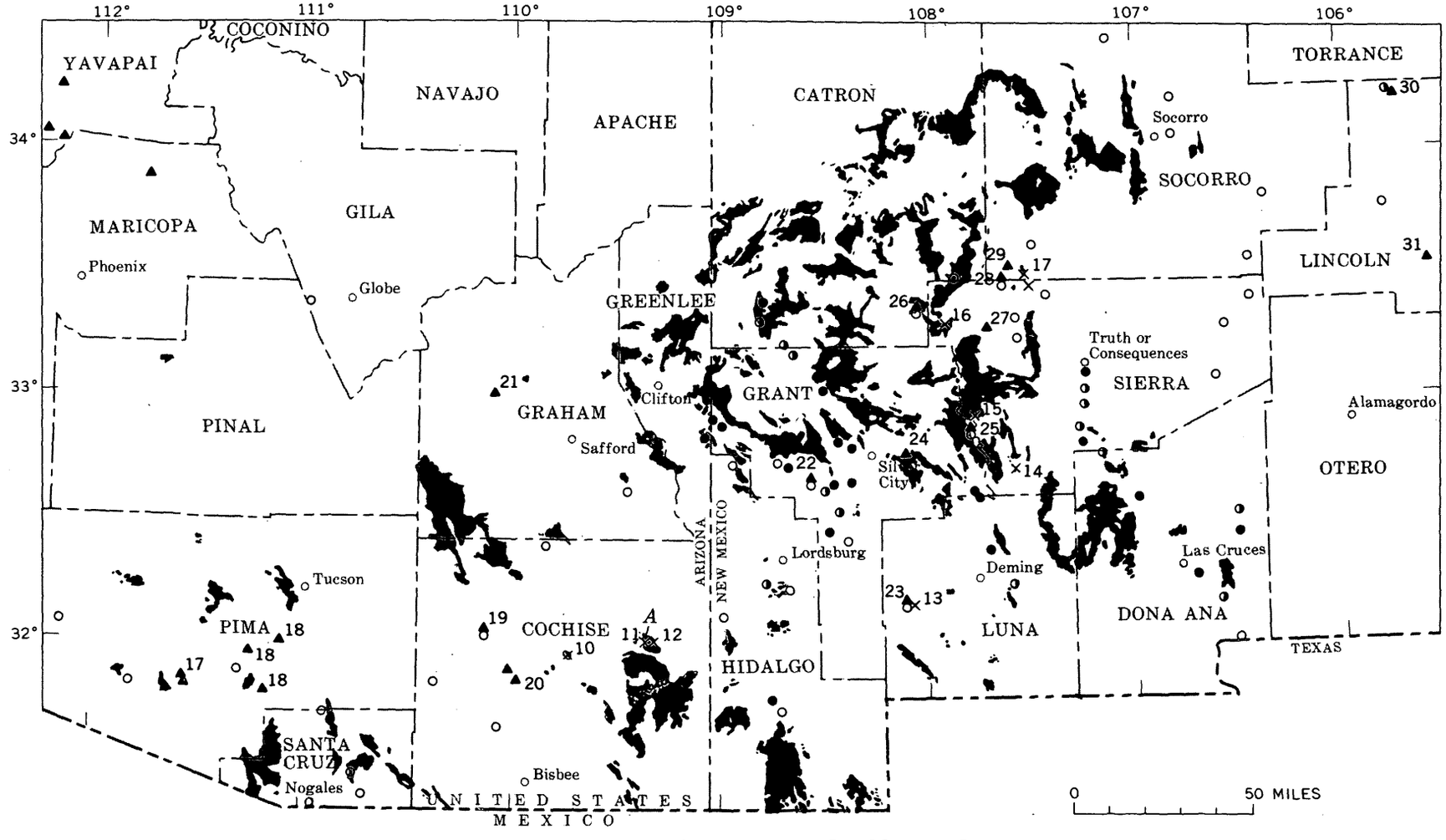


FIGURE 3.—Beryllium and fluorite occurrences in southeastern Arizona and southwestern New Mexico. Dark-gray areas are rhyolitic volcanic rocks, based on geologic maps of Arizona counties (Arizona Bureau of Mines, 1958–60), geologic maps of northwestern and southwestern parts of New Mexico (Dane and Bachman, 1957, 1961), and other sources. Beryllium occurrence: ▲, based on Warner and others (1959), McCrory and O'Haire (1961), Griffitts and others (1962), and other sources; numbers refer to occurrences described in table 1. Fluorite occurrence (some localities only approximate): ●, more than 1,000 tons fluorspar production; ◑, less than 1,000 tons fluorspar production; ○, fluorite mineral occurrence; adapted from Peters (1958), Rothrock and others (1946), and other sources. Fluorine- or beryllium-rich rhyolite or granite: ×, based on Coats and others (1962), other sources, and this report; numbers refer to localities described in table 2. *A*, Chiricahua area.

TABLE 1.—*Beryllium occurrences in east-central Nevada, west-central Utah, southeastern Arizona, and southwestern New Mexico*

| Locality (figs. 2 and 3) | Type of deposit | BeO (percent) | Reserves (tons) | Remarks | References |
|---|---|---|---|---|---|
| **Nevada** | | | | | |
| 1. Sawmill Canyon, Quinn Canyon Range, Nye County. | Beryl in granite | | | | Griffitts (1964b, p. 75). |
| 2. Troy Canyon, Grant Range, Nye County. | Beryl in pegmatite | | | Near scheelite mines | Griffitts (1964b, p. 71). |
| 3. Cherry Creek Mountains, White Pine County. | | 0.1 | | In bleached quartz monzonite near scheelite mines. | Griffitts (1964b, p. 74). |
| 4. Mount Wheeler and Jeppson deposits, Snake Range, White Pine County. | Phenacite and beryl in veins in limestone. | .75 | 100,000+ | With scheelite and fluorite near granitic stock. | Stager (1960), Griffitts 1964b, p. 74). |
| 5. Strawberry Creek, Snake Range, White Pine County. | Beryl in pegmatite-aplite dike. | | | | Griffitts (1964b, p. 71). |
| 6. East side of Snake Range, White Pine County. | Beryllian idocrase in tactite | | | | Griffitts (1964b, p. 75). |
| **Utah** | | | | | |
| 7. Goshute Indian Reservation, Juab County. | Beryl in pegmatite | | | | Griffitts (1964a, p. 75). |
| 8. Trout Creek, Deep Creek Range, Juab County. | Beryl in veins | | | With scheelite near granitic stock | Griffitts (1964a, p. 74–75). |
| 9. Rodenhouse Wash, Gold Hill area, Deep Creek Range, Tooele County. | Bertrandite(?) in silicified quartz monzonite. | 0.5 | Millions | With quartz, calcite, and adularia in fracture zone 2 miles long. | Do. |
| 10. Honeycomb Hills, Juab County | Bertrandite(?) in altered rhyolitic tuff. | .75 | | With fluorite and montmorillonite | McAnulty and Levinson (1964). |
| 11. Granite Mountain, Tooele County | Beryl in pegmatite | .001–.01 | | | Griffitts (1964a, p. 75). |
| 12. Dugway district, Dugway Range, Tooele County. | | .04–.3 | | Near tungsten deposits, in fault zone in limestone. | L. S. Hilpert (written commun., 1965). |
| 13. Spor Mountain, Thomas Range, Juab County. | Bertrandite in altered rhyolitic tuff. | .5 | Millions | With fluorite, montmorillonite. At least 6 deposits ½–2 miles long. | Staatz and Griffitts (1961), Staatz (1963), Griffitts (1964a, p. 75). |
| 14. West side of Keg Mountains, Juab County. | | .03–.2 | | In dark crystalline volcanic rock | L. S. Hilpert (written commun., 1965). |
| 15. Skull Valley, Tooele County | Beryl in pegmatite | | | | Griffitts (1964a, p. 75). |
| 16. Sheeprock Mountains, Tooele County | Beryl in granite | .01–.1 | Millions | Wolframite- and fluorite-bearing deposits near berylliferous granite contact. | Cohenour (1963b, p. 12), Griffitts (1964a, p. 75). |
| **Arizona** | | | | | |
| 17. Baboquivari Peak, Pima County | Beryl in veins | | | Veins in granitic rock | Griffitts and others (1962). |
| 18. Sierrita Mountains, Pima County | | | | Near scheelite-bearing deposits. Garnet tactite at nearby Pima and Helvetia districts contains 0.001–0.002 percent BeO (Warner and others, 1959, p. 103–105). | McCrory and O'Haire (1961). |
| 19. Little Dragoon Mountains, Cochise County. | Beryl in veins | 0.001–0.05 | | With scheelite in quartz monzonitic stock. | Warner and others (1959, p. 97–98). |
| 20. Gordon and Abril mines, Dragoon Mountains, Cochise County. | | .004–.04 | | Garnet tactite near granitic stock | Warner and others (1959, p. 96–97). |
| 21. Goodwin Wash, Graham County | | | | | McCrory and O'Haire (1961). |
| **New Mexico** | | | | | |
| 22. Long Lost Brother claim, Big Burro Mountains, Grant County. | | 0.002 | | Fluorspar vein | Warner and others (1959, p. 114). |
| 23. Victorio district, Victorio Mountains, Luna County. | Beryl in veins, helvite in garnet tactite. | .003–.2 | | With scheelite and fluorite in tactite, wolframite in quartz veins, near granitic stock. | Warner and others (1959, p. 122–125). |
| 24. Groundhog mine, Central mining district, Grant County. | | .002 | | Garnet tactite | Warner and others (1959, p. 118). |
| 25. Grandview mine, Black Range, Grant County. | Helvite in veins | .001–.02 | | With fluorite, near quartz monzonitic stock. | Warner and others (1959, p. 114–116). |
| 26. Taylor Creek, Black Range district, Catron County. | | .002 | | With cassiterite and fluorite in porphyritic rhyolite. | Warner and others (1959, p. 109). |
| 27. Midnight mine, Apache No. 1 district, Sierra County. | | .01 | | Copper-rich quartz vein | Warner and others (1959, p. 128). |
| 28. Iron Mountain district, Sierra Cuchillo, Sierra County. | Helvite in tactite | .2–.7 | 200,000± | With fluorite and scheelite, near rhyolite, granite, aplite intrusive rocks. | Jahns (1944, p. 76). |
| 29. Monticello Box, Sierra Cuchillo, Socorro County. | Bertrandite in vein | .001–1.0 | | In hydrothermally altered rhyolite and latite. | U.S. Geol. Survey (1964, p. A9–A10). |
| 30. Gallinas district, Gallinas Mountains, Lincoln County. | | .008 | | With fluorite in breccia near syenite porphyry. | Warner and others (1959, p. 121). |
| 31. Capitan district, Capitan Mountains, Lincoln County. | | .005 | | In contact zone around "granite aplite" stock. | Do. |

TABLE 2.—*Beryllium- and fluorine-rich igneous rocks in east-central Nevada, west-central Utah, southeastern Arizona, and southwestern New Mexico*

| Locality (figs. 2 and 3) | Rock type | Field sample No. (USGS lab. No.) | Be (ppm) | F (percent) | Remarks | References |
|---|---|---|---|---|---|---|
| **Nevada** | | | | | | |
| 1. Schell Creek Range, White Pine County. | Porphyritic rhyolite dikes | 60D414, 60D501 | 3 | 0.12 | See table 3. Near normal in Be and F content but otherwise chemically like Be- and F-rich rhyolites. | H. Drewes (written commun., 1963). |
| **Utah** | | | | | | |
| 2. Honeycomb Hills, Juab County. | Topaz-bearing rhyolite flow. | DRS-105-61 (D100-56Z; 297981) | 7 | 0.79 | See table 3 | New analysis. |
| 3. Spor Mountain area, Thomas Range, Juab County. | Topaz-bearing rhyolite flow. | DRS-107-61 (297982), DRS-108-61 (297983; D101188W) | 13 | .90 | Semiquantitative spectrographic analyses by J. C. Hamilton. Be content is average of analyses of 2 samples. F content determined on DRS-108-61 by V. C. Smith. 30 ppm Sn, 500 ppm Li also present. | Do. |
| 4. Northern Little Drum Mountains, Millard County. | Topaz-bearing rhyolite plugs. | DRS-183-63 (D101211W), DRS-186-63 | 21 | 1.75 | Neutron-activation analysis by D. R. Shawe. Be content is average of analyses of 2 samples. F content determined on DRS-183-63 by V. C. Smith. | Do. |
| 5. Northern Thomas Range, Juab County. | Rhyolitic glass, younger volcanic group.[1] | SC-14-54, WJC-23-54 | 15 | .29 | See table 3 | Staatz and Carr (1964, p. 110), Staatz (written commun., 1963). |
| 6. Central Thomas Range, Juab County. | Porphyritic rhyolite and rhyolite tuff, older volcanic group.[1] | SO-11-52, WJC-24-54 | 20 | .47 | do | Do. |
| 7. Northern Thomas Range, Juab County. | Topaz-bearing rhyolite flow, younger volcanic group.[1] | CS-23-55, CS-24-55, WJC-124-55 | 20 | .18 | do | Do. |
| 8. Southern Thomas Range, Juab County. | Topaz-bearing rhyolite flow, younger volcanic group.[1] | SO-10-52 | 15 | .27 | do | Do. |
| 9. Dividend, East Tintic Mountains, Utah County. | Eocene Packard Quartz Latite, tuff (Morris and Lovering, 1961, p. 124). | DRS-1-63 | 6 | ---- | Neutron-activation analysis by D. R. Shawe. Be content is unusually high for quartz latite; volcanic rocks of this composition (70 percent silica) average 2 ppm Be (Shawe and Bernold, 1966, table 1). | New analysis. |
| **Arizona** | | | | | | |
| 10. Sulphur Hills, Cochise County. | Black vitrophyre, probably base of welded tuff in Miocene or Pliocene Volcanics (Gilluly, 1956, p. 116–118). | 55C60 | 8 | 0.21 | Sample collected by R. R. Coats. | Coats and others (1962), R. R. Coats (written commun., 1965). |
| 11. Chiricahua National Monument, Cochise County. | Rhyolite Canyon Formation,[2] member 6, welded tuff. | 2 | ---- | .49 | See table 3 | Enlows (1955, p. 1233). |
| | Rhyolite Canyon Formation,[2] member 6, welded tuff. | Ch-5 (I4208) | 10 | .14 | See table 3. Sample collected by D. W. Peterson. | New analysis. |
| 12. Chiricahua National Monument, Cochise County. | Rhyolite Canyon Formation,[2] member 8, welded tuff. | SL-2 (305450), SL-3 (305451), SL-5 (305452). | 6 | ---- | Semiquantitative spectrographic analyses by J. C. Hamilton. Be content is average of analyses of 3 samples. Samples collected by D. W. Peterson. | New analyses. |
| **New Mexico** | | | | | | |
| 13. Victorio Mountains, Luna County. | Granitic plug | DRS-106-62 (D101190W). | 12 | 0.38 | Neutron-activation analysis for Be by Walter Duke. F content determined by V. C. Smith. | New analysis. |
| 14. Lake Valley, Mimbres Mountains, Sierra County. | Mimbres Peak Formation,[3] rhyolite flow. | 7 | ---- | ---- | See table 3. No data on Be and F content but rock is chemically like Be- and F-rich rhyolite of sample 15. | Jicha (1954, p. 50). |
| 15. Emory Pass, Black Range, Grant County. | Rhyolitic vitrophyre dike, probably related to Mimbres Peak Formation.[3] | 55C22 | 10 | .34 | Probably same rock type as 14; Be and F data included with rock 14 in table 3. Sample collected by R. R. Coats. | Coats and others (1962). R. R. Coats (written commun., 1965). |
| 16. Round Mountain, Black Range, Sierra County. | Topaz-bearing rhyolite flow | ---- | ---- | ---- | Contains cassiterite; similar cassiterite-bearing rhyolite flows widespread for 30 miles to the north. | Fries and others (1942, p. 309). |
| 17. Alamosa River, Sierra Cuchillo, Socorro and Sierra Counties. | Rhyolite flows | DRS-146-63 (D101203W), DRS-147-63. | 9 | .12 | Neutron-activation analyses by D. R. Shawe. Be content is average of analyses of 2 samples. F content determined on DRS-146-63 by V. C. Smith. | New analyses. |

[1] Of Staatz and Carr (1964).
[2] Of Enlows (1951).
[3] Of Elston (1957).

TABLE 3.—*Chemical composition of beryllium- and fluorine-rich volcanic rocks*

[Localities shown in figs. 1 and 2. Descriptions given in tables 1 and 2]

| | A | B | C | D | E | F | G | H | I | J | K | L | M |
|---|---|---|---|---|---|---|---|---|---|---|---|---|---|
| Locality No. | 1 | 2 | 5 | 6 | 7 | 8 | | 11 | 11 | 14 | | | |
| Rock type and locality | Porphyritic rhyolite, Schell Creek Range, Nev. | Topaz-bearing rhyolite, Honeycomb Hills, Utah | Rhyolitic glass, Thomas Range, Utah | Porphyritic rhyolite and rhyolite, Thomas Range, Utah | Topaz-bearing rhyolite, N. Thomas Range, Utah | Topaz-bearing rhyolite, S. Thomas Range, Utah | Average F-Be-rich rhyolite, Nevada-Utah | Welded rhyolite tuff, Chiricahua National Monument, Ariz. | Welded rhyolite tuff, Chiricahua National Monument, Ariz. | Rhyolite, Mimbres Peak, N. Mex. | Average F-Be-rich rhyolite, Arizona-New Mexico | Average alkali rhyolite (Nockolds, 1954) | Average calcalkali rhyolite (Nockolds, 1954) |
| **Chemical analyses** | | | | | | | | | | | | | |
| $SiO_2$ | 76.08 | 73.98 | 73.80 | 73.39 | 75.59 | 76.54 | 74.89 | 74.55 | 76.49 | 76.50 | 75.85 | 74.57 | 73.66 |
| $Al_2O_3$ | 12.86 | 13.35 | 12.12 | 13.33 | 12.35 | 12.16 | 12.65 | 11.16 | 12.08 | 11.46 | 11.57 | 12.58 | 13.45 |
| $Fe_2O_3$ | .28 | .72 | .71 | .89 | .80 | .92 | .71 | 1.51 | 1.51 | 1.12 | 1.38 | 1.30 | 1.25 |
| FeO | .40 | .16 | .27 | 1.06 | .23 | .37 | .43 | .00 | .05 | .43 | .16 | 1.02 | .75 |
| MgO | .16 | .04 | .09 | .29 | .24 | .14 | .18 | .16 | .11 | .25 | .17 | .11 | .32 |
| CaO | .79 | 1.53 | .80 | 1.17 | .93 | .78 | .97 | 1.53 | .26 | .68 | .82 | .61 | 1.13 |
| $Na_2O$ | 3.27 | 3.87 | 3.03 | 3.07 | 3.32 | 3.50 | 3.28 | 3.11 | 3.87 | 3.43 | 3.47 | 4.13 | 2.99 |
| $K_2O$ | 4.74 | 4.61 | 5.00 | 5.32 | 5.08 | 4.97 | 4.99 | 4.66 | 4.85 | 4.46 | 4.66 | 4.73 | 5.35 |
| $H_2O^+$ | .42 | .31 | 3.15 | .44 | .25 | .11 | .84 | .76 | .11 | .63 | .50 | .66 | .78 |
| $H_2O^-$ | .55 | .05 | .44 | .22 | .39 | .05 | .34 | 1.15 | .16 | .33 | .55 | | |
| $TiO_2$ | .05 | .02 | .11 | .13 | .11 | .09 | .09 | .11 | .12 | .12 | .12 | .17 | .22 |
| $P_2O_5$ | .02 | .05 | .01 | .05 | .01 | .02 | .02 | .02 | .00 | .02 | .01 | .07 | .07 |
| MnO | .06 | .06 | .06 | .06 | .04 | .05 | .05 | .12 | .07 | .09 | .09 | .05 | .03 |
| $CO_2$ | .03 | .72 | .01 | .12 | .35 | .16 | .20 | .04 | .01 | | .03 | | |
| Cl | .01 | .01 | .11 | .01 | .09 | | .05 | .08 | .01 | | .05 | | |
| F | .12 | .79 | .29 | .47 | .18 | .27 | .31 | .49 | .14 | [1].34 | .32 | | |
| Subtotal | 99.84 | 100.27 | 100.00 | 100.02 | 99.96 | | 100.00 | | 99.84 | | | | |
| Less O | .05 | .33 | .15 | .20 | .10 | | .14 | | .06 | | | | |
| Total | 99.79 | 99.94 | 99.85 | 99.82 | 99.86 | 99.86 | 99.86 | [2] 99.99 | 99.78 | 99.52 | | 100.00 | 100.00 |
| **Semiquantitative spectrographic analyses** [3] | | | | | | | | | | | | | |
| B | 0.0008 | 0 | | 0.003 | | 0.0015 | 0.0015 | | 0.003 | | | | |
| Ba | .001 | 0.003 | | .01 | | .0002 | .004 | | .0015 | | | | |
| Be | .0003 | .0007 | 0.0015 | .002 | 0.002 | .0015 | .0015 | | .001 | [1].001 | 0.001 | | |
| Co | 0 | 0 | | | | | | | .02 | | | | |
| Cr | .00015 | 0 | | .0007 | | .0002 | .0003 | | 0 | | | | |
| Cu | .00015 | .0005 | | .0015 | | .0006 | .001 | | .0002 | | | | |
| Ga | .002 | .005 | | .0035 | | .0015 | .003 | | .005 | | | | |
| La | 0 | .003 | | .007 | | .006 | .003 | | .01 | | | | |
| Li | .015 | .02 | | | | | .02 | | 0 | | | | |
| Mo | 0 | 0 | | 0 | | 0 | 0 | | 0 | | | | |
| Nb | .003 | .003 | | .01 | | .005 | .005 | | .005 | | | | |
| Nd | 0 | 0 | | | | | | | .015 | | | | |
| Ni | 0 | 0 | | .001 | | .0004 | .0005 | | 0 | | | | |
| Pb | .002 | .007 | | .004 | | .006 | .004 | | .005 | | | | |
| Sc | .0007 | 0 | | 0 | | 0 | 0 | | 0 | | | | |
| Sn | .0007 | .002 | .0009 | .005 | .0005 | 0 | .0015 | | 0 | | | | |
| Sr | .005 | .002 | | .0005 | | .0003 | .001 | | .0015 | | | | |
| V | 0 | 0 | | .001 | | 0 | .0002 | | 0 | | | | |
| Y | .002 | .01 | | .008 | | .005 | .005 | | .01 | | | | |
| Yb | .0002 | .0015 | | .001 | | .0007 | .001 | | .0015 | | | | |
| Zr | .005 | .005 | | .009 | | .01 | .008 | | .05 | | | | |

A. Average of 2 chem. analyses; C. L. Parker, analyst. Average of 2 spectro. analyses; P. R. Barnett, analyst.
B. 1 chem. analysis; C. L. Parker, analyst. 1 spectro. analysis; J. C. Hamilton, analyst.
C. Average of 2 chem. analyses; E. J. Tomasi, analyst. Average of 2 spectro. analyses; P. R. Barnett, analyst.
D. Average of 2 chem. analyses; E. J. Tomasi and L. M. Kehl, analysts. 1 spectro. analysis, except Be and Sn values based on 2 analyses; P. R. Barnett, analyst.
E. Average of 3 chem. analyses; M. K. Balazs, analyst. Average of 3 spectro. analyses; P. R. Barnett, analyst.
F. 1 chem. analysis; L. M. Kehl, analyst. 1 spectro. analysis; P. R. Barnett, analyst.
G. Analyses are average of cols. A–F.
H. 1 chem. analysis; L. D. Trumbull, analyst.
I. 1 chem. analysis; D. F. Powers, analyst. 1 spectro. analysis; J. C. Hamilton, analyst.
J. 1 chem. analysis; H. B. Wiik, analyst.
K. Analyses are average of cols. H–J.
L. Average of 21 chem. analyses.
M. Average of 22 chem. analyses.

[1] See "Remarks," table 2, loc. 15.
[2] Includes 0.54 percent $SO_3^{-1}$.
[3] Results are reported in percent to the nearest number in the series 1, 0.7, 0.5, 0.3, 0.2, 0.15, 0.1, and so forth; these numbers represent approximate midpoints of group data on a geometric scale. About 30 percent of the assigned groups for semiquantitative results include the quantitative values.

a similar contrast in the Be content, for the average tuff has 3–4 ppm Be (Shawe and Bernold, 1966, table 3), yet the one sample analyzed here has 10 ppm Be.

## SUGGESTIONS FOR PROSPECTING

At Spor Mountain, Utah, the host rock of the beryllium deposits is a thick widespread unit of water-reworked rhyolitic volcanic debris, which contains numerous carbonate pebbles eroded from Paleozoic formations in the region. The unit's permeability permitted passage of a large volume of mineralizing solutions, and its chemical nature—possibly high calcium carbonate content—induced precipitation of ore minerals. Similar rocks elsewhere in the beryllium belts are worthy of exploration.

Three favorable places seem to be the Keg Mountains (east of the Thomas Range in fig. 2) in the Nevada–Utah belt, the area of the Tertiary volcanic Datil Formation of southwestern New Mexico (which is much of the northern part of the volcanics shown in New Mexico in fig. 3), and the Chiricahua area of southeastern Arizona (vicinity of rock localities 11 and 12, fig. 3). In the Keg Mountains, 5–15 miles east of the Thomas Range, tuffaceous rhyolitic sedimentary rocks are widespread in the vicinity of fluorine- and beryllium-rich rhyolite. Volcanic sedimentary rocks are interbedded with rhyolitic rocks of the Datil Formation in southwestern New Mexico (for example, Jahns and others, 1955, p. 94), and where they cover ancient hills of Paleozoic carbonate rocks that provided debris to the sediments, they have much the same environment as at Spor Mountain. Sabins (1957, p. 1325, 1326) found a small quantity of tuffaceous sediments, together with fresh-water limestone and Paleozoic carbonate cobbles in andesitic conglomerate, in the Chiricahua area in the vicinity of the Rhyolite Canyon Formation of Enlows (1951), and these also may be favorable sites for mineralization.

## REFERENCES


Arizona Bureau of Mines, 1958, Geologic map of Graham and Greenlee Counties.

——— 1959a, Geologic map of Cochise County.

——— 1959b, Geologic map of Pinal County.

——— 1960, Geologic map of Pima and Santa Cruz Counties.

Coats, R. R., Barnett, P. R., and Conklin, N. M., 1962, Distribution of beryllium in unaltered silicic volcanic rocks of the western conterminous United States: Econ. Geology, v. 57, p. 963–968.

Cohenour, R. E., 1963a, The beryllium belt of western Utah, *in* Utah Geol. Soc., Guidebook to the geology of Utah: no. 17, p. 4–7.

——— 1963b, Beryllium and associated mineralization in the Sheeprock Mountains [Utah], *in* Utah Geol. Soc. Guidebook to the geology of Utah: no. 17, p. 8–13.

Dane, C. H., and Bachman, G. O., 1957, Preliminary geologic map of the northwestern part of New Mexico: U.S. Geol. Survey Misc. Geol. Inv. Map I–224.

——— 1961, Preliminary geologic map of the southwestern part of New Mexico: U.S. Geol. Survey Misc. Geol. Inv. Map I–344.

Dasch, M. D., 1966, Fluorine, *in* U.S. Congress, Senate Comm. on Interior and Insular Affairs, Mineral and water resources of Utah: U.S. 88th Cong., 2d sess., p. 162–168.

Elston, W. E., 1957, Geology and mineral resources of the Dwyer quadrangle, Grant, Luna, and Sierra Counties, New Mexico: New Mexico Bureau of Mines and Mineral Resources Bull. 38, 86 p.

Enlows, H. E., 1951, The igneous geology of Chiricahua National Monument, Arizona [summary]: Tulsa Geol. Soc. Digest, v. 19, p. 105–107.

——— 1955, Welded tuffs of Chiricahua National Monument, Arizona: Geol. Soc. America Bull., v. 66, p. 1215–1246.

Fries, Carl, Jr., Schaller, W. T., and Glass, J. J., 1942, Bixbyite and pseudobrookite from the tin-bearing rhyolite of the Black Range, New Mexico: Am. Mineralogist, v. 27, p. 305–322.

Gilluly, James, 1956, General geology of central Cochise County, Arizona: U.S. Geol. Survey Prof. Paper 281, 169 p.

Griffitts, W. R., 1964a, Beryllium, *in* U.S. Congress, Senate Comm. on Interior and Insular Affairs, Mineral and water resources of Utah: U.S. 88th Cong., 2d sess., p. 71–55.

——— 1964b, Beryllium, *in* U.S. Congress, Senate Comm. on Interior and Insular Affairs, Mineral and water resources of Nevada: U.S. 88th Cong., 2d sess., Doc. 87, p. 70–55.

Griffitts, W. R., Larrabee, D. M., and Norton, J. J., 1962, Beryllium in the United States: U.S. Geol. Survey Mineral Inv. Resource Map MR–35.

Hintze, L. F., 1963, Geologic map of southwestern Utah: Utah Geol. and Mineralog. Survey.

Horton, R. C., 1961, An inventory of fluorspar occurrences in Nevada: Nevada Bur. Mines Rept. 1, 31 p.

Jahns, R. H., 1944, Beryllium and tungsten deposits of the Iron Mountain district, Sierra and Socorro Counties, New Mexico: U.S. Geol. Survey Bull. 945–C, p. 45–79.

Jahns, R. H., Kottlowski, F. E., and Kuellmer, F. J., 1955, Volcanic rocks of south-central New Mexico: New Mexico Geol. Soc., Guidebook of south-central New Mexico, p. 92–95.

Jicha, H. L., Jr., 1954, Geology and mineral deposits of Lake Valley quadrangle, Grant, Luna, and Sierra Counties, New Mexico: New Mexico Bur. Mines and Mineral Resources Bull. 37, 93 p.

McAnulty, W. N., and Levinson, A. A., 1964, Rare alkali and beryllium mineralization in volcanic tuffs, Honey Comb Hills, Juab County, Utah: Econ. Geology, v. 59, p. 768–774.

McCrory, F. J., and O'Haire, R. T., 1961, Map of known metallic mineral occurrences of Arizona: Arizona Bur. Mines.

Morris, H. T., and Lovering, T. S., 1961, Stratigraphy of the East Tintic Mountains, Utah: U.S. Geol. Survey Prof. Paper 361, 145 p.

Nockolds, S. R., 1954, Average chemical composition of some igneous rocks: Geol. Soc. America Bull., v. 65, p. 1007–1032.

Peters, W. C., 1958, Geologic characteristics of fluorspar deposits in the Western United States: Econ. Geology, v. 53, p. 663–688.

Rothrock, H. E., Johnson, C. H., and Han, A. D., 1946, Fluorspar resources of New Mexico: New Mexico Bur. Mines and Mineral Resources Bull. 21, 239 p.

Sabins, F. F., Jr., 1957, Geology of the Cochise Head and western part of the Vanar quadrangles, Arizona: Geol. Soc. America Bull., v. 68, p. 1315–1342.

Shawe, D. R., and Bernold, Stanley, 1966, Beryllium content of volcanic rocks: U.S. Geol. Survey Bull. 1214–C, 11 p.

Staatz, M. H., 1963, Geology of the beryllium deposits in the Thomas Range, Juab County, Utah: U.S. Geol. Survey Bull. 1142–M, 36 p.

Staatz, M. H., and Carr, W. J., 1964, Geology and mineral deposits of the Thomas and Dugway Ranges, Juab and Tooele Counties, Utah: U.S. Geol. Survey Prof. Paper 415, 188 p.

Staatz, M. H., and Griffitts, W. R., 1961, Beryllium-bearing tuff in the Thomas Range, Juab County, Utah: Econ. Geology, v. 56, p. 941–950.

Stager, H. K., 1960, A new beryllium deposit at the Mount Wheeler mine, White Pine County, Nevada: U.S. Geol. Survey Prof. Paper 400–B, p. B70–B71.

Stokes, W. L., 1963, Geologic map of northwestern Utah: Utah Geol. and Mineralog. Survey.

Tagg, K. M., and others, compilers, 1964, Geologic map of Nevada, *in* U.S. Congress, Senate Comm. on Interior and Insular Affairs, Mineral and water resources of Nevada: U.S. 88th Cong., 2d sess., Doc. 87, facing p. 12.

U.S. Geological Survey, 1964, Geological Survey Research 1964, Chapter A: U.S. Geol. Survey Prof. Paper 501–A, 367 p.

Warner, L. A., Holser, W. T., Wilmarth, V. R., and Cameron, E. N., 1959, Occurrence of nonpegmatite beryllium in the United States: U.S. Geol. Survey Prof. Paper 318, 198 p.

Whitebread, D. H., and Lee, D. E., 1961, Geology of the Mount Wheeler mine area, White Pine County, Nevada: U.S. Geol. Survey Prof. Paper 424–C, p. C120–C122.

# RECENT FAULTING AT PROPOSED DAMSITES IN THE ERETAN AREA, WEST JAVA, INDONESIA

By REED J. ANDERSON, La Paz, Bolivia

*Work done in cooperation with the Indonesian Geological Survey*

*Abstract.*—Two proposed damsites in the foothills of West Java were investigated in 1963 as part of the preliminary study for a large reservoir project intended to provide irrigation storage and flood control.

The damsites are underlain by Miocene shale, marl, and sandstone and Pleistocene volcanic breccia and tuff. The sedimentary rocks are soft and weak and have been badly deformed by compressive tectonic forces. The volcanic rocks are relatively undisturbed, but at both damsites they are cut by faults believed to be active, and they are highly susceptible to weathering. Evidence of active faulting includes extremely young topography, little modified by erosion; earthquake activity, shown by instrumental records and the reports of local inhabitants; and the chronic problem of landslides in the area. Work on the reservoir project has been suspended because of these conditions.

The northern coastal plain near the Tjimanuk River [1] in West Java is a chronic problem area because of heavy flooding during each rainy season and severe drought during each dry season. In 1962 the Irrigation Department, an agency of the Indonesian Ministry of Public Works and Power, began preliminary investigations of potential damsites on the Tjimanuk River with the hope of providing about 1 billion cubic meters of storage to irrigate 90,000 hectares (about 350 square miles) of riceland and to reduce destructive flooding in the coastal plain.

In early 1963 the Geological Survey of Indonesia (GSI) was requested to make a geologic feasibility study of damsites in the Eretan area. At that time the author was working with the GSI as an advisor in engineering geology, as part of the technical-assistance program of the U.S. Agency for International Development. The study, which was made with the assistance of Ir. Rudiman of the GSI's Engineering Geology–Hydrology Branch, resulted in detailed information concerning foundation areas of the damsites and a geologic map at a scale of 1:5,000. Detailed studies and mapping were confined to the area surrounding the damsites; a reconnaissance study on a regional basis was necessary to interpret the geology, but regional geologic mapping and the defining of stratigraphic units were beyond the scope of the study.

The investigation included 2 alternate potential damsites located about 7 and 8½ kilometers, respectively, north of the town of Darmaradja, near the village of Eretan (fig. 1). In this report they will be referred to as damsite A, the downstream site, and damsite B, the upstream site. Between the two sites are a diversion dam, control structure, and tunnel that are being used to generate electric power at Parakankondang. The damsite area can be reached from Wado or Kadipaten by a road that is sometimes accessible only to 4-wheel-drive vehicles.

The studies of Koolhoven [2] provided helpful background information on the geology of the damsites and surrounding areas. Other information was obtained from Dr. Gan Tjiang Liang and Dr. Tjia Hong Djin (written and oral commun., 1963), who were carrying on geologic mapping and other research in the area. Information was also available from test pits that

[1] The prefix "Tji" in the local language of West Java means flowing water and is applied to all streams regardless of size. Translating to English is difficult and will not be attempted except for those streams that should clearly be designated as rivers. The current Indonesian practice in English-language reports, which the author follows, is to use the full name followed by the English noun; thus, Tjimanuk River.

[2] W. C. B. Koolhoven, 1935, Verslag van een Tocht in de afdeelingen Soemedang en Madjalengka, Bladen 42 en 48 (West Java) in Juli/Augustus 1935 [Report of an expedition in the Soemedang area of the Madjalengka region, quadrangles 42 and 48 (West Java) in July and August 1935]: Unpublished report 10/G/35 on file at Indonesia Geological Survey library, 25 p.

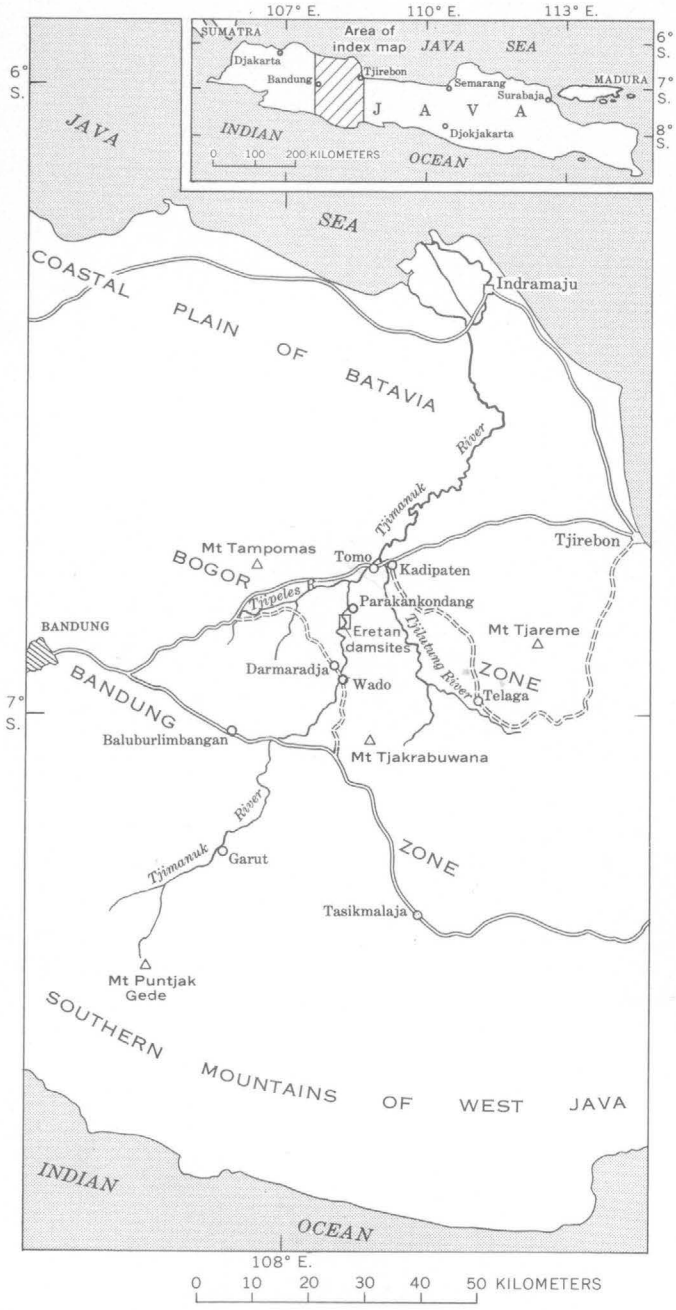


FIGURE 1.—Index map showing location of Eretan damsites and features of the Tjimanuk River drainage basin in West Java.

were put down as part of a study by Ir. Grufron Achmad and Ir. Darmawan of the Bandung Institute of Technology.

## PHYSIOGRAPHY

The Tjimanuk River is one of the major rivers of West Java. It heads about 1,500 meters above sea level on the north slope of Mt. Puntjak Gede, just north of the southern mountains of West Java and about 20 km southwest of Garut. It flows generally northeast and discharges into the Java Sea about 60 km northwest of Tjirebon. Its largest tributary, the Tjilutung River, joins it on the northern coastal plain near Tomo. The river's course, which cuts across northwest-trending structures, shows little structural control except locally.

The headwater area is a high volcanic plateau 800 to 900 m above sea level which is surrounded and partly divided by volcanoes that rise prominently to heights of 2,200 to more than 2,800 m. To the north, between Baluburlimbangan and Wado, another relatively flat plateau lies at an altitude of about 550 m. It is surrounded by volcanoes that rise abruptly to altitudes of 1,000 to 1,800 m. Farther downstream the land surface drops off steeply to the broad Darmaradja topographic basin, which is surrounded by low, gently sloping hills. North of this shallow basin is a narrow belt of greater relief and steeper topography in which the damsites are located. Still farther downstream are the lowest foothills of northern Java, an area of low relief and gently sloping topography, and north and northeast of Tomo the northern coastal plain slopes gradually to the Java Sea.

## REGIONAL GEOLOGY

Bemmelen (1949, p. 27, 28) divides West Java into four structural and physiographic belts. From south to north these are (fig. 1): the southern mountains of West Java, the Bandung zone, the Bogor zone, and the coastal plain of Batavia (Djakarta). The southern mountains and the coastal plain are not important for this discussion, but the structural features of the Bandung and Bogor zones are important in understanding the geology of the region around Eretan. The Bandung zone represents the top and northern flank of the geanticline of Java, which, according to Bemmelen (1949, p. 27, 645), has broken down along a longitudinal fault system and slid northward, compressing the Bogor zone into a complex anticlinorium of strongly folded Tertiary strata. The regional trend of rocks in this anticlinorium is difficult to determine because of the complexity of secondary folding, but according to H. D. Tjia, S. Asikin, and T. L. Gan (written and oral commun., 1963) its axis passes through the mouth of the Tjinambo River just south of damsite B and strikes N. 75°–80° W (fig. 2). The secondary folds are a distinct series of anticlines and synclines; anticlinal or homoclinal ridges are separated by synclinal or homoclinal valleys. Most of the ridges along the east side of the Darmaradja basin that are underlain by sedimentary rocks are structural ridges.

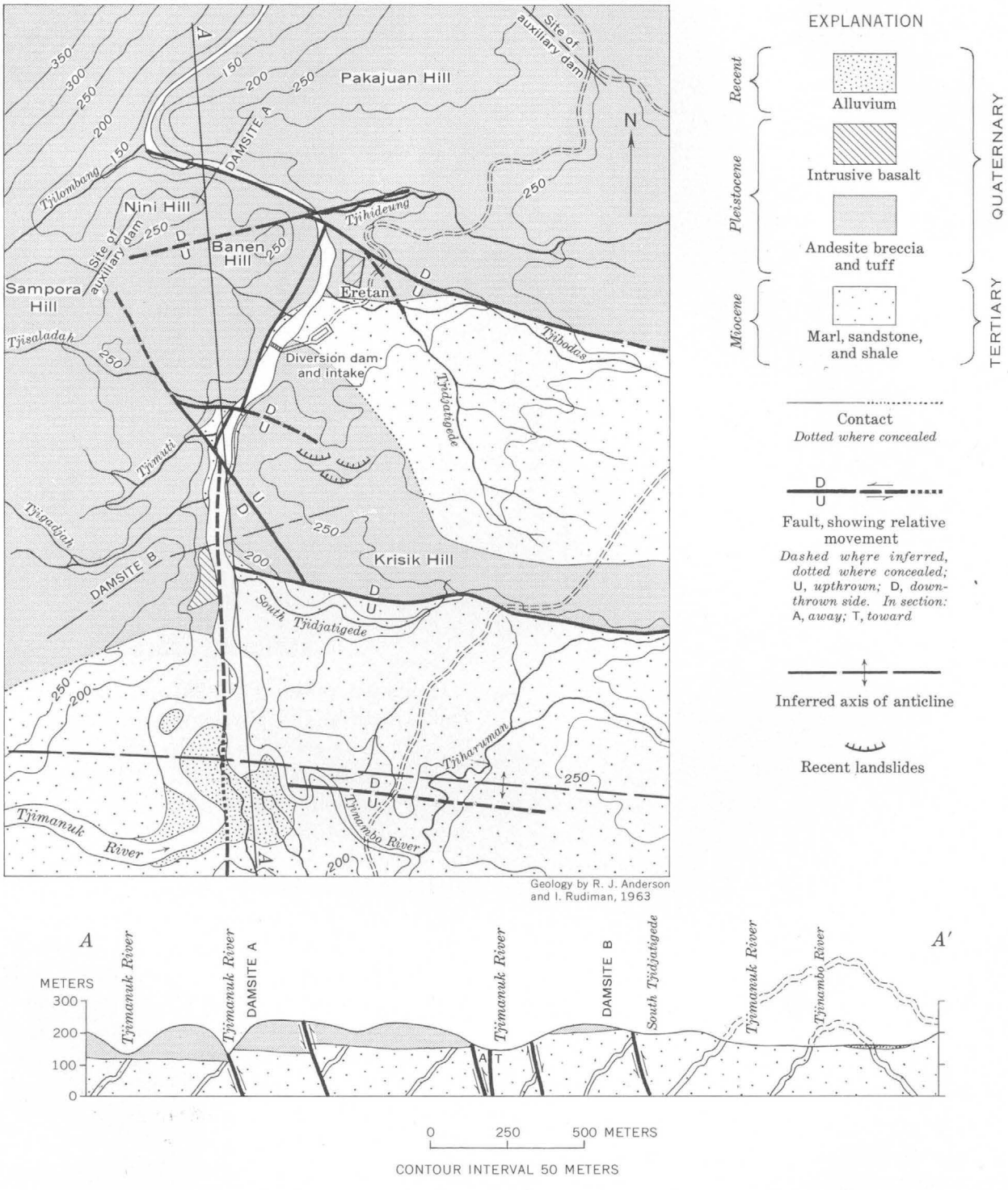


FIGURE 2.—Geologic map and generalized geologic section at potential Eretan damsites in West Java.

Rocks of the region are cut by a series of parallel thrust and reverse faults that are probably associated with the northward sliding of the Bandung zone. Bemmelen (1949, p. 651) describes a thrust fault that can be traced from the west foot of Tjareme volcano northwestward for a distance of about 70 km. Tjareme and Tampomas volcanoes are most likely located on a major fault zone that passes just north of the damsites. Some geologists believe this fault zone is still active; it may be related to recent earthquake activity in the region and to the other more local faults discussed in another section of this report. Other less extensive

thrust or reverse faults are near the damsites and in the proposed reservoir area. Those which were found in the mapped area—near the mouth of the Tjinambo River, on the south side of Krisik Hill, and near the channel of the Tjibodas—are shown on figure 2.

There are also two major tear faults nearby. One has offset structures south of the mapped area and seems to have offset a marl layer near damsite B. It seems to follow the Tjimanuk River channel to or beyond Eretan. The second one is outside the limits of figure 2.

Sedimentary rocks of Miocene and Pliocene age and volcanic rocks of Pleistocene and Recent age are exposed in the damsite region. The most widespread types are Quaternary breccias and tuffs that have accumulated from eruptions of the volcanoes Tjareme, Tampomas, and Tjakrabuwana; these rocks overlie a thick sequence of Miocene and Pliocene shale, marl, sandstone, and conglomerate that contains a few limestone lenses and intercalations of tuff and breccia. The sedimentary rocks are exposed in the core and south limb of an anticlinorium, and some are repeated in the north limb. They occupy a belt extending from Wado to Tomo (fig. 1); the outcrop pattern of each rock unit parallels the regional structural trend, which is slightly north of west. Exposed at the foot of the volcanic plateau southeast of Wado are the Tjidadap (Ludwig, 1933, p. 13–15) or Upper Halang beds[3] (Haar, 1934, p. 16–19); they are underlain to the north by the Lower Halang beds (Haar, 1934, p. 16–19) and the Pemali beds (Haar, 1934, p. 10–12). North of the damsites, thrust faulting has interrupted the sequence on the north limb of the anticlinorium, and the northern facies of the Tjidadap beds and the Kaliwangu beds (Ludwig, 1933, p. 18, 19) and the Tjiherang beds (Bemmelen, 1949, p. 651–653) are exposed. The rocks units are tabulated in table 1. A detailed description of the geology is given in another report, in preparation by the author, on engineering-geology investigations of the damsites.

TABLE 1.—*Stratigraphic units of the lower Tjimanuk River basin*

[Modified from Bemmelen, 1949, p. 649]

| Age | Rock unit | Description | Thickness (meters) |
|---|---|---|---|
| Recent | Alluvium | Stream-channel and terrace deposits, lake beds, a few lahars (landslide or debris-flow deposits of water-saturated volcanic debris) from active volcanoes. | |
| | Unconformity | | |
| Pleistocene | Volcanic rocks | Tuff, breccia, lava, and intrusive rocks, mostly andesitic. | [1] 200–300 |
| | Unconformity | | |
| Pliocene | Tjiherang beds | Conglomerate and tuffaceous sandstone. | 500–1, 000 |
| | Kaliwangu beds | Shale, marl, tuffaceous sandstone, conglomerate, and breccia. | 750–1, 000 |
| | Unconformity | | |
| Miocene | Tjidadap beds | Northern marine facies of shale. | 1, 200–1, 500 |
| | | Southern volcanic facies (Upper Halang beds) of breccia, tuffaceous sandstone, and conglomerate. | 1, 800–2, 500 |
| | Lower Halang beds | Claystone, tuffaceous sandstone and breccia. | 1, 500 |
| | Pemali beds | Shale, marl, quartz sandstone, limestone, small amount of breccia and tuff. | 2, 300–3, 200 |

[1] In vicinity of Eretan.

## GEOLOGY OF THE DAMSITE AREA

The area (fig. 2) is underlain by the Pemali beds, which, at the damsites, are predominantly bluish- to greenish-gray or light-yellow-brown soft, poorly indurated shale and marl (calcareous claystone) that contain thin interbeds of fine-grained friable sandstone and impure limestone. In much of the area these sedimentary rocks are capped by a layer of Pleistocene volcanic rock 200 to 300 m thick; but the sedimentary rocks are exposed in the channel of the Tjimanuk River and in the area between Krisik Hill and the Tjibodas.

The volcanic rocks are composed of a thick basal layer of breccia which forms the steeper part of the gorge immediately adjacent to the river, and of an overlying sequence of intercalated tuff, tuff-breccia, and breccia which forms the more gently sloping parts

[3] Formal stratigraphic names have not yet been established in Indonesia, although considerable stratigraphic work has been done by Dutch geologists and recently by Indonesian geologists. Stratigraphic names in this report are those currently in most general use.

of the canyon walls. The breccia is composed of andesite fragments, mostly in the size range of 1 to 15 centimeters, cemented together in a matrix of tuff; it is commonly moderately well indurated. Two distinct tuff layers are present, both of which are soft, poorly cemented, and highly susceptible to weathering; and in some places there are similar rocks which contain sufficient rock fragments to be called tuff-breccia. These rocks are red to light yellow brown or white and are fine to medium grained; some appear to be quite permeable. There are also at least two separate layers of breccia. Their difference is very noticeable in the lower west slope of Krisik Hill, where they have been brought together by faulting. One has a sandy matrix and weathers gray or brown; the other has a finer grained matrix and weathers red or light yellow.

The Pemali beds are in the core and flank of an anticlinorium. Their gross structure is shown in the generalized section on figure 2; however, on a local scale they are tightly folded and intricately faulted. There is no apparent preferred orientation of these local structures, although most of them seem to be related to regional tectonic movements that formed the Bandung and Bogor zones. In both areas where the Pemali beds are exposed (north and south of Krisik Hill) there are numerous tight folds; some of these folds are overturned, and some are accompanied locally by thrust faults. Most of the faults have displacements of less than 1 m to perhaps 3 or 4 m. The minor folds and faults are not shown on figure 2.

In contrast to the Pemali beds, the overlying volcanic rocks are not folded and are horizontal or, locally, are slightly tilted as a result of faulting.

In addition to the faults mentioned previously, both damsites are cut by faults that are apparently not of regional extent. A small fault follows the channel of the Tjihideung, apparently cuts the northwest side of Banen Hill, and continues through the saddle between Sampora Hill and Nini Hill, the location of a proposed auxiliary dam. Overburden covers the fault where it crosses the Tjimanuk River, but a short distance downstream there is a localized tilting of tuffaceous layers that indicates relative downward movement of the northwest block. A breccia layer is also higher in Banen Hill (alt 280 m) than its presumed correlative layer in Nini Hill (217 m) or in Pakajuan Hill (less than 220 m). There is also evidence of faulting in the channel of the Tjidjatigede. This evidence is difficult to evaluate because of poor exposures and the extreme deformation of the Pemali beds, but it is of particular interest because local inhabitants reported that earthquake activity in 1960 was centered in the channel. The fault follows the channel of the Tjidjatigede, where it apparently joins the fault in the Tjibodas, and continues down the Tjimanuk River channel through damsite A.

A fault cuts through the east abutment of damsite B about 175 m from the river channel. It trends northwest and is expressed topographically by three saddles, including the one between Sampora Hill and Nini Hill. Where it crosses the river it has offset a sandstone bed on the east bank. On the west side of the river it is expressed by a steep, narrow ravine that marks a sharp contact between red soil and gray-brown soil. A branch of this fault also offsets the sandstone bed in the river channel and extends westward to an area where landslides have been a chronic problem in the past.

## EVIDENCE OF RECENT FAULTING

A first view of the damsite area creates a strong impression that the topography is very young. Banen Hill appears to have been chopped off on two sides. It is a high, steep, pyramid-shaped knob that has been modified very little by erosion. The west wall of the Tjilombang also gives the impression of being a recent fault scarp. The slope, which is 200 m high, is bare of the usual vegetation, and landslides and slumps have occurred recently.

It seems reasonable to assume that the landslides have been triggered by earthquake activity related to faults. Landslides at the downstream end of the Parakankondang power tunnel, which involves the movement of some rock, have made it necessary to realine the tunnel, and operating personnel of the power station believe the tunnel subsequently has been affected by earth movement that has decreased the efficiency of the plant. This movement is probably also related to fault activity.

Local inhabitants of Eretan and nearby villages reported that earthquake activity has shaken the area frequently in the past few years, causing a large number of people to leave the area. Specifically, they mentioned earthquakes which resulted in the formation of low scarps along the Tjibodas in 1956, along the Tjihideung and the Tjisaladah on two separate occasions in 1958, and along the Tjidjatigede in 1960.

The information supplied by local inhabitants is supported by earthquake data published by the Meteorological and Geophysical Institute in Djakarta. During the years 1954–59, for which complete earthquake data are available, 21 recorded earthquakes originated in the lower Tjimanuk River basin very close to the damsites. During the latter half of 1955, the most active period, 13 earthquakes originated in

the area. It is significant that this same period was also one of pronounced landslide activity in the vicinity of Eretan.

## SIGNIFICANCE OF THE INVESTIGATION

The study has shown that it would be very costly and probably hazardous to attempt the construction of a major reservoir project at either of the two Eretan damsites because of recent fault activity and the probability of continued earth movement. Work on the damsites was suspended after an informal report describing foundation conditions was submitted to the Irrigation Department, and a search has been made to find other damsites on the Tjimanuk River to replace the Eretan sites.

The problems at the Eretan sites also emphasize the need for extreme caution and careful engineering-geology studies at the Tjipeles River damsite, which is located only 8 km to the west in an area that is also known to be active seismically.

Finally, the study points up the facts that certain areas of Indonesia are extremely active seismically, and that earthquake activity must be taken into consideration in the investigations of building sites and the design of larger structures. Feasibility and design studies should not only consider the stability of foundations and the presence or absence of active faults, but also the maximum intensities that can be expected from nearby or even relatively distant epicenters. The results of the study also emphasize the value of geologic studies at the beginning of large engineering projects to prevent wasted expense on engineering and construction work at building sites that are geologically unstable.

## REFERENCES

Bemmelen, R. W. van, 1949, The geology of Indonesia, v. 1A. General geology of Indonesia and adjacent archipelagoes: The Hague, Netherlands Govt. Printing Office, Indonesian Bur. Mines spec. ed., 732 p.

Harr, C. ter, 1934, Toelichting bij Blad 58 (Boemiajoe): Dienst Mijnd. Ned Indié, p. 16–19. [Explanatory text for quadrangle 58 (Boemiajoe)—Geological map of Java, 1:100,000, Netherlands East Indies (Indonesia) Bur. Mines]

Ludwig, O., 1933, Toelichting bij Blad 30 (Poerwakarta): Dienst Mijnd. Ned Indië, 45 p. [Explanatory text for quadrangle 30 (Poerwakarta)—Geological map of Java, 1:100,000, Netherlands East Indies (Indonesia) Bur. Mines]

Meteorological and Geophysical Institute, Djakarta, 1957, Earthquakes in Indonesia for the years 1948–55: Ser. A, no. 45, 72 p.

——— 1958, Earthquakes in Indonesia 1956: Ser. A, no. 46, 20 p.

——— 1961, Earthquakes in Indonesia 1957–58: Ser. A, no. 47, 31 p.

——— 1962, Earthquakes in Indonesia 1959: Ser. A, no. 48, 10 p.

211-690 O—66——15

# DETERMINATION OF MICROQUANTITIES OF MERCURY IN SULFIDE ORES BY PENFIELD TUBE–DITHIZONE AND SEMIQUANTITATIVE SPECTROGRAPHIC METHODS

By JOSEPH I. DINNIN and HELEN W. WORTHING, Washington, D.C.

*Abstract.*—Microquantities of mercury can be determined by either of two methods described. In the chemical method, mercury is volatilized in a Penfield tube, and the separated mercury dissolved and determined colorimetrically with dithizone. In the semiquantitative spectrographic method, mercury is volatilized using a deep electrode crater and a short exposure time. Both methods are applied to the analysis of mixtures of cinnabar and sphalerite.

The use of mercury-halo methods as a guide to the location of sulfide ore deposits (Saukov, 1946; Williston, 1964) has led to increased interest in the geochemistry of mercury and has fostered a need for better methods for the determination of trace amounts of mercury in sulfide minerals. Although a number of methods are available for the determination of mercury in geologic materials the methods are primarily designed for the analysis of rocks and soils and are not directly applicable to the analysis of sulfide minerals.

Sulfide minerals are likely to contain relatively high concentrations of elements such as copper and silver which interfere in the colorimetric dithizone method for the determination of mercury. Zinc and lead, although not very troublesome in moderate concentrations, require special treatment when present as major components of a mineral; trace elements such as gold, platinum, and palladium are more likely to be present in significant quantities. Although there are a number of methods available for the chemical and physical separation of mercury or for masking of interferences, the methods, albeit effective, are more involved than desirable when applied to the separation of microgram amounts of mercury from milligram or gram amounts of other compounds.

*Acknowledgment.* — Paul Barton, U.S. Geological Survey, furnished a large supply of mercury-free sphalerite for use in this investigation and guided and helped in the manufacture of the solid solutions of mercury in sphalerite.

## PENFIELD TUBE–DITHIZONE DETERMINATION

Chemical treatments for dissolving large samples of sulfide minerals and for the isolation of mercury or the masking of interferences require the use of relatively large amounts of reagents, each of which may be a source of mercury contamination. Elimination of the danger from reagent contamination makes attractive the various distillation procedures which take advantage of the volatility of mercury and its compounds. Although usually used for the volatilization of large amounts of mercury (Fahey, 1937), distillation procedures have also been applied to the determination of small amounts of it.

In the chemical procedure proposed here mercury is volatilized by heating the sample in a Penfield tube. A sample is heated to 800°C or higher, to assure the volatilization of any mercury compound that might be present. Mercuric sulfide rapidly diffuses into the adjacent cooler portion of the tube and condenses on the wall. Sulfides of most other metals are relatively nonvolatile, and only insignificant quantities will accompany the mercury. Removal of the bulb containing the remaining sample provides a means of separating almost all the known interferences from the mercury in the tube. The tube then serves as a convenient container for the dissolution of the sublimed mercuric sulfide.

Although the use of a Penfield tube was arrived at independently, the technique has since been found to have been developed by Aydin'yan (1960) and used for the determination of mercury in soils (Vasilevskaya and Shcherbakov, 1963) and coal (Aydin'yan, 1961), in each instance using lead peroxide as a flux. The method is in some respects similar to the campsite

method described by Ward and Bailey (1961) in which a sample is heated with ammonium iodide in a test tube, unreacted sample spilled out, and the condensed sublimate used for the colorimetric determination of mercury.

The colorimetric method used in the present study for the determination of mercury is based upon the work of Friedeberg (1955) and Yamamura (1960) and take advantage of the use of EDTA for the elimination of interferences and the presence of acetate for the stabilization of the color.

### Reagents

Aqua regia: 3 parts concentrated hydrochloric acid and 1 part concentrated nitric acid (v/v).

Dilute nitric acid: 0.01*N*

Hydroxylamine hydrochloride solution: 10 percent (w/v).

Mixed reagent: Dissolve 18.6 g of disodium ethylene-diaminetracetate dihydrate (EDTA) and 95 g of chloracetic acid in 600 ml of water and sufficient concentrated ammonium hydroxide to attain a final pH of 7. Filter and dilute to 1 liter with water.

Dithizone stock solution: 0.01 percent in carbon tetrachloride (w/v).

Dithizone reagent solution: 0.0005 percent in carbon tetrachloride (w/v). Prepare by dilution of the stock solution.

Stock mercury solution, 1 mg per ml: Dissolve 135.4 mg mercuric chloride in 100 ml 1*N* sulfuric acid.

Mercury standard solution, 10 $\mu$g per ml: Dilute 2.0 ml of the mercury stock solution to 200 ml with 1*N* sulfuric acid.

### Procedure

With the aid of a thistle tube or long-stemmed funnel, quantitatively transfer to the bulb of a Penfield tube a weighed portion of sample estimated to contain no more than 5 $\mu$g of mercury. Cover the open end of the tube with a capillary stopper and place the tube in a jacket filled with crushed ice. Heat the bulb to approximately 700°C with a gas-fired burner equipped with a heat-localizing chimney. Rotate the tube occasionally while heating for approximately 8 minutes. Remove the burner and heat the bulb to approximately 800–900°C with a gas-oxygen torch and maintain the temperature, rotating the tube continuously, for approximately 2 minutes. Seal off the bulb end of the tube and remove the bulb.

Add 1 ml of aqua regia and insert the tube, closed end down, into a bath of warm water. Gradually heat the water to near boiling and maintain at approximately 90°C for 10 minutes. In increments, add 0.01*N* nitric acid to the tube, mixing the solution after each addition. Place the tube in a bath of cold water until the temperature is lowered to 20–30°C. With the aid of a fine stream of water quantitatively transfer the contents of the tube to a 30-ml beaker. Add 1 ml of hydroxylamine hydrochloride solution, and stir. After 10 minutes add 5 ml of mixed reagent and adjust the pH of the solution to 2.7±.1 with $NH_4OH$, using a pH meter.

Using a minimum of water, quantitatively transfer the solution to a 60-ml separatory funnel. Add 5.00 ml of the dithizone reagent solution and shake vigorously for 1 minute. After the phases have separated completely, transfer a portion of the lower layer of the solution to a clear, dry 10-mm spectrophotometer cell. Measure the absorbance of the solution at 510 millimicrons against a reagent blank similarly extracted. Compute the mercury content by comparing the absorbance of the solution with the absorbance of standard solutions of mercury similarly extracted.

### Test of chemical procedure

Particles of cinnabar ranging in weight from 44 to 223 $\mu$g were weighed on a microbalance, transferred to respective Penfield tubes, and the mercury evolved by the technique described under "procedure." Aliquots of each diluted aqua regia solution were taken, and the mercury in each was determined by dithizone extraction and compared to the absorbance of aliquots of a standard solution of mercury. Over 95 percent of the mercury was recovered in each instance.

In the absence of samples of sphalerite or other sulfide minerals of known mercury content, mixtures of cinnabar and sphalerite were prepared to serve as standard samples. Three 50-g samples were prepared so as to contain as much as 40 parts per million of mercury. Each sample was ground in an automatic mortar and pestle for 1½ hours, and then mixed on a mixing cloth. Ten-gram splits were individually ground for half an hour and recombined by mixing on a mixing cloth. Portions of each sample were, over a period of several weeks, analyzed for mercury by the described procedure. The results are given in table 1. The average coefficient of variation is approximately 3.5 percent.

Because a mixture of cinnabar and sphalerite is probably not representative of the physical form of the ingredients as they exist in natural materials, an attempt was made to duplicate the natural state of the mineral assemblage. Three 10-g mixtures of sphalerite and cinnabar were prepared, containing respectively, 15.3, 35.4, and 113 ppm of mercury. The mixtures were heated in evacuated sealed quartz tubes in a furnace at 800°C for 2 weeks. Under these conditions the gaseous mercuric sulfide was expected to diffuse into the lattice of the sphalerite and, upon cooling, to form a solid solution of the two minerals. After cooling to room temperature, the melts were removed from the tubes, and portions of the finely

TABLE 1.—*Results of the Penfield tube-dithizone determination of mercury in synthetic mixtures of sphalerite and cinnabar*

[In parts per million]

| Mercury content | Sample | | |
|---|---|---|---|
| | 1 | 2 | 3 |
| Theoretical | 11. 3 | 22. 8 | 41. 0 |
| Determined | 11. 5 | 21. 1 | 35. 3 |
| | 11. 1 | 23. 5 | 42. 0 |
| | 11. 7 | 22. 9 | 35. 3 |
| | 11. 1 | 23. 8 | 33. 3 |
| | ---------- | 22. 1 | 34. 7 |
| | ---------- | ---------- | 34. 8 |
| | ---------- | ---------- | 34. 7 |
| | ---------- | ---------- | 36. 3 |
| Average, determined | 11. 4 | 22. 7 | 36. 2 |

ground mixtures were analyzed for mercury by the Penfield tube-dithizone technique. No significant differences were found in the mercury recovered from the samples before and after heat treatment.

### Use of fluxes

The use of fluxes has been found to be unnecessary for the quantitative distillation of mercury from sphalerite. Although fusion with sodium carbonate has been advocated for the quantitative removal of mercury from many materials, the technique apparently applies only to large quantities of mercury. When sphalerite containing 1 to 5 $\mu$g of mercury is fused with sodium carbonate in a Penfield tube, only 40 to 60 percent of the mercury is recovered. Fusion with sodium peroxide yields a recovery of only 60 to 70 percent of the mercury. Lead peroxide reacts violently with sphalerite even at low temperature, and much of the reaction mixture is usually carried into the neck of the Penfield tube.

In the presence of significant amounts of pyrite it is necessary to use lead tetroxide or lead monoxide as a flux to prevent the distillation of free sulfur into the cooled portion of the tube (F. S. Grimaldi, oral commun., 1965).

### Temperature and duration of heating

The temperature and duration of heating were varied over a wide range, but no significant differences were found in the amount of mercury recovered by increase in ignition temperature or longer duration of heating. Maintaining a temperature of 600–700°C for 5 minutes is adequate for the quantitative recovery of mercury from 300 mg of sample. A total of 10 minutes and a higher temperature are specified in the procedure to provide a margin of safety in the distillation of mercury from large portions of sample.

### Application of the chemical method

The Penfield tube-dithizone method has been applied to the determination of microquantities of mercury in sphalerite, galena, limestone, barite, and native silver. The experimental results found in the application of the method to a series of synthetic samples of sphalerite suggest that the method is reliable for the determination of mercury in sulfide minerals and may have a wider application to the determination of mercury in many geologic materials which upon ignition do not evolve large amounts of water or other volatile constituents that may physically or chemically interfere with the recovery of mercury.

## SPECTROGRAPHIC DETERMINATION

The chemical method is ordinarily used for the analysis of samples previously known to contain significant concentrations of mercury. The detectable concentrations of mercury are usually found by routine spectrographic analysis of the samples. In some instances, the spectrographic determination alone is requested on samples, and difficulty is experienced if the usual methods are used for the preparation of electrodes and exposures of the photographie plate.

The ease of volatility of mercury and its compounds presents a problem in mercury determination by spectrographic methods. In an arc, sudden excitation of a sample vaporizes mercury rapidly, and the brief duration of the volatilization results in an incomplete recording of mercury concentration due to the lag in photographic-plate response. To overcome this difficulty, a spectrographic procedure suggested by J. D. Fletcher (Fryklund and Fletcher, 1956) was tested. It was reasoned that a deeper electrode crater than previously used would promote a slower release of mercury into the arc stream, gradually enough to permit the emitted energy from the volatilized mercury to be recorded on the photographic plate. A short exposure time, sufficient for the vaporization of mercury, produces a spectrum almost free of continuum and free of emission from less volatile elements.

### Procedure

A 21-foot Wadsworth-mount grating spectrograph, with a 5 A per millimeter dispersion in the first order, was used for the analyses. Approximately 5 ppm of mercury can be detected in sphalerite when such an instrument is used with the following conditions:

| | |
|---|---|
| Sample weight | 50 mg. |
| Electrode shape | Cup, 8 mm deep by 5 mm in diameter (sample tamped into the cavity). |
| Current | 12 amperes. |
| Exposure time | 45 seconds. |

| | |
|---|---|
| Intensity control | 100 percent transmission of radiant energy. |
| Standards | Mercury (sphalerite matrix). |
| Wavelength of analytical line. | 2635.5A. |
| Intensity measurement | Visual comparison. |

Depending on the amount of mercury present in a sample, the amount of recorded transmission of radiant energy is adjusted to produce line intensities suitable for visual comparison of sample and standard spectra recorded on the same spectrographic plate. In comparison with recording 100 per cent of emitted radiant energy for samples containing 5 ppm of mercury, only 10 percent of the transmitted energy is recorded for samples containing approximately 1 per cent of mercury; lines 3125.7A, 3131.6A and (or) 4358.4A are used.

### Test of spectrographic procedures

Mixtures of cinnabar and sphalerite were used as standards for the spectrographic determination of mercury in sphalerite. The comparative results obtained in the analysis of five sphalerite samples by the chemical and spectrographic procedures described in this paper are shown in table 2. Although the spectrographic method is intended for use as a semiquantitative procedure, the results appear to be more than adequate for use as a screening technique.

TABLE 2.—*Comparative results of the determination of mercury in sphalerite by Penfield tube-dithizone and spectrographic methods*

[In percent]

| Sample | Lab. No. | Penfield tube-dithizone method | Spectrographic method |
|---|---|---|---|
| 1 | 159600 | 0. 018 | 0. 02 |
| 2 | ---------- | . 012 | . 005 |
| 3 | ---------- | . 017 | . 01 |
| 4 | 162530 | . 017 | . 01 |
| 5 | 162531 | . 013 | . 01 |

## REFERENCES


Aydin'yan, N. Kh., 1960, Determination of small amounts of mercury in natural objects: Trudy In-Ta geol. rudnykh mestorozhd, petrografii, mineralog. i geokim. Izd. AN SSSR, no. 46.

——— 1961, Determination of mercury in coal: Byull Nauchno-Tekh. Inform. Min. Geol. i Okhrany Nedr Akad. Nauk SSSR, v. 4, p. 70–71; Anal. Abstracts, v. 11, no. 4243.

Fahey, J. J., 1937, Determination of mercurous chloride and total mercury in mercury ores: Indus. and Eng. Chemistry, Anal. ed., v. 9, p. 477–478.

Fryklund, V. C., and Fletcher, J. D., 1956, Geochemistry of sphalerite from the Star mine, Coeur d'Alene district, Idaho: Econ. Geology, v. 51, p. 223–245.

Friedeberg, Harold, 1955, Separation and determination of microgram quantities of silver, mercury, and copper with dithizone: Anal. Chemistry, v. 27, p. 305–306.

Saukov, A. A., 1946, Geokhimiya rtuti [Geochemistry of mercury]: Tr. AN SSSR, Min. Geokh. ser., no. 17.

Vasilevskaya, A. Ye, and Shcherbakov, V. P., 1963, Determination of mercury in soils: Pochvovedeniye, v. 217, p. 343–350.

Ward, F. N., and Bailey, E. H., 1961, Camp and sample-site determination of traces of mercury in soils and rocks: Am. Inst. Mining, Metall., and Petroleum Engineers Trans., v. 217, p. 343–350.

Williston, S. H., 1964, The mercury halo method of exploration: Eng. and Mining Jour., v. 165, p. 98–101.

Yamamura, S. S., 1960, Simplified colorimetric determination of mercury: Anal. Chemistry, v. 32, p. 1896–1897.

# AN IMPROVED METHOD FOR RECOVERY OF BROMOFORM USED IN MINERAL SEPARATIONS

By WILLIAM M. TURNER, Beltsville, Md.

*Abstract.*—A continuous flow of fresh water circulates through a recovery bottle of simple design to separate solvent from bromoform-rich washings. Two groups of experiments show that the process may increase the recovery of bromoform, as compared with recovery by conventional methods, and that it obtains the same degree of purity. In addition, this new method eliminates the manual operations involved in the conventional methods. The method has also been found to be suitable for the recovery of methylene iodide.

An improved method of recovering heavy liquids from wash solutions was developed during studies of heavy minerals separated from a large number of sandstone samples from the Oriskany Group. Although 10 percent or less of the total heavy liquid used in any mineral separation is treated by solvent washing, loss can be great when many samples are processed. It was recognized that recovery of bromoform from bromoform-solvent washings by the conventional method—repeatedly adding water to the bromoform-solvent solution in a large bottle, shaking the bottle, and decanting water and solvent—was the least efficient step in the heavy-mineral separations. Thus a new method, which utilizes a continuous flow of water through a recovery bottle, was developed.

The conventional method and variations of it (Twenhofel and Tyler, 1941, p. 81; Milner, 1940, p. 52; Krumbein and Pettijohn, 1938, p. 322) depend upon the fact that solvent and water are more soluble than solvent and bromoform. Although the principle is sound, the technique has several shortcomings. Among these are (1) the lengthy manual operations required for agitating and emptying the bottle to recover the bromoform, and (2) the loss of bromoform resulting from its incomplete separation from the solvent solution, its being carried away in the water, and its evaporation.

The new method, here termed the continuous-flow bromoform-recovery process, differs from conventional separation methods in that water is never mixed with or passed through the impure solvent-bromoform mixture, but instead circulates above it. The process virtually eliminates manual operations and the loss of bromoform by evaporation, and it appreciably reduces loss of bromoform left in solution in the solvent and loss by mechanical transport by the moving water.

This paper describes the continuous-flow apparatus and two groups of experiments that were made to test its efficiency.

## THE CONTINUOUS-FLOW BROMOFORM-RECOVERY APPARATUS

### Description

The continuous-flow bromoform-recovery apparatus consists of a wide-mouth large-volume glass bottle with a glass stem, or drain, attached as near as possible to its base and with a four-hole rubber stopper in its mouth, through which pass a long-stemmed glass funnel and three glass tubes (fig. 1).

Drain *A* is used to draw off the bromoform; the flow is controlled by a pinch clamp on a bromoform-resistant rubber tube that is attached to the stem. Tube *B*, an air-bleeding valve, is equipped with a stopcock and terminates immediately inside the bottle. Tube *C*, with attached rubber hose, is the fresh-water inlet; it, also, terminates immediately inside the bottle. Funnel *D*, the inlet for the washings, terminates about 3 inches above the bottom of the bottle. Tube *E*, the water–solvent drain, terminates about 4 inches above the bottom of the bottle and has a rubber hose, about equal to the length of the funnel stem, attached to its outer end.

### Operation

The empty bottle is filled with tap water through the fresh-water inlet, with the air-bleeding valve open. When the bottle has been filled as far as its neck, the

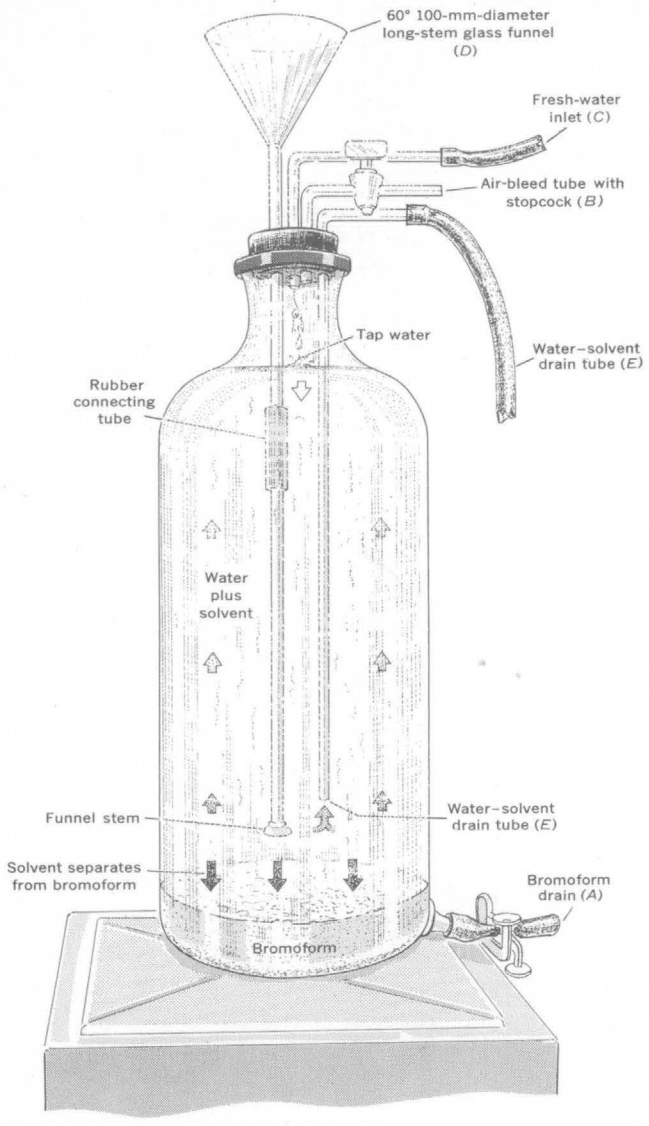


FIGURE 1.—Diagram of the continuous-flow bromoform-recovery apparatus, showing the separation of bromoform, bromoform plus solvent, and water plus solvent.

stopcock is closed so that water begins to issue from the hose attached to the water-solvent drain tube.

Bromoform-solvent washings are introduced into the water-filled bottle through the funnel. The funnel should be fitted with a piece of filter paper to insure that the washings are clear as they enter the bottle, thus eliminating later filtering. As the wash solution emerges from the base of the funnel stem, a large portion of the solvent separates immediately from the bromoform and dissolves in the water.[1] Because of its relatively low density,[2] the water-solvent solution rises in the bottle while the bromoform and the remainder of the solvent, which have a higher density, settle to the bottom. With tap water being introduced at the top, the water and solvent in the bottle are displaced downward and escape through the drain tube. As the water and solvent circulate above the bromoform-rich layer in the bottom of the bottle, solvent continually leaves the bromoform and is carried away in the moving water, and purified bromoform accumulates in the bottom of the bottle.

After the addition of washings, the water flow into the bottle is reduced to a trickle and left at this rate for several hours (as, for example, overnight). Afterward the bromoform is drawn off through the bromoform drain and is ready for immediate use.

## EFFICIENCY OF THE METHOD

The efficiency of the continuous-flow recovery method was tested by comparison with the conventional method in two sets of experiments.

*Experiment 1.*—In the first experiment, heavy minerals of 105 samples were separated in bromoform. The light-mineral fractions from a first group of samples were thoroughly cleansed with solvent (acetone), the washings collected, and bromoform recovered from the washings in conventional fashion. The light fractions from a second group of samples were cleansed with acetone, and the bromoform from these washings was recovered in the continuous-flow recovery bottle. A third group of bromoform separates was washed with methanol and recovered by the continuous-flow method. The results are presented in table 1.

Table 1 shows that the volume of bromoform recovered from the washings by the continuous-flow method is 20 to 35 percent greater than that recovered by conventional means. It also appears that the use of methanol instead of acetone as a solvent may increase the efficiency of the continuous-flow method by as much as 10 percent. The bromoform recovered by this process is of sufficient purity and specific gravity to be reused immediately or to be blended with the stored reserve.

*Experiment 2.*—To investigate further the relative efficiency of the two methods in terms of percentage of bromoform recovered from solvent-bromoform wash solutions, a second experiment consisting of a statistical comparison of these two methods was carried out by analysis-of-variance techniques (Eisenhart, 1947, p. 15;

[1] Both acetone and methanol are soluble in all proportions in water. Bromoform is relatively insoluble, losing only about 0.319 grams in 100 cm of water at 30°C. (Handbook of Chemistry and Physics, p. 538, 586, 687.)

[2] Density of acetone ($CH_3COCH_3$) = 0.792 g per ml, at 20°C. Density of methanol ($CH_3OH$) = 0.796 g per ml, at 20°C. Density of bromoform ($CHBr_3$) = 2.84–2.98 g per ml, at 20°C.

Scheffé, 1959, chap. 7). In performing the experiment, solutions of methanol and bromoform and of acetone and bromoform were used. No mineral fractions were involved in the experiment.

TABLE 1.—*Comparison of bromoform recoveries from bromoform–solvent washings by the conventional method and by variations of the continuous-flow method*

| Experiment No. | Method and solvent used | Number of samples treated | Total weight of samples separated (g) | Total volume of bromoform dissolved in solvent (ml)[1] | Total volume of bromoform recovered (ml)[1] | Volume percent of bromoform recovered[2] | Average specific gravity[3] |
|---|---|---|---|---|---|---|---|
| 1 | Conventional (acetone). | 57 | 1,031.0 | 585 | 222 | 38 | 2.84 |
| 2 | Continuous-flow (acetone). | 17 | 234.3 | 162.5 | 91.5 | 56 | 2.84 |
| 3 | Continuous-flow (methanol). | 31 | 623.1 | 375 | 247 | 66 | 2.84 |

[1] Total volume of bromoform dissolved in solvent was determined by subtracting the quantity of bromoform recovered by filtration from the total volume of bromoform used.

[2] Approximately 90 percent of the bromoform used in heavy-mineral-separation techniques is generally drawn off, filtered, and stored in pure form for later use. Solvents are used to recover the remaining 10 percent of the liquid that adheres to the light-mineral grains and apparatus. Thus the volume percent of total bromoform recovered actually ranges from 94 percent by the conventional washing method using acetone (experiment 1) to 97 percent using the continuous-flow process and methanol (experiment 3).

[3] Average specific gravity was controlled by immersing glass cubes of known specific gravity in a beaker filled with purified bromoform.

The experimental design is a two-way classification (methods and solvents) in which three replicate determinations of different solvent-bromoform proportions (4:1, 1:1, 1:4) were assigned within each method-solvent class. The order in which the replicate determinations were made was determined from random-number tables. Twelve observations, in terms of percentage of bromoform (2.848+ sp gr) recovered by each method, were obtained and recorded (table 2) together with the totals for methods and solvents. Table 2 shows a recovery range of 91 to 97.7 percent by conventional methods and a range of 96 to 100 percent by the continuous-flow method.

Table 3 presents the analysis of variance for bromoform-recovery methods. The variance ratio ($F$) for sources of variation arising from the interaction of solvents and methods (row 3, $B \times A$) is not significant at the 10-percent level. This indicates that any sources of variation arising from solvents and methods do not arise because of their interaction. Presumably they may arise because of inherent advantages of one solvent over the other or of one method over the other.

The variance ratio arising from solvent effects is less than 1, which in turn is very much less than the variance ratio at the 10-percent level with (1,8) degrees of freedom. Solvent effects, therefore, are not significant; we conclude that one solvent is as easily separated as the other from bromoform in the recovery process, or that bromoform is separated with equal ease from either solvent.

TABLE 2.—*A statistical two-way classification (methods and solvents) with three replicates showing percentages of bromoform recovered*

[Data coded. Percent=10(×)]

| Method | Replicate | Solvent: bromoform | Solvent | | $\sum_{1}^{t} x_i$ | |
|---|---|---|---|---|---|---|
| | | | Acetone | Methanol | | |
| Conventional | 1 | 4 : 1 | 910 | 950 | | |
| | 2 | 1 : 1 | 977 | 972 | | |
| | 3 | 1 : 4 | 972 | 957 | | |
| | $\sum_{1}^{3} x_i$ | | 2,859 | 2,879 | 5,738 | |
| Continuous-flow | 1 | 4 : 1 | 960 | 960 | | |
| | 2 | 1 : 1 | 1,000 | 980 | | |
| | 3 | 1 : 4 | 980 | 1,000 | | |
| | $\sum_{1}^{3} x_i$ | | 2,940 | 2,940 | 5,880 | |
| | $\sum_{1}^{6} x_i$ | | 5,799 | 5,819 | 11,618 | $\sum_{1}^{12} x_i$ |

Sources of variation arising from method effects are not significant at the 5-percent level with (1,8) degrees of freedom. From a strict statistical point of view (in which the 5-percent level is considered as the maximum limit of acceptability), the methods would not be significantly different from one another. The $F$ ratio for sources of variation arising from method effects is, however, significant at the 10-percent level; this significance indicates that the new method is at least equal to and probably better than the old method. It is important to note that it is not significantly worse than the old method. Since the interaction term is not significant, the sums of squares of the interaction error may be combined to give a better estimate of the error variance. The new $F$ ratios will be 0.066 and 3.24. In this case the between-methods variance is not significant at the 10-percent level.

## SUMMARY AND CONCLUSIONS

Both experiments show that the continuous-flow bromoform-recovery method is at least as efficient as the conventional methods of recovering bromoform, and may be more efficient. Further, it is easier to use and requires no time-consuming manual operations. Use of the continuous-flow recovery bottle, however, does require that sufficient quantities of bromoform be kept on hand to carry out mineral-separation experiments during the period when part of the bromoform is being recovered from the solvent.

TABLE 3.—*Analysis of variance for comparison of bromoform-recovery methods*

| Number of items | Source of variation | Degrees of freedom | Sum of squares | Mean square | Variance ratio ($F$) | $F.10$ | $F.05$ |
|---|---|---|---|---|---|---|---|
| $M$ 2 | Between solvents ($A$) | $(m-1)$ 1 | $\sum_{1}^{a}\left(\sum_{1}^{be}x_i\right)^2\Big/_{be}-CT=34$ | 34/1=34 | <1 | 3.46 | |
| $P$ 2 | Between methods ($B$) | $(p-1)$ 1 | $\sum_{1}^{b}\left(\sum_{1}^{ae}x_i\right)^2\Big/_{ae}-CT=1{,}681$ | 1,681/1=1,681 | 3.52* | 3.46 | 5.32 |
| | ($B\times A$) Methods × solvents (interaction) | $(P-1)(M-1)$ 1 | $\sum_{1}^{ab}\left(\sum_{1}^{e}x_i\right)^2\Big/_{ae}-CT=857$ | 857/1=857 | 1.79 | 3.46 | |
| 3 | Among replicates (error) | $PM(r-1)$ 8 | By differences $-CT=3{,}814$ | 3,814/8=476.75 | | | |
| 12 | Total | $(MPG-1)$ 11 | $\sum_{1}^{abe}(x_i)^2-CT=6{,}386$ | | | | |

NOTE.—Correction term $(CT)=\left(\sum_{1}^{abe}x_i\right)^2\Big/_{abe}=11248160$.

Variance ratio ($F$) determined by dividing mean squares by mean-square error among replicates (476.75).
*Most significant number.

From the analysis-of-variance of methods and solvents used in the recovery of bromoform from solution in acetone and in methanol, it is evident that bromoform can be separated as easily from one solvent as from the other. This is significant because it means that the cheaper of the two solvents (methanol) can be used with no decrease in efficiency of operation.

Although these experiments were performed using bromoform, the continuous-flow method has also been found to be suitable for the recovery of methylene iodide.

## REFERENCES

Eisenhart, Churchill, 1947, The assumptions underlying the analysis of variance: Biometrics, v. 3, p. 1–21.

Krumbein, W. C., and Pettijohn, F. J., 1938, Manual of sedimentary petrography: New York, Appleton-Century-Crofts, Inc., 549 p.

Milner, H. B., 1940, Sedimentary petrography, 3d ed.: London, Thomas Murby and Co., 666 p.

Scheffé, H., 1959, The analysis of variance: New York, John Wiley and Sons, Inc., 477 p.

Twenhofel, W. H., and Tyler, S. A., 1941, Methods of study of sediments, 1st ed.: New York, McGraw Hill Book Co., Inc., 183 p.

# QUANTITATIVE SPECTROCHEMICAL DETERMINATION OF MINOR ELEMENTS IN APATITE

By CLAUDE L. WARING and NANCY CONKLIN,
Washington, D.C., Denver, Colo.

*Abstract.*—A quantitative spectrochemical method for determination of 29 minor elements in apatite is described in which an apatite sample, with germanium dioxde added as an internal standard and as an excitation buffer, is mixed with graphite and consumed in a d-c arc. The spectrum is recorded, densitometric determinations are made, and the concentrations of elements are obtained from working curves. Precision is excellent for most of the elements. The data show good agreement with chemical and spectrographic determinations made in other U.S. Geological Survey laboratories.

The minor-element content of apatite is important in the study of chemical differentiation of igneous rocks and in the study of chemical precipitation in marine waters or through biological processes. It thus becomes of interest to obtain quantitative data on many of the elements which are substituents in this mineral.

To obtain this information a method was developed to determine the percentage concentration of 29 of these minor elements when they occur above the spectral sensitivity limits. A sample of apatite, with added germanium dioxide (as an internal standard), and graphite is consumed in a direct-current arc. The spectrum is recorded, densitometric determinations are made, and the concentrations of the elements are obtained from working curves.

The method differs from the one conventionally employed in the U.S. Geological Survey laboratories for the analysis of silicate rocks (Bastron and others, 1960) in that an internal standard is used (Brode, 1939, p. 80). The same amount of germanium dioxide is added to the standards and to the samples to serve both as an internal standard and as an excitation buffer. The internal-standard procedure is an aid in compensating for variations in excitation conditions.

## APPARATUS

The spectrograph used is the Wadsworth-mount grating type, covering a wavelength range from 2,250 A to 4,750 A on two 25.4-centimeter plates, thus having a reciprocal linear dispersion of 5 A per millimeter.

The densitometer is capable of measuring differences in transmittance with a standard deviation of not more than 0.2 percent in the 10–90-percent transmittance range.

The lower electrode is a ¼-inch graphite rod 1½ inches long cut to a 0.225-inch outside diameter. The wall thickness is cut to 0.015-inch, and the cup is cut to a 0.180-inch depth, including a 120° cone.

The upper electrode is a ⅛-inch rod cut to a 1½-inch length.

## STANDARDS

To carry out the work, standards were prepared for 29 elements, using pure tricalcium phosphate as a base. Spectrochemical analysis of the tricalcium phosphate showed it to be free of the elements in table 1, within a detectability of $< 1$ part per million. The elements and their ranges were suggested by semiquantitative analysis of a representative number of apatite samples from different geologic environments.

TABLE 1.—*Elements added to tricalcium phosphate for standards*

| | | | | |
|---|---|---|---|---|
| Al | Dy | La | Pr | Tm |
| B | Er | Mg | Sc | V |
| Ba | Fe | Mn | Si | Y |
| Ce | Gd | Na | Sm | Yb |
| Cr | Ho | Nd | Sr | Zr |
| Cu | In | Pb | Ti | |

## EMULSION CALIBRATION

The elements in table 1, in oxide form, were ground into the tricalcium phosphate to synthesize the standards in the 0.5–0.0001-percent range. Another addition was 3.8 percent fluorine as spectrochemically pure cal-

cium fluoride to make the standards equivalent to fluorapatites.

The emulsion calibration curves are prepared by a variation of the two-line method suggested by the American Society for Testing Materials (1964). Exposure conditions are the same as those selected to analyze samples. An apatite with iron content of 0.1 percent is used, and iron lines 3037.38 A and 3047.60 A are employed. Transmissions of the two iron lines and the germanium internal standard (2829.0 A) are taken as if they are the unknown elements sought. Their intensity ratios are calculated using the emulsion calibration curve. Experimentation shows that any variation of the intensity ratios greater than 0.05, that is, 3037.38 A = 1.20±0.05 and 3047.6 A = 1.45 ±0.05, is sufficient emulsion change to require a new curve to be drawn. Two arcings are made on each plate for the purpose of checking the emulsion calibration curve.

TABLE 2.—*Spectral lines of minor elements determined in apatite*

| *Element* | *Lines (A)* | *Concentration (percent)* |
|---|---|---|
| Al | 2660.36 | 0.001– 0.68 |
| B | 2496.78 | .001– .1 |
| Ba | 4554.04 | .001– .1 |
| Ce | 3201.71 | .084– 1. |
| Cr | 4254.35 | .00004– .005 |
| Cu | 3247.54 | .0001– .1 |
| Dy | 3308.89 | .001– .1 |
| Er | 3230.58 | .001– .05 |
| Fe | 2788.10 | .03– .6 |
| Gd | 3032.85 | .036– .1 |
| Ho | 3398.98 | .001– .05 |
| In | 3256.09 | .0005– .05 |
| La | 3337.49 | .01– .5 |
| Mg | 2779.83 | .0035– .26 |
| Mn | 2576.10 | .005– .20 |
| Na | 3302.32 | .002– .15 |
| Nd | 3285.09 | .001– .1 |
| Pb | 2833.07 | .001– .05 |
| Pr | 4241.02 | .001– .1 |
| Sc | 3372.15 | .0005– .01 |
| Si | 2516.12 | .06– 1. |
| Sm | 3183.92 | .005– .01 |
| Sr | 3464.46 | .003– .29 |
| Ti | 3088.02 | .1– .6 |
| | 2646.64 | .001– .1 |
| Tm | 3226.81 | .001– .1 |
| V | 3110.71 | .005– .4 |
| Y | 3195.62 | .008– .30 |
| Yb | 3289.37 | .005– .4 |
| Zr | 3391.98 | .001– .27 |
| | 3279.26 | .03– .50 |
| Ge | 2829.01 | Internal standard |

## SPECTRAL LINES

The spectral lines shown in table 2, are selected because their intensity ratios fit the desirable part of the working curves and have the possibility of determining 29 elements on one arcing of the sample.

## PROCEDURE FOR SAMPLES

A 15-milligram sample of apatite is weighed and placed in a boron carbide mortar to which 5 mg of germanium dioxide and 15 mg of graphite are added. The mixture is then thoroughly ground to a fine powder and transferred to the electrode cup. The electrode is tamped with a special tool which leaves a center hole for gases to escape. The sample is arced to completion (130 seconds) using 15 amperes of direct current and permitting 16 percent of the light to enter the spectrograph. Standards and reference material are arced in the same manner. The spectra are recorded on Eastman III-0 emulsion, which was calibrated previously by the two-line method.

After processing the plate, densitometric determinations are made, intensity ratios are obtained, and the final results are calculated from previously drawn working curves.

## PRECISION AND ACCURACY

To obtain a general idea of the precision of the method, 10 arcings of the same sample of apatite were completed, and the average concentration and standard deviations were calculated for 14 elements (table 3). The standard deviations were found to be sufficiently low.

TABLE 3.—*Average concentration and standard deviation for 10 arcings, in percent*

| *Element* | *Average concentration* | *Standard deviation* |
|---|---|---|
| Al | 0.152 | 0.004 |
| Fe | .200 | .009 |
| Mg | .112 | .001 |
| Na | .045 | .001 |
| Ti | .104 | .003 |
| Mn | .050 | .001 |
| Y | .130 | .004 |
| Yb | .013 | .004 |
| La | .060 | .006 |
| Zr | .055 | .003 |
| Gd | .035 | .002 |
| Sc | .0022 | .0001 |
| Ce | .121 | .002 |
| Sr | .015 | .003 |

TABLE 4.—*Comparative data on two samples of apatite*

| Element | Sample 1 [1] | | | | Sample 2 [2] | | |
|---|---|---|---|---|---|---|---|
| | 1 | 2 | 3 | 4 | 1 | 3 | 4 |
| Si | ------ | ------ | 0.070 | 0.064 | ------ | ------ | ------ |
| Al | ------ | <0.01 | .0014 | .0012 | ------ | 0.16 | 0.15 |
| Fe | ------ | .035 | .036 | .040 | ------ | .17 | .20 |
| Mg | ------ | <.01 | .0040 | .0035 | ------ | .06 | .10 |
| Na | ------ | .13 | ------ | .15 | ------ | ------ | ------ |
| Mn | 0.15 | .12 | .15 | .11 | 0.056 | .055 | .050 |
| Cu | <.0007 | ------ | .0006 | .0005 | .0007 | .0004 | .0002 |
| La | .18 | ------ | .070 | .16 | .05 | .046 | .06 |
| Sr | ------ | ------ | .15 | .12 | ------ | .021 | .015 |
| Y | .22 | ------ | .14 | .23 | .10 | .07 | .13 |
| Yb | .017 | ------ | .014 | .011 | .008 | .005 | .01 |
| Zr | <.005 | ------ | .0033 | .0028 | .06 | .048 | .055 |
| Gd | .07 | ------ | ------ | .075 | .03 | ------ | .035 |
| Ti | ------ | ------ | ------ | ------ | .011 | .14 | .10 |
| V | ------ | ------ | ------ | ------ | .004 | ------ | .005 |
| Ba | ------ | ------ | ------ | ------ | <.0005 | .0003 | .0003 |

1. Spectrographic analysis by Nancy Conklin and A. T. Myers.
2. Chemical analysis by Leoniece Beatty and W. W. Brannock. No analysis made of sample 2.
3. Spectrographic analysis by R. Mays.
4. Spectrographic analysis by C. L. Waring.

[1] Apatite (field No. ONT-1) from Faraday Township, Ontario (R. A. Gulbrandsen, written commun., 1966).
[2] Apatite (field No. GP-84) from Boulder Creek Granodiorite, Colorado, submitted by David Gottfried.

The data on accuracy are limited, due to the lack of carefully analyzed samples of apatite. Results on two apatites by chemical and spectrographic methods using techniques different from those reported here are given in table 4. Two to four comparisons are shown for 16 elements. The agreement among the various procedures is generally very good.

## REFERENCES

American Society for Testing Materials, 1964, Recommended practices for photographic photometry, *in* Methods for emission spectrochemical analysis, 4th ed.: p. 67–90.

Bastron, Harry, Barnett, P. R., and Murata, K. J., 1960, Method for the quantitative spectrochemical analysis of rocks, minerals, ores and other materials by a powder d-c arc technique: U.S. Geol. Survey Bull. 1084–G, p. 165–182.

Brode, W. R., 1939, Chemical spectroscopy: New York, John Wiley and Sons.

# HYDROLOGIC CHARACTERISTICS OF THE ALLUVIAL FAN NEAR SALINAS, PUERTO RICO

By N. E. McCLYMONDS and P. E. WARD,
Mineola, N.Y., Morgantown, W. Va.

*Work done in cooperation with the Puerto Rico Water Resources Authority*

*Abstract.*—The alluvial fan of the Río Nigua (known locally as the Río Salinas) is an important source of groundwater supply in the vicinity of Salinas, P. R. Study of data from wells indicates that the thickness texture of the alluvial deposits, the specific capacity of wells, and the mineralization of the ground water are related to the configuration of the bedrock surface beneath the fan; the thickest and most permeable deposits are in valleys in the bedrock surface, and the thinnest and least permeable deposits are above the intervening ridges. Recognition of this relationship affords a basis for selecting the parts of the area with the greatest potential for the development of large ground-water supplies.

Logs and other data from water wells tapping an alluvial fan on the south coastal plain of Puerto Rico (fig. 1) indicate that both the areal distribution and the chemical quality of large ground-water supplies are related to the configuration of the buried bedrock surface. Recognition of this relationship affords a basis for selecting the parts of the area with the greatest potential for additional wells of high yield.

The alluvial fan has an area of 12 square miles, and its surface slopes gently seaward from the base of the mountains that lie to the north (fig. 2). The sediments composing the fan were derived from an area of about 50 square miles and were transported to the fan by Río Nigua (known locally as Río Salinas) and its tributaries. The west boundary of the fan is less than a mile from the present course of Río Nigua, and the east boundary is at the base of the low hills as much as 4 miles from the river.

The fan is economically important because it stores and transmits large quantities of water. During 1961, ground water was withdrawn from the alluvium in the fan at an average rate of 23 million gallons per day (26,000 acre-feet for the year) without apparent adverse effects. About 50 wells were in use, and their yields ranged from 300 to 3,000 gallons per minute. The fan is recharged by influent seepage from Río Nigua and its tributaries, and from water used for the irrigation of sugarcane, which is supplied via canals and by wells. Part of the canal water is from Río Lapa and Río Majada, but most of it is from two lakes east of Salinas outside the area of figure 2.

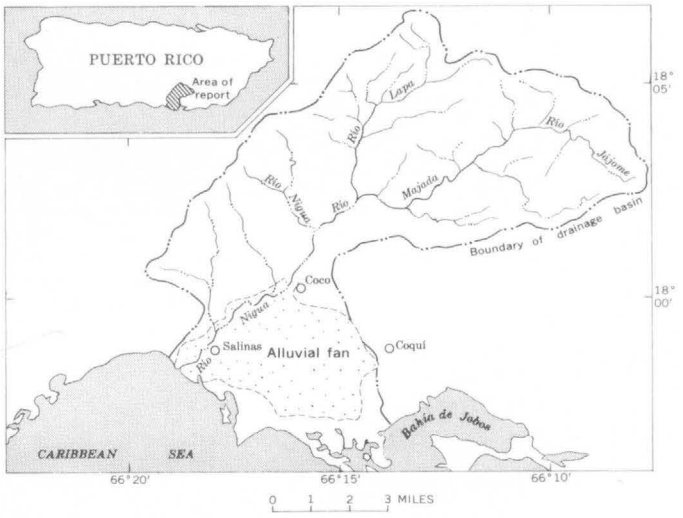


FIGURE 1.—Location of the alluvial fan and boundary of the drainage basin of Río Nigua.

Data from 68 wells, used in this study, include drillers' logs (38 wells), and statistics on specific capacity (27 wells) and specific conductance of the ground water (44 wells). Topographic maps were used for horizontal and vertical control and for preparing figure 2.

U.S. GEOL. SURVEY PROF. PAPER 550-C, PAGES C231-C234

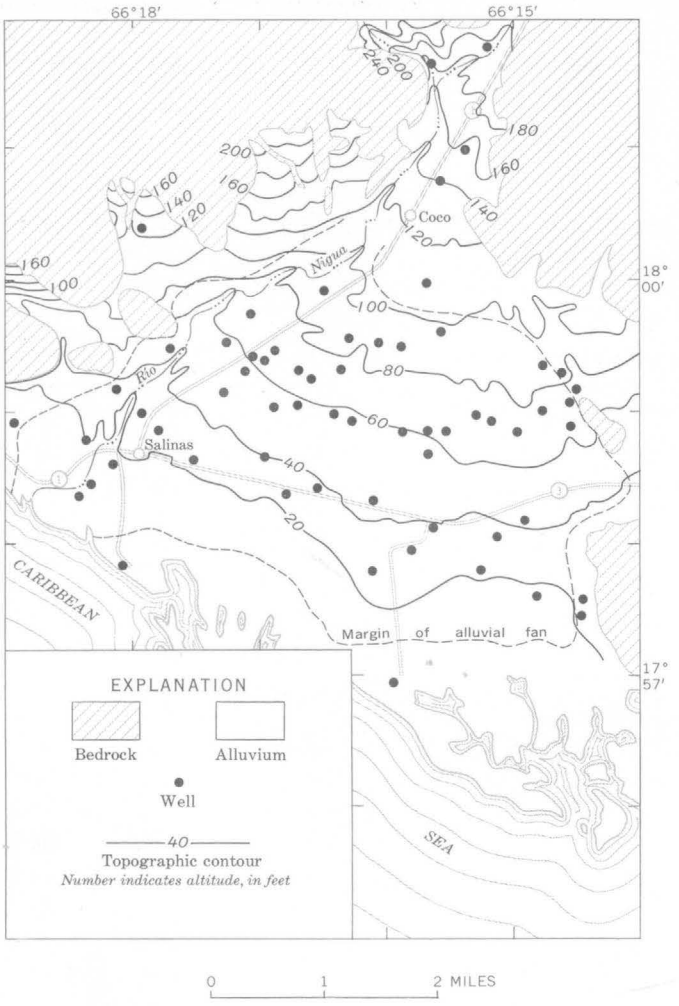


FIGURE 2.—Distribution of bedrock and alluvium at the land surface near Río Nigua, topography of the fan, and location of wells. Contour interval 20 feet.

The drillers' logs were used to determine the thickness, extent, and lithology of the alluvium. The thickness of the material was especially difficult to ascertain because only a few of the logs reported "hard rock" (interpreted to be bedrock). Below depths ranging from 130 feet in the northern part of the fan to 170 feet in the southern part, only clay and tosca were reported by the drillers. The term "tosca" is used commonly by drillers in Puerto Rico to denote silty clay, weathered silty limestone, or other weathered rock. Because much of the material reported as clay or tosca in the Salinas area is believed to represent either weathered bedrock or a zone immediately above the bedrock, it was assumed that little or no permeable unconsolidated material lies below the clay or tosca. Figure 3, which shows the altitude of the base of permeable water-bearing sediments, probably reflects rather closely the configuration of the underlying bedrock surface, even though the contour lines may not conform to it exactly.

The principal, and perhaps the most important, buried features indicated by the contour lines in figure 3 are two major valleys separated by a low ridge. One of the valleys lies beneath the central part of the fan and the other lies beneath the eastern part. The existence of a separating ridge is established by two well logs that recorded "hard rock" at depths of less than 100 feet. Another ridge and a minor valley seem to underlie the western part of the fan, near Salinas. The buried bedrock features of the western part are not well defined because none of the logs indicate that the wells were drilled to hard rock.

The interpretation of the presence and positions of the buried ridges and valleys is of particular hydrologic interest because the relative proportions of coarse and fine materials in the alluvium, as indicated by the drillers' logs, seem to be areally related to the

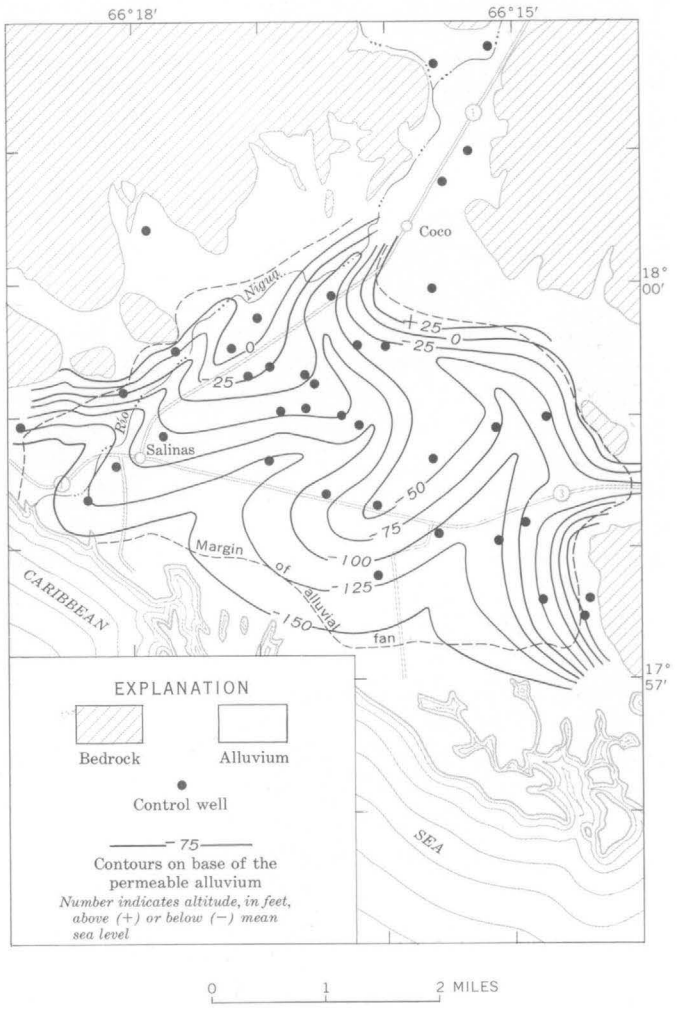


FIGURE 3.—Configuration of the base of permeable alluvium under the fan. Contour interval 25 feet.

subsurface topography. The percentage of sand and gravel in the alluvial-fan deposits commonly decreases southward, away from the source rocks in the uplands. However, it has been found, in addition to this general trend, that sand and gravel constitute a larger proportion of the sediments within the major buried valleys than in other parts of the fan, and that locally they are in extensive beds. The alluvium penetrated in wells in the northern part of the central buried valley was reported to contain as much as 70 percent sand and gravel, whereas the alluvium over the small southeastward-trending ridge west of that valley contains 30 to 40 percent sand and gravel.

The significance of this pattern of abundance of sand and gravel deposits, with respect to water supply, lies in the areal distribution of values of specific capacity (fig. 4). The specific capacity of a well, its yield in gallons per minute per foot of water-level drawdown, is related directly to the transmissibility of the water-bearing sediments tapped by the well. Because transmissibility is a function of both the thickness and texture of the water-bearing sediments, and because these characteristics of the alluvial fan seem to be related to the configuration of the bedrock surface, the areas in which wells have higher specific capacities may be expected to overlie the principal bedrock valleys, and the areas in which wells have lower specific capacities to overlie bedrock ridges. (These conclusions are based on the assumption, believed to be reasonable, that the wells are of comparable efficiency, so that their specific capacities can be compared.) Figure 4 shows two areas in which wells have specific capacities exceeding 125 gallons per minute per foot. The eastern of these areas overlies the eastern buried valley (compare figures 3 and 4), and the western area overlies the axis and the west side of the central buried valley.

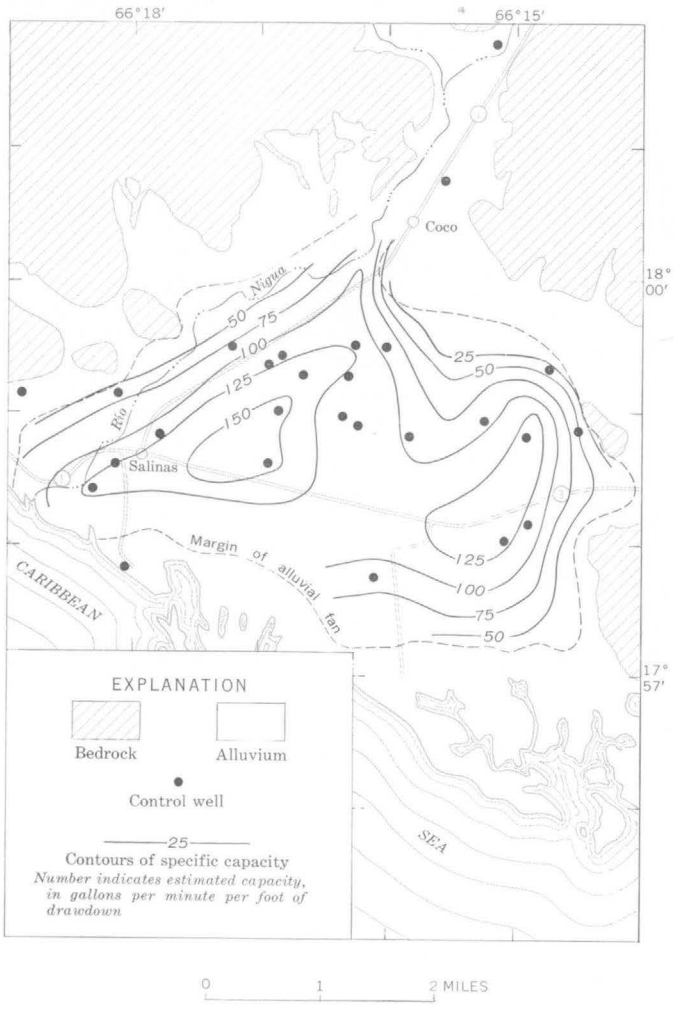


FIGURE 4.—Specific capacity of wells. Contour interval 25 gallons per minute per foot of drawdown.

Differences in the total dissolved-solids content of the ground water, as indicated in figure 5 by lines of equal specific conductance, also seem to be related to the configurations of the bedrock surface. A plausible explanation for this relationship is that the ground water in the deeper sediments (those restricted to the buried valleys) tends to be more mineralized than the ground water in the shallower sediments (those coextensive with the fan). Thus wells tapping the full thickness of the alluvium in the bedrock-valley areas yield a blend of both the more and the less mineralized water, whereas wells tapping the alluvium overlying the bedrock ridges yield only the less mineralized water. Quite possibly the water in the deeper sediments has percolated farther and has been in storage longer than that in the shallower sediments and thus has had more opportunity to dissolve minerals from the sediments with which it has come into contact. Furthermore, the water in the shallower sediments is more subject to dilution (or freshening) by water infiltrating from the land surface. The diluting effect of seepage from Río Nigua is particularly noticeable in that the least mineralized ground water in the fan is near the river. Seepage from precipitation and seepage from the irrigation-water distribution system also dilute the shallower ground water. The specific conductance of the water in the Río Nigua commonly is between 400 and 500 micromhos, depending on the flow; that of the irrigation water, most of which is derived from Lago Carite and Lago Patillas (both several miles east of the fan), generally is less than 150 micromhos. The high specific conductance of the ground water in the extreme southeastern part of the fan probably reflects the locally high alkalinity of the

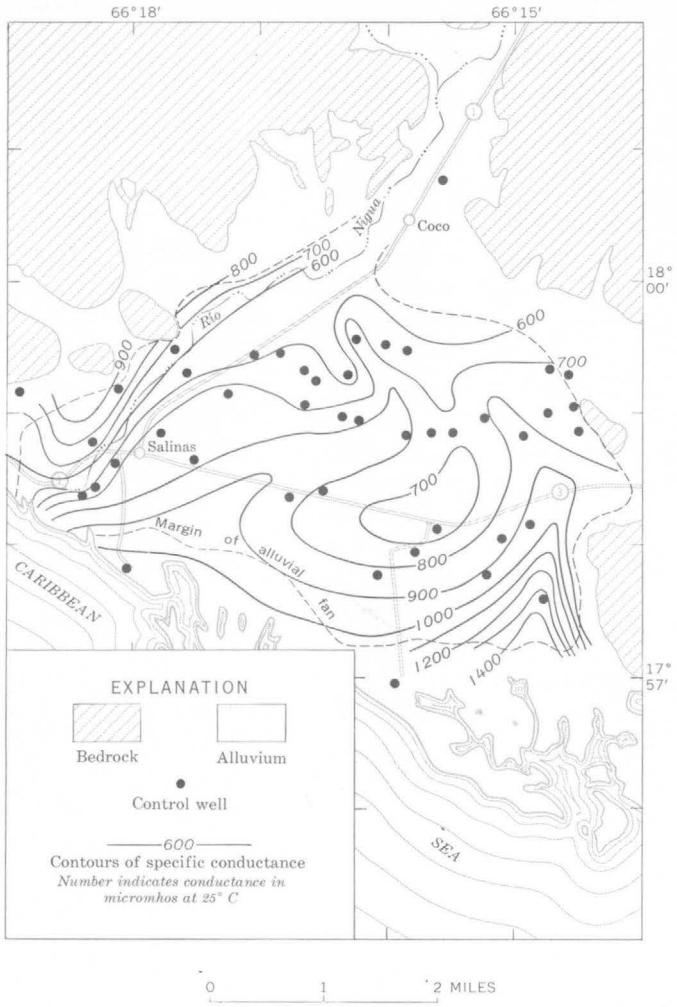


FIGURE 5.—Specific conductance of ground water in the alluvial fan. Contour interval 100 micromhos.

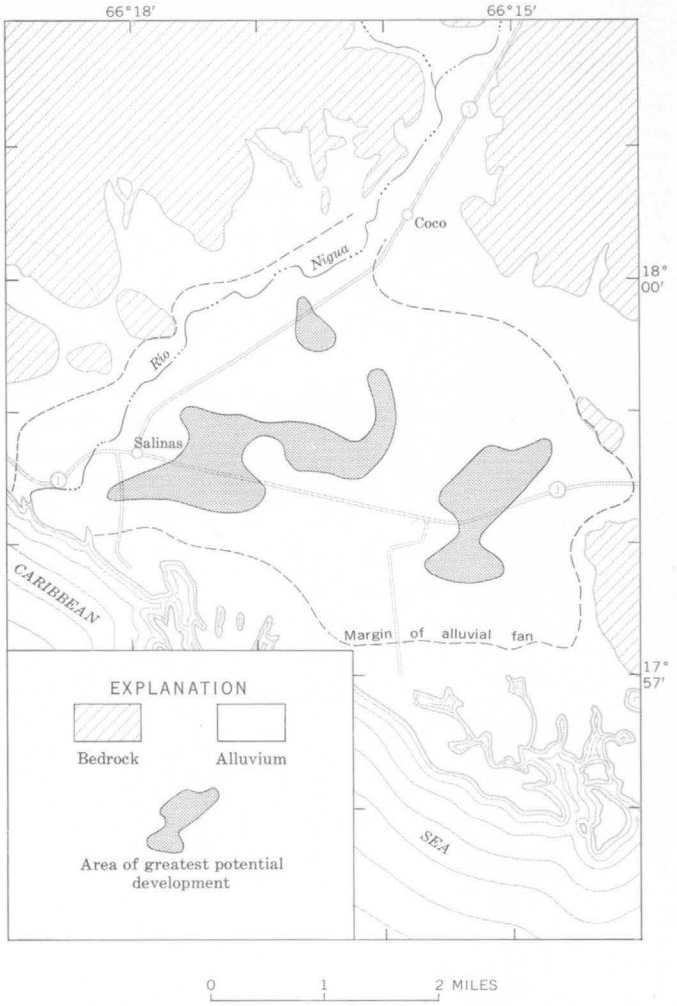


FIGURE 6.—Areas on the alluvial fan where the potential for future development of large ground-water supplies is greatest

soils through which recharge water from the surface must infiltrate.

Recognition of the relation of the availability and chemical quality of the ground water to configuration of the bedrock provided the basis for delineation of areas (fig. 6) in which large yields from wells can be expected and in which development of the ground-water resources currently is negligible. If future high-yield wells are concentrated in these areas, fuller development of the water in the alluvial fan can be realized with minimum detrimental effect on existing well installations. Increased use of the ground water will result in salvage of water that otherwise would be discharged through evapotranspiration or by outflow into the sea.

# RELATIONSHIPS OF FRESH AND SALTY GROUND WATER IN THE NORTHERN ATLANTIC COASTAL PLAIN OF THE UNITED STATES

By JOSEPH E. UPSON, Washington, D.C.

*Abstract.*—Mapping of the boundaries between fresh and salty water in selected aquifers in the northern Atlantic coastal plain of the United States reveals that the limit of salty water and the configuration of the present coastline correspond closely only in the late Pleistocene and Recent deposits. In successively older aquifers the correspondence is progressively less. Here the salt-water boundaries are believed to be controlled chiefly by the circulation patterns of the fresh water in the aquifers, notably the locations of discharge zones. Also, in Maryland and Delaware large lenses of fresh water that might represent Oligocene and Pliocene episodes of terrestrial conditions are lacking. Thus, hydrodynamic adjustment of the boundaries has been rapid enough to keep pace with the general relative changes of sea level since Cretaceous and Eocene times.

Sea-water contamination of fresh ground water by encroachment into coastal aquifers is an ever-present fear of users and distributors of potable water in coastal areas. Along the Atlantic coastal plain, with its hundreds of square miles of low-lying areas underlain by unconsolidated water-bearing sediments, there are many instances of contamination or threatened contamination of a good water supply; and there are one or two instances where contamination has been expected but has not taken place. In some aquifers, salty water occurs many miles from the sea, and at some localities near the shore a deep well penetrates alternating bodies of fresh and salty ground water. These differences and seeming anomalies are thought to stem from differences in the circulation pattern of fresh ground water in the different aquifers, controlled at least in part by the principal intake and discharge areas for each aquifer. Proximity to the present shoreline is a controlling factor only in the shallowest aquifers.

This paper deals with the coastal plain in Long Island, New York, New Jersey, Delaware, and Maryland (fig. 1). The purpose is to describe the occurrence of "salty" ground water and to show that its limits are determined by the flow pattern of the fresh ground water.

In this paper salty water is taken to be that having 250 parts per million or more of Cl ion. Within large areas in the older formations the salinities of the salty water are low, a few hundred to about a thousand parts per million of Cl ion, suggesting that the zones of transition between fresh water and water with salinity near that of sea water (about 18,000 parts per million of Cl ion) are very broad. Also, even though

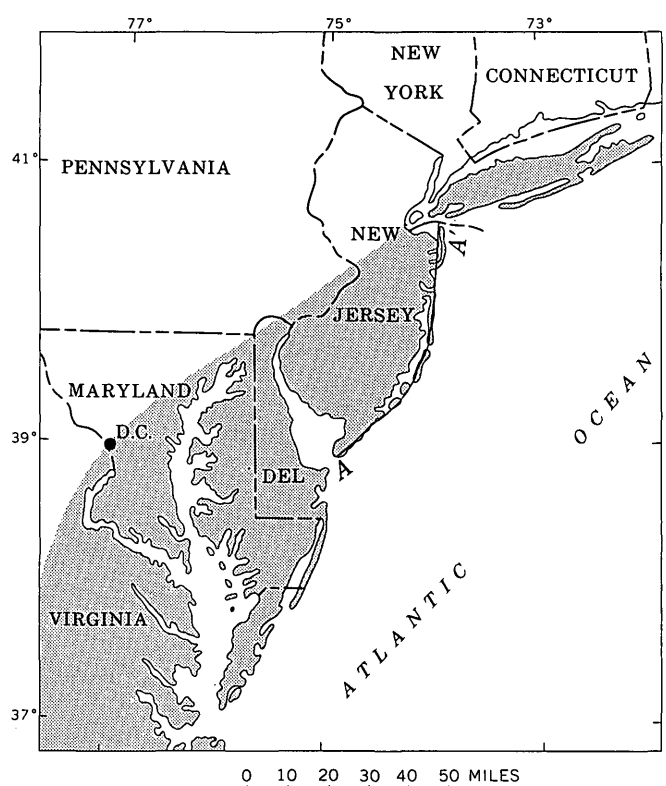


FIGURE 1.—Area underlain by coastal-plain sediments (shaded) along the northern Atlantic coast. *A-A'*, line of section shown on figure 2.

the water does have more than ordinary concentrations of chloride, much of it contains predominant sodium bicarbonate and hence is not of typical sea-water composition. Nevertheless, there is no other reasonable source for chlorides, and consequently water having 250 ppm or more of Cl ion is considered to originate either from the present sea, or from the sea of an earlier geologic time.

## GEOLOGIC FORMATIONS AND AQUIFERS

The coastal-plain sediments range in age from Cretaceous to Pleistocene and, in the area considered, contain representatives of all the intervening epochs except the Oligocene and perhaps the Pliocene. The formations into which these sediments are divided contain aquifers which yield the water pumped for use. Salty water is known to occur somewhere in the seaward parts of most of the aquifers, only some of which are discussed here. Those discussed are shown in table 1 together with their approximate age and a general statement of their mode of origin.

## BOUNDARIES OF THE SALTY WATER

The approximate locations of the boundaries between fresh and salty ground water for certain of these coastal-plain aquifers in Long Island, N.Y., New Jersey, Delaware, and Maryland (fig. 5), their distribution pattern, and other data suggest that the salt-water boundaries are a reflection of, and are dependent upon, the circulation of the fresh water in the different aquifers. This idea is inherent in theoretical considerations of fresh-water–salt-water relationships as described recently and fully by Henry (1964), wherein the shape and position of a theoretical fresh–salt-water interface is shown to be determined primarily by what Henry (1964, p. C59) calls the discharge parameter of the containing deposits. This parameter takes into consideration the permeability and thickness of the

TABLE 1.—*Selected geologic formations and aquifers in the northern Atlantic coastal plain*

[Sources of geologic and hydrologic data are given on figure 5]

| Age | Delaware and Maryland | | | New York and New Jersey | | |
|---|---|---|---|---|---|---|
| | Stratigraphic unit | Aquifer | Origin | Stratigraphic unit | Aquifer | Origin |
| Pleistocene | Columbia group | Several | Predominantly continental, with marine intervals | Pleistocene deposits (includes Cape May Formation in New Jersey) | Several | Predominantly continental, with marine intervals |
| Pliocene | Interval of erosion or fluviatile deposition (continental conditions) | | | | | |
| Miocene | Yorktown and Cohansey [1] Formations | Pocomoke and Manokin | Estuarine and marine | Cohansey Sand [1] | ---------- | Estuarine and marine. |
| | Choptank Formation | Frederica and Nanticoke (part) | Marine<br>Marine | Kirkwood Formation (in New Jersey only) | Rio Grande water-bearing zone of Gill; Atlantic City 800-foot sand | Marine. |
| Oligocene | Interval of erosion or nondeposition (continental conditions) | | | | | |
| Eocene [3] | Piney Point Formation | ---------- | Marine | (Not identified) | ---------- | ---------- |
| Upper Cretaceous. | Magothy and upper part of Raritan Formation | ---------- | Continental and marine | Englishtown Formation (in New Jersey)<br>Magothy [2] and upper part of Raritan Formation | ----------<br>---------- | Marine, except continental in Long Island. |

[1] Age of the Cohansey Sand is Miocene(?) and Pliocene(?).

[2] Includes Magothy(?) of Long Island now properly referred to as Magothy Formation and Matawan Group undifferentiated (Perlmutter and Todd, 1965, p. I3 and pls. 7 and 8.

[3] Deposits of Paleocene age are not distinguished from deposits of Upper Cretaceous or Eocene age.

aquifer, and its discharge, which in turn is related to the hydraulic head. This concept has not been applied to field relationships on a large scale.

That the circulation pattern of the fresh water, rather than the density of the salt water, might control the position of the fresh-water–salt-water interface first occurred to the writer several years ago while making a study of the predevelopment conditions of salty ground-water occurrence on the New Jersey coast. This study showed that at a number of places there is more than one salt-water body in the vertical section.

The occurrence of salty ground water beneath the New Jersey barrier beach from Sandy Hook to Cape May is shown on figure 2. The upper of the two sections contains a plot of old wells, drilled before 1900, for which either initial hydraulic head or presence of salty water, or both, are recorded.[1]

[1] Annual Reports of the (New Jersey) State Geologist for 1876 to 1901, inclusive: New Jersey Geol. Survey, 1876–1902.

The lines of heavy dots on figure 2 represent, to the south, the approximate initial head in the lower aquifer of the Kirkwood Formation (Miocene), the so-called Atlantic City 800-foot sand; and, to the north, in the Wenonah, Mount Laurel, and Englishtown Formations (Cretaceous) which comprise, or are in hydraulic continuity with, the so-called 550-foot sand at Asbury Park.

The initial head along most of the shore in the Kirkwood Formation had an altitude of about 25 feet, but to the north the head declined, suggesting a discharge zone in the vicinity of Berkeley. The initial head in the Wenonah, Mount Laurel, and Englishtown was about 50 feet above mean sea level. There was also a discharge area to the north, but these data do not show it. These features were recognized 35 years ago by David G. Thompson (1928, 1930).

The occurrence of salty water suggests the presence of two bodies of salty ground water: a shallow one in

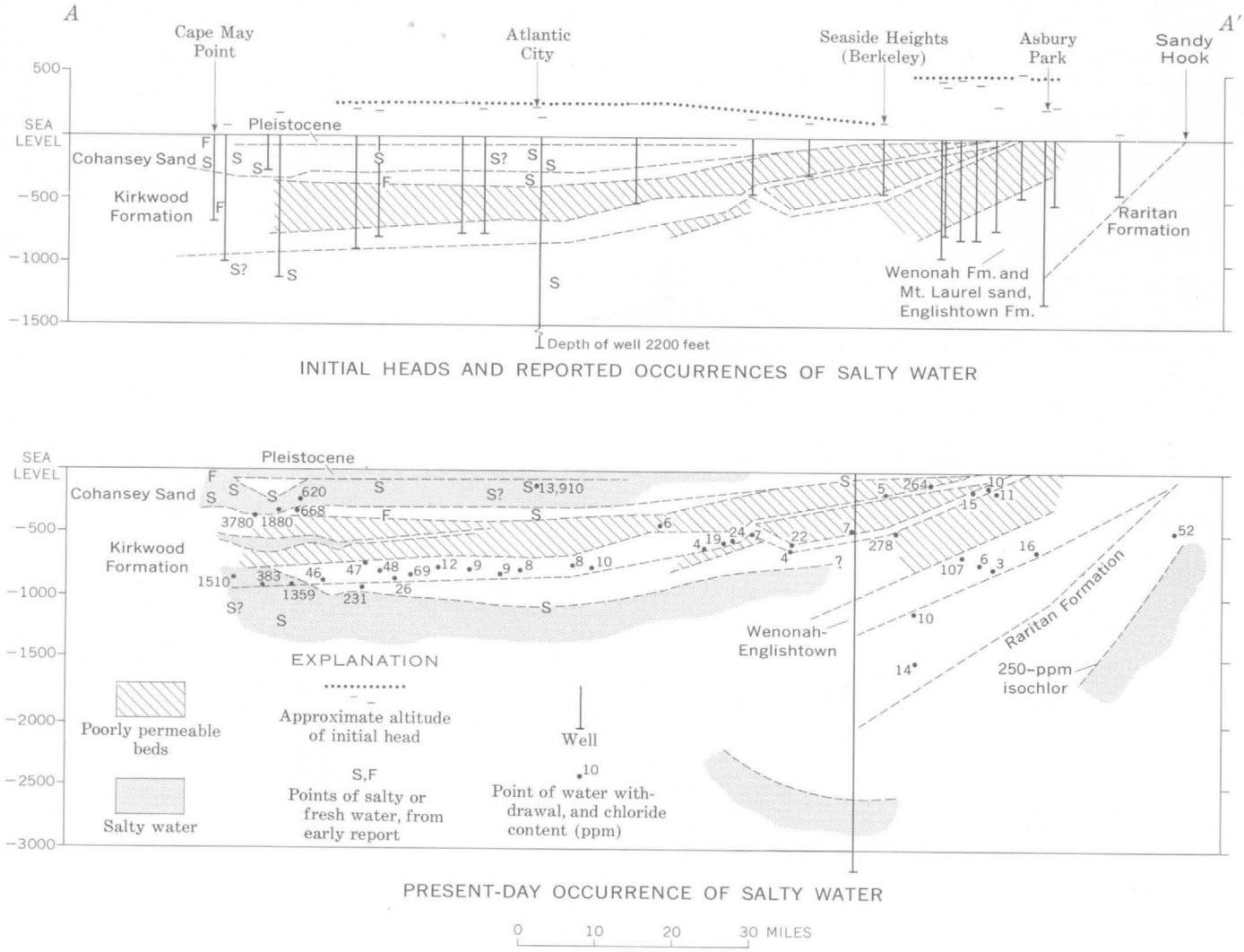


FIGURE 2.—Ground-water head and occurrence of salty water along the New Jersey coast.

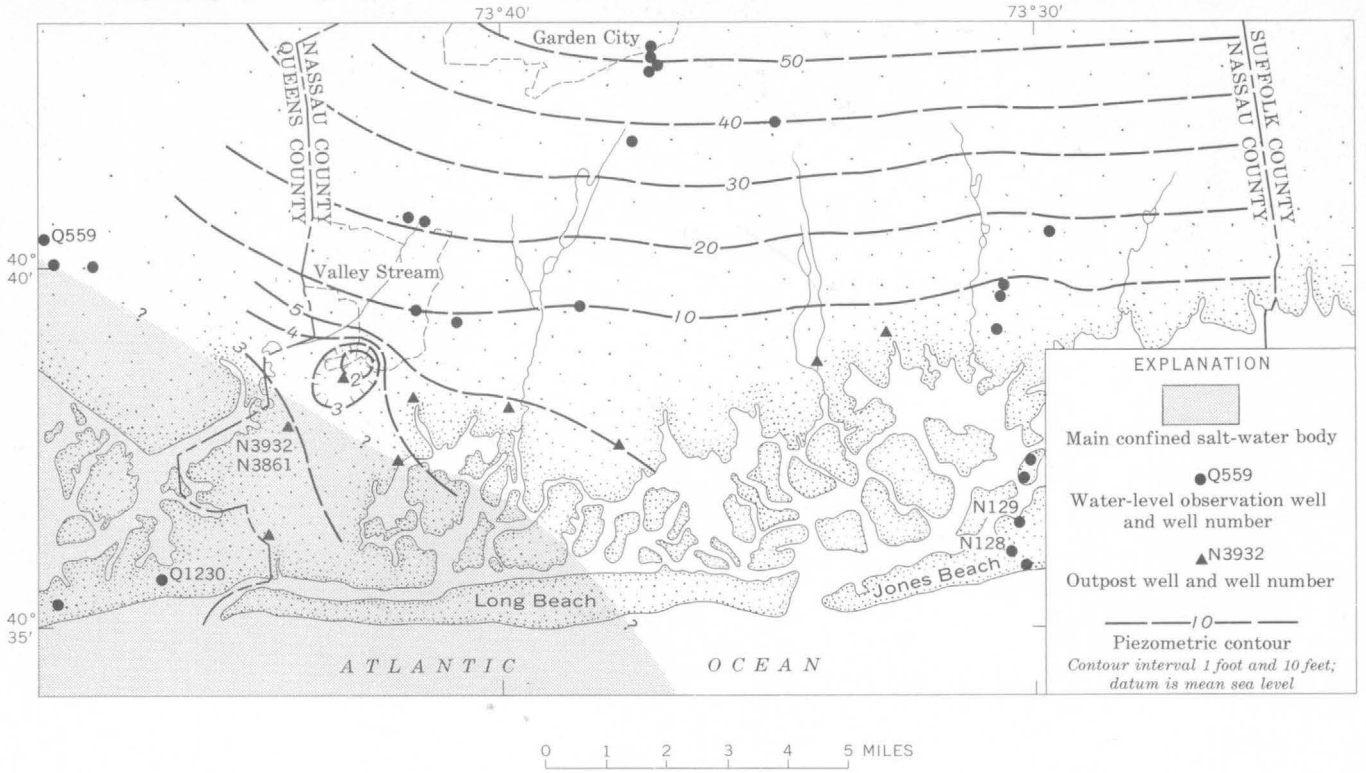


FIGURE 4.—Piezometric contours and the main salt-water body in the Magothy(?) Formation in southwestern Nassau County, Long Island, N.Y., (from Perlmutter and others, 1959) (reproduced by permission of Economic Geology and the authors).

water moves generally parallel to the bedding, past the salt water, along the flow surface toward discharge points to the north and south. This would certainly be true where the aquifer is overlain by tight confining beds or where the head is about the same as in overlying aquifers. In shallower aquifers or in others overlain by incompletely confining beds, some water discharges by upward leakage wherever the hydraulic gradient is favorable. In that case, there is a strong cross-bed component to the flow lines. Water is still moving along the interface, but in a vertical rather than horizontal sense. This is surely the case with much of the Magothy(?) of Long Island, and probably with some of the younger aquifers farther south.

## REGIONAL PATTERNS OF THE SALT-WATER BOUNDARIES

The approximate location of the salt-water boundaries in several formations is shown on figure 5. They are based upon quality-of-water data; upon maps of individual aquifers such as the Manokin (fig. 3); and, for the speculative offshore positions, upon the general parallelism of the boundaries and the piezometric contours.

The boundary in the Cretaceous (Magothy Formation in Maryland and Delaware, and Raritan in New Jersey) is placed about midway between the boundary in the older Cretaceous sediments as drawn by William Back (written commun., 1961) and that in the upper Eocene (Piney Point) as drawn here. The line is controlled by only a few points, except in western Long Island, where there are many. The boundary for the lower Kirkwood aquifer is extended from Gill's (1962) mapping across the tip of Cape May County, N.J., parallel to the initial piezometric contours as restored. There has been a huge drop in head along the whole coast from Atlantic City, N.J., southward, so the boundary now may be somewhat closer to the shore. The boundary in the Englishtown Formation is drawn farther seaward than in the Kirkwood because the initial head in the aquifer was higher. In this region, too, a large cone of depression created by pumping near Asbury Park, N.J., and to the south probably has caused some landward shift of the interface from its initial position.

As shown on figure 5, the salt-water boundaries in successively younger formations lie successively farther seaward in Maryland and Delaware and are more and more nearly coincident with the shape of the present-day Delaware-Maryland peninsula. The boundary in the Pleistocene deposits lies along the present shore in an irregular pattern. In New Jersey and on Long Island the boundaries are independent of the present

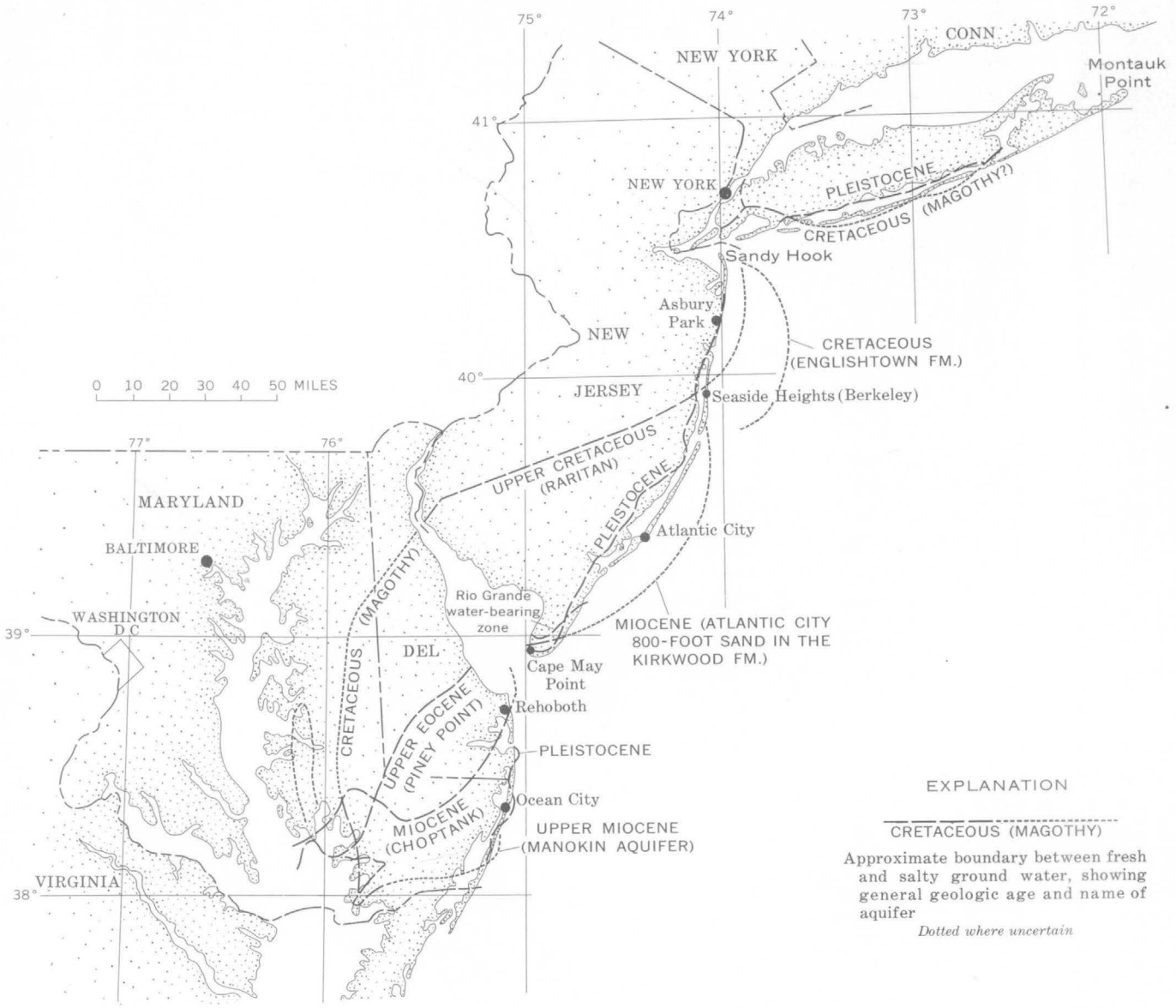


FIGURE 5.—Boundaries between fresh and salty water in selected aquifers. Salinity data and differentiation of formations based on data in Lusczynski and Swarzenski (1962), Marine and Rasmussen (1955), Overbeck and others (1958), Perlmutter and Crandell (1959), Rasmussen and others (1957, 1958, and 1960), Seaber (1962), Slaughter (1962); and on other authorities cited in the text.

shoreline except in the Pleistocene deposits, in which the boundary roughly corresponds to the lagoons.

As thus approximated and restored, the patterns of the salt-water boundaries seem to reflect the main zones of localized discharge from the aquifers. This is shown most noticeably by the boundaries in the Choptank-Kirkwood aquifers of Delaware and southern New Jersey, and in the Englishtown-Magothy(?) aquifers of northern New Jersey and Long Island. The Choptank Formation is roughly the equivalent of the Kirkwood (W. C. Rasmussen, written commun., June 26, 1963). The water-bearing zone may be the equivalent of either of the Kirkwood aquifers. Flanking Delaware Bay, the boundary in the Choptank curves inland toward the north, and that in the Kirkwood curves in from the east, the two seemingly headed for a meeting beneath the central part of the bay. The Delaware River probably had a Pleistocene channel comparable to the Pleistocene channel of the Susquehana (Hack, 1957, fig. 6). In the channel the base of a Pleistocene fill probably cuts the Choptank-Kirkwood aquifers in about mid-bay, and thus makes a good outlet for discharge there.

Similarly the outer part of New York Harbor is bordered by the Englishtown Formation in New Jersey, and its approximate equivalent, the middle part

of the Magothy(?) Formation of Long Island. The salt-water boundaries in these units extend northwestward and westward, respectively, seemingly headed for a juncture beneath the outer part of New York Harbor. In, and off the mouth of, the harbor, the aquifers come in contact with overlying Pleistocene deposits. These deposits are known to be permeable in the vicinity of Jamaica Bay, N.Y., and they doubtless transmit water in the area beneath New York Harbor.

Data on the Raritan are available for only about half of the New York Harbor area. In New Jersey the salt-water boundary of the Raritan suggests discharge into New York harbor. There is probably a somewhat similar boundary off Long Island, but, for the Lloyd Sand Member of the Raritan Formation, which is the Raritan aquifer on the New York side, there are few data on either the piezometric level or the water salinity. On the other hand, figure 2 shows that the Englishtown and Raritan come close together beneath Sandy Hook, N.J. The two formations are truncated by Pleistocene or Recent deposits beneath New York Harbor at nearly the same place, and the respective outlets for fresh-water discharge must be near each other.

In Maryland, the boundaries in the Piney Point Formation (upper Eocene) and in the Choptank (Miocene) parallel the general pattern of the piezometric contours. The contours suggest discharge to streams leading into Chesapeake Bay or into the marshland bordering the Bay. The extreme southwestern part of the boundary in the Choptank is not closely controlled, but is approximately as drawn. That it does not extend farther north along Chesapeake Bay to the area of outcrop of the formation along the Choptank River may be because of upward leakage of fresh water into the Choptank aquifer from the deeper lying Piney Point.

The boundary in the Piney Point lies farther seaward near Chesapeake Bay than does that in the Choptank. The rather sharp bend in the trace of the boundary at the edge of the Bay is thought to point toward a discharge zone lying somewhat farther north. Extending a little west and north from this sharp bend is a narrow area in the marshland along the east side of Chesapeake Bay where several wells have more-than-ordinary concentrations of chloride. This area may separate two discharge zones of the Piney Point—one from the east, and one from the west.

The broad bend in the boundary of the salty water in the Raritan and Magothy aquifers between southern New Jersey and eastern Maryland probably reflects the discharge of fresh water in the upper part of Delaware Bay. In general, however, there are so few data controlling the position of the boundary in these formations that it cannot at present be correlated with discharge zones any more closely.

The last boundary to be discussed is that in the Pleistocene deposits. The location is not very well controlled in detail, but it must be at least approximately as shown. It coincides closely with the present shore alinement, as it should, because the salt water was emplaced during the rise in sea level that accompanied the retreat and waning of the Wisconsin glacial ice. It occurs generally not far landward of the barrier beach. The details of its distribution are probably also controlled by the pattern of ground-water movement, as in the deeper aquifers, but the detailed pattern is too intricate to be delineated by the data available. This shallowest salt-water body is generally overlain by a thin surficial lens of fresh water.

Beneath the barrier beach, the presence of the salt-water body seems to depend chiefly on the absence of confining beds of Sangamon age. These are clays and silts of the Pamlico Formation in Maryland and Delaware, the Cape May Formation in New Jersey, and the Gardiners Clay on Long Island. Where these confining beds are present, the salty water mainly lies above them. Where absent, the salty water extends deep in the section—from about sea level down through the Pleistocene deposits, and at places into the Miocene formations. For example, on Long Island fresh water occurs nearly everywhere beneath the Gardiners Clay, with salty water above. In New Jersey, most of the Cape May Formation is permeable, and, at least in the southern half of the coast, salty water extends down into the Cohansey nearly everywhere. However, in a reach in southern Cape May County, N.J., certain estuarine clay beds have fresh water beneath them.

The pattern of boundaries suggests that the flow pattern in general and the location of the discharge zones in particular control the position of the salt-water boundaries. This conclusion leads to the inference that the boundaries are in at least approximate equilibrium with the fresh water.

This inference is strengthened by the relationship of the boundaries to one another in the regions between the discharge zones in the estuaries, such as in the Delaware-Maryland peninsula. Here, in vertical section, the boundaries in the successively older aquifers are both deeper and farther landward. In a general way they lie along a single smooth curve, concave landward, without marked irregularities. The geologic sequence traversed by this curve contains at least two major episodes of continental conditions with the predominantly marine sequence, one in the Oligocene and one in the Pliocene. Were the bound-

aries markedly out of equilibrium one might expect to find within the salty water large lenses of fresh water representing these terrestrial episodes of the geologic history. This seems not to be the case. Whether or not the boundaries are in precise equilibrium depends on the relative head of fresh and of salty water.

## HYDRAULIC-HEAD RELATIONSHIPS

Theoretically, equilibrium between fresh water and sea water in a coastal region requires that the hydraulic head of the fresh water be at least high enough to balance the head of salt water in the vicinity, considering the difference in density, and assuming that in the aquifers, at some seaward point, water of sea-water density fills the interstices from the sea floor down throughout the aquifer concerned. Let us take the density of sea water at Atlantic City, N.J., as being representative of open-coast sea water along the Atlantic coast. At Atlantic City the water has a mean specific gravity of approximately 1.023 (U.S. Coast and Geodetic Survey, 1957), corresponding to a salinity of 31,500 ppm or to a chloride concentration of about 17,400 ppm. This means that for every 100 feet of depth below sea level, the fresh water must have a head of 2.3 feet or more above sea level, or else the sea water will move landward.

At some localities the fresh-water head before being disturbed by withdrawals was equal to, or more than enough to balance, the head of sea water at the depth at which the fresh water is observed. For example, in the Kirkwood aquifer at Atlantic City (fig. 2) the initial head of fresh water at depths around 800 feet was about 25 feet above sea level; using the figures in the previous paragraph, 18.4 feet would be about enough theoretically to balance the head of sea water. Similarly, for the Englishtown Formation at Asbury Park, N.J. (fig. 2), the initial head of the fresh water was nearly 50 feet at depths of 700–800 feet, whereas at that depth, about 17 feet of head would have been enough. The present head at these localities, after several decades of withdrawals, is of course much lower than was the initial head.

Along the south shore of Long Island, N.Y., the fresh-water head is now, and perhaps was initially, too low to maintain equilibrium with the head of sea water. Two deep wells at Jones Beach on Long Island (Perlmutter, and others 1959, p. 430) are examples. In these wells the head has fluctuated around 8 feet above sea level since 1929 and 1933, respectively. The wells are 1,000 feet deep; and to be in approximate equilibrium the head should be at least 23 feet above sea level. There is no record of what the head at this place was before any pumping in the vicinity, but it has remained at about its present level for a considerable time.

At some other places data are inconclusive. For example, figure 3 shows the head in the Manokin aquifer along the Atlantic shore in Maryland to be 5 feet, or less, above sea level. The top of the aquifer here is around 300 feet below sea level; hence the fresh-water head should be around 7 feet above sea level. The piezometric contours are based on observations made mostly in the early 1940's or before, but no really early observations (near the beginning of withdrawals) are known. The initial head might have been somewhat higher. Similar data for the Choptank aquifer in eastern Maryland suggest that the head is a foot or so higher than necessary to balance salt water at the depth of the aquifer. Thus, although not precise, the data suggest that, except for the Long Island locality, the fresh-water bodies are nearly or quite in equilibrium with the nearby sea.

## CONCLUSIONS

The analysis presented in this paper indicates that the circulation pattern of the fresh ground water in general and the location of the discharge zones in particular control the locations of salt-water boundaries in coastal regions. In the parts of the aquifers that are overlain by confining beds, as between the major drowned river valleys or estuaries of the northern Atlantic coastal plain, the salty water is deeper or farther seaward in the aquifers that have a higher head. In such areas the fresh-water movement is extremely slow; it may be largely an imperceptible upward leakage, perhaps in part a slow drift laterally toward the main discharge points. In these regions, then, the salt-water boundaries are probably practically horizontal, and because the movement of the fresh water is extremely slow, it has been possible for the zones of transition to become thick vertically, and hence apparently broad horizontally. The means for developing the thick transition zones is in part the dispersion mechanism, mainly resulting from tidal fluctuations, identified and described by Cooper (1959), and in part the larger-scale movements accompanying the changes in sea level over geologic time.

Along the margins of the drowned river valleys, however, where post-Pleistocene fill in erosional channels lies against the edges of the aquifers, fresh ground water can escape much more readily, and the salt-water boundaries are near these escape zones. The movement of fresh water is more rapid and the transition zones correspondingly narrower. Here, also, differences in the head of fresh water in the different aquifers can cause local areas of overlap on the map.

The general patterns of the boundaries also suggest that hydrodynamic adjustment of the positions of the salt-water boundaries has been rapid enough to keep pace, at least approximately, with the relative changes of sea level that have taken place since the Late Cretaceous. Crude measurements of fresh-water head related to the depth of the aquifers at most places, show either a substantially greater head than needed to balance sea water or a head "deficient" by only a few feet below the head required to maintain theoretical equilibrium.

The boundary in the Pleistocene formations is doubtless in equilibrium, unless locally influenced by withdrawals, because, owing to the relatively high permeability of the deposits, there was little resistance to the advancement of the sea-water wedge through the deposits as the edge of the sea moved landward in post-Wisconsin time. Fresh water already in the unconfined aquifers would simply be lifted up and floated off to sea until lost by mixing.

An additional conclusion of a more practical nature is that along the barrier beach of the northern Atlantic coastal plain, except very near the land surface, salty water probably occurs downward into the uppermost confining bed. Below that, at many places, fresh water may occur in one or more zones. Still deeper, moderately saline water may be found, especially in pre-Cohansey formations remote from discharge areas. This water of moderate salinity may underlie broad areas, and if penetrated by a well, should not necessarily be taken to indicate that the aquifer is being contaminated by direct movement from the present sea.

## REFERENCES


Barksdale, H. C., and others, 1958, Ground-water resources in the tri-state region adjacent to the lower Delaware River: New Jersey Dept. Conserv. and Econ. Devel., Div. Water Policy and Supply, Spec. Rept. 13, 190 p.

Cooper, H. H., Jr., 1959, A hypothesis concerning the dynamic balance of fresh water and salt water in a coastal aquifer: Jour. Geophys. Research, v. 64, no. 4, p. 461–467; *and in* Cooper, H. H., Jr., Kohout, F. A., Henry, H. R., and Glover, R. E., 1964, Sea water in coastal aquifers: U.S. Geol. Survey Water-Supply Paper 1613-C, p. C1–C12.

Gill, H. E., 1962, Ground-water resources of Cape May County, N. J.; Salt-water invasion of principal aquifers: New Jersey Dept. Conserv. and Econ. Devel., Div. Water Policy and Supply, Spec. Rept. 18, 171 p.

Hack, J. T., 1957, Submerged river system of Chesapeake Bay: Geol. Soc. America Bull., v. 68, no. 7, p. 817–830.

Henry, H. R., 1964, Interfaces between salt water and fresh water in coastal aquifers, *in* Cooper, H. H., Jr., Kohout, F. A., Henry, H. R., and Glover, R. E., Sea water in coastal aquifers: U.S. Geol. Survey, Water-Supply Paper 1613-C, p. C35–C70.

Lusczynski, N. J., and Swarzenski, W. V., 1962, Fresh and salty ground water in Long Island, N.Y.: Am. Soc. Civil Engineers Proc., Jour. Hydraulics Div., v. HY–4, no. 3207, p. 173–194.

Marine, I. W., and Rasmussen, W. C., 1955, Preliminary report on the geology and ground-water resources of Delaware: Delaware Geol. Survey Bull., no. 4, p. 336.

Overbeck, R. M., Slaughter, T. H., and Hulme, A. E., 1958, The water resources of Cecil, Kent, and Queen Annes Counties (Maryland): Maryland Dept. Geology, Mines, and Water Res. Bull. 21, 478 p.

Perlmutter, N. M., and Crandell, H. C., Jr., 1959, Geology and ground-water supplies of the south-shore beaches of Long Island, New York: New York Acad. Sci. Annals, v. 80, art. 4, p. 1060–1076.

Perlmutter, N. M., Geraghty, J. J., and Upson, J. E., 1959, The relation between fresh and salty ground water in southern Nassau and southeastern Queens Counties, Long Island, New York: Econ. Geology, v. 54, no. 3, p. 416–435.

Perlmutter, N. M., and Todd, Ruth, 1965, Correlation and Foraminifera of the Monmouth Group (Upper Cretaceous), Long Island, New York: U.S. Geol. Survey Prof. Paper 483–I, 24 p.

Rasmussen, W. C., Slaughter, T. H., and others, 1955, The water resources of Somerset, Wicomico, and Worcester Counties (Maryland): Maryland Dept. Geology, Mines, and Water Res. Bull. 16, 533 p.

——— 1957, The water resources of Caroline, Dorchester, and Talbot Counties (Maryland): Maryland Dept. Geology, Mines, and Water Res. Bull. 18, 465 p.

Rasmussen, W. C., Groot, J. J., and Depman, A. J., 1958, High-capacity test well developed at the Air Force Base, Dover, Delaware: Delaware Geol. Survey, Rept. Inv. 2, 36 p.

Rasmussen, W. C., Wilkens, R. A., Beall, R. M., and others, 1960, Water resources of Sussex County, Delaware: Delaware Geol. Survey Bull. 8, 228 p.

Seaber, P. R., 1962, Cation hydrochemical facies of ground water in the Englishtown Formation, New Jersey: Art. 51 *in* U.S. Geol. Survey Prof. Paper 450–B, p. 124–126.

Slaughter, T. H., 1962, Beach-area water supplies between Ocean City, Maryland, and Rehoboth Beach, Delaware: U.S. Geol. Survey, Water-Supply Paper 1619–T, 10 p.

Thompson, D. G., 1928, Ground-water supplies of the Atlantic City region: New Jersey Dept. Conserv. and Development, Div. of Water, Bull. 30, 139 p.

Thompson, D. G., 1930, Ground-water supplies in the vicinity of Asbury Park (New Jersey): New Jersey Dept. Conserv. and Development Bull. 35, 50 p.

U.S. Coast and Geodetic Survey, 1957, Density of sea water at tide stations, Atlantic Coast, North and South America (5th ed.): U.S. Coast and Geod. Survey Pub. 31–2 (with data through 1956), 72 p.

# CHEMICAL EFFECTS OF IRRIGATION-RETURN WATER, NORTH PLATTE RIVER, WESTERN NEBRASKA

By G. V. GORDON, Lincoln, Nebr.

*Abstract.*—The return of irrigation water to the North Platte River by ground-water discharge was the main cause of a 27-percent increase in the dissolved-solids content of the river water during 1964, in a period of low flow in the 60-mile reach between the Wyoming-Nebraska boundary and Bridgeport, Nebr. The effects of irrigation return were most pronounced in the reach of the stream in which the flow was least. The irrigation-return water from south of the river generally was of poorer quality than that from north of the river; this difference may be due to differences in the quality of the applied irrigation water and in the nature of the soils in these two parts of the basin.

Deterioration of the chemical quality of water in the 60-mile reach of the North Platte River between the Wyoming-Nebraska boundary and Bridgeport, Nebr., has for some years concerned local water users and State officials. Because the North Platte River provides water for the irrigation of many thousands of acres of land in western and south-central Nebraska, a continued deterioration of its water quality could eventually have an adverse effect on the economy of the area. Possible causes of the deterioration are (1) inflow of municipal-waste effluent, (2) return flow of irrigation water to the stream by ground-water discharge, and (3) the inflow of wastes from the processing of sugar beets. The purpose of the investigation described in this paper was to determine the effects of irrigation return.

## METHODS OF STUDY

Fieldwork for the investigation was done during the period August 17–20, 1964. This was considered to be a good time for the investigation because the flow of the river was being maintained almost wholly by return flow from irrigation, and because the quality of the river water was not being affected by the processing of sugar beets, which occurs later in the season (October–December).

Water samples for this investigation were obtained at 4 sites along the North Platte River, at 6 sites on major canals, and at 25 sites on natural or artificial drains whose flow was maintained wholly or in part by irrigation return (fig. 1). Streamflow-gaging stations were in operation at the 4 river sites and at 16 of the sites on drains, and water discharges for times of sampling were computed from the gaging records. Where no gaging stations were in operation, discharge measurements were made at the time of sampling. Water samples from many of the smaller drains were collected by D. J. Neely, hydrographer for the Nebraska Department of Water Resources.

## SOURCE AND VOLUME OF FLOW OF THE NORTH PLATTE RIVER

The North Platte River has its source in the high mountains in north-central Colorado. As it flows northward and then southeastward through Wyoming, its flow is augmented by that of the Medicine Bow, Sweetwater, and Laramie Rivers and a number of smaller streams. During this course, its flow is also regulated by a series of storage reservoirs, Seminoe Dam and Guernsey Dam being the upstream and downstream facilities, respectively. In Wyoming, the North Platte River provides water for municipal, industrial, and irrigation use and, in turn, receives wastes resulting from those uses. Ordinarily, by the time the water in this river reaches Nebraska, it already has been used extensively.

Within the reach of the river studied, no rain fell just prior to or during the period of fieldwork; moreover, precipitation had been below average earlier in the summer. It was therefore assumed that no overland runoff was entering the river during the period of investigation. All the inflow to the river was either (1) municipal-waste effluent or (2) ground water; both occurred as discharge directly into the river or

U.S. GEOL. SURVEY PROF. PAPER 550-C, PAGES C244-C250

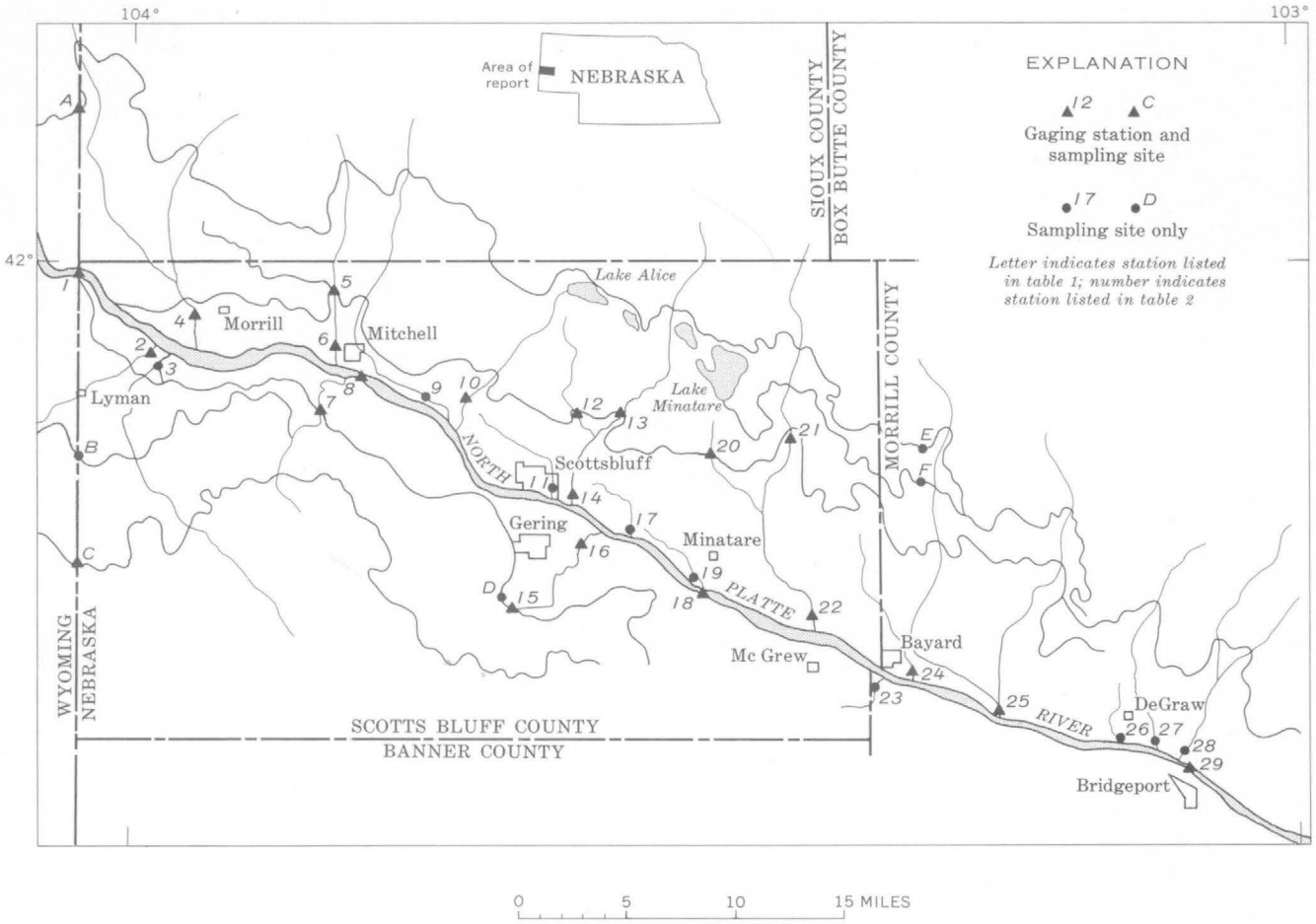


FIGURE 1.—North Platte River, tributary drains, and irrigation canals in western Nebraska, with locations of sampling sites.

into streams and manmade drains that empty into the river.

If we assume that the average daily volume of municipal-waste effluent is 50 gallons per person, the effluent from all the municipalities in this reach (combined population in 1960, 24,315) totals only 1.9 cubic feet per second, or less than 1 percent of the total flow of 287 cfs at Bridgeport (169 cfs in the main channel and 118 cfs in the Browns Creek channel) at the time of sampling for this investigation. Furthermore, because effluent from the municipalities in this reach generally contains less than 1,000 parts per million of dissolved inorganic solids (which is only about 500 ppm more than the content in the river water at the upstream end of the reach), the effects of municipal effluent on the chemical quality of the river water must be very small indeed. Therefore, any significant change in the chemical quality of streamflow within the reach at the time of study can be attributed to the chemical quality of the ground-water inflow.

All or nearly all the ground-water inflow to the North Platte River is discharge from the zone of saturation in the unconsolidated sediments that underlie the irrigated terrace lands on both sides of the river (Wenzel and others, 1946, p. 120). Although precipitation is the source of some water in the zone of saturation, seepage from irrigation constitutes a much larger part; in fact, were it not for the recharge from irrigation seepage, ground-water inflow to the river would be small, and it ordinarily would be negligible at the time of year that this study was made. For this reason, ground-water inflow to the river in this reach may be regarded as consisting almost wholly of irrigation return, and the effect of ground-water inflow on the chemical quality of the streamflow may be attributed principally to the chemical quality of the irrigation return.

At the time of this study, the flow of the North Platte River at the State boundary was 1,160 cfs, and within the reach between the boundary and the town of Mitchell the measured inflow totaled 77 cfs. Because most of the streamflow in that reach was diverted for irrigation, the flow at Mitchell was only 156 cfs. Between Mitchell and Minatare, measured inflow to

the river was 126 cfs. However, diversions for irrigation in this reach were nearly as great as inflow, so that the total flow near Minatare was only 164 cfs (49 cfs in the main channel and 115 cfs in Ninemile channel). Measured inflow to the river between Minatare and Bridgeport totaled 310 cfs, but diversions for irrigation in this segment of the valley decreased streamflow to 287 cfs at the downstream end of the study reach. From these figures it is apparent that the flow of the North Platte River at successive downstream sites consisted of irrigation return in progressively greater proportions.

## QUALITY OF IRRIGATION AND RETURN WATERS

Data in table 1 represent the chemical quality of canal water that is used for irrigation in the area, and data in table 2 represent the quality of water in the North Platte River and in irrigation drains that are tributary to the river. Each sampling site was assigned a reference letter or number that serves to identify the site in figure 1.

Three of the canals listed in table 1 divert water directly from the North Platte River: the Interstate Canal and the Fort Laramie Canal about 35 miles upstream from the Wyoming-Nebraska boundary, in Wyoming, and the Mitchell-Gering Canal at the boundary. The water conveyed by Horse Creek Lateral is diverted from Horse Creek—a natural tributary of the North Platte River draining a long narrow segment of upland that lies east of the Laramie Range in Wyoming. Any flow in Horse Creek below the point of diversion, which is about 5 miles southwest of Lyman, Nebr., is a result of irrigation return. Water in the Interstate High Line Canal and the Government Low Line Canal is derived from Lake Alice and Lake Minatare, respectively. These two lakes are supplementary storage reservoirs for water diverted from the North Platte River into the Interstate Canal.

The water in all the canals except the Horse Creek Lateral was of the calcium sodium sulfate type and contained from 462 to 522 ppm of dissolved solids. The water in the Horse Creek Lateral was of the sodium calcium sulfate type and contained 541 ppm of dissolved solids. Sodium, sulfate, phosphate, and boron concentrations in the water from the Horse Creek Lateral were somewhat greater than those in the water from other canals. The canal water was very similar in chemical quality to water in the North Platte River at the Wyoming-Nebraska boundary; some was of slightly better quality, and some was of slightly poorer quality.

Irrigation return in the area (table 2) was definitely more mineralized and of more variable chemical character than the canal water used for irrigation (table 1). On the north side of the river the return water was generally of a calcium bicarbonate or calcium sodium bicarbonate type, and its dissolved solids ranged from 539 to 720 ppm and averaged 616 ppm. On the south side of the river the return water was generally of a sodium bicarbonate type, and its dissolved solids ranged from 597 to 867 ppm and averaged 766 ppm.

The weighted-average composition of the water from tributary drains is shown in table 3. The drainage from the south side, besides being more mineralized, contained almost twice as much boron as the drainage from the north side. In contrast, the drainage from the south contained appreciably less silica than the drainage from the north. Although concentrations of the major anions (bicarbonate, sulfate, and chloride) were greater in drainage from south of the river, their relative proportions were almost the same as those in drainage from north of the river. Both the concentrations and the relative proportions of the major cations (calcium, magnesium, and sodium), however, were considerably different in drainage from opposite sides of the river.

One explanation for the difference in chemical quality of irrigation return from opposite sides of the river is the small, but nevertheless apparent, difference in the quality of the applied water. Chemical analyses of applied water (table 1) indicate that sodium comprised a greater part of the cationic composition of water on the south side of the river than it did on the north side. Consequently, one would expect sodium to comprise a correspondingly greater part of the cationic composition of irrigation return from the south side (table 3).

The difference in sodium percentage (percentage reacting value) in drainage from opposite sides of the river is greater than one might expect, however. If allowance were made for the irrigation water to undergo some base exchange (wherein calcium and magnesium ions originally present in the water would be exchanged for sodium ions released from the soil), thereby increasing its sodium concentration, the sodium percentage in drainage from the north side would seem to be low. Apparently, irrigation water on that side does not undergo base exchange to the extent that it does on the south side. A possible explanation may lie in a difference in the soils on each side of the river. Soil surveys made jointly by the U.S. Department of Agriculture and the University of Nebraska indicate a more widespread occurrence of calcareous soils north of the river (Hayes and others, 1920, soil map). These calcareous materials may inhibit base exchange

TABLE 1.—*Chemical analyses of water from canals in western Nebraska*

[Results in parts per million except as indicated]

| Reference letter (see fig. 1) | Canal [1] | Date of collection (1964) | Temperature (°F) | Silica ($SiO_2$) | Iron (Fe) | Manganese (Mn) | Calcium (Ca) | Magnesium (Mg) | Sodium (Na) | Potassium (K) | Bicarbonate ($HCO_3$) | Carbonate ($CO_3$) | Sulfate ($SO_4$) | Chloride (Cl) | Fluoride (F) | Nitrate ($NO_3$) | Phosphate ($PO_4$) | Boron (B) | Dissolved solids (residue on evaporation at 180°C) | Hardness as $CaCO_3$ | Noncarbonate hardness as $CaCO_3$ | Percent sodium | Sodium adsorption ratio | Specific conductance (micromhos per cm at 25°C) | pH |
|---|---|---|---|---|---|---|---|---|---|---|---|---|---|---|---|---|---|---|---|---|---|---|---|---|---|
| A | Interstate Canal at Wyoming-Nebraska boundary (N). | Aug. 20 | 68 | 9.5 | 0.01 | 0.02 | 65 | 21 | 59 | 4.2 | 176 | 1 | 201 | 16 | 0.4 | 0.4 | 0.09 | 0.07 | 480 | 249 | 103 | 34 | 1.6 | 709 | 8.3 |
| B | Horse Creek Lateral on Wyoming-Nebraska boundary (S). | Aug. 19 | 68 | 13 | .01 | .03 | 59 | 21 | 85 | 5.8 | 205 | 0 | 219 | 18 | .5 | 1.2 | .11 | .11 | 541 | 232 | 64 | 44 | 2.4 | 811 | 7.8 |
| C | Fort Laramie Canal at Wyoming-Nebraska boundary (S). | do | 72 | 9.0 | .02 | .02 | 63 | 20 | 58 | 4.4 | 169 | 0 | 198 | 15 | .4 | .5 | .07 | .06 | 468 | 239 | 100 | 34 | 1.6 | 701 | 7.8 |
| D | Mitchell-Gering Canal at siphon under Gering drain (S). | do | 68 | 14 | ------ | ------ | 65 | 21 | 72 | 6.1 | 208 | 0 | 207 | 17 | .4 | 1.8 | .09 | .07 | 522 | 248 | 77 | 38 | 2.0 | 778 | 7.8 |
| E | Interstate High Line Canal near Bayard (N). | Aug. 20 | 65 | 8.7 | ------ | ------ | 59 | 20 | 57 | 4.6 | 153 | 0 | 206 | 15 | .4 | .0 | .06 | .08 | 462 | 228 | 103 | 35 | 1.6 | 686 | 7.9 |
| F | Government Low Line Canal near Bayard (N). | do | 65 | 6.9 | ------ | ------ | 63 | 23 | 59 | 5.8 | 198 | 0 | 192 | 17 | .4 | .0 | .07 | .09 | 484 | 252 | 90 | 33 | 1.6 | 726 | 8.1 |

[1] N, canal on north side of river; S, canal on south side of river.

TABLE 2.—*Chemical analyses of water from the North Platte River and tributary drains in western Nebraska*

[Results in parts per million except as indicated]

| Reference number (see fig. 1) | Station [1] | Date of collection (1964) | Temperature (° F) | Discharge (cfs) | Silica ($SiO_2$) | Iron (Fe) | Manganese (Mn) | Calcium (Ca) | Magnesium (Mg) | Sodium (Na) | Potassium (K) | Bicarbonate ($HCO_3$) | Carbonate ($CO_3$) | Sulfate ($SO_4$) | Chloride (Cl) | Fluoride (F) | Nitrate ($NO_3$) | Phosphate ($PO_4$) | Boron (B) | Dissolved solids: Residue on evaporation at 180° C | Dissolved solids: Tons per day | Hardness as $CaCO_3$ | Noncarbonate hardness as $CaCO_3$ | Percent sodium | Sodium adsorption ratio | Specific conductance (micromhos per cm at 25° C) | pH |
|---|---|---|---|---|---|---|---|---|---|---|---|---|---|---|---|---|---|---|---|---|---|---|---|---|---|---|---|
| 1 | North Platte River at Wyoming-Nebraska State line | Aug. 19 | 70 | 1,160 | 14 | 0.01 | 0.04 | 71 | 19 | 65 | 5.8 | 206 | 0 | 198 | 16 | 0.4 | 1.6 | 0.08 | 0.06 | 509 | 1,590 | 257 | 88 | 35 | 1.8 | 757 | 7.9 |
| 2 | Horse Creek near Lyman (S) | do | 65 | 47 | 20 | | | 51 | 18 | 200 | 11 | 425 | 0 | 261 | 27 | .8 | 6.8 | .23 | .24 | 867 | 110 | 200 | 0 | 67 | 6.2 | 1,240 | 8.0 |
| 3 | Lane drain near Lyman (S) | Aug. 17 | 62 | 3.4 | 52 | | | 40 | 13 | 214 | 13 | 420 | 0 | 230 | 27 | .7 | 5.2 | | .23 | 860 | 7.89 | 155 | 0 | 73 | 7.5 | 1,210 | 8.1 |
| 4 | Sheep Creek near Morrill (N) | Aug. 20 | 57 | 4.2 | 54 | | | 78 | 18 | 59 | 10 | 250 | 0 | 168 | 14 | .6 | 7.2 | .09 | .09 | 557 | 6.32 | 268 | 63 | 31 | 1.6 | 766 | 8.1 |
| 5 | Dutch Flats drain near Mitchell (N) | do | 61 | 18 | 32 | | | 84 | 22 | 60 | 10 | 251 | 0 | 196 | 17 | .4 | 5.8 | .18 | .08 | 575 | 27.9 | 300 | 94 | 29 | 1.5 | 835 | 7.7 |
| 6 | Dry Spottedtail Creek at Mitchell (N) | do | 67 | 16 | 44 | | | 84 | 20 | 62 | 9.6 | 271 | 0 | 182 | 17 | .5 | 7.4 | .14 | .11 | 584 | 25.2 | 292 | 70 | 31 | 1.6 | 817 | 8.0 |
| 7 | Brown Canyon drain near Mitchell (S) | Aug. 19 | 65 | 6.5 | 27 | | | 58 | 16 | 103 | 10 | 242 | 0 | 213 | 19 | .5 | 6.0 | .28 | .15 | 597 | 10.5 | 210 | 12 | 50 | 3.1 | 865 | 7.6 |
| 8 | North Platte River at Mitchell | Aug. 20 | 57 | 156 | 32 | 0.00 | .05 | 75 | 18 | 119 | 8.1 | 336 | 0 | 217 | 21 | .5 | 6.6 | .11 | .14 | 669 | 282 | 261 | 0 | 49 | 3.2 | 988 | 8.1 |
| 9 | Wet Spottedtail Creek (N) | Aug. 18 | 78 | 15 | 40 | | | 78 | 21 | 74 | 15 | 273 | 0 | 192 | 18 | .6 | 6.0 | | .12 | 624 | 25.3 | 280 | 56 | 35 | 1.9 | 867 | 7.7 |
| 10 | Tub Springs near Scottsbluff (N) | Aug. 20 | 66 | 2.5 | 48 | | | 84 | 21 | 67 | 10 | 291 | 0 | 174 | 18 | .5 | 5.8 | .08 | .12 | 594 | 4.01 | 297 | 58 | 32 | 1.7 | 829 | 8.0 |
| 11 | Scottsbluff drain No. 1 (N) | Aug. 19 | 68 | 9.4 | 8.8 | | | 88 | 26 | 93 | 16 | 345 | 0 | 206 | 20 | .6 | 11 | | .15 | 720 | 18.3 | 327 | 44 | 37 | 2.2 | 1,000 | 7.8 |
| 12 | Hale drain near Scottsbluff (N) | Aug. 20 | 60 | 18 | 48 | | | 67 | 20 | 80 | 8.5 | 253 | 0 | 182 | 16 | .4 | 9.1 | .34 | .15 | 576 | 28.0 | 248 | 41 | 40 | 2.2 | 808 | 7.7 |
| 13 | Winter Creek at Tri-State Canal near Scottsbluff (N) | do | 60 | 49 | 60 | | | 82 | 16 | 59 | 7.1 | 245 | 0 | 167 | 17 | .5 | 9.6 | .11 | .12 | 570 | 75.4 | 272 | 71 | 31 | 1.6 | 765 | 8.1 |
| 14 | Winter Creek near Scottsbluff (N) | do | 64 | 41 | 53 | | | 80 | 19 | 68 | 8.5 | 260 | 0 | 176 | 18 | .5 | 7.8 | .15 | .14 | 587 | 65.0 | 277 | 64 | 34 | 1.8 | 807 | 8.0 |
| 15 | Gering drain at Mitchell-Gering Canal, near Gering (S) | Aug. 19 | 63 | 33 | 30 | | | 68 | 18 | 96 | 8.1 | 252 | 0 | 207 | 20 | .5 | 6.3 | .17 | .18 | 611 | 54.4 | 242 | 35 | 45 | 2.7 | 874 | 7.6 |
| 16 | Gering drain near Gering (S) | do | 61 | 47 | 39 | | | 63 | 17 | 128 | 9.5 | 314 | 0 | 196 | 23 | .5 | 12 | .22 | .22 | 676 | 85.8 | 225 | 0 | 54 | 3.7 | 963 | 7.9 |
| 17 | Scottsbluff drain No. 2 (N) | do | 65 | 11 | 48 | | | 80 | 24 | 108 | 18 | 364 | 0 | 195 | 24 | .8 | 8.8 | | .22 | 712 | 21.1 | 298 | 0 | 42 | 2.7 | 1,020 | 7.6 |
| 18 | North Platte River near Minatare (Ninemile channel) | Aug. 20 | 69 | 115 | 38 | 0.00 | .04 | 81 | 19 | 109 | 10 | 336 | 0 | 201 | 26 | .5 | 7.9 | .21 | .17 | 669 | 208 | 282 | 6 | 45 | 2.8 | 979 | 8.2 |
| 19 | Fairfield seep (N) | Aug. 19 | 73 | 6.5 | 31 | | | 78 | 24 | 107 | 13 | 336 | 0 | 206 | 28 | .5 | 2.7 | | .21 | 696 | 12.2 | 294 | 18 | 43 | 2.7 | 997 | 7.6 |
| 20 | Alliance drain near Minatare (N) | Aug. 20 | 59 | 32 | 53 | | | 84 | 17 | 61 | 11 | 241 | 0 | 188 | 16 | .6 | 3.3 | .17 | .12 | 574 | 49.6 | 278 | 80 | 31 | 1.6 | 790 | 8.0 |
| 21 | Ninemile drain near Minatare (N) | do | 59 | 60 | 63 | | | 81 | 16 | 52 | 8.3 | 234 | 0 | 161 | 15 | .6 | 7.4 | .12 | .12 | 539 | 87.3 | 268 | 76 | 29 | 1.4 | 731 | 7.9 |
| 22 | Ninemile drain near McGrew (N) | do | | 180 | 56 | | | 86 | 20 | 64 | 11 | 269 | 0 | 187 | 17 | .7 | 8.1 | .13 | .12 | 600 | 292 | 295 | 74 | 31 | 1.6 | 830 | 8.1 |
| 23 | Cleveland drain (S) | Aug. 19 | 72 | 7.6 | 42 | | | 77 | 18 | 150 | 12 | 370 | 0 | 230 | 36 | .6 | 7.1 | | .25 | 800 | 16.4 | 268 | 0 | 53 | 4.0 | 1,140 | 7.6 |
| 24 | Bayard Sugar Factory drain near Bayard (N) | Aug. 20 | 59 | 7.3 | 49 | | | 87 | 22 | 84 | 16 | 321 | 0 | 201 | 20 | .7 | 9.9 | .17 | .15 | 662 | 13.0 | 309 | 46 | 36 | 2.1 | 946 | 7.9 |
| 25 | Red Willow Creek near Bayard (N) | do | 57 | 79 | 51 | | | 88 | 19 | 80 | 12 | 303 | 0 | 197 | 20 | .6 | 9.6 | .17 | .14 | 658 | 140 | 299 | 51 | 36 | 2.0 | 913 | 7.7 |
| 26 | DeGraw drain (N) | do | 59 | 1.8 | 44 | | | 81 | 17 | 72 | 10 | 268 | 0 | 178 | 18 | .6 | 5.6 | | .13 | 572 | 2.78 | 271 | 51 | 36 | 1.9 | 825 | 7.7 |
| 27 | Indian Creek (N) | do | 59 | 18 | 47 | | | 88 | 14 | 65 | 10 | 258 | 0 | 174 | 20 | .5 | 5.9 | | .13 | 584 | 28.4 | 277 | 65 | 33 | 1.7 | 806 | 7.4 |
| 28 | Upper Dugout Creek (N) | do | 58 | 9.7 | 45 | | | 84 | 16 | 50 | 8.4 | 254 | 0 | 148 | 16 | .5 | 2.8 | | .11 | 540 | 14.1 | 276 | 68 | 28 | 1.3 | 739 | 7.5 |
| 29 | North Platte River at Bridgeport (main channel) | do | 71 | 169 | 47 | 0.00 | .05 | 84 | 19 | 86 | 11 | 298 | 0 | 204 | 22 | .5 | 6.3 | .21 | .15 | 647 | 295 | 287 | 43 | 38 | 2.2 | 898 | 8.2 |

[1] Stations listed in downstream order. N, flow into river from north; S, flow into river from south.

TABLE 3.—*Weighted-average composition of water from tributary drains*

| Unit of expression | Silica ($SiO_2$) | Calcium (Ca) | Magnesium (Mg) | Sodium (Na) | Potassium (K) | Bicarbonate ($HCO_3$) | Sulfate ($SO_4$) | Chloride (Cl) | Fluoride (F) | Nitrate ($NO_3$) | Boron (B) | Dissolved solids |
|---|---|---|---|---|---|---|---|---|---|---|---|---|
| **Drainage from north side of the North Platte River (401 cfs)** | | | | | | | | | | | | |
| Parts per million | 51 | 85 | 20 | 71 | 11 | 280 | 187 | 18 | 0.6 | 8.0 | 0.13 | 616 |
| Equivalents per million | ------ | 4.24 | 1.64 | 3.09 | .28 | 4.59 | 3.89 | .51 | .03 | .13 | ------ | -------- |
| Percentage reacting value | ------ | 45.8 | 17.7 | 33.4 | 3.0 | 50.2 | 42.5 | 5.6 | .3 | 1.4 | ------ | -------- |
| **Drainage from south side of the North Platte River (112 cfs)** | | | | | | | | | | | | |
| Parts per million | 31 | 58 | 17 | 161 | 10 | 364 | 228 | 25 | 0.6 | 8.9 | 0.23 | 766 |
| Equivalents per million | ------ | 2.89 | 1.40 | 7.00 | .26 | 5.97 | 4.75 | .70 | .03 | .14 | ------ | -------- |
| Percentage reacting value | ------ | 25.0 | 12.1 | 60.6 | 2.3 | 51.5 | 41.0 | 6.0 | .03 | 1.2 | ------ | -------- |
| **Drainage from north and south sides (combined) of the North Platte River (513 cfs)** | | | | | | | | | | | | |
| Parts per million | 47 | 79 | 19 | 90 | 11 | 299 | 196 | 20 | 0.6 | 8.2 | 0.15 | 649 |
| Equivalents per million | ------ | 3.94 | 1.56 | 3.92 | .28 | 4.90 | 4.08 | .56 | .03 | .13 | ------ | -------- |
| Percentage reacting value | ------ | 40.6 | 16.1 | 40.4 | 2.9 | 50.5 | 42.1 | 5.8 | .3 | 1.3 | ------ | -------- |

and thereby contribute substantially to the calcium bicarbonate character of the drainage from north of the river.

Irrigation-return water that was discharged into the North Platte River between the State boundary and Bridgeport was of poorer quality than the river water at the boundary. The dissolved-solids content of irrigation-return water was as much as 70 percent greater, and the concentrations of bicarbonate, nitrate, phosphate, and boron were all higher than in river water at the State boundary.

The greatest change in the quality of river water occurred in the reach between the State boundary and Mitchell. The river water increased in the concentration of every constituent except iron and magnesium. Increases were substantial in the concentrations of sodium, bicarbonate, nitrate, and boron; the increase in total dissolved solids was 160 ppm. In this reach, large amounts of water were diverted into the Mitchell-Gering, Tri-State, and Enterprise Canals, and a large proportion of the inflow to the river (Horse Creek and Lane drain) was significantly poorer in quality than the river water at the State boundary.

The least change in the quality of river water occurred in the reach between Mitchell and Minatare. The dissolved-solids content of river water at the sampling site near Minatare was the same as that at Mitchell. Although most ions showed small increases in their concentrations, bicarbonate remained unchanged and sodium and sulfate decreased. The most conspicuous change was in phosphate, which increased from 0.11 ppm at Mitchell to 0.21 ppm near Minatare. Very probably the increase in phosphate concentration reflects the high phosphate content of the fertilizers that are used in this area.

Most of the irrigation return in the reach between Minatare and Bridgeport was of better quality than the river water near Minatare. River water at Bridgeport showed a decrease in the concentration of dissolved solids because of decreases in the concentrations of sodium, bicarbonate, chloride, nitrate, and boron. Calcium, potassium, and sulfate concentrations increased slightly. It seems likely that the quality of irrigation return in this reach of the river is better because a much smaller volume of water is diverted from the river for irrigation here than in the reach from the State boundary to Mitchell.

Over the entire reach of the North Platte River between the State boundary and Bridgeport, total dissolved solids increased 27 percent, sodium increased 32 percent, and bicarbonate 45 percent. Sulfate increased only 3 percent. The concentrations of phosphate and boron more than doubled, and the concentrations of silica and nitrate more than tripled. The only constituents to show consistent increases in concentration downstream were silica, calcium, and potassium. The consistent increase in calcium is reflected in the increase in hardness; magnesium remained nearly unchanged throughout the reach.

Increases in the concentrations of the major ions and in the concentration of boron reflect the leaching effect of irrigation water on the more soluble salts in the

TABLE 4.—*Chemical analyses, in parts per million, of drainage water from Broadbalk wheatfield at Rothamsted, England*

[Results recomputed by author from original reporting units]

| Treatment | Silica ($SiO_2$) | Iron (Fe) | Calcium (Ca) | Magnesium (Mg) | Sodium (Na) | Potassium (K) | Sulfate ($SO_4$) | Chloride (Cl) | Nitrate ($NO_3$) | Phosphate ($PO_4$) | Dissolved solids |
|---|---|---|---|---|---|---|---|---|---|---|---|
| Unfertilized | 11 | 4.0 | 70 | 3.1 | 4.5 | 1.4 | 30 | 11 | 15 | 0.4 | 246 |
| Fertilized | 25 | 1.9 | 103 | 4.8 | 7.9 | 3.7 | 88 | 21 | 33 | 1.0 | 408 |
| Percentage increase (+) or decrease (−)[1] | +127 | −52 | +47 | +55 | +76 | +164 | +193 | +91 | +120 | +150 | +66 |

[1] Percentages computed by author.

soils. Increases in the concentrations of potassium, nitrate, and phosphate reflect in part the presence of these constituents in fertilizers. The effect of fertilizers on drainage water from cultivated fields is illustrated in table 4, the data for which were obtained by A. Voelcker (Robinson, 1949, p. 36) from the Broadbalk wheatfield at Rothamsted, England. The wheatfield had been under continuous cultivation for 80 years, and after fertilizers were applied the concentrations of silica, potassium, sulfate, nitrate, and phosphate in the drainage water increased 100 percent or more. With the exception of sulfate, these same constituents increased nearly 100 percent or more in the water of the North Platte River between the Wyoming-Nebraska State boundary and Bridgeport. The increase in the concentration of sulfate is very small (3 percent), probably because sulfate fertilizers (chiefly ammonium sulfate) comprise only a small percentage of the total quantity of fertilizers used in this part of the North Platte Valley (Nebraska Dept. Agriculture and Econ. Devel., 1964, p. 19).

## SUMMARY

The data obtained during the period August 17–20, 1964, indicate an increase of 27 percent in dissolved solids and a change in water type from calcium sodium sulfate to calcium sodium bicarbonate in the North Platte River between the Wyoming-Nebraska boundary and Bridgeport during a period of low flow. The available evidence indicates that the increase and the change were due mostly to irrigation return. During periods of medium and high flows, the percentage increase is undoubtedly much less.

## REFERENCES

Hayes, F. A., Hawker, H. W., Davis, M.D., and Seabury, V. H., 1920, Soil survey of Morrill County, Nebr.: U.S. Dept. Agriculture, Bur. Soils, 69 p.

Nebraska Department of Agriculture and Economic Development, 1964, Report of commercial fertilizers and economic poisons, June 30, 1964–December 31, 1964: 70 p.

Robinson, G. W., 1949, Soils: New York, John Wiley & Sons, Inc., 573 p.

Wenzel, L. K., Cady, R. C., and Waite, H. A., 1946, Geology and ground-water resources of Scotts Bluff County, Nebr.: U.S. Geol. Survey Water-Supply Paper 943, 150 p.

# WATER-QUALITY VARIATIONS IN THE CUYAHOGA RIVER AT CLEVELAND, OHIO

By M. E. SCHROEDER and C. R. COLLIER, Columbus, Ohio

*Work done in cooperation with the Ohio Department of Health*

*Abstract.*—The quality of water in the navigable portion of the Cuyahoga River at Cleveland, Ohio, varies with the length, depth, and width of this 5-mile reach of the stream. Near the river mouth the water is stratified during periods of low flow, when the water, which contains large volumes of industrial and municipal wastes, overlies the cooler and less mineralized water from Lake Erie. Water-quality conditions are further complicated by the irregular and unpredictable changes in water levels in the river due to seiche and wind action on Lake Erie.

Understanding of the variability of water-quality conditions throughout the length and depth of the channel is required in order to interpret data from water-quality monitoring and sampling in the navigable portion of the Cuyahoga River at Cleveland, Ohio. The navigation channel of the Cuyahoga River at Cleveland extends 5.1 miles upstream from the mouth of the river (station 500, fig. 1). The channel averages about 150 feet in width and is maintained at a minimum depth of 23 feet. Heavy indiustrial complexes line both sides of the channel, and industrial and municipal outfalls are scattered along its length. The water quality in the channel is a result of the intrusion and incomplete mixing of lake water with the river and outfall water.

Measurements of specific conductance, water temperature, and dissolved oxygen were made at various depths in the navigable channel in 2 traverses along the centerline, and in 3 cross sections, on October 20–21, 1964, to determine the water quality during a period of low streamflow. To provide information on the changes in the quality of the river water during the time of the traverse, recording conductivity meters were installed at the Republic Steel Corp. water intake, 1.2 miles upstream from the head of navigation, and at the E. I. DuPont de Nemours and Co. intake (station 722) at the turning basin, 4.2 miles upstream from the mouth. A water-quality monitor recorded conductivity, temperature, pH, and dissolved oxygen of the water at the Center Street bridge.

## STREAMFLOW AND WATER-LEVEL FLUCTUATIONS

The average discharge of the Cuyahoga River as it entered the navigation channel was 189 cubic feet per second on October 20, 1964, and 162 cfs on October 21. Over a long period these discharges are exceeded between 80 and 90 percent of the time. The only significant additional inflow is that contributed by the Cleveland Southerly sewage-treatment plant. Along the navigation channel, large volumes of water are withdrawn by industry, primarily for cooling, and returned to the channel. Passage of the river water through the navigation channel is slow because the cross section of the channel is large and because seiching which occurs frequently in Lake Erie tends to obstruct the flow near the mouth of the river.

The water level of Lake Erie fluctuated continuously during the study. Lake levels shown on figure 2 were taken from the hydrograph of the lake gage (upper center, fig. 1) in the east basin at the foot of East 9th Street, Cleveland, operated by the U.S. Army Engineer District, Lake Survey, Corps of Engineers. The hydrograph for October 20 is irregular and fluctuates over a 0.57-foot range in lake level. Part of the fluctuation is believed to have been caused by a north wind; seiching apparently caused part of the variation, although no pattern is evident. On October 21 the range in lake level was 1.50 feet, and the hydrograph is even more irregular than that for the previous day.

The fluctuation in the level of Lake Erie also affects

U.S. GEOL. SURVEY PROF. PAPER 550-C, PAGES C251-C255

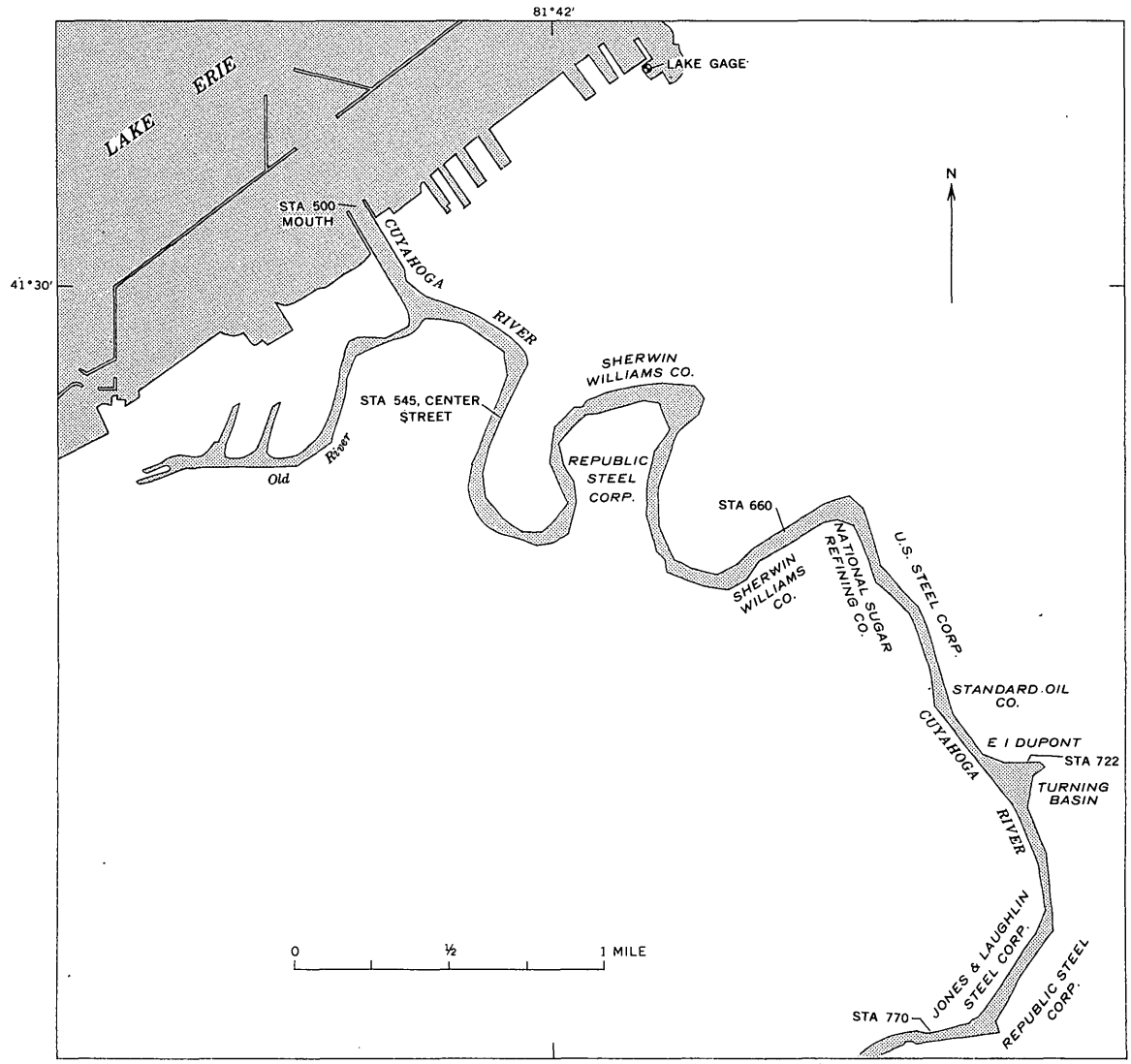


FIGURE 1.—Map of the navigation channel of the Cuyahoga River at Cleveland, Ohio. (Base from U.S. Army Engineer District, Lake Survey, Chart 354.)

the water level in the navigation channel of the Cuyahoga River. At Center Street bridge (station 545), 0.86 mile upstream from the mouth, water levels below an arbitrary reference point were measured by tape during the traverses. Comparison of these measurements with the hydrograph of the lake level (fig. 2) shows that the water-level fluctuation at Center Street bridge closely resembles that of the lake. (This figure illustrates only the similarity of the fluctuations in water level at the two sites, because an arbitrary datum was used for the reference point at Center Street bridge.)

## VARIATIONS IN WATER QUALITY IN THE CHANNEL

The continuous records of specific conductance at the Republic Steel intake (fig. 1), upstream from the head of navigation, and at the DuPont intake at station 722, farther upstream, indicated no significant change in the water quality in those reaches of channel during the traverses. The range in specific conductance at the Republic Steel Corp. intake was from 1,200 to 1,230 micromhos during the October 20 traverse and from 1,200 to 1,220 micromhos during the October 21 traverse. At the DuPont intake the conductance ranged from 1,280 to 1,300 micromhos during the October 20 traverse; on October 21 the conductance at this site was constant at 1,480 micromhos.

At Center Street bridge, the water quality, as indicated by specific conductance at a depth of 5 feet, changed continuously and erratically. During the October 20 traverse it ranged from 1,050 to 1,240

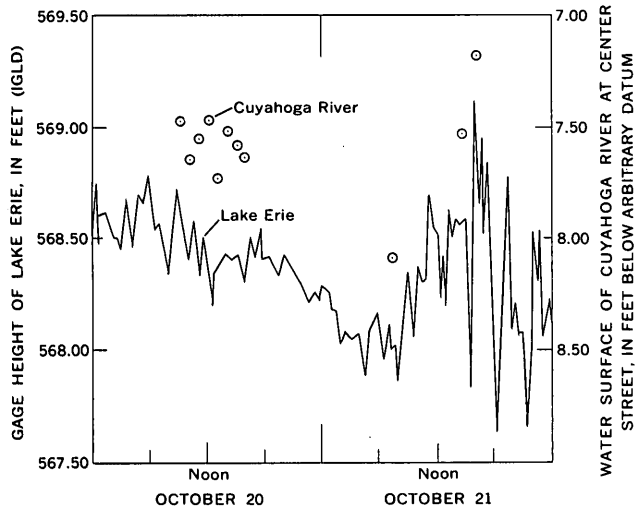


FIGURE 2.—Fluctuations in level of Lake Erie at Cleveland (graph), and of the Cuyahoga River at Center Street bridge in Cleveland (circled points), October 20–21, 1964. Gage height of Lake Erie based on International Great Lakes Datum, and that of Cuyahoga River on an arbitrary datum.

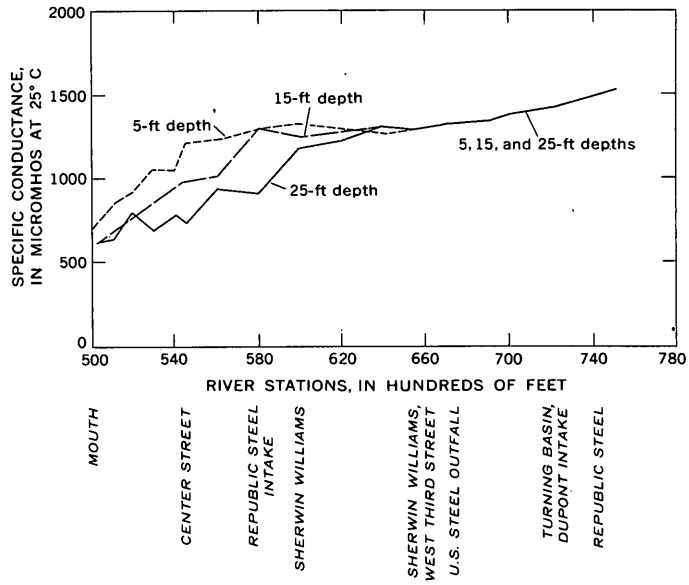


FIGURE 3.—Specific-conductance profiles made at three depths along the centerline of the Cuyahoga River at Cleveland, October 21, 1964.

micromhos, and during the October 21 traverse it ranged from 950 to 1,240 micromhos.

Conductivity, temperature, and dissolved-oxygen traverses were made from a boat at about midchannel, starting at the mouth (station 500) and extending to the head of navigation (station 770). Measurements were made at 1,000-foot intervals along the channel, and at each 5-foot increment of depth. At the Center Street bridge (station 545), at station 717 (just downstream from the turning basin), and at station 722 (at the turning basin), measurements were also taken halfway between the center and each side of the channel, to determine the cross-sectional variation in water quality.

The traverses show that the water in the upper reaches of the channel is well mixed and of uniform quality, whereas in the lower 2-mile reach the water quality changes both with depth and with distance from the mouth. The specific-conductance data for October 21, 1965, are shown on figure 3. For clarity, only the data for the 5-, 15-, and 25-foot depths are shown. Upstream from the vicinity of station 640, differences in specific conductance of the water at various depths are small, indicating nearly complete mixing of the river water with the industrial and municipal wastes contributed along this reach.

Downstream from station 640, and progressively toward Lake Erie, there was a continuous improvement in the quality of the river water. The improvement was due to the dilution and mixing of the river water with lake water. However, mixing was not complete, and the quality of water in the navigable channel depended significantly on depth. The general reduction in the specific conductance of the water with depth is shown in figure 3. The colder and less mineralized lake water had intruded upriver under the warmer and more mineralized river water.

The improvement in water quality from station 640 to Lake Erie is also indicated by the temperature profiles in figure 4. Upstream from station 640 the temperature was nearly uniform, both longitudinally and at the various depths. From station 640 to the mouth of the Cuyahoga River there was a general

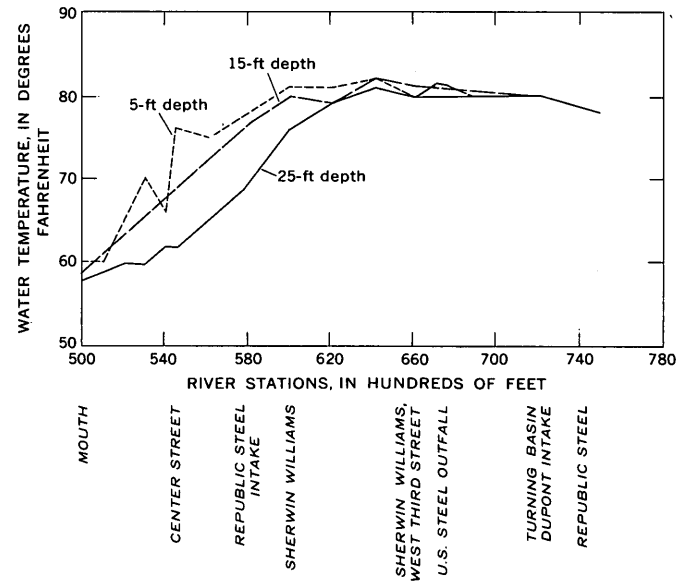


FIGURE 4.—Water-temperature profiles made at three depths along the centerline of the Cuyahoga River at Cleveland, October 21, 1964.

reduction in temperature, with cooler water near the lake and at depths.

The higher water temperatures in the navigation channel are the result of the heat load in the water contributed by industrial and municipal waste outfalls in the Cleveland area. Thus at Independence, upstream from the reach affected by heavy waste disposal, the thermograph record showed a range in water temperatures from 55°F to 57°F, as compared with a range from 78°F to 86°F measured in the upper navigation channel.

Because of their difference in temperature the water in the navigation channel and that in Lake Erie are of different density. When the lake water moves upstream, due to seiche or to wind, it tends to move under the warmer and less dense river waters. This upstream movement of Lake Erie water in the Cuyahoga River is similar to the upstream movement of sea water into a tidal estuary. In tidal estuaries, the sea water is more mineralized and therefore denser that the fresh water, and stratification occurs as the river water passes over the sea water. The Cuyahoga River is more mineralized than Lake Erie, but because of its higher temperature the river water is less dense and tends to flow over the lake water.

The stratification of the water which was observed during this study in the downstream reach of the navigation channel of the Cuyahoga River probably persists throughout the summer months, when the temperature difference between lake water and river water is significant. During periods of high water discharge, or when the temperature differential of the lake and river is small, the stratification is probably altered or destroyed. During high-flow periods there would be little or no movement of lake water upstream into the channel, and water-quality differences throughout the channel should be small. Moreover, when the temperature differential is small, the density difference and resulting stratification should be reduced. During periods when the temperatures are similar, the river water—because it is more mineralized than lake water—may even be denser, and may pass under the lake water.

Lateral variations in water quality were also observed in the downstream reach of the navigable channel. Six series of conductivity measurements at 5-foot increments of depth were obtained at the one-quarter points across the channel at Center Street bridge (station 545). In each series of measurements, differences were noted in the specific conductance at a given depth, with the lower conductance occurring generally at midchannel. These measurements also indicated the incomplete mixing of the river water (containing waste water from municipal and industrial outfalls) with lake water. The discharges from the outfalls evidently tend to follow along the sides of the channel.

The passage of ships and tugs provides some mixing of the water, but does not completely destroy the vertical stratification or lateral differences in the water quality. This mixing was observed at Center Street bridge, where a cross-sectional measurement made immediately after passage of a loaded ore freighter moving upstream indicated that water in the left (west) one-third of the channel was temporarily well mixed below a depth of 10 feet. Also, the common appearance of black sludge and bottom sediments at the water surface after passage of freighters shows that the bottom water is overturned.

Cross-sectional measurements taken at station 717 and in the turning basin at station 722, where there is no vertical stratification of the water (see figs. 3 and 4), showed no lateral variation. The conductivity measurements indicated a uniform water quality both laterally and vertically.

The dissolved-oxygen content of the water was deficient throughout the navigation channel during the study. However, a measurement above the navigation channel, at Independence, showed a dissolved-oxygen concentration of 6.4 parts per million, or 57 percent saturation. This satisfactory dissolved-oxygen concentration is due, at least in part, to aeration of the water as it passes over several riffles upstream from Independence. The oxygen was soon depleted, however, when the river received the municipal- and industrial-waste load in the Cleveland area. Measurements of dissolved oxygen there showed that all sections of the navigation channel more than about 1 mile upstream from the mouth had 0.0 ppm of dissolved oxygen. The anaerobic conditions in the channel were also shown by gas bubbles, which were seen to rise and break at the surface in some reaches. Within about 1 mile of the mouth, the intruded lake water provided some dissolved oxygen. At Center Street bridge, the dissolved-oxygen concentration at the 5-foot depth ranged from 0.0 to 1.9 ppm on October 20, and from 0.1 to 1.2 ppm on October 21. At station 500, at the river mouth, lake water contributed considerable dissolved oxygen. The concentrations at the 5-foot depth were 2.8 ppm (30-percent saturation) on the morning of October 20, and 5.0 ppm (50-percent saturation) on the morning of October 21.

## CONCLUSIONS

The study indicated that water from Lake Erie intrudes the navigation channel of the Cuyahoga River, and that stratification of the lake and river water occurs. Seiches, wind, and probably fluctuations in streamflow and lake levels affect both the extent of the intrusion and the degree of stratification of the water. In the upstream reaches of the channel the water is apparently well mixed, and samples representative of the cross section at a given site may be obtained at verticals near midstream, or possibly from large-volume water intakes. In the downstream reaches, where stratification occurs, sampling at several verticals in the cross section and at several depths is necessary to define water-quality conditions in a given cross section.

211-690 O—66——18

# A HYDRAULIC SQUEEZER FOR OBTAINING INTERSTITIAL WATER FROM CONSOLIDATED AND UNCONSOLIDATED SEDIMENTS [1]

By FRANK T. MANHEIM, Woods Hole, Mass.

*Abstract.*—A squeezer based on designs developed by P. A. Kriukov has been constructed, using fabricated and commercially available parts, and used with a standard laboratory press to recover interstitial water from sediments. Analyzable amounts of water were extracted from as little as 2 g of relatively compact sediment at pressures of 3,000 to 9,000 psi (approximately 200 to 600 kg/cm$^2$). Extraction of water from most samples of core materials from Recent to Paleocene sediments was completed in 3 minutes. The residue after squeezing is in the form of a compact pellet which may be further dried to determine total water content of the original sample. The present work confirms Soviet experience, with similar squeezers, that pressure does not appreciably affect the composition of extracted waters when proper precautions are observed.

With the recent rise of interest in the composition of interstitial waters of sediments, a number of methods have been employed by Western workers for extracting pore fluids for geologic study. These methods include leaching (Emery and Rittenberg, 1952; Kullenberg, 1952; Swarzenski, 1959), centrifugation (Powers, 1957; Rittenberg and others, 1963), immiscible-liquid displacement (Scholl, 1963), gas displacement (Lusczynski, 1961), low-pressure mechanical squeezing (Shepard and Moore, 1955; Siever, 1962), and low-pressure gas-mechanical squeezing (Hartmann, 1965; Raymond Siever, oral commun., 1965). Except for leaching, these methods are best suited for use with Recent sediments or other relatively unconsolidated sediments. In the Soviet Union, on the other hand, hydraulic squeezers of the Kriukov type (Kriukov, 1947; Kriukov and Komarova, 1954) have been used extensively for both unconsolidated and consolidated sediments. For example, interstitial water has been squeezed from Jurassic claystones containing 9 percent water by wet weight (Buneev and others, 1947).

Centrifugation, low-pressure squeezing, and other methods proved inadequate to deal with the small, partially compacted core sections from holes drilled in the Atlantic Ocean bottom off Florida (JOIDES, 1965). A small squeezer of the Kriukov type, constructed with minor modifications, proved effective in extracting water from several hundred core samples weighing from 2 to 15 grams. To my knowledge, this type of squeezer has not been used before in the United States, and its simplicity of operation and its capability for handling even small samples of relatively compact sediments recommend it for wider usage. To this end, details of construction and operation are reported in this paper; no originality in basic design is claimed.

*Acknowledgments.*—Thanks are due Mrs. Heidi Richards, of the Woods Hole Oceanographic Institution, who carried out a number of experiments with the apparatus, and to Jack Brennan, of the Woods Hole Oceanographic Institution, who constructed the equipment. The manuscript was improved by criticism from K. O. Emery, of the Woods Hole Oceanograhpic Institution, and R. H. Meade, B. F. Jones, and H. A. Olsen, of the U.S. Geological Survey.

## CONSTRUCTION

The squeezer utilizes a commercially available cylinder and ram (made by the Carver Co., Summit, N.J.) to which a machined base with a filtering element and fluid outlet is fitted. Construction details are shown in figure 1. The filter unit consists of a stainless steel screen and a perforated steel plate contained in a circular recess in the steel filter holder. Alternatively, a porous (sintered) metal plate may be used to replace both screen and perforated plate. The top surface of the filter should be flush with the outer rim of the holder so that it may support one or more paper filter disks. Fine-grained, hardened laboratory

[1] Contribution No. 1805 of Woods Hole Oceanographic Institution.

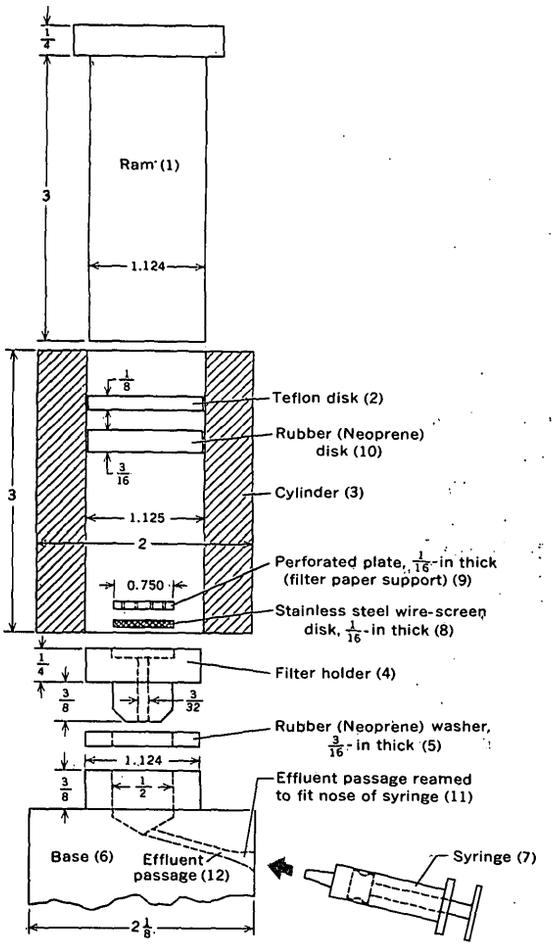


FIGURE 1.—Drawing showing components of hydraulic squeezer. All dimensions in inches. (Base is about 2½ inches in height.)

filters give a visually clear effluent, but membrane or micro filters may be used to assure maximum freedom from suspended matter. The lower part of the filtering assembly, fitted with a rubber washer, protrudes into a recess in the steel base; when pressure is applied the gasket is squeezed against the cylinder and prevents leakage of water around the filter unit. The space in the recess and the diameter of the outflow boring are kept small so that little fluid can collect in the squeezer itself. All metal parts in the filter base are made of Iron and Steel Institute No. 303 stainless steel. The Carver cylinder and ram are chrome-plated steel. If maximum corrosion resistance must be maintained, the cylinder and ram should also be machined of a good grade of stainless steel, because the chromium will abrade in time, exposing corrodible steel. Rubber and Teflon disks just below the piston prevent loss of fluid upward when pressure is applied. The rubber, Teflon, and filter-paper disks are punched out with an arbor punch and can be made as needed.

The present design permits insertion of a disposable syringe (preferably plastic) directly into the base of the squeezer to receive fluid. The narrow effluent hole is reamed out to permit fitting of the standard "Luer" taper of the syringe nose.

A larger squeezer has also been constructed using a 2¼-inch Carver cylinder and piston. The design is similar to that shown in figure 1, except that the filter plate is increased in thickness to give greater strength. The effluent line remains small. Because the cross-sectional area of the cylinder bore of the small squeezer is about 0.88 inch, a 10-ton laboratory press exerting its maximum load of 20,000 pounds will apply a pressure of about 22,000 pounds per square inch to the sediment. However, a 20,000-lb load will apply only about 5,000 psi in the large unit. The large squeezer should therefore be used with a higher capacity press when more compact sediments are to be squeezed.

## OPERATION

Figure 2 illustrates the manner in which the squeezer is operated. In sequence the steps in squeezing a sample are as follows: The filter holder with its gasket is placed in the recess of the filter base. The screen, perforated plate (or porous disk), and 2 or 3 filter-paper disks are positioned. The cylinder is seated over the filter unit so that it rests firmly on the base. Sediment is then quickly transferred into the cylinder through the top, followed by the Teflon and rubber disks. The Teflon and rubber disks can be placed above the sample in either order to obtain a leak-free pressure transfer, but placing the Teflon disk below the rubber disk gives a cleaner seal than the reverse order shown in figure 1. The piston is depressed as far as it will go into the cylinder, and the whole unit put in the press for squeezing. Pressure is applied gradually at first, and when the first drop of interstitial fluid is seen the syringe is seated in its hole in the base (effluent passage in figure 1). The squeezed-out liquid moves the plunger of the syringe back as the liquid is expelled, and there is minimum opportunity for evaporation. When the desired amount of liquid has been obtained the syringe is removed and capped.

Measurement of the amount of extracted interstitial water may be made (1) by weighing, or (2) volumetrically, with an accurately calibrated syringe. The preferred method in the present work has been to weigh the syringe on a single-pan semimicro balance having a precision of 0.1 milligram. After the syringe is emptied of the liquid the syringe is capped and

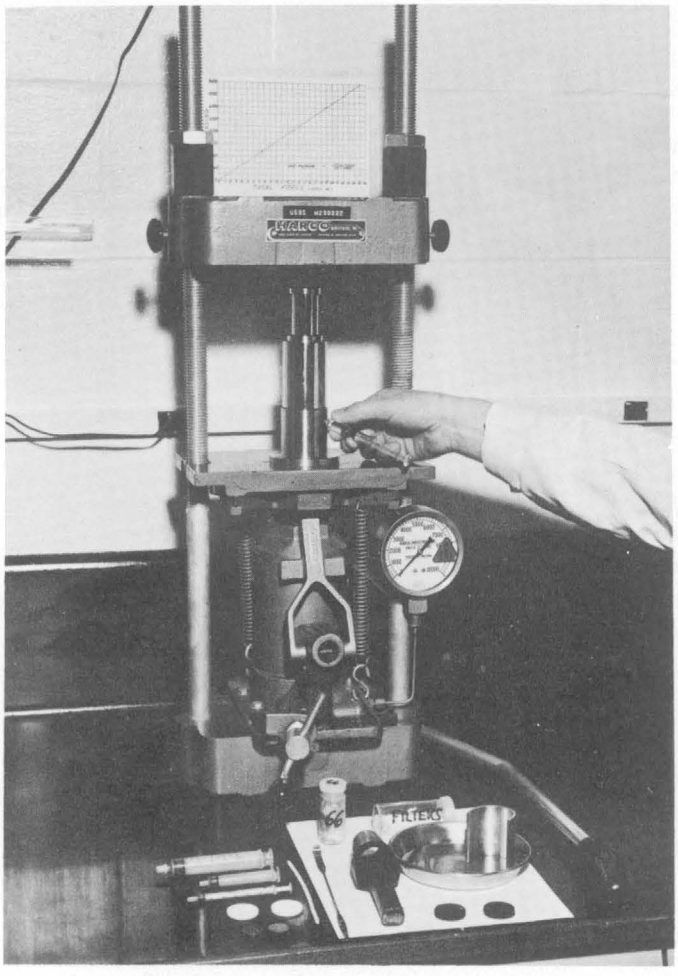

FIGURE 2.—Hydraulic squeezer set up for operation. The accessories on the bench include the following: several sizes of disposable syringes, perforated plate, Teflon and rubber gaskets, filter disks, arbor punch, and half-round steel holder. The half-round holder is used to support the squeezer while the sediment plug and filter plate are being pushed out of the piston after extraction is completed. The arbor punch is used to punch out rubber and Teflon gaskets and filter-paper disks.

weighed again to determine the amount of liquid. For 1 milliliter of sample the weighing precision is approximately ±0.01 percent (relative), whereas for 0.1 ml the precision is ±0.1 percent. Weighing has the following advantages: (1) temperature corrections for volumetric apparatus are eliminated, (2) the measuring precision for small amounts of fluid is better than can be achieved by volumetric methods, and (3) the proper units for weight-weight (‰ (grams of chlorine per kilogram of sea water)) determinations are obtained without specific gravity measurements. Experience has shown that evaporation losses, probably the largest potential cause of error in this procedure, can be held to 0.1 percent, which is consistent with routine rapid operation. If this level of accuracy is sufficient, conversion of weights to in vacuo units need not be carried out.

After extraction of the liquid the parts of the apparatus are rinsed with distilled water and (except for rubber parts) with acetone. The acetone helps dry the unit quickly in preparation for the next sample. The squeezing and washing operations together can be completed in 5 to 10 minutes.

## DISCUSSION

### Sampling

Samples which were taken immediately after the recovery of the core or sediments and were placed in airtight containers may be stored for some time if proper precautions are observed. Good results have been obtained when moistened laboratory tissue was wrapped in polyvinyl chloride film (kitchen-type plastic wrap) and placed above the sediment in glass sample vials with tightly fitting plastic closures. The film helps take up condensation space in the vials, and the moist tissue hinders evaporation from the sediment. When kept chilled (not frozen) such samples can be kept several months without appreciable evaporation. Sampling technique must, of course, be based on the individual problem and on the elements for which analysis is desired. Experience has shown that even relatively permeable cores can yield uncontaminated fluid if the outer parts of the cores are discarded in sampling. Lusczynski (1961) used fluorescein dye in drilling fluid so that contamination of cores could be more readily detected.

### Determination of total water content

Frequently it is desirable to determine the total water content of samples from which interstitial water is extracted. After squeezing by the present procedure practically all of the sediment remains as a firm to hard, flattened disk; loss of sediment by smearing on cylinder walls and other surfaces is usually low (less than 1 percent). The original water content may be determined by finding the difference between the weight of the sediment before squeezing and the weight of the compressed disk, plus any scrapings, after oven drying at 110°–120°C. To minimize exposure of the sediment to evaporation, the first weighing should be done with the sample container closed, and the container and cover should be reweighed after removal of the sediment to be squeezed. The squeezed and dried pellet is available for further studies.

### Influence of squeezing pressure

Soil scientists have long appreciated that squeezing pressure may influence the composition of pore solu-

tions extracted from sediment. Northrup (1918) pointed out that pressure may affect liquid-solid equilibria within the sediment in a variety of ways, and that it may cause solution or precipitation effects. Recent studies have suggested that, above a few thousand pounds per square inch, molecular (salt) filtration may take place when liquids are squeezed through clay membranes (for example, see Von Engelhardt and Gaida, 1963).

Detailed studies by Kriukov and his coworkers (Kriukov and Komarova, 1956; Tsyba and Kriukov, 1959; and Kriukov, 1964) have shown, however, that in normal practice the composition of water extracted by the present type of apparatus is not appreciably influenced by squeezing pressure until adsorbed or semi-liquid layers poor in electrolytes begin to be squeezed from the sediments at high pressures. An example of the variation in composition of extracts from a sodium bentonite clay subjected to successively higher squeezing pressures is given in figure 3. The pressure at which the drop in chloride occurred in extracts from the sample (at about 50 to 60 percent of water removed, fig. 3) is given by Kriukov and Komarova (1956) as about 600 kilograms per square centimeter or about 8,500 psi. The corresponding threshold for chloride in 0.86*N* NaCl was about 1,400 kg/cm² or 20,000 psi (also in sodium bentonite), whereas for fresher waters the influence of pressure on composition was noted at lower pressures. Sodium bentonite is especially sensitive to pressure effects, in part because of its large capacity for adsorbing water. Studies cited in Kriukov and Zhuchkova (1963) indicate that the pressure threshold for influence on the composition of interstitial water is shifted to higher pressures for ordinary sediments. The results of the above work may be applied to the present squeezer, because it differs from Kriukov's apparatus only in details of construction and in the technique for withdrawal of effluent, but not in operating principle.

In the interests of accuracy and speed, pressure should be applied gradually at first, and the pellet thickness should be kept small with respect to the diameter. Samples of 2 to 15 grams having from 20 to 60 percent bulk water were squeezed in approximately 3 minutes each. When samples of sediment of such size that the thickness of the compacted pellet is greater than ¼ to ⅛ of the diameter are squeezed rapidly, dense sediment layers may be formed next to the filter paper while the opposite end of the sample remains moist. Such behavior slows recovery and may, under some conditions, give rise to irregular compositional effects on the extracted fluid.

In any event, it is desirable to squeeze sediments, representing the range of materials to be studied, at different pressures, and to analyze the extracts. The chloride concentrations of successive extracts from two widely different sediment types are shown in table 1. Sample 1, from the Florida-Hatteras slope (U.S. Atlantic coast), contained a large proportion of finely divided carbonate. Sample 2, from the Gulf of Maine, contained more than 50 percent clay minerals, chiefly illite and mixed-layer montmorillonitic clays. The slightly lower chlorinity of the initial aliquot from sample 1 may be due to condensation, in the exit tube, of moist air initially pressed out of the sample chamber. This would result in slight dilution of the initial water fractions. Sample 2 is an average of replicate squeezings from two clayey mud samples which had been homogenized by kneading in a bag of kitchen-type plastic wrap. No further water could be obtained

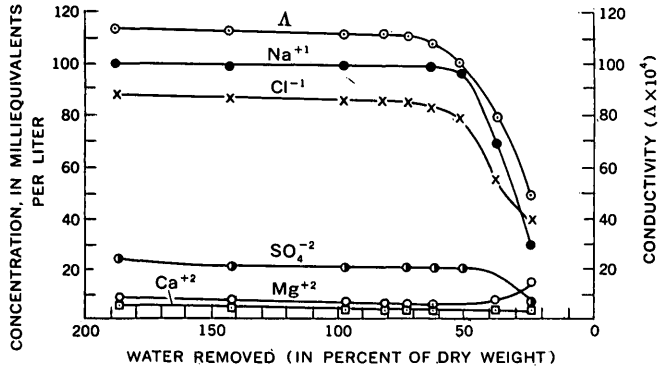


FIGURE 3.—Concentration of $Na^{+1}$, $Cl^{-1}$, $SO_4^{-2}$, $Mg^{+2}$, and $Ca^{+2}$, and conductivity of solution, in extracts from bentonite squeezed at different pressures (from Kriukov and Komarova, 1956). Sodium concentration is calculated from glass-electrode measurements of sodium-ion activity. Concentration is given in milliequivalents per liter, and conductivity (Λ) in reciprocal ohms (mhos) per centimeter.

TABLE 1.—*Analyses of successive extracts from marine sediments from the Florida-Hatteras slope and the Gulf of Maine*

Chloride determined by gravimetric titration with potassium chromate endpoint]

| Pressure (psi) | Cl (‰) | |
|---|---|---|
| | Sample 1 | Sample 2 |
| 580 | 19. 77 | |
| 750 | | 17. 87 |
| 1,250 | 19. 83 | |
| 1,500 | | 17. 90 |
| 2,500 | 19. 83 | |
| 3,000 | | 17. 85 |
| 3,920 | 19. 84 | |
| 5,180 | 19. 85 | |
| 6,000 | | 17. 87 |
| 7,780 | 19. 85 | |
| 9,000 | | 17. 90 |
| 12,000 | | 17. 93 |

1. Florida-Hatteras slope.
2. Gulf of Maine.

even on raising squeezing pressure to 21,000 psi. The last samples squeezed have a slightly higher chloride content than earlier ones. However, membrane-salinometer (Sanders and others, in press) determinations on the residual cake suggest that the remaining water has a lower chlorinity than the analyzed aliquots. This would be in accordance with Kriukov's finding of electrolyte-poor, "adsorbed" water in the last waters squeezed out of sediments. Replicate determinations of Cl on homogenized muds do not usually differ by more than 0.04 ‰, part of which may be due to inhomogeneity in the mud and part to analytical error.

### Limitations and applications

The present method is not applicable to crystalline rocks, nor to sediments too dense to be formed into a flat cylinder under available pressure. In order to avoid squeezing out electrolyte-poor adsorbed water from sediments, "safe" squeezing pressure limits should be determined experimentally for sediments typical of the range of materials to be studied. This is particularly applicable to sediments having very dilute pore waters. Coarse, permeable sands or calcarenites are poorly compressible and are likely to have been contaminated in drilling or coring. However, should one wish to obtain the interstitial water of a poorly compressible but permeable material, this can be done with a modified technique suggested by Scholl (1963; and oral commun., 1965). The sediment is placed in the cylinder and tamped down with the piston (no rubber and Teflon disk, but a filter paper aids in avoiding sticking). Then a fluid such as the epoxy plasticizer recommended by Scholl (1963) is poured in. The rubber and Teflon disks and the piston are introduced, and the pore water is squeezed out in the normal manner, squeezing being stopped when or before the immiscible liquid begins to appear in the effluent.

In addition to being used in study of pore fluids in marine sedimentary strata, squeezers of the type described here may potentially be useful in groundwater investigations. Lusczynski and Swarzenski (1962) pointed out the usfulness of studies of interstitial water for such work, particularly in areas of saline-water infiltration. The present squeezer offers the possibility of making water extraction more convenient, and of extending the technique to relatively compact materials and very small samples such as may be obtained in sidewall cores. Improved extraction techniques may facilitate the analysis of interstitial water as a technique complementary to electrical-log evaluation and to flow and pumping tests. Whereas the most permeable parts of aquifers may not always be amenable to interstitial-water analysis, some of these zones grade transitionally into less permeable strata that are suitable for analysis and may carry water of the same quality. By studying the water in transitional beds, fresh-water aquifers have been detected (work still in progress) in marine strata under the Atlantic Ocean many miles east of the Florida coast.

## REFERENCES


Buneev, A. N., Kriukov, P. A., and Rengarten, E. V., 1947, Opyt otzhimaniya rastvorov iz osadochnykh gornykh porod [Attempt to squeeze solutions from sedimentary rocks]: Akad. Nauk SSSR Doklady, v. 57, no. 7, p. 707–709.

Emery, K. O., and Rittenberg, S. C., 1952, Early diagenesis of California basin sediments in relation to origin of soil: Am. Assoc. Petroleum Geologists Bull., v. 36, p. 735–806.

Engelhardt, Wolf, von, and Gaida, K. H., 1963, Concentration changes of pore solutions during the compaction of clay sediments: Jour. Sed. Petrology, v. 33, p. 919–930.

Hartmann, Martin, 1965, An apparatus for the recovery of interstitial water from Recent sediments: Deep-Sea Research, v. 12, p. 225–226.

JOIDES (Joint Oceanographic Institutions Deep Earth Sampling Program), 1965, Ocean drilling on the continental margin: Science, v. 150, p. 709–716.

Kriukov, P. A., 1947, Metody vydeleniya pochvennykh rastvorov [Methods of extracting soil solutions] *in* Sovremenny metody fizikokhimicheskogo issledovaniya pochv [Modern methods for physicochemical studies of soils]: v. 2, p. 3–15, Moscow.

——— 1964, Pochvennye, ilovye i gornye rastvory [Interstitial waters of soils, muds, and sedimentary rocks]: Aftoreferat dissertatsii, Moscow, Institut Geokhimii i Analiticheskoi Khimi Akademiya, Nauk, SSSR [Author's summary of dissertation for degree of Doctor of Chemical Sciences], p. 1–57, published by Institut Geologii i Geofiziki, Sib. Otdel. Akademii Nauk, SSSR, Novosibirsk.

Kriukov, P. A., and Komarova, N. A., 1954, Ob otzhimanii vody iz glin pri sverkhvysokikh davleniyakh [On the squeezing out of waters from clay at very high pressures]: Akad. Nauk SSSR Doklady, v. 99, no. 4, p. 617–619.

Kriukov, P. A., and Komarova, N. A., 1956, Issledovanie rastvorov pochv, ilov i gornykh porod [Studies on the interstitial waters of soils, muds and rocks]: Mezhdunarodnomu kongressu pochvovedov, 2nd Komissiya, Doklady VI, p. 151–184 (Moscow).

Kriukov, P. A., and Zhuchkova, A. A., 1963, Fiziko-khimicheskie yavleniya, svyazannye s vydeleniem rastvorov iz gornykh porod [Physico-chemical conditions associated with the squeezing out of solutions from rocks]: Sovremennye predstavleniya o svyazannoi vode v porodakh (Sbornik), Izdatel'stvo Akad. Nauk SSSR, Moscow, p. 95–105.

Kullenberg, Borje, 1952, On the salinity of the water contained in marine sediments: Oceanog. Inst. Goteborg Medd., no. 21, 37 p.

Lusczynski, N. J., 1961, Filter-press method of extracting water samples for chloride analysis: U.S. Geol. Survey Water-Supply Paper 1544–A, 8 p.

Lusczynski, N. J., and Swarzenski, W. V., 1962, Fresh and salty ground water in Long Island, N.Y.: Am. Soc. Civil Engineers Proc., Hydraulics Div. Jour., v. 88, p. 173–194.

Northrup, Z., 1918, The true soil solution: Science, v. 47, p. 638–639.

Powers, M. C., 1957, Adjustment of land derived clays to the marine environment: Jour. Sed. Petrology, v. 27, p. 355–372.

Rittenberg, S. C., Emery, K. O., Hulsemann, Jobst, Degens, E. T., Fay, R. C., Reuter, J. H., Grady, J. R., Richardson, S. H., and Bray, E. E., 1963, Biogeochemistry of sediments in experimental Mohole: Jour. Sed. Petrology, v. 33, p. 141–172.

Sanders, H. L., Mangelsdorf, P. C., Jr., and Hampson, G. R., in press, Salinity and faunal distribution in the Pocasset River, Massachusetts: Limnology and Oceanography.

Scholl, D. W., 1963, Techniques for removing interstitial water from coarse-grained sediments for chemical analysis: Sedimentology, v. 2, p. 156–163.

Shepard, F. P., and Moore, D. G., 1955, Central Texas coast sedimentation: Am. Assoc. Petroleum Geologists Bull., v. 39, p. 1463–1593.

Siever, Raymond, 1962, A Squeezer for extracting interstitial water: Jour. Sed. Petrology, v. 32, p. 329–331.

Swarzenski, W. V., 1959, Determination of chloride in water from core samples: Am. Assoc. Petroleum Geologists Bull., v. 43, p. 1995–1998.

Tsyba, N. P., and Kriukov, P. A., 1959, Sravnenie metodov issledovaniya gornykh rastvorov (Comparison of methods for studying the interstitial water of sedimentary rocks): Gidrokhimicheskie materialy, v. 24, p. 273–81.

# AUTOMATIC BATTERY CHARGER FOR FIELD USE

By THOMAS O. DANDO, Washington, D.C.

*Abstract.*—A new, automatic battery charger, designed and developed by the USGS Topographic Division, relieves field engineers of the attendant care required to properly recharge batteries used with electronic equipment. The unit can recharge, simultaneously, as many as three 12-volt batteries to their full capacity in an overnight period.

Field engineers of the Topographic Division of the U.S. Geological Survey engaged in control surveys rely on rechargeable storage batteries as a source of power for their equipment. For recharging the batteries, the engineers have begun using a new automatic charger, developed by the Geological Survey.

The unit (fig. 1), equipped with solid-state components, is physically small (8×10×8 inches), which makes it convenient for field use. It is capable of withstanding extremes of temperature, shock, and vibration commonly met in field environments. It has the capacity to charge three 12-volt batteries simultaneously and to recharge them fully in an overnight period. Moreover, it adapts to either lead-acid or nickel-cadmium batteries. The most important advantage of the new charger is that it provides a controlled-rate charge which will cut off automatically when the batteries reach rated voltage.

## DEVELOPMENT

The need for the charger became apparent in 1963 after a study of the causes of numerous reported battery failures. Analysis of the problem indicated that proper charging would provide much longer battery life and more dependable service. Contrary to popular conception, Division engineers found that recharging a battery properly is not a simple procedure. Regardless of the type, a battery must usually be recharged every day after normal work hours. Connecting a battery to a conventional charger and leaving it for any arbitrary length of time almost assuredly results in either undercharging it, with loss in dependability, or overcharging it, with damage to the cells.

The lead-acid battery is relatively inexpensive and able to withstand charging abuse, but because of its weight, it is seriously limited in many field situations. The nickel-cadmium battery, on the other hand, is compact, lightweight, and therefore extensively used in the field. With proper treatment it has almost indefinite life. However, it is very expensive and easily damaged by improper charging. Consequently, the ability of the charger to save money, by assuring reliable service and long life for nickel-cadmium batteries, has already been demonstrated in field use.

In a review of the commercial battery chargers on the market, design engineers found that, for field use, none had all the features desired—compactness, rugged construction, automatic operation, and the capability of handling, simultaneously, both lead-acid and nickel-cadmium batteries. These considerations led to the fabrication, in February 1965, of the first production model of the new charger.

## GENERAL CONSTRUCTION AND OPERATION

The circuitry is housed in a metal case, whose front face provides a mount for the control switches, indicator lamps, fuses, and output jacks (fig. 1). Inside the case, room is provided for storage of a power cable, battery leads, and spare parts. The storage space is accessible by means of a hinged back cover. On the inside face of the cover are printed a circuit diagram and a set of operating instructions.

The unit has three charging channels. One channel is designed for nickel-cadmium, 12-v batteries only, but each of the other two channels is adaptable, by a switch, to either nickel-cadmium or lead-acid 12-v batteries. The channels can function separately or simultaneously. A battery to be charged is connected to the charger on the proper channel, and the charger is turned on. A red indicator lamp shows that the battery is accepting current. As the battery voltage rises,

U.S. GEOL. SURVEY PROF. PAPER 550-C, PAGES C262-C264

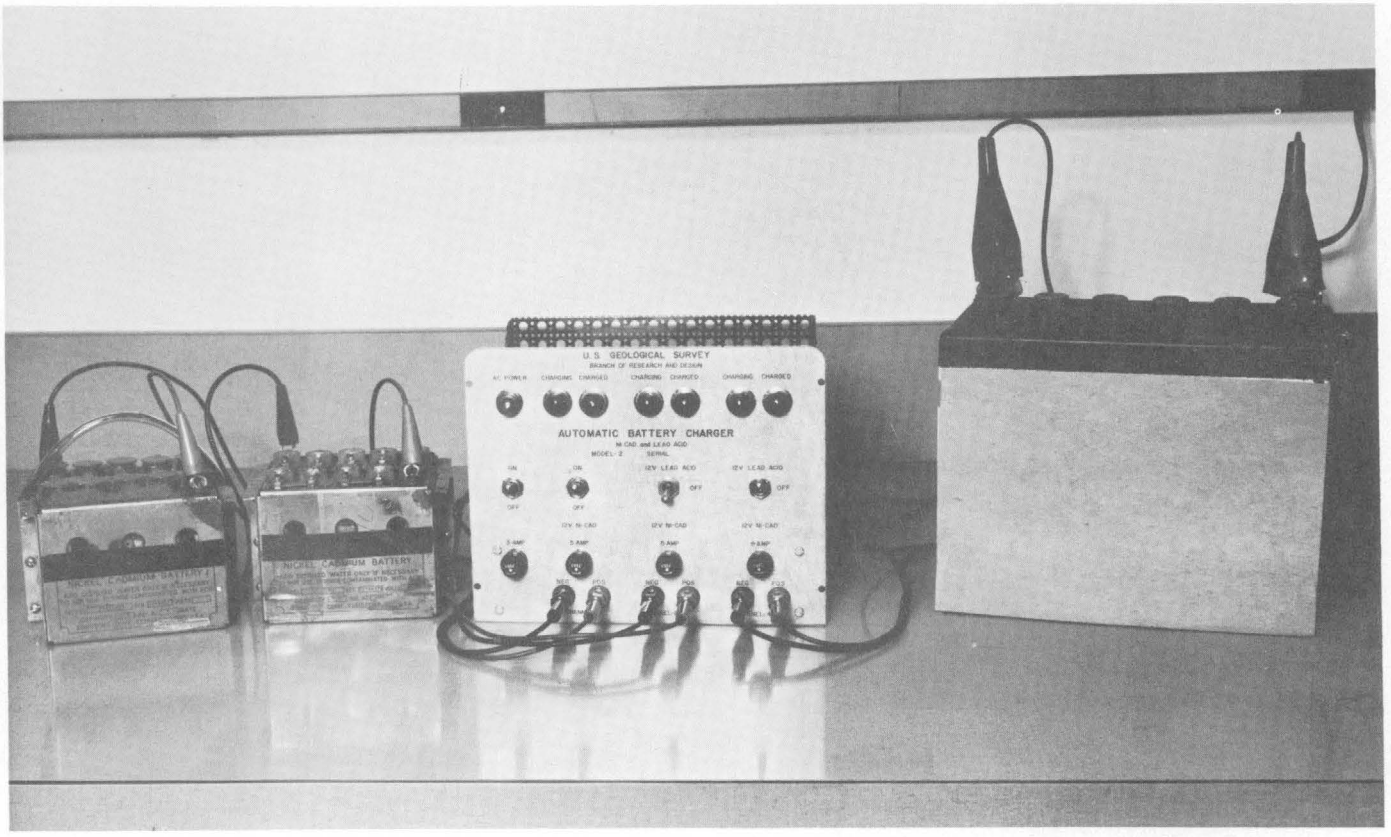


FIGURE 1.—Charger (with the case removed) connected to two nickel-cadmium batteries and a lead-acid battery.

control circuits cause the charging current to diminish. This prevents overcharging which would result in gassing of the battery cells. When the battery reaches rated voltage, the charging stops and a green "charged" lamp lights. If the battery, because of a bad cell, will not accept a charge, the two indicator lamps pulsate rapidly on and off.

If the charged battery is left on the charger, a low external circuit drain and internal battery leakage cause it to slowly discharge a small fraction of its total capacity. When this drain lowers the charge to a preset point, the sensors again switch the system to "charge." This cycle continues as long as the battery is connected to the charger.

## ELECTRICAL CIRCUITS

The circuit layout in schematic form is shown in figure 2. Channel 3 is not included because it is identical with channel 2. A detailed explanation of channel 1 follows: With the line switch $S_1$ closed, the step-down transformer $T_1$ reduces the 110–v a–c supply to 12 v a–c. Silicon rectifiers $CR_1$ and $CR_2$ convert this to full-wave pulsating d–c voltage with an effective value of about 15 v; actual pulse amplitude varies from 0 to about 18 v.

With a discharged battery attached to output terminals $J_1$ and $J_2$ and channel switch $S_2$ closed, a voltage develops across the voltage divider network $R_3$ and $R_5$. This makes the gate of silicon-controlled rectifier $SCR_1$ more positive than its cathode. With this condition, $SCR_1$ conducts, thus admitting a charge to the battery. By its nature, a silicon-controlled rectifier will conduct, once fired by a gate pulse, as long as the anode is positive with respect to the cathode. Although the cathode of $SCR_1$ is tied to the positive battery terminal, with a pulse-type input the gate and anode are more positive than the cathode for part of each cycle. Thus $SCR_1$ conducts intermittently. As the battery voltage increases, conduction time decreases. Hence, the rate of charging is inversely proportional to the battery voltage. This automatic charge-rate taper prevents overcharging. No current-limiting resistors are needed in series with the battery because the transformer output is filtered by capacitors $C_1$ and $C_2$ to avoid high peak voltages.

While charging progresses, a positive potential on

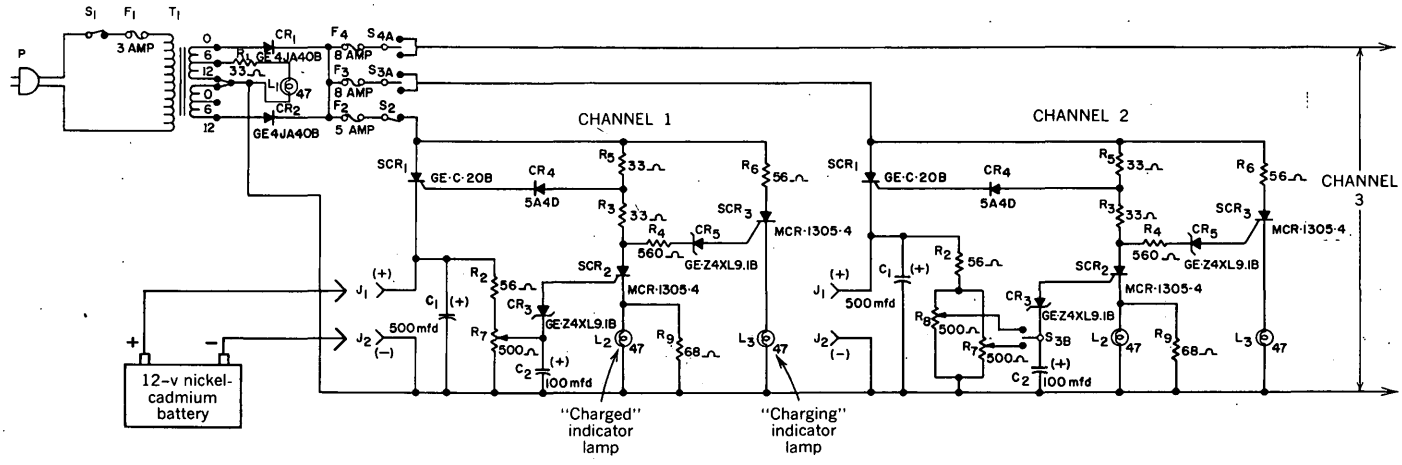


FIGURE 2.—Circuit diagram of charger (channels 1 and 2).

the gate makes $SCR_3$ conduct, lighting the "charging" indicator lamp $L_3$. Resistor $R_4$ limits the gate current and prevents it from being overdriven. Zener diode $CR_5$ is a reference diode; the breakover voltage at which it conducts is established in its construction. Thus $CR_5$ sets the voltage level at which $SCR_3$ fires. $R_6$ is a voltage-dropping resistor that limits the voltage across lamp $L_3$. Although the lamp's operating voltage is 24 v, the series resistor $R_6$ reduces the lamp voltage appreciably below this amount and increases the life of the lamp. This design is an important feature of all the lamp circuits.

When the battery reaches full voltage, a sensing circuit acts to stop the charging current flow. (A fully charged, nominal-12-v lead-acid battery has a terminal voltage of about 13.8 v, and a nickel-cadmium battery has a terminal voltage of 14.5 v.) The battery potential develops across $R_2$ and $R_7$ in parallel with the battery. Being a high resistance net, this path consumes little power. Capacitors $C_1$ and $C_2$ across the resistances act as filters for the load (the battery) and zener-diode sensor $CR_3$. In this case (for a nominal-12-v nickel-cadmium battery) a 9-v zener diode was selected, and the potentiometer was set for a potential of slightly above 9 v when the battery is at full potential. When the battery reaches full charge, the 9-v potential between the sliding contact of $R_7$ and a ground point causes zener diode $CR_3$ to conduct.

This triggers $SCR_2$ into conduction, which in turn lights the "charged" indicator lamp $L_2$. Even more important, conduction in this path redistributes the voltage drop across the divider network $R_3$ and $R_5$. The voltage at the junction of $R_3$ and $R_5$, and consequently at the gate of $SCR_1$, is now below the cathode potential of $SCR_1$ and therefore stops conduction to the battery. The voltage across zener diode $CR_5$ falls below its breakover voltage, thus removing the gate signal from $SCR_3$. Under this condition, when the pulse input to $SCR_3$ falls to zero, $SCR_3$ stops conducting and the "charging" indicator lamp $L_3$ is turned off. The lamp remains off until conduction through $L_2$ ceases. Resistor $R_9$ in parallel with $L_2$ serves to keep the channel operating even if $L_2$ burns out.

If the battery remains connected to the charger, the battery voltage drops a small amount because of internal leakage and a small flow through $R_2$ and $R_7$. This drain, though small, eventually lowers the battery voltage enough to block $CR_3$ and stop conduction through $SCR_2$. This restarts a charging cycle to maintain the battery at full potential.

The sensing networks for channels 2 and 3 differ only slightly from that of channel 1. Switch $S_{3B}$ adapts channel 2 to either type of battery. Potentiometer $R_8$ is provided to change the cutoff voltage to match the slightly lower voltage of the lead-acid battery. Otherwise, the circuits are the same.

The new charger has proved to be a dependable, money-saving piece of equipment, capable of properly charging the light but expensive nickel-cadmium batteries and assuring their long life.

# SUBJECT INDEX

[For major headings such as Economic geology," Geophysics," Paleontology," see under State names or refer to table of contents]

# AUTHOR INDEX





U.S. GOVERNMENT PRINTING OFFICE: 1966 O—211-690